Natural Disaster Science and Mitigation Engineering:
DPRI Reports

Tetsuya Sumi
Sameh A. Kantoush
Mohamed Saber *Editors*

Wadi Flash Floods

Challenges and Advanced Approaches for Disaster Risk Reduction

OPEN ACCESS

Springer

Natural Disaster Science and Mitigation Engineering: DPRI Reports

Because of the high concentration of population in urban habitats and the strong linkage to infrastructures that support a modern urban lifestyle, natural disasters such as fl oods, typhoons, earthquakes, tsunamis, landslides, and volcanoes always create new areas of severe damage whenever they occur. Japan is a "disaster country" of sorts: the Japanese have had to survive many different kinds of natural disasters and consequently they have accumulated a substantial body of knowledge in the phenomenology and mitigation of natural disasters. This series of books presents recent advances in all aspects of natural disasters and related mitigation technologies developed in Japan to be shared with the international community.

The areas covered in this series include

1. Earthquake risk
2. Strong motions and damage prediction for urban structures
3. Volcanic eruptions
4. Ground failures
5. Climate and water disasters
6. Fire and environmental disasters
7. Disaster management and mitigation

More information about this series at http://www.springer.com/series/11773

Tetsuya Sumi · Sameh A. Kantoush ·
Mohamed Saber
Editors

Wadi Flash Floods

Challenges and Advanced Approaches for Disaster Risk Reduction

Springer

Editors
Tetsuya Sumi
Water Resources Research Center (WRRC)
Disaster Prevention Research Institute (DPRI)
Kyoto University
Uji, Kyoto, Japan

Sameh A. Kantoush
Water Resources Research Center (WRRC)
Disaster Prevention Research Institute (DPRI)
Kyoto University
Uji, Kyoto, Japan

Mohamed Saber
Water Resources Research Center (WRRC)
Disaster Prevention Research Institute (DPRI)
Kyoto University
Uji, Kyoto, Japan

This book was funded by the Water Resources Research Center (WRRC) of the Disaster Prevention Research Institute (DPRI) at Kyoto University, which provided support for publishing the book as Open Access through Springer. In addition, the book has been professionally edited using financial support from Springer's DPRI book series at DPRI, Kyoto University. The editors highly appreciate the financial support from WRRC and DPRI.

ISSN 2196-4394 ISSN 2196-4408 (electronic)
Natural Disaster Science and Mitigation Engineering: DPRI Reports
ISBN 978-981-16-2903-7 ISBN 978-981-16-2904-4 (eBook)
https://doi.org/10.1007/978-981-16-2904-4

This Springer imprint is published by the registered company Springer Nature Singapore Pte Ltd.
The registered company address is: 152 Beach Road, #21-01/04 Gateway East, Singapore 189721, Singapore

To academics, researchers, engineers, students, professionals, and decision-makers who are interested in flash flood risk reduction and sustainable water management for improving secure development in arid and semiarid regions

Preface

Introduction

Over the last two decades, a number of studies, research papers, and contributions have been published on wadi system issues. The first specific and original book was presented by Sen in 2008, and it was named "Wadi hydrology." In this book, the author highlighted the wadi terminology to provide a definition for arid basins and addressed the assessment methodologies from different aspects of water resources with innovative and distinctive concepts. Additionally, UNESCO IHP established the "Global Network on Water and Development Information for Arid Lands (G-WADI)" in 2004. It was originally initiated to strengthen the capacity to manage water resources in arid and semiarid regions and build an effective global community through the integration of networks, centers, organizations, and individuals (https://gwadi.org/). Although many previous studies have focused on arid environment characteristics and rainfall-runoff modeling, water management, and disaster risk reduction, the current situation is still challenging due to climate change impacts and global warming. Therefore, we present this book as an attempt to continue the efforts of previous researchers and scientists to develop a tangible and sustainable management process that considers all water resource aspects in arid and semiarid regions.

Wadi flash floods (WFFs) have recently become more frequent and devastating, and they result in significant economic, property, and life losses, as well as environmental degradation. The wadi systems of arid and semiarid regions face various challenges that hamper water resource management for secure sustainable development. Among these, challenges are data limitations (availability and quality), dual disaster events (floods and droughts), water shortage (quantity and quality), improper management (water and sediment), and weak comprehensive understanding of the WFF processes and appropriate WFF approaches (models, strategies, and planning). Although several research studies focused on the use of WFFs to mitigate flash floods in some arid regions based on impact modeling (Saber et al. 2010, 2015, 2017, 2018, 2019, 2020a, b; Saber 2010; Kantoush et al. 2011;

Cools et al. 2012; Moawad 2013; Sumi et al. 2013; Abdel-Fattah et al. 2015; Saber and Habib 2016; Youssef et al. 2016; Abdel-Fattah et al. 2016; Abuzeid et al. 2016; Abdel-Fattah et al. 2017; Abdel-Fattah et al. 2018; Saber and Yilmaz 2018; Al-Mamari et al. 2019; Abdrabo et al. 2020; Prama et al. 2020; Abdel-Fattah et al. 2021), the spatiotemporal variability in both the magnitude and frequency of flash floods is still not well understood and has not been scientifically evaluated, especially in terms of climate change. In this book volume, a comprehensive vision and research directions are introduced with the goal of enhancing the scientific understanding of natural disaster science and WFF mitigation. The book stresses the urgent need to develop sustainable approaches and methods to simulate and forecast WFFs by focusing on water management, climate change impacts, disaster risk reduction, society and environmental development.

The book includes selected high-quality papers from five series of the International Symposium on Flash Floods in Wadi Systems (ISFF) that were held in 2015, 2016, 2017, 2018, and 2020 in Japan and Egypt, Oman, Morocco, and Japan, respectively. The main merit of this comprehensive book is its focus on research and technical papers as well as case study applications in different regions worldwide (see the global maps, Fig. 1) that cover many topics and answer several scientific questions.

The main factors that lead to increases in wadi flash floods in terms of frequency and intensity must be identified to develop robust forecasting programs and proper mitigation strategies for flash flood risk reduction. Additionally, the hydrological characteristics, such as rainfall spatiotemporal variability, infiltration processes, runoff generation, and surface and subsurface water interactions, must be investigated along with geomorphological, topographical, and geological features. This approach represents an optimal method of overcoming the identified issues.

Water resources are highly scarce in arid and semiarid regions; therefore, water management is a must. There are challenges in water resource management related

Fig. 1 Target regions and country applications reported in the WFF textbook

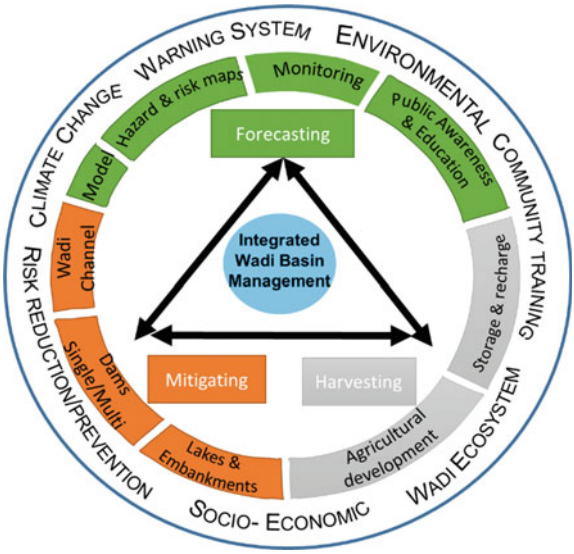

Fig. 2 Governing factors and issues for wadi flash flood management

to the increases in population, agricultural areas, and water demand. Moreover, the hydrological conditions in such regions are not only extremely variable but also affected by climate change. Due to the absence of water management and sustainable mitigation strategies, the development of effective hydrological models is desperately needed to overcome wadi system problems. Therefore, we propose a multidisciplinary approach relying on the addressed factors (Fig. 2). Such a proposed research strategy focuses on WFF modeling, mitigation, and harvesting as well as the related socioenvironmental issues. We propose an integrated strategy based on multidisciplinary research according to the following issues:

- **Innovative approaches**: What factors are missing in the existing approaches for flash floods? How can we enhance the forecasting and mitigation of models and methodologies?
- **Databased networks**: What are the existing challenges of observation and monitoring networks for modeling and forecasting? How can we enable these ungauged wadi basins?
- **Teamwork**: What are the existing global and national networking programs for research collaboration? How can we start efficient networks that include researchers, professionals, engineers, and stakeholders from different countries?
- **Risk reduction and sediment management**: How can we propose flash flood risk reduction approaches based on innovative hydrological models and mitigation actions?
- **Water harvesting and water management**: How can we integrate methods for surface and subsurface water management for water harvesting and groundwater recharge?

- **Society and environment**: How can we develop wadi societies and communities by involving the local population in research project implementation?
- **Decision making, planning, and governance**: How can we improve the existing national and global plan for wadi society development?

Overview of the Wadi Flash Flood Textbook

The main purpose of this book is to bring together research studies, developments, and application-related flash flood topics on wadi systems in arid regions. In this book, the authors and contributors (engineers, researchers, and professionals) have introduced their recent scientific findings to develop proper, applicable, and innovative tools for mitigation, forecasting, and water management as well as society development. The main contents include recent scientific achievements and findings, which are introduced in 22 chapters under seven main research themes as follows:

Part I. Wadi Flash Flood Challenges and Strategies
Part II. Hydrometeorology and Climate Changes
Part III. Rainfall-Runoff Modeling and Approaches
Part IV. Disaster Risk Reduction and Mitigation
Part V. Reservoir Sedimentation and Sediment Yield
Part VI. Groundwater Management

Uji, Kyoto, Japan

Tetsuya Sumi
Sameh A. Kantoush
Mohamed Saber

References

Abdel-Fattah, M., Kantoush, S. A., Saber, M., & Sumi, T. (2021). Evaluation of Structural Measures for Flash Flood Mitigation in Wadi Abadi Region of Egypt. J Hydrol Eng, 26(2), 04020062

Abdel-Fattah, M., Kantoush, S., & Sumi, T. (2015). Integrated management of flash flood in wadi system of egypt: Disaster prevention and water harvesting. 京都大学防災研究所年報. B= Annu Disas Prev Res Inst. B, 58(B):485–496

Abdel-Fattah, M., M. Saber, et al. (2017). "A Hydrological and Geomorphometric Approach to Understanding the Generation of Wadi Flash Floods." Water 9(7): 553

Abdel-Fattah, M., S. A. Kantoush, et al. (2018). "Rainfall-Runoff Modeling For Extreme Flash Floods In Wadi Samail, Oman." J Jpn Soc Civ Eng Ser B1 (Hydraul Eng) 74(5)

Abdel-Fattah M, Kantoush S, Saber M., & Sumi T. (2016). "Hydrological modelling of flash flood at wadi samail, Oman." 京都大学防災研究所年報. B= Disaster Prevention Research Institute Annuals. B 59 no. B:533–541

Abdrabo, K. I., Kantoush, S. A., Saber, M., Sumi, T., Habiba, O. M., Elleithy, D., & Elboshy, B. (2020). Integrated Methodology for Urban Flood Risk Mapping at the Microscale in Ungauged Regions: A Case Study of Hurghada, Egypt. Remote Sens 12(21):3548

Abuzied, S., Yuan, M., Ibrahim, S., Kaiser, M., & Saleem, T. (2016). Geospatial risk assessment of flash floods in Nuweiba area, Egypt.J Arid Environ 133:54–72

Al-Mamari, M. M., S. A. Kantoush, et al. (2019). "Real-Time Measurement of Flash-Flood in a Wadi Area by LSPIV and STIV." Hydrology 6(1):27

Cools, J., Vanderkimpen, P., Afandi, G. E., Abdelkhalek, A., Fockedey, S., Sammany, M. E., ... & Huygens, M. (2012). An early warning system for flash floods in hyper-arid Egypt. Nat Hazards Earth Syst Sci 12(2):443–457

Kantoush, S. A., Sumi, T., Kojiri, T., Saber, M., Elshennawy, I., Awad, H., & Sefelnaser, A. (2011). JE-HydroNet: Modern Methodologies for the Management, Monitoring and Planning of Integrated Water Resources in the Nile Delta of Egypt. In Proceedings of the 34th World Congress of the International Association for Hydro-Environment Research and Engineering: 33rd Hydrology and Water Resources Symposium and 10th Conference on Hydraulics in Water Engineering (p. 3928). Engineers Australia.

Moawad, M. B. (2013). Analysis of the flash flood occurred on 18 January 2010 in wadi El Arish, Egypt (a case study). Geomatics, Natural Hazards and Risk, 4(3):254–274

Prama, M., Omran, A., Schröder, D., & Abouelmagd, A. (2020). Vulnerability assessment of flash floods in Wadi Dahab Basin, Egypt. Environ Earth Sci, 79(5):1–17

Saber, M. (2010). Hydrological Approaches of Wadi System Considering Flash Floods in Arid Regions. Kyoto, Graduate School of Engineering, Kyoto University

Saber, M. and E. Habib (2015). Flash floods modelling for wadi system: Challenges and trends. Landscape Dynamics, Soils and Hydrological Processes in Varied Climates: 317–339

Saber, M., & Yilmaz, K. K. (2018). Evaluation and bias correction of satellite-based rainfall estimates for modelling flash floods over the Mediterranean region: application to Karpuz River Basin, Turkey. Water, 10(5), 657

Saber, M., Abdrabo, K. I., Habiba, O. M., Kantosh, S. A., & Sumi, T. (2020). Impacts of triple factors on flash flood vulnerability in Egypt: urban growth, extreme climate, and mismanagement. Geosciences, 10(1), 24.

Saber, M., Kantoush, S., Sumi, T., Abdel-Fattah, M., Alharrasi, T., Koshiba, T., ... & Almamari, M. (2018). Field investigation on wadi system in arid regions: Flash flood indicators and sedimentation impacts. 京都大学防災研究所年報. B= Disaster Prev Res Inst Ann. B, 61 (B):722–731

Saber, M., Kantoush, S., Sumi, T., Ogiso, Y., & Alharrasi, T. (2019). Reservoir Sedimentation at Wadi System: Challenges and Management Strategies. 京都大学防災研究所年報. B= Disaster Prevention Research Institute Annuals. B, 62(B):689–699

Saber, M., S. A. Kantoush, et al. (2020). "Assessment of spatiotemporal variability of water storage in Arabian countries using global datasets: implications for water resources management." Urban Water J 1–15

Saber, M., S. Kantoush, et al. (2017). "Assessing flash floods prone regions at wadi basins in Aswan, Egypt." 京都大学防災研究所年報. B= Disaster Prev Res Inst Annuals. B 60(B):853–863

Saber, M., T. Hamaguchi, et al. (2015). "A physically based distributed hydrological model of wadi system to simulate flash floods in arid regions." Arab J Geosci 8(1):143–160

Saber, M., T. Hamagutchi, et al. (2010). "Hydrological modeling of distributed runoff throughout comparative study between some Arabian wadi basins." Annu J Hydraul Eng Jpn Soc Civil Eng, Japan Society of Civil Engineers 54:85–90

Sumi, T., Saber, M., & Kantoush, S. A. (2013). Japan-Egypt hydro network: science and technology collaborative research for flash flood management. J Disaster Res 8(1):28–36

Acknowledgements

The main contents of this book are collected from research papers, technical studies, and case studies presented at the ISFF conferences series; therefore, we would like to express our deep gratitude to all of the participants and authors for their worthy contributions to this book. Special gratitude is extended to the reviewers and experts who have generously helped and contributed significantly to improving the quality of the submitted book chapters based on their constructive comments and suggestions. Additionally, the editors greatly appreciate the financial support from DPRI for publishing this book in Springer's DPRI book series.

Summary

The chapters of the book are summarized in this section. The WFF book contains six themes and a total of 22 chapters focused on several topics associated with arid and semiarid regions. The first theme (Part I) is "WFF Challenges and Strategies," and it includes three chapters (Kantoush et al. 2021; Loudyi and Fekri 2021; and Boutaghane et al. 2021) that define the research gaps, directions, strategies, and challenges at the regional scale of the MENA region and the country scale, such as Morocco and Algeria.

Kantoush et al. (2021) (Chap. 1) provide a state-of-the-art scientific basis in terms of integrated flash flood management, and it mainly highlights the research gaps and emerging research methodologies that can contribute to guiding the management of WFFs in the Middle East and North African (MENA) arid areas. The chapter also discusses the importance and objectives of the international symposium on flash floods (ISFF) project and the different dimensions of flash flood phenomena, causes, and resulting impacts in the MENA region. This chapter highlights that flash flood disasters in arid environments are associated with several challenges related to flash flood features, arid environment characteristics, and data and methodology limitations. At the country scale, two chapters address local strategies. The second chapter addresses flood risk management practices in Morocco by Loudyi and Fekri (2021) (Chap. 2). In this chapter, the phenomenon of floods in Morocco is discussed, and the evolution of approaches to assess flood risk, related technical and governance aspects, and best practices for managing floods are highlighted. This chapter provides holistic insights into flood risk management in Morocco. The authors stated that the engagement of citizens and other public stakeholders within a participatory approach is recommended for better communication of flood risk preparedness and resilience enhancement, and it indicates that the involvement of international organizations, such as OECD and WB, and international collaboration in research can also offer a great opportunity for improving flood risk assessment in the country. The third chapter by Boutaghane et al. (2021) (Chap. 3) highlights the strategies for flood analysis and mitigation in Algeria. The flood monitoring network is also addressed by highlighting the data availability and quality and implementing the first forecasting and early warning

system. The authors stated that there are problems with the length of historical datasets obtained from hydrometric and pluviometric monitoring networks.

The second theme (Part II) is "Hydrometeorology and Climate Changes," and it includes two chapters. The first study by Nayak and Takemi (2021) (Chap. 4) focuses on the impact of climate change on temperature and precipitation in India. The study introduces a comprehensive assessment of future climate change in terms of the climatologies, distribution patterns, annual cycles, and frequency distributions of temperature and precipitation over India. The results indicate that some desert regions in the west and tropical humid climate types in the central and south regions of the country show possible temperature increases of 4–5 °C while the temperatures over the subtropical humid climates in the north and east regions of the country show increases of 3–4 °C. The second chapter by Belarbi et al. (2021) (Chap. 5) presents an analysis of the hydrological behavior of watersheds in the context of climate change in Algeria. The study focused on the temporal evolution of the rainfall-runoff relations in four basins in northwestern Algeria. The results show that in the four basins, rainfall deficits started in 1974/1975 and continue to the present with annual variability. The authors stated that such changes, which are characterized by downward trends, have motivated them to pay more attention to the proper functioning of completed or planned projects with the challenge of attaining sustainable management of water resources in the region to mitigate persistent drought. Both studies in India and Algeria highlight the importance of understanding climatic variability and its impacts on water resources as well as its relation with different climatic environments, and they also provide insights to understand climatic dynamics and variability.

The third theme (Part III) is "Rainfall-Runoff Modeling and Approaches," and it includes five chapters (Tügel et al. 2021; Holzbecher et al. 2021; Abdelmoneim et al. 2021; Al-mamari et al. 2021; and Banihabib and Vaziri 2021). Tügel et al. (2021) (Chap. 6) investigated flash floods in the region of El Gouna in Egypt by using a 2D robust shallow water model that incorporates time-dependent infiltration to find the most realistic infiltration settings for this desert area. The study concluded that in addition to the overestimation of infiltration, the DSM lacked accuracy and resolution because some important topographical features were not well captured. The authors recommended extending their research work to include infiltration measurements with a rainfall simulator to better represent the natural conditions during heavy rainfall events and to investigate the effect of surface sealing and improve the DSM. Holzbecher et al. (2021) (Chap. 7) introduced smart technology for an early warning system that includes hydrological sensors, remote sensing, sensor networks, data integration, hydrodynamic simulation and visualization, decision support and early warning systems and the dissemination of information to decision-makers and the public. Two case studies are presented in Australia and Oman with similar flood characteristics. The case of the flash flood guidance system of Oman shows that technical issues associated with flood warning systems can be addressed and resolved.

Abdelmoneim et al. (2021) (Chap. 8) presented a study on different global precipitation estimations based on satellite products (PESPs) with high resolution as

the input to the distributed Hydrological River Basin Environmental Assessment Model (Hydro-BEAM) to investigate the potential effects on streamflow predictions over the Blue Nile basin (BNB). A comparison of PESPs with observed gauge data reveals that the performance of the TRMM 3B42 V7 product is the most precise in terms of monthly precipitation estimates. Flash flood monitoring is not well implemented in arid regions; therefore, Al-Mamari et al. (2021) (Chap. 9) highlighted the importance of implementing innovative monitoring techniques that can use noncontact measurements to extract accurate information and data from wadi channels. Two different image-based techniques were applied in Oman. The first is photogrammetry processing to quantify postpeak flood discharge by using a drone survey to build a digital elevation model (DEM) that is calibrated and validated by a field survey. In the second method, they combined the previous technique with the large-scale particle image velocimetry (LSPIV) technique to measure flash flood discharge by installing a fixed camera at the site. The results show acceptable agreement between the applied techniques and the real observations, and it will represent a good step to measure and monitor flash floods indirectly. An additional study by Banihabib and Vaziri (2021) (Chap. 10) focused on using an experimental rainfall simulator to generate temporally varied rainstorms. A rainstorm simulator was designed and built using cascading tanks to generate rainstorm hyetographs that cannot be obtained using traditional rainfall simulators, and the results and numerical model showed that the instrument can simulate the temporal distributions of rainstorms with an accuracy of 95%.

The fourth theme (Part IV) is "Disaster Risk Reduction and Mitigation," and it includes four chapters (Abdrabo et al. 2021; Huq et al 2021; Saber et al. 2021; Saeed and Mills 2021). Abdrabo et al. (2021) (Chap. 11) presented a review study to address the role of urban planning and landscape tools concerning flash flood risk reduction within arid and semiarid regions. The chapter stated that the application of the urban planning approach for FRR in arid and semiarid regions has not yet received adequate attention and concluded that integration of a DRR strategy with both structural and nonstructural mitigation measures in spatial planning could be much more effective than applying the approaches separately. The second chapter by Huq et al. (2021) (Chap. 12) focuses on assessing the vulnerability of flash floods in the urban city of Dhaka, Bangladesh. The study addresses the importance of various factors, including social, economic, structural, institutional, political, geographic, and environmental factors, for measuring the specific nature of people's vulnerability levels to different hazards. The results show that slum inhabitants are more vulnerable to flash flood hazards than nonslum inhabitants. Additionally, Saeed and Mills (2021) (Chap. 13) explored the flash flooding risk in the Saudi Arabian city of Jeddah with a particular focus on the Abruq Ar Rughamah neighborhood. The results show that most of the area, especially the unplanned area, is located along a natural flood path. This paper concludes that it is important to develop a risk management strategy that includes limiting urban expansion in flood-prone areas and redesigning neighborhoods to increase flood resilience. The last chapter on this theme was introduced by Saber et al. (2021) (Chap. 14), who presented a comparison study at Wadi Uday in Oman and Sume Basin in Paraiba,

Brazil. The climatic characteristics are reviewed for both regions, and the rainfall-runoff inundation model (RRI) was used to simulate the discharge and flood inundation of recent flood events in the study areas. This simulation highlighted the severity and frequency of recent flash flood events to better assess the current mitigation measures in arid and semiarid basins. The findings indicated that flash floods tend to be more severe and extreme in arid regions than in semiarid regions despite the lower frequency of flash floods and the water scarcity in arid regions. Distributed dams also proved to be more effective in preventing flash floods in arid regions than in semiarid regions

The fifth theme (Part V) is "Reservoir Sedimentation and Sediment Yield," and it includes five chapters (Saber et al. 2021; Holzbecher and Hadidi 2021; Djoukbala et al. 2021; Adam and Suleiman 2021; Banihabib and Tanhapour 2021). In arid and semiarid environments, little attention has been focused on sedimentation assessments and impacts associated with flash floods, especially in the MENA region, with hyperarid conditions. Saber et al. (2021) (Chap. 15) highlighted the integration of field investigation and modeling as well as remote sensing techniques to understand the sediment dynamics in hyperarid reservoirs in Oman. This chapter presents an international collaboration project implemented in Oman focusing on monitoring and observing sedimentation and its impacts on infiltration in the Asserin Reservoir, Wadi Mijlas, Oman. Detailed field investigations were conducted, including drone surveys, pedon analysis, and infiltration tests, and questionnaires about flash floods were also implemented. The detailed field survey is highly important for assessing sediment transport and sedimentation impacts on infiltration. Holzbecher and Hadidi (2021) (Chap. 16) introduced a multiphysics approach that coupled shallow water equations (SWEs) representing water height and velocity with equations for suspended particulate matter and bed loads by using COMSOL Multiphysics software. The study examined the capability of the numerical approach to simulate basic processes that change the bottom elevation of a water body. However, this study demonstrated that basic phenomena associated with sediment transport, such as scour creation and sediment deposition, can be captured by a 2D coupled multiphysics approach. Sedimentation in Algeria is associated with a high level of challenges, especially in the northern and central basins. Therefore, Djoukbala et al. (2021) (Chap. 17) aimed to estimate the eroded and transported sediment yields from the whole Hodna Basin area by two approaches. In the first model, the eroded yield is estimated by mapping erosion using the Revised Universal Soil Loss Equation (RUSLE). In the second approach, the data of the gauged subbasins are extrapolated to the ungauged areas based on homogeneous factors that influence the water erosion-sediment transport process. The results of the two methods showed that high eroded and transported sediment yield values were observed in the basin.

Sedimentation is also a challenging issue in Sudan due to its impacts on the operations of reservoirs and irrigation networks, as highlighted by Adam and Suleiman (2021) (Chap. 18). This study discusses the sediment management practices used in the Khashm el-Girba Dam, which crosses the Atbara River in Eastern Sudan, and their impacts on maintaining reservoir capacity. Practices

including operation policy (OP), trap efficiency (TE), sluicing, sediment sluicing, and flushing operation (FO) were discussed. The authors stated that the adopted management practices succeeded in removing a considerable amount of silt and maintaining the lifetime of the reservoir. Determining the precipitation intensity threshold of debris flood occurrence was addressed by Banihabib and Tanhapour (2021) (Chap. 19). In this study, a laboratory model was employed to determine the precipitation intensity threshold at which debris floods occur using a set of factors, including sediment layer thickness, bed slope, grain mean diameter, length of sediment, precipitation intensity, and time of debris flood occurrence.

The sixth theme (Part VI) is "Groundwater Management," and it includes three chapters (groundwater in arid regions is an important and basic water resource for different uses in most arid regions). Ebraheem et al. (2021) (Chap. 20) presented geophysical methods to determine the locations of saturated fractures and karsts and the thicknesses of the unconsolidated materials in the wadis. The locations of the two production wells were determined in the Wadi Ham and Ain Madab Springs areas in the UAE for feeding the spring during drought seasons. The authors indicated that to avoid losses of spring water, water should be transported by pipes or by the construction of sealed small canals toward the bathing pool. Overexploitation of groundwater has led to declining water levels in many aquifers in arid regions, as stated by Sherif et al. (2021) (Chap. 21). This study was conducted to evaluate the effect of the Wadi Bih Dam on groundwater resources and to provide data on the hydrodynamics of the aquifer. The results showed that the additional recharge provided by dam storage does not balance groundwater extraction; thus, the present exploitation regime is not sustainable. To achieve sustainable management of the groundwater resources in Wadi Bih, an integrated solution must be pursued considering demand management as well as options for further mitigating the impacts of groundwater abstraction. In terms of water quality and the impact of groundwater overpumping, Saber et al. (2021) (Chap. 22) investigated the environmental impacts of the increasing groundwater level through field observations and chemical analyses of the groundwater wells in the Faris Area, Aswan. The results revealed that the use of flood irrigation systems in the upper newly reclaimed land area in the study area is the main cause of the decreasing groundwater levels, which have led to remarkable environmental degradation in the city. Additionally, the water quality also drastically changed due to the overpumping of groundwater.

In conclusion, the presented chapters comprehensively and significantly highlight different scientific research disciplines related to wadi flash floods, including climatology, hydrological models, new monitoring techniques, remote sensing techniques, field investigations, international collaboration projects, risk assessment and mitigation, sedimentation and sediment transport, and groundwater quality and

quantity assessment and management. These collections of chapters could provide valuable guidance and scientific content not only for academics, researchers, and students but also for decision-makers in the MENA region and worldwide.

Mohamed Saber
mohamedmd.saber.3u@kyoto-u.ac.jp

Sameh A. Kantoush
kantoush.samehahmed.2n@kyoto-u.ac.jp

Tetsuya Sumi
sumi.tetsuya.2s@kyoto-u.ac.jp

Reviewers List

Mohamed Abdel-Fattah, Military Technological College, Sultanate of Oman
Takahiro Sayama, Kyoto University, Japan
Reinhard Hinkelmann, Technische Universität Berlin (TUB), Germany
Mitsuteru Irie, Miyazaki University, Japan
Hitoshi Tanaka, Tohoku University, Japan
Kazuki Yamanoi, Kyoto University, Japan
Ali Al-Maktoumi, Sultan Qaboos University, Oman
Takahiro Koshiba, Kyoto University, Japan
Franziska Tuegel, Technische Universität Berlin (TUB), Germany
Koichi Unami, Kyoto University, Japan
Tetsuya Takemi, Kyoto University, Japan
Nohara Daisuke, Kyoto University, Japan
Hesham Eldardiry, University of Washington, Seattle, USA
Ashraf M. Elmoustafa, Ain Shams University, Egypt
Hassan Ayad, Hassan II University of Casablanca, Morocco
Ekkehard Holzbecher, German University of Technology in Oman (GUtech), Oman
Anis Chkirbene, Borj Cedria Technopark, Tunisia
Ahmed Hadidi, German University of Technology in Oman (GUtech), Oman
Cherifa abdelbaki, Université de Tlemcen, Algérie
Dalila Loudyi, Hassan II University of Casablanca, Morocco
Temur Khujanazarov, Kyoto University, Japan
Hamouda Boutghani, Badji Mokhtar-Annaba University, Algeria
Tayb Boulmaiz, University of Ghardaia, Algeria.
Sohei Kobayashi, Wenzhou University, China

Contents

About the Editors

Tetsuya Sumi is a professor at the Water Resources Research Center, Disaster Prevention Research Institute, Kyoto University, Japan. He has a degree in civil engineering from Kyoto University. Subsequently, he worked for the Japanese Ministry of Construction. His specialties are hydraulics and dam engineering, with particular emphasis on integrated sediment management for reservoir sustainability and river basin environment improvement. He has contributed to several international associations and conferences, such as IAHR, ISRS, and ISE. He organized the 2nd International Workshop on Sediment Bypass Tunnels in 2017 in collaboration with ETH-Swiss and NTU-Taiwan. He recently conducted a general report of Q100 "Reservoir Sedimentation and Sustainable Development" at the 26th ICOLD Congress, Vienna, Austria, July 2018.

Sameh A. Kantoush is currently an associate professor at Disaster Prevention Research Institute (DPRI), Kyoto University. He received his master's and doctorate degrees in civil and environmental engineering from Saga University in Japan and the Swiss Federal Institute of Technology Lausanne (EPFL) in Switzerland, respectively. Prior to joining Kyoto, he served at the German University in Cairo (GUC) as an associate professor in the Civil Engineering Program. He is a member of the Japan Society of Civil Engineers (JSCE) and Syndicate of Engineers in Egypt. The industrial expertise of Dr. Kantoush is predominantly in infrastructure projects at multinational consulting firms

in many countries. His research interests span the fundamentals of shallow flow and sediment transport, wadi flash floods, reservoir sustainability, ecohydraulics, dam impacts, and sediment management techniques.

Mohamed Saber is currently working as a Specially Appointed Associate Professor at the Disaster Prevention Research Institute (DPRI), Kyoto University. He has a Ph.D. in Hydrology from Kyoto University, Japan, and has worked as an assistant professor at the Geology Department, Faculty of Science, Assiut University, Egypt. He has experience working and holding different positions, such as a senior researcher, Water Resources Research Center Disaster Prevention Research Institute, Kyoto University, Japan; a visiting professor, Geological Engineering, Middle East Technical University, Turkey; a postdoctoral researcher, the University of Louisiana at Lafayette, LA, USA; a postdoctoral researcher, Kyoto University; and a research assistant, GCOE_ARS Project, Kyoto University, DPRI, Japan. He participated in more than 50 different publications and supervised more than 20 undergraduate, professional diploma, master's, and doctorate students. His research interests are mainly focused on wadi hydrology, flood forecasting and risk management, hydrometeorological analysis and climate change, water resources management, reservoir sedimentation management, and remote sensing and GIS applications, as well as machine learning techniques in flash flood risk assessment.

Part I
Wadi Flash Flood Challenges and Strategies

Chapter 1
Integrated Strategies for the Management of Wadi Flash Floods in the Middle East and North Africa (MENA) Arid Zones: The ISFF Project

Sameh A. Kantoush, Mohamed Saber, Mohammed Abdel-Fattah, and Tetsuya Sumi

Abstract Sustainable management of wadi flash flood (WFF) risks is desperately needed to secure development in wadi systems. Due to rapid flow generation with sudden high flood peaks, spatiotemporal variability of rainfall occurrence, and poorly sited rapid development, most Middle East and North Africa (MENA) region have no comprehensive proper protection from WFFs. In arid regions, single mitigation measures, including storage dams, recharge dams, artificial lakes and embankments, are implemented, although soft mitigation measures are not dominant, such as early warning systems. The single management strategy under climate change impacts is not adequate to reduce flash flood risks; an integrated strategy is required. The objective of the international symposium on flash floods (ISFF) project has been to develop scientific understanding of WFFs in wadi systems; monitor, model, and mitigate; issue warnings; and plan urban development by discussing and networking the strategies in the MENA region. To achieve this goal, the project defines priorities for future research challenges and potential projects for WFFs. This chapter provides a state-of-the-art scientific basis in terms of integrated flash flood management. Further, priorities are defined for the main research gaps, and the emerging research methodologies can contribute to guide the management of WFFs in such regions.

Keywords Wadi flash floods · ISFF · Flood risk management · MENA region

S. A. Kantoush (✉) · M. Saber · T. Sumi
Disaster Prevention Research Institute, Kyoto University, Goka-sho, Uji City, Kyoto 611-0011, Japan
e-mail: kantoush.samehahmed.2n@kyoto-u.ac.jp

M. Abdel-Fattah
Civil Engineering and Quantity Surveying Department, Military Technological College, P.O. Box: 262, P.C: 111, Muscat, Oman

T. Sumi et al. (eds.), *Wadi Flash Floods*, Natural Disaster Science and Mitigation Engineering: DPRI Reports, https://doi.org/10.1007/978-981-16-2904-4_1

1.1 Introduction

'*Wadi*' is an Arabic word that is commonly used to refer to dry stream channels and ephemeral streams or valleys typically in arid zones, such as in the Middle East and North Africa (MENA) countries (Jackson and Bates 1997; Sen 2008). In the past (before the year 2003, usually in late October or November), rainfall in the wadis can be described as episodic, varying widely on spatial and temporal scales, with many years receiving no precipitation at all. Recently, in the last 10 years, wadi flash floods (WFFs) in arid regions have become catastrophic and more frequent due to climate change impacts. In direct response to intense and usually sudden rains, WFFs can produce enough runoff such that wadis flow for some distance within the basin, but the flow often does not reach the coast because of high transmission losses, as documented by El Bastawesy et al. (2009), who analyzed pre- and post-flood remotely sensed data. Therefore, water harvesting of flash flood water can be a significant approach to mitigate some potential wadis.

Floods are natural disasters worldwide; however, their adverse impact is superior in developing countries (Alcántara-Ayala 2002). It was recently reported by the United Nations Office for Disaster Risk Reduction (UNISDR) that Arabian countries were affected by many disasters (approximately 270) over the last 30 years, resulting in over 150,000 deaths and influencing approximately 10 million people (Guha-Sapir et al. 2016). Recently, WFFs have been extreme and frequent in most of the MENA arid zone, resulting in substantial economic and property losses. For instance, flash floods struck Egypt, Jordan, and Saudi Arabia 39 times from 1900–2016, causing 1,508 casualties and significant damages exceeding 1.8 billion USD (De Vries et al. 2018). For instance, October 2016 flash floods left 26 dead people and tens of millions of USD in damages in Ras Gharib City (Abdel-Fattah et al. 2017). Due to extreme precipitation in Sudan during a 6-h period on 7 August 2013, the Humanitarian Aid Commission (HAC) estimated that 499,900 people countrywide had been impacted and more than 85,385 houses were destroyed in the affected states, with Khartoum State experiencing the worst effects (IFRC 2013). Flash floods in Oman are often caused by more severe phenomena, which include tropical cyclones that bring massive devastation to infrastructure and the loss of human life. Oman was also hit by an extreme cyclone in July 2007 that killed 54 people, and property damage was assessed at 3.9 billion USD (Al Khatry and Helmi 2008; Al Barwani 2015). In October 2018, the increased frequency of extreme rainfall events associated with various flash floods triggered widespread destruction in most of the MENA region, including Jordan, Kuwait, Qatar, Saudi Arabia, the UAE, Morocco, Tunisia, Algeria, Mauritania, Sudan and Oman. Because previous experience of such disasters in arid regions is limited, proper planning and management are now required. Events such as those in Egypt (2010), Oman (2007), Yemen (2008), Jordan (2012), and Bahrain (2008) ensure that WFFs remain the leading meteorological disaster causing death and property damage. These floods destroy the main infrastructure, such as buildings, villages, agricultural lands, roads, power towers, and pipelines, and they injure and kill humans and

animals (Murata et al. 2015; Abdel-Fattah et al. 2018). In 2018, wadi flooding trapped tourists and forced 4,000 tourists to evacuate to safe places within 1 h before the peak flood reached the historic site of Petra, Jordan (Guardian 2018). Sirens blared minutes before extreme flash flooding after heavy rainfall approached Petra (historical city, dating back to 9,000 B.C.). The last deadly flash flood hit Petra in 1963, when 22 French tourists and a local guide were killed by flash floods (Laure Van Ruymbeke 2018).

Monitoring, modelling and early warning of WFFs are difficult, especially in ungauged wadis. Furthermore, the lack of a complete data archive of pre- and post-WFF events across the MENA region obstructs efforts to mitigate the flooding risk (Viglione and Rogger 2014; Saber and Habib 2015). Most of the published studies regarding WFFs have focused on the geology, geomorphology, and hydrogeology of wadi systems (Moneim 2005; Elewa and Qaddah 2011; Abdelkareem and El-Baz 2015). The other flash-flood-related features of wadi systems, such as integrated management, hydrological modelling, and risk assessment, have not been sufficiently addressed. Unfortunately, modelling the response of wadis to rainfall is challenging due to the lack of data and to special characteristics of wadis; consequently, developing powerful hydrological models is difficult (Wheater et al. 2007). Different rainfall modelling tools and methodologies have been widely used, but most of them were originally established for humid environments; nevertheless, arid and semi-arid regions facing severe water resources scarcity and flash flood threats have received little attention. The lack of high-quality observations is hindering the development in arid regions (Pilgrim et al. 1988). Precipitation events are spatiotemporally irregular, highly variable and localized. Flow measurements are lacking or uncertain. Moreover, some of the developed hydrological models that were constructed for humid conditions cannot be easily adapted to arid environmental conditions (Cools et al. 2012). Generally, in humid environments, during the dry seasons, flow discharge increases downstream and groundwater contributes to river systems, whereas in arid environments, the opposite is valid, the surface flow is reduced because the groundwater table is usually depressed (Sen 2008). For these reasons, the hydrological processes of arid lands differ from those of humid lands and present particular challenges. Developing hydrological models and methodologies is urgently needed in arid and semi-arid regions. According to many previous studies, nonrioting and measuring of flow is mostly problematic in arid regions for numerous reasons (Rodier and Roche 1978; Kilpatrick and Cobb 1985; Pilgrim et al. 1988; Lange et al. 1999; Lin 1999; Abushandi and Merkel 2011) and can be summarized as follows: (1) during flash floods, there is a rapid rising and falling of the water level; (2) it is difficult to install monitoring devices in the target area; (3) appropriate natural control sectors are nonexistent, artificial control in wadis is expensive; (4) extreme physical and climatologic circumstances exist; (5) sediment transport, moving rocks and debris can damage the installed instruments; (6) access is difficult due to few drivable roads, especially during the rainy and flooding seasons; (7) the population density in arid environments is typically low; (8) there is insufficient awareness of the

importance of flooding studies and monitoring; and (9) the devices for flood measurement are expensive, especially in developing countries.

Not all flash floods are destructive, and the harvest of floodwater and rainfall-runoff for human and livestock usage and agricultural development should be considered by management in the construction of underground dams, artificial lakes, recharge dams and off-stream structures. Structures located unwisely in wadis are vulnerable to damage, and residents and tourists may be killed or injured, as vividly illustrated by the November 2009 floods in Jeddah (BBC 2009). Unfortunately, culverts, dams and other flood mitigation structures that have been designed and constructed in many wadis put significant numbers of people at risk. In the MENA region, very few researchers have considered the different alternatives for flash flood mitigation. Al-Weshah and El-Khoury (1999) compared various mitigation measures, including terracing, storage dams, construction of check, and afforestation, as well as different combinations of these measures using hydrological modelling tools. A master plan was proposed by McLane and Wüst (2000) to mitigate the flooding impact on the archaeological tombs of the Valley of Kings. An integrated approach using GIS and remote sensing was proposed for flash flood mitigation and water resource management in Safaga, Red Sea, Egypt. In this study, the prone area for flood risk was identified and mapped, the appropriate locations for dam construction were determined, and highly potential sites for water recharging were determined. Additionally, various rainfall-runoff analyses and discharge forecasting were conducted, and the inundation areas were identified. To date, no comprehensive proper strategies for mitigating and managing water resources have been developed in wadi basins. Establishing guidelines and integrated methods for the management and mitigation of wadis for potential future development projects is urgently needed to utilize floodwater as an additional water resource in arid areas.

The ISFF project is focused on disaster risk reduction (DRR) by discussing existing mitigation strategies for flash flood protection and consequent proper floodwater management (water harvesting) in arid countries in Egypt, Oman, Saudi Arabia, Yemen, Sudan, Jordan, and Morocco. Priorities will be defined for future research challenges, gaps, and potential projects for flash floods in wadi systems. ISFF projects have different objectives: (1) to initiate a networking platform for sharing knowledge, data, and experience among researchers, scientists, and authorities in the MENA countries, (2) to boost collaboration among researchers in both fundamental and applied sciences, and (3) to transfer Japanese technologies to the MENA region for FF protection and water harvesting.

The current chapter aims to present the current status of wadi flash floods in some parts of the MENA region, provide a state-of-the-art summary of current management and existing WFF mitigation strategies, present and discuss the approach of integrated flash flood management, and discuss the main research challenges to be addressed in future years.

1.2 ISFF Project

The ISFF project was originally initiated by The Water Resources Research Center (WRRC) and the Global Alliance of Disaster Research Institutes (GADRI) of the Disaster Prevention Research Institute (DPRI), Kyoto University, to discuss the research outcomes of the MENA region and to establish research projects with several Arabian countries, including Morocco, Tunisia, Jordan, Egypt, Morocco, Oman, Saudi Arabia, Tunisia, Sudan, and Jordan. The first ISFF was organized at Kyoto University from 14 to 15 October 2015. The main purpose was to bring together researchers, scientists, and experts from governmental and private organizations in Japan, Sudan, Saudi Arabia, Egypt, Jordan, Oman, and Europe to initiate a scientific platform to discuss different topics related to flash floods, including hydrometeorology, flood disasters, and risk management, and to boost the foundation of joint research cooperation programmes. The ISFF was established to fill the current gaps in flash flood knowledge and to confirm a proper integrated strategy for water resource management in wadi systems. Several related topics have been addressed from different aspects, including water harvesting, mitigation measures (structural and non-structural), hydrological modelling, and early warning systems.

The main outcomes of the first ISFF symposium were drawing a roadmap for the next five years to support and continue the efforts of organizations and governments and to implement more scientific research and propose guidelines for assessing, mitigating and utilizing flash floods. In the symposium, a training course under the framework agenda of the UNESCO Japanese Fund-In-Trust (JFIT) project was organized with the title "Urgent Capacity Development for Managing Natural Disaster Risks of Flash Floods in Egypt, Jordan, Sudan and Yemen". Many participants from developing countries joined the course, which focused on flash flood management and prediction using the integrated flood analysis system (IFAS) and the rainfall-runoff-inundation (RRI) model designed by the International Centre for Water Hazard and Risk Management (ICHARM), Japan. This training was planned to foster the participants' awareness of WFF risk assessment and management.

Based on the road map, the second ISFF was organized and hosted by the TUB, El Gouna campus, Egypt, with the support of the UNESCO project. The third ISFF was organized in 2017 at GUTech in Muscat, Oman. It was mainly concentrating on flood risk mitigation, management, and assessment. The fourth ISFF was organized in 2018 at Hassan II University, Casablanca, Morocco. From 25 to 28 February 2020, the fifth ISFF was organized and hosted at WRRC, DPRI, Kyoto University, Japan. The fifth ISFF symposium was focused on wadi flash flood challenges in arid regions and especially "Disaster Risk Reduction and Assessment for the Flood Prone Urbanized & Archaeological Wadis in Middle East and North Africa MENA Region". During the symposium, a special seminar on flash flood risk at UNESCO World Heritage Sites (WHS) was held on 26 February 2020. Due

to COVID-19, the number of participants was limited, with approximately 87 from 12 countries. The sixth ISFF will take place in Amman, Jordan, from 26 to 30 September 2021. The continuity of such ISFF special annual meetings is desperately needed to overcome the water-related challenges in the MENA region.

1.3 Extreme WFF Events and Disasters in Wadi Systems in the MENA Region

The arid areas in the MENA region are typically hot and dry deserts (Fig. 1.1a) with rare to intermittent rainfall. However, the climate is variable according to the topography of each country (compare Fig. 1.1a–c), and extreme rainfall events are a crucial part of the region's climate (De Vries et al. 2018). Various examples of different wadi climates in Egypt, Morocco, and Oman are shown in Fig. 1.1. The infrequent storms recharge the freshwater storage, supporting agriculture and sustainable development, as shown in Wadi Samail (Fig. 1.1c). However, they can also be transformed into deadly and economical disasters in a short time. Flash floods in arid wadis are distinguished from other types of urban and river flooding by the following characteristics: (1) the dry stream channel is characterized by the absence of base flow (Fig. 1.1a) (Abdel-Fattah et al. 2018); (2) wadi surface runoff presents discontinuous flow due to short-duration rainfall events with highly localized spatial extent (Wheater et al. 1991; Saber 2010; Saber et al. 2010a, b, 2015); (3) the flow volume from single events is high, starting with low flow before the ascending hydrograph and increasing to the maximum peak of discharge before flow recession (Knighton and Nanson 1997; Saber and Habib 2015); (4) the evaporation rate, permeability of the desert, recharge of ground surfaces, sediment yield and slope are high; (5) plants and organic material are scarce, and soils are thin and poorly developed (McIntyre and Al-Qurashi 2009; Camarasa-Belmonte 2016); and (6) monitoring (rainfall, water level and discharge rates), accurate prediction, planning and strategies are lacking.

Extreme WFFs in the MENA region are characterized by high spatiotemporal variability in terms of frequency and intensity (Saber et al. 2017a, b, 2020). In the wadi systems of Arabian countries, a total of 50 flood events were recorded between 2000 and 2018, as shown in Fig. 1.2. The regional events in 2010, 2015, and 2018 affected more than one country. For instance, a single event in November 2018 affected Kuwait, the UAE, Oman, Qatar, Saudi Arabia, and Jordan, and extreme impacts occurred in most of the region. Figure 1.2 shows the total number of events in each country in the MENA region. More events occur in Saudi Arabia and Jordan due to cyclones.

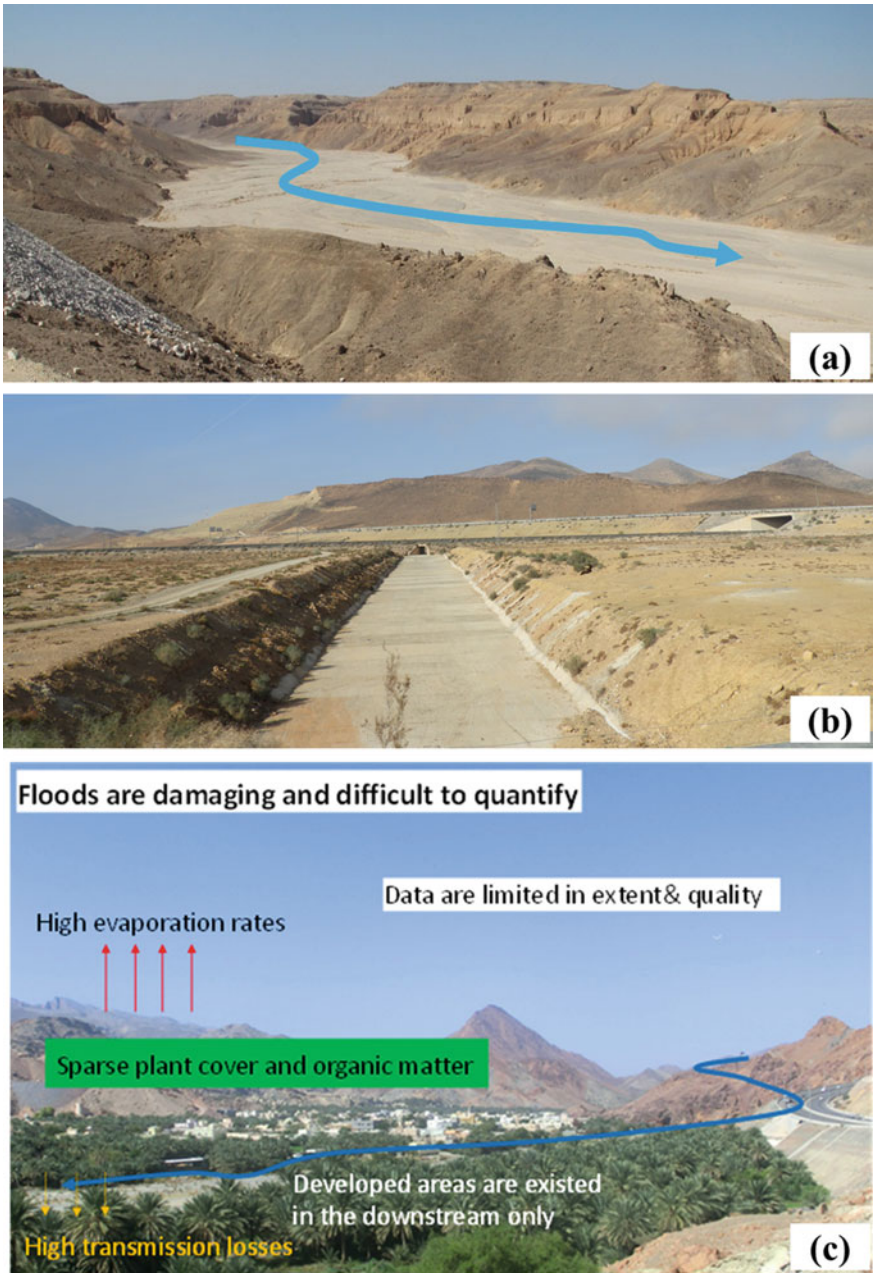

Fig. 1.1 Arid wadis system in **a** Wadi Qena (Egypt), **b** Oued (Wadi) El-Abed (Morocco) and **c** Wadi Samail (Oman)

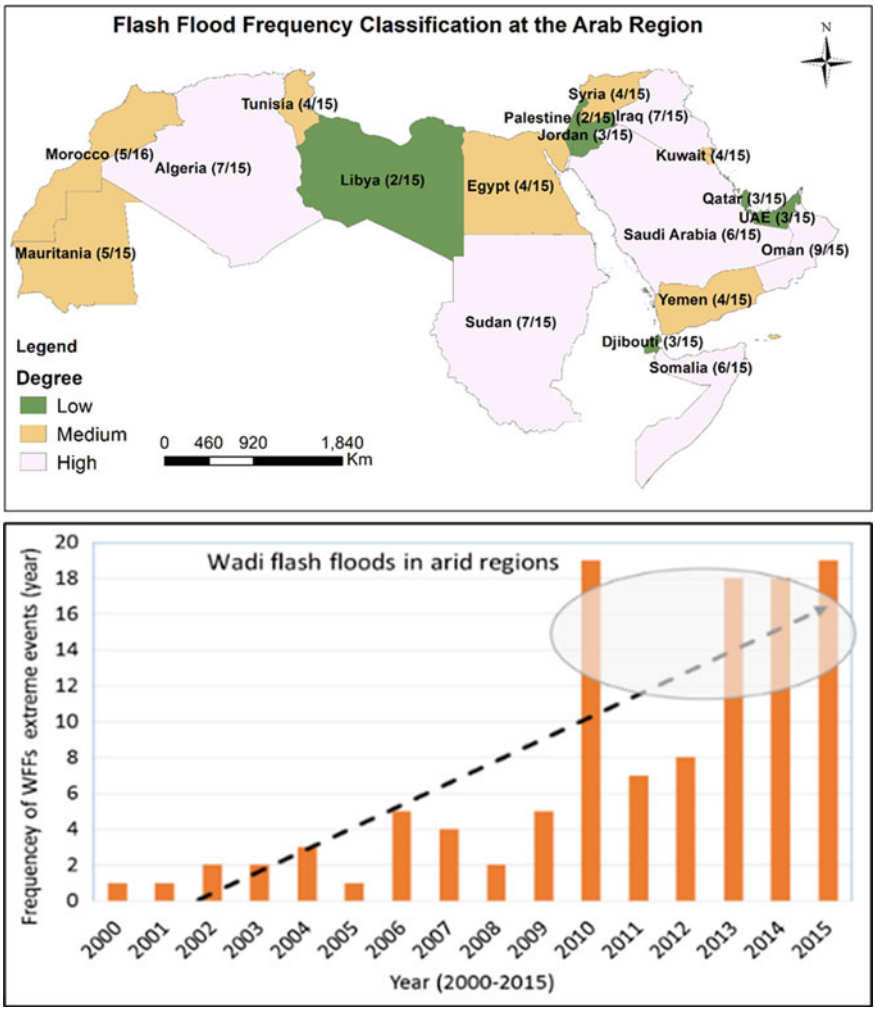

Fig. 1.2 Extreme flash floods events in the Arab region (2000–2018) showing the degree of flood frequency (upper panel) and the increasing trend in floods within the last two decades (lower panel)

1.4 Spatial and Temporal Distributions of Wadi Flash Flood Events

A recent study by De Vries et al. (2018) reported that tropical-extratropical interactions are the main drivers of extreme precipitation events in the MENA region. Therefore, understanding the variability of extreme rainfall events that mostly form flash floods is crucial to improving physically based forecasts and DRR. Figure 1.3

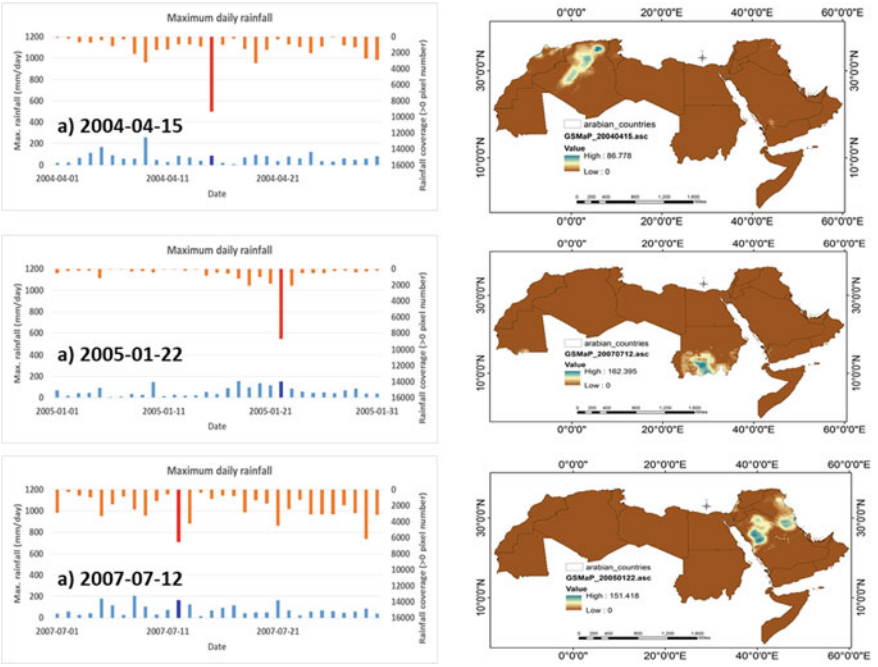

Fig. 1.3 Comparative analysis of 3 selected extreme events identified based on the maximum rainfall per day

shows the maximum spatial (Algeria, Arabian Peninsula, and Sudan) and temporal rainfall for three extreme events based on satellite rainfall datasets. The high variability in spatial coverage and intensity for the daily time series was investigated. Spatially, the first event over the northeastern part of the region produced a maximum rainfall rate of approximately 86.778 mm/day, the second event affected the Arabian Peninsula with 151.40 mm/day, and the third event over Sudan involved approximately 162.4 mm/day. These WFFs were highly variable depending on the climate and topography of each region.

1.5 Rainstorms and Tropical Cyclones from the Indian Ocean

MENA countries represent different climatic, hydrological, land use, and observational characteristics and storm types. WFFs in most of the region are produced by convective clouds at the end or beginning of winter and summer, when hot air masses cause heavy rainfall connected with thunderstorms except for the Arabian Peninsula, which is affected additionally by tropical cyclones. Most of these cyclone tracks develop over the Indian Ocean and Arabian Sea from April to June

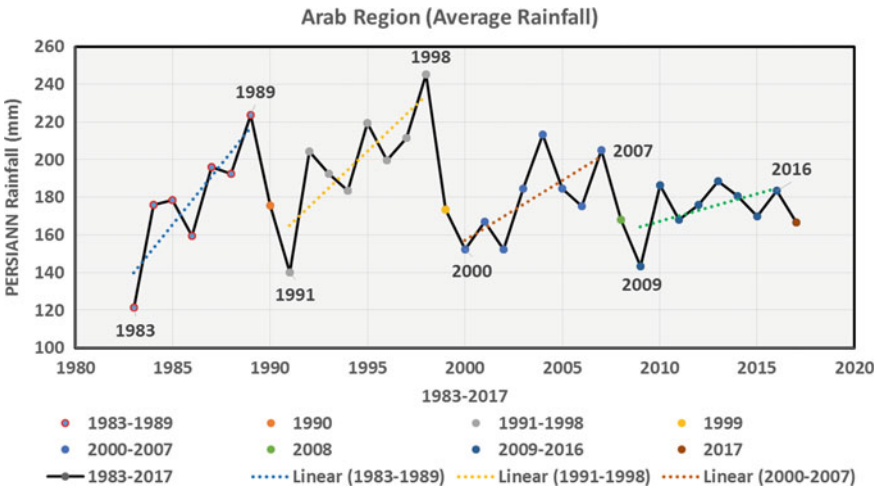

Fig. 1.4 Annual average rainfall over the Arabian countries from PERSIANN data

and October through December. For instance, Egypt has a very dry and arid climate with low annual average rainfall (<50 mm), whereas Oman has semi-arid to arid climatic conditions and a higher annual average rainfall of 50–350 mm. In Oman, WFFs are mainly discharged to coastal drainage systems. Figure 1.4 shows the annual average spanning 35 years over Oman associated with the total rainfall during cyclones. Records show that severe damage occurred in Oman in 1989, 1997, 2002, 2003, 2007, 2010, 2015 and 2016 (Al Barwani 2015) due to WFFs. The most extreme rainfall events that occurred in Oman were due to tropical cyclones Gonu-2007 and Phet-2010 (Al Barwani 2015; MRMWR 2015), which caused 56 fatalities with 6 billion USD of economic losses. Several wadis (W. Kabir, W. Aday and W. Samail) in Oman have experienced flash floods with huge impacts on the human life, infrastructure and property (Al-Rawas and Valeo 2008). Detailed hydrological research studies are desperately required to assess flash flood risks and propose effective mitigation measures in the MENA region.

1.6 Impacts of Extreme Event Occurrences on Management

Flash floods in arid environments can be dangerous because when rain falls on unabsorbent or clay soils, the amount of runoff increases and exceeds the wadi channel capacities (Saber 2010). Topographic factors play a significant role in the evolution of rainfall that causes flash floods. There are different issues that have a critical impacts on the occurrences of flash floods, including rainfall intensity and duration, topography, soil conditions and terrain. Topographic features, such as

steep slopes, highland terrains and narrow valleys, increase the flash flood probability and accelerate surface runoff. The surface runoff is also affected by shallow watertight geological and saturated soil layers. Urbanized and affiliated construction with water-tight materials are supposed to generate runoff several times greater than that in natural coverage terrains (meadows, fields, and forests). Another flash flood hazard source is transported sediments and debris during flooding. Debris flow impacts can be explained as follows (Hungr et al. 1987): (1) hazards of the direct and indirect influence of high-energy, coarse-grained debris that can adversely affect structures and (2) hazards of debris deposits associated with the flood waters leading to the erosion of vulnerable surfaces and consequently flood damage.

The rapid increases in urbanization, population, and touristic and economic developments have pushed residences to build in vulnerable risk zones, including wadi flood plains. Figure 1.5 shows the present status of flash floods in different countries in the MENA region and different times of flood events. Flash flood management and the determination of flood-prone regions are extremely important due to residential development on hill slopes and at outlets of wadis as well as the lack of previous studies addressing flood hazard assessment given the infrequent occurrence of rainfall and the absence of well-defined watercourses. In general, most low-lying urban centres are flood-prone areas, which consequently require assessment and management using advanced techniques. Many cities have been affected by such flash flood events, such as Taba in Sinai and Wadis Abu-Shieha,

Fig. 1.5 **a** The affected areas by flash floods in Rafah, Sinai, Egypt, on 20 January 2010 (© Photo courtesy AF) and **b** Taba and Nweba flash flood in May 2010 (© El-Masry Elyoum)

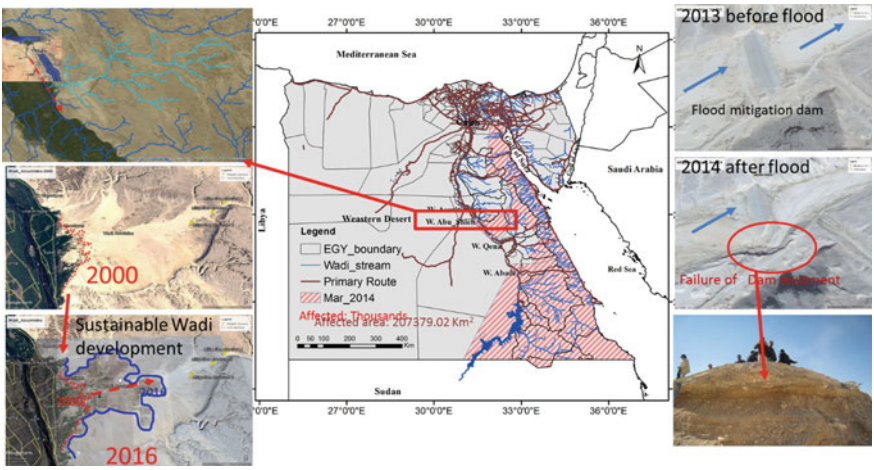

Fig. 1.6 The downstream delta of Wadi Abou Sheih along the river Nile, showing the extension of urbanization and agriculture reclamation (left panel) and the affected mitigation dams (right panel). Modified from Saber et al. (2017a, b)

Sohag, Aswan and Kom ombo along the River Nile. Wadi AbuShiha, one of the most important wadis in the Eastern Desert of Egypt, has suffered from many flash floods. It is characterized by many sub-basins (Fig. 1.6) in the downstream region, with many urbanized areas and agricultural reclamation projects. The downstream delta of the wadi is very large and has many new sites of urbanization, agriculture reclamation started in 2000, and the extension of agricultural lands increased to cover a much larger area in front of the outlet of the wadi, which is prone to flash floods, as shown in Fig. 1.6 (Saber et al. 2017a, b). Due to the importance of this downstream development in the wadi, the government constructed three mitigation dams (Fig. 1.6). However, after the 2014 flash flood, the first dam was broken at the abutment. Considering the climate change impacts and increased urbanization and reviewing the wadi management according to the occurrence of events are important, as well as enhancing the design codes for integrated management.

In summary, several factors contribute to flash flood risk, including human intervention and non-human actions. The flash flooding phenomenon is one of the most difficult natural hazards to predict and manage. As a result, responding appropriately is challenging for the concerned communities and authorities, and response plans are also essential (APFM 2007). During a flash flood, the water levels in streams rise suddenly, and the flow velocity can be very high. The strength of the water can be strong enough to uproot trees, move boulders, and destroy buildings and bridges located in its pathway. Water flowing often changes the morphology and riverbed characteristics and can consequently appear in locations where it usually does not. Water at a depth of 1 m depth and speed of 1.0 m/s can pose a destructive threat for an adult person; flash floods often flow at very high speeds, and a water level of merely a dozen cm can be very hazardous (APFM

2007). Early warning systems could be the significant element in dropping the risk to human lives and their properties. Conventional forecasting approaches cannot provide satisfactory warning, and people have insufficient time to move away from the floods.

1.7 Hydrological Measurements of Wadi Systems and Flash Flood Forecasting

Forecasting of WFFs is only the beginning to correctly design flood mitigation structures and develop efficient warning systems (Abdel-Fattah et al. 2018). Few wadis in the MENA region are equipped with hydrological monitoring stations for rainfall, water level and discharge rates (Al-Mamari et al. 2019). Therefore, calibrating and validating the computed runoff discharge and inundation depths in wadi systems are difficult. Such limited data availability in the wadi systems has resulted in the improper design and selection of mitigation structures, such as embankments, culverts, dams and drainage systems (Al-Mamari et al. 2019). Thus, the development of hydrological monitoring techniques is needed in the MENA region to improve wadi management and utilize measurements for prediction and evaluation. Figure 1.7 depicts an integrated list of the potential sensors and techniques to monitor spatial rainfall variations with rainfall radar and for continuous monitoring

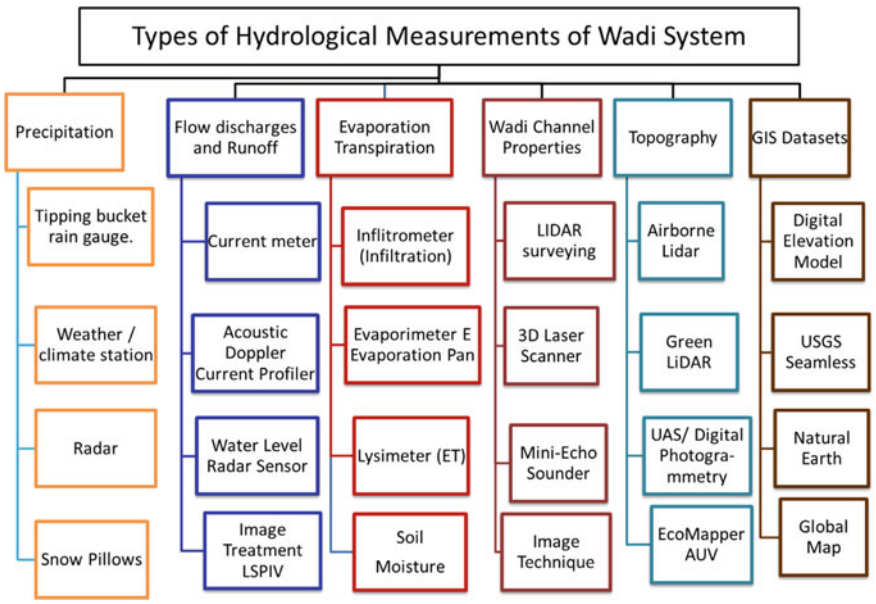

Fig. 1.7 Ad hoc hydrometric network and potential hydrological sensors/techniques

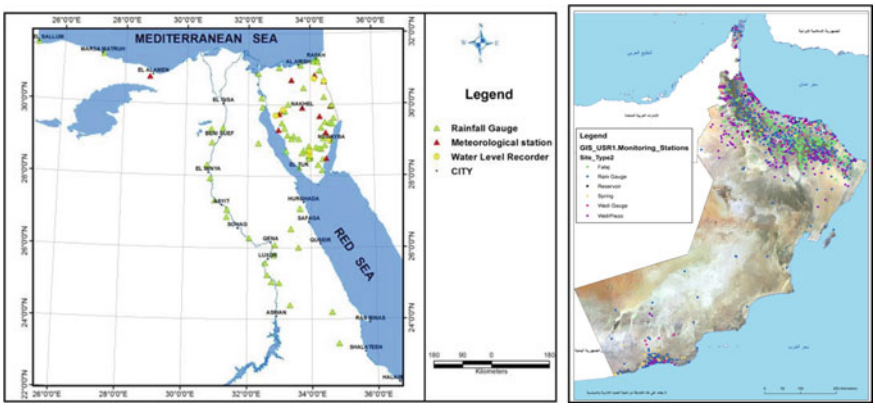

Fig. 1.8 Available wadi monitoring stations in Egypt (left panel) and Oman (right panel). *Sources* The National Water Research Center in Egypt and Ministry of Regional Municipalities and Water Resources in Oman

of water levels, soil moisture and infiltration using radar sensors and ultrasonic devices to measure flow velocities and calculate discharges. Moreover, the available techniques for the direct measurement of evaporation rates and remote sensing systems produced spatial datasets for different applications in hydrology (Tomsett and Leyland 2019). Wadis present various challenges to installing rain gauges and measuring flow, Therefore, there are a limited number of wadi monitoring stations in Oman and Egypt except for the rain gauges, water flow, and ground water wells (Fig. 1.8).

1.8 Image-Based Techniques

Monitoring systems that use recorded videos have the advantage of capturing real-time floods so that the flow discharge can be computed, which can help in flood management. The implementation of large-scale particle image velocimetry (LSPIV), which is an image-based technique, was recently accomplished for the first time in Oman at Wadi Samail (Al-Mamari et al. 2019). Various fixed cameras have been installed on the bridges crossing the wadi channel, and they can record the surface flow movements. LSPIV based on drone images is now common in many applications among the river engineering community, such as for time-averaged surface velocities. The rapid development of unmanned aerial systems (UASs) has allowed us to measure streamflow in real-time with high spatial and temporal variations (Tauro et al. 2016). To capture valuable information about the river hydraulic conditions during flash floods in humid environments, a UAS was successfully utilized by Perks et al. (2016). The potential of UASs during low-flow conditions was demonstrated by Detert and Weitbrecht (2015).

A considerable amount of literature on using photogrammetric techniques to monitor riverbed morphology and riverbanks has been published (Brasington and Smart 2003; Bird et al. 2010).

1.9 Risk Assessment Methods

El Shamy (1992) developed a method to evaluate the flash flood possibility and groundwater recharge in several sub-basins, employing various geomorphometric parameters, such as the drainage density, drainage frequency, and bifurcation ratio. This model has since been adopted by many studies (Youssef and Hegab 2005; El-Behiry et al. 2006; Arnous et al. 2011; Abdel-Lattif and Sherief 2012; Abdalla et al. 2014). Abdel-Fattah et al. (2017) proposed a consistent methodology applied to assess flash floods in Wadi Qena, where field data are limited. Flash flood consequences include environmental and economic issues because these floods may cause impairment to urbanized and agricultural regions as well as lead to the loss of human lives (Merz et al. 2010). The increasing frequency of destructive flash floods requires an ongoing enhancement in the identification and mapping of flood hazards (Kundzewicz and Kaczmarek 2000; Ebert et al. 2009). Al Saud (2010) used high-resolution satellite images to identify the 2009 flood damage in Jeddah City, KSA. Omran et al. (2011) used the standardization of morphometric parameters with the same weight for basin-based flash flood hazard assessment in Wadi Dahab, Sinai Peninsula, Egypt. The same method was applied in Wadi Al Lith (Bajabaa et al. 2014) and at Wadi Rabigh, Wadi Yanbu, Wadi Khulais, Wadi Jizanhe, Wadi Baish, and Wadi El-Qunfza in the KSA (Shi 2014). By integrating geomorphology and geology along with remote sensing techniques and field observations, geomorphological hazard assessments based on GIS have been performed in several areas in Egypt, including the area between Quseir and Safaga near the Red Sea, using the El-Shamy model (Youssef et al. 2009), and along the Katherine-Feiran road in South Sinai (Youssef et al. 2011).

To reduce the flood damage impacts of FF hazards, proposing proper dam sites have been proposed for several urban areas. The probability of flood hazards has been estimated for different catchments based on geomorphometric features (El Shamy 1992). Further, geomorphometric-based studies have been conducted to assess FF risk levels in many basins. For instance, El-Magd et al. (2010) used remote sensing data and GIS tools combined with morphometric parameters to assess FF hazards in the Abu Dabbab wadi basin. Then, all the datasets were integrated as inputs for a hydrological model to estimate surface runoff and identify the flood risk levels.

Sen et al. (2013) proposed a procedure for establishing flood inundation maps in the southwestern Kingdom of Saudi Arabia using surveyed cross-sections of the flood plain. The main geological hazards, flash flood causes, and main rainfall events in the KSA were summarized by Youssef and Maerz (2013). An analytical hierarchical process (AHP) was used by Elkhrachy (2015) to estimate the flood

hazard index in Najran, Saudi Arabia, employing the main controlling parameters of flash floods, such as the channel discharge, soil type, drainage density, surface roughness, surface slope, distance from main streams and land use. An AHP was further used by Youssef et al. (2015) to utilize variant geological, geomorphological, and geographical features in an approach to understand the effects of urban development in Wadi Al-Aska, Jeddah, KSA. Abuzied et al. (2016) used multi-source geospatial data with remote sensing techniques, GIS analyses, and field investigations to evaluate flash flood hazards in the Nuweiba area based on basin morphometric analysis and hydrological modelling indices using the Soil Conservation Services (SCS) method.

1.10 Wadi Hydrological Modelling and Approaches

The major limitation of furthering our understanding of wadi flood events is that in most wadis, hydrological measurements do not exist. Most researchers have conducted flash flood analyses using simplified hydrological models. These models mathematically represent various hydrological processes, such as surface and groundwater processes, and are essential tools for water resources management (Abdel-Fattah et al. 2017). Hydrological models are desperately needed due to the limited measurements and the intricacy of hydrological systems (Beven 2011). The selection of the hydrological model approach relies on the number of measured parameters and the required observational data for the input model parameters and catchment characteristics (Abushandi 2011). Most WFFs in arid regions have been studied using lumped or semi-distributed models with very few applications based on distributed models because these models are data-driven. Various challenges remain to validate and calibrate the developed models in arid regions (Cools et al. 2012; Abdel-Fattah et al. 2018), to improve the reliability of the results, and to conduct a sensitivity analysis of the model parameters.

1.11 Utilized Hydrological Models in Arid Areas

Few hydrological models have been adopted and developed for flash flood modelling in wadis, such as the applied models in wadis in Oman, including the RRI model (Abdel-Fattah et al. 2018), the KINEROS2 model (Al-Qurashi et al. 2008), and the IHACRES model (McIntyre and Al-Qurashi 2009), as well as the soil water assessment tool (SWAT) in the UAE (Al Mulla 2005; Abushandi and Merkel 2011) and the HEC-HMS model in Oman, the West Bank-Palestine and the UAE (Al-Rawas and Valeo 2008; Shadeed and Almasri 2010; Sherif et al. 2010).

In addition to the aforementioned studies, several trials have been conducted, such as that by Al-Weshah and El-Khoury (1999), who applied and calibrated the HEC-1 model utilizing the SCS and curve number (CN) methods in the Petra

region, Jordan, and further used these hydrological modelling tools to determine the impact of several mitigation scenarios. Abdulla et al. (2002) developed a watershed model for a simple single event to predict surface runoff in the western part of Iraq. In Saudi Arabia, a geomorpho-climatic model has been adopted (Al-Turbak 1996), in which rainfall duration and intensity are estimated in three catchments from the infiltration parameters. In Palestine, (Lange et al. 2000) focused on the rainfall-runoff modelling of single flood events. It was stated that the analysis of a single storm event is highly recommended to understand extreme floods in arid environments. The HEC-HMS model and the spatial water budget model (SWBM) were employed in the Zarqa River Basin to manage water resources (Al-Abed et al. 2005; Abushandi and Merkel 2011; Dawod et al. 2011, 2012), and the SCS and CN methods in GIS have been used to assess flash floods, to determine the impacts of some basin geomorphometric parameters on the estimated flood characteristics in the Makkah metropolitan region, and to classify the flood hazard degree on city roads.

Foody et al. (2004) predicted sites at risk from high peak flows accompanying flash flooding in wadis intersecting the Idfu-Marsa Alam road (near the Red Sea) using the HMS model and field observations of the soil texture and infiltration capacity. This study was further updated using the same model setting by Ghoneim and Foody (2013) to investigate the impact of flood sites, areal coverage, and rainfall depth. El Bastawesy et al. (2009) presented an integrated method using ArcGIS and remote sensing data for modelling flash floods, where Landsat images can be used to distinguish flooded and non-flooded areas. The physical hydrological parameters, including rainfall, infiltration, land use and soil types, must be taken into consideration. Flash flood simulations for some rainfall events at wadis of the River Nile were conducted by Saber et al. (2010a, b) using Hydro-BEAM integrated with remote sensing and satellite datasets. In the study of Ismail et al. (2010), GIS, morphometric parameters and rainfall-runoff modelling based on flood routing processing (FRP) were integrated and employed to simulate the flow discharge at Wadi Abu Ghusun, the Eastern Desert, Egypt. Kehew et al. (2010) reconstructed extreme flash floods in Wadi Isla, South Sinai, Egypt, using palaeohydrological indictors related to flood velocity and discharge, such as the size of boulders transported within the wadi. Additionally, the calibrated SWAT model was used to estimate the amount of rainfall required to generate a flood. The flood hazard levels and ground recharge potentiality have been assessed at W. Abadi (Ibrahim et al. 2011). Based on field measurements of paleo-flood events and the rating curve, the peak flow of the January 2010 flash flood event was estimated, and this discharge peak was then used for model calibration. Hydrological modelling conducted in Wadi Hodin used the HEC-1 model by Soussa (2012) and the SCS method to calculate the losses. Hadadin et al. (2013) used routing and Snyder synthetic unit hydrograph methods to estimate the peak flow in 12 main basins in Jeddah City, KSA. Fathy et al. (2015) developed a lumped model for arid watersheds and compared the results with those from the watershed modelling system (WMS). This model was applied to W. Sudr in the Sinai Peninsula. The peak runoff discharge of six basins in western Saudi Arabia was estimated by Shi (2014) using three

empirical models (Farquharson's model, Nouh's model and Al-Subai's model) and the Snyder unit hydrograph. Moreover, Abuzied (2016) conducted hydrological modelling at Wadi Watier using the SCS method.

1.12 Surface Runoff Interaction with Groundwater

Many studies have examined groundwater recharge due to rainfall events and surface runoff. For instance, Gheith and Sultan (2002) estimated groundwater recharge in the alluvial aquifers of several wadis in the Eastern Desert of Egypt (W. El-Arish, W. Asyuti, W. Tarfa, W. Qena, and W. Hammamt). In this study, a hydrological model that considers the spatiotemporal rainfall distribution, appropriate sub-basin unit hydrographs and infiltration parameters were utilized to calculate initial and transmission losses and runoff. The model incorporated geological and meteorological datasets along with remote sensing and GIS techniques. Milewski et al. (2009) modelled runoff and groundwater recharge based on remote sensing datasets by focusing on the heavy rainfall events between 1998 and 2007 for the main wadis of the Sinai Peninsula and Eastern Desert. In the studied catchments, the annual precipitation, runoff, initial losses, and recharge through transmission losses were assessed. This approach has also been utilized to calculate the annual groundwater recharge at the Nubian Sandstone aquifer, South Sinai (Sultan et al. 2011). A proper example of cost-effective and practical integrated solutions, including geophysics, geochemistry, and modelling, that utilize global remote sensing datasets and web-based GIS technologies was proposed by Becker et al. (2012) for the wadis of the Eastern Desert and Sinai Peninsula, Egypt. The study implemented approaches to develop a conceptual model for hydrogeological settings in different aquifers to assess the annual runoff and recharge using a hydrologic model of the main watersheds.

The potential sites for surface runoff recharge in Sinai have been determined using an integration of GIS, remote sensing, and watershed modelling to introduce a multi-criteria decision support system that includes several parameters, such as the flood volume, average overland flow distance, lineament frequency density, soil infiltration, and morphometric parameters. The potential areas for rainwater harvesting have been determined based on such criteria by conducting weighted spatial probability modelling. The potential sites for water harvesting have been determined by applying Finkel-SCS rainfall-runoff approaches (Elewa et al. 2012). Furthermore, the same approach has been utilized to recommend proper dam locations for flood management and control at Wadi El-Arish. Technical considerations and design criteria have been introduced for the planned mitigation structures (Elewa et al. 2013).

To estimate surface runoff and groundwater recharge, the relationship between runoff and rainfall has been assessed depending on paleo-flood indicators. Two methods have been tested to evaluate the relationships between rainfall and runoff at the El-Hawashyia basin and Ghazala sub-basin in the Gulf of Suez, Egypt. Some

morphometric parameters with direct effects on flooding have been analyzed to evaluate the flood risks, and their relationship with flash floods has been investigated (Masoud 2013).

Al Zayed et al. (2013) assessed the potential of flood water harvesting at Wadi Watier in South Sinai, Egypt. The study was conducted based on the integrated guidelines of water resource management (IWRM). Thus, physical and environmental investigations along with social and institutional analyses were conducted. The flow discharge was calculated using the Hydrologic Engineering Centre (HEC-1) model; then, the potential sites were determined in ArcGIS by combining several factors, including slope, geology and land use.

Therefore, a new methodology urgently needs to be proposed to address the abovementioned challenges, to assess and predict flash flood disasters in arid wadis, and to evaluate the various flood mitigation strategies.

1.13 Mitigation Measures Against Wadi Flash Floods

Substantial efforts have been undertaken by governments and the private sectors of the MENA countries to enhance flash flood mitigation structures and early warning systems, while WFFs continue to be one of nature's worst killers in this region. Within the ISFF project, we can conclude that critical infrastructure and houses are newly allocated by the government and are often located in wadi channels because the wadi floors are flat and construction material is available. We find that this infrastructure is constructed in the path of flooding leading to a narrow channel to convey floodwaters along streams, in addition to the existence of important infrastructure and houses situated on higher lands. Such settlements are also affected by floods because the population chooses flood-sensitive economic, cultural and social activities (McBain 2012; Sayers et al. 2013). Understanding the contribution of structural and non-structural measures on flood risk reduction could support proper decision making and future planning (Shah 2015). Usually, the main structural measures in wadis rely on an 'embankment only' option that has been broadened to integrate other options, such as improvements to drainage channels, diversion dykes, detention and flood storage dams.

Flood risk reduction can be accomplished by controlling the flood magnitude flood-prone areas (Heidari 2009), where flood mitigation measures can be categorized into non-structural and structural measures (Hansson et al. 2008; Heidari 2009). Non-structural measures refer to non-engineering actions, such as increasing preparedness through early warnings, using insurance, land use, restricting development, planning and operating flood control reservoirs (Hansson et al. 2008; Shah et al. 2015). Structural defence strategies can be either conventional measures, such as dams and levees, or extensive ecosystem-specific measures, such as restoration of natural conditions (Hansson et al. 2008). Furthermore, structural measures can be important for managing water and controlling hazardous floods (Ho et al. 2017).

Flood mitigation strategies should consider the following issues (HEC 1998; Heidari 2009): (1) a proper implementation approach for flood control; (2) an appropriate site for facility installation; (3) an appropriate facility size; and (4) effective maintenance and operation of the facilities. In Egypt, most highways, roads and other infrastructure have been constructed across wadis that surround the main cities. Currently, no inclusive proper protection from flash floods is applied at most wadis in Egypt. Although comprehensive protection from flood risks is not feasible, the flood disaster risk could be decreased by (1) reducing the exposure by preventing or moving the development activities in areas where the hazards are high, such as floodplains; (2) reducing vulnerability by establishing resilient infrastructure standards and design and sound disaster preparedness measures; and (3) reducing the hazard itself, in some cases, by the construction of flood mitigation measures.

1.14 Structural Measures

Based on the spatial scale, structural mitigation measures can be categorized into distributed and concentrated measures. Several past studies have discussed distributed structural measures for flood mitigation (Andoh and Declerck 1997; Montaldo et al. 2004; Emerson et al. 2005; Kurz et al. 2007; Ravazzani et al. 2014; Thomas 2015). The main goal of distributed structures is to alleviate the flow peak and store excess floodwaters in the upstream sub-basins to reduce the discharge in the downstream areas (Montaldo et al. 2004; Thomas 2015). Distributed reservoirs have been shown to reduce the flow peak magnitudes based on distributed models (Chennu et al. 2007; Del Giudice et al. 2014), semi-distributed models (Ramireddygari et al. 2000; Leblois et al. 2010) and analytic analyses (Del Giudice et al. 2014). Various studies have also used cost–benefit analysis for flood mitigation scenarios (Heidari 2009) or multi-criteria decision-making techniques (e.g., Ahmad and Simonovic 2006; Mostafazadeh et al. 2017). The reductions in the flow peak in these related studies vary extensively within the range from 0.3 to 36% (Emerson et al. 2005; Mostafazadeh et al. 2017; Ravazzani et al. 2014; Thomas 2015); however, in some cases of dry dams, the reduction in the flow peak was less than 50% (Chennu et al. 2007). Onusluel Gul et al. (2010) studied the use of concentrated dams to evaluate the impact of flood mitigations on a downstream area using a combination of hydraulic and hydrologic modelling. However, the direct advantage of structural control measures, i.e., the sustainable efficiency of the structural flood control measures, cannot be maintained. For instance, several areas within large flood control projects have been affected by flooding immediately after their establishment. Further, flood mitigation measures often appeal to new development in flood-prone areas (McBain 2012; Shah et al. 2015).

Several measures have been adopted in Egypt to mitigate flash floods, such as the integration of detention and obstacle dams as well as artificial lakes, leading to well water management and flood mitigation. A field investigation was conducted

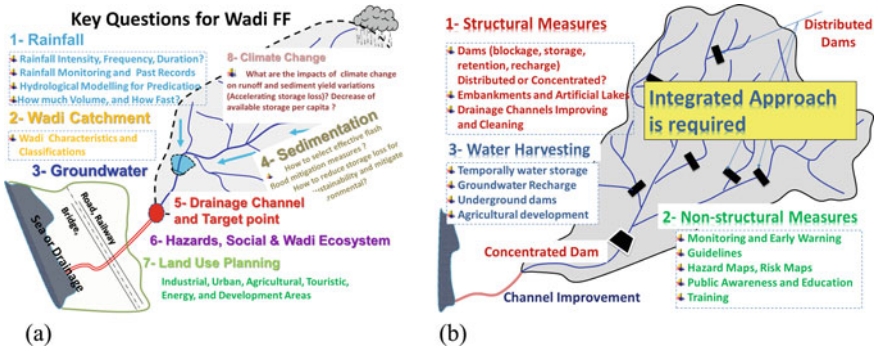

Fig. 1.9 The main challenges of wadi systems (**a**) and the requirement of an integrated approach (**b**)

by researchers and experts from both Kyoto University and the Japan Dam Engineering Center (JDEC) to investigate some wadi basins from 22 to 29 November 2014 along the Red Sea coast and the Eastern Desert, Egypt. The main purpose of such field investigations was to evaluate the current geological, hydrological, operational and structural conditions of the present flood control mitigation dams. This could be helpful for the selection of suitable integration measures and their structural design criteria as well as to clarify possible collaboration on selected pilot projects.

The Egyptian government makes master plans for water harvesting and flash flood mitigation, including long-term and short-term plans for low- and high-risk wadi basins. Different flood management structures have been implemented in Egypt, such as storage dams, obstacle dams, artificial lakes, diversion dykes, embankments, and artificial drainage channels, as indicated in Fig. 1.5. The proper selection of mitigation measures and their design are usually proposed based on the expected volume of flood water, risk and hazard degree, the prone and affected areas, and return periods.

Figure 1.9 shows the different characteristics of the main flash flood management and mitigation structures in both Egypt and Oman: (1) obstacle dams (less than 4–6 m) simply reduce the flood velocity, whereas (2) retention dams (approximately 10 m) and artificial lakes (2–4 m) are mainly for water harvesting and flood retention.

1.15 Non-structural Measures

Non-structural flood control measures have been widely applied to decrease the flow peak via land-use changes, early warning, and reducing flood vulnerability and exposure (Tapsell et al. 2002; White and Richards 2007; Richards et al. 2008; Shah 2015). Recently, these strategies have been followed by increasing efforts for

appropriate risk management to reduce flood hazards (McBain 2012; Sayers et al. 2013).

Unlike the immediate visualization of the advantages of structural flood defences, quantifying the efficiency of non-structural measures is often difficult. Owing to non-structural flood control measures, the adaptation and response of vulnerable communities to flood disasters vary widely and are influenced by several factors, such as community susceptibility and resilience to flooding. Additionally, the efficiency of non-structural flood control measures is sensitive to socio-economic changes and governmental arrangements (Dawson et al. 2011). However, non-structural control measures provide flexible flood mitigation measures for adapting to changes in river systems, climatic change and socio-economic impacts, which can hinder sustainable environmental development (Kundzewicz 2002).

1.16 Preparedness and Emergency Planning

The purpose of the preparedness stage is to provide the essential decision support system for the case in which the present flood protection system fails (Plate 2002). Obviously, there is no technical solution that is unconditionally safe in the context of flood control (Plate 2002). Even if the system always performs as expected, offering protection against any conceivable flood is rarely possible (Plate 2002). A residual risk always remains due to failure of technical systems or due to infrequent floods that surpass the design flood level. It is important to understand the flood risk in terms of safety and communication approaches for a better present and future development (Shah et al. 2015).

1.17 Education and Modification of Human Actions

The WRRC and the GADRI of the DPRI, Kyoto University, initiated ISFF and established several research projects to assess flash flood hazards and risks, to offer effective methodologies and techniques, and to highlight transdisciplinary approaches in the MENA region.

1.18 Integrated Wadi Flash Flood Management and Strategies

Efficient and sustainable flood mitigation measures (structural and non-structural) vary significantly according to the planning framework (Shah et al. 2015). In the short term, several structural flood management projects have confirmed their

efficiency for mitigating floods; such contributions have led to confidence in protecting people from flooding impacts by engineering structures (Shah et al. 2015). In the long term, however, some structural control measures have been found to be inefficient during catastrophic flood events (Shah et al. 2015) due to unplanned developments, land-use changes, growing production levels, population growth, transportation and consumption, which have led to increased flood hazards (Jonkman et al. 2003). Flood fatalities have continued to increase; thus, more advanced approaches for flood risk management are needed (Hall and Penning-Rowsell 2011; Sayers et al. 2013; Shah et al. 2015).

In the early decades of the twentieth century, extreme flooding events motivated researchers and scientists to develop basin-scale flood mitigation measures and coordination policies for mitigating floods instead of local flood mitigation measures (Shah et al. 2015). Flood risk management is a constant adaptive management process (Hall and Penning-Rowsell 2011; Sayers et al. 2013); thus, dynamic sustainability approaches and concepts that involve adaptative interventions for accomplishing a suitable outcome via problem-solving and nonstop learning are highly recommended (Newman 2005; Scoones et al. 2007).

1.19 Recommendations and Feedback from ISFF Participants

A single management strategy is not sufficient to reduce flash flood risks; nevertheless, integration approaches for flood risk management are needed in wadi systems. The proposed integrated management approach (Fig. 1.10) addresses the development of strategic methodologies to assess the capability of mitigating flash floods and managing water resources using effective strategies and hydrological modelling (Kantoush et al. 2011; Sumi et al. 2013). Reducing flood disaster risk is a crucial concern for many countries worldwide. The management and mitigation of flooding remains a challenging task in many developed and developing countries (Shah et al. 2015), and existing global efforts and technological advancements still fall short. In most arid wadis, no comprehensive proper mitigation strategies for flash floods have been proposed. This situation is mainly due to the relatively low flood frequency compared to that of humid regions. With progress in international collaboration and data sharing, flood management strategies and approaches can be transferred from other experiences or countries and applied in arid wadi systems with customization for the unique characteristics of wadi systems, including the socio-economic situation. In this chapter, a critical review of the concepts, strategies and practices of flood risk management reveal new dimensions for developing and proposing sustainable and efficient management strategies in wadi systems.

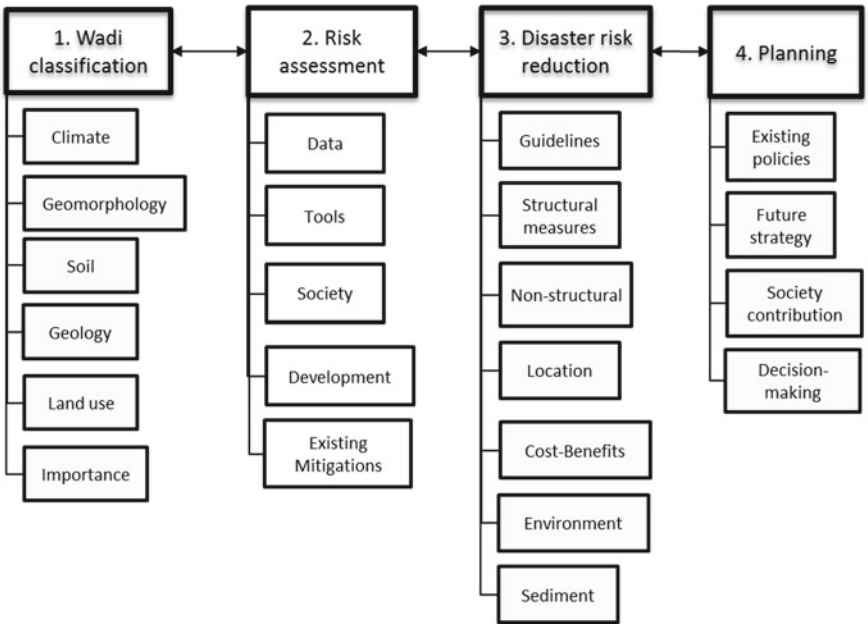

Fig. 1.10 Key components of integrated wadi flash flood management

1.20 Research Challenges

The current research has left several gaps, where more research and development need to be implemented to minimize future wadi flash flood risks. The main questions and challenges that are facing wadi systems are summarized in Fig. 1.9. Some such challenges are also addressed in the following sections.

1.21 Methods

The proposed approaches require further calibration and validation in the ungauged wadis of Egypt using rainfall and wadi flow observations in addition to applying similar approaches in other wadis with an extensive range of hydrological basin characteristics. In some models, such as the Hydro-BEAM model, kinematic wave models have been used, which are appropriate for steep slopes but do not work well in flat areas. Therefore, other techniques, such as diffusive and dynamic wave models, may provide better results. Moreover, the current time step adjustment in the Hydro-BEAM model is manually determined, consuming excess simulation time; therefore, an adaptive scheme for the Hydro-BEAM time step is recommended. The RRI model still does not have a stable groundwater module (under

development), which is recommended to be included and validated. Due to data limitations, the RRI model inundation outputs have not been calibrated and should be considered in the future for a more comprehensive evaluation of the RRI model in wadi systems. The performance of more hydrological models should be compared and assessed to identify the best option in wadi systems. Fieldwork to investigate the infiltration capacity of different land-use types can be used to better calibrate hydrological models. Wadi channel transmission losses should be considered in future RRI models because these processes are essential in wadi systems. Defining flood events by a return period using frequency analysis (Stedinger 1993) has evolved from the application of simple methods to intricate ones to assess probabilistic flood scenarios considering the exceedance probability (Merz and Thieken 2004) and uncertainties (Merz et al. 2008; Wu et al. 2011; Shah et al. 2015); therefore, current flood risk assessments should be updated based on the return period. Other important criteria, including the effect of structural measures on the landscape, society, environment and habitat diversity, should be considered along with the addressed factors. Additionally, the developed dam standards should be updated to investigate water infiltration and siltation in reservoirs. Different methods of flash flood water harvesting should be proposed and adapted for sustainable water management. The proposed approaches for determining dam design and locations (dam height, reservoir volume and area) using digital elevation model data should be validated using field surveys. Moreover, the long-term prediction of climate change and anthropogenic impacts (such as land-use changes) on wadi flash foods is necessary.

1.22 Mitigation Measures

Focusing on soft flood mitigation measures (early warning systems and social awareness) helps minimize the loss of human life and infrastructure damage caused by flash floods. The evaluation of sediment transport during wadi flash flooding is also recommended because sediment has a severe impact on mitigation structures, which increases the flash flood risk and decreases the efficiency of flood mitigation structures. Therefore, studying this factor and linking it with wadi characteristics, such as geomorphometry and soil type, are important. Detailed flood risk assessment based on more land use and geomorphological features is highly advised. This study recommends an integrated approach for all wadi systems that includes 'dynamic sustainability' concepts for proper flood management planning (Fig. 1.10). Stakeholders and decision-makers have various options and approaches for flood-prone communities by sharing experiences and knowledge around the world (Shah et al. 2015). Therefore, we highly recommended that a database contains the available data from all wadi systems and be accessible to any researcher.

1.23 Conclusions

Flash floods are damaging natural disasters and are an important source of water in arid areas, where flash floods can provide renewable freshwater, mainly for groundwater recharge. Therefore, using a proper decision support system based on efficient approaches could help manage infrequent floods. A flash flood can be created within a short time after a rainfall event, especially under certain geological and topographical conditions, such as steep topography with shallow, impermeable soils, bare rock and rare or sparse vegetation. The majority of the Great Sahara of North Africa and the Arabian Peninsula consists of hyper-arid environments with limited precipitation, where most countries suffer from water scarcity.

Flash flood disasters in arid environments are associated with several challenges that originate from many characteristics of a flash flood itself, arid environment characteristics, and data and methodology limitations. The different dimensions of flash flood phenomena, reasons and resulting impacts have been discussed in detail. Despite these challenges, several hydrological, geomorphological and disaster management aspects have been discussed in the context of wadi systems in this chapter.

References

Abdalla F, El Shamy I et al (2014) Flash floods and groundwater recharge potentials in arid land alluvial basins, southern Red sea coast, Egypt. Int J Geosci 2014

Abdel-Fattah M, Saber M et al (2017) A Hydrological and geomorphometric approach to understanding the generation of Wadi flash floods. Water 9(7):553

Abdel-Fattah M, Kantoush SA et al (2018) Rainfall-runoff modeling for extreme flash floods in Wadi Samail, Oman. J Jpn Soc Civ Eng Ser B1 (Hydraul Eng) 74(5)

Abdel-Lattif A, Sherief Y (2012) Morphometric analysis and flash floods of Wadi Sudr and Wadi Wardan, Gulf of Suez, Egypt: using digital elevation model. Arab J Geosci 5(2):181–195

Abdelkareem M, El-Baz F (2015) Analyses of optical images and radar data reveal structural features and predict groundwater accumulations in the central Eastern Desert of Egypt. Arab J Geosci 8(5):2653–2666

Abdulla FA, Amayreh JA et al (2002) Single event watershed model for simulating runoff hydrograph in desert regions. Water Resour Manage 16(3):221–238

Abushandi E (2011) Rainfall-runoff modeling in arid areas. PhD Thesis. https://citeseerx.ist.psu.edu/viewdoc/download?doi=10.1.1.458.8955&rep=rep1&type=pdf

Abushandi E, Merkel B (2011) Rainfall estimation over the Wadi Dhuliel arid catchment, Jordan from GSMaP_MVK+. Hydrol Earth Syst Sci Discuss 8(1):1665–1704

Abuzied S, Yuan M et al (2016) Geospatial risk assessment of flash floods in Nuweiba area Egypt. J Arid Environ 133:54–72

Ahmad S, Simonovic SP (2006) An intelligent decision support system for management of floods. Water Resour Manage 20(3):391–410

Al-Abed N, Abdulla F et al (2005) GIS-hydrological models for managing water resources in the Zarqa river basin. Environ Geol 47(3):405–411
Al-Mamari MM, Kantoush SA et al (2019) Real-Time measurement of flash-flood in a Wadi area by LSPIV and STIV. Hydrology 6(1):27
Al-Qurashi A, McIntyre N et al (2008) Application of the Kineros2 rainfall–runoff model to an arid catchment in Oman. J Hydrol 355(1–4):105
Al-Rawas GA, Valeo C (2008) Issues with flash flood modeling in the capital region of Sultanate Oman. Geomatics Eng Schulich Sch Eng Univ Calgary 1–11
Al-Turbak A (1996) Geomorphoclimatic peak discharge model with a physically based infiltration component. J Hydrol 176:1–12
Al-Weshah RA, El-Khoury F (1999) Flood analysis and mitigation for Petra area in Jordan. J Water Resour Plan Manage 125(3):170–177
Al Barwani A (2015) Flash flood mitigation and harvesting Oman case study. In: First international symposium on flash floods (ISFF), Kyoto, Japan
Al Khatry A, Helmi T (2008) The effect of Gonu cyclone on recharging groundwater aquifers—sultanate of Oman. In: The first international conference on water resources and climate change in the MENA region, Muscat, The Sultanate of Oman
Al Mulla M (2005) Application of a hydrological model in a data-poor arid region catchment: a case study of Wadi Ham
Al Saud M (2010) Mapping potential areas for groundwater storage in Wadi Aurnah Basin, western Arabian Peninsula, using remote sensing and geographic information system techniques. Hydrogeol J 18(6):1481–1495
Al Zayed IS, Ribbe L et al (2013) Water harvesting and flashflood mitigation-Wadi Watier case study (South Sinai, Egypt). Int J Water Resour Arid Environ 2(2):102–109
Alcántara-Ayala I (2002) Geomorphology, natural hazards, vulnerability and prevention of natural disasters in developing countries. Geomorphology 47(2–4):107–124
Andoh RYG, Declerck C (1997) A cost effective approach to stormwater management? Source control and distributed storage. Water Sci Technol 36(8–9):307–311
APFM (2007) Guidance on flash flood management: recent experiences from Central and Eastern Europe
Arnous MO, Aboulela HA et al (2011) Geo-environmental hazards assessment of the north western Gulf of Suez, Egypt. J Coast Conserv 15(1):37–50
Bajabaa S, Masoud M et al (2014) Flash flood hazard mapping based on quantitative hydrology, geomorphology and GIS techniques (case study of Wadi Al Lith, Saudi Arabia). Arab J Geosci 7(6):2469–2481
BBC (2009) Flood deaths in Saudi Arabia rise to around 100. BBC
Becker D, Sultan M et al (2012) Integrated solutions for hydrologic investigations in arid lands. Geosphere 8(6):1588–1605
Beven KJ (2011) Rainfall-runoff modelling: the primer. Wiley, Chichester, West Sussex, United Kingdom
Bird S, Hogan D et al (2010) Photogrammetric monitoring of small streams under a riparian forest canopy. Earth Surf Proc Land 35(8):952–970
Brasington J, Smart R (2003) Close range digital photogrammetric analysis of experimental drainage basin evolution. Earth Surf Proc Land J Br Geomorphol Res Group 28(3):231–247
Camarasa-Belmonte AM (2016) Flash floods in Mediterranean ephemeral streams in Valencia Region (Spain). J Hydrol 541:99–115
Chennu S, Grésillon J et al (2007) Efficiency of distributed flood mitigation measures at watershed scale. In: WaReLa scientific conference on integrated catchment management for hazard mitigation, Trier, Germany
Cools J, Vanderkimpen P et al (2012) An early warning system for flash floods in hyper-arid Egypt. Nat Hazards Earth Syst Sci 12(2):443–457
Dawod GM, Mirza MN et al (2011) GIS-based spatial mapping of flash flood hazard in Makkah city, Saudi Arabia. J Geogr Inf Syst 3(03):225

Dawod GM, Mirza MN et al (2012) GIS-based estimation of flood hazard impacts on road network in Makkah city, Saudi Arabia. Environ Earth Sci 67(8):2205–2215
Dawson RJ, Ball T et al (2011) Assessing the effectiveness of non-structural flood management measures in the Thames Estuary under conditions of socio-economic and environmental change. Glob Environ Change 21(2):628–646
De Vries AJ, Ouwersloot HG et al (2018) Identification of tropical-extratropical interactions and extreme precipitation events in the Middle East based on potential vorticity and moisture transport. J Geophys Res Atmos 123(2):861–881
Del Giudice G, Rasulo G et al (2014) Combined effects of parallel and series detention basins for flood peak reduction. Water Resour Manage 28(10):3193–3205
Detert M, Weitbrecht V (2015) A low-cost airborne velocimetry system: proof of concept. J Hydraul Res 53(4):532–539
Ebert A, Kerle N et al (2009) Urban social vulnerability assessment with physical proxies and spatial metrics derived from air-and spaceborne imagery and GIS data. Nat Hazards 48(2):275–294
El-Behiry M, Shedid A et al (2006) Integrated GIS and remote sensing for runoff hazard analysis in Ain Sukhna Industrial area, Egypt. Earth Sci 17(1)
El-Magd IA, Hermas E et al (2010) GIS-modelling of the spatial variability of flash flood hazard in Abu Dabbab catchment, Red sea region, Egypt. J Remote Sens Space Sci 13(1):81–88
El Bastawesy M, White K et al (2009) Integration of remote sensing and GIS for modelling flash floods in Wadi Hudain catchment, Egypt. Hydrol Process 23(9):1359–1368
El Shamy IZ (1992) Recent recharge and flash flooding opportunities in the Eastern Desert, Egypt
Elewa HH, Qaddah AA (2011) Groundwater potentiality mapping in the Sinai Peninsula, Egypt, using remote sensing and GIS-watershed-based modeling. Hydrogeol J 19(3):613–628
Elewa H, Qaddah A et al (2012) Determining potential sites for runoff water harvesting using remote sensing and geographic information systems-based modeling in Sinai. Am J Environ Sci **8**(1):42–55
Elewa HH, Ramadan EM et al (2013) Runoff water harvesting optimization by using RS, GIS and Watershed modelling in Wadi El-Arish, Sinai. Int J Eng Res Technol **2**(12):1635–1648
Elkhrachy I (2015) Flash flood hazard mapping using satellite images and GIS tools: a case study of Najran city, Kingdom of Saudi Arabia (KSA). Egypt J Remote Sens Space Sci 18(2):261–278
Emerson CH, Welty C et al (2005) Watershed-scale evaluation of a system of storm water detention basins. J Hydrol Eng 10(3):237–242
Fathy I et al (2015) Runoff hydrograph modeling for arid regions: case study—Wadi Sudr-Sinai. Int Water Technol J IWTJ 5:58–68
Foody GM, Ghoneim EM et al (2004) Predicting locations sensitive to flash flooding in an arid environment. J Hydrol 292(1–4):48–58
Ghoneim E, Foody GM (2013) Assessing flash flood hazard in an arid mountainous region. Arab J Geosci 6(4):1191–1202
Guardian T (2018) Jordan: flash floods kill 12 and force tourists to flee. The Guardian
Guha-Sapir D, Below R et al (2016) EM-DAT: the CRED/OFDA international disaster database
Hadadin N et al (2013) Hydrological analysis for floodplain hazard of Jeddah's drainage Basin, Saudi Arabia. Arab J Sci Eng 38(12):3275–3287
Hall JW, Penning-Rowsell EC (2011) Setting the scene for flood risk management. Flood Risk Sci Manage 1–16
Hansson K, Danielson M et al (2008) A framework for evaluation of flood management strategies. J Environ Manage 86(3):465–480
HEC (1998) Flood damage reduction analysis: HEC-FDA user's manual, vol 72. Davis, CA
Heidari A (2009) Structural master plan of flood mitigation measures. Nat Hazards Earth Syst Sci 9 (1):61–75

Ho M, Lall U et al (2017) The future role of dams in the United States of America. Water Resour Res 53(2):982–998
Hungr O, Morgan G et al (1987) Debris flow defenses in British Columbia. Debris Flows/Avalanches Process Recogn Mitig. Geol Soc Am Rev Eng Geol 7:201–222
Ibrahim SM, Masoud MH et al (2011) Hydrology of Wadi Abadi-Eastern Desert-Egypt. Assiut Univ J Geol 40(2):1–31
IFRC (2013) Sudan: floods emergency appeal n° MDRSD018, IFRC (Published in 13 August 2013)
Ismail YL, Othman AA et al (2010) Impact of flash flood on development potentials of Wadi Abu Ghusun, Eastern Desert, Egypt. Kuwait J Sci Eng 37(2 A):111–134
Jackson JA, Bates R (1997) Glossary of geology: Alexandria. Va Am Geol Inst 769
Jonkman SN, van Gelder P et al (2003) An overview of quantitative risk measures for loss of life and economic damage. J Hazard Mater 99(1):1–30
Kantoush SA, Sumi T et al (2011) JE-HydroNet: modern methodologies for the management, monitoring and planning of integrated water resources in the Nile delta of Egypt. In: 34th IAHRWorld congress, 33rd hydrology and water resources symposium and 10th conference on hydraulics in water engineering, Australia
Kehew AE, Milewski A et al (2010) Reconstructing an extreme flood from boulder transport and rainfall-runoff modelling: Wadi Isla, South Sinai, Egypt. Glob Planet Change 70(1–4):64–75
Kilpatrick FA, Cobb ED (1985) Measurement of discharge using tracers, Department of the Interior, US Geological Survey
Knighton A, Nanson G (1997) Distinctiveness, diversity and uniqueness in arid zone river systems. In: Thomas DSG (ed) Arid zone geomorphology: process, form and change in drylands, 2nd edn. Wiley, pp 185–203
Kundzewicz ZW (2002) Non-structural flood protection and sustainability. Water Int 27(1):3–13
Kundzewicz ZW, Kaczmarek Z (2000) Coping with hydrological extremes. Water Int 25(1):66–75
Kurz B, Wang X et al (2007) An evaluation of basinwide, distributed storage in the Red river basin: the Waffle® concept, vol 23. Energy & Environmental Research Center, University of North Dakota. Accessed Nov 2011
Lange J, Leibundgut C et al (1999) A noncalibrated rainfall-runoff model for large, arid catchments. Water Resour Res 35(7):2161–2172
Lange J, Liebundgut C et al (2000) The importance of single events in arid zone rainfall-runoff modelling. Phys Chem Earth Part B Hydrol Oceans Atmos 25(7–8):673–677
Laure Van Ruymbeke (2018) APN news. https://apnews.com/article/db926fe441be475cb653ab1cfe7ee199
Leblois E, Poulard C et al (2010) Design of dry dams at watershed scale: lessons learnt from sensitivity analyses using a simple but consistent rainfall-runoff model. Balwois, Ohrid, France
Lin X (1999) Flash floods in arid and semi-arid zones. Technical documents in hydrology, UNESCO
Masoud M (2013) The possible impact of the prevailing physiographic features of selected catchments upon their hydrological characteristics, Egypt (comparative study). Aust J Basic Appl Sci **7**(14):324–347
McBain W (2012) Twenty-first century flood risk management. Flood risk: planning, design and management of flood defence infrastructure. ICE Publishing, pp 7–22
McIntyre N, Al-Qurashi A (2009) Performance of ten rainfall–runoff models applied to an arid catchment in Oman. Environ Model Softw 24(6):726–738
McLane J, Wüst R (2000) Flood hazards and protection measures in the Valley of the Kings. CRM-WASHINGTON 23(6):35–38
Merz B, Thieken AH (2004) Flood risk analysis: concepts and challenges. Österr Wasser Abfallwirtsch 56(3–4):27–34
Merz B, Kreibich H et al (2008) Flood risk analysis: uncertainties and validation. Österr Wasser Abfallwirtsch 60(5–6):89–94

Merz B, Hall J et al (2010) Fluvial flood risk management in a changing world. Nat Hazards Earth Syst Sci 10(3):509–527
Milewski A, Sultan M et al (2009) A remote sensing solution for estimating runoff and recharge in arid environments. J Hydrol 373(1–2):1–14
Moneim AA (2005) Overview of the geomorphological and hydrogeological characteristics of the Eastern desert of Egypt. Hydrogeol J 13(2):416–425
Montaldo N, Mancini M et al (2004) Flood hydrograph attenuation induced by a reservoir system: analysis with a distributed rainfall-runoff model. Hydrol Process 18(3):545–563
Mostafazadeh R, Sadoddin A et al (2017) Scenario analysis of flood control structures using a multi-criteria decision-making technique in Northeast Iran. Nat Hazards 87(3):1827–1846
MRMWR (2015) Oman, Ministry of Regional Municipalities and Water Resources
Murata M, Ozawa H et al (2015) Post Aswan High Dam flash floods in Egypt: causes, consequences and mitigation strategies. Bull Cent Collab Community Naruto Univ Educ 29:173–186
Newman L (2005) Uncertainty, innovation, and dynamic sustainable development. Sustain Sci Pract Policy 1(2)
Omran A, Schroder D et al (2011) Flood hazard assessment in Wadi Dahab, Egypt based on basin morphometry using GIS techniques. GI_Forum Program Committee
Onusluel Gul G, Harmancioglu N et al (2010) A combined hydrologic and hydraulic modeling approach for testing efficiency of structural flood control measures. Nat Hazards 54(2):245–260
Perks MT, Russell AJ, Large ARG (2016) Technical note: advances in flash flood monitoring using unmanned aerial vehicles (UAVs). Hydrol Earth Syst Sci 20:4005–4015
Pilgrim D, Chapman T et al (1988) Problems of rainfall-runoff modelling in arid and semiarid regions. Hydrol Sci J 33(4):379–400
Plate EJ (2002) Flood risk and flood management. J Hydrol 267(1–2):2–11
Ramireddygari S, Sophocleous MA et al (2000) Development and application of a comprehensive simulation model to evaluate impacts of watershed structures and irrigation water use on streamflow and groundwater: the case of Wet Walnut Creek Watershed, Kansas, USA. J Hydrol **236**(3–4):223–246
Ravazzani G, Gianoli P et al (2014) Assessing downstream impacts of detention basins in urbanized river basins using a distributed hydrological model. Water Resour Manage 28 (4):1033–1044
Richards J, White I et al (2008) Local planning practice and flood risk management in England: is there a collective implementation deficit? Environnement Urbain/Urban Environ 2:11–20
Rodier J, Roche M (1978) River flow in arid regions. Hydrom Prin Pract 453
Saber M (2010) Hydrological approaches of Wadi system considering flash floods in arid regions. Kyoto, Graduate School of Engineering, Kyoto University
Saber M, Habib E (2015) Flash floods modelling for wadi system: challenges and trends. Landscape Dyn Soils Hydrol Process Varied Climates 317–339
Saber M, Hamaguchi T et al (2010a) Flash flooding simulation using hydrological modeling of Wadi basins at Nile river based on satellite remote sensing data
Saber M, Hamagutchi T et al (2010b) Hydrological modeling of distributed runoff throughout comparative study between some Arabian wadi basins. Annu J Hydraul Eng Jpn Soc Civil Eng 54:85–90
Saber M, Hamaguchi T et al (2015) A physically based distributed hydrological model of wadi system to simulate flash floods in arid regions. Arab J Geosci 8(1):143–160
Saber M, Kantoush S et al (2017a) Assessing flash floods prone regions at wadi basins in Aswan, Egypt. 京都大学防災研究所年報. B= Disaster Prev Res Inst Annuals B 60(B):853–863
Saber M, Kantoush S et al (2017b) Assessing flash floods prone regions at Wadi basins in Aswan, Egypt. Annu Disaster Prev Res Inst 60 B:427–437

Saber M, Kantoush SA et al (2020) Assessment of spatiotemporal variability of water storage in Arabian countries using global datasets: implications for water resources management. Urban Water J 1–15

Sayers P, Yuanyuan L et al (2013) Flood risk management: a strategic approach. Asian Development Bank, GIWP, UNESCO and WWF-UK

Scoones I, Leach M et al (2007) Dynamic systems and the challenge of sustainability

Sen Z (2008) Wadi hydrology. CRC Press, New York

Sen Z, Khiyami HA et al (2013) Flash flood inundation map preparation for wadis in arid regions. Arab J Geosci 6(9):3563–3572

Shadeed S, Almasri M (2010) Application of GIS-based SCS-CN method in West Bank catchments, Palestine. Water Sci Eng 3(1):1–13

Shah AA (2015) Assessing the influence of watershed characteristics on the flood vulnerability of Jhelum Basin in Kashmir Himalaya by Gowhar et al., 2015. Nat Hazards 77(3):2139–2143

Shah MAR, Rahman A et al (2015) Challenges for achieving sustainable flood risk management. J Flood Risk Manage 7

Sherif MM, Mohamed MM et al (2010) Rainfall runoff modeling of three Wadis in the Northern area of UAE. J Hydrol Eng 16(1):10–20

Shi Q (2014) Flood hazard assessment along the Western regions of Saudi Arabia using GIS-based morphometry and remote sensing techniques

Soussa H et al (2012) Flood hazard in wadi Rahbaa area, Egypt. Arab J Geosci 5(1):45–52

Stedinger JR (1993) Frequency analysis of extreme events. In: Handbook of hydrology, vol 18

Sultan M, Metwally S et al (2011) Modern recharge to fossil aquifers: geochemical, geophysical, and modeling constraints. J Hydrol 403(1):14–24

Sumi T, Saber M et al (2013) Japan-Egypt hydro network: science and technology collaborative research for flash flood management. J Disaster Res 8(1):28–36

Tapsell SM, Penning-Rowsell EC et al (2002) Vulnerability to flooding: health and social dimensions. Philos Trans Royal Soc Lond A Math Phys Eng Sci 360(1796):1511–1525

Tauro F, Porfiri M et al (2016) Surface flow measurements from drones. J Hydrol 540:240–245

Thomas NW (2015) Simulating the hydrologic impact of distributed flood mitigation practices, tile drainage, and terraces in an agricultural catchment. Ph.D, Graduate College, Iowa, The University of Iowa

Tomsett C, Leyland J (2019) Remote sensing of river corridors: a review of current trends and future directions. River Res Appl 35(7):779–803

Viglione A, Rogger M (2014) Flood processes and hazards. Hydro Meteorol Hazards Risks Disasters 3–33

Wheater HS, Butler AP et al (1991) A multivariate spatial-temporal model of rainfall in southwest Saudi Arabia. I. Spatial rainfall characteristics and model formulation. J Hydrol 125(3–4):175–199

Wheater H, Sorooshian S et al (2007) Hydrological modelling in arid and semi-arid areas. Cambridge University Press

White I, Richards J (2007) Planning policy and flood risk: the translation of national guidance into local policy. Plan Pract Res 22(4):513–534

Wu S-J, Yang J-C et al (2011) Risk analysis for flood-control structure under consideration of uncertainties in design flood. Nat Hazards 58(1):117–140

Youssef A, Hegab M (2005) Using geographic information systems and statistics for developing a database management system of the flood hazard for Ras Gharib area, Eastern Desert, Egypt. In: The fourth international conference on the geology of Africa

Youssef AM, Maerz NH (2013) Overview of some geological hazards in the Saudi Arabia. Environ Earth Sci 70(7):3115–3130

Youssef AM, Pradhan B et al (2009) Geomorphological hazard analysis along the Egyptian Red Sea coast between Safaga and Quseir. Nat Hazards Earth Syst Sci 9(3):751–766

Youssef AM, Pradhan B et al (2015) Use of geological and geomorphological parameters in potential suitability assessment for urban planning development at Wadi Al-Asla basin, Jeddah, Kingdom of Saudi Arabia. Arab J Geosci 8(8):5617–5630

Youssef AM, Pradhan B, Hassan AM (2011) Flash flood risk estimation along the St. Katherine road, southern Sinai, Egypt using GIS based morphometry and satellite imagery. Environ Earth Sci 62(3):611–623

Chapter 2
Flood Risk Management Practices in Morocco: Facts and Challenges

Dalila Loudyi, Moulay Driss Hasnaoui, and Ahmed Fekri

Abstract From ancient flood management practices driven by agricultural activities to dam's policy for water resources management including flood protection, to the National Strategy for Natural Disaster Risk Integrated Management; Morocco has come a long way in flood risk management. This chapter describes the recurrent flooding phenomenon plaguing the country along with progress in flood risk assessment approaches in terms of technique, governance, and best practices. An extensive number of research articles, administrative documents, consultancy, and international organizations reports are analyzed to give a holistic up-to-date insight into flood risk management in Morocco and present a comprehensive and critical view from a scientific perspective. Information and data were collected from a range of various sources and synthesized to integrate all scientific and governance aspects. Though analysis of this landscape shows progresses made by the Government to protect the population and reduce flood risk, it also shows shortcomings and challenges still to be overcome. Thus, a SWOT analysis was carried out for scoping and identifying the strengths, weaknesses, opportunities, and threats pertaining to this issue. The analysis reveals various success and failure factors related to three major components: governance, risk assessment approaches, and flood risk mitigation measures sustainability.

Keywords Flood risk management · Morocco · SWOT · Flood risk assessment · Flood control measures

D. Loudyi (✉)
Water, Environment and Climate Change Laboratory Team, Faculty of Science and Technology, Hassan II University of Casablanca, Mohammedia, Morocco
e-mail: dalila.loudyi@fstm.ac.ma

M. D. Hasnaoui
Water Resources Division, Ministry of Equipment, Transport, Logistics and Water, Rabat, Morocco

A. Fekri
Applied Geology, Geomatics and Environment Laboratory, Faculty of Sciences Ben Msik, Hassan II University of Casablanca, Casablanca, Morocco

T. Sumi et al. (eds.), *Wadi Flash Floods*, Natural Disaster Science and Mitigation Engineering: DPRI Reports, https://doi.org/10.1007/978-981-16-2904-4_2

Acronyms

AAL	Average Annual Loss
ABH	Hydraulic/River Basin Agency
ACAPS	Insurance and Social Security Regulatory Authority
AUA	Al Hoceima Urban Agency
AUT	Taounate Urban Agency
CAU	Urbanization Aptitude Map
CVC	Coordination and Monitoring Center
DEM	Digital Elevation Model
DGE	General Directorate of Water
DGM	General Directorate of Meteorology
DGPC	Civil Protection Directorate
DGRN	Natural Disasters Risk Management Directorate
DRPE	Water Research and Planning Directorate
EMDAT	The OFDA/CRED International Disaster Database, www.emdat.be—Université catholique de Louvain—Brussels, Belgium
FFWS	Flood Forecasting and Warning System
FLCN	Fund to combat Effects of Natural Disasters
FSEC	Fund of Solidarity against Catastrophic Events
GIS	Geographical Information System
HCEFLCD	High Commissioner for Water, Forests and the Fight against Desertification
IDF	Intensity-Duration-Frequency
IPCC	Intergovernmental Panel on Climate Change
JICA	Japan International Cooperation Agency
LEC	Loss Exceedance Curve
LTE	Long-Term Evolution
LYDEC	Lyonnaise des Eaux of Casablanca, water utility
MAD	Moroccan Dirham (10 MAD is about 1 USD)
MI	Ministry of Interior
MnhPRA	Morocco natural hazards Probabilistic Risk Analysis
OECD	Organisation for Economic: Co-operation and Development
ONE	National Office for Energy
ONEE	National Office for Energy and Drinking Water (merger of former ONE and ONEP)
ONEP	National Office for Drinking Water
ORMVA	Regional Agricultural Development Office
ORSEC	Local Emergency Response Plan
PCC/RCC	Provincial/Regional Coordination Center
PDAIRE	Master Plan for Integrated Water Resources Management
PNE	National Water Plan
PNI	National Flood protection Plan
PPRI	Prevention Plan against Flood Risk
RCM	Regional Climate Models

SCO	Western mega-drainage channel of Casablanca city
SDACR	Master Plan for Risk Analysis and Coverage
SNE	National Water Strategy
UAV	Unmanned Aerial Vehicle
UNDP	United Nations Development Programme
UNDRO	United Nations Disaster Relief Coordinator—UNDRO
UNDRR	United Nations Office for Disaster Risk Reduction
UNEP	United Nations Environment Programme
UNESCO	United Nations Educational, Scientific and Cultural Organization
UNISDR	United Nations International Strategy for Disaster Reduction
WB	World Bank

2.1 Introduction

As a country with an agriculture-based economy under arid to semi-arid climate conditions, Morocco has traditionally developed its agriculture on its vast and plentiful floodplains due to their water availability and favorable topography for many types of crops. Consequently, many Moroccan farmers have built up flood management practices based on floodwater control for irrigation. For example, the use of dikes designed to erode in a controlled manner during a flood event and spread floodwaters was part of ancestral irrigation knowledge. In fact, floods have always been regarded as a relief from water scarcity for agriculture and a gift of nature that ensures prosperity and the well-being of local populations. However, there has been a paradigm shift driven by an increase in urbanization and the fading of traditional agriculture that have turned floods into an impediment to modern societal development. Gradually, protecting cities and farmlands in the vicinity of watercourses from floods in addition to mitigating recurrent droughts has become a governmental priority. As a consequence, at an early stages of the country independence, Morocco developed a dam's policy which began in 1967 (Jouve 2006). The policy aimed at the design and construction of two to three dams each year in order to irrigate one million hectares by the year 2000, secure drinking water supply, mitigate flood risk and produce hydropower. This dam's policy, designed initially for drought control and agricultural development, led to important investments in the water sector that rapidly proved to be beyond the state budget capacities. It raised the question of water cost, tariffication issues of water services (i.e. drinking water, irrigation, and energy), and the respective cost sharing between the state and users. As an institutional response to this problem, a hydrological landscape-based division was introduced in 1995 by the water law 10-95, creating nine catchment agencies, called Hydraulic Basin Agencies (ABH) that provide administrative, financial, and technical framework for integrated water resources assessment and management at regional levels. Hence, in 1999, the first ABH of Oum Er Rbia (ABHOER) was created, followed by Sebou (ABHS), Tensift

(ABHT), Bouregreg-Chaouia (ABHBC), Moulouya (ABHM), and Souss-Massa-Draa (ABHSMD) in 2000; Loukkos (ABHL) in 2001; Guir-Ziz-Rheris (ABHGZR) and Sakia el Hamra-Oued Eddahab (ABHSO) in 2009. In 2016, a tenth ABH was created by dividing the Souss-Massa-Draa catchment into two separate administrative entities that are known as Souss-Massa ABH (ABHSM) and Draa Oued Noun ABH (ABHDON). This was due to the extent of this territory and its numerous water challenges which include both droughts and floods (Fig. 2.1). This set of ABHs serves as the regional administrative framework for water management planning including flood risk management. Moreover, between 1951 and 2019, Morocco experienced more than 80 flood events showing that despite the success of many dams in ensuring flood protection, many of them are still unable to prevent downstream flooding (e.g. Wahda 2008; Guelmim 2014; El Malleh 2002). Besides revealing the persistent lack of structural and non-structural measures in many Moroccan zones, the recurrent flooding raised the question of new risk management approaches. This chapter describes the phenomenon of floods in Morocco, the existing approaches to assess flood risk, their related technical and governance aspects, and the adopted best management practices. An analysis of the existing approaches will be carried out and recommendations for improving it will be provided.

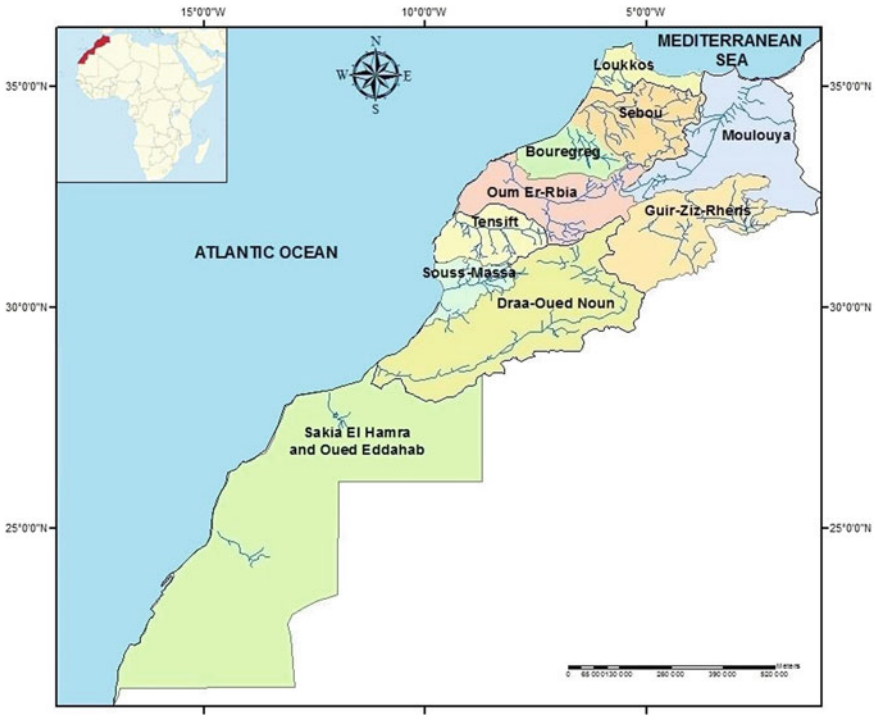

Fig. 2.1 The ten Hydraulic Basin Agencies (ABHs) boundaries for regional integrated water management and planning in Morocco

2.2 Overview of Flood Events in Morocco

2.2.1 Flood Events Historical Data

In the past twenty years, Morocco was hit by multiple natural disasters such as Al Hoceima earthquake (February, 2004), Taourart-Akchour landslide in the Rif mountains (November, 2010) and floods that affected large cities such as Mohammedia (November 2002), Tangier (October 2008, December 2009, January 2013), Casablanca (November 2010 and January 2013), plains such as Gharb (2008) and, lately, desertic areas of Guelmim and Sidi Ifni in southern Morocco (November, 2014), Laayoune–Saquia Al Hamra (October, 2016) and Taroudant (2019). Disasters history shows that, since 1970, floods are events that impacted the most people in Morocco and caused important economic damages (Fig. 2.2). An inventory of past flood events over Moroccan territory with their damages for the last fifty years is shown in Table 2.1.

Many international database resources can be found for recording flood events in Morocco. A research dedicated resource is the EM-DAT database of the University of Louvain for all disasters (EM-DAT 2020). On an administrative level, the Moroccan department of environment used to update regularly the United Nation Disaster Risk Reduction (UNDRR) system DesInventar Sendai database with information on floods, landslides, forest fires, droughts, and earthquakes (DesInventar Sendai 2014). Currently, natural disaster management is the responsibility of the Ministry of Interior leading to a new approach of data communication on disasters.

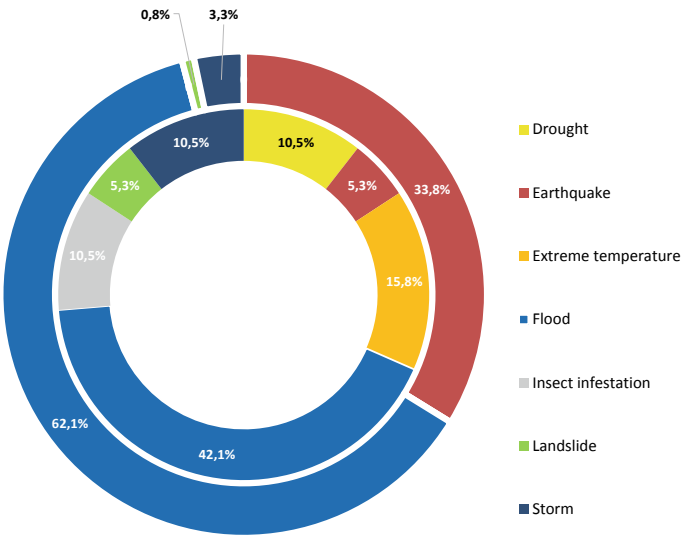

Fig. 2.2 Reported natural disaster events in Morocco 1970–2020: frequency (internal ring); number of deaths (external ring) (*Source* EM-DAT)

Table 2.1 Inventory of past flood events over Moroccan territory and related damages 1970–2020

Year	Date	Location	Flood causes	Deaths	Economic damages
1970	22 January	Northern region		11	USD 30 million
1975	21 April	Western provinces		10	
1979	25 October	Ouarzazate		16	
1985	07 January	Guelmim	33–65 mm/53 min, Oum Laachar wadi		
1995	01 April	Tata	Akka wadi	18	2 wounded, 4 missing, and 350 families homeless; as well as destruction of 655 homes, about USD 9 million
1995	17–19 August	Ourika valley	Ourika wadi	730	USD 9 million
1995	04 September	Taza-Taounate	Amlil wadi	43	
1996	21 Jan. to 01 Feb.	Beni Mellal		25	USD 55 million
1997	28–29 September	El Hajeb		60	
2000	22 December	Martil plain—Tetouan		6	
2001	23–26 December	Settat-Essaouira		15	USD 2.2 million
2002	24–29 November	Mohammedia, Berrechid, Settat, Fez		80	17 wounded, 26 missing, 44 industrial units, fire at la SAMIR oil refinery, 1334 homes damaged, many hectares of agricultural land and livestock lost; USD 200 million
2003	17–18 November	Nador—El Hoceima		35	
2006	26–28 May	Errachidia		6	
2006	26 May	Merzouga	112 mm/3 h, El Beida and Tisserdmine wadis		140 houses and hotels, deterioration of Taouz–Merzouga road and ONEP (National Office for Drinking Water) water supply pipes of Merzouga and Taouz villages

(continued)

Table 2.1 (continued)

Year	Date	Location	Flood causes	Deaths	Economic damages
2006	25–27 October	Essaouira—Safi		11	
2008	26–28 February	Marrakech		9	
2008	23 Oct. to 03 Nov.	Tanger		30	Industrial units important damages
2009	1–12 February	Al Gharb region		29	400 homes and 100,000 ha of land destroyed
2009	25–26 December	Middle Draa Valley		5	
2010	27 November	Bouskoura	195 mm/ 24 h		Schools, national phosphate production company (OCP) headquarter, several buildings, and Roads are flooded
2010	09 March	El Ksiba, Taza, Midelt, Khénifra	200 mm/ 24 h with a max of 25 mm/1 h	10	
2010	25 Oct. to 06 Nov.	Tiflet, Al Hoceima, Khenifra area, Ouezzane, Bouznika, Ouarzazate, Zagora, Salé, Rabat, Casablanca		32	USD 29 million
2012	31 October	Taroudant, Agadir	84–100 mm/ 12 h		
2013	29 August	Tetouan, M'diq	31 mm/3 h		
2014	28–30 November	Guelmim region/Sidi IfnI	Bousafen and Oum el Achar wadis	60	More than 32 fatalities and damages due to inundations
2016	4–5 May	Taroudant-Ouarzazate	Azkrou wadi	4	
2017	23 February	Sale-Rabat	120 mm/ 24 h with a max 65 mm/ 1 h		National Road n°6—Lâarjate road partly destroyed
2018	17 August	Zagora			
2018	25–26 September	Tata			
2019	28 August	Taroudant region		8	200 homes destroyed
2019	08–09 September	Errachidia	Damachine wadi	17	27 wounded

2.2.2 Flood Types Description

An analysis of historical flood events in Morocco shows that the nature of these floods can be classified as follows:

- Wadi floods of large catchments, with an area generally greater than 10,000 km^2, where watercourses gradually take over their banks. Such is the case of Moulouya, Sebou, Oum Er Rbia, Tensift, Souss, Drâa, and Ziz wadis.
- Flash floods of the main tributaries of large wadis, with a rise time between 6 and 24 h. It is the case of Moulouya tributaries (e.g. Melloulou, Za), Sebou tributaries (e.g. Ouergha, Beht), Oum Er Rbia tributaries (e.g. El Abid, Tessaout, Lakhdar), Tensift tributaries (e.g. N'Fis), Souss tributaries (e.g. Issen), Drâa tributaries (e.g. Dadès, Ouarazazte, N'Ait Douchéne) and Ziz tributaries (e.g. Rhéris, Todgha).
- Flash floods of the coastal Mediterranean wadis (e.g. Nekor, El Had, Lao, Emsa, Martil) and coastal Atlantic wadis (Mharhar, El Hachef, Loukkos, Bouregreg, Ykem, Cherrat, El Mellah, Nfifikh, Tamdrost, Ksob, Tamri, Massa). Their related watersheds surfaces range generally between 300 km^2 and 3000 km^2, with a rise time of one to few hours.
- Semi-flash floods of medium-sized plains with flat water flow, on the plains located at the foothills of Rif and the Atlas Mountains. Slopes abruptly diminish and the conveyance capacity of wadis from high mountains to their foothills then decreases sharply (e.g. Tamdrost, Mazer, Issyl).
- Torrential flash floods of small mountain basins in Rif and Atlas, characterized by steep slopes, generally with rugged, unvegetated, and impervious lands, where the heaviest daily maximum rains are recorded (e.g. Ourika, Rhéraya, Toghdra, Nfis, Fnideq, Charâa valleys). The rise time of these type of floods is less than one hour and often applies to urban areas that are large (e.g. Marrakech, Mohammedia, Settat, Berrechid, Béni Mellal, Errachidia, Oujda) and located in the vicinity of wadis.
- Urban stormwater floods, generated by rainfall on impervious parts of the city or runoff of small upstream basins (e.g. Tangier, Casablanca, Fez, Azrou, El Hajeb).

Based on the sixty years record of flood events in Morocco, the National Water Plan of Morocco (PNE 2015) reported that the main reasons can be broadly summarized in the following points:

- rapid and uncontrolled development of urbanization in flood-prone areas,
- lack of integrating flood risk in urban planning documents,
- lack of maintenance of watercourses,
- insufficient sections of hydraulic structures to convey floodwater (e.g. channels, culverts, nozzles). They generally suffer from an undersizing which is sharply exacerbated in urban areas,
- localized solutions to flood-prone areas without any integrated approach: most structural measures in urban areas are carried out without considering neither

works located immediately upstream nor for possible downstream impacts. The problem aggravates even more with development work on a long stretch of a watercourse (e.g. recalibration, containment, undergrounding),
- deficiencies in maintenance of underground hydraulic structures (e.g. culverts, nozzles, pipes) that are often the default solutions for flood control in urban area based on their sewage networks,
- poor knowledge of the flood dynamic (meteorological conditions, role of the oceans, fine spatial and temporal distribution of precipitation, rainfall-runoff relationship, watershed morphology role, landcover, and the land use, flood probability, climatic drivers, etc.). This is particularly true at local levels,
- climate change and increase of intensity of extreme rainfall episodes. Indeed, despite its arid and semi-arid climate, Morocco has experienced in the past 30 years an increase in the frequency of flood events.

2.2.3 Climate Change and Extreme Rainfall Trends

Due to its geographical location and geomorphological features, Morocco's climate is Mediterranean in the north and arid in the south and southeast. Average annual temperature is 17.5 °C, and average annual precipitation is 318.8 mm with yet a great interannual, seasonal and spatial variability (Fig. 2.3). Precipitation patterns vary interannually from 50 mm to 100 mm in dry years and 300 m to 400 m in wet years (Driouech 2010). Alternation of wet and dry episodes that can last several years is a defining feature of climatic and hydrological regimes of Morocco. Figure 2.4 shows the monthly distribution of temperature and precipitation for the period 1901–2016 (WB 2016). Morocco's rainy season extends from October through April, often resulting in devastating floods. High-intensity precipitations occur mainly in November to February, but can also occur in summer as a thunderstorm on the Atlas and Rif mountains.

According to the Intergovernmental Panel on Climate Change (IPCC), average annual precipitation will decrease in most of the Mediterranean region between −4% and −27%. Number of rainy days is also expected to decrease with an increased risk of drought (IPCC 2007).

Climate change scenarios with 50 km resolution on Moroccan territory were performed by Driouech 2010 using ARPEGE-RV model. They showed that there will be a high spatial variability in magnitude evolution of extreme winter rainfall. The north-west and east of the country as well as part of the middle and high Atlas would not undergo significant changes. Yet, south of Morocco would experience less intense precipitation and the central coastal area would witness a relative increase in amplitude of heavy precipitation events. The number of extreme rainfall events, on the other hand, would decrease throughout the territory (Fig. 2.5a).

With higher resolution of 12 km, two simulations for two of 30 years each (1971–2000 and 2021–2050) were carried out with ALADINClimat to assess future

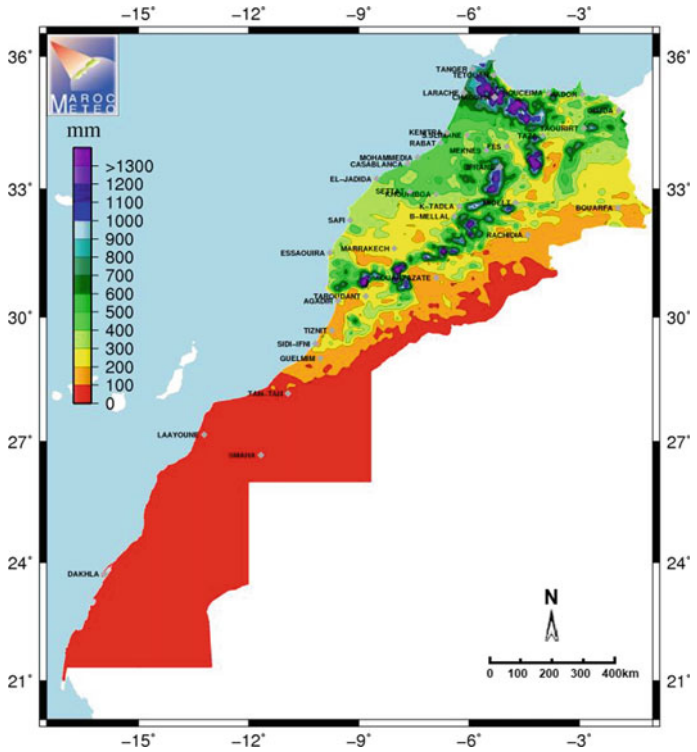

Fig. 2.3 Annual mean precipitations in Morocco for the period 1981–2010 (*Source* DGM 2017)

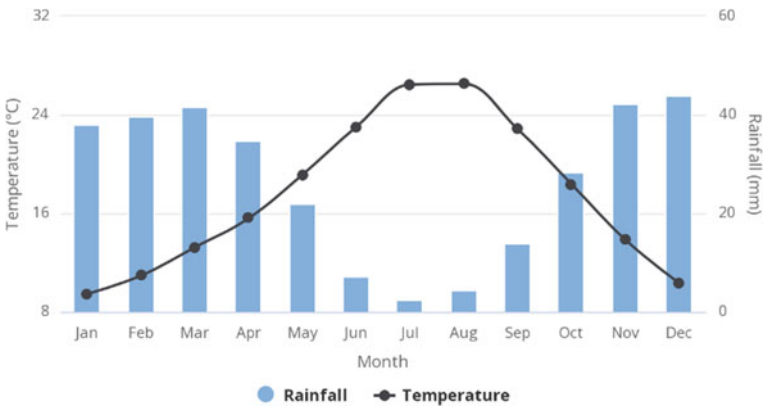

Fig. 2.4 Average monthly temperature and rainfall in Morocco for the period 1901–2016 (*Source* WB 2016)

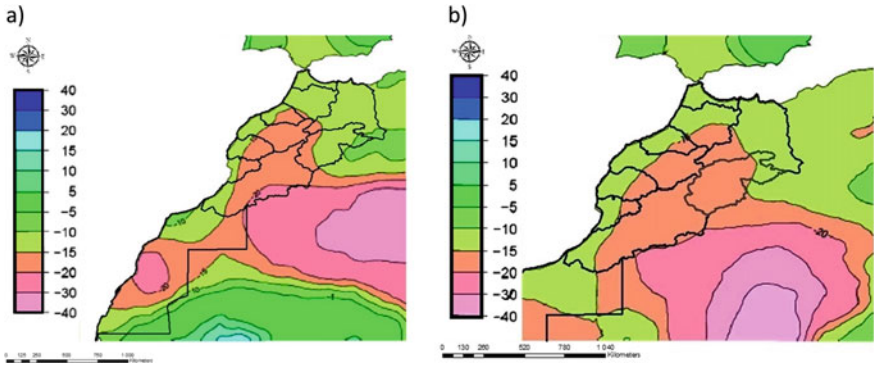

Fig. 2.5 Variation (in %) of extreme rainfall events numbers for A1B scenario winter season, for 2021–2050 based on 1971–2000 record simulated change **a** by ARPEGE-RV-50 km resolution, **b** by ALADINClimat-12 km resolution (Modified from Driouech 2010)

changes in the northern half of Morocco. The results showed that winter precipitation would decrease by −10% to −15% over most of the northern part of the country where there will also be an increase in the maximum period of drought and a decrease in the number of wet days. Extreme rainfall events would not undergo significant amplitude evolutions on all the zone west of the Atlas Mountains and the extreme north. Yet, they will decrease in number from −10% to −20% on the whole northern part of Morocco covered by the domain of the model (Fig. 2.5b). Average spring precipitation is expected to increase by +5% to +20% over the northern half of the country with the exception of the northwest coastal region between Tangier and Casablanca, which is not expected to change significantly. The drying up of the north of the country in summer is also forecast by large majority of regional climate models (RCMs). In autumn, practically the entire area west of the Atlas Mountains would not change in terms of average precipitation.

Sinan and Belhouji (2016) estimated an overall decrease in annual precipitation totals varying on average between 10% and 30% depending on the scenario chosen and regions for horizon 2080–2100. Average annual temperatures will concomitantly increase on average between +2 and +5 °C depending on the chosen scenario and the region considered. The impact of these variations on water resources volume is expected to have an overall downward trend ranging from −7.6% to −40.6%.

2.2.4 Hydrological Impact of Climate Change

Rainfall–runoff process is tightly influenced by watersheds geomorphological and hydrological characteristics. Moroccan landscape can broadly be divided into two categories: mountains and plains. Most of Moroccan wadis cross plains that are

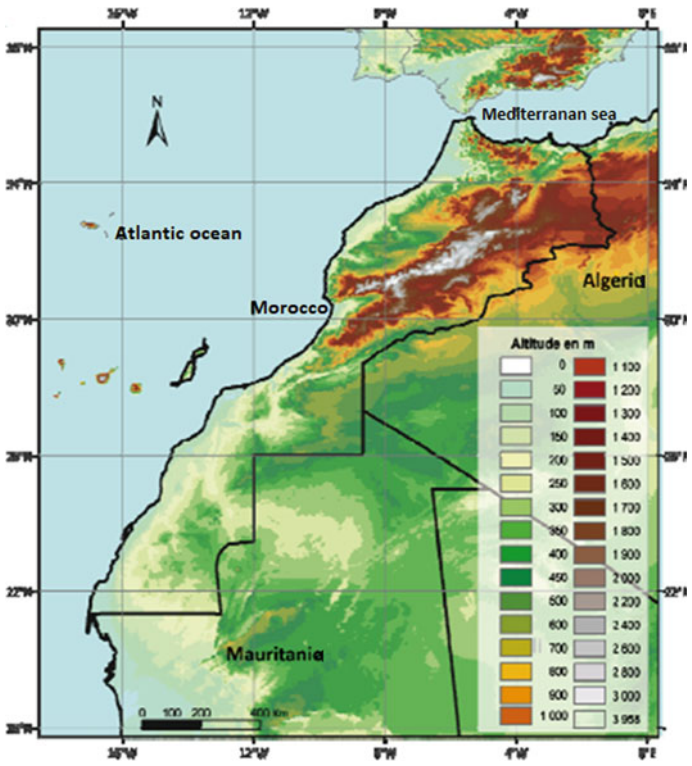

Fig. 2.6 Digital elevation model (DEM) map of Morocco (*Source* Singla 2009)

generally alluvial. Coastal and inland plains are large between the Atlantic Ocean and the Atlas Mountains, and get narrower on northern coastlines between the Mediterranean Sea and the Rif mountains (Fig. 2.6). In the South, plains and desert hills lay from the Anti-Atlas Mountains to the Moroccan southern Sahara. Rif Mountains in the North of the country, culminate at 2456 m. As for the Atlas chain (i.e. Middle Atlas, High Atlas and Anti-Atlas), it extends from the North-East to the South-West and its highest point is 4165 m. The mountains thus play the role of climatic barriers, regulating the rainfall over the northern part of the country.

At catchment level, few studies have tackled the impact of climate change on rainfall-runoff relationship in Morocco. Driouech et al. (2010) assessed the impact of climate change on Moulouya catchment of 55,500 km^2 surface north east Morocco. The GR2M hydrologic model was run using ARPEGE-Climat model output scenarios with 50–60 km resolution. Between 1958 and 2000, monthly flows showed a clear downward trend mainly attributed to a decrease in rainfall and an increase in evapotranspiration (ET). By 2050, winter flow discharges are projected to decrease by −20 to −30%, those of other seasons would decrease less (on average +7 to +10%).

In Diekkrüger et al. (2012), climate scenarios showed that Drâa catchment, a 28,400 km^2 basin in south eastern Morocco, will face a decrease in rainfall of 30 ± 11 mm and an increase in temperature up to 1.4 ± 0.7 °C up to 2050. Rainfall variability and evapotranspiration will increase which results in a reduced vegetation coverage amplifying rainfall effects. Consequently, an increase in the erosion rate up to 21 ± 17% is expected.

On the Oum Er Rbia catchment, a basin with a total area of 36,972 km^2, Azhari and Loudyi (2019) built up statistical downscaling scenarios to predict future climate. The models showed an increase in temperature fluctuating between 0.8% and 15.4%, and a decrease in precipitation that varies from 3% to 16.4%. The impact of these variations was simulated using the hydrologic model HEC-HMS resulting in a decrease of runoff discharge ranging from 48.4% to 57.1% over the basin area.

On a smaller scale, Marchane et al. (2017) carried out five regional climate models to evaluate future changes in precipitation and temperature over Rheraya watershed, a sub-basin at the Tensift catchment of 225 km^2 surface located in the High Atlas Mountains of Morocco. The models were developed through the Med-CORDEX initiative, according to the two emissions scenarios RCP4.5 and RCP8.5. The future projections for the period 2049–2065 under the two scenarios indicate higher temperatures (+1.4 °C to +2.6 °C) and a decrease in total precipitation (−22% to −31%). The hydrological projections under these climate scenarios indicate a significant decrease in surface runoff (−19% to −63%, depending on the scenario and hydrological model) mainly caused by a significant decline in snow amounts and increased temperature.

Seif-Ennasr et al. (2016) found that, under RCP8.5 scenario, temperatures in the Chtouka Ait-Baha sub-basin in the Souss Massa catchment, will increase up to 2 °C during 2030–49 and up to 5 °C during 2090–2100 compared to baseline (1986–2005). Precipitation will also decrease down to −30% for the period 2030–2049 as well as to −60% for 2080–2099 period. Subsequently, hydraulic simulations showed that water deficit at the basin will triple by year 2050 due to the reduction of aquifer recharge and dam's storage.

Many ABHs are still carrying out studies on the impact of climate change on their water resources within the process of updating their Master Plan for Integrated Water Resources Management, (e.g. Sebou, Souss Massa). Mitigation and adaptation measures are being identified as a result of these studies so that they can be included in the investment program drawn by the Master Plan of each of the ten Moroccan ABHs.

Research and technical studies show that there is a general trend to a decreasing total annual rainfall and an increase in temperature for next fifty years at national and local levels. However, no study has made a downscaling to simulate the trend in the intensity of extreme rainfall events, especially for short durations of few hours, that are often the cause of flash floods. Runoff is also expected to decrease as a natural consequence of decreasing rainfall in most catchments of the country. An exception can be the northern catchments of Loukkos and Sebou given the possible increase in precipitation pattern, the size, and shape of their watersheds having rapid hydrological responses especially those in Rif mountainous areas.

2.3 Flood Risk Management Framework

2.3.1 Management Approach

As an arid and semi-arid country, the unexpected occurrence of flash floods was first handled in a crisis management manner. The frequency of events and their generated damages urged the government to prepare a strategy for flood management moving from crisis management to risk management (Fig. 2.7). Indeed, in a study published by OECD 2017 on risk management policies in Morocco, it was clear that a reactive approach did not enable an upstream preparation and identification of management, financial, and logistics needs for emergency situations, and therefore, pushed decision-makers to seek a proactive management approach.

2.3.2 Institutional, Legal, and Policy Frameworks

Morocco's institutional and legislative frameworks for flood risk management are broad and progressive. As the management approach was evolving from crisis management to proactive management, many institutions have seen their role changing by necessary legislative and regulatory updates. The nature of flood risk as an inter-sectorial field, correlating natural disaster, water management, environment, and public safety, has produced a wide array of actors involved in its planning and management as shown in Fig. 2.8. Introduction of the main flood management stakeholders is given below.

(a) **National and regional institutions**

The General Directorate of Water (DGE): Water resources planning is mainly the responsibility of the Water Department in Morocco. Within this department, the Directorate of Water Research and Planning (DRPE) is in charge of integrated

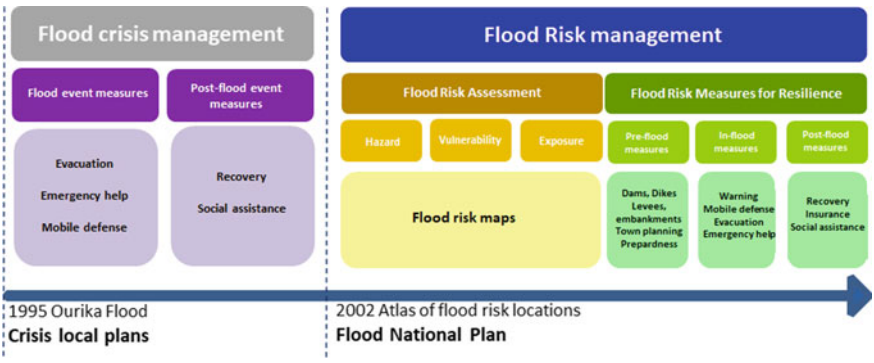

Fig. 2.7 Flood risk management framework

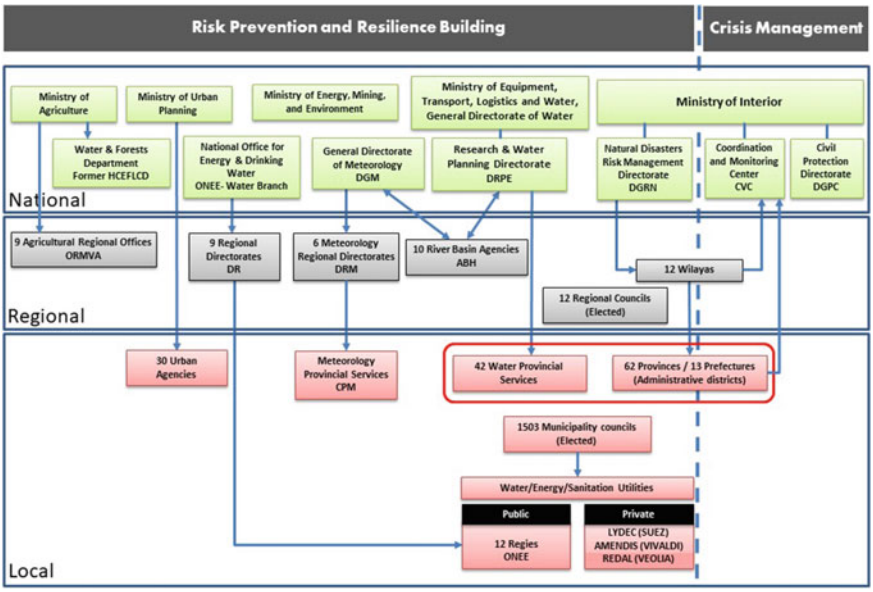

Fig. 2.8 Flood risk management institutional stakeholders in Morocco

water resources management including extreme events of droughts and floods management. The DRPE has always been involved in flood risk assessment and mitigation in addition to administrative support and coordination at national level for regional river basin agencies, namely ABHs. Of note, since 1992, the water department shifted jurisdiction between different ministries such as Ministry of Agriculture, Ministry of Equipment, Ministry of Land use Planning and Ministry of Energy, Mines and Environment. Since 2017, this department has been part of the Ministry of Equipment, Transport, Logistics and Water converted to the General Directorate of Water (DGE) since 2020. The DGE outlines the National Water Strategy, the National Water Plan, and the National Flood Protection Plan.

Ministry of Interior (MI): Natural disaster crisis management has always been handled by the Ministry of Interior. Later, the MI created the Monitoring and Coordination Center (CVC), in 2008, that oversees processes related to emergency situations and disaster crisis management. In particular, it leads decisions and actions relating to risk and threat prevention, coordination of disaster event operations, and recovery actions. The MI holds also the Civil Protection Directorate (DGPC) which is the official body carrying out operations on the ground when a disaster happens.

In 2020, the government created within the MI a central Directorate for Natural Disasters Risk Management (DGRN) to enhance efficient coordination between various and multi-level stakeholders. The DGRN is in charge of collecting information for optimizing operations during disaster events and crisis situations. This

directorate is also responsible for the preparation of emergency plans, called ORSEC that are launched when disasters occur, including but not limited to floods.

Recently, the MI announced the creation of Flood Risk Management Center incorporating operational monitoring , warning, and assistance for flood management. The project is financed by the Fund to combat Effects of Natural Disasters (FLCN) that was created earlier in 2009. Initially, four pilot zones were targeted by this project for their flood history, namely Ourika valley, El Ghrab plain, Guelmim desertic area, and the coastal city of Mohammedia. A Provincial/Regional Coordination Center (PCC/RCC) will be installed in the administration representing the MI locally (Prefecture, Province or Region). The PCC/RCC will ensure coordination between the MI, the DGE, the General Directorate of Meteorology (DGM), the DRPE, the regional ABHs, and international organization partners.

General Directorate of Meteorology (DGM): It is an independent institution that is in charge of managing rainfall stations and meteorological radar networks throughout the Moroccan territory. Besides It has the responsibility of weather forecasting at national and regional levels, collecting, analyzing, and providing meteorological data, satellite images to different public and private operators.

Hydraulic Basin Agency (ABH): At catchment level, the river basin agency, called Hydraulic Basin Agency (ABH) is the main regional water authority in Morocco. There are ten ABHs that cover all Moroccan watersheds. Each ABH coordinates its actions with the DGE within a collaborative approach for flood maps updates and flood control measures selection and adoption. The ABH has the responsibility of preparing the Master Plan for Integrated Water Resources Management including flood risk assessment, mitigation measures identification, and implementation of action plan in partnership with related stakeholders. The ABH also establishes Flood Atlas that identifies flood-prone areas within the catchment territory, manages its own hydrometeorological stations and flood warning networks, and performs its data monitoring and processing.

There are other ministries, institutions, and commissions that are involved in the management of flood risk either at assessment level or implementation of mitigation and adaptation measures level. For instance, the Ministry of Land Use and Urban Planning and its regional representations are in charge of including flood mapping in planning document. The former High Commissioner for Waters and Forests (HCEFLCD), now called Waters and Forests Department within the Ministry of Agriculture, is in charge of erosion control upstream, a serious problem that reduces the efficiency of flood control structural infrastructures (i.e. dams, dykes, drainage systems). The Ministry of Agriculture, the Department of Environment, water and sewerage utilities, and elected regional and local councils are other examples of stakeholders involved in flood control measures implementation.

(b) **Legal framework for flood risk management**

Water law 36-15: The DGE and ABHs carried out an assessment of the previous water law 10-95 enforcement in consultation with stakeholders and civil society. In the previous law 10-95, that prevailed for twenty years, only a section, under

transitional provisions chapter, was dedicated to flood control. It provided weak framework limited to specific measures for flood and drought risks and regulated the implementation of measures for flood control. The study of this law revealed many shortcomings as it proved to be no longer adapted to the socio-economic changes of the Moroccan context. Among these shortcomings, weak provisions related to flood protection were highlighted. Therefore, the law needed to be updated to respond to the requirements of sustainable development and climate change conditions. In 2016, the new water law 36-15 was adopted. Flood provisions within this law were introduced as a legal measure to respond to national and international organizations call to adopt a new proactive approach for flood risk management in Morocco. As a result, this law is the first one to dedicate a whole chapter to floods. It gives provisions regarding (1) protection and flood risks prevention, (2) flood sensing, monitoring and warning, and (3) flood event management. The new water law 36-15 brought more specifications on the roles of stakeholders and diverse provisions on tools for flood risk management. Yet, this law states the obligation of addressing risk assessment through the production of flood Atlas by each ABH. The flood Atlas aims at identifying flood-prone areas according to three levels of flood risk (low, medium, and high) and possibly indicating flood hazard frequencies. For high and medium flood risk areas, the law states the obligation of preparing Flood Risk Prevention Plan within a participatory approach involving others public stakeholders for the plan implementation. These plans are established for a twenty years period and can be revised as necessary.

So far, some ABHs have produced their flood Atlas whereas others have made progress on projects for local mapping of flood-prone zones in order to establish their own flood Atlas.

Another novelty of the water law 36-15 is the introduction of Integrated Systems for Flood Monitoring and Warning as a responsibility of each ABH. It should be fulfilled in cooperation with the DGM for data exchange. These systems contain rainfall-runoff models that allow the follow up of hydrological situation and flood risk prevention.

Insurance law 110-14 amending insurance code and establishing coverage scheme of disaster events: Following the recommendations of the World Bank, Morocco adopted in 2016 the new law 110-14 amending the Insurance Code to introduce a new coverage scheme of disaster events consequences. This law was first effectively implemented on 2020 as a financial measure to increase territories resilience to disasters including flood events. The new law also established the Fund of Solidarity against Catastrophic Events (FSEC) to allow compensation for victims of disaster events whether they are natural or man-made hazards.

(c) **Strategy and plans**

National Water Strategy (SNE): In 2009, the National Water Strategy (SNE) was established as a framework for implementing water action plans to respond to water demand under climate change and increasing constraints, in a sustainable manner

for the 2010–2030 period (SNE 2009). The SNE is structured around the following six axes: (1) demand management and water resources recovery, (2) supply management and water availability development, (3) water resources protection and conservation (4) mitigation of vulnerability to water-related risks and adaptation to climate change, (5) regulatory and institutional reforms advancement and (6) upgrading Information Systems and capacity and resources building. Within the fourth axis, the SNE outlines actions for improving protection of people and property against floods through the following actions:

- finalizing actions described in the National Flood Protection Plan aiming at protecting vulnerable sites each year;
- integrating flood risk in land use planning, urban planning, and catchment management plan;
- improving knowledge in the field of weather forecasting and urban hydrology;
- developing flood warning systems and emergency plans; and
- developing financial mechanisms (i.e. insurance and natural disaster funds).

For the fulfillment of Morocco dam's policy, the SNE also sets the objective of building about sixty large dams by 2030 with a total storage capacity of 7 Billion m^3. These dams have to meet the needs of water demand and flood control. The strategy aims also at building one thousand small and medium-sized dams by 2030 in order to support irrigation development, provide livestock water and protect against flooding. Another flood measure outlined in the SNE is rainwater harvesting by setting up pilot projects at small scale in each catchment before extending it to a larger regional scale.

National Flood Protection Plan (PNI): Following the 1995 Gharb plain floods that endangered national food security, and their successive recurrence, the DGE released the National Flood protection Plan in 2002, commonly called PNI (2002). The plan was aimed at reducing flood risk through (1) a detailed diagnostic of flood events, (2) an analysis of current institutional framework and suggestions for improving it, and (3) proposal of an action plan, its content, funding, cost, timetable, and implementation.

The PNI drew up an inventory of around 400 flood-prone sites, which were subject of consultation at the level of the ABHs along with various public departments. Within the framework of a partnership with the relevant parties, in particular the MI, the DGE started in 2003 the implementation of the PNI outcomes. One hundred sites were hence concerned with flood control measures by building small dams and developing watercourses.

Due to increasing flood events frequency, the DGE realized in 2010 an update of the PNI to include new flood-prone sites to reach a total of 1032 sites based on field visits (Fig. 2.9). A second update of the PNI is being currently undergone by the DGE and should be released shortly. The new PNI aims at drawing up a progress report on vulnerable sites processing and updating data and information regarding flood black points and flood control action plans (DRPE 2019).

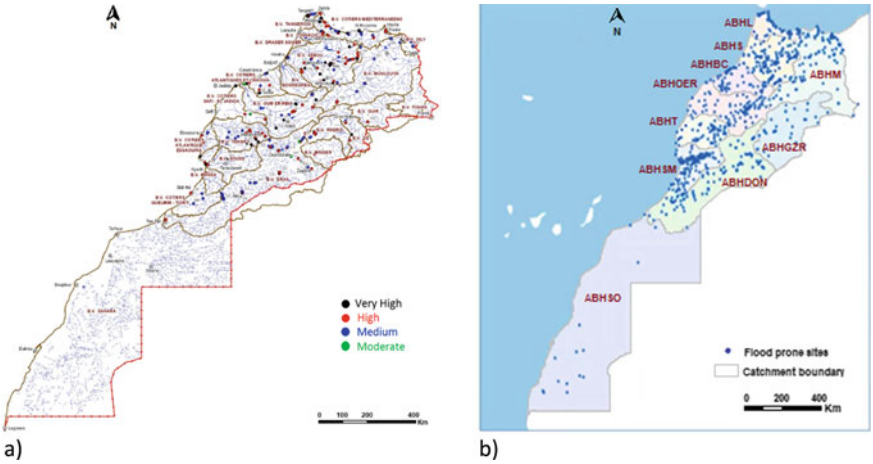

Fig. 2.9 Flood-prone zones according to **a** PNI 2002; **b** PNI 2010 (*Source* PNI 2002, 2010)

National Water Plan (PNE): The National Water Plan, commonly called in Morocco PNE, was developed in 2015 by the DGE, formerly part of the Ministry of Energy and Mines. The plan draws up an inventory of water resources, presents the main directions of water policy, sets the plan of actions to be undertaken in the medium and long terms, the accompanying measures as well as a plan for their monitoring and financing. These actions relate to water demand management and development of water resources, water supply management and development, protection of water resources and the natural environment, and adaptation to climate change along with support actions (PNE 2015). The PNE used to be established for a period of at least twenty years. It could be subject to periodic reviews every five years and whenever exceptional circumstances required its update. The recent water law 36-15 has extended the PNE planning period horizon to thirty years and its update to ten years.

With regard to flood risk, the PNE gives orientations about action plan for flood control including structural and non-structural measures. To mitigate floods harmful impacts, structural actions to be taken related to the continued implementation of the PNI recommended control measures and their updates according to the current PNI update study carried out by the DGE. The PNE underlines the implementation of non-structural actions based on the following main provisions:

- reform of the legislative framework governing the management of flood risk;
- delineation of areas at flood risk and the establishment of flood risk maps by ABHs;
- articulation of planning and land use documents in order to control land use in areas at flood risk;

- strengthening prevention by improving knowledge in the field of hydrometeorological forecasting and the development of flood forecasting, and emergency plans;
- development and strengthening of financial mechanisms (insurance and funds for natural disasters), consultation, and coordination.

Master Plan for Integrated Water Resources Management (PDAIRE): Each of the ten ABHs is required, under the previous and the current water laws, to elaborate its Master Plan for Integrated Water Resources Management, commonly called in Morocco PDAIRE. This plan is a road map for regional water resources management at catchment level for the next thirty years. It can be revised every ten years unless exceptional circumstances occurrence requires its amendment before this deadline. Its main objective is to respond quantitatively and qualitatively to current and future water demands of various users in the ABH catchment area. With regard to flood, one of the plan objectives is to assess flood risk within the basin in order to develop a regional strategy in a holistic approach that is consistent with the PNI, and contributes to the implementation of the SNE 2010–2030 directives along with the PNE 2020–2050. The PDAIRE presents a diagnosis of flood risk in its territory, and its action plan for flood control including program of structural and non-structural measures for flood mitigation, capital cost, funding plan, and timeline for implementing the selected measures. The PDAIRE also establishes limits of banned areas for any development that may disturb floodwater flow. To do so, the ABH conducts studies for identifying flood-prone areas, and priority sites for mitigation measures. The studies can be conducted using ABH's own resources or within contracts with consultant companies using the tender process. The first PDAIREs were developed in late eighties. Following the enforcement of water law 10-95 and later on law 36-15, many of the ABHs have updated or are in the process of updating their PDAIRE as stated by water law and its related regulations.

Within this framework, many other flood control studies and atlases of flood-prone zones were developed by the ABHs at local and regional levels. Accordingly, all flood black spots in each catchment were identified, and actions plans and partnerships were established. Hence, the PDAIRE is an important tool for updating the PNE, the National Urban Development Plan and the National Land use Plan in a bottom-up approach building national policies on the basis of regional level feedbacks.

Emergency Response Plan (Plan ORSEC): The Emergency Response Plan, commonly called ORSEC, is a document drawn up at the level of each prefecture and province under the responsibility of the Wali or Governor. The plan fixes, in advance, the course of action to be followed for the organization of rescue and relief of population and property in the event of a disaster including floods. The ORSEC ensures unity of command, tasks assignments, and coordination of actions and means. It gives also a complete inventory of human and material resources likely to be mobilized if necessary. In the event of a disaster, the alert is triggered by the Wali/Governor who gives the ORSEC warning for crisis management. He informs

in particular, the Cabinet of the Ministry of Interior and the General Directorate of Civil Protection.

Master Plan for Risk Analysis and Coverage (SDACR): This document is prepared by the regional, provincial and prefectural commands of Civil Protection that is the national body in charge of emergency actions and relief during a disaster event. The SDACR draws up an inventory of specific risks in the region that Civil Protection services must face. It determines also the objectives of coverage of these risks by civil protection services. This document has a real database related to risk management for a better preparation of major crisis situations likely to compromise citizens safety, health, and sanitation. It is also a basic technical reference allowing the General Directorate of Civil Protection (DGPC) to develop and plan investment in equipment, and necessary actions for crisis management.

National Strategy for Natural Disaster Risk Integrated Management: Following the recommendation of OECD (2019), Morocco is in the process of elaborating its National Strategy for Natural Disaster Risk Integrated Management with the support of the World Bank. This strategy will be built upon the following five areas of action: (1) strengthening the governance of natural risk management, (2) improving knowledge and assessment of natural risks, (3) building resilience and prevention of natural risks, (4) disaster prevention for rapid recovery and better reconstruction, and (5) promoting scientific research, international cooperation, and capacity building. These areas correspond to the country priorities as well as to international reference frameworks such as the OECD recommendation on critical risk governance (OECD 2014), and the Sendai framework for disaster risk reduction (UNISDR 2015). Its adoption will also establish a monitoring and evaluation framework to measure progress towards improving Morocco's resilience.

2.4 Technical Aspects of Flood Risk Assessment Methods

2.4.1 The PNI Assessment Method

The PNI is the only document dedicated to flood risk strategy at national level. It gives a better understanding of flood risk in the Moroccan territory through a classification of observed flood types and the identification of vulnerable sites. The PNI (2002) study defined about 400 most vulnerable sites to flood in Morocco (Fig. 2.9a). The methodology used in the PNI (2002) and 2010 for risk mapping is a matrix that crosses hazard and vulnerability. The various risk components, as internationally defined by UNESCO, recalling the definition of the Office of United Nations Disaster Relief Coordinator—UNDRO (Varnes 1984), are computed using the following expression:

$$R_t = H_t \times V \times E$$

in which: R_t is the risk associated with a return period t for the zones for which hydraulic models have been performed; H_t represents the hazard associated with a return period t over a given space; E is the element at risk (person or asset exposed to the risk when the hazard H_t occurs) on a given area and V is vulnerability defined as the potential for the element at risk E to undergo H_t hazard. In this method, vulnerability V is considered as the average damage that element E can suffer when it is exposed to the hazard H_t.

(a) **Flood hazard** in Morocco has been described through two main components: average velocity and average height in wadis floodplains. The maximum daily precipitation maps were drawn up from the results of statistical adjustment (Gumbel distribution) of the 375 rainfall gauging stations of the ABHs (PNI 2002). GIS was used to represent the maximum daily precipitation values of these 375 positions for return periods of 10, 25, 50, and 100 years in all watersheds. Therefore, mean runoff depths were extracted for each sub-basin related to each of the above return periods using an Inverse Distance Weighted (I.D.W.) interpolation method.

The 390 sites identified in the PNI (2002) study were ranked in five categories describing the hydraulic type of site flooding. This classification was based on the cause of flooding, the morphology of the site, and the availability of topographic data. Hydraulic calculations were then adapted to each category.

The maximum daily runoff depth was calculated for 10-year return period, for all the ABHs, based on data collected from 150 hydrometric stations, using probabilistic approaches such as the Gradex method and has also been mapped across the Moroccan territory. Hydraulic modeling was generally performed using HEC-RAS software. However, these models have only been carried out for sites with available topography maps at the scale 1/5000 or 1/2000 before 2002. For sites with sparse data and coarse topographic map, the experts referred to the testimony of residents as a first approach for hazard assessment. For small watersheds with time of concentration of one hour or less, daily precipitation measurements were not representative of the rainfall intensity variation. The Montana equation, largely used in Morocco, was applied to daily rainfall to extract rainfall for shorter periods using the expression:

$$I(t, T) = a(T) \times t^{b(t)}$$

where I is the mean rainfall intensity for a duration t and a return period T, a and b are regional parameters calculated using statistical methods. In 2002, the flood assessment study was carried out despite the absence of long-period consecutive daily runoff measures for large catchments, and complete hydrographs for small watersheds. In order to reconstruct missing hydrologic data, such as peak flows or flood hydrographs in the flood-prone and ungauged sites, the maximum daily

rainfall for a return period is computed as well as the rainfall for the same return period for a duration equal to 3 times the watershed concentration time. The Soil Conservation Service Curve Number SCS-CN is used for rainfall-runoff modeling.

The resulting hazard maps showed that the most important hazards were found on the Rif mountains, the Mediterranean coastal watersheds within the Loukkos catchment, and Sebou sub-basins with parts laying on the Rif mountains. On the Atlas Mountains, either on the upper basin of the Oum Er Rbia or on the upper Tensift catchments, maximum daily precipitation and runoff were less significant, which does not mean that flood risk was lower, especially on the Tensift basin. Indeed, daily rainfall values did not correctly translate the hourly intensities which can occur in these parts of the country, especially during summer thunderstorms, as they were very poorly measured by the rain gauging network in place. The hazard was then classified into four categories as shown in Table 2.2.

(b) **Flood vulnerability** was evaluated in a qualitative manner with regard to the importance and type of assets as shown in Table 2.3.

Flood risk was then assessed as a combination of hazard and vulnerability previous classifications. A matrix for flood risk classification was developed using five levels of risk, ranging from low risk to very high risk (Table 2.4). Example of hazard and risk maps developed in the PNI is shown in Fig. 2.10 for El Gara town, southeast Casablanca city in Morocco.

The level classes remain qualitative so that experts who have visited the sites can inform these classes even if they do not have concise data (calculations, reports) related to the strongest events recorded in recent years. Hence, another risk assessment approach was adopted in the PNI for sites where calculations were not made and flood hazard was assessed following residents' testimony. Six exposure categories were considered: Human exposure (H), Constructions/buildings (C), Infrastructures (I), Agriculture (A), Environment (Ev), and Economy (Ec). They correspond to the categories most often encountered on Moroccan territory, although it is extremely rare that only one is encountered at a given site. However, they have the advantage of paving the way to estimating the damage and assigning an economic value to the damage (Table 2.5).

For mapping purpose at national level, and for all type of assessment methods, only four types of risk were used. Thus Construction (C), Infrastructure (I) and

Table 2.2 Hazard classification in the PNI (2002)

Velocity (m/s)	Height (m)			
	<0.3	0.30–0.80	0.80–1.50	>1.50
<0.50	LH	MH	HH	HH
0.50–1.00	MH	MH	HH	**VHH**
1.00–2.00	HH	HH	**VHH**	**VHH**
>2.00	HH	**VHH**	**VHH**	**VHH**

Source PNI (2002)
LH Low Hazard, *MH* Medium Hazard, *HH* High Hazard, *VHH* Very High Hazard

Table 2.3 Vulnerability classification used in the PNI (2002)

Low vulnerability (LV)	• Desert areas • Brownfields	• Forest areas • Natural areas
Medium vulnerability (MV)	• Extensive agricultural areas • Arable lands	• Secondary infrastructure • Household landfills
High Vulnerability (HV)	• Intensive agricultural areas • Irrigated agricultural areas • Vegetable and fruit crops areas • Palm groves	• Sparsely populated areas • Low activity areas • Main infrastructure • Non-toxic industrial landfills
Very High Vulnerability (VHV)	• Heavily populated areas • Important activity areas • Highly touristic areas	• Camping sites • Toxic industrial landfills

Source PNI (2002)

Table 2.4 Risk classification used in the PNI (2002)

Vulnerability	Hazard			
	LH	MH	HH	VHH
LV	LR	LR	MR	MR
MV	LR	MR	MR	HR
HV	MR	HR	VHR	VHR
VHV	MR	VHR	VHR	EHR

Source PNI (2002)
LR Low Risk, *MR* Medium Risk, *HR* High Risk, *VHR* Very High Risk, *EHR* Exceptional High Risk

Agricultural (A) risks were grouped under a same section called "Social Risk" (S). The highest risk of these three categories gives the degree of social risk (S = Max [C, I, A]).

A five level Global Risk (GR) index was defined as a quantitative value assigned for each risk category as follows:

If Max (H, S, Ev, Ec) = 0 → GR = 0—Minor
If Max (H, S, Ev, Ec) > 0:

If Max (H + 1, S, Ev, Ec) = 1 → GR = 1—Low
If Max (H + 1, S, Ev, Ec) = 2 → GR = 2—Medium
If Max (H + 1, S, Ev, Ec) = 3 → GR = 3—High
If Max (H + 1, S, Ev, Ec) = 4 → GR = 4—Very high

Consequently, a Global Risk cannot be low unless there is no human risk (H = 0). An example of the GIS-based map built upon these considerations is shown in Fig. 2.11.

In order to better rank quantitatively each of the flood-prone sites with regard to the importance of their risk exposure, the following scores were assigned to each of the risk levels:

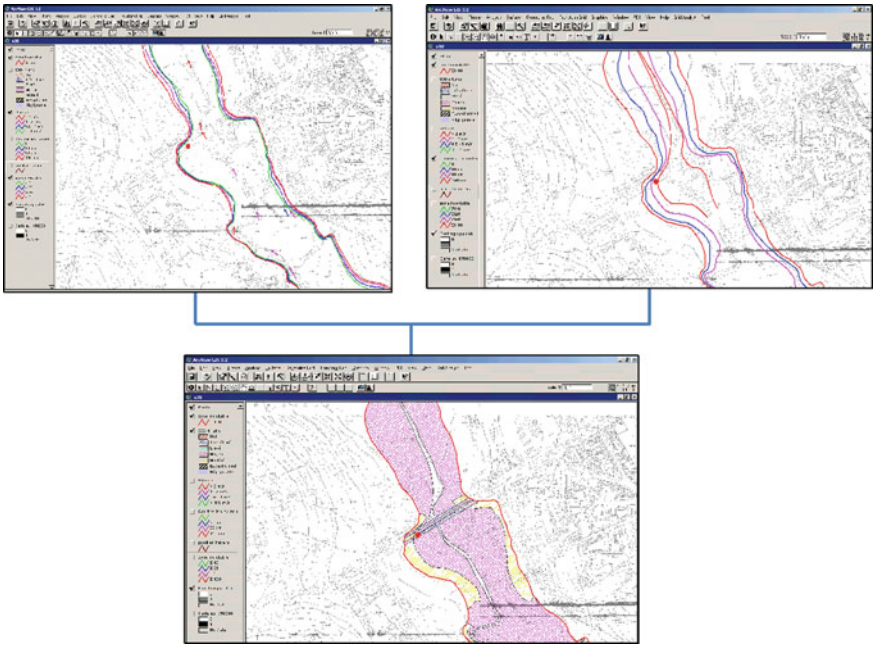

Fig. 2.10 Example of flood maps developed in PNI, case of El Gara town site **a** hazard map and velocities, **b** flood depths map, **c** flood risk map (*Source* PNI 2002)

1 for low risk; 2 for medium risk; 3 for high risk; 5 for very high risk

and weight coefficients for each of the different types of risk:

Human risk (H): 10; Construction risk (C): 7; Infrastructure risk (I): 7; Agricultural Risk (A): 6; Environmental Risk (Ev): 8

The Economic risk (Ec) was not taken into account directly because it is not independent of other risks. It is in fact strongly linked to them and it is rather through the sum of the weighted ratings assigned to each site that an idea on the importance of the economic risk can be made. In the 2010 PNI update, economic criteria were discarded as it is very subjective and time-dependent value.

Using these assessment criteria for each category (H, C, I, A, Ev, Ec) and assigned weighting coefficients, the 391 sites were ranked downward according to their scores in PNI (2002). This ranking allowed to identify 50 most priority sites to be protected against flood risk in Morocco and therefore to facilitate the elaboration of investment plans at national and regional levels.

In the first method, hazard (i.e. height and velocity) assessment approach was probabilistic and therefore risk assessment was also probabilistic within certain limits of simplification as certain vulnerability elements are variables (e.g. disaster arriving day or night, a weekday or a holiday, house inhabited or not during the

Table 2.5 Categories of exposure and their classification

Nature	Level			
	Low	Medium	High	Very high
Human: H	Risk of injuries —Isolated persons for long-duration flood	Risk of victims (1 to 10 victims)	Risk of victims (10 to 50 victims)	Risk of victims (more than 50 victims)
Constructions: C	Less than 50 cm flood heights and less than 50 affected dwellings with little or no damage	Less than 50 cm flood heights with more than 50 affected dwellings Or more than 50 cm flood heights with less than 50 affected dwellings and moderate damage	Flood heights between 50 cm and 1 m with houses and assets damaged	More than 1 m flood heights—destroyed houses
Infrastructures: I	Roads (secondary roads—paths—streets) flooded for a short time with less than 20 cm flood height—no damage	Roads (main/secondary roads—paths—streets) flooded with flood height between 20 and 50 cm with traffic interrupted for few hours—low structure damages	Roads and bridges flooded with more than 50 cm flood heights; traffic interrupted for few hours to few days. Significant structure damages	Roads and bridges flooded with more than 1 m flood heights. Destroyed structures, traffic interrupted for few days to few weeks. Dykes and networks (water, energy, and telecommunication) heavily damaged with distribution service interruption for many days
Agricultural: A	Flooding of meadows, forest areas, and small extensive agricultural areas—little or no damage	Flooding of large extensive agricultural areas and small intensive agricultural areas—average damage	Flooding of large intensive agricultural areas and medium irrigated areas —significant damage to soil, crops, and structures	Flooding of intensive agricultural areas or agricultural areas with high crops added value and high local economic impact (fruit—palm groves) Very significant damages—infrastructure destroyed—plantation losses—erosion or significant soil sedimentation

(continued)

Table 2.5 (continued)

Nature	Level			
	Low	Medium	High	Very high
Economic: Ec	Some recovery actions (street sweeping—sediment removal—washing carpets—floors—walls—paintings, etc.) Less than MAD 100,000 damage cost	Damages cost (private and public) comprised between MAD 100,000 and MAD 1,000,000	Direct and indirect damages cost (Job losses—rescue operations—relocation—medical and social assistance) comprised between MAD 1,000,000 and MAD 10,000,000	Direct and indirect damages cost higher than MAD 10,000,000 Dh
Environmental: Ev	Return to the river of floating bodies, traces of oil products washed out by flood from the pavements washed, fertilizer agricultural	Vulnerable zones (wetlands) flooded and polluted	Spill in the natural environment (streams—lakes—ponds—reservoirs) common toxic products harmful to flora, fauna and exceeding sanitary standards for water intended for human consumption	Spill in the natural environment of highly toxic products which can destroy partially or totally the flora and fauna and cause a break in consumption of water for domestic use

Source PNI (2002)
MAD Moroccan Dirham (10 MAD is about 1 USD)

event). Yet, in the second method, more simplified, the risk is no longer probabilistic but rather refers to the most significant event observed in recent years. Given the current level of investigation, this approach is yet sufficient to properly identify the areas at greatest risk and to undertake a prioritization of actions. Other international bodies, such as the World Bank, Euro-Mediterranean Partnership, and UNDP, also carried out studies about flood risks in Morocco (WB 2011a, b; SEEE/UNDP 2008; SEEE 2008; EMWIS 2005). These disparate studies came up with interesting results and solutions but in either very broad or fragmented way.

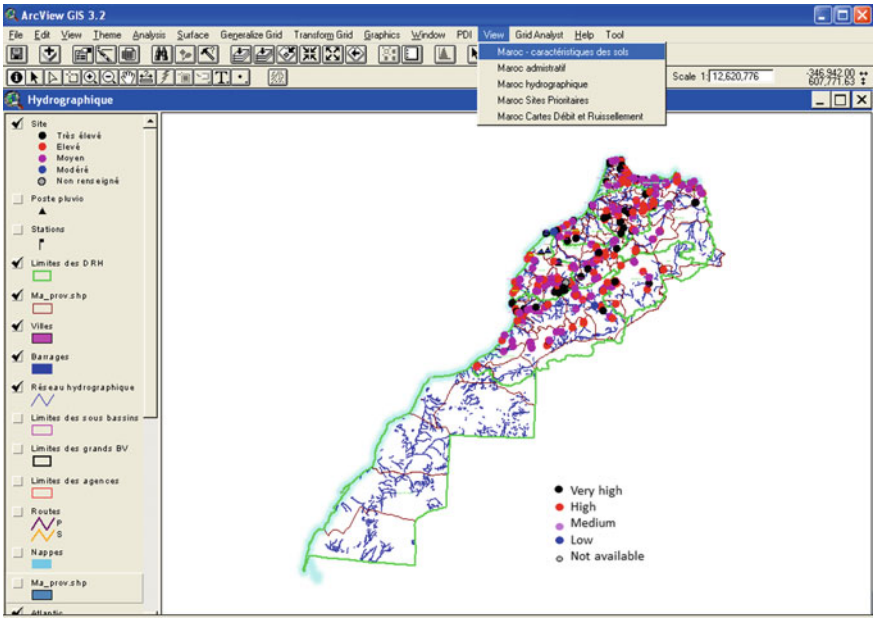

Fig. 2.11 Overview of GIS database output map for flood risk assessment developed in PNI 2002 (*Source* PNI 2002)

2.4.2 The PDAIRE Method

As mentioned in Sect. 2.3.2c, each ABH prepares its Master Plan for Integrated Water Resources Management (PDAIRE) that has to include a component on 'Flood protection', describing flood related-actions carried out by each ABH since 2002 and offering more concise details of outlined measures than the PNI.

Most ABHs have led their field investigation to identify prone flood areas within their territory to comply with the PDAIRE directives and to establish their Atlas of flood-prone zones as requested by water law 36-15 (e.g. Atlas of flood-prone areas of Tensift catchment, ABHT 2007). Based on information available on entire sections of valleys, the atlas of flood-prone zones consist of an informative map of historical flood events, hazard map (i.e. probability, extent, intensity) complemented by other information on the wadi beds geomorphology and floodplains exposure. The Atlas provides the basis for flood risk management as it is the main regional document that produces:

- Information for decision-makers of water planning and urban planning;
- Identification of vulnerability (e.g. housing, public services, economic activities, roads) subject to different hazards; and floodplains to be protected;
- Identification of flood mitigation measures.

PDAIRE has considered a different way of hazard assessment. For example, in ABHBC (2007), floods where classified according to the time of rise t_r, which refers to time from the start of rainfall excess to the peak of the hydrograph. According to this classification, the sub-catchments of the basin were ranked as medium-rise floods or slow rise floods. The flood hazard in this catchment was assessed for six urban watersheds (Casablanca, Nfifekh, El Mellah, Bouskoura, Merzeg, and Bouregreg sub-basins catchments and Berrechid plain). Climate change parameters that were considered are (1) extreme precipitations: based upon daily precipitation data and new design storm of 10 to 100 year-return periods; and (2) sea level: to assess boundary conditions downstream of certain coastal streams and sewage systems. For flood hazard assessment in urban basin, design storms used for modeling the sewer networks are based on Intensity-Duration-Frequency (IDF) curves of observed rainfall at the Casablanca-Anfa station. The effect of climate change on stream discharges was evaluated using Gradex method, in consistence with the method used in the PDAIRE surface water resources assessment studies.

For vulnerability assessment, the ABHBC used the same methodology as in the PNI considering the six exposure criteria: Human exposure, Buildings, Infrastructures, Agriculture, Environment, and Economy. Five levels of risk ranging from minor risk to very high risk were defined accordingly. The output of this analysis is a map showing risk level for several parts of the basin (Fig. 2.12). This result gives an indication of the exposure of the catchment to different risk categories ranging from very high flood risk to low flood risk. Urban flood vulnerability of Casablanca city was analyzed using parameters such as density, building quality, number of floors and social level, economic activities. The current and 2030-future flood vulnerability maps were given based on extreme precipitation change (2002–2050). The same approach was used to assess flood risk in an urban planning touristic project in the city of Rabat (WB 2011a).

Other ABHs such as Sebou, Moulouya, Loukkos, have also led their studies for flood protection and suggested structural and non-structural measures that were later adopted within their PDAIRE and the PNI updating processes. Given the important cost of flood control measures, financial support of different public and private entities, and sometimes within international cooperation, are sought by the ABHs to implement these measures.

2.4.3 The MnhPRA Assessment Method

During the period 2010–2012, a project coordinated by the Moroccan Ministry of General Affairs and Governance, with the support of the World Bank, the Global Facility for Disaster Reduction and Recovery, and the Swiss Agency for Cooperation and Development, developed an open-source new GIS analysis tool called Morocco natural hazards Probabilistic Risk Analysis (MnhPRA) for disaster modeling. Using advanced probabilistic risk assessment approach, this program

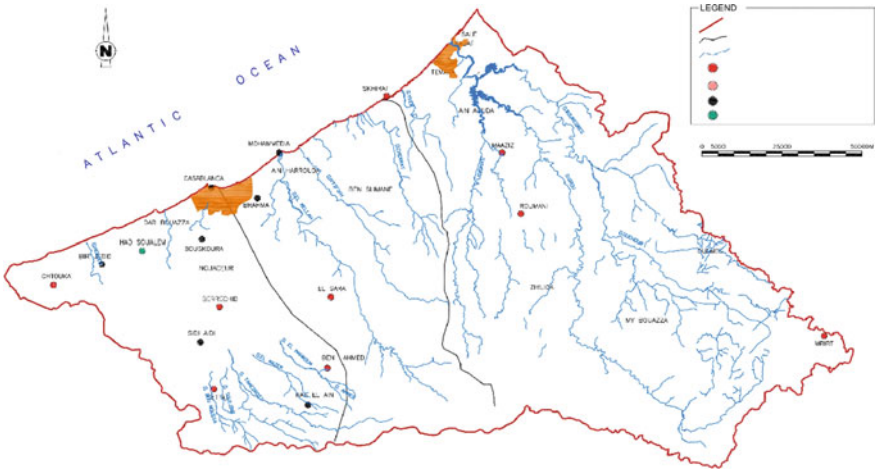

Fig. 2.12 Map of flood-prone zones and their different levels of risk in Bouregreg-Chaoui catchment (*Source* ABHBC 2007)

generates a detailed analysis of return periods on the basis of advanced risk models (Michel-Kerjan et al. 2014). MnhPRA is built upon four basic modules for disaster modeling that are hazard, inventory, vulnerability, and loss (Fig. 2.13):

- Module 1 (M1): The risk of the hazard phenomenon is calculated by first assessing the occurrence and frequency of events using a set of stochastic events, a set of simulated events characterizing observed or scientifically

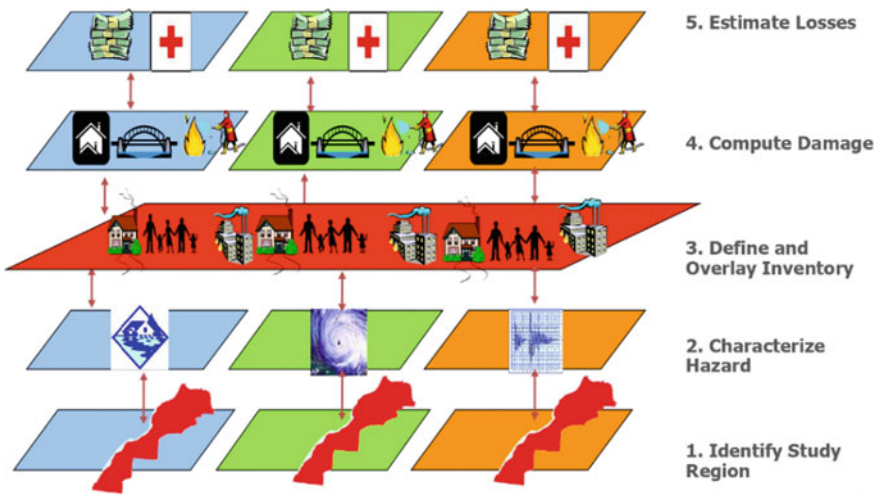

Fig. 2.13 MnhPRA risk analysis process (*Source* Scawthorn 2017)

modeled events and their probability of occurrence. Secondly, the severity of events is calculated based on data of rainfall stations at each site of nine catchments that are: Loukkos, Sebou, Moulouya, Bouregreg and Chaouia, Tensift, Oum Er Rbia, Souss, Draa – Oued Noun, and Guir-Ziz-Gheris.

- Module 2 (M2): The inventory of assets at risk is characterized. The portfolio includes the entire built environment of Morocco (e.g. residential, commercial, industrial, public infrastructure). The inventory is based on a combination of data collection through field visits and satellite information.
- Module 3 (M3): Vulnerability is quantified to evaluate the way in which assets or infrastructures at risk identified in the inventory module (M2) will react physically under the events generated in risk module (M1). Vulnerability functions represent the relationships between the intensity of the risks (e.g. Flood depth) at the site and the level of damage.
- Module 4 (M4): Disaster losses are calculated assuming that the only uncertainty is the occurrence of an event. For example, the occurrence of floods in Casablanca follows a certain mathematical process which has been specified in the risk module at first, then its severity is calculated in the second part of the risk module (M1) across the whole city. Vulnerability module (M3) then calculates the average damage ratio at each site given the characteristics specified in the inventory module (M2). Finally, the loss module examines damages according to the values of exposure and calculates the total losses on this site producing a Loss Exceedance Curve (LEC) that gives the annual probability to a disaster aggregated loss to be exceeded yearly.

The tool provides also an economical estimation of flood damages using the Average Annual Loss (AAL) for any type of inventory for a selected hazard in a selected location. According to the analysis of risk assessment based on MnhPRA tool, in the next 20 years, there is a 95% chance of flood in Morocco causing losses estimated at MAD 5 billion, and a 65% chance of an event causing losses of about MAD 25 billion. Floods remain fairly frequent and building losses are about 75% of the AAL (93% in the case of earthquake and only 50% in the case of tsunami).

MnhPRA can also assess potential flood mitigation measures, the best solution being the one which total cost is the lowest. The total cost is calculated as the sum of capital cost and damages cost.

Over forty flood risk mitigation scenarios were assessed using MnhPRA, based on a cost-benefit analysis (WB 2012). The measures range from flood warning systems to elevating buildings for protection against floods. The scenarios considered high-risk areas such as Kenitra province for floods. According to the MnhPRA based analysis, the highest Benefit-Cost-Ration (BCR) flood mitigation scenarios over Moroccan territory were:

- Flood warning system for Ouregha sub-basin (BCR = 54.3)
- Culverts on railway lines in Gharb plains (BCR = 34.6)
- Mitigation of 46 residential buildings for floods in new township near Kenitra (BCR = 8.2)

- Mitigation of 47 government buildings for floods in new township near Kenitra (BCR = 7.2)
- Risk assessment for floods in new township near Kenitra (BCR = 5.7)
- Mitigation of school buildings for floods in new township near Kenitra (BCR = 4.2)

MnhPRA is the first tool that brought an economic analysis of flood measures in Morocco. The damage is calculated in a quantitative way, unlike the previous approaches, where damages were assessed in a qualitative manner. However, although this probabilistic model has been widely disseminated to the flood risk management stakeholders, in particular through organization of training sessions, it was noted that it is not used in almost all organizations visited by the Court of Auditors (Cour des comptes 2016). Except the Insurance and Social Security Regulatory Authority (called ACAPS) and few private insurances companies, MnhPRA model is not very widely used in particular within the flood risk management public stakeholders (e.g. ABHs, Urban planning agencies, etc.). Besides, till 2019, none of the regional administrations or provinces has developed a flood risk management integrated information system (WB 2019). The same year, the WB released a loan for Morocco to support the country in development of its National Strategy for Natural Disaster Risk Integrated Management with the objective of adopting it within 2020 calendar. One of the main expected outcomes of this strategy is to develop an Integrated Information System for Disaster Risk Management based on the adoption of cooperation framework to enhance flood risk management and early warning systems in the country.

2.4.4 The OECD Approach

In 2016, the OECD released a study on risk management policies in Morocco that has highlighted the country main advancements in this subject but also the main shortcomings of these policies (OECD 2016). The study made over thirty recommendations about the whole risk management cycle including, risk assessment, risk prevention, preparedness, emergency responses, and buildings. As a result, the Moroccan government, with the support of Swiss cooperation, asked the OECD to provide the necessary expertise for implementing these recommendations for the period 2017–2018. Hence, the OECD launched a capacity building program for local and national stakeholders about knowledge and risk assessment enhancement (OECD 2017a). The main outcome of these training was to raise the awareness of parties on the urgent need for: (1) the development of a shared GIS database from data institutions producers such as DGM, ABHs, Urban Planning Agencies, Wilayas as a common and integrated platform for national risk assessment; (2) capacity building in hydraulic modeling for ABHs and mapping tools for many parts of the Moroccan territory; (3) flood vulnerability atlas for all the ABHs based on hydrological modeling and high-resolution Digital Elevation Models

(DEM) and/or satellite images and LiDAR in a consistent way with the GIS platform.

Within this framework, the OECD organized training sessions and produced a guide on knowledge and natural disaster risk assessment in Morocco (OECD 2018). The guide introduced the concept of exposure and thus defined the risk as:

$$\textbf{Risk} = \textbf{Hazard} \times \textbf{Vulnerability} \times \textbf{Exposure}$$

- **Hazard** is defined by its intensity and frequency. Floods intensities with 50 and 100 years return period should be adopted.
- **Vulnerability** is ranked within four categories: Physical (e.g. Building quality) Human and social (e.g. elderly people, isolated and handicap peoples); Economical and financial (e.g. agriculture, tourism) and Environmental (e.g. natural resources). The same classification for vulnerability as in the FNP was adopted. Table 2.3 gives an example of vulnerability levels by economic zones.
- **Exposure** to the hazard is evaluated based on the relative importance of its components (humans, assets, economical activities, historical sites, etc.) such as the population density, assets, economical activities, historical sites, etc., and related threats.
- **Risk is assessed by combining** hazards and vulnerability analysis. It characterizes thus potential impacts of disasters on a given territory. This involves estimating these consequences and defining a risk classification scale according to their relative importance (Fig. 2.14).

In 2019, the OECD carried out an evaluation of risk management advances in Morocco since 2016 and concluded that knowledge of risks is progressing but remains insufficient. However, major progress on prevention with the Fund to combat Effects of Natural Disasters (FLCN) call for projects mechanism can be

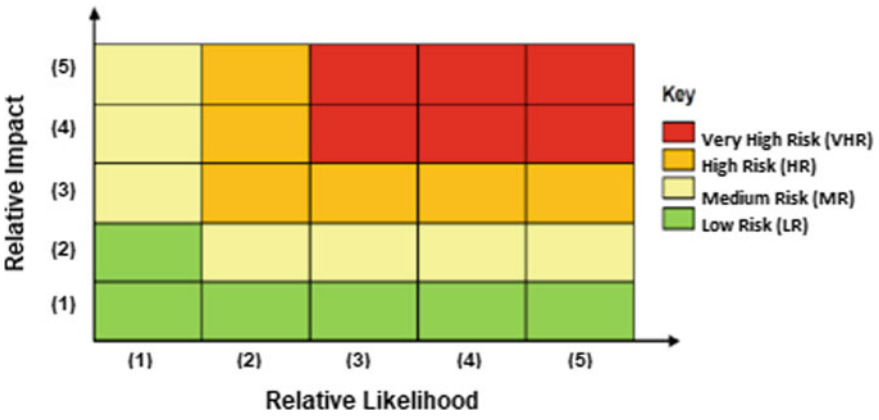

Fig. 2.14 Flood risk assessment matrix (*Source* OECD 2018)

made. There is also a factual need to promote scientific research in the field of risk management and strengthen international cooperation.

2.5 Flood Control Practices

The PNI study (PNI 2002) had estimated the average cost of flood damages at USD 4.2 Million for each flooded site on average. Flood risk assessment over the Moroccan territory has revealed that about 400 sites were exposed and for which protection measures will require in total about USD 2.5 Billion. The plan has identified 50 priority sites using two types of flood control measures, namely structural and non-structural measures. Structural measures include:

- Cleaning operations, recalibration, widening of the wadis crossing structures (bridges, scuppers, culverts, etc.), construction of canals to regenerate the initial wadi corridor, riverbanks protection, damming of wadis, creation of peripheral water diversion canals, construction of dams or weirs for water storage and flood lamination upstream endangered areas, and
- Earthworks, demolition, bank protection, embankment, culverts-bridges-riffles-fords, dams, and related works.

Non-structural measures aim at mitigating floods by controlling vulnerability mainly through:

- Regulation of land use in flood-prone areas through delineation studies and raising public awareness against encroachment upon these areas; and
- Implementation of flood warning systems, maintenance of watercourses, development of watersheds, risk prevention rescue plan, monitoring systems, information, training, and participation.

The total investment cost of operations planned within this program for the shortlisted sites is USD 571.5 Million, in which 79% is dedicated to structural measures. Among these later, 34% of the investment cost is dedicated to dams.

2.5.1 Dams for Flood Control

Thanks to the dam's policy launched in late sixties, Morocco accounted for 145 large dams in 2019 with a total capacity exceeding 18 Billion m^3 (Fig. 2.15), 13 hydraulic water transfer structures (Flow rate: 200 m^3/s, Length 1100 km, Volume 2.5 Billion m^3/year) and over a hundred small dams and reservoirs. Many of these dams are for flood protection (Table 2.6). Dams storage capacity will be increased in 2030 to 27 Billion m^3 with the objective of building 2–3 large dams per year. The choice of dams is part of action plan for developing water supply, meeting local needs, and concurrently, protecting against floods.

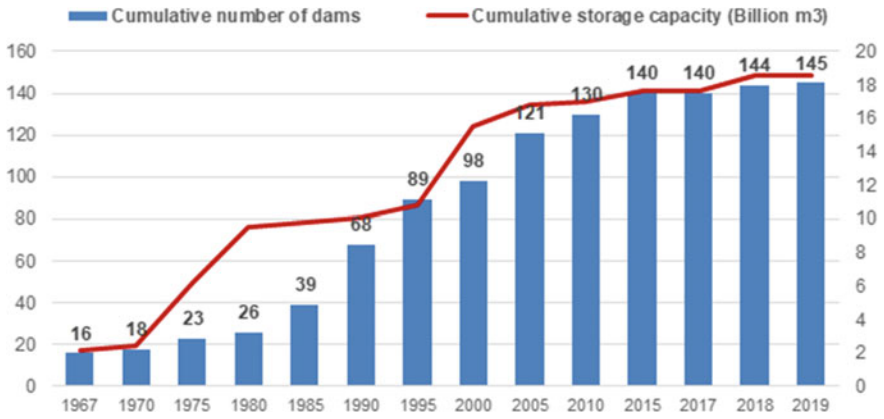

Fig. 2.15 Evolution of built large dams' number and their storage capacity 1967–2019 (*Source* DGE 2020)

Table 2.6 Main flood protection dams in Morocco

Dam	Province	Year	Height (m)	Storage (Mm^3)	Protected zone
Mellah	Ben Slimane	1931	33	8.8	Mohammedia city
El Knsera	Khemissat	1935	68	266	Beht and Moghrane agricultural area
Mohamed V	Oujda	1967	64	700	upstream zones including Saidia port
Hassan Addakhil	Errachidia	1971	85	320	Ziz valley
Mansour Addahbi	Ouarzazate	1972	70	529	Draa valley
Idriss 1er	Taounate	1973	72	1186	El Gharb plain
Sidi Med Ben Abdallah	Rabat	1974	99	1000	Bouregreg valley
Oued El Makhazine	Larache	1979	67	773	Ksar El Kebir city and Loukkos plain
Saquia El Hamra	Laayoune	1995	16	110	Laayoune-Trafaya road
Wahda	Sidi Kacem	1996	88	3800	El Gharb plain
Hassan II	Midelt	2000	91	275	Moulouya upstream
Ahmed El Hansali	Béni Mellal	2001	101	740	Oum Rbiaa upstream
Touizgui Remz	Assa Zag	2007	18	78	Assa Zag city
Al Himer	Settat	2008	38.5	14	Berrechid plain
Koudiat El Garn	Settat	2012	54.5	33	Berrechid plain

Source DGE (2015)

Case study of Wahda dam for El Gharb floodplain control

Located in the northwest of Morocco, El Gharb plain is the largest irrigated agricultural area of the country with an estimated 250,000 ha of potential irrigated land and a total surface of 616,000 ha. It lays from the Pre-Rif hills and the middle Atlas in the north east to Atlantic Ocean in the west passing by the Mamora forest plateau (Fig. 2.16a). With elevations ranging between 0 and 200 m, it is made up of a coastal zone, continental boundaries, and the central alluvial plain of Sebou. Waterways system is made of wadi Sebou and its main tributaries (Beht, Ouergha, etc.) with an annual contribution of 6 Billion m^3, representing 27% of the national potential of water resources. Mean annual rainfall is 600 mm in the coastal part decreasing to 470 mm toward Sidi Kacem in the east (PNE 2015). Climate is Mediterranean type with humid winters and very hot summers. Groundwater resources are estimated at 900 million m^3. Population is about 1.9 Million inhabitants (HCP 2014) with 56% living in rural areas.

This area has experienced several floods. The most devastating ones occurred in the years 1963, 1973, 1989, 1996, 2009, and 2010 generating flooding of several thousand hectares of agricultural land (Fig. 2.16b), damaging infrastructures, destroying houses, and evacuating several affected families. Table 2.7 gives description of El Gharb plain floods most critical recorded damages.

Previous studies, carried out as part of El Gharb plain flood protection, selected the option of constructing Al Wahda dam in 1997 on the Ouergha wadi. The dam has a capacity dedicated for floodwaters storage and evacuation capacity enhancement of the lower Sebou wadi. The dam is the largest one in Morocco with a total capacity of 3800 Mm^3, a total height of 88 m and a silting volume of 58 Mm^3. It is the second-largest dam in Africa after the High Aswan dam in Egypt (UNEP 2008; Arthurton et al. 2008). Al Wahda dam has a positive impact downstream by supplying water for drinking and irrigation and providing 400 Million KW/year of hydropower. Since the dam's completion, flooding has dropped by about 90%. As such, its impoundment came at the right time since it made it possible to laminate the floods of December 1996 and January 1997 and thus avoid damage to infrastructure downstream and crop production.

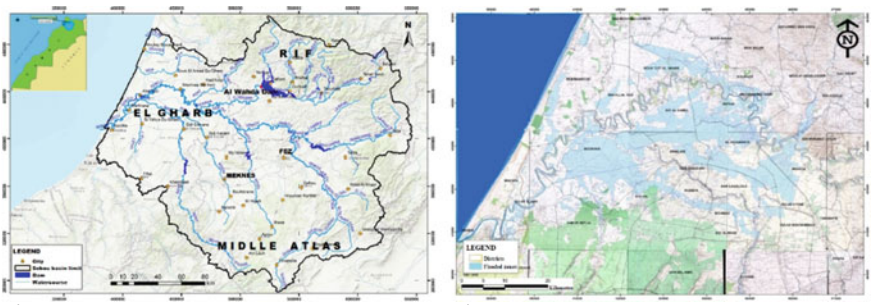

a) b)

Fig. 2.16 El Gharb plain: **a** location (*Source* ABHS 2018); **b** 2009 flood extent (*Source* PNE 2015)

Table 2.7 Historical flood damages in El Gharb Plain, Morocco

Year	Wadis	Damages
1963, 1973, 1989	Sebou	150,000 ha flooded land, roads, and railways cuts
1996	Sebou, Beht, Rdom et Tifelt	Isolation of cooperative El Kheir, 1.200 inhabitants were displaced, 120,000 ha flooded land
2009	Sebou, Beht, Rdom, Tiflet, Smento, Bouchahla	90,000 ha land and transport infrastructures flooded
2010	Sebou, Beht, Rdom, Tiflet, Smento, Bouchahla	110,000 ha land and transport infrastructures flooded

Source PNE (2015)

It has to be noted that despite storing water upstream the Ouergha basin in El Wahda dam, flood risk remained considerable in the plain. Indeed, El Gharb plain had experienced successive flood events in 2009 and 2010 incurring damages estimated at USD 800 Million. A hydraulic model developed by Midaoui et al. (2015) simulated water flow profiles downstream of Wahda dam for flood events of December 19, 2009 to January 15, 2010 with three successive peak flows ranging from 4000 to 6030 m^3/s. The model showed that the dam preparatory management for rainy seasons helped to avoid a flood on December 21, 2009 and another one on January 07, 2010. The dam yet failed to stop flooding on January 14, 2010 as the dam storage had already reached a fill rate of 104%, but the flood extent was significantly mitigated reducing peak flows.

As many large dams in the world, the risk of erosion of Wahda dam had to be controlled. The initial scheme for Ouergha wadi basin water planning, established by the High Water Council in 1988, defined in addition to Wahda dam, 15 medium-sized dams, and 300 small-sized dams and reservoirs to protect the dams from silting. Examples of these protecting dams are Jorf El Ghorab (1991), Essaf dam (1991), Sahla dam (1994), Bouhouda dam (1998), Asfalou (2000). However, in semi-arid region, environmental impacts of dams are particularly emphasized because of the irregular nature of climate and the intensity of erosive forces. Anthropic actions and drought are the main factors in increasing erosion. Many zones vulnerable to erosion were identified. The steep marly slopes of Rif mountains upstream cause erosion of the Ouergha watershed estimated at 98 t/ha/year over an area of 6150 km^2. Hence, the dam loses an annual volume of 0.6 Mm^3 (Albergel 2008). Moreover, according to the HCP (2014), there is an important erosion risk in the watershed of Wahda dam that is drained by Ouergha river. In order to improve knowledge of hydro-geomorphological processes Jaouda et al. (2020) mapped the evolution of soil erosion for the period 1990–2014 using Landsat and radar images. They showed that erosion process is still predominant due to important changes in land use, stating the need for soil conservation measures.

In fact, Wahda dam services are highly important at national level, beside its flood control regional service. It has indeed a strategic role in food-energy-water nexus security, thus solutions to improve Wahda dam longevity and mitigate its reservoir sedimentation have to be found. This was clearly stated in the ABHS revision of its PDAIRE that claimed integrated sustainable solutions to protect the plain from floods based on integrated dam reservoir management as a non-structural measure and development of models for hydrometeorological projections (ABHS 2017). Being directly concerned with flooding of this important agricultural area, the Regional Agricultural Development Office of El Gharb, called ORMVAG, implemented an ambitious program for mitigating flood risk. Indeed, during the period 2009–2013, ORMVAG led cleaning up and dredging operations of all stormwater networks in El Gharb plain, i.e. 4500 km of channels, in order to cope with the rapid siltation of these networks and to preserve its functionality in mitigating floods (Fig. 2.17).

In 2018, a master plan for flood control and management of Sebou catchment was developed within bilateral cooperation between Morocco and South Corea. The main measures and actions outlined in this plan relate essentially to improving dams' reservoirs operation system, implementing flood prevention and warning system, setting standards, and enforcing legal framework of wadis maintenance system.

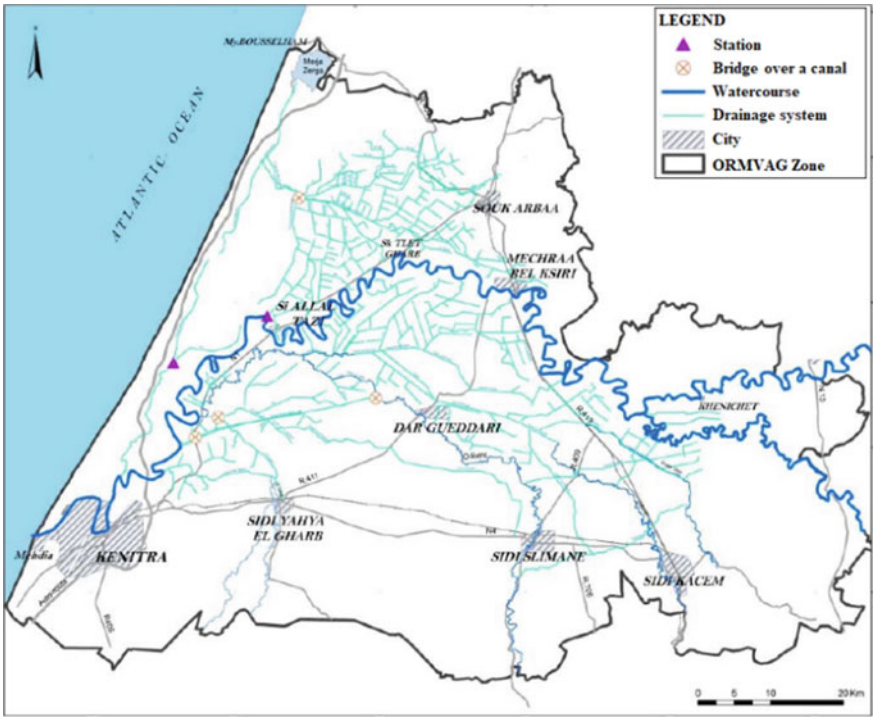

Fig. 2.17 Stormwater drainage system map in El Gharb plain (*Source* ORMVAG 2017)

Wahda dam solution was certainly a great response for flood mitigation in El Gharb plain and development of its agriculture potential for national food security. However, erosion risk had deceased its efficiency, particularly in mitigating flood. This measure has been accompanied by other structural measures and non-structural measures including stormwater systems maintenance, and the plan for the dam reservoir and watercourses maintenance. It has to be highlighted though that a cost-benefit analysis has to be made to update the multilevel usefulness of the dam in order to appraise flood prevention and control options. Exploring new techniques for erosion control, storage capacity enhancement, watercourses recalibration, and flood warning systems are some of the options that could be explored for an optimal flood protection that are economically affordable for public budget.

2.5.2 *Other Structural Measures*

As stated in this section introduction, 79% of the total investment cost for flood control are assigned to structural measures (PNI 2002). In addition to dams, many other structural measures have proved their efficiency in Moroccan practices for flood control. They include embankment protection, spurs and weirs river impoundment, installing culverts, bridges, riffles and fords, demolition operations, and earthworks. An example of a structural measure other than dam, for flood control is the case of the diversion channel Bousekoura Wadi, commonly called SCO.

Case study of SCO diversion channel of Bouskoura wadi Casablanca city flood control

The economic capital of Morocco, Casablanca, is located on the Atlantic coast about 80 km south of the administrative capital Rabat. It is characterized by a semi-arid climate with average temperatures ranging from normal to 12.5 °C in winter to 22 °C in summer. Annual rainfall totals are characterized by high variability and have an annual mean of 427 mm. They can reach values lower than 200 mm or sometimes exceed 800 mm. Increasing number and intensity of extreme rainfall events and rapid urban development have affected the performance of urban drainage systems in this city and its suburbs. Indeed, Casablanca has experienced torrential rains on November 27th, 2010 that reached 195 mm in 24 h, which represents nearly 50% of the precipitation annual average that was totally recorded in only one day. These precipitations have exceeded the network discharge capacity and gave rise to floods that caused significant damage in this strategic city paralyzing many parts of its territory, especially industrial areas and transport infrastructures. However, the low capacity of the stormwater pipes was not the main cause of this dramatic situation. The city was mostly affected by the overflowing of wadi Bouskoura that reached also many basic infrastructures that cross the wadi and riparian areas during the day of November 30th, 2010 (Fig. 2.18). The wadi crosses the city from the East side to the West side, before flowing into Atlantic Ocean

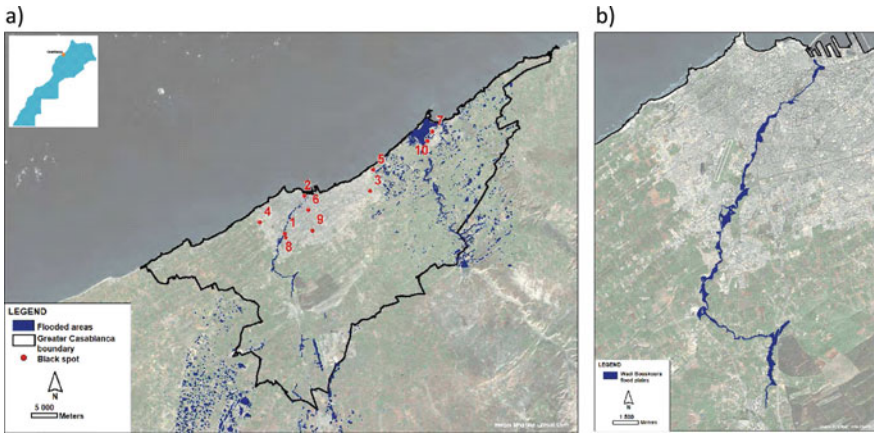

Fig. 2.18 2010 flooded areas in Greater Casablanca **a** 10 black spots causing most frequent floods; **b** map of Bouskoura wadi floodplain (*Source* WB 2011a)

through the stormwater drainage network of the city. In the last two decades, Casablanca has experienced such a rapid economic development in real estate causing the closing off the wadi flow path. Thus, Bouskoura wadi flow cross section at the entrance of the urban area was significantly reduced as the drainage pipe capacity was 2 m^3/s while the 10-year return period discharge was 45 m^3/s.

The World Bank study in 2011 showed that for the period 2010–2030, the net present value of potential economic losses due to natural disaster and the impact of climate change for Casablanca are estimated at 1.39 billion dollars, which most would be associated with flooding (WB 2011c). These losses represent 7% of current gross domestic product (GDP) of Greater Casablanca.

In order to combat the major black spots of overflow in Casablanca, a channelization system, commonly called SCO, has been suggested within the Sewerage Master Plan of Casablanca by the water utility in charge of water supply, sewage systems, and energy in Casablanca, namely LYDEC, a branch of Suez. The suggested measure is a mega-drainage system, called the Super Collecteur Ouest (SCO) combining a 3 km-open channel, for Bouskoura wadi diversion, and a 7 km underground tunnel with 4 m diameter discharging at 65 m^3/s in the Atlantic coast (Fig. 2.19).

The cost of the project implementation was estimated to USD 90 Million which was a heavy investment for the sole public resources. In fact, its implementation was a good example of public-private partnership for flood control measures financing and cost-sharing. The various stakeholders involved in this project funding are shown in Table 2.8.

In November 2018, the SCO proved its efficiency by discharging 30 m^3/s and making western parts of Casablanca floods free. In addition to the protection in the city of Casablanca against floods, this structural measure enables the city managers to protect basic urban infrastructures; to open important spaces to urbanization; to

Fig. 2.19 Wadi Bouskoura channelization with the SCO drainage system for Casablanca flood control (*Source* LYDEC 2014; Casa Aménagement 2020)

Table 2.8 Main Public-Private funding parties of the SCO drainage system for Casablanca flood control

Public-private parties	Financing contribution over 3 years (2015–2017) in USD Million*
State general budget starting in 2014	13.2
Ministry of interior (fund to combat effects of natural disasters-FLCN)	13.2
Ministère of interior (territorial collectivities directorate)	16.4
Water department at the ministry of energy, mines, water, and environment	8.2
Casablanca municipality	15
Greater Casablanca region	10
Cherifian office for phosphates (OCP Group)	8
Anfa urbanization and development agency (AUDA)	5
Hydraulic basin agency of Bouregreg-Chaouia (ABHBC)	1
Total	**90**

Source Casa Aménagement (2020)
*1 USD is equivalent to about 10 MAD

protect existing and planned industrial zones; to relocate rainwater outlets in the western part of Casablanca and to resize Bouskoura wadi outlet.

2.5.3 Flood Warning Systems for Flood Prevention

The PNI (2002) has planned many non-structural measures as a backup for engineering structural solutions. Investment planning had given a small share to these types of measures showing the weak importance given to them. Yet, the occurrence of flood events in areas that were seemingly protected by structural measures such as dams and watercourse recalibration, had drawn attention of flood management stakeholders to the potential of non-structural measures in improving flood prevention and thus resilience of flood-prone areas. Examples of these measures are flood warning systems, rainwater harvesting, legal framework enforcement, etc. In this way, the adoption of the new water law 36-15 was a good example of a legal non-structural measure as it has brought many adjustments and details for a better-integrated water management including floods and drought control (see Sect. 2.3.2). This law had particularly emphasized on flood warning development all over the Moroccan territory. In the same way, many international cooperation projects recommended the enhancement of warning systems. A typical best practice of non-structural measure for flood prevention is the Ourika flood warning system case.

Case study of Ourika valley and flood warning system in the High Atlas Mountains

Ourika watershed is a small sub-basin in the high Atlas Mountains, part of Tensift catchment, South of Morocco. It has a surface of 503 km^2 at Aghbalou gauging station located about 40 km to the Southeast of Marrakech city. It is bordered on the east by the watershed of Zat, and on the west by the Rheraya basin, the plain of Haouz at north, and the High Atlas Mountains to the south (Fig. 2.20). The Ourika basin is characterized by high elevation and steep slopes upstream of the wadi. 75% of the basin is located between 1600 m and 4165 m elevations and slopes can reach 60° to 70°. When intense rains occur, these slopes along with the land surface high imperviousness increase runoff generating the rise of floods (Bennani et al. 2019). The rainy period is October–April and the dry period is May-September with an average annual rainfall at the High Atlas ranging from 600 mm to 800 mm. The hydrological context of the Ourika watershed is influenced by a very marked seasonal and inter-annual irregularity of precipitation and heterogeneity of their spatial distribution (Saidi et al. 2003; Zkhiri et al. 2017). The drainage network is causing serious flooding by the extension of water bodies during periods of heavy rainfall, between July and October generating important damages for populations and infrastructures. The basin experienced many floods in 1984, 1987, 1995 1999, and 2014 that pushed water authorities to seek solutions for flood control. The case of the 17 of August 1995 was particularly severe as more than 200 people lost their

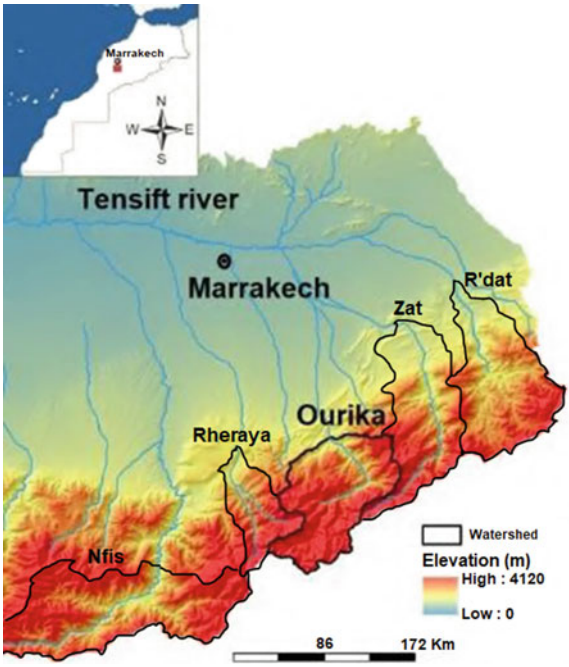

Fig. 2.20 Geographic location of Ourika watershed, Morocco (Modified from Bennani et al. 2019)

lives, many persons were missing, 300 ha of agricultural land were inundated, among which 62 ha were lost, and enormous material damage occurred (Daoudi and Saidi 2008). Besides, this mountainous basin is a touristic area that is massively visited during summer, and many touristic infrastructures, such as hotels and restaurants located nearby the river bed, were affected. The rainfall intensity was about 100 mm/h upstream the Ourika basin having generated a peak flow of 1000 m^3/s within 15 mn. Sediments accumulation has played a major role in aggravating the damages as it initially blocked the runoff by forming a natural dam that has later on collapsed creating a sharp hydrograph downstream and bringing alluvial cones into the wadi. In October 1999, another flood hit the Ourika valley and its neighboring watersheds including R'dat, Zat, Rheraya, and N'fiss. The rainfall and peak discharge reached 103.8 mm/day and 762 m^3/s, respectively. No human causalities were recorded but infrastructure and agricultural areas were damaged.

After the 1995 disaster, structural measures against flood have been implemented in the Ourika basin given its importance in terms of touristic activities and flood exposure. Ministry of Equipment (ME) has mainly concentrated on the Ourika water streams to mitigate occurrence of debris flow as well as to enlarge floodwater carrying capacity. Such measures included riverbed excavation along 12 km to ensure discharge capacity for floodwater, riverbank formation and protection with large gravel and revetment works to protect damaged road linking Marrakech city to Ourika valley. In addition, 27 small check dams were constructed

by the ME in the Ourika basin as of April 2000 to prevent outbreak of debris flow in the eight tributaries of Ourika wadi. Other small dams were built in the main wadi course to reduce the flow speeds and bank erosion as well as sediment transport. However, upstream of check dams were still causing important raise of water level increasing flood risk. In order to complement this set of structural measures and improve flood mitigation efficiency, other non-structural measures were added. Indeed, the High Commissioner for Water, Forests, and the Fight against Desertification (HCEFLCD) implemented a master plan of reforestation in order to mitigate erosion risk. A reforestation of two watersheds of Ourika and R'dat was carried out with a total treated surfaces of 2093 ha in Ourika basin and 3389 ha in the R'dat basin during the period 2000–2006.

All these measures were tightly reliant upon a good knowledge of hydro-meteorological conditions. Besides, the safety of the population required a good warning system in this mountainous and yet highly touristic area. Therefore, in march 2000, Moroccan government sought the support of the Japan International Cooperation Agency (JICA) to conduct a study for implementing a Master Plan for Flood Forecasting and Warning System (FFWS) for Atlas Region (JICA 2004). Thus, in 2001, five new hydrological stations were installed in the Ourika basin and another one in Rheraya basin as they were badly hit by the disaster (Fig. 2.21a). These stations were equipped with a VHF/FM and/or a HF/SSB radiotelephone to report flood information to the regional water authority. Two data transmission stations, four monitoring posts, and a warning post located at Ighref were also implemented. In addition, for a better integrated regional management of water resources, Tensift Hydraulic Basin Agency ABHT was created in 2000 having the responsibility, among others, of flood management. The ABHT included in its

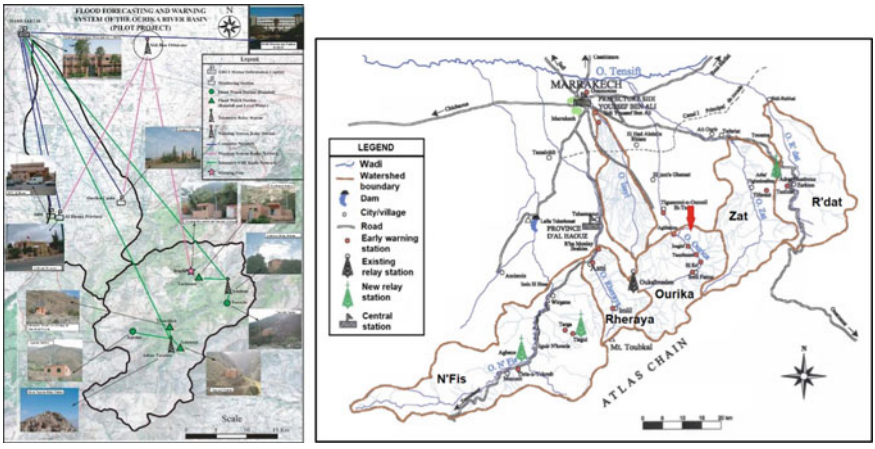

Fig. 2.21 Flood forecasting and warning system (FFWS) for the high Atlas: **a** FFWS stations in Ourika valley 2004, **b** FFWS stations in all Tensift High Atlas sub-catchments 2010 (*Source* JICA 2004)

PDAIRE the FFWS by extending it to five other watersheds, namely Rdat, Zat, Rheraya, Issyl, and Nfis (Fig. 2.21b). Since 2007, the ABHT has financed the telemetry network extension to 16 sites, including 3 rainfall stations and 13 rainfall-limnometric stations (ABHT 2010). The Ourika valley FFWS played a successful role in the detection and warning of ten floods between 2003 and 2012. During the 2014 floods, which affected Al Haouz province, no loss of life was recorded despite some property damages. In addition to providing an efficient early warning system, this project has raised local populations awareness toward emergency procedures. Currently, when flooding occurs, many local volunteers are tasked with warning tourists, keeping them informed, and helping them evacuate (OECD 2017b).

In its PDAIRE, the ABHT has assessed a total of 88 flood-prone areas over Tensit catchment territory. To tackle this problem, a program for flood risk protection was planned for the period of 2010–2020 and 2021–2030. 15% of the total budget of this program is dedicated to non-structural measures that are basically consisting of land use regulation in flood zones through delineation studies, awareness raising of the population, and the extension of flood forecast and warning systems. The ABHT has nowadays 42 hydrometeorological stations, 7 control posts, 7 transmission relays and 18 alarm posts. 98% of hydrological stations are equipped with telemetry. Data transmission is ensured by Radio across all sites. In 2019, the ABHT began to install redundancy networks with LTE wireless broadband (ABHT 2019).

2.5.4 Other Non-structural Measures

Most of the PDAIREs have integrated non-structural measures in their financial plans for flood control. In addition to flood warning systems, these measures include watercourses maintenance, watersheds management, contingency plans, information, training, and coordination. These choices were made based on the PNI (2002) recommendations. However, the PNE (2015) recalled that other measures should be contained in action plans for flood control, such as:

- reform of the legislative framework governing the management of flood risk;
- delineation of areas at flood risk and their mapping for each catchment;
- linkage between planning and land use development documents in order to control land use in areas at flood risk;
- flood prevention enhancement by improving knowledge in the field of hydrometeorological forecasting and the development of flood forecasting and warning and emergency plans;
- reinforcement of financial mechanisms (i.e. insurance and funds for natural disasters mitigation), in addition to consultation and coordination.

These new non-structural measures are being integrated into the latest update of the PNI. In the meanwhile, many governmental bodies have already taken actions for

implementing such measures. Some successful examples of these achievements are the new water 36-15 enactment, the creation of the FLCN fund for mitigating natural disaster impacts, production of new maps of aptitude for urbanization, and recently the creation of the Fund of Solidarity against Catastrophic Events (FSEC).

Legislative measure: Law 36-15

A good example of legislative measures for flood management is the new law 36-15, enacted in 2016. As introduced in paragraph, this law gives provisions of flood control, prevention, and management in a more detailed way that was absent in the previous water law 10-95. The new water law emphasizes on the management of water-related risks in particular floods and water scarcity. For floods, the law dedicated many articles on protection and prevention of flood risks, detection, monitoring, warning and management of flood events, and the implementation of water information system (Table 2.9). This legislative measure is a very important step in adapting the legal framework and therefore the administrative action to climate change related risks including floods. Similar efforts are still to be continued through the publication of pending implementation instruments of this law related to the novel documents that it provided. This is particularly the case of:

Table 2.9 Comparison of flood provisions between law 10-95 and the new law 36-15

Law 10-95	Law 36-15
– ABH liability for implementing flood prevention and control measures (art.20)	– Flood definition (art.3)
– Flood control infrastructures and prohibited construction areas (art.94-97)	– ABH liability for identifying and realizing flood prevention and control measures (art.80)
	– **Atlas of Flood prone areas** based on three-level risk classification (art.118)
	– **Plans for Flood Risk Prevention** to be prepared by ABH for medium and high flood risk areas in coordination with related stakeholders (art.118)
	– **Integrated Flood Monitoring and Warning Systems** to be implemented in all flooding streams (art.121-122)
	– **Communication** between General Directorate of Meteorology and ABH for providing necessary metrological forecast to the Integrated monitoring and warning systems (art.121)
	– **Vigilance committees'** creation at national and regional levels for flood events management (art.123)

- The procedures for establishing and approving Flood Risk Prevention Plans. These plans are made for a period of 20 years.
- The conditions and procedures for establishing and operating Integrated Flood Monitoring and Warning Systems to be implemented in all flooding streams.
- The composition and operating procedures of the new Vigilance Committees that will be established at national and regional levels for flood events management chaired by the governmental authority in charge of the Interior.

Financial measure: The FLCN fund

Another successful measure is the implementation of the Fund to combat the effect of Natural Disasters, called FLCN. The fund was created in 2009, with the support of the WB and the assistance of the OECD, and put under the auspices of the MI. Initially, the fund was mainly dedicated to cover emergency response and post-disaster reconstruction; it has gradually evolved into prevention financing. Thus, the fund has launched call for projects every year since 2015 in order to support projects of public stakeholders involved in risk management, namely the ministerial departments, public institutions, and companies, or territorial community elected councils. During the 2015–2018 period, the fund hence co-financed a total of 97 projects, through these calls, supporting both structural and non-structural measures for disaster prevention. In 2019, call submission, 75 applications were received, most of them from territorial community councils, and 46 projects were related to structural measures and 29 for non-structural measures.

For flood disaster prevention, the fund is supporting structural measures such as infrastructures for flood control or elevation of public infrastructures exposed to flood (e.g. public buildings, bridges, airports, ports), and non-structural measures such as plans for flood risk mitigation, warning systems, resilience regulations improvement and structures to monitor their application in urban and land use planning, floor risk mapping. For flood disaster prevention, the fund is supporting structural measures such as infrastructures for flood control or elevation of public infrastructures exposed to flood (e.g. public buildings, bridges, airports, ports), and non-structural measures such as plans for flood risk mitigation, warning systems, flood risk mapping, resilience regulations improvement and structures to monitor their application in urban and land use planning.

Most of the disaster control projects supported so far by the FLCN are related to flood control and related measures led by ABHs for studying and implementing flood protection measures in flood-prone areas, or installation of new radars for data monitoring and automation of meteorological stations investigated by DGM, or urbanization aptitude mapping undertaken by the Ministry of Urban Planning or Urban Agencies. Examples of such projects funded by the FLCN are:

- Modernization of meteorological services within the framework of the VIGIOBS project (Issara et al. 2010). The number of automatic weather stations has thus increased from 50 to more than 200, and the number of radars from 6 to 8. The FLCN has mobilized funding of USD 13.5 million over the period 2010–2012 for this project.

- The SCO diverting channel of Bouskoura wadi. This project has reduced floods of the city of Casablanca and Bouskoura. The FLCN mobilized 14% of the total budget for this project for the period 2015–2017.

The FLCN measure has enabled Moroccan state to have a specific financial tool for risk management. This fund will leverage other sources of funding as the FLCN contributes up to 50–70% of the total cost of eligible projects (MI 2020).

Urban planning measure: Urbanization Aptitude Map

Al Hoceima, a city in north Morocco on the Mediterranean shores, has experience successive natural disasters that are floods in 2003, the devastating earthquake of 2004, and landslides in 2008. As a response, the MI launched with the support of the WB a program on Integrated Disaster risk management and Resilience to assess Morocco's exposure to natural risk hazards and suggest recommendations for mitigating these risks. Following these program recommendations, the first urbanization aptitude map, called CAU, was elaborated in 2012 for Al Hoceima city. It is a major decision-making tool for earthquake-Flood and landslide risks management as it represents a real basis for the preparation and updating of urban planning documents and the regulation of land use and planning for this city. In 2017, 62% of urban planning documents of Al Hoceima city have incorporated the provisions of the CAU (Al Hoceima Urban Agency, AUA 2017). Following the implementation of the FLCN financial tool and the launch of its calls for proposals in 2015, a governmental program for elaborating 31 CAUs through the Moroccan territory was established for the period 2016–2021, thus many urban agencies received this fund support to elaborate their maps.

Regarding the risk of flooding, urbanization aptitude maps are based on the exploitation of Flood Atlas maps elaborated by the ABH and more detailed studies on most vulnerable sites. Therefore, these maps involve the implementation of the classification and mapping of flood risk based on field investigations concerning the areas at stake; analysis of hydro-meteorological data; a hydro-geomorphological study, and hydraulic modeling of urbanized areas. Different types of hazard maps, including flood maps, are then crossed and synthesized under a single cartographic document that is the CAU. This map defines five urban area classes:

- *Constructible areas*: Areas deemed to have no significant natural risk;
- *Constructible areas under technical conditions*: Low-risk areas, which can be built under conditions for carrying out general improvements;
- *Constructible areas under special conditions*: Medium-risk areas, which can be built under specific measures to be taken by urban and real estate developers;
- *Non-constructible areas:* Areas at high risk.
- *Non aedificandi areas*: presenting risks of flood, landslide, or earthquake which cannot be rectified.

Figure 2.22 shows an example of an urbanization aptitude map of Taounate city, northern Morocco (AUT 2017). The ongoing generalization of these maps to the whole Moroccan territory is a good example of compelling administrative planning tools as a non-structural measure for flood risk management.

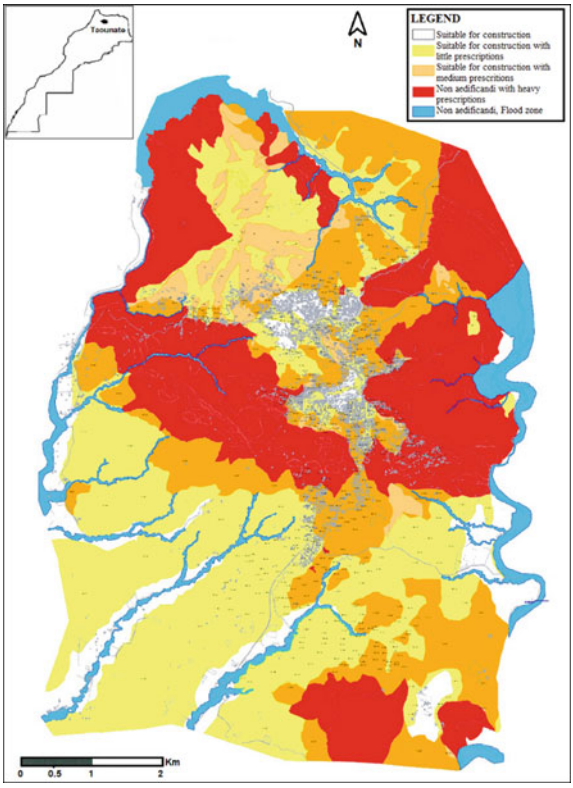

Fig. 2.22 Taounate city urbanization aptitude map (*Source* AUT 2017)

2.6 Swot Analysis and Recommendations

In this work, many research articles, administration documents, consultancy, and international organizations reports were analyzed to give a holistic insight on flood risk management in Morocco and form a critical view from a scientific perspective. Information and data were collected from different sources to come up with one document that integrates all scientific and governance aspects of flood risk management in Morocco. Analysis of this management landscape shows the important advances made by the Government to protect the population and prevent flood risk, but also the shortcomings that were or are still to be overcome. Given the variety of these aspects, a SWOT analysis (Hill and Westbrook 1997) was carried out for scoping and identifying the strengths, weaknesses, opportunities, and threats related to flood risk management in Morocco. Results are shown in Fig. 2.23. The analysis revealed various flood risk management success and failure factors related to three major components that are: governance, risk assessment approaches, and flood risk mitigation measures sustainability.

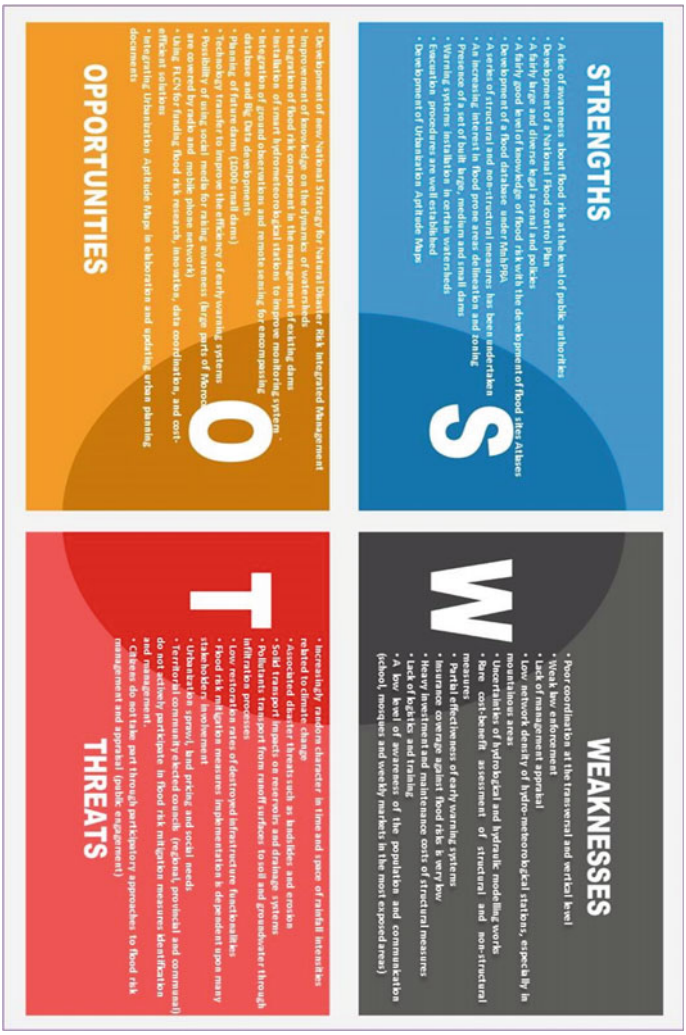

Fig. 2.23 SWOT analysis of flood risk management in Morocco 2020

Governance issues: In general, Morocco has made considerable progress in managing the risk of one of the most costly and adverse disasters for the past fifty years that is flood. The existence of legal arsenal, flood dedicated national plan (PNI), and integration of flood prevention and control in regional water agencies plans are all premises of a real awareness of public authorities and an advantageous framework for flood risk management. The paradigm shift from reactive to proactive approach in flood risk management, thrusted by international organizations, is also another positive advance in the process of risk management. However, the multiplicity of stakeholders, the poor coordination at transversal and vertical

levels, the weak law enforcement, particularly in the delineation and use of flood-prone areas are still impediments to the improvement of this management. The appraisal process is not implemented yet as a common practice for updating and adapting the development of flood risk management strategies. The prevention approach is still being developed but in an unequal manner between the ten ABHs (flood atlases, PDAIRE updates) despite the provisions of the newly elaborated water law. Indeed, on legislative level, the water law 36-15 has undoubtedly the merit of introducing for the first-time provisions dedicated to flood management. However, many of its implementation instruments are still pending generating discrepancies in flood prevention actions implementation.

The ongoing development of a risk management national strategy is a good opportunity to come up with solutions for these discrepancies and deficiencies. The MI leading this strategy is indeed the right department that can coordinates effectively flood prevention and control as it does for flood emergency and crisis management. The recent trainings, communication efforts, and the positive responses of stakeholders are good indicators of the potential of this leadership. Moreover, the financial hurdles that most of the implementation parties were facing in terms of heavy investment and/or maintenance costs of structural and non-structural measures, were largely reduced by the creation of the FLCN under the MI management. The call for proposals launched each year by the FLCN receives indeed increasing numbers of proposals from a variety of eligible public institutions and consolidates the role of this ministry in the coordination challenge.

The newly created Provincial Coordination Centers in the four locations, cited in Sect. 2.3.2, are also expected to improve local coordination between the multiple stakeholders and advocate for the creation of new directives for better legal responsibilities description and differentiation.

Among the 96 projects financed by the FLCN through calls for proposals over the period 2015–2018, only one project was investigated by a consortium of three research institutions. The project was on natural risk study in the central Rif. A special interest should be given to research institutions to encourage more interaction between the different stakeholders for advancing research on natural risk assessment. Indeed, flood risk is a particularly transversal issue involving many administrations and data providers. The FLCN can be a good framework for promoting collaboration between different partners.

Flood Atlas maps and their updates by ABHs are an essential prerequisite for urbanization aptitude maps (CAU) elaboration by urban agencies. The absence or lack of accuracy of such maps may affect the development of such map, essential to harness the rapid development of land use and urbanization sprawl. Therefore, the process of updating such maps should be adapted to urban planning requirements. The fact that many projects financed by the FLCN were dedicated to elaborating Urbanization Aptitude Maps proves the urgent need for these documents. However, a close look at the process of establishing such document shows that it goes through a hydrological and hydraulic modeling work for accurate risk assessment. This part should be closely coordinated with ABHs for more technical and accurate risk assessment and to avoid redundancy in flood risk studies.

Although flood-prone zones atlases have been produced at the scale of each ABH, these documents remain very general and only informative. They were not followed by the implementation of Prevention Plan against Flood Risk (called PPRI), a document that is more concise and should give accurate delimitation of flood zones, heights, and velocity reached at different points in these zones, identification of exposure and risks, and recommendations for suitable measures for future urbanization (DRPE 2013). Accelerating the production of pending implementation instruments of related provisions in law 36-15 will certainly help in the elaboration of these plans.

Technical issues: another strength of Moroccan flood risk management is the development of flood risk modeling since nineties despite the lack of data in terms of time and spatial distribution. Modeling works, mostly carried out by ABH and the Water Department gave a fairly primary assessment of flood risk at national and catchment scales that formed the basis for establishing PNI, PNE, catchment's flood atlas, and selecting flood control measures and their integration in budget planning. Since the launch of the program for establishing 31 urbanization aptitude maps (CAU) by the land use and urban planning ministry, many urban agencies performed their own flood risk modeling downscaled to their urban action perimeters. However, accuracy of these studies is a real weakness for the following reasons:

- Hazard assessment: no study has made a downscaling to simulate future trends of extreme rainfall events intensities, especially for short durations of few hours, that are often the cause of flash floods. Table 2.1 gives indications on duration of extreme precipitations that caused floods.
- Rainfall-runoff processes are often estimated based on stochastic methods and calibrated with discharge measurements when they exist. Estimates of design floods are often missing to initiate any hydraulic modeling for water infrastructures in the region (Zemzami et al. 2012). IDF curves are often used to estimate future rainfall intensities based on the Talbot-Montana model (Moujahid et al. 2018). However, these curves need to be updated by DGM for each meteorological station as climate change has considerably affected their accuracy.
- In mountainous areas, floods are greatly affected by geomorphological and hydrographic characteristics of watersheds. Steep slope, dense drainage network, compact shape, unvegetated surface, low infiltration soils increase the rainfall-runoff process paving the way to important floods in upstream basins (e.g. Ourika, Upper Moulouya, Rif, etc.). Therefore, catching these characteristics in fine detail is crucial for an accurate hydraulic modeling and flood risk assessment. Indeed, Bennani et al. (2019) analyzed the impact of two digital elevation models (DEM), with 30 m and 4 m spatial resolution on the accuracy of hydraulic models of Ourika watershed. They showed that a realistic representation of topography is essential to simulate flood in areas where data are scarce. The development of remote sensing public resources is a good opportunity for hydraulic modeling improvement. However, their resolution is not

always sufficient to accurately describe the geomorphological characteristics of mountainous watersheds.

- In both versions of the PNI, the primary recommendation was the improvement of flood risk knowledge. An accurate scientific risk assessment requires indeed a good knowledge of hazard and vulnerability. However, it became clear from the technical approaches adopted in PNI and Flood Atlases so far, that data sparsity and short records, and lack of high-resolution topography maps hampered the development of more accurate risk maps. It was obvious that, in 2002, with the pressing need for a more preventive flood policy, accuracy of maps was not a priority. Yet, it is clear that the present development of technology and data resources, including satellite and UAV data and the advent of big data, machine learning, and more broadly artificial intelligence, can develop a better risk assessment knowledge and thus, help decision makers in optimizing investment in flood protection measures. It can also overcome the obstacle of data exchange and communication between various and large arrays of institutional stakeholders.
- Vulnerability assessment needs to be refined in urban areas. The newly developed Urbanization Aptitude Maps are certainly an opportunity to come up with deficiencies in urban vulnerability assessment as it is strongly linked to urban and real estate factors.
- Exposure was not considered in the PNI and PDAIRE first editions as the knowledge about this risk element was not fully acquired. Vulnerability was assimilated as exposure. Besides, exposure data are often collected from various institutions with different levels of availability. In fact, a fair good coverage of social data, urban data, land use is available. However, economical value is still a weak link in the process of exposure assessment.
- MnhPRA is a good GIS-based tool for a first assessment of risk in Morocco. However, this tool is not accessible to researchers so that a scientific and technical improvement of this tool can be performed. In addition, law 36-15 provision about the implementation of a new Integrated Systems for Flood Monitoring and Warning could be a good opportunity for linking this system to MnhPRA to improve its accuracy and usage in partnership with the scientific research community.
- So far, there is no standard in Morocco defining reference or threshold hazards. The 2016 water law 36-15 states that flood risk atlases should define three levels of hazards—low, medium, and high—without fixing the related return period. In Europe, the 100-years return period that has long served as a reference is now considered to be the average level. In the OECD guide for Morocco (OECD 2018), return periods of 10–20 years, 50 years, and 100 years were recommended.

Mitigation measures, sustainability, and resilience issues

Many measures have proven their efficiency in flood control, such as the SCO channel for protecting Casablanca city and the new El Malleh dam for Mohammedia city. In fact, the set of dams realized within the dam's policy is a

major asset for Morocco's water resources integrated management strategy including flood protection. In the PDAIREs, the primary implemented flood protection measures were the traditional engineering ones, generally consisting of programs of dams, levees, and channels building. Cost estimation of these measures is usually based upon the method used in the PNI (2002), where investment costs were computed using a classification of sites according to the size of the urban area and flood vulnerability, and the estimation of a cost class ratio based on previous sites studies. However, no cost-benefit analysis has been integrated into the process of selecting mitigation options. Besides, the environmental and social impacts of large dams and structural measures are often neglected. Indeed, these large infrastructures generally require substantial land provisions and real estate acquisition, generating adverse social impact and important threat to flood control measures acceptance. Moreover, erosion is another serious threat to Moroccan dams as their silting puts the sustainability of these structures in jeopardy. Erosion affects also the hydraulic performance of drainage and sewage systems (e.g., El Gharb). Maintenance of these structural measures can be a hurdle to water managers that seriously affects their performance in protecting against floods in the long term.

Large reservoirs have the advantage of economy of scale but they are costly to build and maintain, and they can result in massive social and environmental disturbances. Cost-benefit analyses should be required for flood risk studies done by ABHs and DGE for a better investment adjustment and sustainable protection.

Lessons from neighboring countries should be drawn. Indeed, Aswan High Dam offered Egyptians a way to control runoff from the Nile and to provide a stable water supply but hard-pressed the country financially and politically to secure funding. The dam successfully stopped damage from seasonal flooding but blocked sediment that floodwater brought with it to replenish the Nile Delta and therefore, increased its vulnerability to erosion (Syvitski 2008; Verner 2012). For flood control channel in Sfax city, Tunisia, water deterioration in the channel is firstly related to contaminated groundwater drained by the channel and secondly to anthropogenic inputs (Dahri et al. 2014). The sustainability of flood measures, particularly structural ones, should be integral part of options selection. For instance, enhancing dam's sustainability can be achieved by prospecting new ways of designing dams. Indeed, studies in Spain and China showed that hybrid connection of check dams' system can generate the largest decrease in flood magnitude better than the parallel system and to a lesser degree, the series of dam system. The construction of check dams is an important instrument in holding sediment from reaching downstream infrastructure and for reducing flood amplitude in a cascading way (Boix-Fayos et al. 2008; Yuan et al. 2019). Leichao 2020 showed that the sediment interception efficiency of check dams can be greatly reduced under extreme rainstorms when these dams are poorly managed. They concluded that management and construction technology standards of check dams for flood and erosion control should be improved to keep up the efficiency of dams' systems.

The need for future dams may be obvious for flood control as extreme rainfall-runoff are varying under climate change. However, the random character of climate change poses also the risk of oversizing these structures and therefore

reducing their efficiency. Yet, the succession of long sequences of drought in 1980–1985; 1991–1995; 1998–2002; 2004–2008, asserts the need for dams to alleviate drought impact on water resources, drought events being considered as natural disasters far more damaging economically and socially than floods in Morocco. Therefore, updating national and regional water policies (PNI, PDAIREs) is a good opportunity to reassess the role of existing or new dams, primarily designed for hydropower or irrigation, with the additional purpose of flood mitigation. Hence, cost-benefit analyses should be a necessary step in defining program of dams' construction and should integrate all services provided by large dams including water availability, hydropower generation, and flood control.

Besides, relying on dams alone for long-term protection is a real threat to flood resilience. Indeed, the examples of al Wahda dam built in 1996 that failed in protecting Al Ghrab plain against the 2010 floods, the Assif El Krayma hill dam built in 2012 that failed in protecting Sidi Ifni city in Moroccan desert against 2014 floods, have demonstrated how much it was dangerous to rely solely on these types of measures for flood control. Indeed, non-structural measures are required to accompany structural ones for a better resilience. The Ourika case is a good example of combination of structural and non-structural measure for flood risk management and resilience enhancement. However, a close look at numbers and investment shares in non-structural measures shows their low consideration in regional planning, highlighting a weakness of flood risk management in Morocco. Update of flood risk management plans should be an opportunity to consider the benefit of these measures and increase their shares in investment planning. As these measures often require a public engagement to ensure their long-term efficiency, absence of citizen involvement in decision-making may be a threat to the sustainability of such measures. Nevertheless, the provision of law 36-15 for preparing new Flood Risk Prevention Plan for high and medium risk areas is the right opportunity to stimulate the engagement of citizens and other public stakeholders within a participatory approach for a better communication, flood risk preparedness and resilience enhancement. Lastly, the involvement of international organizations, such as OECD and WB, was a good opportunity for Moroccan government to advance its flood risk management strategy. International cooperation in research can also offer a great opportunity for improving flood risk assessment in Morocco and developing innovative solutions for flood prevention and control.

References

ABHBC (2007) Etude du Plan Directeur d'Aménagement Intégré des Ressources en Eau du Bassin Hydraulique du Bouregreg et de la Chaouia. Rapport sous Mission I-2: Evaluation quantitative des ressources en en eau et des écosystèmes. Hydraulic Basin Agency of Bouregreg and Chaouia report

ABHS (2017) Gestion du risque d'inondation dans le bassin du Sebou. Hydraulic Basin Agency of Sebou communication. In: OECD workshop on risk prevention in Morocco, Fez, Morocco

ABHS (2018) Surface water resources. Hydraulic Basin Agency of Sebou [online]. Available at: http://www.abhsebou.ma/presentation-du-bassin/eaux-de-surface/. Accessed: 16 April 2020

ABHT (2007) Atlas des zones inondables. Hydraulic Basin Agency of Tensift document [online]. Available at: http://www.eau-tensift.net. Accessed: 18 April 2020

ABHT (2010) Plan Directeur d'Aménagement Intégré des Ressources en Eau des bassins du Tensift, Ksob et Igouzoulen,. Hydraulic Basin Agency of Tensift PDAIRE document

ABHT (2019) Rôle des Agences de Bassins dans la prévention et la gestion du risque naturel d'inondations. Hydraulic Basin Agency of Tensift communication, in Workshop for Training and Informing Focal Points in charge of Risks Management, Marrakech, Morocco [online]. Available at: https://www.gestionrisques.ma/. Accessed: 11 April 2020

Albergel J (2008) Place des petits barrages dans la mobilisation des eaux de surface et dans la lutte contre l'érosion au Maghreb et au Moyen-Orient. In: Roose É et al (ed) Efficacité de la gestion de l'eau et de la fertilité des sols en milieux semi-arides, pp 31–43. Paris, AUF, EAC, ENFI, IRD

Arthurton R, Le Tissier M, Snoussi M, Kitheka J, Shaghude Y, Kane A, Flöser G, Kremer H (2008) AfriCat: LOICZ—global change assessment and synthesis of river catchment—coastal sea interactions and human dimensions in Africa. LOICZ Reports & Studies No. 30

AUA (2017) La carte d'aptitude à l'urbanisation de la province d'Al Hoceima. Al Hoceima Urban Agency communication. In: OECD workshop on risks prevention in Morocco, Fez, Morocco

AUT (2017) Documents d'urbanisme entre planification urbaine et gestion des risques -Etude géotechnique et carte d'aptitude à l'urbanisation de la ville de Taounate. Taza Urban Agency communication. In: OECD workshop on knowledge and risk assessment in Morocco, Rabat, Morocco

Azhari M, Loudyi D (2019) Downscaling climate projections and hydrologic responses for regional water resources assessment: case of the Oum Er Rbia river basin, Morocco. J Eng Res Appl 7:49–58

Bai L, Wang N, Jiao J, Chen Y, Tang B, Wang H, Chen Y, Yan X, Wang Z (2020) Soil erosion and sediment interception by check dams in a watershed for an extreme rainstorm on the Loess Plateau, China. Int J Sedim Res 35:408–416

Bennani O, Tramblay Y, Simon G, Frédéric L, Saidi ME (2019) Flood hazard mapping using two digital elevation models: application in a semi-arid environment of Morocco. Eur Sci J 15:338–359

Boix-Fayos C, Vente DJ, Martínez-Mena M, Barbera GG, Castillo V (2008) The impact of land use change and check-dams on catchment sediment yield. Hydrol Process 22(25):4922–4935

Casa Aménagement (2020) Infrastructures: protection of the city of Casablanca from the floods of Oued Bouskoura [online]. Available at: https://www.casa-amenagement.ma/en/nos-projets/super-collecteur-ouest. Accessed: 20 April 2020

Cour des Comptes (2016) Evaluation de la gestion des catastrophes naturelles. The Kingdom of Morocco court of auditors summary report [online]. Available at: http://www.courdescomptes.ma/. Accessed: 30 March 2020

Dahri N, Atoui A, Abida H (2014) Environmental impact assessment of a flood control channel in Sfax City, Tunisia. Int J Sci Eng 7(1):23–29

Daoudi L, Saidi MEM (2008) Floods in semi-arid zone: example of the Ourika (High Atlas of Marrakech, Morocco). Int Sci J Altern Energy 5(61):117–123

DesInventar Sendai (2014) Disaster information management system. United Nations office for disaster risk reduction, UNDRR [online]. Available at: https://www.desinventar.net/DesInventar/. Accessed: 29 April 2020

DGE (2015) Plan National de l'Eau: Rapport Géneral. Moroccan General Directorate of Water report

DGE (2020) Data directly collected from the Moroccan General Directorate of Water

DGM (2017) Les données et les informations météorologiques/climatiques. National Meteorological Direction of Morocco communication. In: OECD workshop on knowledge and risk assessment in Morocco, Rabat, Morocco

Diekkrüger B, Busche H, Klose A, Klose S, Rademacher C, Schulz O (2012) Impact of global change on hydrology and soil degradation—scenario analysis for the semi-arid Drâa catchment (South Morocco). In: Bogardi KJ et al (eds) River basins and change, pp pp 21–26. GWSP and UNESCO-IHE [online]. Available at: http://www.gwsp.org/fileadmin/documents_news/GWSP_12_01_E-Lernbuch_Complete_RZ5.pdf. Accessed: 1 April 2020

Driouech F (2010) Distribution des précipitations hivernales sur le Maroc dans le cadre d'un changement climatique: descente d'échelle et incertitudes. PhD thesis, Institut National Polytechnique de Toulouse, France [online]. Available at: https://oatao.univ-toulouse.fr/7237/, Open Archive Toulouse Archive Ouverte. Accessed: 3 April 2020

Driouech F, Mahe G, Deque M, Dieulin C, El Heirech T, Milan M, Benabdelfadel A, Rouche N (2010) Evaluation d'impacts potentiels de changements climatiques sur l'hydrologie du bassin versant de la Moulouya au Maroc. In Proceedings of the sixth world FRIEND conference, vol 340, pp 561–567. IAHS Pub, Fez, Morocco

DRPE (2013) Etude d'actualisation du plan national de protection contre les inondations. CID/ISL report RM12-70 for the Moroccan Water Department

DRPE (2019) Rôle de la Direction de la Recherche et de la Planification de l'Eau dans la Gestion des Risques d'Inondations. Moroccan research and water planning directorate, DRPE communication. In: Workshop for training and informing focal points in charge of risks management, Marrakech, Morocco [online]. Available at: https://www.gestionrisques.ma/. Accessed: 10 April 2020

EM-DAT (2020) The OFDA/CRED international disaster database, Université Catholique de Louvain, Brussels, Belgium [online]. Available at: https://www.emdat.be/. Accessed: 20 April 2020

EMWIS (2005) Base de données SIG du plan national de protection contre les inondations et impacts des ouvrages de protection sur l'environnement. In: Seminar of information on SEMIDE: euro-mediterranean information system on know-how in the water sector, Rabat, Morocco [online]. Available at: http://www.emwis.org/. Accessed: 22 April 2020

HCP (2014) Moroccan population census, high commissioner for planning in Morocco report [online]. Available at: https://www.rgph2014.hcp.ma/Note-sur-les-premiers-resultats-du-Recensement-General-de-la-Population-et-de-l-Habitat-2014_a369.html. Accessed: 11 May 2020

Hill T, Westbrook R (1997) SWOT analysis: it's time for a product recall. Long Range Plan 30 (1):46–52

IPCC (2007) Summary for policymakers. In: Solomon S et al (eds) Climate change 2007: the physical science basis. Contribution of working group I to the fourth assessment report of the intergovernmental panel on climate change. Cambridge University Press, Cambridge, United Kingdom and New York, NY, USA

Issara S, Merrouchi R, Nouni N (2010) Intensification and automation of Moroccan meteorological observation network for the improvement of weather forecasting and warning system. National meteorological direction of Morocco (DMN) poster presentation. In: TECO-2010—WMO technical conference on meteorological and environmental instruments and methods of observation, Helsinki, Finland

Jaouda I, Akhssas A, Ouadif L, Bahi L, Elkasri J, Souidi H, Soussi H (2020) Study of soil erosion risks using remote sensing in Ouergha River watershed (Morocco). In: Akhssas et al (eds) The 7th international congress on water, waste and environment, Salé, Morocco. E3S Web of conferences 150 [online]. Available at: https://www.e3s-conferences.org/. Accessed: 15 April 2020

JICA (2004) The master plan study on flood forecasting and warning system for Atlas region in the Kingdom of Morocco. Japan International Cooperation Agency final report, volume 2 main report [online]. Available at: https://openjicareport.jica.go.jp/pdf/11750825_01.PDF. Accessed: 2 May 2020

Jouve A (2006) Les trois temps de l'eau au Maroc: l'eau du ciel, l'eau d'Etat, l'eau privée. Confluences Méditerranée 58(3):51–61

Lydec (2014) Schéma Directeur d'Assainissement. Aménagements de renforcement du réseau d'assainissement existant des zones urbanisées des communes de Casablanca et Mohammedia
Marchane A, Tramblay Y, Hanich L, Ruelland D, Jarlan L (2017) Climate change impacts on surface water resources in the Rheraya catchment (High Atlas, Morocco). Hydrol Sci J 62 (6):979–995
MI (2020) Ongoing projects, ministry of interior national portal for Morocco's integrated disaster risk management and resilience program. Available at: https://www.gestionrisques.ma/Realisations/projets_en_cours.aspx. Accessed: 05 May 2020
Michel-Kerjan E, Scawthorn C, Baeumler AEN, Banerjee A, Rondot P, Medouar M, Mahul O, Boudreau L, Davila-Bonazzi A, Dana J (2014) Building Morocco's resilience: inputs for an integrated risk management strategy. World Bank report 83782 [online]. Available at: http://documents.worldbank.org/curated/en/703601468060288949/Building-Moroccos-resilience-inputs-for-an-integrated-risk-management-strategy. Accessed: 7 April 2020
Midaoui A, Lahrach A, Chaouni A, Bourak A, Benaabidate L, Boukharas L (2015) Integration of GIS and HEC-RAS in floods modeling of the Ouergha river, northern Morocco. Eur Sci J ESJ 11:196–204
Moujahid M, Stour L, Agoumi A, Saidi A (2018) Regional approach for the analysis of annual maximum daily precipitation in northern Morocco. Weather Climate Extremes 21:43–51
OECD (2014) Recommendation of the council on the governance of critical risks. Meeting of the organisation for economic co-operation and development council at ministerial level, Paris, France [online]. Available at: http://www.oecd.org/gov/risk/Critical-Risks-Recommendation.pdf. Accessed: 8 May 2020
OECD (2016) OECD review of risk management policies Morocco. The organisation for economic co-operation and development, OECD Publishing, Paris [online]. Available at: https://www.oecd-ilibrary.org/governance/oecd-review-of-risk-management-policies-morocco_9789264276482-en. Accessed 23 April 2020
OECD (2017a) Mieux évaluer les risques au Maroc: Quels besoins? Quels outils? Quelle gouvernance? The organisation for economic co-operation and development report presentation, in OECD workshop on knowledge and risk assessment in Morocco, Rabat, Morocco
OECD (2017b) OECD review of risk management policies Morocco. The organisation for economic co-operation and development, OECD Publishing, Paris [online]. Available at: https://www.oecd.org/gov/oecd-review-of-risk-management-policies-morocco-9789264276482-en.htm. Accessed 21 April 2020
OECD (2018) Guide pratique: Connaitre et évaluer les risques de catastrophes naturelles au Maroc. The organisation for economic co-operation and development document at the national portal for Morocco integrated disaster risk management and resilience program. Available at: https://www.gestionrisques.ma/telecharger/guides.aspx. Accessed 15 April 2020
OECD (2019) Gestion des risques au Maroc: Progrès réalisés et enjeux pour l'avenir. The organisation for economic co-operation and development evaluation report at the national portal for Morocco integrated disaster risk management and resilience program. Available at https://www.gestionrisques.ma/web/files/Rapport_d_evaluation_OCDE.pdf. Accessed: 19 May 2020
ORMVAG (2017) Le Plan Agricole Régional de Rabat-Salé-Kénitra: Un modèle de gouvernance territoriale pour un développement durable. Regional Agricultural Development Office of El Gharb communication. In: 5th international seminar SESAME, agropolis international, Montpellier, France [online]. Available at: https://www.agropolis.fr/actualites/retour-seminaire-international-sesame-5-2017.php. Accessed 3 May 2020
PNE (2015) Plan National de l'Eau, Moroccan Water Department document
PNI (2002) Étude du Plan National de Protection contre les Inondations et impacts des ouvrages de protection sur l'environnement. Moroccan State Secretary in charge of water, Summary report
PNI (2010) Étude d'actualisation du Plan National de Protection contre les Inondations. Moroccan General Directorate of Water report

Saidi MEM, Daoudi L, Aresmouk M, Blali A (2003) Rôle du milieu physique dans l'amplification des crues en milieu montagnard: exemple de la crue du 17 août 1995 dans la vallée de l'Ourika (Haut-Atlas, Maroc). Sécheresse 14(2):1–8

Scawthorn C (2017) Modèle d'évaluation probabiliste multi-risques MnhPRA et la voie à suivre, communication. In: OECD workshop on knowledge and risk assessment in Morocco, Rabat, Morocco

Seif-Ennasr M, Zaaboul R, Hirich A, Caroletti GN, Bouchaou L, El Morjani Z, Beraaouz E, McDonnell RA, Choukr-Allah R (2016) Climate change and adaptive water management measures in Chtouka Aït Baha region (Morocco). Sci Total Environ 573:862–875

SEEE (Secrétariat d'État chargé de l'Eau et de l'Environnement), Environment Department (2008) Étude pour la réalisation d'une cartographie et d'un Systèmed'Information Géographique sur les risques majeurs au Maroc. Mission 1: Identification des risques - Le risque d'inondation

SEEE (Secrétariat d'Etat chargé de l'Eau et de l'Environnement). SEEE/UNDP/DEPP/HYDRAUMET (2008) Rapport Étude V&A s/ SCN, Mission III: Adaptation.Projet SCN-CC/00047842/2006. Étude vulnérabilité et adaptation du Maroc face aux changements climatiques. Rapport de synthèse - Mission 1 : Étude de lavulnérabilité

Sinan M, Belhouji A (2016) Impact of the climate change on the climate and the water resources of Morocco on horizons 2020, 2050 and 2080 and measures of adaptation. La Houille Blanche 4:32–39

Singla S (2009) Impact du changement climatique global sur les régimes hydroclimatiques au Maroc: tendances, ruptures et effets anthropiques sur les écoulements. Master Thesis, Université de Montpellier 2 [online]. Available at: https://www.documentation.ird.fr/hor/fdi:010055323, All rights reserved. Accessed: 13 May 2020

SNE (2009) Stratégie Nationale de l'Eau. Moroccan state secretary in charge of water document [online]. Available at: http://www.environnement.gov.ma/PDFs/EAU/STRATEGIE_EAU.pdf. Accessed: 10 May 2020

Syvitski JPM (2008) Deltas at risk. Sustain Sci 3:23–32

UNEP (2008) Africa: Atlas of our changing environment. Division of early warning and assessment (DEWA), United Nations environment programme. Nairobi, Kenya [online]. Available at: http://www.unep.org/dewa/africa/africaAtlas/PDF/en/Chapter3b.pdf. Accessed: 7 April 2020

UNISDR (2015) Sendai framework for disaster risk reduction 2015–2030. United Nations office for disaster risk reduction publication UNISDR/GE/2015—ICLUX EN5000 1st edition, Geneva, Switzerland [online]. Available at: https://www.undrr.org/publication/sendai-framework-disaster-risk-reduction-2015-2030. Accessed: 05 May 2020

Varnes D (1984) Landslide hazard zonation: a review of principles and practice. Natural hazards 3, commission on landslides of the IAEG, UNESCO, Paris, France

Verner D (2012) Adaptation to a changing climate in the Arab countries: a case for adaptation governance and leadership in building climate resilience. MENA development report. World Bank, Washington, DC [online]. Available at: https://openknowledge.worldbank.org/handle/10986/12216. Accessed: 8 April 2020

WB (2011a) Adaptation au changement climatique et aux désastres naturels des villes côtières d'Afrique du Nord. Phase 1: Évaluation des risques en situation actuelle et à l'horizon 2030 pour la ville de Casablanca. World Bank report, Egis BCEOM International/IAU-IDF/BRGM, GED 80823T

WB (2011b) Adaptation au changement climatique et aux désastres naturels des villes côtières d'Afrique du Nord. Phase 1: Évaluation des risques en situation actuelle et à l'horizon 2030 pour la vallée du Bouregreg. World Bank report, Egis BCEOM International/IAU-IDF/BRGM, GED 80823T

WB (2011c) Climate change adaptation and natural disasters preparedness in the coastal cities of North Africa. World Bank report, Egis BCEOM International/IAU-IDF/BRGM, GED 80823T

WB (2012) What if scenario analysis report, Morocco natural hazards probabilistic risk analysis and national strategy development. The Ministry of General Affairs and Governance, prepared by RMSI Ltd

WB (2013) Building Morocco's resilience: inputs for an integrated risk management strategy public. World Bank working paper. Available at: http://documents.worldbank.org/curated/en/2014/01/19226575/building-moroccos-resilience-inputs-integrated-risk-management-strategy. Accessed: 10 April 2020

WB (2016) Climate change knowledge portal. World Bank group [online]. Available at: https://climateknowledgeportal.worldbank.org/country/morocco. Accessed: 15 April 2020

WB (2019) Morocco—disaster risk management development policy loan with a Catastrophe deferred drawdown option project. World Bank Group document, Washington, DC [online]. Available at: http://documents.worldbank.org/curated/en/500751580292321681/Morocco-Disaster-Risk-Management-Development-Policy-Loan-with-a-Catastrophe-Deferred-Drawdown-Option-Project. Accessed: 6 May 2020

Yuan S, Li Z, Li P, Xu G, Gao H, Xiao L, Wang F, Wang T (2019) Influence of check dams on flood and erosion dynamic processes of a small watershed in the loss plateau. Water 11:834

Zemzami M, Benaabidate L, Layan B, Dridri A (2012) Design flood estimation in ungauged catchments and statistical characterization using principal components analysis: application of Gradex method in Upper Moulouya. Hydrol Process 27(2):186–195

Zkhiri W, Tramblay Y, Hanich L, Berjamy B (2017) Regional flood frequency analysis in the High Atlas mountainous catchments of Morocco. Nat Hazards 86:953–967

Chapter 3
Flood Analysis and Mitigation Strategies in Algeria

Hamouda Boutaghane, Tayeb Boulmaiz, El Khansa Lameche, Abdelouahab Lefkir, Mahmoud Hasbaia, Chérifa Abdelbaki, Ahmed Walid Moulahoum, Mehdi Keblouti, and Abdelmalek Bermad

Abstract Floods are frequent hazard in Algeria. They cause severe casualties, destroy infrastructures, and impair economies. In the past decades, Algeria experienced devastating floods. The dominant type of occurring floods are flash floods, which tend to be not well documented and studied in Algeria. This chapter presents a brief introduction to the flood phenomena within the Algerian climatic and management context, based on databases, scientific publications, and local technical reports. Existing studies about floods are reviewed. It also provides an analysis of the most disastrous floods that occurred in the past decades. Of the most noteworthy flash floods, a highlight of the Bab El Oued flash flood occurring in a heavily

H. Boutaghane (✉)
LSH Laboratory, Badji Mokhtar-Annaba University, P.O. BOX 12, 23000 Annaba, Algeria
e-mail: hamouda.boutaghane@univ-annaba.dz

T. Boulmaiz
Materials, Energy Systems Technology and Environment Laboratory, Ghardaia University, Ghardaia, Algeria
e-mail: boulmaiz.tayeb@univ-ghardaia.dz

E. K. Lameche
Larbi Ben M'Hidi University, Oum El Bouaghi, Algeria

A. Lefkir
Laboratory of TPiTe Ecole Nationale Supérieure des Travaux Publics, Algiers, Algeria
e-mail: a.lefkir@enstp.edu.dz

M. Hasbaia · A. W. Moulahoum
CEHSD Laboratory, University of M'sila, 166 Ichebilia, 28000 M'sila, Algeria
e-mail: mahmoud.hasbaia@univ-msila.dz

C. Abdelbaki
EOLE Laboratory, University of Tlemcen, Tlemcen, Algeria
e-mail: cherifa.abdelbaki@pauwes.dz

M. Keblouti
Abdelhafid Boussouf University Center, P.O. BOX 26, RP, 43000 Mila, Algeria

A. Bermad
CEME Laboratory, Ecole Nationale Polytechnique D'Alger, El Harrach, Algeria
e-mail: abdelmalek.bermad@g.enp.edu.dz

T. Sumi et al. (eds.), *Wadi Flash Floods*, Natural Disaster Science and Mitigation Engineering: DPRI Reports, https://doi.org/10.1007/978-981-16-2904-4_3

urbanized setting and the M'zab Valley flash flood, which took place in a UNESCO World Heritage Site. The monitoring network in Algeria is presented and data availability is discussed. The implementation of the first forecasting and early warning system are also presented. Different aspects of flash floods were presented including the effect of the increase of urbanization, the influence of climate change and the adopted strategies of flood risk management. Heavy and increasing urbanization and population growth increased the flood vulnerability and this trend must be mitigated.

Keywords Flash flood · Vulnerability · Integrated flood risk management · Algeria

3.1 Introduction

Floods are a worldwide natural phenomenon and are considered as one of the most severe weather-related disasters. They can damage societies, impair economies, harm the environment, and cause tragic human casualties. 47% of all weather-related disasters are caused by floods, impacting 2,3 billion persons, and killing 156,000 others with estimated economic losses of 662 billion (US $).

In recent decades, occurring floods were dominated by devastating flash floods especially observed in Mediterranean countries (Gaume et al. 2016; Llasat et al. 2013, 2010) and the MENA zone (WorldBank 2014). From 1900 to 2011, 15 MENA countries were affected by 213 floods, killing almost 19,000 peoples and impacting 8.6 million others. Flash floods are also generated by extreme rainfall over a short time period (Price et al. 2011)

Floods have been a permanent scientific interest with many developments done in different associated relating topics. The main challenge of scientists is to better understand the phenomenon and develop a model strategy for flood risk management. Several instructive reviews dealing with floods appeared: (Hammond et al. 2015; Mignot et al. 2019; Nkwunonwo et al. 2020; Teng et al. 2017).

Llasat et al. (2010) and Gaume et al. (2016) have collected and analyzed information about 55 events of extreme floods that happened during the period between 1990 and 2006 and 172 extreme flood events (period 1940–2015) respectively in Mediterranean countries. They found a contrast in the magnitude and impact of extreme events between the West and East parts of Mediterranean region. Floods occur in Northern Africa with reduced frequencies, but with a high number of fatalities, they are often devastating. The most dramatic event in Mediterranean and MENA regions occurred in Algiers (2001, 900 killed) (Gaume et al. 2016).

Algeria is part of MENA countries and the most exposed to natural disasters (62 hazards, between 1980 and 2010) with 58% of them as floods (WorldBank 2014). Floods are among the most important natural hazards in Algeria. Significant

fatalities, damage to buildings, and the loss of roads and urban infrastructure have been induced.

In this chapter, the focus is made on the flood analysis and mitigation strategies in Algeria: what is known and what can be done. A synthesis of several scientific publications and research projects on this theme is presented. Different aspects of flood analysis and their evolution in relation to urbanization and climate change are discussed.

3.2 Reviewed Studies on Floods

The flood research is the first step to a better comprehension of the phenomenon for improving management. It needs a good study of meteorological data and climate change, in particular precipitation, and good knowledge of the vulnerability of watersheds and cities and exposure to flooding in those territories to tackle flood problems (Loudyi and Kantoush 2020). The studies reporting the floods in Algeria are increasing in recent years. This research focused on three themes: (1) flood hazard mapping, (2) hydraulic and hydrologic modelling (3) some specific flood event analysis (Table 3.1).

Several studies have been carried out with the aim of generating flood risk maps based on hydrological and hydraulic simulation (Astite et al. 2015; Yamani et al. 2016; Abdessamed and Abderrazak 2019 and Hafnaoui et al. 2020) or hydrogeomorphological approach (Cheikh lounis et al. 2015; ZaÏri 2018; Mimouni et al. 2019; Bourenane et al. 2019). By using PLUTON as a hydrological model and HecRas for flood simulation, Astite et al. (2015) delimitated flood risk areas in El Harrach river, the most important in Algiers city. Several flooding events resulting from the growth of the population and municipalities expansion over the natural space of El-Harrach River, have been identified in this coastal region. On the semiarid Ain-Safra River, which is located in Southwest of Algeria, a similar study was carried out (Abdessamed and Abderrazak 2019). The simulation was also carried out for the purpose of testing the retaining concrete walls built by local officials, as well as other proposed security measures. Results showed that for 100-years floods there are some overflows, although the measures given remain insufficient for 1000-years. Both studies (Astite et al. 2015 and Abdessamed and Abderrazak 2019) were focused on the frequency related to return periods to indicate flooded zones, furthermore, Hafnaoui et al. (2020) have proposed a system based on the suggested values of rainfall. (40, 60, 80, and 100 mm) to identify flood-prone zones. The idea was to use the flood hazard map with weather warnings released by the National Office of Meteorology (NOM) in order to identify the area exposed to flood. Contrary to the simulated flood using mostly the HecRas software, Bourenane et al. (2019) performed an investigation based mainly on field survey, aerial photographs, and satellite images analyze in addition of other information sources to identify the flood plains of historical events. The use of such approaches is more effective since it is based on real events (historical floods),

Table 3.1 Summary of reviewed studies on floods in Algeria

Study area City/ Catchment/ Wadi	Method/approach	Tools	References
Flood hazard and mapping			
El Baydh	Hydrological analysis and hydraulic simulation	ArcGIS, HEC-RAS	Hafnaoui et al. (2020)
Constantine	Hydro geomorphological approach	GIS	Bourenane et al. (2019)
Wadi M'zab	Vulnerability and risk analysis	GIS	Mimouni et al. (2019)
Ain-Safra	Hydrologic and hydrologic modeling	HEC-HMS, WMS, HEC-RAS, and GIS	Abdessamed and Abderrazak (2019)
Chlef	Multi criteria analysis	GIS	Zaïri (2018)
Wadi Kniss	Hydro geomorphological approach	GIS	Cheikh lounis et al. (2015)
Wadi El Harrach	Floods cartography on urban environment	PLUTON ArcGis, HEC-GeoRAS, HEC-RAS	Astite et al. (2015)
Ghardaia	Cartography the flooded area event of (2008)	(SOGREAH) HEC-RAS	Yamani et al. (2016)
Hydraulic and hydrologic modelling			
Wadi Bechar	Hydrologic modeling of floods	GR1A, GR2M (IRSTEA)	Bekhira et al. (2018)
Wadi Mekkera	Deterministic modeling for the identification of the flood	HEC- HMS, Muskingum-Cunge	Benmansour and Haddouche (2019)
	Simulation of flood generation in the semi-arid region	MERCEDES (IRD)	Maref and Seddini (2018)
	Study of the uncertainty	HEC-HMS, GLUE approach	Lehbab-Boukezzi et al. (2016)
	propagation of floods model Muskingum and QdF model	HyfranPlus (INRS-ETE) Author program	Abbes and Meddi (2016)
	Hydrodynamic modeling describes the flash floods that characterize semiarid zones	Numerical simulation: P.G. and V.L. schemes	Korichi et al. (2016)
	Identification of potential risk areas	Numerical simulation: BSV equations, RKDG finite element scheme.	Atallah et al. (2016)
Wadi Ksob	Study of the Wadi Ksob flood of the 1994	Hydrodynamic simulation Code Rubar20 (IRSTEA)	Hasbaia et al. (2015)

(continued)

Table 3.1 (continued)

Study area City/ Catchment/ Wadi	Method/approach	Tools	References
Specific flood event analysis			
Bab El Oued	Analyzing the influence of urbanization and the meteorological hazard (event of 2001)	RuiCells	Menad et al. (2012)
Saf-Saf Basin	Study of the exceptional floods (1984, Skikda)	Analysis and description	Boulghobra (2012)

contrary to the first approach (hydrological and hydraulic simulation) which is based on projected events and unperfect models. However, the hydrogeological approach requires an enormous amount of data and more time, especially for the field survey.

The major observation is the missing of scientific contribution about urban flooding despite the prevalence of this type of flood. Urban sewer systems are not well studied, and only rural areas are analyzed. It could be due to the difficulty of this kind of study and the gap of available data.

The choice of the hydrological model is conditioned by the availability of climatic data. The hydrologic studies were just a statistical adjustment of time series or a simple rainfall-runoff transformation. The time step of available data is typically daily which is not suitable for rapidly occurring phenomenon. HEC-RAS, a 1-D Hydraulic model was commonly used and one of the simplest existing flood models. This simplicity is related to the considerable negligence of essential elements of flood hydraulics (Nkwunonwo et al. 2020).

The topographic information is generally extracted from low resolution (30 m × 30 m) digital elevation models (DEMs) given by SRTM products, which does not successfully capture the fluvio-morphological characteristics of the wadis that are narrow in nature.

Hydrological and hydraulic modelling of the flood inundation is an essential tool for better flood risk management. However, the unavailability of adequate data and detailed information needed by the researchers slows the flood modelling development in Algeria. These difficulties must be overcome firstly.

3.3 Flood Inventory in Algeria

The information about floods in this chapter was collected from different types of sources: technical reports, scientific publications, and databases. In order to inventory historical floods and their effects in Algeria, several works were carried

out. They provide information about fatalities, a brief description of the induced damage, and refer to other characteristics of floods (rain, flow, and water depth). Sardou et al. (2016) developed a flood's catalogue of north-western Algeria for the period between 1847 and 2014. They documented 127 events and found that 62.20% are classified as flash floods (Sardou et al. 2016).

The Civil Protection (CP) has the most complete information of occurred flood events since 1921. The main statistics of CP database are recapitulated in Fig. 3.1 and Table 3.2. Another inventory was produced and documented by the Algerian National Agency of Water Resources (ANRH) of the events from 1970 until 2000 (Lahlah 2000).

Other information was collected from the Dartmouth global archive of large flood events (dartmouth.edu) and the major flood events in FloodList (floodlist.-com). Globally, information of events characteristics is partial and often not accurate. One of the EM-DAT criteria to qualify hazards as disastrous is that the number of casualties must exceed 10 (Gaume et al. 2016): Table 3.3 and (Fig. 3.2) present the disastrous floods in Algeria.

By analyzing (Fig. 3.2), October is the month with the highest flood occurrence with 1141 recorded casualties (87% of the total death toll). In addition, most events are occurring in autumn and winter, appearing more frequently in the central regions of the country (Fig. 3.3).

ANRH agency classifies the main causes of floods in three major types: (i) exceptional weather situation (heavy rain, torrential rain), (ii) anthropogenic factors

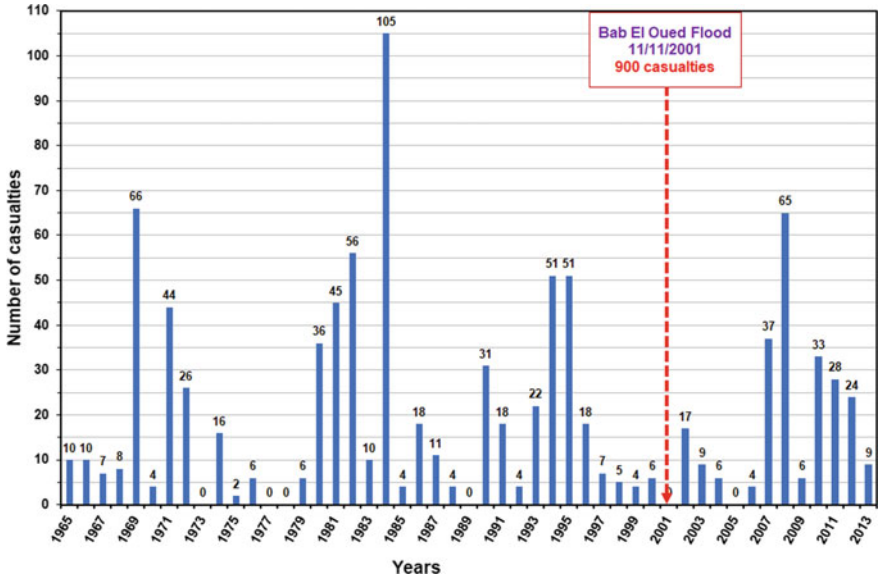

Fig. 3.1 Evolution of the number of flood-related casualties in Algeria (CP database, period 1965–2013)

Table 3.2 Statistics of floods occurred in Algeria from 1965 to 2013(CP database)

Parameters	Value
Number of events	1306
Event with human casualties	607
Total number of human casualties	1849
Number of casualties (period 2000–2011)	1014
Event with more than 10 casualties	27
Average number of casualties every year	10:20

Table 3.3 Disastrous floods with more than 10 casualties (1965–2013)

No.	Locations	Date	Casualties
1	Chlef	06/10/1966	63
2	Mascara (Ouled Sidi Ali)	01/01/1969	10
3	Biskra	01/09/1969	28
4	Batna	09/10/1969	28
5	Tizi Ouzou (Azzazga)	12/10/1971	40
6	Tizi Ouzou	28/03/1974	52
7	Alger	01/01/1980	11
8	Sétif (El Eulma)	01/09/1980	44
9	Tiaret (Sougueur)	24/09/1980	15
10	Annaba	11/11/1982	47
11	Djelfa (Birine)	22/08/1983	10
12	Ain Temouchent	01/01/1984	33
13	Jijel	29/12/1984	29
14	Skikda	30/12/1984	11
15	Ain Defla (Bordj El Amir Khaled)	01/01/1986	13
16	Sétif (Ain Azel)	06/02/1990	19
17	Relizan (Oued-Rhiou)	20/10/1993	22
18	BordjBou Arréidj	23/09/1994	16
19	Laghouat	28/10/1995	40
20	Adrar	14/01/1999	12
21	Chlef (Tedjna)	11/10/2001	15
22	Algiers (Bab El Oued)	11/10/2001	900
23	Tamanrasset, Reggane	09/08/2003	13
24	M'sila region	19/04/2007	13
25	Ghardaïa	01/10/2008	50
26	Béchar	08/10/2008	12
27	El Bayadh	01/10/2011	11

(iii) and geographic location (city crossed by Wadi or city at the foot of mountains). These three types are interconnected (Bahlouli 2010; Lahlah 2000). During the last decades, the Algerian authorities initiated 575 actions with an amount of 227 billion

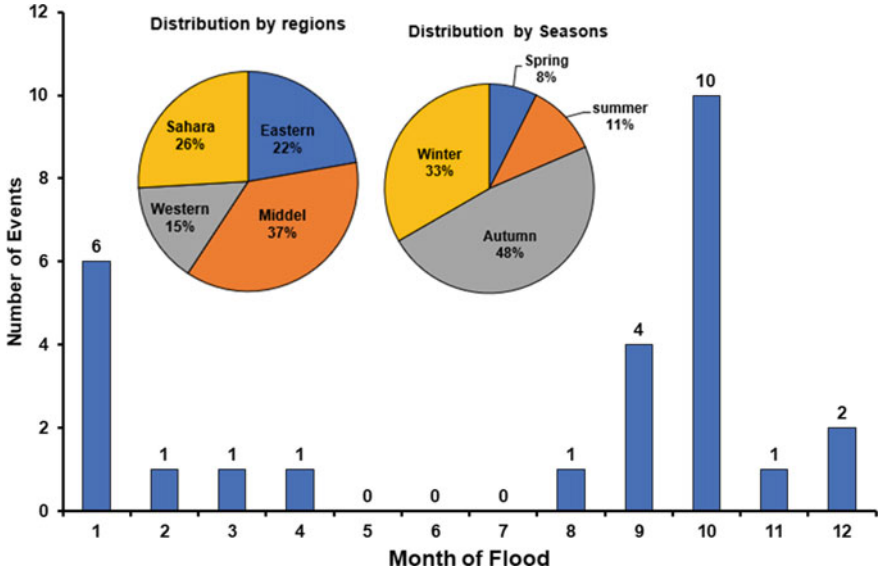

Fig. 3.2 Monthly, seasonal, and regional distributions of the disastrous floods in Algeria (1965–2013)

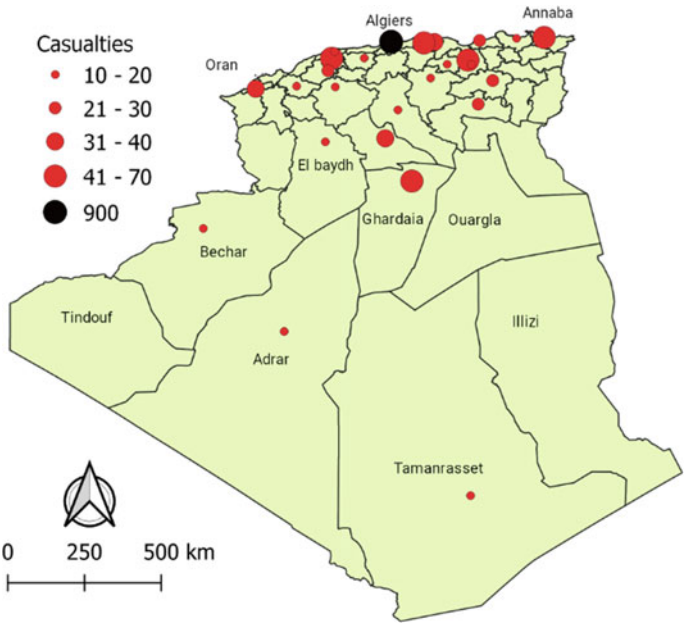

Fig. 3.3 Map of disastrous floods in Algeria (1965–2013)

DZD (1.75 billion US$) to mitigate floods. Hundreds of cities and locations were protected and an important number of Wadis were managed (MRE 2018).

3.4 Notable Flash Floods in Algeria

The two catastrophic flash flood events that marked the country during the 2000s are the Bab El Oued flash flood (2001, urban flash floods) and the Wadi M'zab flash flood (2008, UNESCO World Heritage Site flash floods).

3.4.1 Bab El Oued Flash Flood (Urban Flash Flood)

Bab El Oued is a municipality of Algiers that is located on the northern coastal façade. From 9th to 10th of November 2001, Bab El Oued was devastated by the worst flash flood in the Mediterranean and MENA regions (Gaume et al. 2016). This disaster caused 900 fatalities, 423 injuries, and catastrophic material damages estimated to exceed 300 million US$. Of the 38 floods disasters that hit North Africa from 1975 until 2001, 31% of the casualties died in this flood (Brauch 2003). This sad record tells of the gravity of this disaster.

Bab El Oued district is at the output of the Wadi Koriche catchment (9 km^2) (Fig. 3.4). This catchment is heavily urbanized in its downstream part and on the upstream ridges. Despite the inconvenient steep slopes, these areas were gradually urbanized in an uncontrolled manner (Fig. 3.5). Urbanization occupies approximately two-thirds of the watershed; the remaining third is occupied by forests and low vegetation areas (Menad et al. 2012).

Algiers was struck by a heavy rain during 36 h reaching 263 mm (Bouzaréah rainfall station). If the rains with remarkable intensities seem to be frequent in this region, this rain accumulation which has been widely studied (Argence et al. 2006, 2008; Menad et al. 2012; Thomas et al. 2011), has never been recorded before since 1908 (Menad et al. 2012). The associated return period of this exceptional event is 200 years (Cheikhlounis et al. 2009).

Menad et al. (2012) using the reduced discharges method (Gaume et al. 2009), suggest the value of the specific flow as 9–14 $m^3/s/km^2$. According to Gaume et al. (2016), the extreme peak discharge of the Bab El Oued flash flood is the greatest in the Mediterranean region (Fig. 3.6).

There is an agreement that effects generated by the heavy rainstorm were accentuated by heavy urbanization, degradation of cover of vegetation, and accumulation on the slopes of earth embankments which constituted mudslides (Fig. 3.7). The sediment volume was estimated from 0.8 to 1 million m^3 (Boutaoutaou 2007; Cheikhlounis et al. 2009; Menad et al. 2012).

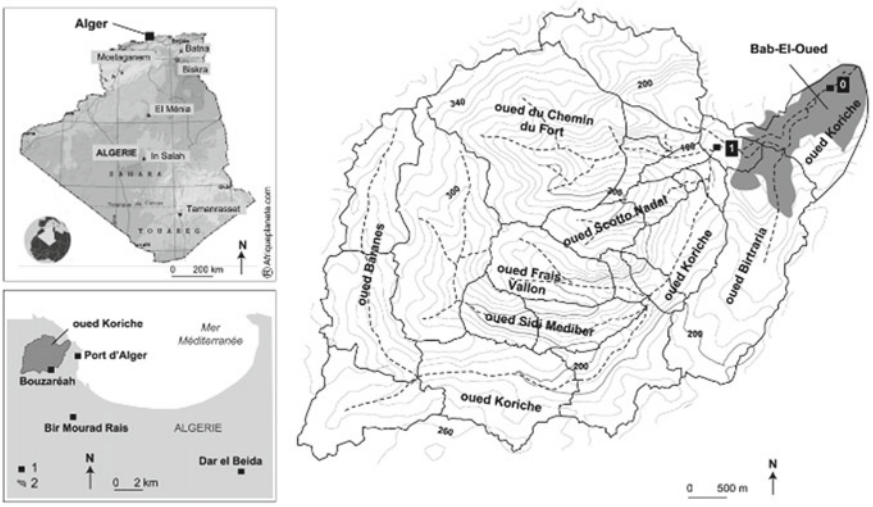

Fig. 3.4 Wadi Koriche catchment (Menad et al. 2012)

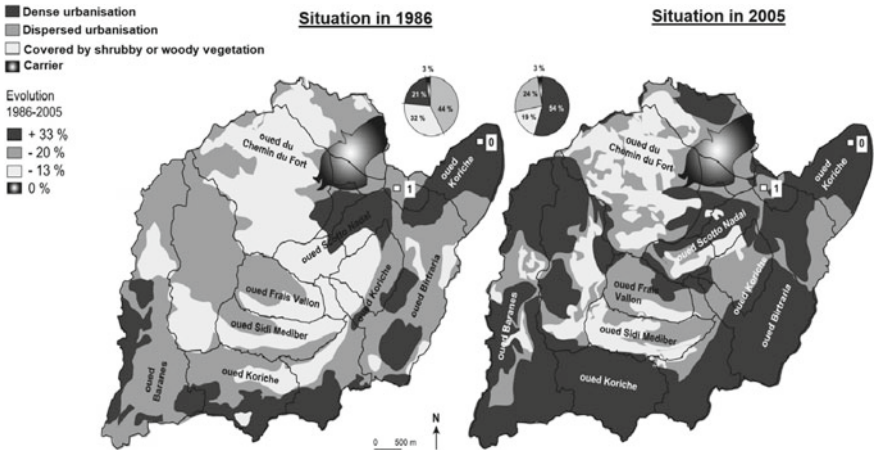

Fig. 3.5 Land cover change in the Oued-Koriche catchment (Menad et al. 2012)

3.4.2 Wadi M'zab Flash Flood (UNESCO World Heritage Site)

Ghardaïa is situated about 600 km south of Algiers in northern-central Algeria and lies on the left bank of M'zab River (Fig. 3.8). In 1982, for its settlement influencing urban planning, for its Ibadi cultural values, and a settlement tradition that has prevailed to the present century, the M'zab valley was registered as cultural property under the UNESCO World Heritage List (Sub-catchment).

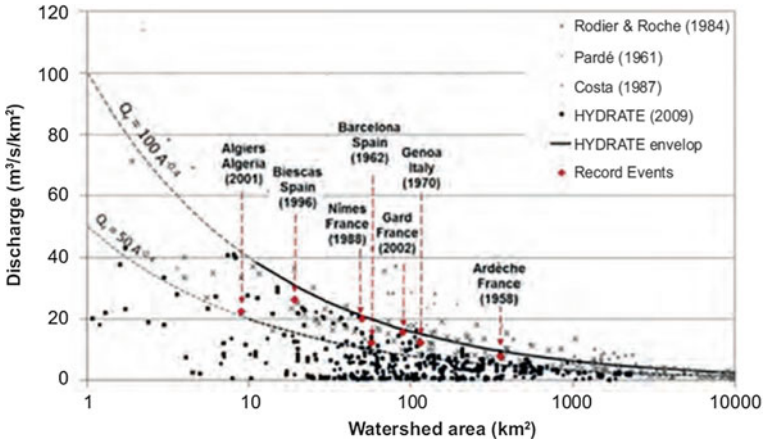

Fig. 3.6 The peak discharge of the Bab El Oued flash floods related to estimated world records since 1940 (Gaume et al. 2016)

Fig. 3.7 Flash floods of Bab El Oued (November 10, 2001)

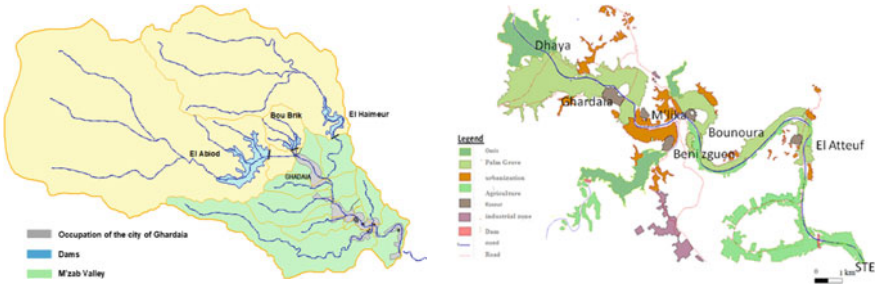

(b) Sub-catchment map *(a) Soil occupation map (Yamani et al. 2016)*

Fig. 3.8 Wadi M'zab-Ghardaia region

Fig. 3.9 Flash flood of Wadi M'zab in October 01, 2008

Ghardaïa is one of the most-arid regions affected by floods. The region lived, in October 1st, 2008, an extreme flood with a maximum discharge of 1600 m^3/s and a water depth exceeding 8 m (Fig. 3.9). Several studies in the literature can be found about this catastrophic event (Bendoudj et al. 2014; Bourenane et al. 2019; Yamani et al. 2016). This catastrophe resulted in an estimated number of 50 victims and 86 injured while leaving thousands homeless (MRE 2018).

The damage would have been more dramatic if the alert had not been launched at 4 A.M. from the ancestral alert system called: Oumanaa Al Sayel (flash flood sentinel) which is a community-based system for the management of the watershed. This system was designed in 1273. It is a very ingenious hydraulic system based on the principle of full and fair exploitation of rain water and its accurate distribution in all oasis groves. It also includes towers and installations that enable permanent monitoring of floods to prevent flood hazards (Ali Taleb and Souad 2020; Benmamar et al. 2016; Khelifa and Remini 2019).

According to the ANRH agency, the measurements of precipitations in the two days of the event accumulated to 79.7 mm, almost equaling the yearly precipitation. Floods were caused by heavy rains generating a water accumulation along 2 km of wadis and mudslides overrun the riverbanks of Wadi M'Zab. The floods were aggravated when a dam break took place 20 km upstream of the city releasing more than 900 m^3/s (Mimouni et al. 2019). The Algerian Space Agency (ASAL) has mapped the inundated areas of the event of October 1, 2008, using high-resolution satellite images and surface terrain model enhanced by GPS data (Benhamouda 2012) (Fig. 3.10).

The flood event value is extreme but still included in anticipated rainfall and discharge region statistics. The aggravation of the event comes from the huge amounts of deposits that raised the wadi bottom (1.50 m in some sections). The dam break had a secondary effect. Mimouni et al. (2019) concluded in their analysis of flood hazard of the Wadi M'zab valley, that there is an increase in the vulnerability due to the accelerating urbanization. This generates a serious problem in risk management. The ancestral alert system, despite being rudimentary and traditional, had a major role in reducing the damage.

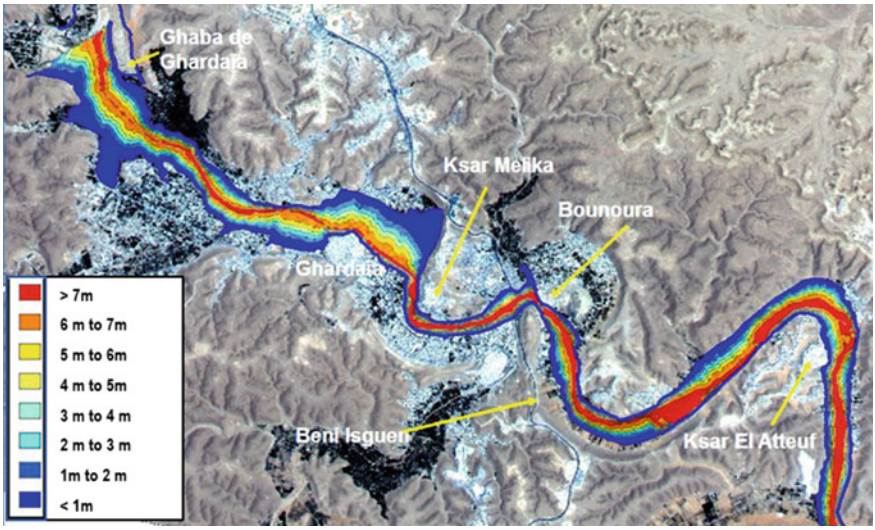

Fig. 3.10 Analysis and mapping of flooded areas in October 1st, 2008 (Benhamouda 2012)

3.5 Monitoring and Data Availability in Algeria

Algerian has an area of 2.38 million km^2 and it is divided in 17 large hydrographic basins. Two national organizations have a network of monitoring stations (Figs. 3.12 and 3.14). The two organizations are the National Office of Meteorology (NOM) and the Algerian National Agency of Water Resources (ANRH).

The network wish is currently managed by ANRH (Taibi 2012) is made of:

- 220 hydrometric stations (water level, Discharge, Sediment Concentration, Salinity, Sampling for river water quality analysis).
- 50 complete climatological station.
- 200 rain gauges (Rainfall intensity).
- 860 rainfall stations (Daily rainfall).

The network is almost entirely manual. With a view to future improvement, the ANRH have undertaken the task to automate the stations so that data is easily collected and transmitted (Figs. 3.11 and 3.12).

The ONM uses the following networks and types of stations (Halimi 2016):

- 84 professional observation stations, thirty-two (32) of which are in aerodromes. This network is distributed according to the international standards of the World Meteorological Watch (V.M.M) networks.
- 300 Climatological stations, of which 100 are automatic stations.
- 07 weather radars (200 km, radius) distributed in the north of territory (Fig. 3.13). This network comes with satellite resources to complete the

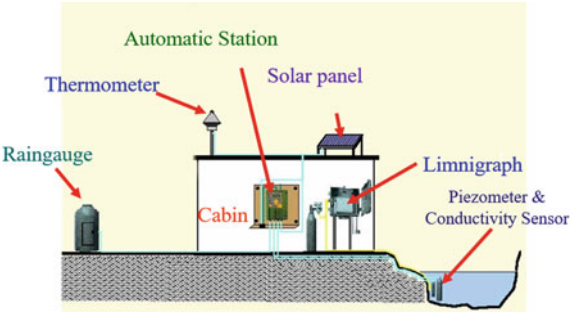

Fig. 3.11 An automatic station ANRH

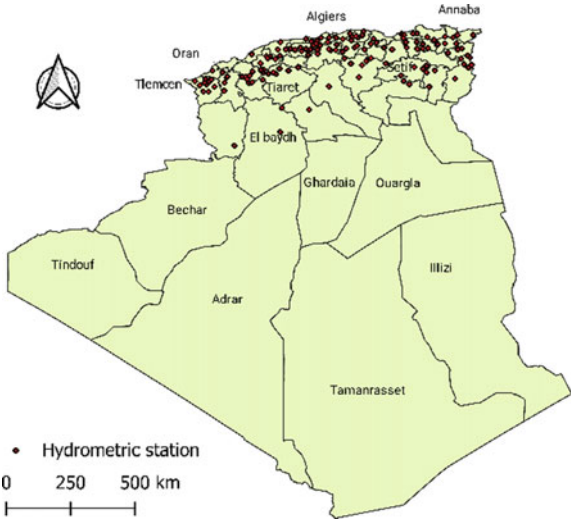

Fig. 3.12 Hydrometric stations in Algeria

meteorological observation network for monitoring cloudy systems (oriented towards aviation hazards) and rainy systems for agriculture, hydrology, and civil protection (Keblouti et al. 2015) (Fig. 3.14).

The quality of the data obtained from these two sources is reliable that is considered being collected with the necessary rigor. There is a problem with the length of the historical datasets provided both from hydrometric and pluviometric monitoring networks. Monitoring stations tend to be frequently interrupted, decommissioned, or simply abandoned. This leads to the presence of discrepancies and the occurrence of randomized gaps in the datasets which limits the availability of long synchronous time-series to capture long-term patterns.

It is important to note that most of hydrometric stations are implemented outside of urban areas, intended for water resource management purposes. However, no monitoring systems are dedicated to flood measurements.

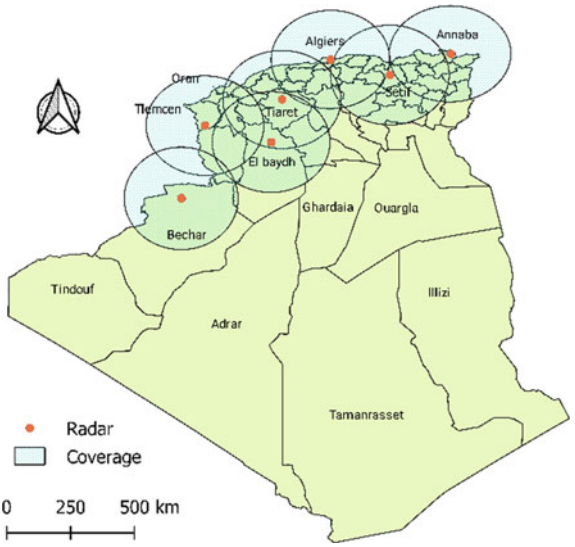

Fig. 3.13 Algerian weather radar network

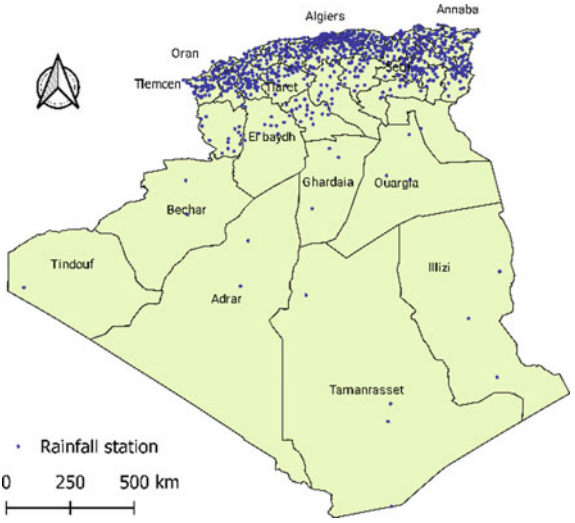

Fig. 3.14 Rainfall stations in Algeria (ONM & ANRH)

It would therefore be highly desirable to build a "national hydrometeorological network", endowed with stable and sufficient human, material, and financial resources to ensure the sustainability of the activity as well as the reliable quality of the data. To this end, it is therefore essential to bring together all the means to ensure continuous operational maintenance of the network. It would also be appropriate to strengthen the radar network, will supplement precipitation data, for purposes of flood prevention, warning systems, and real-time flood monitoring.

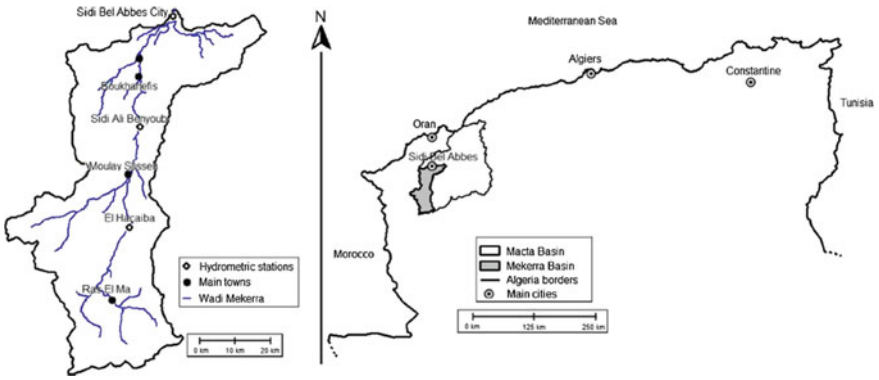

Fig. 3.15 Location of the Mekerra basin and its main gauging stations (Korichi et al. 2016)

3.6 Forecasting and Early Warning Systems

The Ministry of Water Resources (MRE) had a project intended to install warning systems in several cities of the country. The first operation of this type was initiated as a pilot project in Mekerra Basin and was implemented during the period 2009–2010 (Fig. 3.15).

A Flood Prediction Unit (UPI) has been established to manage flood forecasting processes in river basins. This unit is currently estimated to predict the floods of the Wadi Mekerra (basin of the Oued Mekerra), as a first step, then will be gradually generalized throughout the Algerian territory. Flood forecasting and warning systems integrate real-time management and data collection (automatic hydro-pluviometric stations) and apply and integrate hydrological and hydraulic models to provide forecasts of flows and levels. Water in the main sites of Oued Mekerra. The monitoring sytems is managed by ANRH.

The main goal of this project is to upscale rules and to establish procedures of flood risk forecasting and warning systems based on the results obtained and tested on a pilot case.

Flood Forecasting and Warning Monitoring Regulations exist nowadays which include:

- The context of the pilot project,
- The regulatory framework and the administrative framework,
- The basic hydrological elements and the definition of alert levels, maps, and tables to be consulted in the event of an alert by the organs of the ORSEC plan (Algerian emergency plan), the structure of the UPI (Flood Prediction Unit), and all stakeholders in the alert procedure, the current activity of the UPI, the activation of a standby state,

- The preparation of forecasts by the UPI on standby—alert communications, current data management—the relationship between the UPI and the ANRH including comments and recommendations.

Currently, according to the information collected, the system installed in Wadi Mekerra is not operational and no other system is installed.

3.7 Urbanization and the Increase in Vulnerability

Clearly, floods occur from natural processes, but they are not a natural disaster. Heavy rainfall is the flash floods trigger; all things considered, the damages depend on land use and expanded urbanization. The disasters that occurred in the last two decades showed the impact of urbanization in the improved cost of flash floods (Sect. 3.5).

Over time, Algeria has been subjected to rapid socio-economic modifications, which have resulted in urbanization concentration and population growth. The Algerian population expanded from about 11.3 million in 1960 to almost 43 million in 2019, quadrupling in 50 years. A disproportionate spatial redistribution has resulted in this demographic development. The population of the coastal areas and valleys is focused on the cities. In 2018, 90% of the population is located on 13% of the country's area. The urbanization rate went from 30.5% in 1960 to 72% in 2019 (Fig. 3.16).

Algeria experienced in the last decades, successive drought sequences and a higher urban need. Progressively, the limits of the wadis are unprotected, and urban settlement tend to occupy the wadi beds. In other cases, the main wadis-bed had been disturbed: piped, derived, or buried (Fig. 3.17). The increase in impervious areas results in changes in the hydrology of watershed (Shuster et al. 2005).

The disastrous consequences were the result of inconsiderate occupation of wadi beds (Freddy et al. 2016). These changes have induced a highly imperviousness and anthropogenic influences and growth in the urban vulnerability.

3.8 Floods and Climate Change

The climate variability and climate change remain the main causes of the frequent recurrence of floods over time. Algeria is considered North Africa's most sensitive country to climate change (Schilling et al. 2020). Several studies have been carried out on the assessment of climate change in some regions involving Algeria: (Tramblay et al. 2013)used an Extreme Precipitation (EP) index in the Maghreb region and concluded that in most stations, the rules of stationarity remain valid. The same conclusion has been reached by (Kharin et al. 2013) and (Ghenim and Megnounif 2016). In fact, the first showed that non-significant change occurred in

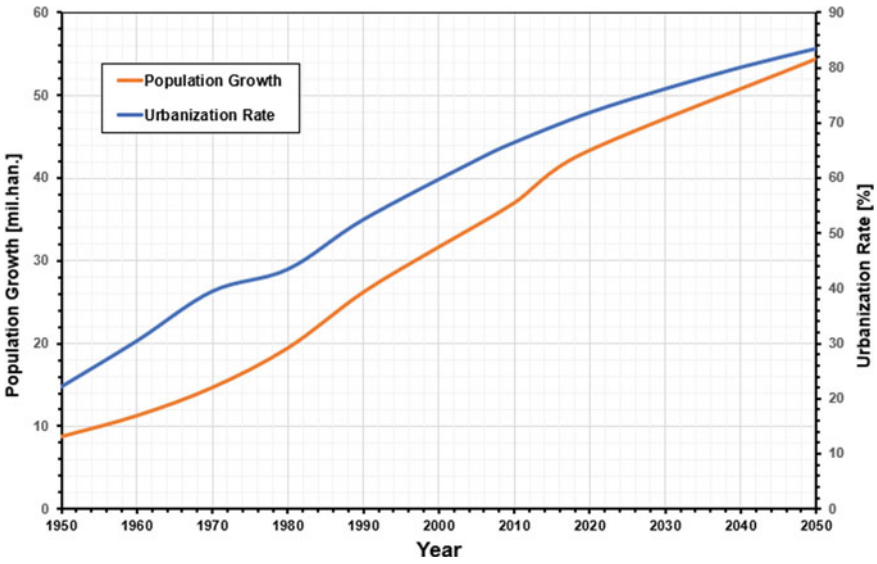

Fig. 3.16 Population growth and changes in urbanization rate

(b) *Aerial photography of Sidi Kaci city, El Tarf (2015)* (a) *Aerial photography of Sidi Kaci city, El Tarf (2004)*

Fig. 3.17 An example of the effect of urbanization: imperviousness anthropogenic influences generating a flood (Abdelmadjid et al. 2018)

EP by using Coupled Model Intercomparison Project 5 (CMIP5) models of global climate for the Representative Concentration Pathway (RCP) 8.5 scenarios, while the latter who studied the variability and trend of EP, found that no significant trend exists over 35 stations in northern Algeria. These findings support the idea that in Algeria, the EP is more influenced by local climatic processes and orography (Ghenim and Megnounif 2016; Tramblay et al. 2013).

3.9 Integrated Flood Risk Management Strategy in Algeria

The most human losses (1014, 77.64%) and economic damage occurred during the period between 2000 and 2011. This was a turning point for Algeria in flood protection. Consequently, the (MRE) has developed the National Flood Protection Strategy (NFPS) based on the deep analysis of the fifty most frequently flooded sites in different portions of the country. The NFPS categorized the flood types for the fifty sites as represented in (Fig. 3.18) (MRE 2018).

Rapid floods can be considered a sub-category of flash floods. Noticeably 1/3 of flood events are a flash floods and 56% of the events have significant sediment depositing risk, which makes them more devastating. The NFPS identified 689 areas with potential flooding risk (MRE 2018). Five level risks were retained in the NFPS (Fig. 3.19).

The NFPS promotes the Integrated Flood Risk Management (IFRM); as a strategic tool that allows an improved perception of the problem of flood risk management in a thorough and systematic manner (Fig. 3.20).

The IFRM is the main flood risk management policy adopted in Algeria for 2030. It encompasses the three main action areas, namely (i) preventive management measures (Preparation, Protection, Adaptation, Mitigation), (ii) control of the situation (limiting the extent of the phenomenon by managing the event), and (iii) recovery or post-flood measures to return to normal economic, social and environmental activity as quickly as possible (MRE 2018). The NFPS represents a major advance in the field of flood protection in Algeria.

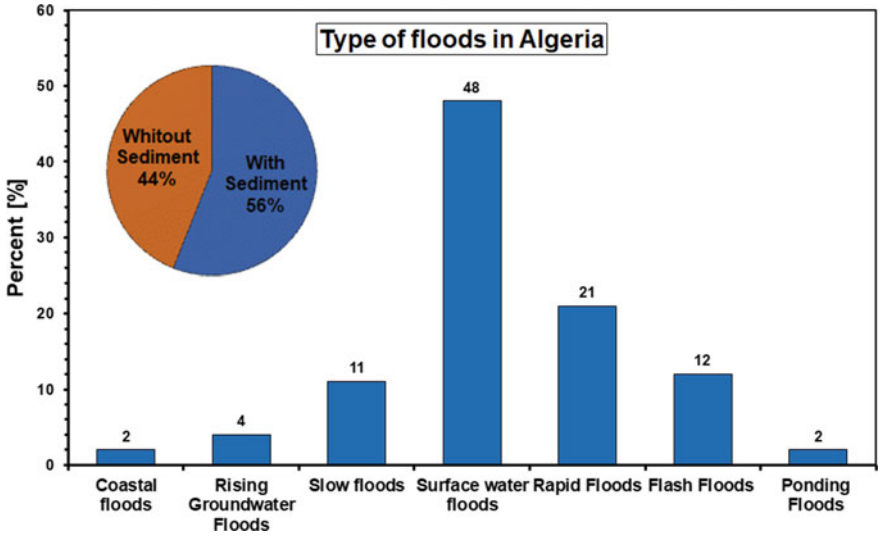

Fig. 3.18 Types of floods in 50 most frequent flooded areas

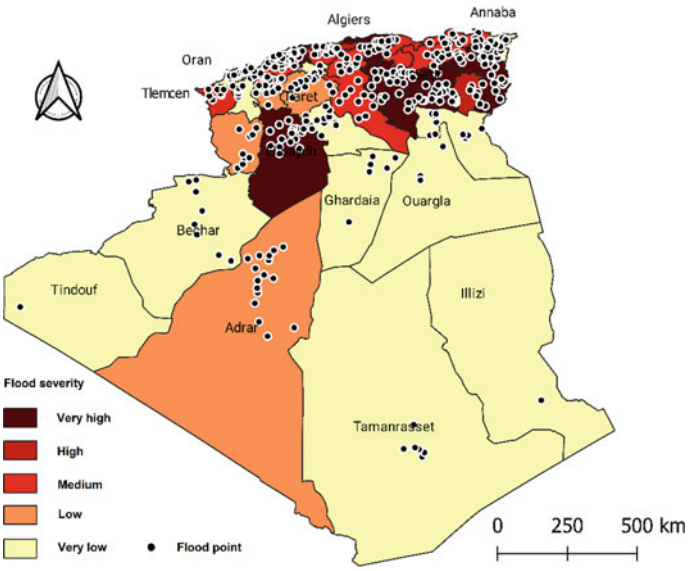

Fig. 3.19 Localization and classification of potential risk in the 689 areas

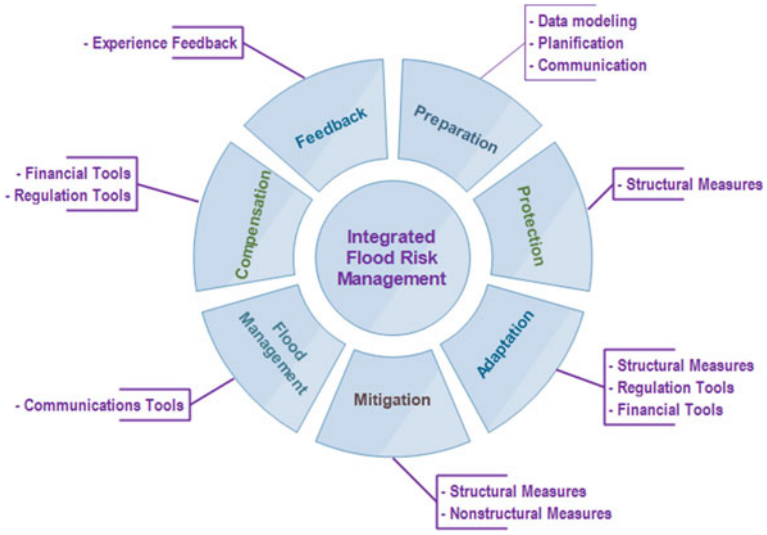

Fig. 3.20 Summary of the IFRM

3.10 Conclusion

The knowledge of floods, especially of flash floods is very limited in Algeria, such events are not well researched and documented in the country. This chapter aims to provide a clear insight and useful information on them for future studies.

Flood history in Algeria was recapped and the disastrous flood events were listed. Clearly, the country is very affected by floods with 1306 events and 1849 casualties. The most disastrous floods typically occur in autumn and winter, appearing more frequently in the central regions of the country. Information about floods is very important, which is why it is necessary to develop specific and detailed catalogs for historical floods. The two recent catastrophic flash floods are highlighted. The first is the Bab El Oued flash flood (2001). This is the deadliest event occurred in Mediterranean and MENA regions. This urban flash flood is an important case study. The second is the Wadi M'zab flash flood (2008) which occurred in UNESCO World Heritage Site of the valley of M'zab. The lesson to remember is that a rudimentary warning system can be very beneficial to reduce casualties.

In Algeria, 90% of population is concentrated in 13% of the country's area. The population growth and increase in urbanization are the drivers of the increasing vulnerability. This trend is projected to continue until 2050 and its effects need to be mitigated. In Algeria, the influence of climate change on floods is inexistent. The extreme precipitation is more influenced by local climatic erratic processes and orography. Modelling of the flood inundation can be a helpful tool for a better flood risk management strategy. All studies focused on rural regions. The used approaches and selected models are limited by the data availability.

The National Floods Protection Strategy have a big challenge to promote the Integrated Flood Risk Management, adopted in 2018 as the main Policy for 2030.

Acknowledgements We would like to express our deepest thankfulness to the MRE technical support. This work was established with the support of the MESRS-PRFU project to examine the possible effects of climate change on heavy rainfall, flooding, and urban drainage systems.

References

Abbes ASB, Meddi M (2016) Study of propagation and floods routing in north-western region of Algeria. Int J Hydrol Sci Technol 6:118–142. https://doi.org/10.1504/ijhst.2016.075578

Abdelmadjid B, Lekouaghet I, Boutaghane H (2018) Protection study against the flooding of the city of Sidi Kassi-North East Algeria. Paper presented at the 4th International Symposium on Flash Floods in Wadi Systems, 04–06 December 2018, Casablanca, Morocco

Abdessamed D, Abderrazak B (2019) Coupling HEC-RAS and HEC-HMS in rainfall–runoff modeling and evaluating floodplain inundation maps in arid environments: case study of Ain Sefra city, Ksour Mountain. SW Algeria Environ Earth Sci 78:586. https://doi.org/10.1007/s12665-019-8604-6

Ali Taleb B, Souad B-L (2020) Quantitative analysis and efficiency assessment of floodwater harvesting system in Arid Region: case of Touzouz ephemeral stream. Mzab Valley Water Res 47:54–64. https://doi.org/10.1134/s0097807820010029

Argence S, Lambert D, Richard E, Söhne N, Chaboureau JP, Crépin F, Arbogast P (2006) High resolution numerical study of the Algiers 2001 flash flood: sensitivity to the upper-level potential vorticity anomaly. Adv Geosci 7:251–257. https://doi.org/10.5194/adgeo-7-251-2006

Argence S, Lambert D, Richard E, Chaboureau J-P, Söhne N (2008) Impact of initial condition uncertainties on the predictability of heavy rainfall in the Mediterranean: a case study. Q J R Meteorol Soc 134:1775–1788. https://doi.org/10.1002/qj.314

Astite S, Medjerab A, Belabid N, El Mahmouhi N, El Wartiti M, Kemmou S (2015) Cartography of flood hazard by overflowing rivers using hydraulic modeling and geographic information system: Oued El Harrach case (North of Algeria) Revista de Teledetección 44:67–79. https://doi.org/10.4995/raet.2015.3985

Atallah Mh, Hazzab A, Seddini A, Ghenaim A, Korichi K (2016) Hydraulic flood routing in an ephemeral channel: Wadi Mekerra. Algeria Model Earth Syst Environ 2:1–12. https://doi.org/10.1007/s40808-016-0237-0

Bahlouli L (2010) Majors risks related to water. In: CRSTRA (ed) Drought: analysis and strategies adaptation, pp 44–74. Biskra, Algeria 21 et 22 Novembre 2010 (In Frensh)

Bekhira A, Habi M, Morsli B (2018) Hydrological modeling of floods in the Wadi Bechar watershed and evaluation of the climate impact in arid zones (southwest of Algeria). Appl Water Sci 8:185. https://doi.org/10.1007/s13201-018-0834-3

Bendoudj A, Touaibia B, Hubert P (2014) Flood's in the M'zab Valley (South Algeria): genesis and prediction. Le journal de l'eau et de l'environnement 24&25:20–34

Benhamouda F (2012) Spatial tool and GIS for flood prevention and management: experience and perspectives. In: Using space technology to serve the water sector, Alger, pp 18–30 (in Frensh)

Benmamar S, Poulard C, Berreksi A, Paquier A, Sioussiou R (2016) From the hydraulic system of ancestral M'Zab to Sustainable Urban Drainage Systems for the management of floods. Paper presented at the Novatech 2016, 9th International conference on Planning and technologies for sustainable URBAN WATER management, Lyon, France

Benmansour N, Haddouche D (2019) Deterministic modeling of the Mekerra wadi for the identification of the flood zone of Sidi Bel-Abbès (North-West Algeria) TSM 4:59–66. https://doi.org/10.1051/tsm/201904059

Boulghobra N (2012) The exceptional inundations of December 1984 in the Saf-Saf basin and Skikda city (North-eastern Algeria): Origins; spread and impacts Geographia Technica 7:14–22

Bourenane H, Bouhadad Y, Guettouche MS (2019) Flood hazard mapping in urban area using the hydrogeomorphological approach: case study of the Boumerzoug and Rhumel alluvial plains (Constantine city, NE Algeria). J Afr Earth Sci 160:103602. https://doi.org/10.1016/j.jafrearsci.2019.103602

Boutaoutaou D (2007) Debris flow and the Bab El Oued disaster. Paper presented at the Seminar on climate-related natural disasters, INRF, Oran, Algeria

Brauch HG (2003) Towards a fourth phase of research on human and environmental security and peace: conceptual conclusions. In: Security and Environment in the mediterranean. Springer-Verlag, pp 919–953

Cheikh lounis G, Chatelain JL, Mimouni O, Machane D (2015) Assessment of flood risk in Kniss Wadi catchment in Urbain Area Algiers—Algeria. In: Cham, 2015. Engineering geology for society and territory—volume 3. Springer International Publishing, pp 459–462

Cheikhlounis G, Machane D, Belhai D, Chatelain J-L, Dahmani K, Bichi N (2009) Floods and mudflows on November 11, 2001 in Bab El Oued, (Algiers). In: the 6th European congress on regional geoscientific cartography and information systems. Munich, pp 328–331

Freddy V, Saidi MEM, Douvinet J, Fehri N, Nasrallah W, Menad W, Mellas S (2016) Urbanization and land use as a driver of flood risk, pp 563–575

Gaume E et al (2009) A compilation of data on European flash floods. J Hydrol 367:70–78. https://doi.org/10.1016/j.jhydrol.2008.12.028

Gaume E, Borga M, Carmen Llasat M, Maouche S, Lang M, Diakakis M (2016) Mediterranean extreme floods and flash floods. In: The mediterranean region under climate change a scientific update. IRD Éditions, Marseille, France, pp 133–144. https://doi.org/10.4000/books.irdeditions.23181

Ghenim AN, Megnounif A (2016) Variability and trend of annual maximum daily rainfall in Northern Algeria. Int J Geophys 2016:6820397. https://doi.org/10.1155/2016/6820397

Hafnaoui MA, Madi M, Hachemi A, Farhi Y (2020) El Bayadh city against flash floods: case study. Urban Water J 1–6. https://doi.org/10.1080/1573062x.2020.1714671

Halimi L (2016) Presentation of the weather and climate observation network in Algeria availability of observed data. Paper presented at the climasouth seminar Algeria, Algeria, 11 et 12 Janvier 2016

Hammond MJ, Chen AS, Djordjević S, Butler D, Mark O (2015) Urban flood impact assessment: a state-of-the-art review. Urban Water J 12:14–29. https://doi.org/10.1080/1573062x.2013.857421

Hasbaia M, Adoui H, Paquier A (2015) Simulation of semiarid stream flow using the 1D model (Rubarbe), Case of Ksob Wadi in Algeria. Proc Environ Sci 25:120–126. https://doi.org/10.1016/j.proenv.2015.04.017

Keblouti M, Ouerdachi L, Berhail S (2015) The use of weather radar for rainfall-runoff modeling, case of Seybouse watershed (Algeria). Arab J Geosci 8:1–11. https://doi.org/10.1007/s12517-013-1224-7

Kharin VV, Zwiers FW, Zhang X, Wehner M (2013) Changes in temperature and precipitation extremes in the CMIP5 ensemble. Clim Change 119:345–357. https://doi.org/10.1007/s10584-013-0705-8

Khelifa A, Remini B (2019) The sharing of flood waters in the Ksours of Ghardaia and Berriane (Algeria) hydraulic study. GeoScience Eng LXV:44– 57. https://doi.org/10.35180/gse-2019-0011

Korichi K, Hazzab A, Atallah M (2016) Flash floods risk analysis in ephemeral streams: a case study on Wadi Mekerra (northwestern Algeria). Arab J Geosci 9:589. https://doi.org/10.1007/s12517-016-2624-2

Lahlah S (2000) Inventory of flood zones in Algeria—first approach

Lehbab-Boukezzi Z, Boukezzi L, Errih M (2016) Uncertainty analysis of HEC-HMS model using the GLUE method for flash flood forecasting of Mekerra watershed. Algeria Arab J Geosci 9:751. https://doi.org/10.1007/s12517-016-2771-5

Llasat MC et al (2010) High-impact floods and flash floods in Mediterranean countries: the FLASH preliminary database. Adv Geosci 23:47–55. https://doi.org/10.5194/adgeo-23-47-2010

Llasat MC, Llasat-Botija M, Petrucci O, Pasqua AA, Rosselló J, Vinet F, Boissier L (2013) Towards a database on societal impact of Mediterranean floods within the framework of the HYMEX project Nat Hazards Earth. Syst Sci 13:1337–1350. https://doi.org/10.5194/nhess-13-1337-2013

Loudyi D, Kantoush SA (2020) Flood risk management in the Middle East and North Africa (MENA) region. Urban Water J 17:379–380. https://doi.org/10.1080/1573062x.2020.1777754

Maref N, Seddini A (2018) Modeling of flood generation in semi-arid catchment using a spatially distributed model: case of study Wadi Mekerra catchment (Northwest Algeria). Arab J Geosci 11:116. https://doi.org/10.1007/s12517-018-3461-2

Menad W, Douvient J, Arnaud-Fassetta G (2012) Evaluating the influence of urbanised areas face to are markable meteorological hazard: the flood event of 9–10 November 2001 at Bab-el-Oued (Alger, Algeria). Géomorphol Relief Processus, Environn 3:337–350 (In French)

Mignot E, Li X, Dewals B (2019) Experimental modelling of urban flooding: a review. J Hydrol 568:334–342. https://doi.org/10.1016/j.jhydrol.2018.11.001

Mimouni O, Merchichi A, Lounis GC, Taleb B, Tahalaitit EH (2019) Flood hazard evaluation in Mzab Valley (Ghardaia—Algeria). In: Cham, 2019. IAEG/AEG annual meeting proceedings, San Francisco, California, 2018—volume 5. Springer International Publishing, pp 113–122

MRE (2018) Flood prevention strategy. Paper presented at the national meeting on disaster risk management, 22 et 23 Octobre 2018 (In Frensh)

Nkwunonwo UC, Whitworth M, Baily B (2020) A review of the current status of flood modelling for urban flood risk management in the developing countries. Sci Afr 7:e00269. https://doi.org/10.1016/j.sciaf.2020.e00269

Price C et al (2011) Using lightning data to better understand and predict flash floods in the Mediterranean. Surv Geophys 32:733. https://doi.org/10.1007/s10712-011-9146-y

Sardou M, Maouche S, Missoum H (2016) Compilation of historical floods catalog of northwestern Algeria: first step towards an atlas of extreme floods. Arab J Geosci 9:455. https://doi.org/10.1007/s12517-016-2490-y

Schilling J, Hertig E, Tramblay Y, Scheffran J (2020) Climate change vulnerability, water resources and social implications in North Africa. Reg Environ Change 20:15. https://doi.org/10.1007/s10113-020-01597-7

Shuster WD, Bonta J, Thurston H, Warnemuende E, Smith DR (2005) Impacts of impervious surface on watershed hydrology: a review. Urban Water J 2:263–275. https://doi.org/10.1080/15730620500386529

Taibi R (2012) Presentation of the ANRH ABH. http://www.abhcsm.dz/Comm_Coll_2012/Mr.TAIBI_Rachid_ANRH_Alg%C3%A9rie.pdf. Accessed 28/09/2020

Teng J, Jakeman AJ, Vaze J, Croke BFW, Dutta D, Kim S (2017) Flood inundation modelling: a review of methods, recent advances and uncertainty analysis. Environmen Model Softw 90:201–216. https://doi.org/10.1016/j.envsoft.2017.01.006

Thomas W, Baier F, Erbertseder T, Kaästner M (2011) Analysis of the Algerian severe weather event in November 2001 and its impact on ozone and nitrogen dioxide distributions. Tellus B Chem Phys Meteorol 55:993–1006. https://doi.org/10.3402/tellusb.v55i5.16392

Tramblay Y, El Adlouni S, Servat E (2013) Trends and variability in extreme precipitation indices over Maghreb countries Nat Hazards Earth. Syst Sci 13:3235–3248. https://doi.org/10.5194/nhess-13-3235-2013

WorldBank (2014) Natural disasters in the Middle East and North Africa: a regional overview

Yamani K, Hazzab A, Sekkoum M, Slimane T, Korichi K, Hazzab A, Atallah M (2016) Flash floods risk analysis in ephemeral streams: a case study on Wadi Mekerra (northwestern Algeria). Arab J Geosci 9:589. https://doi.org/10.1007/s12517-016-2624-2 Modeling Earth Systems and Environment 2:147 https://doi.org/10.1007/s40808-016-0183-x

Zaïri Y (2018) Flood risk mapping in the region of Ouled Ben Abdelkader in the Wilaya of Chlef, Northern Algeria. In, Cham, 2018. Recent advances in environmental science from the Euro-Mediterranean and surrounding regions. Springer International Publishing, pp 879–881

Part II
Hydrometeorology and Climate Changes

Chapter 4
Assessing the Impact of Climate Change on Temperature and Precipitation Over India

Sridhara Nayak and Tetsuya Takemi

Abstract This study explores a comprehensive assessment of future climate change in terms of the climatologies, distribution patterns, annual cycles, and frequency distributions of temperature and precipitation over India by analyzing 190 mega-ensemble experimental results. The results indicate that the annual mean surface temperatures over Indian regions are typically 25 °C or higher in the present climate (1951–2010) and are expected to increase by 3–5 °C in the future climate (2051–2110). Some desert regions in the west and tropical humid climate types in the central and south regions of the country show possible temperature increases of 4–5 °C, while the temperatures over the subtropical humid climates in the north and east regions of the country show increases of 3–4 °C. The precipitation amounts over the arid and semiarid climate types in the western region and over some tropical rainforest climate zones in the southwest region show increases of 0.5 mm d^{-1} in the future climate, and the precipitation amounts over the temperate, rainy climate types in the northeast region show increases of more than 1 mm d^{-1}. This study also discusses future changes in various climatic variables, including vertical velocity, air temperature, specific humidity, cloud cover, and relative humidity.

Keywords Climate change · Indian future climate · Large ensemble · AGCM

S. Nayak (✉) · T. Takemi
Disaster Prevention Research Institute, Kyoto University, Gokasho, Uji, Kyoto 6110011, Japan
e-mail: nayak@storm.dpri.kyoto-u.ac.jp

T. Takemi
e-mail: takemi@storm.dpri.kyoto-u.ac.jp

T. Sumi et al. (eds.), *Wadi Flash Floods*, Natural Disaster Science and Mitigation Engineering: DPRI Reports, https://doi.org/10.1007/978-981-16-2904-4_4

4.1 Introduction

According to the recent reports of the Intergovernmental Panel on Climate Change (IPCC), climate change is anticipated to play a crucial role in increasing or intensifying natural disasters on Earth, particularly extreme weather events (IPCC 2014). Climate change has therefore become one of the major concerns in the world due to its impact on socioeconomic development, and the effects of climate change are mostly reflected in the increase in surface temperature and the changes in precipitation patterns and other climatic features (Pall et al. 2007; O'Gorman and Schneider 2009; Guhathakurta et al. 2011; IPCC 2012, 2014; Takemi et al. 2016).

India is a land of diverse topographies and climate types. The topography in India is characterized by various mountain ranges, plains, high plateaus, coastal plains, and deserts. The mountain ranges of India include the Western Ghats in the southwest, the Eastern Ghats in the southeast, the high Himalayan range in the north, the Aravalli Range in the northwest, and the Vindhya and Satpura Ranges in the central region. The Indo-Gangetic Plains occupy most of the central, eastern and northern parts of India, and the Thar Desert occupies most of the western part. The high plateaus of India comprise the Chota Nagpur Plateau in the east, the Deccan Plateau in the south, and the Malwa Plateau in the west. The coastal plains of India are surrounded by the Bay of Bengal and the Arabian Sea. Because of such topographical and physical variations, the climate of India consists of a wide range of climatic types, from the alpine Himalayan region in the north to the tropics in the south, including tropical rainforest, tropical monsoon, tropical wet, tropical arid, and semiarid, savanna, temperate rainy, steppe, subtropical humid, alpine and desert climate types. The major climate types in India include a desert climate in the west (less than 300 mm $year^{-1}$ rainfall), a wet climate in the tropics (approximately 2000 mm $year^{-1}$ rainfall), a wet-dry climate in the tropics (normally above 18 °C and 1500 mm $year^{-1}$ rainfall), a humid climate in the subtropics (within 0–27 °C and 1000–2500 mm $year^{-1}$ rainfall) and an alpine climate type with glaciers in the north. Therefore, understanding the climates of tropical, subtropical, temperate, and arid/semiarid regions are key to understanding the climate of India. Furthermore, understanding how global climate change affects the climate of India will provide profound knowledge on the impacts of global warming on regional-scale climates.

Occasional occurrences of natural disasters such as droughts, floods, coastal erosion, and landslides are also part of life in this land and cause severe and widespread damage (IPCC 2012, 2014). These disasters are mainly associated with weather extremes and are strongly determined by the temperature and precipitation characteristics over the target areas (e.g., Guhathakurta et al. 2011; Ojha et al. 2013). Therefore, understanding the distributions of temperature and precipitation over India is very important not only for the present climate but also for future developmental planning and decision-making aimed at resisting future climate change issues.

There have been a number of studies (Nayak and Mandal 2012; Kumar et al. 2013; Prakash et al. 2015; Kishore et al. 2016; Akhter et al. 2017; Maity et al.

2017a, b; Nayak et al. 2017, 2018; Nayak and Mandal 2019) that have investigated the distributional patterns and climatologies of temperature and precipitation over the Indian region from observational, reanalysis, and modeled datasets. In a recent study, Nayak et al. (2019) analyzed precipitation and temperature climatologies and distributions over India for the period 1981–2010 and highlighted that the 30-year mean precipitation climatology over India corresponds to ~ 3 mm d^{-1} and the 30-year mean annual temperature over India corresponds to 23.15 °C. The climate signals during the twentieth century over India also confirm remarkable changes in precipitation patterns and an increasing surface temperature trend (Sinha Ray and Srivastava 1999; Sharma et al. 2004; Dash and Hunt 2007; Niyogi et al. 2010). Kothawale and Rupa Kumar (2005) reported an increase in the mean annual temperature over India at a rate of 0.05 °C per decade during the period 1901–2003. Jain and Kumar (2012) documented a warming trend in the annual mean, minimum and maximum temperatures at rates of 0.51, 0.27, and 0.72 °C per century, respectively, from 1901–2007. Rao et al. (2014) also highlighted an increase in the annual minimum temperature over India of 0.24 °C per 10 years during the period 1971–2009. On the other hand, studies of annual precipitation show mixed trends (decreasing over some regions and increasing over some regions) over Indian regions during the period 1901–2003 (e.g., Kothawale and Rupa Kumar 2005; Guhathakurta and Rajeevan 2008). Kumar et al. (2010) also observed similar trends in annual precipitation over Indian regions during the period 1871–2005.

Although many studies are available that have assessed past temperature and precipitation distributions and trends over India, a limited number of studies have focused on future climate changes over India. Kumar et al. (2013) highlighted possible warming over India of 1.5 °C by the end of 2050 and of 3.9 °C by the end of twenty-first century under the SRES A1B climate scenario compared to the temperature in 1970–1999. Patwardhan et al. (2018) also documented a possible increase in surface temperature over India of 4–5 °C towards the end of the twenty-first century under the SRES A1B scenario. Patwardhan et al. (2018) reported increases in summertime (Mar–May) temperatures of 1.6–4.1 °C over the northwest and west-central regions, of 1.7–4.4 °C over the central northeast region, and of 1.2–3.8 °C over the northeast and peninsular regions of India by the 2080s under the SRES A1B scenario with respect to the temperatures recorded in the 1970s. Chaturvedi et al. (2012) highlighted possible increases in precipitation amount over India by 4–5% by 2030 and 6–14% by 2080 under the RCP6.0 and RCP8.5 scenarios compared to the amounts in 1961–1990. Akhter et al. (2017) also documented possible increases in precipitation amounts over various Indian regions during the 2020s, 2050s, and 2080s under the RCP4.5 and RCP8.5 scenarios. Akhter et al. (2017) highlighted increases in precipitation amounts by 12–30% over some regions of northwest India, by 3–30% over some regions of western India, by 5–18% over a few parts of northeast India and by 6–24% over some regions of southern India under the RCP4.5 and RCP8.5 scenarios. All these studies clearly indicate possible increases in surface temperatures and precipitation amounts over Indian regions towards the end of the twenty-first century.

Recently, Mizuta et al. (2017) conducted mega-ensemble global climate simulations for 6000-year historical and 5400-year future (4 °C warming) climates with 100 experiments for the present climate (1951–2010) and 90 experiments for the future climate (2051–2110) by using the Meteorological Research Institute (MRI) Atmospheric General Circulation Model (AGCM) at a 60-km spatial resolution. A number of recent studies (e.g., Endo et al. 2017; Iizumi et al. 2018; Kusunoki 2018; Fujita et al. 2019) have used these mega-ensemble simulations to predict various aspects of the historical climate over different regions of the world and assess future climate change projections. Based on the limited previous studies over India, it is expected that the surface temperatures and precipitation amounts over India would increase in the future climate. Thus, understanding future climate change projections over India has become crucial for future developmental planning and monitoring climate risks. In this sense, the abovementioned mega-ensemble climate simulations should add new insights to future assessments of climate change over India because ensemble analysis always reduces uncertainties in the context of climate risk management. Thus, an attempt is made to explore a comprehensive assessment of climate change over India by analyzing the 190 mega-ensemble experimental results in two climate periods (1951–2010 and 2051–2110) and discussing the climatologies, distribution patterns, annual cycles, and frequency distributions of temperature and precipitation over India in the past 60 years and their future changes in the next 100 years.

4.2 The d4PDF and Analysis Procedures

The hourly precipitation and daily temperature datasets used in this study were obtained from 100 experiments of the present climate (1951–2010) and 90 experiments of the future climate (2051–2110 with +4 °C warming) from MRI-AGCM simulations at a 60-km resolution. A list of these 190 ensemble experiments is given in Table 4.1. This mega-ensemble climate simulation dataset is known as d4PDF (database for policy decision making for future climate change), and the database was collected using various initial conditions and small perturbations of sea surface temperatures (SSTs) for 6000-year historical and 5400-year future (4 °C warming) climate simulations (Mizuta et al. 2017). Here, the 6000-year historical climate simulations refer to 100 ensemble historical experiments comprising

Table 4.1 List of 190 ensemble experiments conducted by AGCM

Model	Climate period	Total number of ensemble experiments	Resolution
MRI-AGCM	Present (1951–2010)	100	60 km
	Future (2051–2110, with 4 °C warming)	90	

Source (Data source) Mizuta et al. (2017)

60 years each, totaling 100 × 60 years of simulations. Similarly, the 5400-year future climate simulations refer to 90 ensemble future experiments comprising 60 years each, totaling 90 × 60 years of simulation.

Asian precipitation-highly resolved observational data integration towards evaluation (APHRODITE) daily temperature and precipitation datasets at a 0.25° × 0.25° grid box for the period 1961–2007 are also used to validate the model-simulated temperature and precipitation results in the present climate. The detailed methods for the preparation of the APHRODITE temperature and precipitation data are described in Yasutomi et al. (2011) and Yatagai et al. (2012), respectively.

As described in the introduction, this study is focused on climate change over India. The topography of India and the surrounding regions is demonstrated in Fig. 4.1. A tropical rainforest climate extends in the southern and western coastal parts of the Indian subcontinent, surrounded by monsoon and savanna climate regions in the central, east, and south. In the north and northeastern parts of India, a rainy temperate climate exists. In the western parts of India, there are steppe and some arid/semiarid climate regions. The tropical humid climate type includes the tropical wet (no dry season), tropical monsoon (short dry season), and tropical wet-dry (dry in winter) climate types. The dry climate consists of subtropical steppe and desert climate types and is mostly arid/semiarid and dry. The humid subtropical (warm summer but no dry season), Mediterranean (dry, hot summer), and west coast (no dry season but warm and cool summer) climate types are included in warm temperate climates.

In the present analyses, the ensemble annual mean climatologies, annual cycles, and frequency distributions of temperature and precipitation over India are first

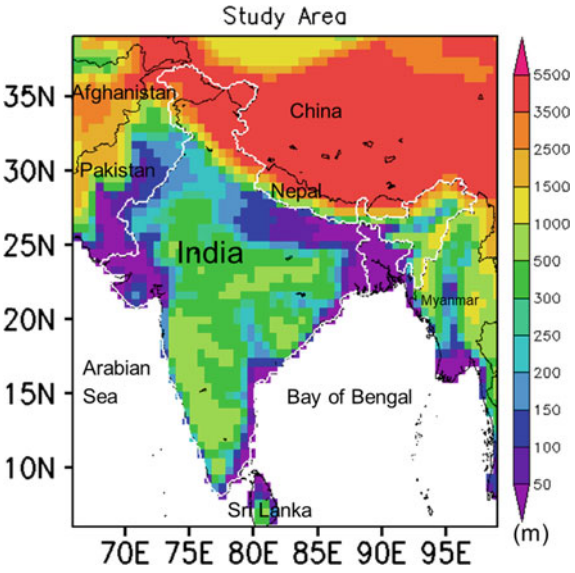

Fig. 4.1 Topography of the area. The Indian Ocean is located with white on the map. *Source* (Data source) Mizuta et al. (2017)

derived for the period 1961–2007 (48 years) from the AGCM simulations and are then compared with the APHRODITE observations to validate the d4PDF results over the Indian region. Then, similar analyses of temperature and precipitation are performed from the AGCM simulations for two climate periods of 60 years each: 1951–2010 for the present climate and 2051–2110 for the future climate. The climatologies of other climatic variables, including the vertical velocity, air temperature, specific humidity, cloud cover, and relative humidity, are also analyzed and discussed in this study.

4.3 Validation of d4PDF Data Over India

Figure 4.2 shows the temperature climatology for the period 1961–2007 from the ensemble mean of the AGCM experiments and that from the APHRODITE observations. The AGCM-simulated temperatures show that the annual mean surface temperatures over Indian regions, except over a few regions of north India, correspond to mostly 25 °C or higher during 1961–2007 (Fig. 4.2a, b). The lowest temperatures, which are approximately 0 °C or less, are noticed over some regions in northern India, and the highest temperatures of approximately 27 °C or greater are seen over some regions in southern and western India during this period. Similar temperature variations are also noticed in the APHRODITE observations except over a few regions in southern and western India (where the temperatures are ~ 2 °C higher). A comparison between the AGCM-simulated climatology and the APHRODITE-observed climatology indicates that the overall temperature climatology over India is well-represented by the model. The individual ensemble climatology also shows similar results, with standard deviations in the range of 0.5–0.15 °C from the means (Fig. 4.2c). A comparison between the temperature climatology from the ensemble mean of the AGCM and that from the observations indicated that the AGCM simulations have an overall cold bias over India. The AGCM shows a large cold bias over the northern and northeastern mountainous areas; however, the magnitude of the model bias over most of the Indian regions is in the range of −1 to 0.5 °C (Fig. 4.2d). The spatial correlation coefficient between the simulated and observed temperature climatologies over India is 0.99.

The distribution of annual mean precipitation over most of the regions in central, eastern, and northeastern India shows approximately 3–5 mm d^{-1} of precipitation during 1961–2007 in the AGCM ensemble simulation and approximately 1–3 mm d^{-1} over most of the other parts of India (Fig. 4.3a, b). A few areas over the northeastern regions, including the Western Ghats, received the highest amounts of precipitation (>7 mm d^{-1}) during this period. The APHRODITE observations also show mostly the same amounts of precipitation over these regions. The precipitation climatology in each individual simulation also shows similar results, with standard deviations within 0.05–0.25 mm d^{-1} compared to the means (Fig. 4.3c). The ensemble mean precipitation climatology obtained by the AGCM shows a wet bias of 0–1 mm d^{-1} over most of the regions of central, eastern, southern, and

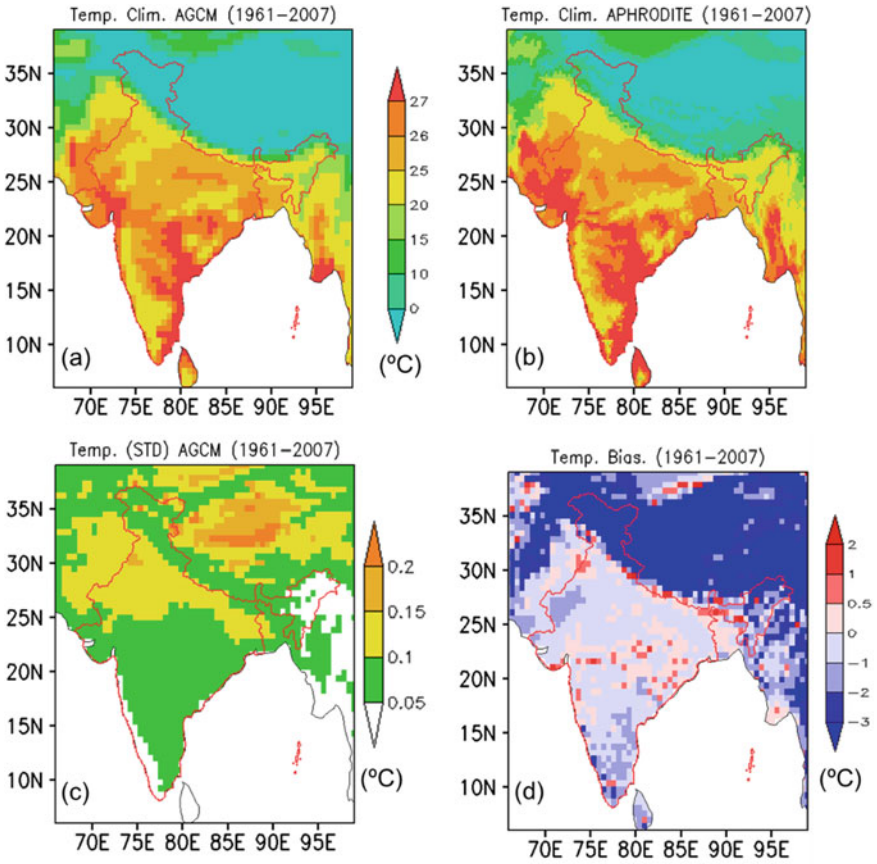

Fig. 4.2 Temperature climatologies derived from **a** the AGCM ensemble mean and **b** APHRODITE for the 1961–2000 period. **c** Standard deviations (STD) of the climatologies of temperature derived from all ensemble members. **d** Model biases in the temperature climatology. *Source* (Data source) Mizuta et al. (2017)

western India, while a large wet bias is noticed over some regions of northern, northeast, and southcentral India (Fig. 4.3d). The spatial correlation coefficient between the simulated and observed precipitation climatologies over India is 0.76.

The annual cycles and normal probability distribution functions (PDFs) of the monthly mean temperatures over India during 1961–2007 from the AGCM model simulations and those from the APHRODITE observations are presented in Fig. 4.4. The monthly mean temperature climatologies over India from the AGCM simulations indicate that the lowest temperature over India corresponds to ∼15 °C during December–January and the highest temperature corresponds to approximately 29 °C in May (Fig. 4.4a). The PDFs from monthly mean temperatures

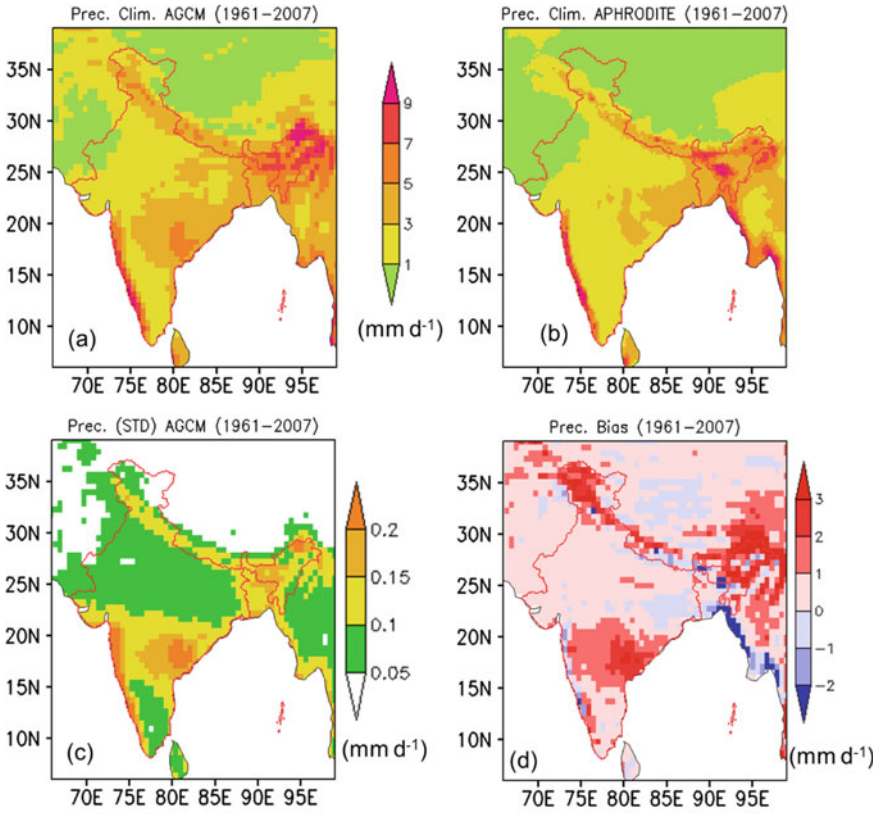

Fig. 4.3 Precipitation climatologies derived from **a** the AGCM ensemble mean and **b** APHRODITE for the period 1961–2000. **c** Standard deviations (STD) of the climatologies of precipitation derived from all ensemble members. **d** Model biases in the precipitation climatology. *Source* (Data source) Mizuta et al. (2017)

indicate that the temperature over India in most of the months remained at approximately 22 °C during 1961–2007 (Fig. 4.4b).

The temperature patterns seen in d4PDF can be confirmed with the observed temperatures from APHRODITE, but the model values are underestimated by approximately 2 °C. Each individual ensemble simulation also shows similar temperature characteristics over India. The annual cycle of the precipitation climatology over India during 1961–2007 shows that India receives the highest amount of precipitation (240 mm or higher) in July (Fig. 4.4c). Both the AGCM model and APHRODITE observations show the same features qualitatively, although the AGCM overestimates the precipitation amount by approximately 20–30 mm in some months. The precipitation amounts for May, June, September, and December are well-captured by the model and have good agreement with the observations. The *p*-value between the observed precipitation amounts and the

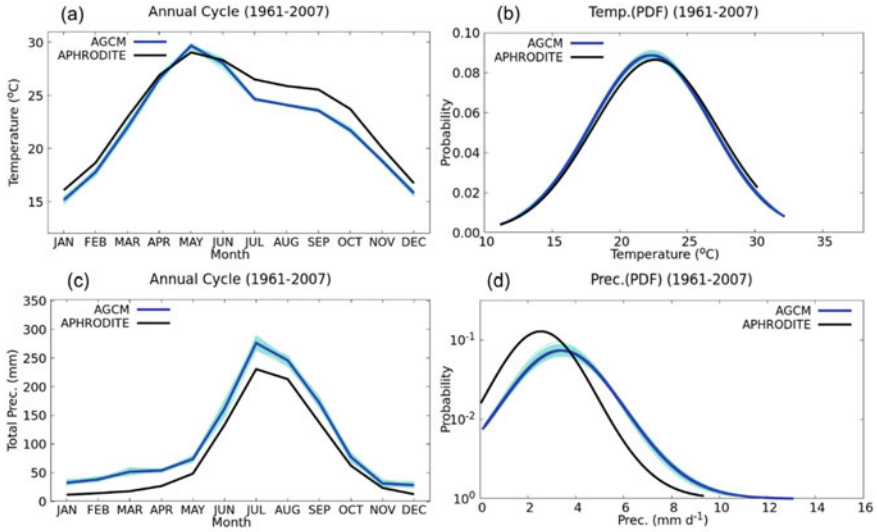

Fig. 4.4 Annual cycles and probability distributions (PDFs) over India derived from the AGCM ensemble and APHRODITE observations for the period 1961–2007. The upper panels (**a**–**b**) correspond to the results for temperature, and the lower panels (**c**–**d**) correspond to the results for precipitation. The thin lines in the figures correspond to the results for each ensemble member. *Source* (Data source) Mizuta et al. (2017)

d4PDF simulations was tested considering the null hypothesis as an equal mean with a 99% significance level; the *p*-value was found to be 0.45, which is sufficiently higher than 0.1. We thus fail to reject the null hypothesis. In other words, the differences between the observed and simulated precipitation amounts are not significant. The PDFs of monthly precipitation intensities in the AGCM simulations show precipitation intensities of approximately 4 mm d^{-1} (or $\sim$120 mm precipitation considering 30 days in a month) in most months, while the precipitation intensities are approximately 3 mm d^{-1} in the APHRODITE observations (Fig. 4.4d). Similar monthly precipitation features over India are also noticed in each individual simulation.

Overall, the AGCM-simulated mean temperature and precipitation climatologies, annual cycles, and frequency distributions are in good agreement with the APHRODITE observations over the Indian region.

4.4 Climate Change Over India Under Global Warming

4.4.1 Projected Changes in Temperature Distribution

The spatial distributions of the temperature climatologies derived from the AGCM ensemble mean for the periods 1951–2010 and 2051–2110 are presented in Fig. 4.5. The annual mean surface temperature over a large part of India is noticed to be mostly 25 °C or higher in the period 1951–2010 and is expected to be mostly 27 °C or higher in the period 2051–2110 over the same regions (Fig. 4.5a, b). The results show a possible warming of 3–5 °C over the entire Indian region in the period 2051–2110 with reference to the period 1951–2010 (Fig. 4.5c). The temperatures over central and northwest India are expected to increase by 4–5 °C in the future climate, while the temperatures over a few regions of north India are projected to rise by 6 °C or more.

Figure 4.6 represents the annual cycles and frequency distributions of the monthly mean temperatures over India in two climate periods and their projected changes. The results indicate that the mean temperature over India in the future climate is expected to vary from ∼20 °C in December–January to 34 °C in May (Fig. 4.6a). Each individual ensemble member also shows a similar pattern of monthly temperature over India. The monthly mean temperature is expected to increase by ∼4 °C during July–September and by ∼5 °C during October–June under the future climate (Fig. 4.6b). The normal probability distribution functions indicate that the monthly temperature over India is expected to shift by approximately +5 °C in the future climate (Fig. 4.6c). The temperatures over India in most months are expected to shift from ∼22 °C in the present to ∼27 °C in the future climate. Similar temperature characteristics are observed in each individual ensemble member. The change in the frequencies of monthly mean temperatures with a 1 °C interval bin between the two climate periods indicates that more months are expected to be warmer (26 °C or higher) in the future climate (Fig. 4.6d).

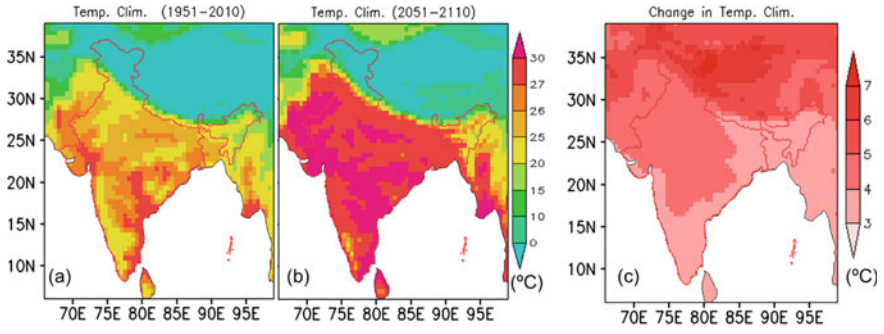

Fig. 4.5 Temperature climatologies from the AGCM ensemble mean for **a** present and **b** future climates and **c** the future temperature changes. *Source* (Data source) Mizuta et al. (2017)

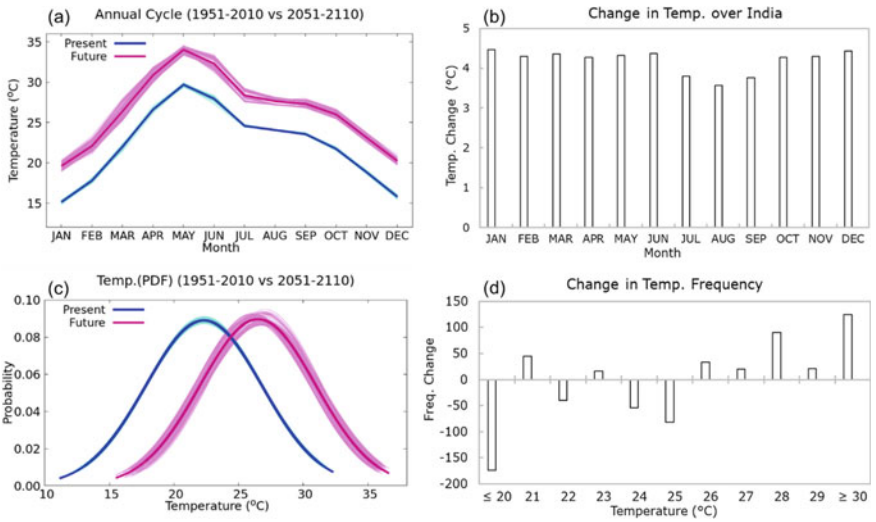

Fig. 4.6 **a** Annual cycles in two climate periods and **b** projected changes in temperature. **c** PDFs in two climate periods and **d** projected changes in the temperature frequencies. The thin lines (a, c) correspond to the results for each ensemble member. *Source* (Data source) Mizuta et al. (2017)

4.4.2 Projected Changes in Precipitation Distribution

Figure 4.7 represents the precipitation climatologies derived from the AGCM ensemble experiments for two climate periods and their future changes. The figure shows that the precipitation distribution patterns in both climate periods (i.e., during 1951–2010 and 2051–2110) are almost the same over all regions of India but with higher magnitudes under the future climate except over the Western Ghats regions (Fig. 4.7a–b). The precipitation amounts increase in the future climate by approximately 0.5–1 mm d^{-1} over almost all regions and decrease by

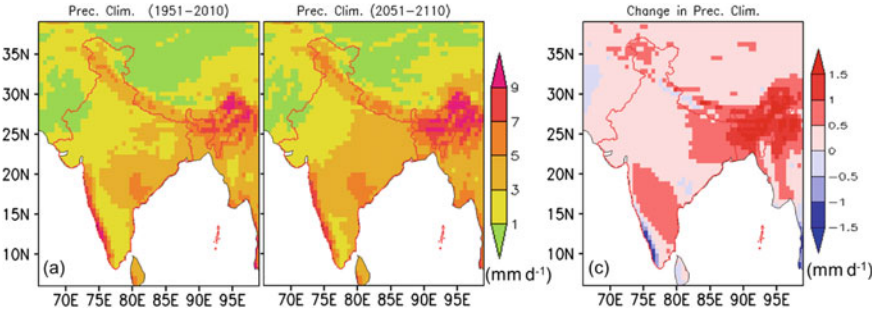

Fig. 4.7 Precipitation climatologies from the AGCM ensemble mean for the **a** present and **b** future climates and **c** their future changes. *Source* (Data source) Mizuta et al. (2017)

approximately 1 mm d^{-1} over the west coast along the Western Ghats (Fig. 4.7c). The northeast regions of India are likely to experience relatively more precipitation in the warming future climate.

The annual cycles and frequency distributions of the monthly total precipitation amounts over India in the present and future climates and their projected changes are illustrated in Fig. 4.8. The results indicate that the total monthly precipitation over India in the future climate is expected to increase to ~300 mm in July with an uncertainty range of 260–340 mm (Fig. 4.8a). The monthly total precipitation amount is likely to increase by 20–40 mm (5–45%) during July–October in the future climate and by 2–13 mm (3–35%) during November–June (Fig. 4.8b). This indicates that India is expected to receive relatively more precipitation in the monsoon season (June–September) under the future climate. The PDFs of the monthly precipitation intensities show peaks at 4 mm d^{-1} in the present and future climates, but the peaks are less frequent in the future (Fig. 4.8c). This indicates a possible reduction in the number of months in the future climate with precipitation amounts of approximately 120 mm. On the other hand, an increase in the number of months with precipitation intensities of 7 mm d^{-1} or higher is expected in the future climate. This indicates the possibility of an increased number of months being wetter in the future climate. Each individual member also shows similar characteristics in their PDFs, although some members do not show large changes in the annual cycles and the frequency patterns of precipitation in the future climate. This uncertainty behavior could be associated with the use of SST perturbations in the

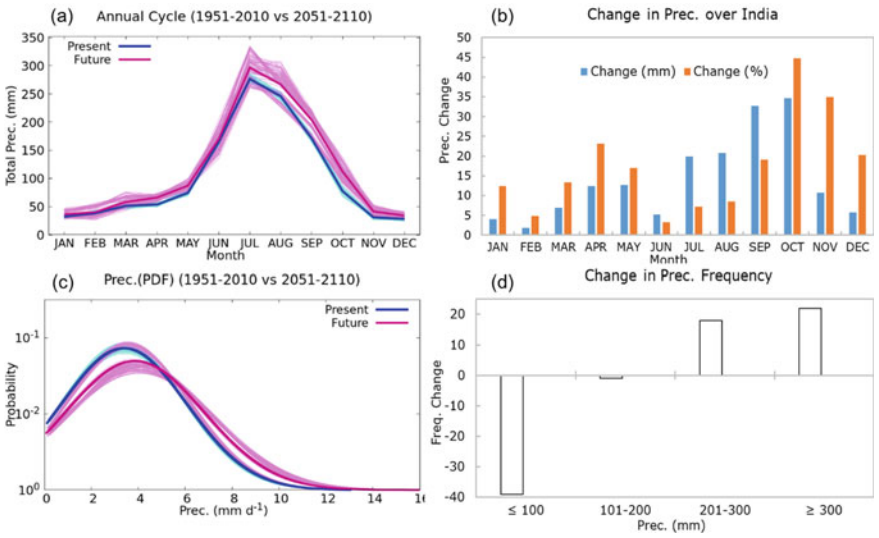

Fig. 4.8 **a** Annual cycles in the two climate periods and **b** projected changes in precipitation. **c** PDFs for the two climate periods and **d** projected changes in the precipitation frequencies. The thin lines (**a**, **c**) correspond to the results for each ensemble member. *Source* (Data source) Mizuta et al. (2017)

simulations (e.g., Mizuta et al. 2017). For instance, Yoshioka et al. (2007) reported that changes in SSTs led to a maximum precipitation variation of -0.23 ± 0.05 mm d^{-1} over north African regions. The changes in the frequencies of monthly total precipitation amounts over India in the two climate periods with 100-mm interval bins indicate a possible increase in the number of months with total precipitation amounts higher than 200 mm in the future climate (Fig. 4.8d). On the other hand, there is a possibility that the number of months with total precipitation amounts lower than 200 mm will decrease in the future climate.

4.4.3 *Projected Changes in Extreme Events*

We analyzed the frequency distributions of daily mean temperatures and precipitation amounts over India as a whole to understand the occurrences of cold and warm days and of light and heavy precipitation days in present and future climates. Figure 4.9 illustrates these PDFs. The results indicated that the daily temperature in the present climate varies in the range of 11–34 °C (Fig. 4.9a), while the daily precipitation varies from no rain up to 20 mm (Fig. 4.9b). The magnitudes of the daily temperatures in the future climate show an increase of 4–5 °C compared to those in the present climate, while the intensities of daily precipitation show increases in precipitation intensities of wet days exceeding ~ 7 mm d^{-1}. The intensities and frequencies of warm events (>25 °C) and strong precipitation events (>25 mm d^{-1}) are expected to increase in the warming future climate, indicating more severe hot days and water-related disasters over India in the future. Each ensemble experiment result also shows the same characteristics of the frequency and intensity of the daily mean temperature and precipitation.

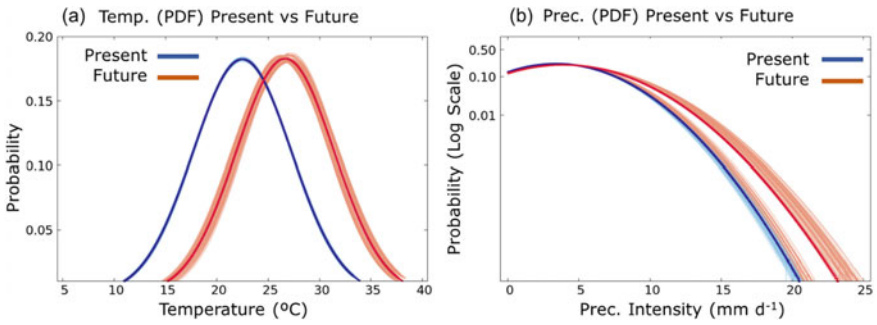

Fig. 4.9 Frequency distributions derived from the daily **a** temperature and **b** precipitation datasets in the AGCM ensemble experimental results for two periods: present climate and future climate. *Source* (Data source) Mizuta et al. (2017)

4.4.4 *Projected Changes in Other Climatic Variables*

This section discusses the climatologies of various climatic variables, including the vertical velocity, specific humidity, relative humidity, air temperature, and cloud cover from 1951 to 2051 and from 2051 to 2110, and their future projections. Here, omega refers to the vertical velocity, which represents the rate of change in pressure in a parcel over time.

Figure 4.10 presents the annual mean omega at 500 hPa derived from the AGCM ensemble means for the two climate periods and their future changes. It shows that omega is negative over almost all Indian regions except over a few regions in eastern India in both climate periods (Fig. 4.10a, b), indicating strong upward air motions over most Indian regions. A few regions in north and northeast India show relatively strong upward air motions in both climates. However, the upward air motion is expected to be weaker over a few regions in south and north India in the warming future climate than in the present climate (Fig. 4.10c).

The annual mean temperature climatologies at 500 hPa during 1951–2010 and 2051–2110 and their projected changes are shown in Fig. 4.11. The temperatures in the upper atmosphere (at 500 hPa) are negative in both climates, with maximum values up to −4 °C in the present climate and up to 0 °C in the future climate (Fig. 4.11a, b). The future changes in temperature (at 500 hPa) during 2051–2110 indicate increases of 4–5 °C over the Indian regions relative to the period 1951–2010 (Fig. 4.11c). The atmosphere under the future climate is expected to be relatively warmer over the western and northern parts of India than in the other Indian regions.

Figure 4.12 illustrates the annual mean specific humidities at 500 hPa in the two climate periods and their future changes. The spatial patterns of specific humidity in both climates are similar over almost all regions of India, but there is an increase in the overall amount of specific humidity in the future climate (Fig. 4.12a, b). The specific humidity over the southern regions of India seems to be more pronounced

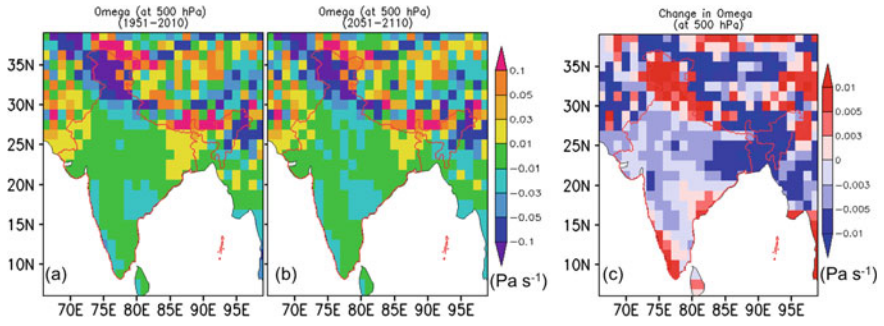

Fig. 4.10 Omega at 500 hPa from the AGCM ensemble mean for the **a** present and **b** future climates and **c** their future change. Negative signs in (**a**–**b**) indicate upward directions. *Source* (Data source) Mizuta et al. (2017)

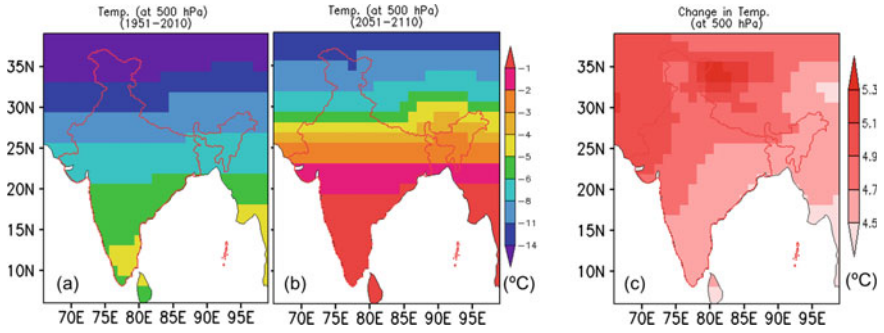

Fig. 4.11 Temperatures at 500 hPa from the AGCM ensemble mean for the **a** present and **b** future climates and **c** their future changes. *Source* (Data source) Mizuta et al. (2017)

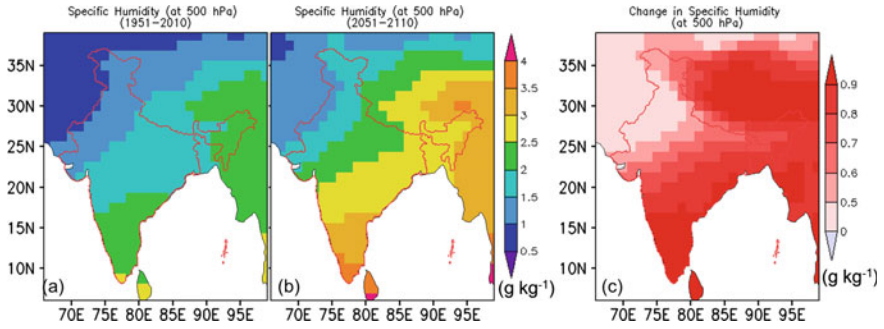

Fig. 4.12 Specific humidities at 500 hPa from the AGCM ensemble mean for the **a** present and **b** future climates and **c** their future changes. *Source* (Data source) Mizuta et al. (2017)

compared to those of other Indian regions. The specific humidity in the future climate is expected to increase over the entire Indian region (Fig. 4.12c). A few regions in western and northern India show relatively low increases in specific humidity in the future climate.

The annual mean relative humidities at 500 hPa in both climates and their future changes are shown in Fig. 4.13. The relative humidities in both climates are maximized over some regions in south and northeast India and minimized in west India (Fig. 4.13a, b). The relative humidities in the future climate are expected to increase over the eastern, central, and western regions of India, particularly in the 12–27 °N latitudinal belt, and to decrease over some regions in southern, northern, and northeastern India (Fig. 4.13c). The spatial patterns of cloud cover at 500 hPa are found to be similar in both climates but with a slightly lower percentage in the future climate (Fig. 4.14a, b). The cloud cover in the future climate is likely to decrease over the entire Indian region, although the magnitude of this decrease is below 2% (Fig. 4.14c).

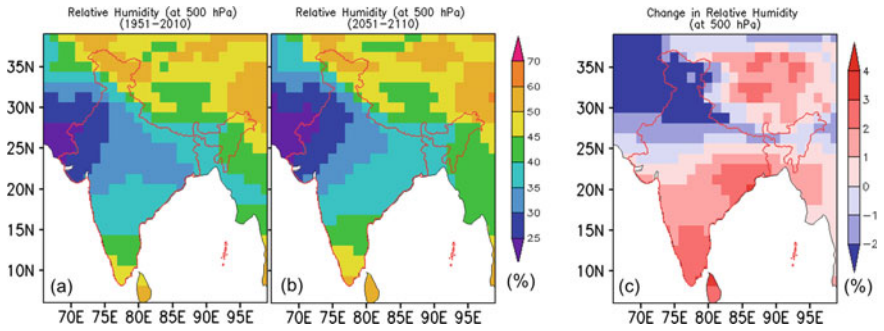

Fig. 4.13 Relative humidities at 500 hPa from the AGCM ensemble mean for the **a** present and **b** future climates and **c** their future change. *Source* (Data source) Mizuta et al. (2017)

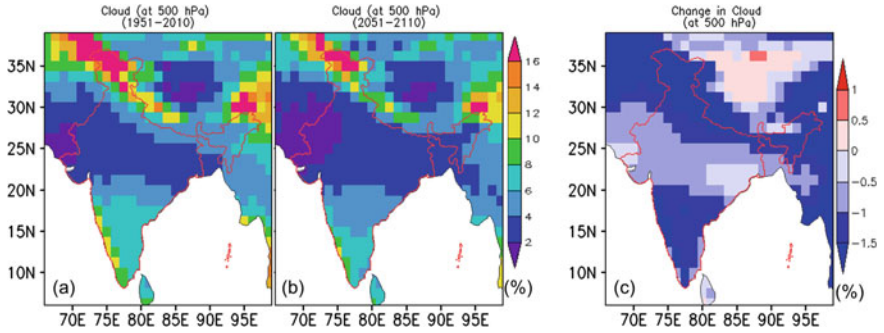

Fig. 4.14 Cloud cover at 500 hPa from the AGCM ensemble mean for the **a** present and **b** future climates and **c** their future changes. *Source* (Data source) Mizuta et al. (2017)

4.5 Discussion

This study considers various aspects of temperature and precipitation characteristics over India in the past 60 years (1951–2010) and their future changes in the next 100 years (2051–2110) by analyzing the results of 190 ensemble experiments. The climatologies, annual cycles, and frequency distributions of temperature and precipitation for the period 1961–2007 from the ensemble means of AGCM experiments over India are first compared with those from the APHRODITE observations to validate the model results. The results indicate that the AGCM-simulated climatologies, annual cycles, and frequency distributions of temperature and precipitation are in good agreement with the APHRODITE observations over the Indian region, although some cold and wet biases are noticed in the temperature and precipitation simulations, respectively (Figs. 4.2 and 4.3). Previous research (e.g., Karmacharya et al. 2017, Nayak et al. 2019) over Indian regions with various climate models has also highlighted similar cold and wet biases in the respective

models used in the studies. Therefore, simulating Indian climatology with complete accuracy has been a long-standing challenge. However, the spatial distribution of the various climate states over India in the d4PDF datasets appear to be quite reasonable (Figs. 4.2 and 4.3). The temperature climatologies over the desert climate type in the west region, the tropical wet and monsoon climate types in the west coast, central and south regions, and the temperate climate type in the north and northeast regions are well-represented in the d4PDF dataset, while those over some tropical wet-dry climate types in the southeast regions are underestimated (Fig. 4.2a, b). The d4PDF dataset reproduced the precipitation climatologies well over tropical rainforests in the south region and the arid and semiarid climate types in the west region, while it overestimated the precipitation amounts over some temperate rainy climate types in the north and northeast regions and tropical monsoon and savanna climate types in the central-east region (Fig. 4.3a, b).

The annual mean surface temperatures over most of the Indian regions are 25 °C or higher in the present climate and are expected to increase by 3–5 °C in the period 2051–2110 (Fig. 4.5). This result is consistent with the multitude of other previous studies over India (e.g., Kumar et al. 2013; Patwardhan et al. 2018). The temperatures over some desert regions in the west of the country and tropical humid climates in the central region show possible increases of 4–5 °C, while those over the subtropical humid climates in the north and east regions show increases of 3–4 °C. An increase of 4–5 °C in the air temperature at 500 hPa is also noticed over the Indian regions during the period 2051–2110 relative to the period 1951–2010 (Fig. 4.11), indicating a possible warmer atmosphere under the future climate. An increase in the temperature of ∼5 °C is expected, particularly during October–June, in the future climate (Fig. 4.6b). The number of months with monthly temperatures of 26 °C or higher is also likely to increase in the future climate (Fig. 4.6d).

The spatial distributions of precipitation over India show maximum precipitation over northeast India and in the regions over the west coast along the Western Ghats in both climate periods. An increase in precipitation of approximately 1 mm d^{-1} is expected in the future climate over most regions of India, while a decrease in precipitation of approximately 1 mm d^{-1} is expected over the west coast regions (Fig. 4.7). The precipitation amounts over the arid and semiarid climate types in the west and in some tropical rainforests in the southwest show increases of 0.5 mm d^{-1} in the future climate, and the precipitation amounts over the temperate rainy climate in the northeast show expected increases of more than 1 mm d^{-1}. Most of the tropical monsoon and savanna climate type regions show possible increases of ∼1 mm d^{-1} in precipitation in the future climate, while some tropical wet regions on the southwest coast indicate possible reductions of ∼1 mm d^{-1}. The monthly precipitation over India in the future climate is expected to increase by 5–45% during the months from July to October (Fig. 4.8b). Previous studies over India (e.g., Sabade et al. 2011; Chaturvedi et al. 2012; Akhter et al. 2017) also highlighted similar magnitudes of precipitation increases in the future climate. The reason for this result could be associated with the upward motion of air, which is expected to be stronger in the future climate, together with increased specific humidity (Figs. 4.10 and 4.12). It is interesting to note that the vertical motion of air

is weaker in the future climate over the Western Ghats regions, possibly because of the decrease in precipitation on the west coast along the Western Ghats. The number of warm days (>25 °C) and strong precipitation days (>25 mm d^{-1}) are also expected to intensify and to occur more frequently in the warming future climate. This indicates the possible occurrence of severe hot days and water-related disasters over India in the future climate. The reason for the increase in strong precipitation days in the future climate may be attributed to the temperature increases over the Indian region, which would increase the specific humidity, according to the Clausius-Clapeyron relationship, and cause more precipitation (e.g., Nayak 2018; Nayak and Takemi 2019).

The omega values at 500 hPa indicate stronger upward motions of air over most of the Indian regions in the future climate (Fig. 4.10). The arid and semiarid climate types in the western part of the country and the temperate rainy climate types in the northeast show stronger vertical velocities in the future climate, while most of the tropical wet in the south indicates weaker vertical velocity in the future climate. The upward motion of air in the future climate is also noticed to be weakened in the north areas, which include mountainous regions. The annual mean temperature climatologies at 500 hPa show a warmer atmosphere over entire Indian regions under future climate (Fig. 4.11). The desert in the west seems to be comparatively warmer in the future compared to the other climate states of India, while some regions in the temperate climate in the east and northeast are expected to be less warm. The specific humidity at 500 hPa also shows an increase of specific humidity over entire Indian region in future climate (Fig. 4.12). The desert, arid and semi-arid climate in the west shows relatively low increase of specific humidity in future climate. The relative humidity at 500 hPa is expected to increase over east, central and west regions of India and decrease over some regions in south, north, and northeast India (Fig. 4.13). Most of the regions of tropical rainforest, monsoon, and savanna in the 12–17 N latitudinal belt show a possible increase of the relative humidity in the future climate, while a possible reduction of the relative humidity is noticed over few regions of temperate rainy climate. The cloud cover at 500 hPa are noticed mostly similar in two climate periods with a small decrease in magnitude in future climate over entire India (Fig. 4.14c). The cloud cover over the desert in the west shows relatively low decrease in the future climate, while the same over most of the tropical wet and monsoon in the south and temperate rainy in the northeast shows relatively more decrease.

The present study with mega-ensemble d4PDF climate simulations shows overall consistency results with previous studies over India in the present climate and future climate. Thus, the present results with the d4PDF dataset with historical 6000-years and future 5400-years climate simulation give an overall confidence to understand the climate of India and its different climate states starting from dry/desert to wet and tropical to temperate. Moreover, this study discussed future changes of various climatic variables which would help to understand the factors behind the climate changes over India. So this study would provide an insight towards the future assessment over Indian climate in order to reduce the uncertainties to monitor climate hazards in India.

4.6 Conclusions

This study investigates a comprehensive assessment of climate change over India from 190 mega-ensemble AGCM experiment results in two climate periods (1951–2010 and 2051–2110). The main focus was on the climatologies, annual cycles, and frequency distributions of temperature and precipitation over Indian region in the past 60 years and their projected future changes in the next 100 years. The model simulated ensemble mean results appeared quite reasonable in simulating climatologies, annual cycles, and frequency distributions of the temperature and precipitation over the Indian region. The temperature over Indian regions during 1951–2010 shows mostly 25 °C or higher and precipitation shows mostly 3–5 mm d^{-1} during this period. Future AGCM simulations show an overall increase of 4–5 °C temperature and 2–45% precipitation over India in the period 2051–2110 with reference to the period 1951–2010. The consistency of these results with previous studies over India would lead to overall confidence in climate change assessments to monitor climate hazards in India in the future.

Declarations

Availability of data and material

The d4PDF data (the database for Policy Decision making for Future climate change) dataset supporting the conclusions of this article is obtained from the Data Integration and Analysis System (DIAS, http://search.diasjp.net/en/dataset). The precipitation and temperature observation dataset supporting the validation of this study is obtained from the Asian Precipitation-Highly-Resolved Observational Data Integration Towards Evaluation (APHRODITE's Water Resources, https://www.chikyu.ac.jp/precip/english/products.html).

Competing interests

The authors declare that they have no competing interest.

Funding

This study was supported by the TOUGOU program Grant Number JPMXD0717935498 funded by the Ministry of Education, Culture, Sports, Science, and Technology, Government of Japan.

Authors' Contributions

SN proposed the topic, designed the study, analyzed the data and drafted the manuscript. TT helped in the interpretation and the construction of the manuscript. All authors read and approved the final manuscript.

Acknowledgments

This study was supported by the TOUGOU program Grant Number JPMXD0717935498 and funded by the Ministry of Education, Culture, Sports, Science, and Technology, Government of Japan. The Japan Meteorological Agency (JMA) is acknowledged for providing the radar/rain gauge-analyzed precipitation product.

References

Akhter J, Das L, Deb A (2017) CMIP5 ensemble-based spatial rainfall projection over homogeneous zones of India. Clim Dyn 49(5–6):1885–1916

Chaturvedi RK, Joshi J, Jayaraman M, Bala G, Ravindranath NH (2012) Multi-model climate change projections for India under representative concentration pathways. Curr Sci 103 (7):791–802

Dash SK, Hunt JCR (2007) Variability of climate change in India. Curr Sci 93(6):782–788

Endo H, Kitoh A, Mizuta R, Ishii M (2017) Future changes in precipitation extremes in East Asia and their uncertainty based on large ensemble simulations with a high resolution AGCM. SOLA 13:7–12

Fujita M, Mizuta R, Ishii M, Endo H, Sato T, Okada Y, Watanabe S et al (2019) Precipitation changes in a climate with 2-K surface warming from large ensemble simulations using 60-km Global and 20-km Regional Atmospheric Models. Geophys Res Lett 46(1):435–442

Guhathakurta P, Rajeevan M (2008) Trends in the rainfall pattern over India. Int J Climatol 28 (11):1453–1470

Guhathakurta P, Sreejith OP, Menon PA (2011) Impact of climate change on extreme rainfall events and flood risk in India. J Earth Syst Sci 120(3):359–373

Iizumi T, Shiogama H, Imada Y, Hanasaki N, Takikawa H, Nishimori M (2018) Crop production losses associated with anthropogenic climate change for 1981–2010 compared with preindustrial levels. Int J Climatol 38(14):5405–5417

IPCC (2012) Managing the risks of extreme events and disasters to advance climate change adaptation. In: Field CB, Barros V, Stocker TF, Qin D, Dokken DJ, Ebi KL, Mastrandrea MD, Mach KJ, Plattner G-K, Allen SK, Tignor M, Midgley PM (eds) A special report of working groups I and II of the Intergovernmental Panel on Climate Change. Cambridge University Press, Cambridge, UK, and New York, NY, USA, 582 pp

IPCC (2014) Climate change 2014: impacts, adaptation, and vulnerability. Part A: global and sectoral aspects. Field CB, Barros VR, Dokken DJ, Mach KJ, Mastrandrea MD, Bilir TE, Chatterjee M, Ebi KL, Estrada YO, Genova RC, Girma B, Kissel ES, Levy AN, MacCracken S, Mastrandrea PR, White LL (eds) Contribution of working group ii to the fifth assessment report of the Intergovernmental Panel on Climate Change. Cambridge University Press, Cambridge, UK and New York, USA, 1132 pp

Jain SK, Kumar V (2012) Trend analysis of rainfall and temperature data for India. Curr Sci 102 (1):37–49

Karmacharya J, Jones R, Moufouma-Okia W, New M (2017) Evaluation of the added value of a high-resolution regional climate model simulation of the South Asian summer monsoon climatology. Int J Climatol 37(9):3630–3643

Kishore P, Jyothi S, Basha G, Rao SVB, Rajeevan M, Velicogna I, Sutterley TC (2016) Precipitation climatology over India: validation with observations and reanalysis datasets and spatial trends. Clim Dyn 46(1–2):541–556

Kothawale DR, Rupa Kumar K (2005) On the recent changes in surface temperature trends over India. Geophys Res Lett 32:L18714

Kumar V, Jain SK, Singh Y (2010) Analysis of long-term rainfall trends in India. Hydrol Sci J 55:484–496

Kumar P, Wiltshire A, Mathison C, Asharaf S, Ahrens B, Lucas-Picher P, Jacob D et al (2013) Downscaled climate change projections with uncertainty assessment over India using a high resolution multi-model approach. Sci Total Environ 468:S18–S30

Kusunoki S (2018) Is the global atmospheric model MRI-AGCM3.2 better than the CMIP5 atmospheric models in simulating precipitation over East Asia? Clim Dyn 51(11–12):4489–4510

Maity S, Mandal M, Nayak S, Bhatla R (2017a) Performance of cumulus parameterization schemes in the simulation of Indian summer monsoon using RegCM4. Atmósfera 30(4):287–309

Maity S, Satyanarayana ANV, Mandal M, Nayak S (2017b) Performance evaluation of land surface models and cumulus convection schemes in the simulation of Indian summer monsoon using a regional climate model. Atmos Res 197:21–41

Mizuta R, Murata A, Ishii M, Shiogama H, Hibino K, Mori N, Kawase H et al (2017) Over 5000 years of ensemble future climate simulations by 60-km global and 20-km regional atmospheric models. Bull Am Meteor Soc 98(7):1383–1398

Nayak S (2018) Do extreme precipitation intensities linked to temperature over India follow the Clausius-Clapeyron relationship? Curr Sci 115(3):391–392

Nayak S, Mandal M (2012) Impact of land use and land cover change on temperature trends over Western India. Curr Sci 102(8):1166–1173

Nayak S, Mandal M (2019) Impact of land use and land cover changes on temperature trends over India. Land Use Policy 89:

Nayak S, Takemi T (2019) Dependence of extreme precipitable water events on temperature. Atmósfera 32(2):159–165

Nayak S, Mandal M, Maity S (2017) Customization of regional climate model (RegCM4) over Indian region. Theoret Appl Climatol 127(1–2):153–168

Nayak S, Mandal M, Maity S (2018) RegCM4 simulation with AVHRR land use data towards temperature and precipitation climatology over Indian region. Atmos Res 214:163–173

Nayak S, Mandal M, Maity S (2019) Performance evaluation of RegCM4 in simulating temperature and precipitation climatology over India. Theoret Appl Climatol 137(1–2):1059–10751

Niyogi D, Kishtawal C, Tripathi S, Govindaraju RS (2010) Observational evidence that agricultural intensification and land use change may be reducing the Indian summer monsoon rainfall. Water Resour Res 46:W03533

O'Gorman PA, Schneider T (2009) The physical basis for increases in precipitation extremes in simulations of 21st-century climate change. Proc Natl Acad Sci 106(35):14773–14777

Ojha R, Nagesh Kumar D, Sharma A, Mehrotra R (2013) Assessing severe drought and wet events over India in a future climate using a nested bias-correction approach. J Hydrol Eng 18(7):760–772

Pall P, Allen MP, Stone DA (2007) Testing the Clausius-Clapeyron constraint on changes in extreme precipitation under CO_2 warming. Clim Dyn 28(4):351–363

Patwardhan S, Kulkarni A, Rao KK (2018) Projected changes in rainfall and temperature over homogeneous regions of India. Theoret Appl Climatol 131:581–592

Prakash S, Mitra AK, Momin IM, Rajagopal EN, Basu S, Collins M, Ashok K et al (2015) Seasonal intercomparison of observational rainfall datasets over India during the southwest monsoon season. Int J Climatol 35(9):2326–2338

Rao BB, Chowdary PS, Sandeep VM, Rao VUM, Venkateswarlu B (2014) Rising minimum temperature trends over India in recent decades: implications for agricultural production. Global Planet Change 117:1–8

Sabade SS, Kulkarni A, Kripalani RH (2011) Projected changes in South Asian summer monsoon by multi-model global warming experiments. Theoret Appl Climatol 103(3–4):543–565

Sharma SK, Bhattacharya S, Garg A (2004) India's initial national communication (NATCOM) to United Nations framework convention on climate change and the forestry sector. Vulnerability and adaptation (Chap 3), Ministry of Environment and Forests, Government of India, pp 59–71

Sinha Ray KC, Srivastava AK (1999) Is there any change in extreme events like droughts and heavy rainfall? Curr Sci 79(2):155–158

Takemi T, Okada Y, Ito R, Ishikawa H, Nakakita E (2016) Assessing the impacts of global warming on meteorological hazards and risks in Japan: philosophy and achievements of the SOUSEI program. Hydrol Res Lett 10(4):119–125

Yasutomi N, Hamada A, Yatagai A (2011) Development of a long-term daily gridded temperature dataset and its application to rain/snow discrimination of daily precipitation. Glob Environ Res 15(2):165–172

Yatagai A, Kamiguchi K, Arakawa O, Hamada A, Yasutomi N, Kitoh A (2012) APHRODITE: constructing a long-term daily gridded precipitation dataset for Asia based on a dense network of rain gauges. Bull Am Meteor Soc 93(9):1401–1415

Yoshioka M, Mahowald NM, Conley AJ, Collins WD, Fillmore DW, Zender CS, Coleman DB (2007) Impact of desert dust radiative forcing on Sahel precipitation: Relative importance of dust compared to sea surface temperature variations, vegetation changes, and greenhouse gas warming. J Clim 20(8):1445–1467

Chapter 5
Analysis of the Hydrological Behavior of Watersheds in the Context of Climate Change (Northwestern Algeria)

Halima Belarbi, Bénina Touaibia, Nadir Boumechra, Chérifa Abdelbaki, and Sakina Amiar

Abstract The aim of this work is to study the temporal evolution of the rainfall-runoff relations of four basins in northwestern Algeria: the Tafna Maritime, Isser Sikkak, downstream Mouilah and Upper Tafna basins. The adopted approach consists of analyzing hydroclimatic variables using statistical methods and testing the nonstationarity of the rainfall-runoff relation by the cross-simulation method using the GR2M model. The results of the different statistical methods applied to the series of rainfall and hydrometric variables show a decrease due to a break in stationarity detected since the mid-1970s and the beginning of the 1980s. The annual rainfall deficits reached average values of 34.6% during the period of 1941–2006 and 29.1% during the period of 1970–2010. The average annual wadi flows showed average deficits of 61.1% between 1912 and 2000 and 53.1% between 1973 and 2009. The GR2M conceptual model simulated the observed hydrographs in an acceptable manner by providing calculated runoff values in the calibration and validation periods greater or less than the observed runoff values. The application of the cross-simulation method highlighted the nonstationarity of the rainfall-runoff relations in three of the four studied basins, indicating downward trends of monthly runoff.

Keywords Precipitation · Runoff · Breakpoint · Nonstationarity · Drought · GR2M model

H. Belarbi (✉)
Institute of Science and Technology, University Center of Maghnia, Tlemcen, Algeria

B. Touaibia
National School of Hydraulics, Blida, Algeria

N. Boumechra · C. Abdelbaki · S. Amiar
Faculty of Technology, University Abou-Bakr Belkaïd, Tlemcen, Algeria
e-mail: cherifa.abdelbaki@pauwes.dz

H. Belarbi · N. Boumechra · C. Abdelbaki
EOLE Laboratory, University Abou-Bakr Belkaïd, Tlemcen, Algeria

T. Sumi et al. (eds.), *Wadi Flash Floods*, Natural Disaster Science and Mitigation Engineering: DPRI Reports, https://doi.org/10.1007/978-981-16-2904-4_5

5.1 Introduction

Water is a common and vital good, and its access, security and control are major challenges. In addition to these challenges, there are other challenges linked to probable changes in extreme climatic events, particularly periods of drought, which are predicted to become intense and persistent over time (Vervier et al. 2004). For all these reasons, the quantification of water resources is of great importance for scientists and water managers around the world (Milano et al. 2013). The importance of research lies in the major challenges represented by meteorological variability and its effect on the hydrological cycle (Goula et al. 2006).

In Algeria, the majority of productive watersheds, representing approximately 75% of the annual flow of surface water, are found in the eastern part of the country along the Mediterranean coast. Much of the rest of the land is subjected to desert conditions in which water scarcity is acute (PNUD-FEM 2003). In addition to the unfavorable geographic position of the country, the population explosion has worsened the situation. Indeed, the available water resources per inhabitant per year, which was 1,500 m^3 in 1962, dropped to 720 m^3 in 1990, 630 m^3 in 1998 and 430 m^3 now, thus reflecting pressure from population growth (Mozas and Ghosn 2013; Safar-Zitoun 2019). Therefore, Algeria is already in a situation of water scarcity (Benblidia and Thivet 2010) that could be amplified by the intensity and pace of climate change (Barnett et al. 2001; Frich et al. 2002). In fact, with regard to estimates of sectoral needs, climate change will place the country in an uncomfortable situation since the maximum volume of water that can be mobilized will reach the limit of the water needs of the country (Rousset and Arrus 2006).

Current climate disturbances are reflected in irregular rainfall and a drought that has become established over several years. This climatic variability, manifested by a drop in rainfall, has been the subject of numerous studies. In 1993, following an analysis of data from 120 rainfall stations, Laborde (1993) was able to highlight a succession of four rainfall phases, including a long deficit phase established at the end of 1973. The most pronounced rainfall deficit was recorded in the western part of the country, where the rainfall hardly exceeded 350 mm on average (Matari et al. 1999; Medejerab and Henia, 2011; Belarbi et al. 2013; Achite et al. 2014; Belarbi et al. 2016, 2019; Khedimallah et al. 2020). According to Aït Mouhoub (1998), while this reduction was on the order of 30% in eastern Algeria, it amounted to more than 50% in the central and western regions of the country. Meddi and Meddi (2009) estimated the deficit at 20% in the central region and more than 36% in the far western region, resulting in a drastic decrease in surface flows. Meddi and Hubert (2003) estimated this reduction at nearly 55% for the basins in the central region and between 37 and 44% in the eastern region, while the deficit varied from 61 to 71% for the basins in the far west.

The objective of this study is to analyze trends in the rainfall-runoff relation, taking four basins in northwestern Algeria as the study area: the Maritime Tafna, Isser Sikkak, downstream Mouilah and Upper Tafna basins. These four basins are of important socioeconomic interest because they supply water to the populations of many municipalities and provide the needs of the agricultural and industrial sectors, which are very active in the region (Kettab 2001). The methodological approach consists, first, of a characterization of hydrometeorological variability using non-parametric statistical tests for trend analysis and, second, of an application of the cross-simulation method starting from the lumped conceptual hydrologic monthly model GR2M over several subperiods.

5.2 Methods and Materials

5.2.1 Study Area

The four basins, which are subbasins of the Tafna basin, occupy the extreme northwest of Algeria (Fig. 5.1).

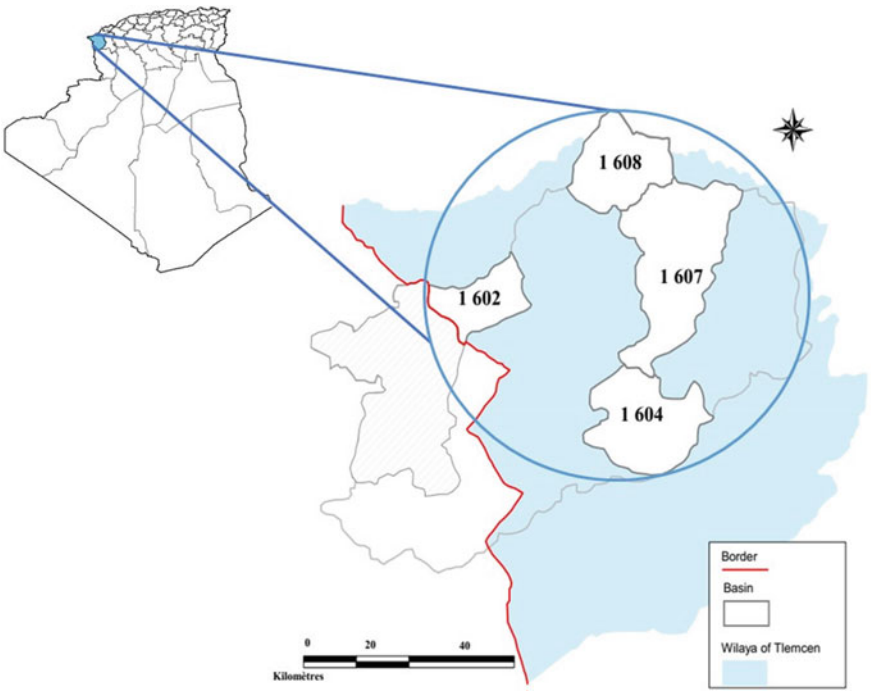

Fig. 5.1 Geographic location of the study area

The Upper Tafna basin (1604) (Fig. 5.1) covers an area of 256 km^2 and has a perimeter of 78 km (Ghenim 2001). Bounded to the north by the plains of Maghnia and Hennaya and to the south by the high Oran plains, this basin is occupied mainly by mountains of the Alpine orogeny formation whose summits culminate at 1465 m above sea level (Tlemcen Mountains). This basin is characterized by steep relief, and 49% of its surface has a slope greater than 25% (Megnounif et al. 2003). The watershed is well-drained with a poorly organized hydrographic network (Rc < 2) (Bouanani 2004). Its mainstream, Oued Sebdou, drains the basin over a length of 28 km (Ghenim et al. 2010). Oued Sebdou begins in Ouled Ouriach at Ghar Boumaaza, at an altitude of 1300 m, but is clearly distinct only around the town of Sebdou at an altitude of 900 m. From Sebdou and up to Sidi Medjahed, the course of Oued Sebdou follows a steep valley established in limestones and dolomites of the Jurassic period. It then follows a southeast/northwest direction until it reaches the Beni-Bahdel dam (Ghenim et al. 2010).

The downstream Mouilah basin (1602) (Fig. 5.1) covers an area of 2650 km^2 and has a perimeter of 230 km. A large portion of its surface is in Moroccan territory. The fairly varied relief in this basin consists of very heterogeneous zones formed by mountains (the Traras Mountains in the northwest and the Tlemcen Mountains in the south), plains and valleys. The slopes are generally very accentuated in the mountains (exceeding 20%) and gentler (between 0 and 10%) on either side of the watercourse (Ghenim et al. 2008). The stream begins in the El Abed region at an altitude of 1250 m, enters Morocco (40 km north of Oujda) and takes the name Oued Isly. Oued Isly becomes permanent downstream near Oujda and is then called Oued Bou-Naïm; Oued Bou-Naïm enters Algeria around Maghnia under the name Oued Mouilah. The confluence of Oued Mouilah with Oued Tafna is located at an altitude of 285 m upstream of the Hammam Boughrara dam at the level of Sidi Belkheir (Dahmani et al. 2006). Oued Mouilah receives on its right bank Oued Ouerdeffou, which forms the meeting of Oued Abbes, Oued Aouina and Oued Mehaguene (Terfous et al. 2001), and on its left bank, it receives Oued Bou-Selit, Oued Ben-Saria and Oued El Aouedj.

The Isser Sikkak basin (1607) (Fig. 5.1) covers an area of 460 km^2 with a perimeter of 116 km. The average altitude in this basin is 475 m. The Isser Sikkak watercourse originates at an altitude of 1190 m on the Terny plateau south of Tlemcen at the source of Aïn-Rhanous. The length of its main thalweg is 55.7 km. This thalweg is reformed from the sources of the El-Ourit waterfalls at an altitude of 800 m and takes the name Oued Saf-Saf downstream from the village of Saf-Saf and then the name Oued Sikkak from the commune of Chetouane. It first follows a deep and steep valley and then continues on the plains of Hennaya.

The Tafna Maritime basin (1608) (Fig. 5.1) has an area of 392 km^2 with a maximum altitude of 713 m and a perimeter of 116 km (ABHOCC 2006). It is the lowest region in the large Tafna watershed and is the region all the waters of Oued Tafna and its tributaries collect.

The types of geological formations that are observed in outcrops in the basins influence the distribution of superficial flows. Following his study, Bouanani (2004) found that almost the entire area of the basins is occupied by permeable to

semipermeable formations, which promote the infiltration of surface water. However, the relative abundance of karst carbonate formations, represented by the Tlemcen and de Terny dolomites in the Upper Tafna (1604) and Isser Sikkak (1607) basins, undoubtedly differentiates the hydrological behavior of these two basins from that of the downstream Mouilah basin (1602), more than half of the surface of which is occupied by Plio-Quarternary alluvium surmounting marl and Miocene sandstone at the level of the Maghnia plain.

The region is characterized by a semiarid climate with two predominant seasons. A cool, wet season extends from October to May with fairly irregular rains; the other season, which is dry and warmer, extends from June to September with low rainfall (ABHOCC 2006).

5.2.2 *Data Description*

Rainfall, temperature and hydrometric data were obtained from the two organizations that are responsible for the hydrometeorological network, namely, the National Agency for Hydraulic Resources (NAHR) and the National Office for Meteorology (NOM).

We needed to select a homogeneous observation period to ensure the statistical consistency of the results. Following quality control and homogeneity tests of the rainfall, hydrometric and temperature data, we selected six rainfall stations arranged over two periods: the first period begins in 1941 and runs until 2006, and the second period begins in 1970 and runs until 2010. The data were represented by observations from four stations arranged over two study periods: First period began in 1912 and ended in 2000, and the second period began in 1973 and ended in 2006. The temperature data were collected from four stations and covered a single study period from 1976 to 2007.

It should also be mentioned that, for the statistical analysis of the hydrometeorological data, a hydrological year beginning on September 1 of year M and ending on August 31 of year $(M + 1)$ was adopted. This decision is justified by the fact that in the Mediterranean area, the rainy season begins in the month of September and ends in May. The maximum rainfall rates are often recorded during winter in the months of November, December and January. It follows that the hydrological year reflects the natural climatic conditions (Sebbar et al. 2011).

The geographic coordinates and the main statistical parameters characterizing the distributions of rainfall data (mm) from the different stations selected are shown in Table 5.1.

Table 5.1 shows that the average annual rainfall over the 1941–2006 period varies between 424.8 (Bensekrane station) and 521.7 mm (Zenata station), with a general average of 470.3 mm. Over the 1970–2010 period, the annual averages fluctuate between 325.5 (Pierre du Chat station) and 565.0 mm (Mefrouche station), with a general average of 409.8 mm. The table also shows that the decade of the 1980s had the highest rainfall deficit in the region. The coefficient of variation (C_v)

Table 5.1 Geographic coordinates and statistical parameters of the selected rainfall stations

ID	Station	Longitude (E) (m)	Latitude (N) (m)	Elevation (m)	Study period	Max (mm)	Min (mm)	Mean (mm)	S_e (mm)	C_v
160702	Bensekrane	142,450	204,650	247	1941–2006	725.0 (1964/65)	184.5 (1944/45)	424.8	120.2	0.283
160403	Beni-Bahdel	115,200	165,500	660		756.1 (1967/68)	187.7 (1987/88)	464.8	137.05	0.295
605310	Zenata	119,670	196,626	247		986.0 (1963/64)	193 (1982/83)	521.7	211.7	0.406
160802	Pierre du Chat	123,100	213,350	60	1970–2010	594.6 (1972/73)	135.4 (1981/82)	325.5	93.6	0.285
160701	Mefrouche	135,750	179,700	1110		931.4 (1973/74)	304.3 (1987/88)	565.0	160.9	0.285
605220	Maghnia	88,100	176,750	428		586.5 (1974/75)	173.2 (1982/83)	338.8	111.9	0.331

S_e Standard deviation; C_v Coefficient of variation

is quite important. The highest variability is noted at Zenata station, with a coefficient of variation equal to 0.406 (1941–2006).

The geographic location, catchment area and various statistical parameters of the mean annual flows are presented in Table 5.2.

According to Table 5.2, the results of the mean annual flow analysis show a high standard deviation and coefficient of variation. Across all stations, the runoff depth varies enormously from year to year. In addition, these results show that the decade of the 1990s was the driest decade. On the other hand, the decades of the 1930s (1912–2000) and the 1970s (1973–2009) were periods of surplus. The coefficient of variation, C_v, varies between 64% and 77%, which means that the variability of the hydrometric series is considered to be very high.

The results of the descriptive analyses of the two quantiles (the minimum and the maximum), mean, standard deviation and coefficient of variation of the temperature time series are shown in Table 5.3.

The long-term averages of the mean annual temperatures range from 17.3 °C (Mefrouche station) to 18.2 °C (Beni-Bahdel station), with an average across all stations of 17.7 °C. The coefficient of variation, C_v, does not exceed 8%, which means that the variability of the temperature time series is considered to be low (Table 5.3).

Potential evapotranspiration is an essential input of the GR2M model. Potential evapotranspiration expresses the evaporative losses of a basin and is used in the production function of the model (Kouassi et al. 2008). The potential evapotranspiration values, which were calculated according to the Thornthwaite formula, cover the period from 1976 to 2007.

5.2.3 *Methodological Approach to Structural Break Detection*

The literature on statistical approaches to time series of hydrometeorological variables is particularly abundant. In this study, we opted for the nonparametric Pettitt and Mann-Kendall (MK) tests. The Pettitt test is renowned for its robustness; it allows the detection of breaks in a time series (a break at time "t" can be defined, generally, by a change or shift in the central tendency of a time series variable) (Braud 2011). To complement the results of the Pettitt test, we used the Mann-Kendall test. This test makes it possible to analyze the existence of a linear trend (upward or downward) in a time series. The robustness of this statistical test has been approved by several comparison tests carried out by Yue and Wang (2004). These two tests were programmed in the Turbo Pascal language. In addition, the results of the applications were represented by the selection of a significance level of 5%.

Table 5.2 Geographic location and statistical characteristics of the selected hydrometric stations

ID	Station	Longitude (E) (m)	Latitude (N) (m)	Elevation (m)	Area (km^2)	Study period	Max (m^3/s)	Min (m^3/s)	Mean (m^3/s)	S_e (m^3/s)	C_v
160801	Pierre du Chat	122,925	213,325	75	6900	1912–2000	21.87 (1932/33)	0.24 (1999/00)	6.52	5.03	0.771
160703	Remchi	122,900	208,850	93	1935		9.74 (1935/36)	0.07 (1999/00)	3.26	3.06	0.696
160202	Pont RN7/A	83,500	182,400	420	1820	1973–2009	1.85 (1979/80)	0.15 (1992/93)	0.85	0.47	0.643
160402	Beni-Bahdel	118,950	163,350	665	600		2.71 (1973/74)	0.31 (2004/05)	0.85	0.62	0.739

S_e Standard deviation; C_v Coefficient of variation

Table 5.3 Temperature stations and their statistical characteristics (°C)

ID	Station	Longitude (E) (m)	Latitude (N) (m)	Elevation (m)	Max Temp (°C)	Min Temp (°C)	Mean Temp (°C)	S_e (°C)	C_v
160403	Beni-Bahdel	115,200	165,500	660	20.3 (1996/97)	15.6 (1976/77)	18.2	1.307	0.072
160701	Mefrouche	135,750	179,700	1110	18.9 (1989/90)	15.5 (2005/06)	17.3	0.915	0.053
605220	Maghnia	88,100	176,750	428	18.5 (2005/06)	16.4 (1980/81)	17.5	0.513	0.029
605310	Zenata	119,670	196,626	247	18.8 (1989/90)	16 (1976/77)	17.9	0.683	0.038

S_e Standard deviation; C_v Coefficient of variation

Pettitt Test

Pettitt (1979) defines the variable $U_{t,n}$ as follows:

$$U_{t,n} = \sum_{i=1}^{t} \sum_{j=t+1}^{n} D_{ij} \tag{1}$$

or

$$D_{i,j} = \operatorname{sgn}(x_i - x_j) = \begin{cases} 1 & \text{si } x_i > x_j \\ 0 & \text{si } x_i = x_j \\ -1 & \text{si } x_i < x_j \end{cases} \tag{2}$$

Pettitt proposed testing the null hypothesis using the K_n statistic, which is defined by the maximum absolute value of $U_{t,n}$ for values of t varying from 1 to $n-1$. From rank theory, k denotes the value of K_n taken over the studied series; under the null hypothesis, the probability of exceeding the value k is given approximately as follows:

$$\Pr(K_n > k) \approx 2 \exp\left[\frac{-6k^2}{(n^3 + n^2)}\right] \tag{3}$$

For a given risk (significance level) α, if the estimated probability of exceedance is less than α, the null hypothesis, H_0, is rejected. The series then includes a localized break at the time when it is observed as $\max\left|U_{t,n}\right|_{t=1,\ldots,n-1}$ (Belarbi et al. 2012).

Mann-Kendall Test

If we consider each element x_i in a time series with (i = 1, …, n), we can calculate the trend statistic, t', of the test, given as follows by Mann (1945), Kendall (1975) and Paturel and Servat (Paturel and Servat 1996):

$$t' = \sum_{i=1}^{n} n_i \tag{4}$$

The mean and variance of the test statistic are calculated, respectively, as follows:

$$E(t') = \frac{n(n-1)}{4} \tag{5}$$

$$V(t') = \frac{n(n-1)(2n+5)}{72} \tag{6}$$

The reduced test statistic is given as follows:

$$u(t') = \frac{[t' - E(t')]}{\sqrt{V(t')}} \tag{7}$$

We seek the probability, α_1, using the reduced centered normal law such that $\alpha_1 = P(|u| > |u(t')|)$, and the null hypothesis is accepted or rejected at level α depending on whether $\alpha_1 > \alpha$ or $\alpha_1 < \alpha$.

When the values of $u(t')$ are significant, we conclude that there is an increasing or decreasing trend depending on whether $u(t') > 0$ or $u(t') < 0$, respectively (Sneyers 1975).

To locate the period when a trend appeared, the test statistic lends itself better to the progressive and retrograde calculations necessary for this purpose. By reversing the direction of the calculation, the obtained variable, $u(t')$, is called a retrograde series. The point of intersection of $-u(t')$ with $u(t')$ indicates the beginning of the trend (Meddi et al. 2005).

5.2.3.1 Analysis of Variability of Meteorological Observations

The moving average method aims to reduce the influence of accidental variations and to eliminate the effect of very short-term fluctuations. This method makes it possible to smoothen random and periodic components without affecting the general movement of the series (Belarbi et al. 2012). The principle of this method is to replace the original series with a series of moving average values defined, in the simplest case, as follows:

$$y_k = \frac{1}{2n+1} \sum_{i=-n}^{n} (y_{k+i}) \tag{8}$$

In addition, to assess the evolution of an annual time series of a meteorological variable, it is advisable to take into account any deviation from the average that corresponds to the surplus or deficit for the year in question compared to the observed long-term average (Bodian 2011). This deficit is calculated as follows:

$$E_i = \frac{(Y_i - \text{Mean})}{\text{Mean}} \times 100 \tag{9}$$

where E_i denotes the deviation from the average (percent); Y_i represents the annual average of the variable recorded during year i; and Y_{mean} indicates the interannual average of the variable recorded over the study period.

5.2.3.2 Hydrological Modeling and Rainfall-Runoff Relation

Modeling the rainfall-runoff relation has become an essential tool for the management of water resources. A number of studies carried out in Algeria using conceptual models have been presented in the hydrological literature. Several models (GR1A, GR2M, GR3M, GR4J, SWAT or even neuro-fuzzy) have been used in the works of these authors.

For this research, we chose the GR2M model developed in the GR (Rural Engineering) model series from CEMAGREF. This global conceptual model has undergone several revisions, proposed successively by Kabouya and Michel (1991), Makhlouf and Michel (1994), Mouelhi (2003) and Mouelhi et al. (2006), which allowed the gradual improvement of the performance of the model.

Indeed, the advantage of using GR2M comes from the small amount of data required (rain, evapotranspiration and flow) for the calibration and simulations. These input data are expressed in depth of runoff (mm). GR2M simulates the flow at the outlet of a watershed using precipitation and evapotranspiration data.

5.2.3.3 Description of the GR2M Model

The GR2M model consists of a production tank that governs the production function, characterized by its maximum capacity, and a reservoir (gravity water) that governs the transfer function (Kouassi et al. 2012). This monthly water balance model contains two free parameters that require calibration (X_1 and X_2). The first parameter (X_1) represents the maximum capacity of the tank (soil). The second parameter (X_2) represents the exchange parameter at the underground reservoir level (gravity water) (Perrin et al. 2007). Two free parameters in a global conceptual model are sufficient to represent the rainfall-runoff relation at the monthly time step (Mouelhi 2003; Makhlouf and Michel 1994).

5.2.3.4 Mathematical Criterion for Optimizing the Model (Nash-Sutcliffe Criterion)

The performance of a model is measured according to the objectives that are set. The same model can be assessed in several ways, the only constraint being the objective of the assessment (Djellouli et al. 2013).

The best-known and best-performing criterion for conceptual models is the Nash-Sutcliffe criterion (Perrin et al. 2007). Indeed, several comparative studies among different forms of criteria have been carried out and have shown that the Nash-Sutcliffe criterion imposes itself as that which, overall, allows the best calibration (Mouelhi 2003). This dimensionless criterion makes it possible to judge the quality of an adjustment and facilitates the comparison of adjustments among different basins whose flows correspond to different orders of magnitude (Kouassi 2007). The criterion is defined by Nash and Sutcliffe (1970) as follows:

$$\text{Nash} = \left[1 - \frac{\sum\left(Q_0^i - Q_C^i\right)^2}{\sum\left(Q_0^i - Q_m\right)^2}\right] \cdot 100 \tag{10}$$

where Q_0^i represents the monthly observed discharge; Q_C^i is the monthly calculated discharge; and Q_m is the average flow observed over the whole observation period without gaps.

The estimation of the Nash-Sutcliffe criterion ranges between $-\infty$ and 100%. The model is considered effective when the estimated streams approach the observed streams, i.e., when the value of the Nash-Sutcliffe criterion is close to 100%. Thus, a performance greater than or equal to 60% can be viewed as acceptable (Perrin 2000). The version of the GR2M model used in this study is available on the CEMAGREF Web site (http://webgr.irstea.fr/modeles/mensuel-gr2m/).

5.2.3.5 Evaluation of the Robustness of the GR2M Model

One of the most commonly utilized methods to assess the robustness of a model is the double-sample technique. This method makes it possible to test the adaptability of models regardless of their complexities (Kouassi et al. 2011).

In the case where there are observations presenting themselves as time series (e.g., monthly or annual time series), it suffices to subdivide the observation period of each watershed into subperiods and perform a calibration over one period and a validation over the rest of the observations while making sure to reserve a period for the model warm-up (Kouassi 2007). This task is repeated such that the model calibrates successively on all the subperiods. The robustness of a model is evaluated by the difference between the value of the Nash criterion in the calibration phase and that in the validation phase (Perrin 2000).

5.2.3.6 Cross-Simulation Approach: Trend Analysis of the Rainfall-Runoff Relation

While many methods to detect trends in hydrological variables such as rainfall and flows are available, there are very few methods capable of detecting trends in rainfall-runoff behavior (Aït-Mesbah 2012). Among these methods, the cross-simulation approach is used because of its robustness for the study of trends in rainfall-runoff relations (Kouamé et al. 2013).

The description of the methodology of this approach is based on the work of Andréassian et al. (2003) and Kouassi et al. (2012).

The methodology begins with the division of the study period into n successive periods of equal lengths. This approach is based on the principle that calibrating a model makes it possible to characterize the hydrologic behavior of the model over

the calibration period (of n subperiods). Then, applying the calibrated model to all the other subperiods while keeping the same parameters, we obtain the flow that would have resulted had the basin remained under the conditions of the calibration period. By renewing this operation after each control, we thus build a trend matrix. In the interpretation of the simulation matrices, each value is replaced by a sign, indicating an increasing or decreasing evolution of the hydrological variable over time. For this study, the target variable that is considered is the monthly average flow, transformed into a measure of the depth of runoff (mm). For this purpose, each value in the matrix is replaced by a (+) or a (−), depending on whether the value is greater or less than the value of the diagonal. The value located on the diagonal represents, for each line, the best reference insofar as it is the closest value to the value that was actually observed (because it is predicted by the model calibrated on the period in question). The comparison is carried out line by line because it is necessary to ensure conditions of equal rainfall. If the (+) values represent the majority, this means that the hydrological variable simulated in the matrix tends to increase over time. If (−) values represent the majority, the opposite is true (Renard Renard 2006; Belarbi et al. 2017).

5.3 Results and Discussions

5.3.1 Results

5.3.1.1 Detection of Breaks in the Rainfall Time Series

The application of the two tests (Mann-Kendall and Pettitt) at a significance level of 5% made it possible to identify a breakpoint in the rainfall time series. The identification of this breakpoint makes it possible to distinguish two periods, a surplus period and a deficit period, in the basins (Table 5.4).

Table 5.4 Statistical tests applied to the time series of annual rainfall totals

Station	Mann-Kendall test			Pettitt test		
	$u(t')$	Significance level	Breakpoint year	Values of K_n	Pr (K_n)	Significant breakpoint
Study period 1941–2006						
Bensekrane	−4.14	−1.96	1976/77	646	0.00025	1976/77
Beni-Bahdel	−3.03	−1.96	1978/79	692	0.00007	1974/75
Zenata	−5.97	−1.96	1976/77	1013	0.00000	1975/76
Study period 1970–2010						
Pierre du Chat	−0.96	−1.96	–	203	0.04614	1980/81
Mefrouche	−2.35	−1.96	1975/76	221	0.02296	1980/81
Maghnia	−1.79	−1.96	–	207	0.03972	1980/81

The Pettitt test, when applied to annual rainfall totals during the 1941–2006 period, confirmed the occurrence of significant breakpoints in the mid-1970s (Table 5.4; Fig. 5.2). However, during the 1970–2010 study period, breakpoints were identified in 1980/81 (Table 5.4; Fig. 5.3).

This break is identified by a peak in the evolution of the Pettitt indices. Over the period from 1941 to 2006 (Fig. 5.2), the Pettitt indices correspond to 646 for the Bensekrane station, 692 for the Beni-Bahdel station and 1013 for the Zenata station. During the period 1970–2010, indices have values of 203 for the Pierre du Chat station, 221 for the Mefrouche station and 203 for the Maghnia station (Fig. 5.3).

By applying the Mann-Kendall test, we detected the existence of a very significant downward break in the time series of the annual rainfall totals of the Bensekrane, Beni-Bahdel and Zenata stations. This abrupt change occurred in the mid- and late 1970s (Table 5.4; Fig. 5.4). During the 1970–2010 study period, a break was identified in the mid-1970s in the rainfall totals from the Mefrouche station (Fig. 5.5). However, the trend in the annual rainfall totals of the Pierre du Chat and Maghnia stations is not significant (the null hypothesis that there is no trend is accepted) (Table 5.4).

A rainfall deficit indicates a negative change or a decrease in the mean annual rainfall, while a surplus means an increase in the mean annual rainfall observed in the time series before and after a breakpoint. The deficits are −50.82% for the Zenata station, −27.76% for the Beni-Bahdel station and −25.16% for the Bensekrane station (period 1941–2006) (Table 5.5). During the period 1970–2006, the deficits exceeded -26% for the Pierre du Chat station and −30% for the Mefrouche and Maghnia stations. Furthermore, the linear regression between the precipitation values and time, which is used to quantitatively describe the possibility of a linear downward or upward trend in the time series, confirms that annual rainfall totals experienced an average decrease. The rainfall totals reached −8.04 mm annually at Zenata station (study period 1941–2006) (Fig. 5.4) and −6.83 mm annually at Mefrouche station (study period 1970–2010) (Fig. 5.5).

These observations corroborate the results of a number of studies, among which we can cite Laborde (1993), Matari et al. (1999), Meddi and Hubert (2003), Meddi

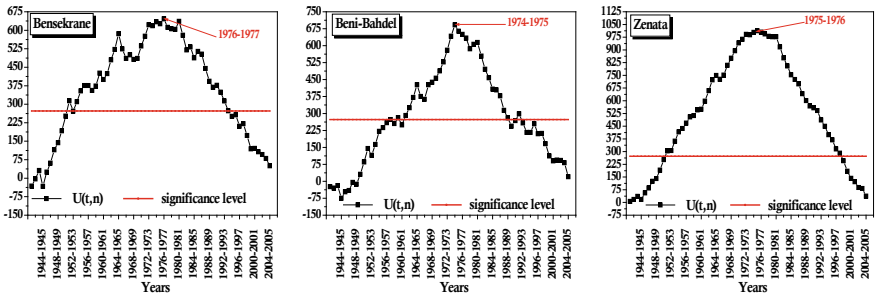

Fig. 5.2 Application of the Pettitt test to the annual rainfall time series data for the period 1941–2006

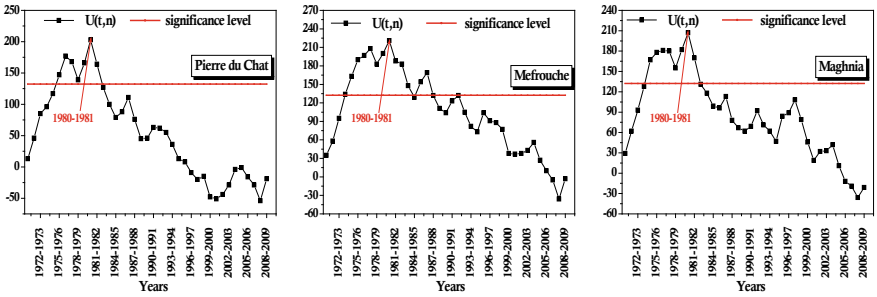

Fig. 5.3 Application of the Pettitt test to the annual rainfall time series data over the 1970–2010 period

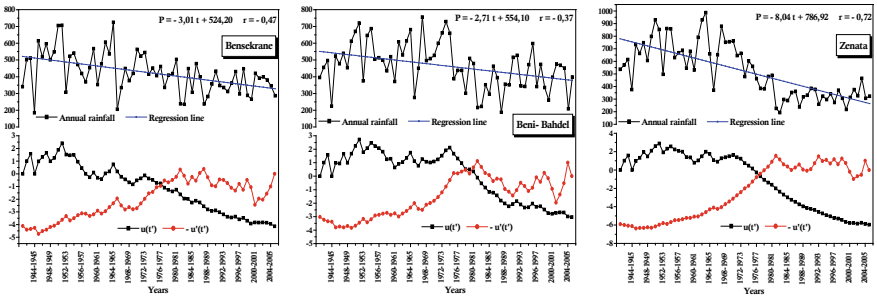

Fig. 5.4 Application of the Mann-Kendall test to the annual rainfall time series data for the period 1941–2006

Fig. 5.5 Application of the Mann-Kendall test to the annual rainfall time series data over the 1970–2010 period

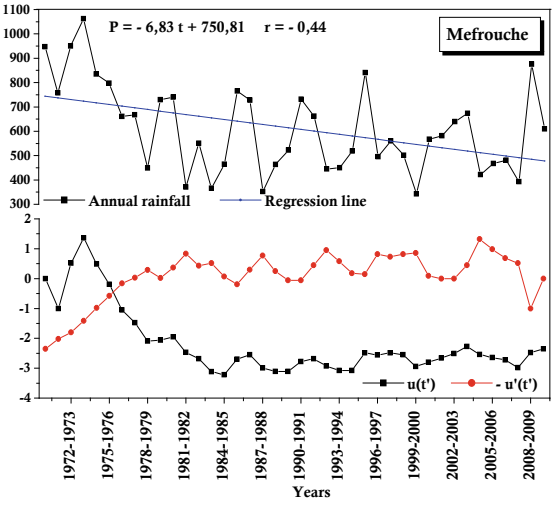

Table 5.5 Rainfall deficits at the various stations studied

Station	Breakpoint year	Study period	Before break	After break	Deficit (%)
			Mean (mm)	Mean (mm)	
Bensekrane	1976/77	1941–2006	478.5	358.1	25.16
Beni-Bahdel	1974/75		535.7	387.0	27.76
Zenata	1975/76		681.6	335.2	50.82
Pierre du Chat	1980/81	1970–2010	403.8	295.8	26.74
Mefrouche	1980/81		781.5	546.2	30.12
Maghnia	1980/81		435.0	302.3	30.51

and Meddi (2009), Belarbi et al. (2013, 2016, 2017), and Sebaibi (2014), which place most of the breakpoints during the 1970s in Algeria, particularly in the western part of the country.

5.3.1.2 Detection of Breakpoints in the Runoff Time Series

The results of the two tests, at a significance level of 5%, on the mean annual flow time series of the Pierre du Chat, Remchi, Pont RN7/A and Beni-Bahdel stations are shown in Table 5.6.

The mean annual flow time series of the Pierre du Chat and Remchi stations analyzed over the period from 1912 to 2000 show a significant break in the mid-1970s (Table 5.6). The results show that the test statistic reached a maximum in 1975/76 for the time series from Pierre du Chat station and in 1974/75 for that of Remchi station (Fig. 5.6).

Table 5.6 Statistical tests applied to the mean annual flow time series

Station	Mann-Kendall test			Pettitt test		
	$u(t\prime)$	Significance level	Breakpoint year	Values of K_n	Pr (K_n)	Significant breakpoint
Study period 1912–2000						
Pierre du Chat	−3.30	−1.96	1994–1995	432	0.16129	1975–1976
Remchi	−4.65	−1.96	1986–1987	619	0.01138	1974–1975
Study period 1973–2009						
Pont RN7/A	1.88	1.96	–	151	0.11534	–
Beni-Bahdel	−3.60	−1.96	1981–1982	195	0.01717	1986–1987

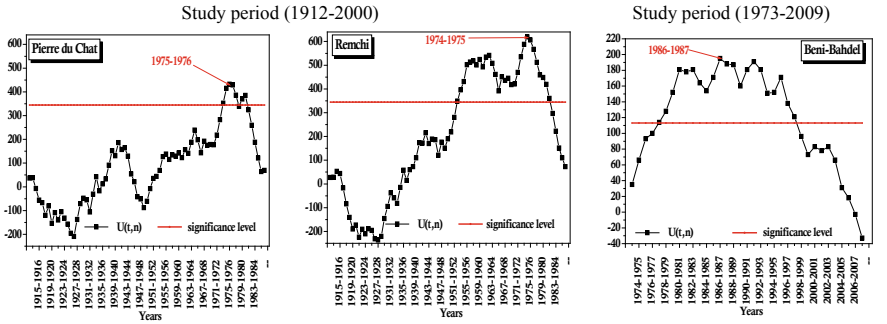

Fig. 5.6 Trends of mean annual flows determined using the Pettitt test

During the 1973–2009 study period, a break in the mean annual flow time series was identified in the mid-1980s for the Beni-Bahdel station (Table 5.6; Fig. 5.6). No break was detected in the discharge time series of the RN7/A Pont station (Table 5.6).

The identification of these structural breaks is an expected consequence following a very significant downward trend in annual average flows during the twentieth century in general and in particular since the mid-1970s and 1980. In addition, the linear regression between the annual average flows and time indicated downward trends in the flows. The average annual drop reached −0.27 mm at the Pierre du Chat station during the study period of 1912–2000 and −1.57 mm at the Beni-Bahdel station during the period from 1973 to 2009 (Fig. 5.7).

The flow deficits calculated before and after the date of the break of each mean annual flow time series were quite significant (Table 5.7).

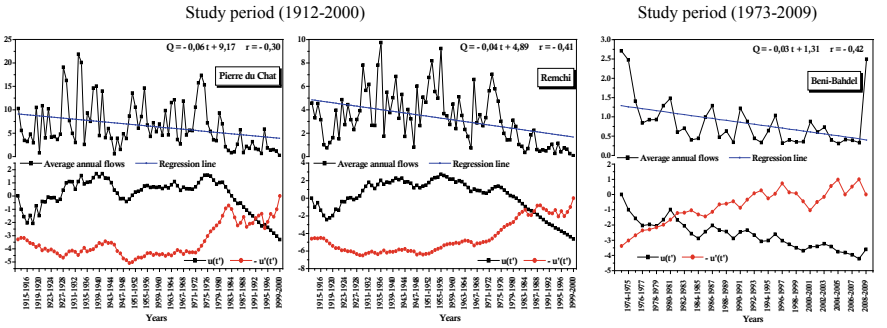

Fig. 5.7 Trends of mean annual flows determined using the Mann-Kendall test

Table 5.7 Hydrometric deficits of the different stations studied

Station	Breakpoint year	Study period	Before breakpoint	After breakpoint	Deficit (%)
			Mean (m^3/s)	Mean (m^3/s)	
Pierre du Chat	1975–1976	1912–2000	7.94	2.75	65.34
Remchi	1974–1975		4.12	1.12	72.86
Beni-Bahdel	1981–1982	1973–2009	1.41	0.66	53.13

5.3.1.3 Study of Interannual Rainfall Variability

Rainfall is very variable from year to year and from one station to another. A very rainy year can be suddenly followed by a dry year without a transition period. This is the case for the Bensekrane station, which received a total rainfall of 725 mm in 1964/65 and only 205.8 mm in 1965/66 (Fig. 5.8). Similarly, the Pierre du Chat station recorded 494.2 mm and 135.4 mm in the 1980/81 and 1981/82 seasons, respectively (Fig. 5.9).

The seven-year moving average curve highlights the excess, normal and deficit periods. The rainfall evolution of the Bensekrane station is characterized by excess, normal and deficit periods (Table 5.8; Fig. 5.8). The surplus period from 1941/42 to 1967/68 had an average rainfall of 485.3 mm, which was 14% higher than the total annual average of 424.8 mm. This surplus was followed by a normal period from 1967/68 to 1977/78; the average rainfall during this period (449.6 mm) was close to the total annual average (424.8 mm). The deficit period began in 1977/78 and ran until 2005/06. During this period, the total annual average rainfall was 358.9 mm.

For the Beni-Bahdel station (Table 5.8; Fig. 5.8), only one excess period was observed, ranging from 1941/42 to 1975/76 with an average annual rainfall of 531.5 mm, followed by the first period of deficit beginning in 1975/76 and running until 1990/91. During this period of deficit, a minimum total rainfall value of

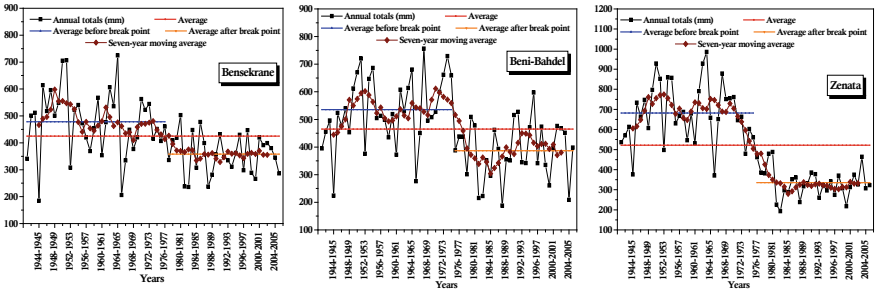

Fig. 5.8 Interannual variability in annual rainfall totals for the period 1941–2006

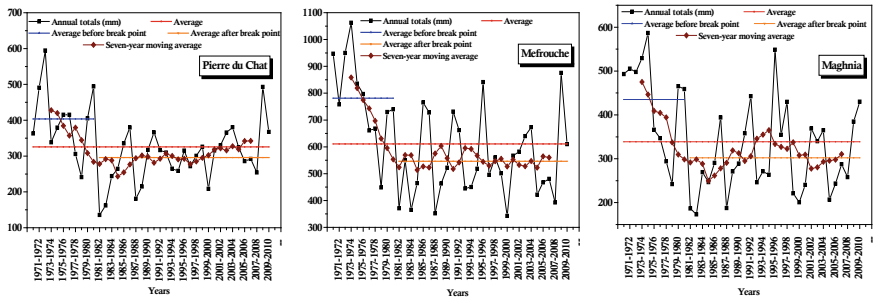

Fig. 5.9 Interannual variability in annual rainfall totals over the period 1970–2010

187.7 mm was recorded (1987/88). The period between 1990/91 and 1997/98 was a normal period with an average rainfall of 442.6 mm, which was close to the total annual average (464.8 mm). Again, a succession of dry years followed this normal period. The second deficit period began in 1997/98 and continued until 2005/06.

For the Zenata station, two contrasting periods were identified (Table 5.8; Fig. 5.8). The first is a surplus period from 1941/42 to 1973/74. During this period, the total rainfall reached a maximum of 986 mm (1963/64). This surplus period was followed by a deficit period that began at the end of the excess period and ran until 2005/06. The total annual average rainfall was 350.6 mm.

The application of the seven-year moving average method highlighted two distinct periods at all the analyzed stations during the 1970-2010 study period. For the Pierre du Chat and Mefrouche stations (Table 5.8; Fig. 5.9), excess periods were observed between 1970/71 and 1977/78, with interannual averages of 412.8 mm for the Pierre du Chat station and 834.8 mm for the Mefrouche station. The other period was a deficit period that began in 1977/78 and ran until 2007/08. The total annual average rainfall values recorded during this period were 295.3 mm and 542.4 mm for the Pierre du Chat and Mefrouche stations, respectively.

The analysis of rainfall data from the Maghnia station (Table 5.8; Fig. 5.9) showed an excess phase that began in 1970/71 and ended in 1980/81. During this phase, the total maximum rainfall between the beginning and the mid-1970s reached 586.6 mm. The deficit phase began at the end of the excess period and ran until 2007/08. During this phase, the average annual rainfall was 294.5 mm.

The results obtained following calculations of the deviations from the means highlight the succession of dry and wet periods.

During the period 1941–2006 (Fig. 5.10), the wettest years corresponded to 1964/65 for the Bensekrane station, 1967/68 for the Beni-Bahdel station and 1963/64 for the Zenata station, with deviations from the mean of 70.7%, 62.7% and 88.9%, respectively. The driest years were 1944/45 for the Bensekrane station, 1987/88 for the Beni-Bahdel station and 1982/83 for the Zenata station.

Over the period of analysis (1970–2010) (Fig. 5.11), the driest years were 1981/82 for the Pierre du Chat station, 1999/00 for the Mefrouche station and 1982/83 for the Maghnia station.

Table 5.8 Different trends at the studied rainfall stations

Station	Beginning of the period	End of the period	Trend	Mean (mm)	Max (mm)	Min (mm)
Study period 1941–2006						
Bensekrane	1941/42	1967/68	Excess	485.3	725.0 (1964/65)	184.5 (1944/45)
	1967/68	1977/78	Normal	449.6	562.7 (1970/71)	335.8 (1977/78)
	1977/78	2005/06	Deficit	358.9	502.7 (1980/81)	**235.8 (1982/83)**
Beni-Bahdel	1941/42	1975/76	Excess	531.5	756.1 (1967/68)	224.3 (1944/45)
	1975/76	1990/91	Deficit	367.7	515.7 (1990/91)	**187.7 (1987/88)**
	1990/91	1997/98	Normal	442.6	597.4 (1995/96)	341.5 (1993/94)
	1997/98	2005/06	Deficit	374.7	476.2 (2001/02)	208.7 (2004/05)
Zenata	1941/42	1973/74	Excess	687.7	986.0 (1963/64)	371.0 (1965/66)
	1973/74	2005/06	Deficit	350.6	602.0 (1974/75)	**193.0 (1982/83)**
Study period 1970–2010						
Pierre du Chat	1970/71	1977/78	Excess	412.8	594.6 (197/73)	305.8 (1977/78)
	1977/78	2007/08	Deficit	295.3	494.2 (1980/81)	**135.4 (1981/82)**
Mefrouche	1970/71	1977/78	Excess	834.8	1062.4 (1973/74)	661.3 (1976/77)
	1977/78	2007/08	Deficit	542.4	841 (1995/96)	342.4 (1999/00)
Maghnia	1970/71	1980/81	Excess	435.0	586.6 (1974/75)	242.1 (1978/79)
	1980/81	2007/08	Deficit	294.5	548.7 (1995/96)	**173.2 (1982/83)**

Bold indicates Minimum annual rainfall totals during the 1980s

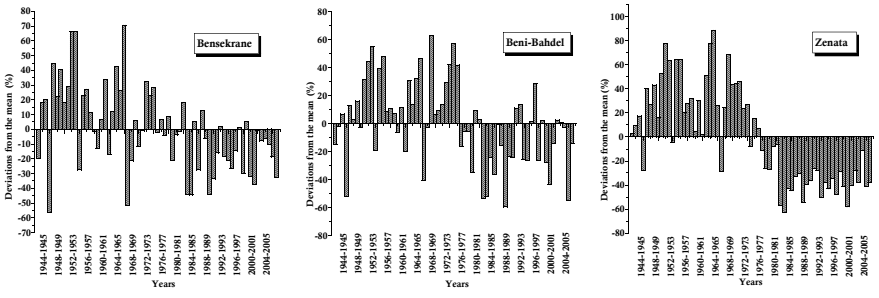

Fig. 5.10 Relative average deviations in annual rainfall for the period 1941–2006

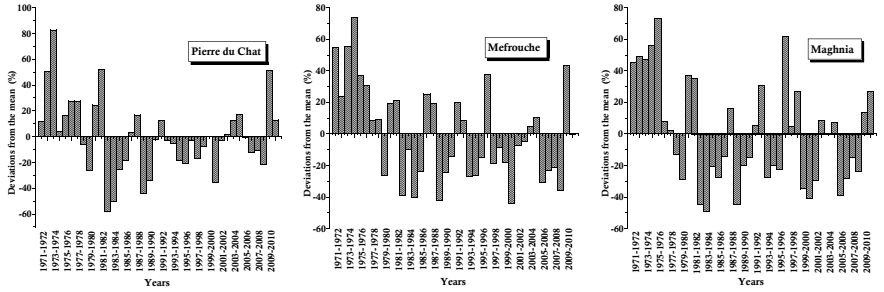

Fig. 5.11 Relative average deviations in annual rainfall over the 1970–2010 period

5.3.1.4 Study of Interannual Hydrometric Variability

The depth of runoff over the basins is marked by high temporal variability. Indeed, the transition from a wet year to a dry year can be very abrupt. For example, for the years 1933/34 and 1934/35, the Pierre du Chat station recorded runoff depths of 90.3 mm and 11.71 mm, respectively. The same case applies for Remchi station, which recorded a water depth of 157.7 mm in 1935/36 and a depth of only 28.1 mm in 1936/37 (Fig. 5.12).

An analysis of the evolution of the average annual flows using seven-year moving averages better illustrates the variability at all the stations (Table 5.9; Fig. 5.12). Figure 5.12 shows that the evolution of flows at the Pierre du Chat station is characterized by alternating periods of rainfall deficits and excesses. A dry period was identified between 1912/13 and 1926/27. The average flow during this period was 5.6 m^3/s with a minimum of 0.8 m^3/s in 1919/20. A wet period followed, lasting from 1926/27 to 1940/41. During this period, the average annual

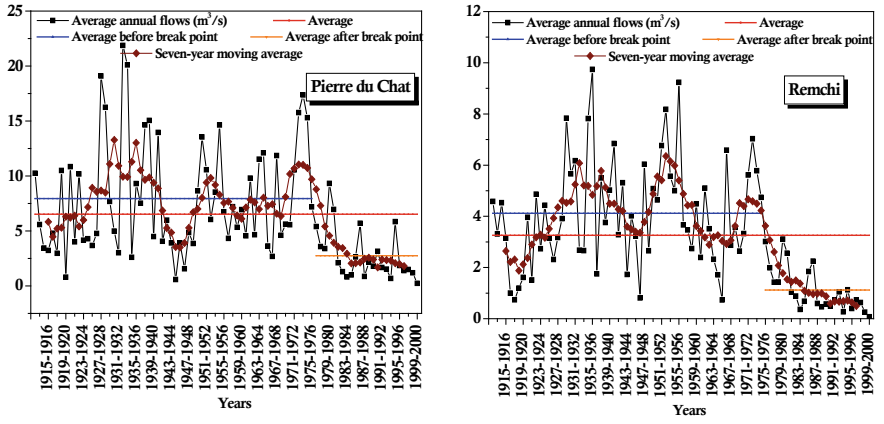

Fig. 5.12 Interannual variability in annual average station flows for the period 1912–2000

Table 5.9 Different trends at the studied hydrometric stations

Station	Beginning of the period	End of the period	Trend	Mean (m^3/s)	Max (m^3/s)	Min (m^3/s)
Study period 1912–2000						
Pierre du Chat	1912/13	1926/27	Deficit	5.6	10.8 (1920/21)	0.8 (1919/20)
	1926/27	1940/41	Excess	11.5	21.9 (1932/33)	2.6 (1934/35)
	1940/41	1949/50	Deficit	4.2	8.7 (1949/50)	0.6 (1944/45)
	1949/50	1975/76	Excess	8.8	17.36 (1973/74)	2.68 (1966/67)
	1975/76	1999/00	Deficit	2.8	9.3 (199/80)	0.2 (1999/00)
Remchi	1912/13	1928/29	Deficit	2.9	0.7 (1917/18)	4.9 (1922/23)
	1928/29	1975/76	Excess	4.5	9.7 (1935/36)	0.7 (1965/66)
	1975/76	1999/00	Deficit	1.04	3.1 (1979/80)	0.07 (1999/00)
Study period 1973–2009						
Pont RN7/A	1973/74	2000/01	Deficit	0.7	1.8 (1979/80)	0.2 (1992/93)
	2000/01	2008/09	Excess	1.3	1.6 (2004/05)	1.02 (2001/02)
Beni-Bahdel	1973/74	1980/81	Excess	1.5	2.7 (1973/74)	0.8 (1976/77)
	1980/81	2007/08	Deficit	0.7	2.5 (2008/09)	0.3 (2004/05

flow reached a value of 11.5 m^3/s. A second dry period occurred between 1940/41 and 1949/50 with a mean annual flow of 4.2 m^3/s. This short deficit phase was limited in time by a sequence of wet years beginning in 1949/50 and extending until 1975/76. The average flow during this period was 8.8 m^3/s. From 1975/76 to 1999/00, a long phase of dry years was established with a maximum flow of 9.3 m^3/s in 1979/80 and a minimum of 0.2 m^3/s in 1999/00.

The evolution of the interannual variability in the mean annual flow at the Remchi station includes three hydrometeorological periods (Table 5.9; Fig. 5.12), starting with an initial dry period between 1912/13 and 1928/29. Over this period, the average annual flow was 2.9 m^3/s, with a minimum of 4.9 m^3/s in 1922/23. The second period was a long sequence of wet years between 1928/29 and 1975/76. During this period, the maximum flow reached a value of 9.7 m^3/s in 1935–1936. The third period was marked by a more intense and more severe drought than the first; this dry period was established in 1975/76 and lasted until 1999/00. The average annual flow dropped to 1.04 m^3/s with a minimum of 0.07 m^3/s in 1999/00.

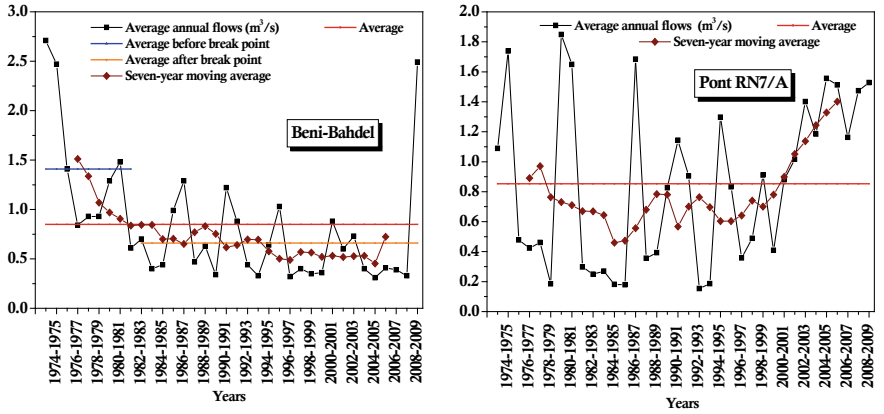

Fig. 5.13 Interannual variability in the annual average station flows over the 1973–2009 period

During the 1973–2009 study period, successions of dry and wet periods were observed at the two studied stations. For the Beni-Bahdel station (Table 5.9; Fig. 5.13), a sequence of wet years was detected during the period from 1973/74 to 1980/81. During this period, the average annual flow was 1.5 m^3/s with a maximum of 2.7 m^3/s in 1973/74. The second period observed at this station was a dry period beginning in 1980/81 and ending in 2007/08; the average annual flow was 0.7 m^3/s with a minimum of 0.3 m^3/s in 2004/05.

On the other hand, the interannual flow variability of the Pont RN7/A station (Table 5.9; Fig. 5.13) was characterized by an initial dry period from 1973/74 to 2000/01 followed by a wet period from 2000/01 to 2008/09. During this wet period, the average annual flow was 1.3 m^3/s.

Figures 5.14 and 5.15 show the deviations of the annual average flows from the mean. For the four stations, the wettest years correspond to 1932/33 for the Pierre du Chat station, 1935/36 for the Remchi station, 1973/74 for the Beni-Bahdel station and 1979/80 for the Pont RN7/A station, with deviations from the mean of 235.3%, 198.5%, 220.4% and 116.8%, respectively.

The driest year corresponded to 1999/00 for both the Pierre du Chat and Remchi stations (Fig. 5.14), 2004/05 for the Beni-Bahdel station and 1992/93 for the Pont RN7/A station (Fig. 5.15). The analysis results also show that the 1930s and 1970s stood out as surplus phases in the region.

5.3.1.5 Evaluation of the GR2M Model Applied to the Four Basins

The breaks in stationarity in the mid-1970s and early 1980s detected during the analysis of the rainfall series introduced a modification of the hydrological functioning of the four basins. Therefore, the choice of calibration periods becomes essential for the specification of the model parameters. In this study, to represent the

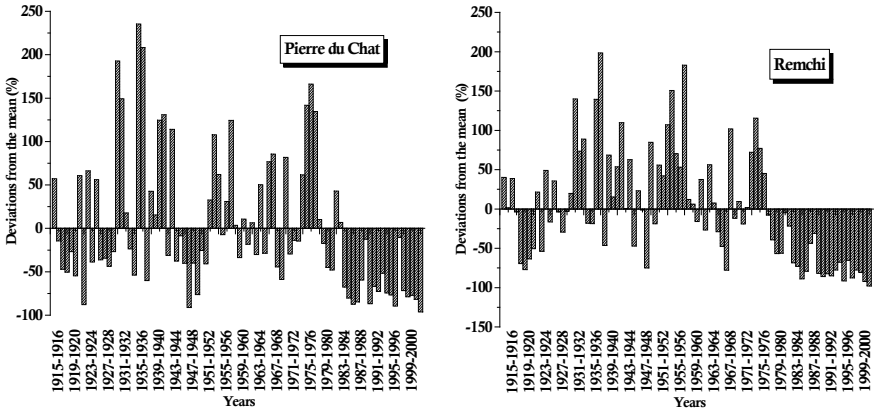

Fig. 5.14 Relative average deviations of annual average flows for the period 1912–2000

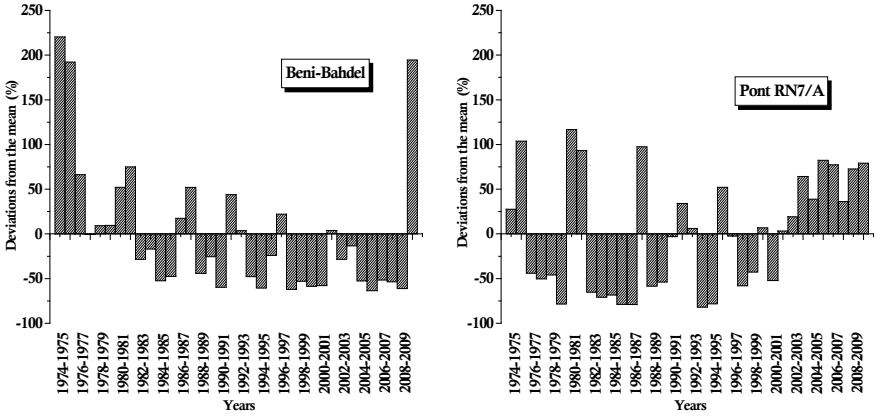

Fig. 5.15 Relative average deviations of annual average flows for the period 1973–2009

modeling results in the calibration and validation phases, we used 2/3 of the data for calibration and 1/3 for validation.

For hydrological modeling of the Tafna Maritime basin (1608), we used potential evapotranspiration data from the Zenata station and rainfall data from the Pierre du Chat station. Potential evapotranspiration data from the Mefrouche station and areal rainfall time series calculated from the Mefrouche and Bensekrane stations were used to model the Isser Sikkak basin (1607). The Upper Tafna basin (1604) was represented by rainfall data and potential evapotranspiration data from the Beni-Bahdel station. Finally, rainfall data series and potential evapotranspiration from the Maghnia station were adopted to represent the downstream Mouilah basin (1602).

Table 5.10 Results of the calibration (1976–1992) and validation (1992–2000) of the GR2M model at the Tafna maritime (1608) and Isser Sikkak (1607) basins for the period 1976–2000

ID	1608	1607	Average
Basin	Tafna maritime	Isser Sikkak	
X_1 (mm)	492.75	699.24	596.0
X_2	0.88	0.72	0.8
Nash calibration (%)	70.3	80.5	75.4
R^2 (%)	58.5	85.0	71.8
Nash validation (%)	74.4	88.5	81.5
R^2 (%)	97.2	90.3	93.8

The monthly flow simulation results for the four basins are shown in Tables 5.10 and 5.11.

According to Tables 5.10 and 5.11, the X_1 parameter varied between 492.75 and 699.24 mm, with an average of approximately 596.0 mm, during the 1976–2000 period and between 88.68 and 295.27 mm, with an average of 192 mm, for the 1976–2006 period. The parameter X_2 oscillated between 0.72 and 0.88 during the 1976–2000 period, with an average of 0.8, and between 0.42 and 0.74 in the 1976–2006 period, with an average of 0.6. These values are less than 1, which indicates that groundwater inflows to the different rivers. Indeed, when X_2 is greater than 1, there is a loss of water from the reservoirs to other watersheds, and vice versa. In the case of the four studied basins, the reservoirs contribute water to the rivers (Koffi 2007).

In general, for the calibration phase, the values of the Nash-Sutcliffe criteria were satisfactory for all four basins. The average performance of the Nash-Sutcliffe criterion was 75.4% for the studied basins during the 1976–2000 period and 77.2% for those analyzed over the 1976–2006 period. For the validation phase, the average values of the obtained Nash-Sutcliffe criteria were 81.5% for the basins modeled during the 1976–2000 study period and 78.7% for those analyzed over the 1976 to

Table 5.11 Results of the calibration (1976–1996) and validation (1996–2006) of the GR2M model at the Upper Tafna (1604) and downstream Mouilah (1602) basins for the period 1976–2006

ID	1604	1602	Average
Basin	Upper Tafna	Downstream Mouilah	
X_1 (mm)	295.27	88.68	192.0
X_2	0.74	0.42	0.6
Nash calibration (%)	78.7	75.6	77.2
R^2 (%)	80.3	86.3	83.3
Nash validation (%)	72.6	84.7	78.7
R^2 (%)	72.8	65	68.9

2006 period. Regarding the coefficient of determination (R^2), the values obtained were as follows: the maximum was 0.833 (1976–2006), and the minimum was 0.718 (1976–2000). In the validation phase, the maximum R^2 was obtained during the 1976–2000 period with a value of 0.938, and the minimum value was 0.689, obtained during the 1976–2006 period.

The different average performance values obtained for the calibration and validation phases of the GR2M model are shown in Table 5.12.

According to the double-sample method, the performance values obtained from the calibration and validation stages, which define the robustness criterion of the model, are acceptable. The range was between −0.4 and −5.9%, with an average of −3.2% for the basins analyzed during the 1976–2000 period. The values varied between −4.6 and +1.9%, with an average of −1.3%, for the basins analyzed over the period from 1979 to 2006. The absolute values of the robustness criterion obtained when the Nash-Sutcliffe criterion was used were less than 10%, which reflects the robustness of the GR2M model Mouelhi version applied to the Tafna Maritime (1608), Isser Sikkak (1607), Upper Tafna (1604) and downstream Mouilah (1602) basins.

Figures 5.16 and 5.17 indicate the hydrographs of the observed and simulated phases for the calibration and validation stages.

Figures 5.16 and 5.17 show that the dynamics of the simulated flows in the calibration and validation phases were fairly consistent with the observed flows. Indeed, the mean monthly runoff depths captured the seasonal variations of the calibration sample (Fig. 5.16). On the other hand, floods were poorly simulated, particularly after 1978, a period marked by the intensification of degradation phenomena in hydrometeorological conditions. These conditions also affected the parameters that constituted the forcing variables of the GR2M model. In the validation phase, the GR2M model underestimated the highest peak flows except in the Upper Tafna basin (1604), where the peak flows were overestimated (Fig. 5.17). On the other hand, the model generated very low flows during the period from 1987 to 1992 in the Tafna Maritime (1608) and Isser Sikkak (1607) basins and from 1988 to 1996 in the Upper Tafna (1604) and downstream Mouilah (1602) basins. These periods coincided with periods of drought.

Table 5.12 Average performance and robustness criterion of the GR2M model

		Average performance calibration	Average performance Validation	Range
Study period 1976–2000				
1608	Tafna Maritime	69.7	70.1	−0.4
1607	Isser Sikkak	79.2	85.1	−5.9
Average		74.5	77.6	−3.2
Study period 1976–2006				
1604	Upper Tafna	77.5	75.6	+1.9
1602	downstream Mouilah	80.9	85.4	−4.6
Average		79.2	80.5	−1.3

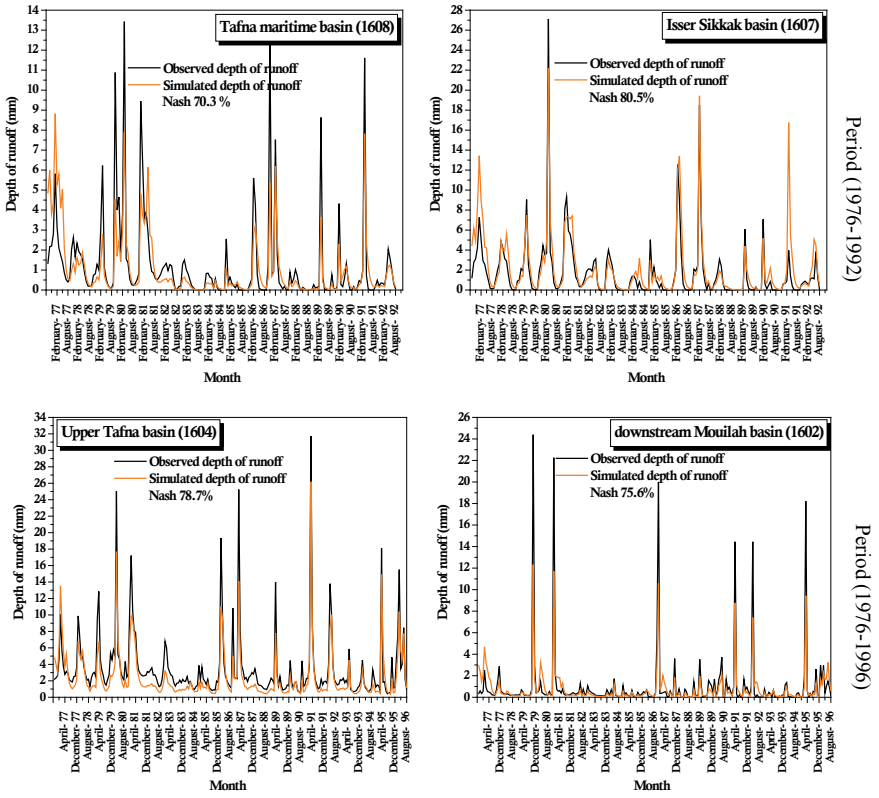

Fig. 5.16 Hydrographs of observed and simulated flows during the calibration phase of the GR2M model

5.3.1.6 Study of the Trend of the Rainfall-Runoff Relation

A matrix of cross-simulations was applied to the simulated annual average water depths, which made it possible to correctly present the rain-runoff relations in the four basins. The constituted periods, of which there were 4 in the 1976–2000 period and 5 in the 1976–2006 period, were in steps of 6 years. The results of this application are shown in Tables 5.13, 5.14, 5.15 and 5.16.

The matrices of cross-simulations were transformed into matrices of standardized simulations and then into sign matrices, as shown in Tables 5.17, 5.18, 5.19 and 5.20. Recall that the gains and losses are indicated in these matrices by "+" and "−" signs, respectively. As we studied the annual average flows in the direction of the progressive evolution of time, the half of each standardized matrix above the diagonal has been taken into account.

In the Tafna Maritime basin (1608), a total of 9 negative signs were recorded versus 3 positive signs. In the Isser Sikkak basin (1607), 11 negative signs were

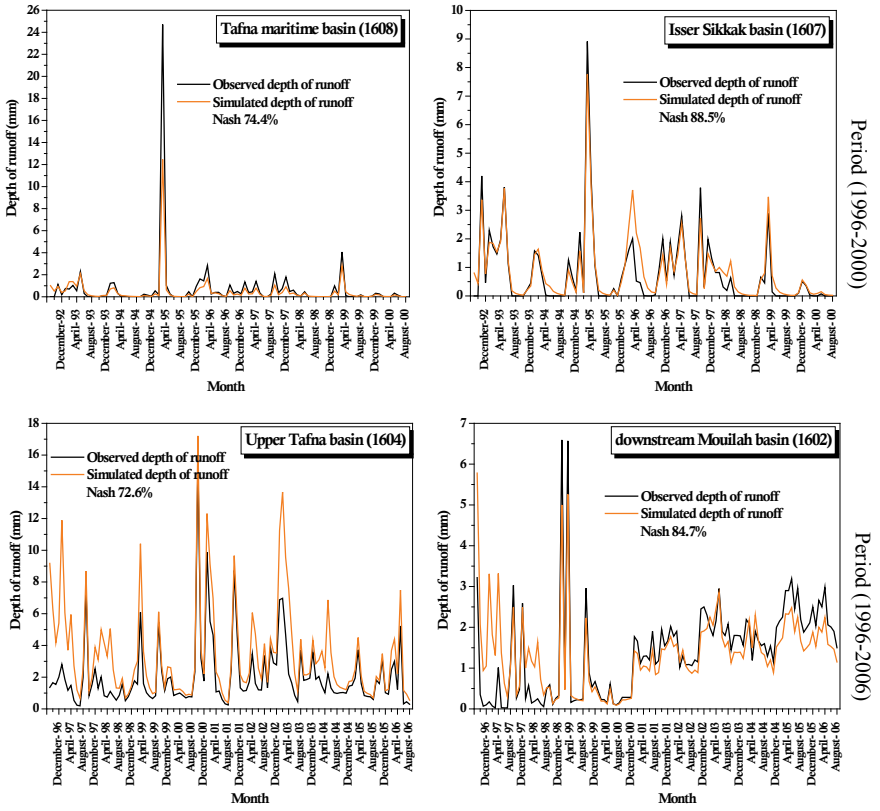

Fig. 5.17 Hydrographs of observed and simulated flows during the validation phase of the GR2M model

Table 5.13 Matrix of cross-simulations of runoff depth (mm) in the Tafna Maritime basin (1608) for the 1976–2000 period

	1976–1982	1982–1988	1988–1994	1994–2000
1976–1982	30.68	8.01	4.92	5.43
1982–1988	18.60	11.25	6.92	7.91
1988–1994	17.15	8.02	8.43	7.03
1994–2000	14.86	6.83	6.39	11.17

recorded versus 1 positive sign. In the Upper Tafna basin (1604), 14 negative signs were recorded versus 6 positive signs. In the downstream Mouilah basin (1602), 4 negative signs were recorded versus 16 positive signs.

Table 5.14 Matrix of cross-simulations of runoff depth (mm) for the Isser Sikkak basin (1607) for the 1976–2000 period

	1976–1982	1982–1988	1988–1994	1994–2000
1976–1982	26.19	18.43	14.05	7.23
1982–1988	27.53	17.13	11.44	7.07
1988–1994	27.21	19.32	6.74	5.62
1994–2000	31.26	20.37	9.26	9.83

Table 5.15 Matrix of cross-simulations of runoff depth (mm) for the Upper Tafna basin (1604) for the 1976–2006 period

	1976–1982	1982–1988	1988–1994	1994–2000	2000–2006
1976–1982	45.80	25.82	30.28	24.18	28.33
1982–1988	44.67	25.04	24.72	20.75	28.24
1988–1994	38.53	28.83	21.36	25.97	27.32
1994–2000	45.40	30.02	27.89	20.50	28.73
2000–2006	39.82	29.01	23.81	20.94	24.13

Table 5.16 Matrix of cross-simulations of runoff depth (mm) the downstream Mouilah basin (1602) for the 1976–2006 period

	1976–1982	1982–1988	1988–1994	1994–2000	2000–2006
1976–1982	11.12	8.10	11.13	10.23	20.28
1982–1988	8.60	5.72	7.08	7.75	21.91
1988–1994	9.09	6.46	7.88	9.89	18.96
1994–2000	9.16	6.88	8.58	9.27	20.75
2000–2006	9.24	6.61	8.22	9.06	20.26

Table 5.17 Sign matrix for the Tafna Maritime basin (1608) for the 1976–2000 period

	1976–1982	1982–1988	1988–1994	1994–2000
1976–1982	30.68	–	–	–
1982–1988	–	11.25	–	–
1988–1994	–	+	8.43	–
1994–2000	–	+	+	11.17

From the results for all the studied basins, it is apparent that the negative signs constitute the majority compared to the positive signs except in the downstream Mouilah basin (1602).

Table 5.18 Sign matrix for the Isser Sikkak basin (1607) for the 1976–2000 period

	1976–1982	1982–1988	1988–1994	1994–2000
1976–1982	26.19	–	–	–
1982–1988	–	17.13	–	–
1988–1994	–	–	6.74	–
1994–2000	–	–	+	9.83

Table 5.19 Sign matrix for the Upper Tafna basin (1604) for the 1976–2006 period

	1976–1982	1982–1988	1988–1994	1994–2000	2000–2006
1976–1982	45.80	–	–	–	–
1982–1988	–	25.04	–	–	+
1988–1994	–	–	21.36	+	+
1994–2000	–	–	–	20.50	+
2000–2006	–	–	+	+	24.13

Table 5.20 Sign matrix the downstream Mouilah basin (1602) for the 1976–2006 period

	1976–1982	1982–1988	1988–1994	1994–2000	2000–2006
1976–1982	11.12	–	+	–	+
1982–1988	–	5.72	+	+	+
1988–1994	–	+	7.88	+	+
1994–2000	+	+	+	9.27	+
2000–2006	+	+	+	+	20.26

The two study periods (1976–2000 and 1976–2006) are both characterized by high hydrometeorological variability. The assumption of the stationarity of the annual runoff time series in the Tafna Maritime (1608), Isser Sikkak (1607) and Upper Tafna (1604) basins can be rejected. Thus, this implies a nonstationarity of the rainfall-runoff relations, manifested by downward trends in the hydrological behavior of these basins. For the downstream Mouilah basin (1602), the stationarity hypothesis is accepted.

5.3.2 Discussions

During the last four decades, 1970–1980, 1980–1990, 1990–2000 and 2000–2010, a persistent decline in rainfall was experienced. The results of the application of the Pettitt and Mann-Kendall tests programmed in the Turbo Pascal language established that there was a significant downward trend at a significance level of 5% that

manifested itself during the mid-1970s and intensified during the 1980s. The rainfall deficit reached an average value of 34.6% during the period from 1941 to 2006; it fluctuated between 26.7 and 30.5% during the 1970–2010 study period. These results confirm the drought that plagues the countries of the southern shores of the Mediterranean. Thus, Sebbar (2013) estimated the rainfall deficit in Morocco to be between 17.8% and 20%. Bahir et al. (2020) estimated this deficit in the upstream part of the Essaouira basin (Morocco) at approximately 14% (1940–2015). In Algeria, Meddi et al. (2009) indicated that since the mid-1970s, deficit years are consistent, and these authors estimated rainfall deficits of 38% in Ain Fekane, 40% in Ras El Ma and 39% in Ben Badis. By analyzing the data of 16 rainfall stations located in the Tafna watershed, Ghenim and Megnounif (2013) found that the breakpoint seen from the middle to the end of the 1970s was sudden and substantial. In their study, observed rainfall deficit was estimated to be between 23 and 36%. Belarbi (2017), who studied the same watershed, showed that in addition to the downward trend and the timing of the breakpoint, the winter and spring rains greatly decreased. The analysis of the various results obtained by the seven-year moving average method confirms that the period after the break is dominated by deficit years beginning from the end of the twentieth century and extending into the early twenty-first century. Of the six stations used for the study of rainfall variability, five stations showed sudden drops in rainfall from 1981 to 1988. This period was marked by a severe drought in the region. This result was confirmed by the work of Meddi and Meddi (2009), who found that the 1980s were defined by the most abrupt and significant fluctuation (in the statistical sense of the term) observed in the northwest region of Algeria; the drop in rainfall amounted to more than 36% over the west of the country. This drop led to a reduction in the runoff contributions of the watersheds and was marked by a significant break in the stationarity of the runoff time series detected in the mid-1970s for the period 1912–2000 and in the mid-1980s for Beni-Bahdel hydrometric station during the period 1973–2009. Indeed, the characteristic synchronization of the breakpoints identified in the rainfall and flow time series underlines the indisputable link that exists between drops in rainfall and decreases in surface runoff (Kouassi et al. 2008). The average hydrometric deficit was estimated at 69.1% over the period 1912–2000 and was estimated to exceed 53% for the Beni-Bahdel station during the period 1973–2009. The runoff deficit was greater than the rainfall deficit, which reflects the intensification of meteorological drought at the level of runoff. The results of the time series analysis of runoff depth using the seven-year moving average method support the results found by change point detection tests. Indeed, the dry periods detected during the 1970s and 1980s coincided with the breaks in stationarity identified by the two statistical tests applied to the runoff time series data at the Pierre du Chat, Remchi and Beni-Bahdel stations. Similarly, an analysis of the results shows that the 1930s and 1970s stand out as surplus phases in the region.

The GR2M model was used to model monthly flows in the Tafna Maritime, Isser Sikkak, Upper Tafna and downstream Mouilah basins. The results show that this model is efficient and robust when applied to these basins. The performance of the model during calibration and validation attained NSE values over 60%. Similarly,

the values of the robustness criteria were less than 10% in absolute value. These results corroborate those previously found. Following these conclusions (performance and robustness), the GR2M model was used to analyze trends in the rainfall-runoff relation by applying the cross-simulation approach. This approach allows the testing of the expression of a stationarity behavior (such as in cases of progressive evolution, cases of sudden disturbances and cases of presumed stability) in rainfall-runoff relations. In our case, the results indicated decreases in the monthly runoff depth in two periods: 1976–2000 and 1976–2006. These results highlighted the nonstationarity of the hydrological response of the Tafna Maritime (1608), Isser Sikkak (1607) and Upper Tafna (1604) basins. This nonstationarity can be attributed to various causes. In some basins, nonstationarity results from the physiographic character of the basin (soils, relief, vegetation, etc.). In other basins, the change is probably due to rainfall variability, which is manifested by decreases in the frequency and quantity of rainfall depths.

5.4 Conclusions

An analysis of the variability of hydrometeorological observations allowed the characterization of the main modifications that the Tafna Maritime, Isser Sikkak, Upper Tafna and downstream Mouilah basins have experienced. Generally, for the four basins, rainfall deficits started in 1974/75 and continue to this day. The severities of these deficits vary from one year to another. However, the repercussions of this reduction in rainfall depth were identifiable in the runoff depth values, which showed clear downward trends detected in the mid-1980s.

Given its performance and robustness, the GR2M model was applied to analyze the trends in the rainfall-runoff relations of the Tafna Maritime and Isser Sikkak basins over the period from 1975 to 2000 and the downstream Mouilah and Upper Tafna basins over the 1976–2006 period. Nonstationarity was observed in the rainfall-runoff relations, characterized by downward trends in the hydrometric behavior of the Tafna Maritime (1608), Isser Sikkak (1607) and Upper Tafna (1604) basins. This decrease was attributed to the modification of the rainfall regime experienced in the region over the past 40 years and to the change in land use following the geographic and morphological modifications of each basin. These modifications, characterized by downward trends, motivate us to pay more attention to the proper functioning of completed or planned projects and challenge us to attain sustainable management of water resources in the region to mitigate persistent drought.

References

ABHOCC (Agence de Bassin Hydrographique Oranais Chott Chergui) (2006) Cadastre hydraulique bassin Tafna. Mission I. Inventaire des ressources en eau et en sols et des infrastructures de mobilisation. Document de synthèse: Ministère de ressources en eau, Algérie

Achite M, Mansour H, Toubal A, Lamrani C (2014) Etude de la variabilité climatique dans le nord-ouest algérien (Bassin de l'oued Mina): approche statistique. Int J Environ Water 3 (1):116–122

Aït Mouhoub D (1998) Contribution à l'étude de la sécheresse sur le littoral algérien par le biais de traitement des données pluviométriques et la simulation Mémoire de Magister Ecole Nationale Polytechnique

Aït-Mesbah S, (2012) Analyse du comportement hydrologique du bassin versant de l'Orgeval: tendance sur les cinquante dernières années Mémoire de Master 2 Université chatet Marie Curie Ecole des Mines de Paris & Ecole Nationale du Génie Rural des Eaux et des Forêts. France. Available from http://m2hh.metis.upmc.fr/archives/

Andréassian V, Parent E, Michel C (2003) A distribution-free test to detect gradual changes in watershed behavior. Water Resour Res 39(9):1252. https://doi.org/10.1029/2003WR002081

Bahir M, Ouhamdouch S, Ouazar D, Chehbouni A (2020) Assessment of groundwater quality from semi arid area for drinking purpose using statistical water quality index (WQI) and GIS technique Carbonates and Evaporites 35(1):27. https://doi.org/10.1007/s13146-020-00564-x

Barnett TP, Pierce DW, Schur R (2001) Detection of anthropogenic climate change in the world's oceans. Science 292(5515):270–274. https://doi.org/10.1126/science.1058304

Belarbi H (2017) Modélisation et régionalisation de la relation «pluie-débit» face au changement climatique: Impact sur les ressources en eau Thèse de Doctorat Université de Tlemcen Algérie

Belarbi H, Matari A, Habi M (2012) Etude des séries temporelles: Application aux données hydro climatologiques Sarrebruck Allemagne Edition Universitaires Européennes ISBN: 3841793169, 9783841793164

Belarbi H, Matari A, Zekouda N (2013) Mise en évidence des changements climatiques à l'aide des variations pluviométriques de la région Nord-Ouest Algérien 5éme Colloque International «Ressources en eau et Développement Durable» Alger Algérie 24 & 25 février 2013

Belarbi H, Touaibia B, Boumechra N, Abdelbaki C (2016) Persistance de la sècheresse pluviométrique au niveau du bassin de la Tafna Le 5éme Colloque International du réseau «Eaux & Climats» Changements globaux et ressources en eau: Etat des lieux. Adaptations et perspectives Fès, Maroc 12& 13 Octobre 2016

Belarbi H, Touaibia B, Boumechra N, Amiar S, Baghli N (2017) Sécheresse et modification de la relation pluie-débit: cas du bassin versant de l'Oued Sebdou (Algérie Occidentale) Journal des sciences hydrologiques 62(1):124–136 http://dx.doi.org/10.1080/02626667.2015.1112394

Belarbi H, Touaibia B, Boumechra N, Amiar S, Abdelbaki C (2019) Analyse de tendance hydrologique de quatre bassins versants dans le Nord-Ouest de l'Algérie VIème Colloque de l'Association francophone de Géographie physique (AFGP) «Géographie physique et gestion des risques et des catastrophes» Arlon Belgique 19–21 septembre 2019

Benblidia M, Thivet G (2010) Gestion des ressources en eau: les limites d'une politique de l'offre Notes d'analyse du CIHEAM et Plan Bleu n°58

Bodian A (2011) Approche par modélisation pluie-débit de la connaissance régionale de la ressource en eau: application au haut bassin du fleuve Sénégal Thèse de Doctorat Université Cheikh Anta Diop Dakar Sénégal

Bouanani A (2004) Hydrologie, transport solide et modélisation. Etude de quelques sous bassins de la Tafna (NW–Algérie) Thèse de Doctorat Université de Tlemcen Algérie

Braud I (2011) Méthodologies d'analyse de tendances sur de longues séries hydrométrologiques Fiche Technique OTHU N°23

Dahmani B, Hadjib F, Allal F (2002) Traitement des eaux du bassin hydrographique de la Tafna (N-W Algeria) Desalination 152:113–124

Djellouli F, Bouanani A, Baba Hamed K (2013) Modélisations pluie-débit par une approche globale: cas du bassin versant d'oued Louza (Oued El-Hammam- Macta) NW algérien Séminaire International sur l'hydrogéologie et l'Environnement Ouargla 5 & 7 Novembre

Frich P, Alexander LV, Della-Marta P, Gleason B, Haylock M, Klein Tank AMG, Peterson T (2002) Observed coherent changes in climatic extremes during the second half of the twentieth century. Climate Res 19:193–212

Ghenim A (2001) Contribution à l'étude des écoulements liquides et des dégradations du bassin versant de la Tafna cas d'Oued Isser, Oued Mouillah et la Haute Tafna Mémoire de Magister Université de Tlemcen Algérie

Ghenim A, Megnounif A (2013) Ampleur de la sécheresse dans le bassin d'alimentation du barrage Meffrouche (Nord-Ouest de l'Algérie). Géographie Physique et Environnement 7:35–49. Disponible http://physio-geo.revues.org/3173

Ghenim A, Seddini A, Terfous A (2008) Variation temporelle de la dégradation spécifique du bassin versant de l'Oued Mouilah (Nord-Ouest Algérien). J des Sciences Hydrologiques 53 (2):448–456

Ghenim A, Megnounif A, Seddini A, Terfous A (2010) Fluctuations hydro-pluviométriques du bassin versant de l'Oued Tafna à Béni-Bahdel (Nord-Ouest algérien) Sécheresse 21(2):115–120

Goula BTA, Savane I, Konan B, Fadika V, Kouadio GB (2006) Impact de la variabilité climatique sur les ressources hydriques des bassins de N'Zo et N'Zi en Côte D'Ivoire (Afrique tropicale humide) Vertigo 7(1):1–12

Kabouya M, Michel C (1991). Estimation des ressources en eau superficielle aux pas de temps mensuel et annuel, application à un pays semi-aride Revue des sciences de l'eau 4(4):569–587

Kendall MG (1975) Rank correlation methods, 4th Edn. Charles Griffin London

Kettab A (2001) Les ressources en eau en Algérie: stratégies, enjeux et vision Desalination 136 (1):25–33. https://doi.org/10.1016/s0011-9164(01)00161-8

Khedimallah A, Meddi M, Mahé G (2020) Characterization of the interannual variability of precipitation and runoff in the Cheliff and Medjerda basins (Algeria). J Earth Syst Sci 129 (1):134. https://doi.org/10.1007/s12040-020-01385-1

Koffi YB (2007) Etude du calage, de la validation et des performances des réseaux de neurones formels à partir des données hydro-climatiques du bassin versant du Bandama blanc en Côte d'Ivoire Thèse de Doctorat Université de Cocody Abidjan

Kouamé KF, Kouassi AM, N'Guessan Bi TM, Kouao JM, Lasm T, Saley MB (2013) Analyse de tendances dans la relation pluie-débit dans un contexte de changements climatiques: cas du bassin versant du N'ZO-Sassandra (Ouest de la Côte d'Ivoire). Int J Inno Appl Studies 2 (2):92–103

Kouassi AM (2007) Caractérisation d'une modification éventuelle de la relation pluie-débit et ses impacts sur les ressources en eau en Afrique de l'Ouest: cas du bassin versant du N'zi (Bandama) en Côte d'Ivoire Thèse de Doctorat. Université de Cocody

Kouassi AM, Kouamé KF, Goula BTA, Lasmi T, Parturel JE, Biemi J (2008) Influence de la variabilité climatique et de la modification de l'occupation du sol sur la relation pluie-débit à partir d'une modélisation globale du bassin versant du N'Zi (Bandama) en Côte d'Ivoire Revue Ivoirienne des Sciences et Technologie 11:207–229

Kouassi AM, Kouamé KF, Koffi YB, Kouamé KA, Oularé S, Biemi J (2011) Modélisation des débits mensuels par un modèle conceptuel: application à la caractérisation de la relation pluie-débit dans le bassin versant du N'zi-Bandama (Côte d'Ivoire). J Africain de Communication Scientifique et Technologique 11:1409–1425

Kouassi AM, N'guessan BTM, Kouamé KF, Kouamé KA, Okaingni JC, Biémi J (2012) Application de la méthode des simulations croisées à l'analyse de tendances dans la relation pluie-débit à partir du modèle GR2M: cas du bassin versant du N'zi-Bandama (Côte d'Ivoire) Comptes Rendus Geoscience 344:288–296. https://doi.org/10.1016/j.crte.2012.02.003

Laborde JP (1993) Carte pluviométrique de l'Algérie du Nord à l'échelle du 1/500000, notice explicative Projet PNUD/ALG/88/021 Alger Agence nationale des ressources hydrauliques

Makhlouf Z, Michel C (1994) A two-parameter monthly water balance model for French watersheds. J Hydrol 162:299–318

Mann HB (1945) Non parametric test against trend. Econometrica 13(3):245–259

Matari A, Kerrouche M, Bousid H, Douguedroit A (1999) Sécheresse dans l'ouest algérien Publications de l'association Internationale de Climatologie 12:98–106

Meddi M, Hubert P (2003) Impact de la modification du régime pluviométrique sur les ressources en eau du nord-ouest de l'Algérie In: Servat E et al (eds) Hydrology of mediterranean and semiarid regions. Wallingford: IAHS Press: IAHS publication 278:229–235

Meddi H, Meddi M (2009) Variabilité des précipitations annuelles du nord-ouest de l'Algérie Sécheresse 20(1):57–65. 10.1684/sec.2009.0169

Meddi M, Meddi H, Ketrouci K, Matari A (2005) Tendance du régime pluviométrique et sècheresse dans le nord-ouest algérien IVe colloque du département de géographie Eau et Espace: ressources, enjeux et aménagements Tunis

Meddi M, Talia A, Martin C (2009) Evolution récente des conditions climatiques et des écoulements sur le bassin versant de la Macta (nord ouest de l'Algérie) Géographie Physique et Environnement 3

Medejerab A, Henia L (2011) Variations spatio-temporelles de la sécheresse climatique en Algérie nord-occidentale Courrier du savoir 11:71–79

Megnounif A, Terfous A, Bouanani A (2003) Production et transport des matières solides en suspension dans le bassin versant de la Haute-Tafna (Nord-Ouest Algérien) Revue des sciences de l'eau 16(3):369–380

Milano M, Ruelland D, Fernandez S, Dezetter A, Fabre J, Servat E, Fritsch JM, Ardoin-Bardin S, Thivet G (2013) Current state Mediterranean water resources and future trends under climatic and anthropogenic changes. Hydrol Sci J 58(3):498–518. https://doi.org/10.1080/02626667.2013.774458

Mouelhi S (2003) Vers une chaîne cohérente de modèles pluie-débit conceptuels globaux aux pas de temps pluriannuel, annuel, mensuel et journalier Thèse de Doctorat ENGREF Cemagref Antony France

Mouelhi S, Michel C, Perrin C, Andréassian V (2006) Stepwise development of a two-parameter monthly water balance model. J Hydrol 318(1–4):200–214. https://doi.org/10.1016/j.jhydrol.2005.06.014

Mozas M, Ghosn A (2013) État des lieux du secteur de l'eau en Algérie Institut de Prospective Economique du Monde Méditerranéen (Etudes & Analyses)

Nash JE, Sutcliffe JV (1970) River flow forecasting through conceptual models Part I—a discussion of principles. J Hydrol 27(3):282–290

Paturel JE, Servat E (1996) Procédure d'identification de «ruptures» dans les séries hydrologiques; modification du régime pluviométrique en Afrique de l'Ouest non sahélienne IAHS Publication 238:99–110

Perrin C (2000) Vers une amélioration d'un modèle global pluie-débit au travers d'une approche comparative Thèse de Doctorat Institut National Polytechnique de Grenoble France

Perrin C, Michel C, Andréassian V (2007) Modèles hydrologiques du Génie Rural (GR) CEMAGREF Disponible. http://www.cemagref.fr/webgr

Pettitt AN (1979) A non-parametric approach to the change-point problem. Appl Stat 28(2):126–135

PNUD-FEM (Programme des Nations Unies pour le Développement—Fonds pour l'Environnement Mondial) (2003) Projet maghrébin sur les changements climatiques Algérie—Libye—Maroc—Tunisie Bilan et perspectives Projet RAB/94/G31

Renard B (2006) Détection et prise en compte d'éventuels impacts du changement climatique sur les extrêmes hydrologiques en France Thèse de Doctorat Institut National Polytechnique de Grenoble France

Rousset N, Arrus R (2006) L'agriculture du Maghreb au défi du changement climatique: quelles stratégies d'adaptation face à la raréfaction des ressources hydriques? Communication à WATMED 3 3éme conférence internationale sur les Ressources en Eau dans le Bassin Méditerranéen Tripoli (Liban)

Safar-Zitoun M (2019) Plan National. Sècheresse Algérie. Lignes directrices en vue de son opérationnalisation Ministère de l'Agriculture du développement rural et de la pêche Direction générale des forêts

Sebaibi A (2014) Potentialités agro-climatiques de la région de Zenata et de Maghnia. Étude d'une longue série climatique Mémoire d'Ingéniorat Université de Tlemcen

Sebbar A (2013) Etude de la variabilité et de l'évolution de la pluviométrie au Maroc (1935–2005): Réactualisation de la carte des précipitations Thèse de Doctorat Université d'Hassan II Mohammedia Maroc

Sebbar A, Badri W, Fougrach H, Hsaine M, Saloui A (2011) Etude de la variabilité du régime pluviométrique au Maroc septentrional (1935–2004) Sécheresse 22(3):139–148. https://doi.org/10.1684/sec.2009.0169

Sneyers R (1975) Sur l'analyse statistique des séries d'observations OMM Note technique n° 143. Genève

Terfous A, Megnounif A, Bouanani A, (2001) Etude du transport solide en suspension dans l'Oued Mouilah (Nord-Ouest Algérien) Revue des sciences de l'eau 14(2):175–185

Vervier P, Amigues JP, Salles D, Gazelle F, and Marmonier P (2004) Gestion de l'eau et la sécheresse. Colloque de Prospective «Sociétés et environnements» Paris France 5 & 6 février. Available from http://www.insu.cnrs.fr/publications/prospective-societe-environnement

Yue S, Wang CY (2004) The Mann-Kendall test modified by effective sample size to detect trend in serially correlated hydrological series. Water Resour Manag J 18(3):201–218

Part III
Rainfall-Runoff Modeling and Approaches

Chapter 6
Validation of Flash Flood Simulations Using Satellite Images and Community-Based Observations—Impact of Infiltration and Small-Scale Topographical Features

Franziska Tügel, Ahmed Hadidi, Ilhan Özgen-Xian, Jingming Hou, and Reinhard Hinkelmann

Abstract This work is aimed at investigating flash floods in the region of El Gouna, Egypt, by using a 2D robust shallow-water model that incorporates the Green-Ampt model to find the most realistic infiltration setting for this desert area. The results of different infiltration settings are compared to inundation areas observed from LANDSAT 8 images as well as to community-based information and photographs to validate the results despite scarce data availability. The model tends to overestimate infiltration in the study area if tabulated Green-Ampt parameters for the dominant soil texture class are considered. Specifically, bare soils with no vegetation tend to develop a surface crust, leading to significantly decreased infiltration rates during heavy rainfalls. Comparing the results of different infiltration settings with the observed data showed that the crust approach or the consideration of sandy clay loam instead of sand led to more plausible results for

F. Tügel (✉) · R. Hinkelmann
Chair of Water Resources Management and Modeling of Hydrosystems, Technische Universität Berlin, Straße des 17. Juni 135, 10623 Berlin, Germany
e-mail: franziska.tuegel@wahyd.tu-berlin.de

R. Hinkelmann
e-mail: reinhard.hinkelmann@wahyd.tu-berlin.de

A. Hadidi
Department of Applied Geosciences, GUtech German University of Technology, Muscat, Oman

I. Özgen-Xian
Geochemistry Department, EESA, Lawrence Berkeley National Laboratory, Berkeley, CA, USA
e-mail: iozgen@lbl.gov

J. Hou
School of Water Resources and Hydro-Power Engineering, Xi'an University of Technology, Xi'an, China
e-mail: jingming.hou@xaut.edu.cn

T. Sumi et al. (eds.), *Wadi Flash Floods*, Natural Disaster Science and Mitigation Engineering: DPRI Reports, https://doi.org/10.1007/978-981-16-2904-4_6

the considered study area than those obtained using the values for sand from two different sources in the literature. Furthermore, small-scale structures, which are not appropriately captured in the original digital surface model, but significantly affect the resulting flow field, have been included based on the available information leading to much more plausible results.

Keywords Shallow water equations · Hydroinformatics modeling system · Green-Ampt Model · Data scarcity · Landsat-8 · Egypt

6.1 Introduction

Flash floods generated by heavy rainfall events occur all over the world, even in desert areas. As they occur very suddenly and have destructive power, flash floods can affect highly developed cities as well as areas with poor infrastructure. This emphasizes how challenging it is to deal with such events. As climate change and enhanced urbanization might lead to increased intensities and frequencies of such events, appropriate mitigation and adaptation measures will become even more important. In arid regions such as the Eastern Desert of Egypt, flash floods are often caused by heavy rainfall in wadi catchments, where high rainfall amounts from a large area quickly accumulate in the wadi streams. Often, cities and settlements are located in the downstream regions of normally dry wadi catchments, and during rare flash flood events, these cities and settlements are immediately at high risk of flooding. Flash floods also affect the Red Sea region of Egypt almost every year, leading to damage to infrastructure and properties and endangering human lives. This work presents a 2D shallow-water model setup for El Gouna, a town of approximately 15,000 inhabitants located along the Red Sea coast of Egypt. The model can be used to analyze the flood areas generated from different rainfall events and to investigate different structural mitigation measure scenarios, such as retention basins and drainage channels. In previous work, a sensitivity analysis on a simplified catchment was carried out, and the results showed that in addition to other parameters, such as friction and rain intensity, infiltration has a strong influence on runoff at the outlet of the catchment (Tügel et al. 2018). In Tügel et al. (2020a), the impacts of infiltration under different parameter sets as well as under different mitigation measure scenarios for the city of El Gouna were studied, and infiltration was represented for different extreme rainfall events. As Hou et al. (2020) showed that the temporal storm resolution plays an important role in obtaining reliable simulation results of inundated areas, a temporal rainfall distribution was incorporated in the model used to study flash floods in El Gouna instead of a simplified approach consisting of a constant average rain intensity, as used in earlier studies, e.g., Tügel et al. (2020a).

The calibration and validation of flash flood models are commonly challenging, as in most cases, no direct measurements of water depths or flow velocities are available due to the sudden occurrence of heavy rainfall. Furthermore, the spatial

distribution of flash floods over a wide land surface instead of at fixed points, as during river floods, exacerbates the challenge of obtaining direct measurements. Therefore, other data sources must be considered to obtain estimations of flood extent and water depth to check the plausibility of simulation results. A useful and widely available source for detecting land cover changes and flood areas are remotely sensed multispectral images, for example, from the Landsat-8 or Sentinel-2 satellites; however, due to their rather coarse temporal resolutions of several days up to weeks, their usability is limited when considering relatively short flood events such as flash floods. In recent years, community-based, crowd-sourced data or so-called citizen science approaches have been used in different studies, for example, for studies on the hydrological modeling of ungauged catchments and flash floods (Starkey et al. 2017) and studies aiming to validate the results of city-scale 2D flood simulations (Yu et al. 2016). Smith et al. (2017) assessed the usefulness of social media for flood risk management, and Liang et al. (2017) investigated the potential contribution of crowd-sourced data such as photographs and messages to real-time flood forecasting.

Infiltration excess represents the main contributor to runoff generation during storm events in arid areas. Especially in rural areas and urban green spaces, infiltration losses cannot be neglected. An appropriate representation of infiltration during heavy rainfall events is important to include the runoff generation in hydrodynamic models and for calculating water depths and flooding areas more realistically. Additionally, due to the increasing interest in sustainable urban drainage systems (SUDS) (e.g., Vergroesen et al. 2014; Ghazal 2018; Hou et al. 2019), the appropriate consideration of infiltration in 2D hydrodynamic rainfall-runoff models is also of great interest for the accurate assessment of the effectiveness of decentralized stormwater management measures such as infiltration basins and trenches. The Green-Ampt model (Green and Ampt 1911) is often used to calculate time-dependent infiltration rates; for example, it is often used in hydrological catchment models. However, only a few studies have coupled a 2D shallow-water model with the Green-Ampt model, such as Esteves et al. (2000) and Xing et al. (2019), which showed the general capability of these methods to simulate rainfall runoff and infiltration processes.

For real-world applications, it is often difficult to estimate the Green-Ampt parameters in terms of the hydraulic conductivity, capillary suction head at the wetted front, and effective porosity of a catchment area, in addition to the initial soil water content of the soil. If runoff measurements are available, the Green-Ampt parameters are often considered as calibration parameters (e.g., Fernández-Pato et al. 2016; Ni et al. 2020). For ungauged areas or during flash floods, direct measurements are usually unavailable, and different methods to estimate the Green-Ampt parameters have evolved and been investigated in recent decades. One well-known contribution is the work of Rawls et al. (1983), in which average parameter sets dependent on the soil texture class and soil horizon were derived from 5000 soil samples. In the manual of the modeling software company Innovyze (2019), other average values are recommended to be used to estimate the

Green-Ampt parameters if no measurements are available, and these estimations refer to different sources, such as Akan (1993).

During heavy rainfall events, soil surfaces can become clogged, which leads to reduced infiltration rates. In particular, on bare, unprotected soils without vegetation in arid regions such as the study area, the kinetic energy of raindrops can cause the formation of a surface seal or crust (Morin and Benyamini 1977; Müller 2007; Nciizah and Wakindiki 2015). Such layers have been observed to be approximately 1 to 5 mm thick (Tackett and Pearson 1965; Sharma et al. 1980). A modified Green-Ampt model in which the hydraulic conductivity is calculated as the effective hydraulic conductivity of the crust and subcrust soil is one simple approach that can be used to account for the effects of a surface crust (Brakensiek and Rawls 1983; Esteves et al. 2000; Nciizah and Wakindiki 2015).

In this study, the results of flash flood simulations of the event that occurred on March 09, 2014 in El Gouna are validated by Landsat-8 images as well as community-based photographs and statements. The most suitable infiltration settings were determined, while the tabulated Green-Ampt parameters from two different sources were considered with and without the consideration of a surface crust of reduced hydraulic conductivity, following the approach of Brakensiek and Rawls (1983). Furthermore, the topographical data were checked due to poor agreement of the model results with the observed data at some locations for the late timesteps. Three major modifications in the original digital surface model (DSM) based on observations from satellite images and photographs were proposed to improve the model results.

6.2 Methods and Materials

6.2.1 Shallow Water Flow Model

To set up a 2D shallow water flow model of the study area, the hydroinformatics modeling system (hms) was used; this system is an in-house software of the Chair of Water Resources Management and Modeling of Hydrosystems, Technische Universität Berlin (Simons et al. 2012, 2014; Busse et al. 2012). In the system, different laws are implemented to calculate the bottom friction, and rainfall and infiltration can be considered for each cell individually through sink/source terms in the mass balance equation. In this study, the turbulent viscosity, *vt*, is set to zero as turbulent effects can usually be neglected in rainfall-runoff simulations. The bottom friction is calculated with Manning's law. The general form of the conservation laws is spatially discretized with a cell-centered finite–volume method, and an explicit forward Euler method is used for the time discretization. The conserved variables, q, for the new time level, $n + 1$, are calculated as shown in Eq. (6.1):

$$\mathbf{q}^{n+1} = \mathbf{q}^{n} - \frac{\Delta t}{A}\sum_{k}\mathbf{F}_{k}^{n}\cdot\mathbf{n}_{k}l_{k} + \Delta t\mathbf{s}^{n} \tag{6.1}$$

where $n + 1$ and n denote the new and old time levels, respectively; $\mathbf{q}$ is the vector of conserved variables; $\mathbf{F}$ is the flux vector over edge k; $\mathbf{s}$ is the vector of source terms; k is the index of a face of the considered cell. The timestep is denoted with Δt; A is the area of the considered cell; $\mathbf{n}$ is the normal vector pointing outward from the face; l is the length of the face.

Equation (6.1) is solved with a second-order MUSCL scheme (Hou et al. 2013). As rainfall-runoff simulations usually deal with small water depths over complex topography and are associated with propagating wet-dry fronts, flow transitions, and high gradients, robust numerical methods are required to prevent numerical problems and instabilities. The implemented HLLC Riemann solver used to compute the fluxes over the cell edges is able to handle discontinuities in the flow field. A total variation diminishing scheme including different slope limiters is used to avoid spurious oscillations (Hou et al. 2013; Özgen et al. 2014). The water depth threshold necessary to consider a cell as dry was set to 10^{-6} m, and at high gradients, the scheme switches from second-order to first-order accuracy (Hou et al. 2013; Murillo et al. 2009).

6.2.2 *Infiltration*

Infiltration processes were represented with the Green-Ampt model. In the model, the calculation of cumulative infiltration is performed iteratively as given in Eq. (6.2); afterward, the infiltration rate is calculated using Eq. (6.3). Equations (6.2) and (6.3) are described as follows:

$$F(t) = Kt + (h_0 - \psi)\Delta\theta\ln\left(1 + \frac{F(t)}{(h_0 - \psi)\Delta\theta}\right) \tag{6.2}$$

$$f(t) = K\left(1 + \frac{(h_0 - \psi)\Delta\theta}{F(t)}\right) = \frac{\mathrm{d}F}{\mathrm{d}t} \tag{6.3}$$

where $F(t)$ denotes the cumulative depth of infiltration; $f(t)$ describes the infiltration rate in terms of the temporal change in the cumulative infiltration depth; K denotes the hydraulic conductivity at the residual air saturation, which is assumed to be 50% of the saturated hydraulic conductivity, K_s (Whisler and Bouwer 1970). The capillary suction head at the wetted front of the soil is given with ψ, h_0 is the ponding water depth, and $\Delta\theta$ is the increase in moisture content calculated by the difference between the effective porosity, n, and the initial moisture content, θ_i. The effective porosity, capillary suction head at the wetted front, and hydraulic conductivity are the so-called Green-Ampt parameters, which can be estimated from the given soil

texture class. There exist different approaches to account for such a crust; a simple approach can be seen in Brakensiek and Rawls (1983), in which the effective hydraulic conductivity of the crust and subcrust soil is calculated by a harmonic mean (Rawls et al. 1990). Table 6.1 shows the Green-Ampt parameters for four different soil texture classes described by Rawls et al. (1983).

Other values of the parameters are given in the user manuals of the hydraulic and hydrologic modeling software XPStorm and XPSWMM of the Innovyze company (2019) based on different sources. These manuals state that higher initial soil moisture deficit values are applicable for very dry conditions, and lower values should be used when wetter initial conditions occur. The values for four different soil texture classes are given in Table 6.2.

Comparing the values from Innovyze (2019) with those from Rawls et al. (1983) shows that the hydraulic conductivity for sand from Rawls et al. (1983) is approximately one order of magnitude higher than the maximum value from Akan (1993), and the value for loamy sand is more than double the one from Akan, while the values are similar for sandy clay loam from Rawls et al. (1983) and for clay loam from Akan (1993). For clay, the value from Rawls et al. (1983) is closer to the minimum value than to the maximum value from Akan (1993). The average capillary suction head values from Rawls et al. (1983) are lower than those from Innovyze (2019) for all soil types except clay, for which the value from Rawls et al. (1983) is almost double that from Innovyze (2019).

If it is expected that the considered soil will generate a surface crust with a lower hydraulic conductivity than the subcrust soil, a modified infiltration model can be used to account for such a crust. There exist different approaches to designing this mode; a simple approach can be seen in Brakensiek and Rawls (1983), in which the effective hydraulic conductivity of the crust and subcrust soil is calculated by a harmonic mean (Rawls et al. 1990):

$$K_{\mathrm{e}} = \begin{cases} K_{\mathrm{c}} & \text{for} \quad Z_f \leq Z_{\mathrm{c}} \\ \frac{Z_f}{\frac{Z_f - Z_{\mathrm{c}}}{K} + \frac{Z_{\mathrm{c}}}{K_{\mathrm{c}}}} & \text{for} \quad Z_f > Z_{\mathrm{c}} \end{cases} \tag{6.4}$$

where K_{e} is the effective hydraulic conductivity, K_{c} is the hydraulic conductivity of the crust, Z_{c} is the crust thickness, and Z_{f} denotes the wetted depth, which is

Table 6.1 Average Green-Ampt parameters

Soil texture class	Effective porosity n (–)	Capillary suction head ψ (cm)	Hydraulic conductivity K (cm/h)
Sand	0.417	4.95	11.78
Loamy sand	0.401	6.13	2.99
Sandy clay loam	0.330	21.85	0.15
Clay	0.385	31.63	0.03

Source Rawls et al. 1983

Table 6.2 Typical values of Green-Ampt parameters given in the user manuals of XPStorm and XPSWMM

Parameter	Typical initial moisture deficit at wilting point (m^3/m^3)	ψ (cm)	K (cm/h)
Reference	(Clapp and Hornberger 1978)	Several; sources not given	(Akan 1993)
Sand	0.34	10.16	0.76–1.14
Loamy sand	–	–	0.76–1.14
Clay loam	0.24	25.40	0.00–0.13
Clay	0.21	17.78	0.00–0.13

Source Innovyze (2019)

calculated by dividing the cumulative infiltration depth from the previous timestep by the soil moisture deficit.

6.2.3 Study Area

El Gouna is a tourist town 25 km north of Hurghada in the Red Sea Governorate of Egypt. It is located inside the catchment of Wadi Bili. The total catchment area of Wadi Bili is approximately 880 km^2, and the wadi flows from the Red Sea Mountains, passes through a narrow channel to the coastal plain of El Gouna and finally drains into the Red Sea. In recent years, the region of El Gouna has been affected by flash floods several times, leading to road and infrastructure damage. Measurements of the rainfall and runoff of the event that occurred on March 09, 2014 were carried out and published in Hadidi (2016). Figure 6.1 shows the location of Hurghada in Egypt (a) and the topography and catchment area of Wadi Bili (b). Panel 1(c) represents the region of El Gouna on the coastal plain, including the location of the discharge measurements collected in 2014 in a narrow valley upstream of where the wadi spreads into a wider delta.

6.2.4 Data for Validation of Results

As it is usually difficult to obtain direct measurements of flash flood events, alternative data sources need be considered to enable a validation of the results. In this study, three different kinds of data are taken into account: multispectral satellite images, pictures taken by the community, and statements from the community.

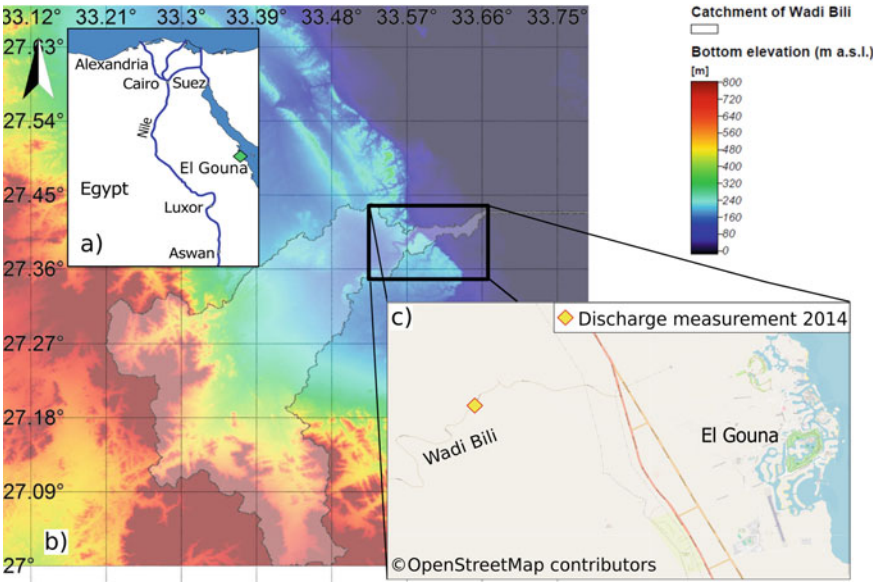

Fig. 6.1 **a** location of Hurghada in Egypt (made with Natural Earth), **b** topography and Wadi Bili catchment (delineated from SRTM DEM and visualized with SAGA GIS), and **c** location of discharge measurements from Hadidi (2016) and the city of El Gouna (map: ©OpenStreetMap contributors)

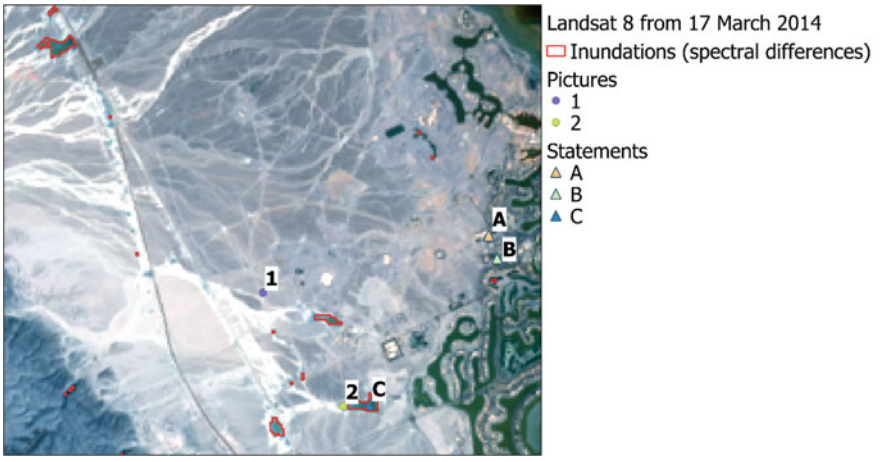

Fig. 6.2 Landsat 8 image from 17 March 2014 indicating the locations of the pictures and statements as well as the inundated areas obtained from automatically detection of land use changes from the spectral distance between Landsat 8 images of 20 February and 17 March 2014 (Landsat 8 image courtesy of the U.S. Geological Survey)

Figure 6.2 shows the locations at which information of these three different sources was obtained; the information types are further described in the next sections.

6.2.4.1 Landsat 8 Images

Images from the Landsat 8 satellite, which was launched in February 2013, are available for the time of the considered flash flood event in El Gouna in March 2014. These images contain eleven different bands with different resolutions; most of them have a resolution of 30 m. The "Semi-Automatic Classification Plugin" (SCP) was used to download the images directly in QGIS (Congedo 2016). As the temporal resolution of 16 days is relatively coarse and, due to excessively high cloud cover during the days of the rainfall event itself, the images of 20 February and March 17, 2014 were chosen as the best images to be compared to detect the inundated areas caused by the event on 9 March 2014. Both images are shown in Fig. 6.3, and when the images are compared, it becomes obvious which areas were still inundated 8 days after the event. Following the SCP documentation, only bands 2–7 were considered, and the band processing tool "Spectral distance" was used to automatically detect land cover changes between 20 February and March 17, 2014. "Spectral angle mapping" was chosen as the distance algorithm, and the distance threshold was set to 10. After vectorizing the results and extracting them for the land surfaces, the polygons of inundated areas observed from the Landsat 8 images are shown with red polygons in Fig. 6.2.

6.2.4.2 Pictures

Another important source of information about the inundated areas and estimated water depths that occurred during the event are pictures that were taken during and

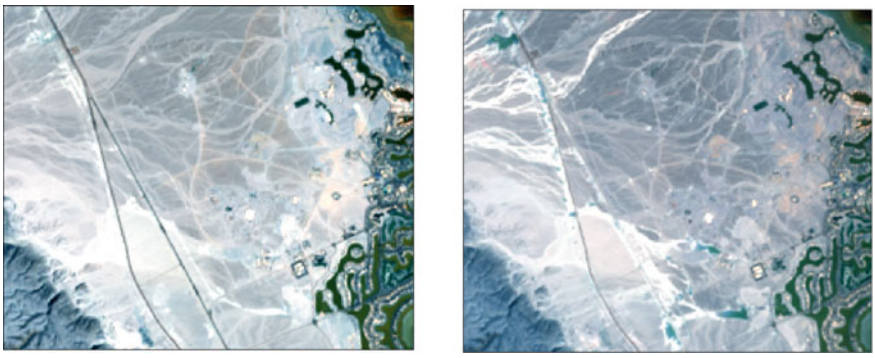

Fig. 6.3 Landsat 8 images from 20 February 2014 (left) and March 17, 2014 (right) (Landsat 8 image courtesy of the U.S. Geological Survey)

after the event. In this study, it was very important to obtain the geographical information on the location where each picture was taken. The best case occurs when the geotag function was activated on the used device while taking the pictures. Another possibility is to locate each picture as precisely as possible by descriptions or through orientation based on striking features in the surroundings. Many pictures were collected from the flash flood event in March 2014, but unfortunately, only very few of them were geotagged. Two of these photos were chosen and are shown in Fig. 6.4. The left panel shows an inundated road with a driving car. The water depth can be estimated to be between 10 and 25 cm, as the car tire seems to be inundated up to less than half of its diameter. The right picture shows an inundated area with some children. The water depth can be estimated to be approximately 25–35 cm as the water goes up to the knees of the children. The locations obtained from the geotags are indicated with circles in Fig. 6.2; 1 indicates the location of the left picture, and 2 indicates the location of the right picture.

6.2.4.3 Statements

The third source of information used in this study are statements from persons who were in El Gouna at the time of the event and observed the inundations in different areas. To gather these statements, requests for information on and pictures of the events were shared in different groups on Facebook and via email. Furthermore, a

Fig. 6.4 Pictures of inundated areas were taken on March 09, 2014, at 15:04 (Picture 1, left) and on March 10, 2014, at 12:49 (Picture 2 right). The right picture was modified for reasons of data protection to make the shown persons unrecognizable. *Source* private

questionnaire was created with KoboToolbox, in which the locations of observed inundations can be directly tagged within the toolbox and pictures can be uploaded.

6.3 Model Setup

To simulate the flood extent, water depths, and flow velocities for the region of El Gouna, a shallow-water model was set up for a domain of approximately 9 km 11 km. The grid consisted of 438,372 rectangular cells of 15 m × 15 m each. To consider the topography of the model area, the digital surface model (DSM) ALOS WORLD 3D (JAXA 2017) was used, as it was concluded in preliminary studies that this model represents the study area better than other freely available digital surface models with the same resolution, 30 m, namely, SRTM, and ASTER GDEM2 (Tügel et al. 2018). To reach smoother gradients between the cells, inverse distance weighted interpolation with an output cell size of 10 m was conducted by using QGIS. As most of the buildings were not included in the original DSM, buildings were incorporated from open street map polygons by increasing the elevation of the original DSM by 10 m. Figure 6.5 shows the interpolated DSM, including buildings, for the model domain. A Manning coefficient of 0.01 $m^{-1/3}$·s was used to represent the friction of bare sand based on the values given in Engman (1986). As an initial condition, the system was considered to be completely dry. The incoming flood wave from the Wadi Bili catchment was taken into account with a boundary condition at the channel cross-section, where Hadidi (2016) carried out flow velocity measurements and estimated the water depths and runoff rates during the event on March 09, 2014. The inflow hydrograph considered in this study, which has a peak discharge of 47.5 m^3/s, was generated from a hydrological model presented in Tügel et al. (2020b) that was calibrated with the hydrograph observed by Hadidi (2016). The temporal distribution of rainfall with a resolution of 10 min that was recorded during the event in 2014 at the weather station at TU Berlin Campus El Gouna was considered a source term for all cells inside the model domain. A total time period of 45 h was simulated to calculate the flow propagation inside the domain.

6.4 Results and Discussion

6.4.1 Simulated Flow Field Without Infiltration

The simulation results include the flood extents, spatial distributions of water depths, and flow velocities every three hours over the total simulation time of 45 h. These outputs enable an analysis of the temporal and spatial developments of the flood event. Figure 6.6 represents the simulated flow velocities, and Fig. 6.7 shows

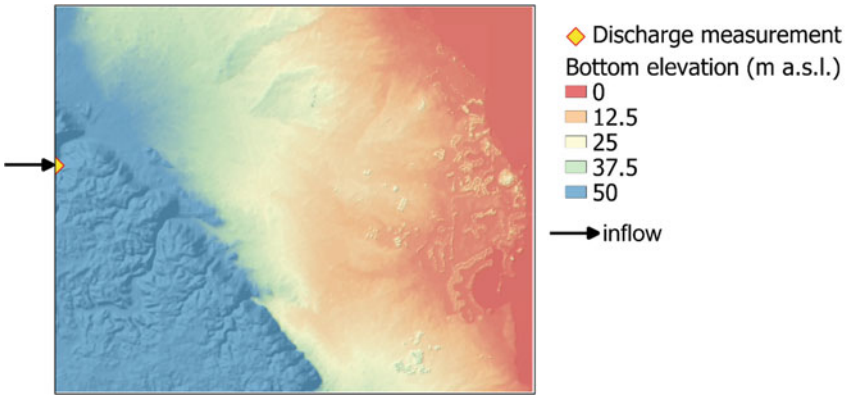

Fig. 6.5 Model domain, location of inflow, and topography from the AW3D digital surface model and incorporated buildings from Openstreetmap polygons

the simulated water depths after 9 h, when the maximum water depths were simulated, in a zoomed-in part of the model domain with open street maps in the background to better locate the inundated areas within the city. The analytical hillshade in the background allows the visualization of elevation and improves the visibility of buildings, which were incorporated in the DSM. The flood came from Wadi Bili at the western boundary of the domain and spread into different flow paths, some of which propagated to the northeastern direction, crossing the model boundaries, and continued beyond the considered domain. Other flow paths propagated to the southeast direction to the city of El Gouna. In addition to the incoming flood wave from the wadi catchment, the rainfall inside the domain also generated streams at different locations, and water accumulated in several depressions. The area around the campus of TU Berlin (denoted by A in Fig. 6.6 and Fig. 6.7) and the area around the student dorms (denoted by B in Fig. 6.6 and Fig. 6.7) were only affected by rainfall inside the domain, and water depths up to 0.20 m were simulated, which agrees well with the statements given for these locations (see Table 6.3); although the time in the first statement was 7 pm, and the timestep shown in the figure is 9 pm. However, the timestep for 6 pm also showed inundations of approximately 0.10 m, which agrees well with the statement that the shoes of individuals were submerged. In the northwest corner of the depicted section, a large flooded area was observed in the Landsat 8 images, where inundations with water depths of approximately 0.20 m were also simulated. At all locations where inundations were observed and reported by at least one of the considered sources, a flooded area with a certain water depth was simulated. Only at location 1 was no water depth simulated although flooded roads were observed at this location, as shown in Picture 1 (Fig. 6.4, left). In the close surroundings of that location, water depths up to 0.50 m were simulated. Additionally, it must be taken into account that the geotags of the pictures might not be very accurate. At location C, where maximum inundations of 2.00 m were reported within the questionnaire,

the maximum simulated water depth was only 0.40 m. On the other hand, Picture 2 (Fig. 6.4, right), which is close to location C, led to an estimated water depth of approximately 0.25–0.35 m, which fits quite well with the simulated water depths. A large flooded area with an overall maximum water depth of approximately 1 m was simulated close to the desalination plant (indicated with a red X in Fig. 6.7), while none of the considered observation sources indicated specifically high water depths at this location. From earlier personal exchanges with staff members of the desalination plant, it is known that inundations were also observed there but not in the range of 1 m. Flow velocities between 0.5 and 2.5 m/s were simulated for most streams. These numbers seem to be reasonable, as during a smaller flash flood event in the same area that occurred on October 27, 2016, flow velocities of approximately 1 m/s were measured by one coauthor in a stream next to the main connection road, which crosses the section shown in Figs. 6.6 and 6.7 from the north-northwest to the south-southeast.

6.4.2 *Infiltration*

As most parts of the model domain consist of natural bare surfaces and mostly sandy soils with high hydraulic conductivities, infiltration should not be neglected. In this section, the obtained results when accounting for infiltration with the Green-Ampt model are represented for different parameter values. Taking into account the average Green-Ampt parameters for loamy sand from Rawls et al. (1983) (see Table 6.1) and an initial moisture content of 0.03 m^3/m^3, assuming very dry soil before the rainfall event, all the water infiltrated before reaching the city of El Gouna (Fig. 6.8 left). Taking into account the parameter values for sand from Innovyze

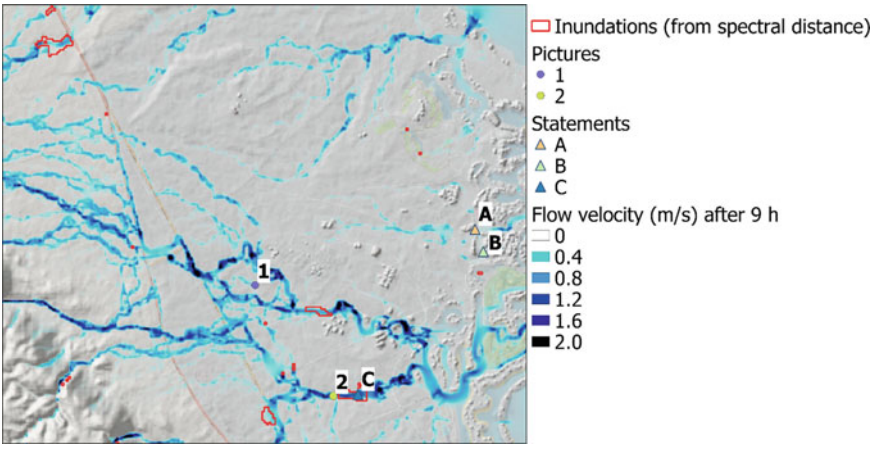

Fig. 6.6 Simulated flow velocities after 9 h of simulated time, including the locations of observations as described in Sect. 6.2.4

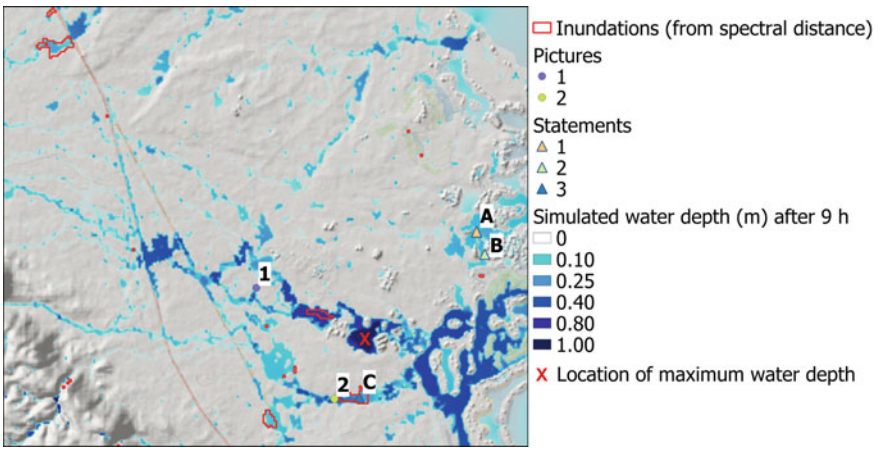

Fig. 6.7 Simulated water depths after 9 h of simulated time, including the locations of observations as described in Sect. 6.2.4

Table 6.3 Statements from the El Gouna community regarding inundated areas and water depths during the flash flood event in El Gouna on March 09, 2014

Location	Statement	Source
A	*The flood kind of receded in about a day. After that, the road was quite bad and slippery We stayed the night in the uni, as we could not move out at all*	Facebook group for students of TU Berlin Campus El Gouna
Between A and B	*I remember that the area between the university and the dorms was flooded* (dorms: location B)	Facebook group for students of TU Berlin Campus El Gouna
Between A and B	*By around 7 pm, I remember our shoes were submerged ankle deep in front of the library building*	Facebook group for students of TU Berlin Campus El Gouna
Between A and B	*The ground where GSpace is currently situated, water stagnation had happened for days*	Facebook group for students of TU Berlin Campus El Gouna
C	*Maximum observed water depth of estimated 2 m near El Gouna cable park*	Questionnaire created with KoboToolbox

(2019) (see Table 6.2), the flood wave propagated slightly further than in the case of loamy sand from Rawls et al. (1983), but most of the area around El Gouna was still completely dry - the local rainfall did not lead to any surface runoff as it directly infiltrated, and most of the locations where inundations were reported from the considered sources (see Sect. 6.2.4) did not show any water depths. Therefore, it can be concluded that both sets of Green-Ampt parameters for sandy soil strongly overestimate infiltration.

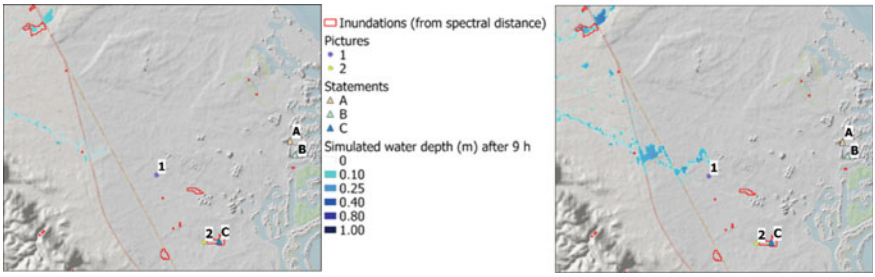

Fig. 6.8 Water depths after 9 h of simulated time for the average Green-Ampt parameter values for loamy sand from Rawls et al. (1983) (left) and for sand from Innovyze (2019) with the minimum hydraulic conductivity value (right)

Figure 6.9 shows the water depths after 9 h as simulated for sandy clay loam from Rawls et al. (1983) and for sand from Rawls et al. (1983), as well as for sand from Innovyze (2019), both accounting for a surface crust (after Eq. 6.4) of 5 mm thickness and a hydraulic conductivity equal to that for clay from Rawls et al. (1983) (see Table 6.1). All three of the simulations show very similar distributions of flooded areas, with some differences in water depths. The simulated flooded areas were still significantly reduced compared to the case without infiltration (Fig. 6.7), but surface runoff also occurred in the city area, leading to inundations in some areas. At most locations where inundations were reported via at least one of the considered sources (see Sect. 6.2.4), significant water depths were simulated. However, at locations, A and B corresponding to the statements that report inundations around Campus El Gouna and the student dorms, only small water depths with a maximum of 0.05 m were simulated. In most parts of the study area, the dominant soil type is sand with pebbles, sometimes combined with mud (Hadidi 2016), but only the parameters for finer soil texture classes, such as sandy clay loam, or the consideration of a surface crust with a reduced hydraulic conductivity led to surface runoff in some areas of El Gouna as it was observed during the event in 2014.

To further investigate the suitability of these three infiltration settings, the temporal development of the water depths inside three of the major ponds that were observed by the Landsat 8 image taken on 17 March are plotted in Fig. 6.10, and the location of each pond is labeled in Fig. 6.9 with P1, P2, and P3. In addition to the results of the three infiltration settings, the water depths that were simulated if no infiltration was considered are shown in Fig. 6.10. It can be seen that at all three locations, the water depth dropped to zero at first for the case of sand from Rawls et al. (1983) with a crust, second for the case of sand from Innovyze (2019) with a crust, and then for sandy clay loam from Rawls et al. (1983). As the crust effect regarding decreased hydraulic conductivity decreases with ongoing time and increasing wetted depth (see Eq. (6.4)), considering the case of sand from Rawls et al. (1983) with a crust again resulted in overestimating infiltration after a certain time. The same effect is valid for the case of sand from Innovyze (2019), but due to

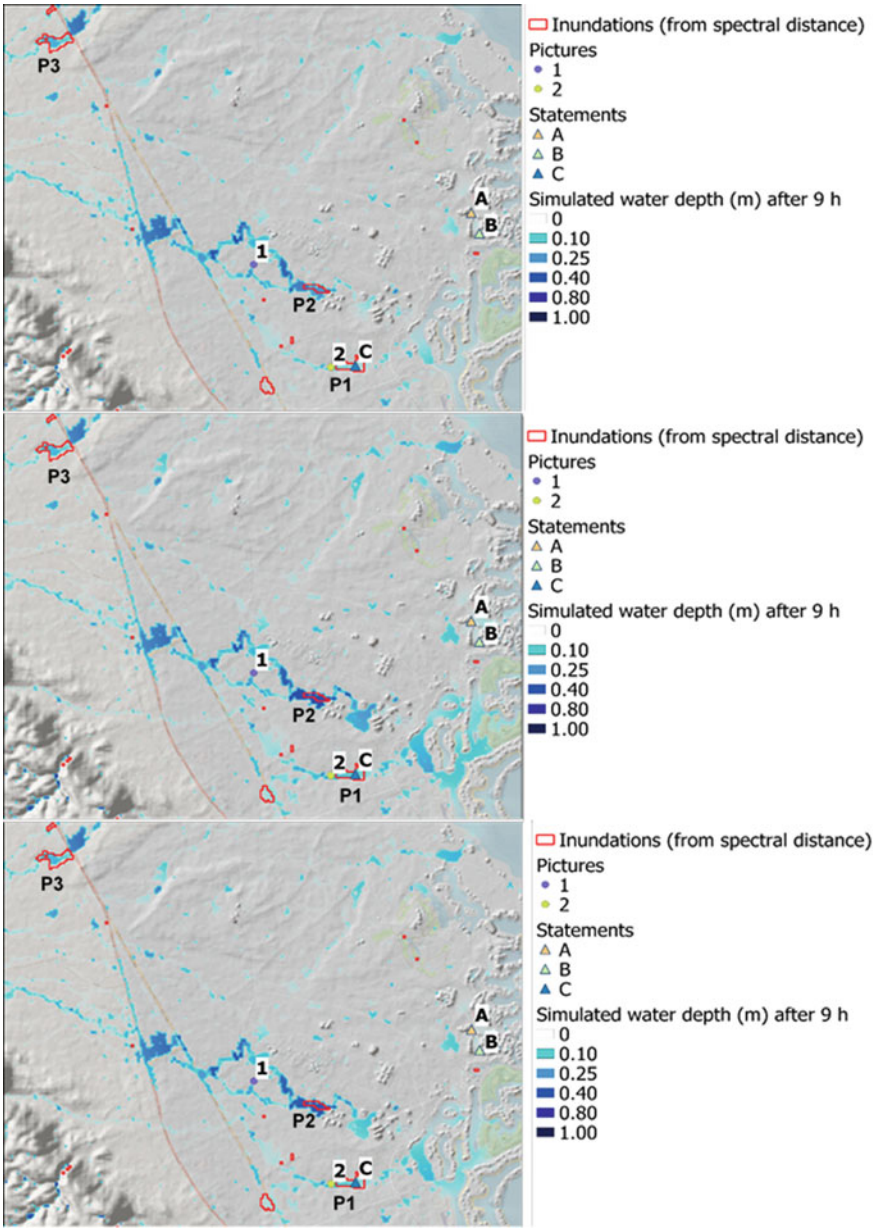

Fig. 6.9 Spatial distributions of water depth after 9 h for the cases of sandy clay loam from Rawls et al. (1983) (top), sand from Rawls et al. (1983) with a surface crust (middle), and sand from Innovyze (2019) with a surface crust (bottom)

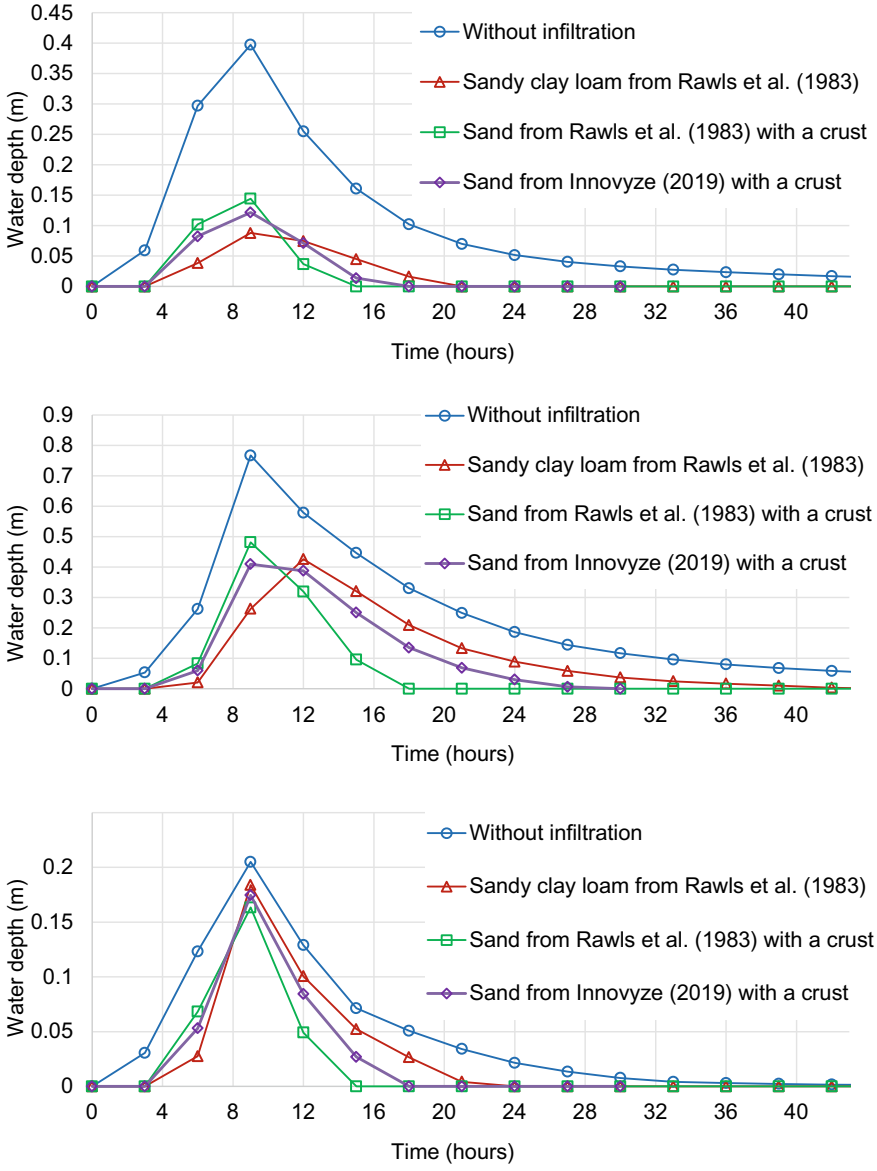

Fig. 6.10 Temporal development of water depths inside pond P1 (top), pond P2 (middle), and pond P3 (bottom); the locations of the ponds are indicated in Fig. 6.9. The temporal resolution is three hours

the smaller hydraulic conductivity of the subcrust sand compared to the values from Rawls et al. (1983) the overestimation of the infiltration is smaller, but the water also completely disappeared after approximately 18 h (P1 and P3) and 28 h (P2).

The results of the case considering sandy clay loam from Rawls et al. (1983) seem to be more reasonable than the two other cases, but in this case, the water still disappeared at all three locations after approximately 21 h (P1), 41 h (P2), and 28 h (P3). The flow velocities for these three infiltration settings were reduced in many areas compared to those simulated in the case without infiltration but still lie between 0.5 and 2.5 m/s in the main streams.

For the case without infiltration, there was still some water present at the locations of the observed ponds P1 and P2, but only in the range of 0.02 m in depth at P1 and 0.05 cm in depth at P2, while at P3, the water disappeared by the end of the simulation time of 45 h. As the ponds were still quite large on March 17, 2014 (eight days after the event), it can be concluded that even the simulation without infiltration seemed to underestimate the water depth at those locations. When looking at the Landsat 8 images of later dates, it becomes obvious that P2 disappeared approximately one month, P1 between one and two months, and P3 approximately five months after the rainfall event. Therefore, in addition to the overestimation of infiltration, an incorrect representation of the topography of the area is most likely another reason for the underestimated water depth obtained in the simulations, as there might be deeper depressions or blockages of the flow paths causing higher water depths and larger flooding areas that are not well-captured in the relatively coarse DSM. The next section further investigates the digital surface model (DSM) and introduces modifications in certain areas based on observations from satellite data as well as from pictures of the area.

6.4.3 Correction of DSM

As shown in the previous section, some characteristics are not well-captured in the DSM, leading to underestimations of water depths; for example, the water depths were underestimated at the locations of several ponds that were observed by Landsat 8 images. If a high-resolution and accurate DSM is not available for a certain study area, the best option would be to carry out field surveys and create a high-resolution DSM, e.g., one derived from laser-scanning data recorded with the help of an unmanned aerial vehicle (UAV). As the necessary capacities for such investigations are not available, the given DSM can also be modified based on observations in the field, from satellite images, or from pictures of the area. Three major modifications were carried out to the DSM of the model domain with regard to the three observed ponds, P1, P2, and P3: (1) the elevation of the main road that crosses the model domain from north-northwest to south-southeast was increased; (2) the wall around Scarab Club El Gouna was incorporated; (3) the dam directly east of pond P1 was incorporated, as observed from satellite images taken in February 2014. The locations of these modifications are presented in Fig. 6.11, and the reasons and explanations for each of the three modifications are given in the following sentences. In Fig. 6.12 (top), the water depths after 45 h are represented when taking into account the original DSM (without infiltration), showing a large pond in the upper-left corner

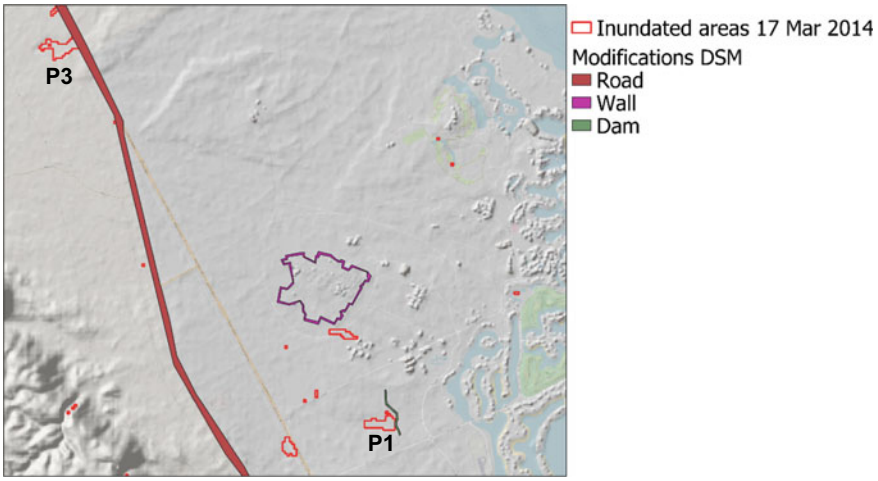

Fig. 6.11 Locations of carried out modifications in the DSM

of the depicted section. In the simulation results, this pond is located east of the road, while pond P3 is located directly on the other side of the road, as observed in the Landsat 8 images. This leads to the conclusion that the road is probably blocking the flow path, resulting in an accumulation of water west of the road instead of east of the road. From pictures taken of the area, it can be seen that the road is slightly elevated and has a high curbstone, while the original DSM shows a small lowering of the road compared to the adjacent area. To better capture the blocking of the flow path through the elevated road, the area of the road was elevated by 0.50 m in the DSM. The second modification incorporated a wall around the Scarab Club El Gouna, which is located north of P2. This wall was not included in the original DSM and might lead to redirections of flows in the corresponding area. The elevation in the area of the wall was increased by 10 m. The third modification was performed east of pond P1, as seen in satellite images from the time before the event in March 2014, when a sand dam was built to block the flow at that location. To include the dam in the DSM, the elevation at the location of the dam was elevated by 1 m. Figure 6.12 (middle) shows the water depths after 45 h taking into account the modified DSM without infiltration, and Fig. 6.12 (bottom) shows the water depths with infiltration considering sandy clay loam from Rawls et al. (1983). For both cases, ponds P1 and P3 are much better captured than in Fig. 6.12 (top), where the original DSM was taken into account, while P2 is slightly better represented with the modified DSM when no infiltration is considered but is not well-captured if infiltration with sandy clay loam is taken into account.

Figure 6.13 shows the temporal development of the water depths at P1, P2, and P3 considering the modified DSM without infiltration (top) and with infiltration through sandy clay loam (bottom). While the water depth considerably increased at P1 and P3 after the modification of the DSM, it remained almost the same at P2

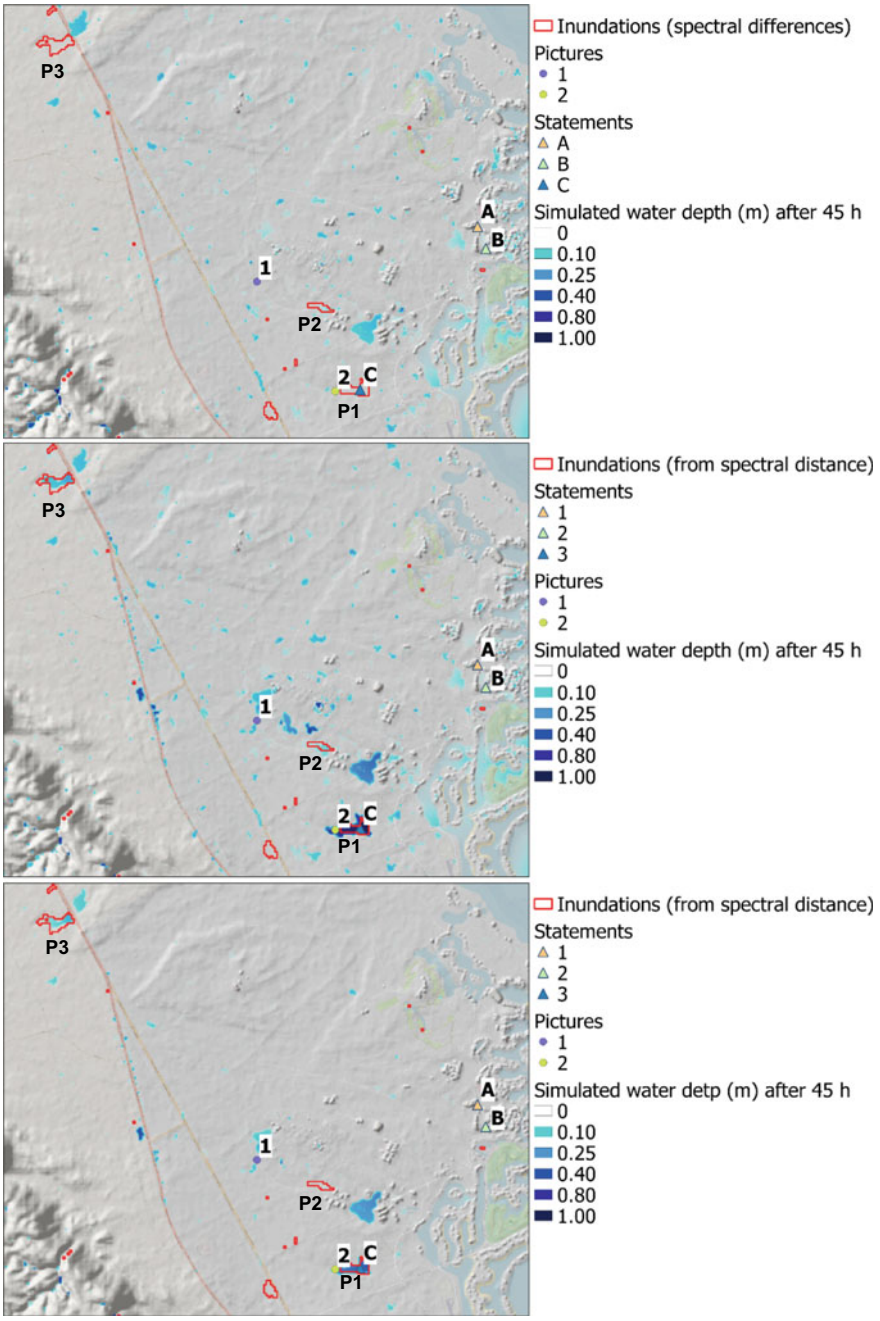

Fig. 6.12 Spatial distributions of water depths after 45 h of simulated time considering the original DSM without infiltration (top), the modified DSM without infiltration (middle), and the modified DSM accounting for infiltration with the Green-Ampt parameters for sandy clay loam from Rawls et al. (1983)

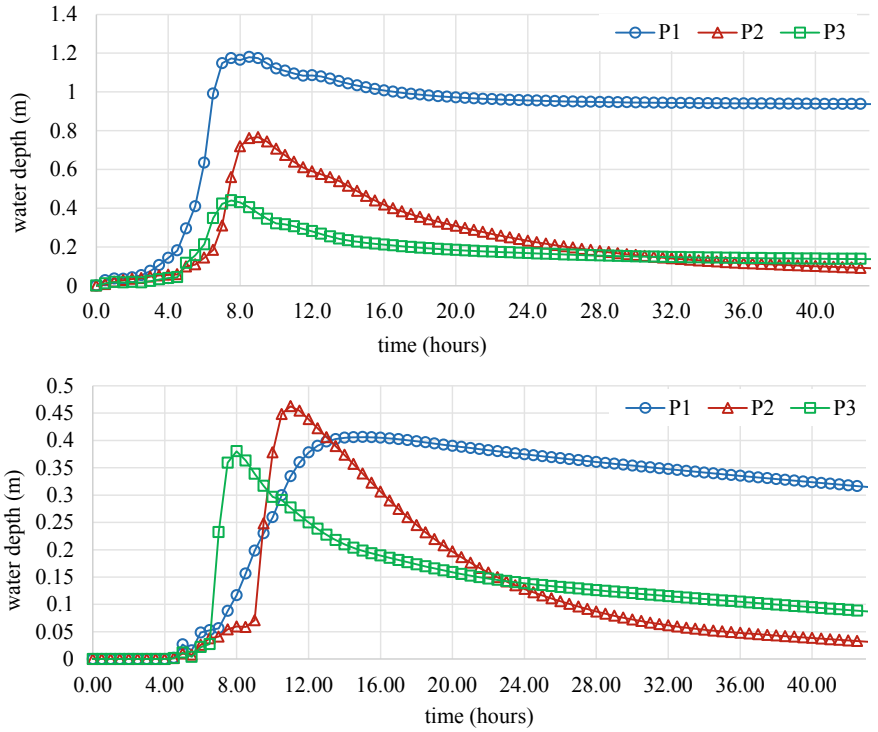

Fig. 6.13 Temporal development of the water depths of ponds P1, P2, and P3 considering the modified DSM without infiltration (top) and the modified DSM with infiltration through sandy clay loam from Rawls et al. (1983); the locations of ponds are indicated in Fig. 6.12; the temporal resolution is 30 min

compared to the water depth calculated with the original DSM, shown in Fig. 6.10. Therefore, the wall around the Scarab Club El Gouna north of P2 had only a very small influence on the water depth at P2. There might be additional features in the area of P2 that are not represented appropriately in the DSM, leading to higher observed water depths than the simulated ones.

Of course, all presented modifications in the DSM are based on strongly simplified assumptions and rough estimations of the modified elevations. Furthermore, there might be further features that are not captured appropriately in the DSM, such as a fourth pond located west of P1 that is also not well-captured in the simulation results as well as inundated areas indicated in statements A and B. In general, the results underline the importance of accurate and high-resolution topographical data, which is unfortunately often not available or not easily accessible. However, as the results could be clearly improved with regard to the observed ponds P1 and P3, it can also be concluded that a careful modification of the DSM to incorporate known features can significantly improve the simulation results. Of course, only available observations, e.g. from satellite images or photographs, can justify these modifications as long as there are no accurate data from topographical surveys available.

6.5 Conclusions

In this study, the flash flood event that occurred on 9 March 2014 in the region of El Gouna, Egypt, was simulated with a robust 2D shallow-water model using the hydroinformatics modeling system (hms), and the results were validated with observations from different sources. As direct measurements of water depths and flow velocities are often not available for flash floods, especially in data-scarce regions such as the region where the study area is located, alternative sources must be taken into account. Here, multispectral images from the Landsat 8 satellite, pictures of inundations taken from the community in El Gouna, and statements from persons who observed the flooded areas during and after the event were collected to compare the simulation results with these observations.

The results after nine hours of simulated time agreed relatively well with most of the observed flooded areas and were plausible in terms of the ranges of water depths and flood extents, while there were a few locations where the model underestimated the observed flood extents and water depths. The simulated flow velocities seem to be plausible compared to the velocities measured during a smaller flash flood event in the same area. As the investigated area consists mostly of bare sand, infiltration should not be neglected and was taken into account with the time-dependent Green-Ampt model. When the Green-Ampt parameters were set to values indicated in two different sources in the literature for the dominant soil types of sand and loamy sand, infiltration was strongly overestimated by the model, while the consideration of a surface crust with a thickness of 5 mm and the hydraulic conductivity of clay or the consideration of the literature-obtained values for sandy clay loam instead of sand led to much better agreements of the simulation results with the observations. For locations where inundations were observed even a few days up to a few months after the rainfall event, most of the water had already drained out of the area by the end of the simulation time of 45 h, even if no infiltration was considered in the model. This led to the conclusion that in addition to the overestimation of infiltration, the DSM lacked accuracy and resolution, so some important topographical features that had significant impacts on the flow paths and the development of flooded areas were not well captured. Three modifications in the DSM were introduced based on observations from satellite images and personal photographs, and the simulation results of the modified DSM agreed much better with the observed flood extents and water depths at the end of the simulation time of 45 h. Nevertheless, the DSM most likely still lacked other important features, so the flood extent and water depth were still underestimated at several locations. Although the DSM needs further improvements, the model results, such as the maps of flooded areas, support the risk assessment, and different structural mitigation measures can be incorporated in the model to investigate their effectiveness for different rainfall events.

Overall, it could be shown that the considered data sources in terms of satellite images and community-based pictures and statements can be used for a rough validation of the model results if no direct measurements are available. A drawback

of using Landsat-8 images is its relatively low temporal resolution, which makes it difficult to examine the extent of floods immediately after rainfall events. Therefore, only flooded areas that remained for a longer time can be observed from these satellite images. Data from the Sentinel-2 satellites that were launched in June 2015 (2A) and March 2017 (2B) have higher temporal resolutions of approximately 5 days and spatial resolutions of 10 m, which makes these data even more suitable for analyzing events that occurred more recently.

Due to the rather low temporal resolution of satellite images and because it remains challenging to estimate water depths from satellite images, community-based information in terms of statements and pictures is also very important for assessing model results if no direct measurements are available. Although the event occurred several years ago at the time the requests were sent to the community, several useful statements were collected. Regarding the collected pictures, the problem was not the number of photos but rather the localizations of their recordings, as most of the photos were not geotagged. Currently, as the usage of smartphones with very good cameras and often automatically activated geotagging has considerably increased in recent years, it is probably much easier to find pictures that include corresponding geospatial information. As the general activity on different social media platforms is also continuously increasing, it is likely that many more pictures and statements from social media communities could be found for more recent flood events, especially with the help of machine learning techniques.

The next steps are to conduct infiltration measurements with a rainfall simulator to better represent the natural conditions during heavy rainfall events and to investigate the effect of surface sealing. These steps will enable more appropriate implementations of infiltration processes in the model. In general, a further improvement of the DSM is needed to achieve more accurate results.

Acknowledgments This work was supported by TU Berlin, Germany. The travel grants of the DFG Research Training Group "Urban Water Interfaces" (GRK 2032/1) are gratefully acknowledged. The simulations were computed on the supercomputers of Norddeutscher Verbund für Hoch—und Höchstleistungsrechnen in Berlin and Göttingen as well as on the HPC cluster of TU Berlin.

References

Akan AO (1993) Urban stormwater hydrology: a guide to engineering calculations. Technomic Pub. Co, Lancaster, Pa

Brakensiek D, Rawls W (1983) Agricultural management effects on soil water processes. Part II: green and Ampt parameters for crusting soils.), pp 1753–1757. Trans ASAE 26(6):1753–1757

Busse T, Simons F, Mieth S, Hinkelmann R, Molkenthin F (2012) HMS: a generalised software design to enhance the modelling of geospatial referenced flow and transport phenomena. In: Proceedings of the 10th international conference on hydroinformatics—HIC 2012, Hamburg

Clapp RB, Hornberger GM (1978) Empirical equations for some soil hydraulic properties. Water Resour Res 14(4):601–604

Congedo L (2016) Semi-automatic classification plugin documentation
Engman E (1986) Roughness coefficients for routing surface runoff. J Irrig Drain Eng 11(1):39–53
Esteves M, Faucher X, Galle S, Vauclin M (2000) Overland flow and infiltration modelling for small plots during unsteady rain: numerical results versus observed values. J Hydrol 228(3–4):265–282
Fernández-Pato J, Caviedes-Voullième D, García-Navarro P (2016) Rainfall/runoff simulation with 2D full shallow water equations: sensitivity analysis and calibration of infiltration parameters. J Hydrol 536:496–513
Ghazal A (2018) Urban flood protection in arid regions King Fahd suburb in Dammam—Saudi Arabia. Master's thesis, TU Berlin Campus El Gouna, Water Engineering
Green W, Ampt G (1911) Studies on soil physics, Part 1, the flow of air and water through soils. J Agric Sci 4:11–24
Hadidi, A (2016) Wadi Bili catchment in the Eastern Desert—flash floods, Geological model and hydrogeology. Dissertation. Fakultät VI—Planen Bauen Umwelt der Technischen Universität Berlin, Berlin
Hou J, Liang Q, Simons F, Hinkelmann R (2013) A stable 2D unstructured shallow flow model for simulations of wetting and drying over rough terrains. Comput Fluids 132–147
Hou J, Zhang Y, Tong Y, Guo K, Qi W, Hinkelmann R (2019) Experimental study for effects of terrain features and rainfall intensity on infiltration rate of modelled permeable pavement. J Environ Manage 177–186
Hou J, Wang N, Guo K, Li D, Jing H, Wang T, Hinkelmann R (2020) Effects of the temporal resolution of storm data on numerical simulations of urban flood inundation. J Hydrol 125100
Innovyze (2019) Help documentation of XPSWMM and XPStorm. Available https://help.innovyze.com/display/xps/Infiltration Accessed 30 April 2020
JAXA (2017) ALOS global digital surface model "ALOS World 3D—30 m (AW3D30)". Available http://www.eorc.jaxa.jp/ALOS/en/aw3d30/index.htm. Accessed 20 Feb 2017
Liang Q, Xing Y, Ming X, Xia X, Chen H, Tong X, Wang G (2017) An open-source modelling and data system for near real-time flood forecasting. In: E-proceedings of the 37thIAHR World Congress, 13–18 Aug, 2017, Kuala Lumpur, Malaysia
Morin J, Benyamini Y (1977) Rainfall infiltration into bare soils. Water Resour Res 13(5): 813–817
Müller E (2007) Scaling approaches to the modelling of water, sediment and nutrient fluxes within semi-arid landscapes, Jornada Basin, New Mexico. Logos Verlag Berlin. PhD thesis submitted 2004 to King's College London, UK
Murillo J, García-Navarro P, Burguete J (2009) Conservative numerical simulation of multi-component transport in two- dimensional unsteady shallow water flow. J Comput Phys 15:5539–5573
Nciizah A, Wakindiki I (2015) Soil sealing and crusting effects on infiltration rate: a critical review of shortfalls in prediction models and solutions. Arch Agron Soil Sci 61(9):1211–1230
Ni Y, Cao Z, Liu Q, Liu Q (2020) A 2D hydrodynamic model for shallow water flows with significant infiltration losses. Hydrol Process 34:2263–2280
Özgen I, Simons F, Zhao J, Hinkelmann R (2014) Modeling shallow water flow and transport processes with small water depths using the hydroinformatics modelling system. CUNY Academic Works, New York
Rawls W, Brakensiek D, Miller N (1983) Green-Ampt infiltration parameters from soils data. J Hydraul Eng 1:62–70
Rawls WJ, Brakensiek DL, Simanton JR, Kohl KD (1990) Development of a crust factor for a Green Ampt Model. Trans ASAE 33(4):1224–1228. https://doi.org/10.13031/2013.31461
Sharma M, Gander G, Hunt C (1980) Spatial variability of infiltration in a watershed. J Hydrol 45 (1–2):101–122
Simons F, Busse T, Hou J, Özgen I, Hinkelmann R (2012) HMS: model concepts and numerical methods around shallow water flow within an extendable modeling framework. In: Proceedings of the 10th international conference on hydroinformatics, Hamburg

Simons F, Busse T, Hou J, Özgen I, Hinkelmann R (2014) A model for overland flow and associated processes within the hydroinformatics modelling system. J Hydroinformatics 16 (2):375–391

Smith L, Liang Q, James P, Lin W (2017) Assessing the utility of social media for flood risk management. J Flood Risk Manage 10:370–380. https://doi.org/10.1111/jfr3.12154

Starkey E, Parkin G, Birkinshaw S, Large A, Quinn P, Gibson C (2017) Demonstrating the value of community-based ('citizen science'). J Hydrol 548:801–817

Tackett J, Pearson RW (1965) Soil science

Tügel F, Özgen I, Hadidi A, Tröger U, Hinkelmann R (2018) Modelling of flash floods in wadi systems using a robust shallow water model—case study El Gouna, Egypt. In: Advances in hydroinformatics. Singapore, Springer

Tügel F, Özgen-Xian I, Marafini E, Hadidi A, Hinkelmann R (2020a) Flash flood simulations for an Egyptian city—mitigation measures and impact of infiltration. Urban Water J 14(5):396–406

Tügel F, Abdelrahman A, Özgen-Xian I, Hadidi A, Hinkelmann R (2020b) Rainfall-runoff analysis of the Wadi Bili catchment in the Red Sea Governorate of Egypt. In: Advances in hydroinformatics. Springer, Singapore

Vergroesen T, Verschelling E, Becker B (2014) Modelling of sustainable urban drainage measures. Revista De Ingeniería Innova 8:1–16

Whisler F, Bouwer H (1970) Comparison of methods for calculating vertical drainage and infiltration for soils. J Hydrol 1:1–19

Xing Y, Liang Q, Wang G, Ming X, Xia X (2019) City-scale hydrodynamic modelling of urban flash floods: the issues of scale and resolution. Nat Hazards 96:473–496

Yu D, Yin J, Liu M (2016) Validating city-scale surface water flood modelling using crowdsourced. Environ Res Lett 11(12):124011

Chapter 7
Advanced Tools for Flood Management: An Early Warning System for Arid and Semiarid Regions

Ekkehard Holzbecher, Ahmed Hadidi, Nicolette Volp, Jeroen de Koning, Humaid Al Badi, Ayisha Al Khatri, and Ahmed Al Barwani

Abstract Technologies concerning integrated water resources management, in general, and flood management, in particular, have recently undergone rapid developments. New smart technologies have been implemented in every relevant sector and include hydrological sensors, remote sensing, sensor networks, data integration, hydrodynamic simulation and visualization, decision support and early warning systems as well as the dissemination of information to decision-makers and the public. After providing a rough review of current developments, we demonstrate the operation of an advanced system with a special focus on an early warning system. Two case studies are covered in this chapter: one specific urban case located in the city of Parramatta in Australia in an area that shows similar flood characteristics to those found in arid or semiarid regions and one case regarding the countrywide Flash Flood Guidance System in Oman (OmanFFGS).

Keywords Flash management · IWRM · Flood early warning systems · OmanFFGS

E. Holzbecher · A. Hadidi (✉) · H. Al Badi
Applied Geoscience Department, German University of Technology in Oman, Muscat, Oman
e-mail: ahmed.hadidi@gutech.edu.om

H. Al Badi
e-mail: h.albadi@met.gov.om

N. Volp · J. de Koning
Nelen & Schuurmans, Utrecht, The Netherlands
e-mail: jeroen.dekoning@nelen-schuurmans.nl

H. Al Badi
Civil Aviation Authority, Muscat, Oman

A. Al Khatri
Ministry of Agriculture, Fisheries, and Water Resources, Muscat, Oman

A. Al Barwani
Oman Water Society, Muscat, Oman

T. Sumi et al. (eds.), *Wadi Flash Floods*, Natural Disaster Science and Mitigation Engineering: DPRI Reports, https://doi.org/10.1007/978-981-16-2904-4_7

7.1 Introduction

There has been a rapid development of a new generation of "smart" tools concerning flood management. Such tools can assist in decision-making in various phases of flood management, ranging from predictions to live monitoring. These tools support and strengthen each other. Monitoring tools based on smart sensor networks provide detailed information about the past and current state of a flood event. Recorded observations enable modeling tools to identify the hot spots of high vulnerability and to predict inundation scenarios (de Risi et al. 2018). These high-risk locations need to be considered in early warning issuances (Wicht and Osinska-Skotak 2016), rescue operations, intervention measures (Webber et al. 2018), and other management decisions. Flood early warning systems (FEWSs) are an integral part of the range of advanced tools.

In arid and semiarid areas, water managers deal with periods of drought and short periods of severe rainfall. Flood hazards can occur quickly and unexpectedly. Therefore, it is important to be able to forecast these events as accurately as possible. Flash floods can endanger communities and vital infrastructures. Early warnings with sufficient lead times would significantly benefit the ability of water managers to warn communities to take the necessary safety precautions. In this situation, the operation of FEWSs can be crucial.

Recent developments in flash flood early warning methods, described in the tool set section below, imply significant improvements for early warning systems. As examples, more detailed explanations and focus will be given in this chapter on two systems: An early warning system set up in the Australian region of the city of Parramatta and a countrywide flash flood guidance system in the Sultanate of Oman. Both systems consist of a combination of tools, including hydrodynamic modeling software and tools used to force models with up-to-date precipitation forecasts, and the tools are connected to decision support systems (DSSs).

7.2 Tool Set for an Urban Area

A survey concerning new tools within the framework of integrated water resources management (IWRM) was recently presented by Holzbecher et al. (2019). The framework contains various aspects concerning water resources management, from measurements and data availability to decision-making platforms. Advanced tools are available and are in development in all areas of IWRM. For example, information about the actual conditions of the real world is improving due to sensor developments, remote sensing techniques, and satellite data. There are increased amounts of easily accessible data thanks to improved storage and sharing options in cloud solutions and better data transfer. Moreover, these data can also be used more efficiently in modeling tools based on new techniques, and models now run with increased computer power. Advances have been made in techniques to optimize

calibration processes and sensitivity studies. New visualization techniques allow much more intuitive images of outcomes, which can also serve as inputs to DSSs. In urban planning, new tools are highly appreciated in discussing, designing, and building means for hazard prevention and mitigation. Flood hazard maps and vulnerability maps can be combined with flood risk maps that enable users and urban planners to identify (new) risk areas (Tingsanchali 2012) and to plan measures for reducing vulnerability.

Early warning systems are integrated in this framework of IWRM tools. In short, FEWSs detect impending disasters, give information to people at risk, and enable those in danger to make decisions and take action (Mileti 1999). According to Manual 21 (Attorney-General's Department 2009) in Australia, effective flood warning systems have six components.

1. Monitor changes in the environment that can lead to flooding.
2. Define the impacts of the detected floods on communities.
3. Construct warning messages containing information about predicted events.
4. Disseminate warnings to organizations and people at risk.
5. Generate appropriate actions of the communities and involved authorities.
6. Review the system after the event to improve the performance of the system.

Early warning systems are an integral part of flood management toolsets and consist of monitoring, modeling, risk analysis, decision-making, and warning. Early warning messages occur at the end of the complex system of components and are related to dissemination and communication with the local community. It is crucial for the acceptance and success of an early warning system that its predictions are as exact as possible. Warnings should be given for at-risk locations in case of inundation. There should be no warnings for locations that are not at risk. A crucial factor for the correct operation of a FEWS is thus the hydrodynamic modeling software that simulates and predicts the development of a flood. In the following section, we briefly describe 3Di as an example of advanced hydrodynamic modeling software belonging to the new generation of IWRM tools.

The 3Di software accepts input data from monitoring systems, performs flood simulations, and delivers forecast results to a data analysis platform called Lizard (Lizard 2020; 3Di 2020). The 3Di system is cloud-based, allows interactions during its simulations, and provides intuitive visualizations. The input data necessary to build a 3Di model consist of vector and raster data that describe the digital elevation model (DEM) and the local structures, obstacles, etc.

The computational core of 3Di computes flow in 1D and 2D based on shallow water equations. The 2D computations make use of the subgrid technique (Casulli 2009). The subgrid technique, illustrated in Fig. 7.1, allows coarse computational cells with the incorporation of high-resolution information. For example, bathymetry (DEM), infiltration, and roughness information can be defined at high resolutions using the subgrid technique (Volp et al. 2013; 3Di 2020). Moreover, the subgrid technique makes the computational core favorable for the computation of flooding and drying cycles.

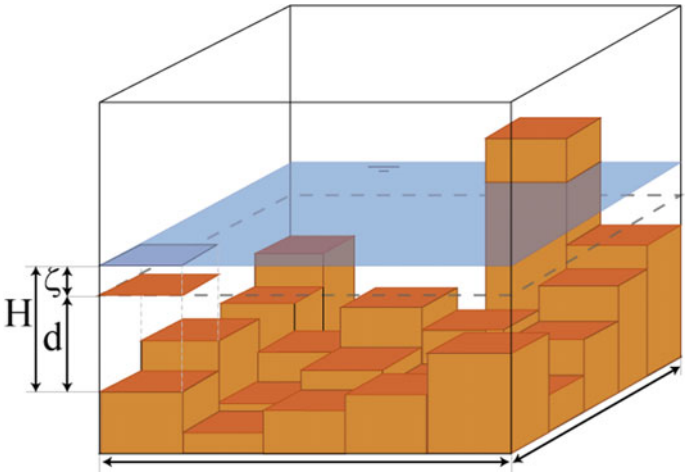

Fig. 7.1 Illustration of a coarse computational cell with varying bathymetry (Volp et al. 2013)

In addition, 3Di supports full interaction with 1D components within the computational domain (Casulli and Stelling 2013). Pipes and structures, such as weirs, are often critical for determining the water distribution. The 3Di model allows these components to be defined within the 2D domain and to be fully integrated in the computations.

The simulations of the 3Di model can be forced in several ways through boundary conditions, precipitation events, and wind. The precipitation information used in the model consists of spatially and temporally varying forecasts and uses the technology of Lizard (2020).

During the initiation phase of an early warning system, the model is calibrated and validated against the model results and measurements. A QGIS environment (QGIS 2020) offers the possibility to fully analyze all variables computed by 3Di, but this analysis can also be done via other means. In addition, the modeled water levels can be depicted live in an aerial view on maps (Fig. 7.2).

The flood forecast results are sent to the cloud-based analytic system. Here, the flood forecast results can be analyzed on interactive flood maps, including the resulting discharges, velocities, and water levels (Fig. 7.3).

In the initiation phase of setting up the early warning system, "observation" locations can be defined, where the forecasted water level results will be analyzed automatically. For these locations, trigger levels are defined. Depending on the level of exceedance and the period of time before the actual event, different warning levels are reached. Per the warning levels, different groups of stakeholders are warned. The stakeholders can be local authorities or residents of certain areas. This service is supported by Lizard Technology (Lizard 2020).

In this setup, various major challenges associated with the development of new tools that were previously mentioned (ITU-T 2014) are addressed: (1) Real-time

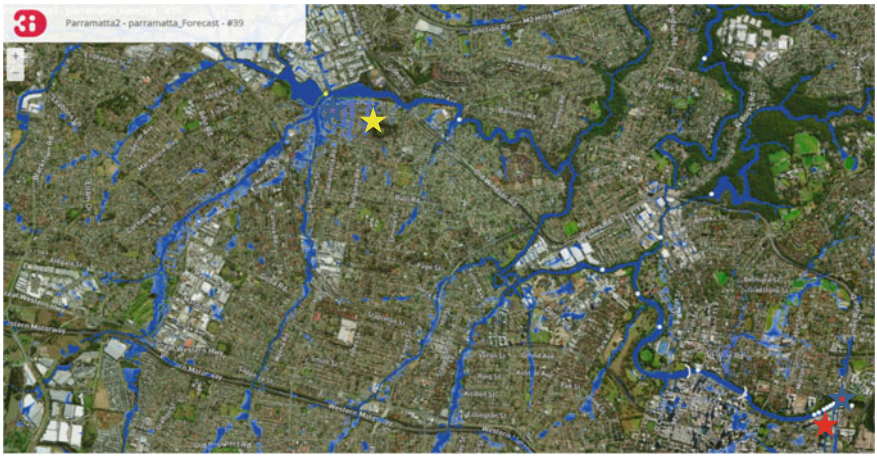

Fig. 7.2 Results simulated by in the live site of 3Di. The yellow star denotes the upstream urban area, and the red star denotes the outflow location. The depth values and discharges can be viewed directly

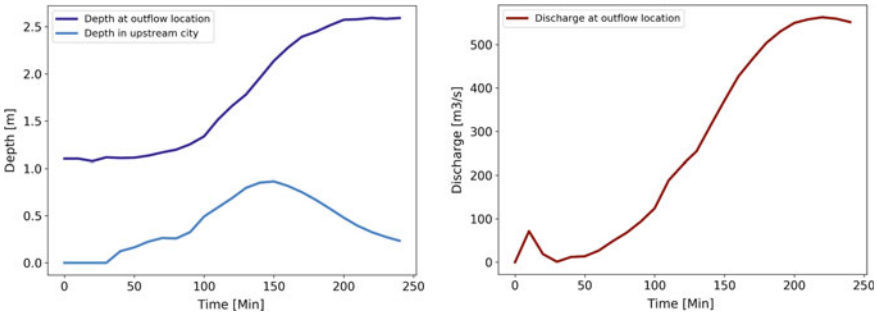

Fig. 7.3 Inundation development at the locations indicated in Fig. 7.2 by the stars; scenario simulated using 3Di

data and measurements are easily collected through sensor networks and low-cost innovative communications and protocols; and (2) better-informed decisions are made through the use of advanced analytics that translate raw data into actionable intelligence.

7.3 Flood Early Warning System in Action

The flash flood forecasting service (FLASH®) that is installed in the Australian city of Parramatta serves here as an example of an early warning system for flash floods on the scale of an urban area (Flash 2020). The city of Parramatta is located near Sydney, and the Parramatta River runs through the city. The region is known to suffer from severe hydrological events. In a recent event, 194 mm of rain fell in 72 h. The majority of precipitation events in the upper watershed show high spatial and temporal heterogeneity, as shown in a study using rainfall semi-variograms (Umakhanthan and Ball 2002).

The flood characteristics in Parramatta are typical of flash flood catchments, such as those seen in wadis in arid and semiarid climates. For the watershed in question, Morrison and Molino (2016) stated that floods arrive quickly and without significant warning time and then recede quickly. The flash flood risk is high, as a relatively small riverbed crosses through a relatively large urbanized area (Fig. 7.4). In a probable maximum flood event, the flooding would be extensive, deep, and fast-flowing and could reach up to several meters deep across wide areas (Morrison and Molino 2016). The DEM in Fig. 7.5 shows the gradual changes in height that serve to focus water flows in a particular direction (Fig. 7.5). Figure 7.6 shows the effect before and after the occurrence of a rainfall event and shows the river in a base flow situation and during a flood event occurring due to a high rainfall event upstream.

The Australian Bureau of Meteorology (BoM) offers new precipitation forecast data every half an hour. Based on these forecasts, which include spatially and temporally varying precipitation data, 3Di computes the resulting water levels and

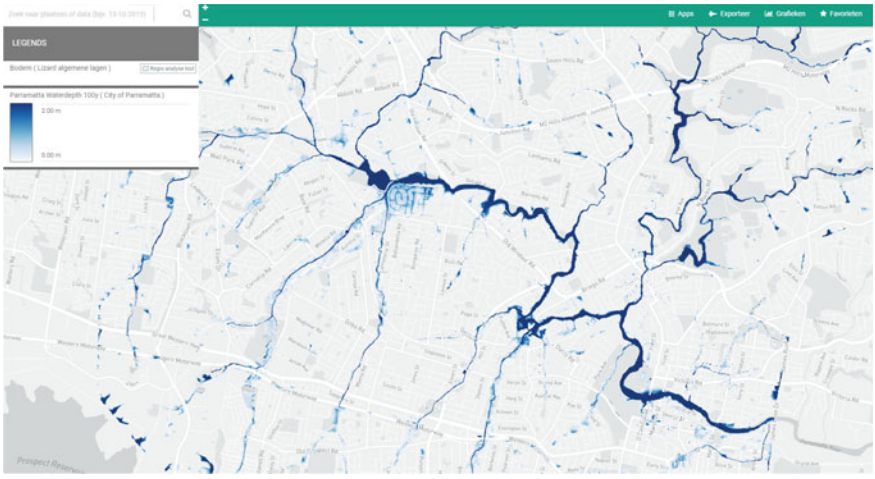

Fig. 7.4 Flood map of the Parramatta region based on a 1-in-100-year precipitation event. The water depth ranges from 0 to 2 m outside the riverbanks

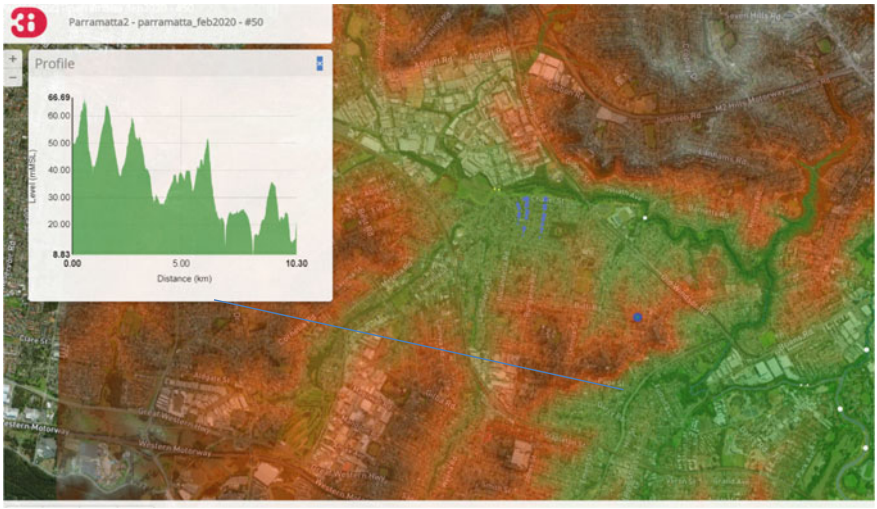

Fig. 7.5 DEM of the Parramatta region with a cross section over the white line

Fig. 7.6 Parramatta River before and after an extreme rainfall event

flows for the next 12 h. The 3Di model can produce accurate and reliable flood forecast results within 15 min (Fig. 7.4).

When 3Di predicts water levels above the trigger levels, messages are sent. The results of the modeling tool can be analyzed interactively by the authorities and decision-makers (Fig. 7.7). The flood maps and warning levels are updated with every new precipitation forecast to offer the best-known information for the involved parties to support their decision-making processes.

This set of tools offers the communities and authorities of the city of Parramatta the time necessary to make the correct decisions and take safety precautions. In the

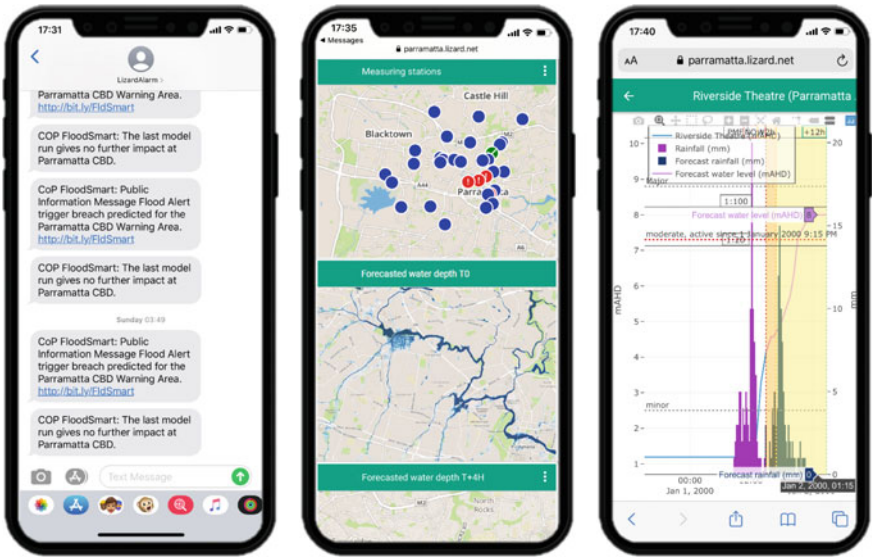

Fig. 7.7 Early warning in three steps: (1) the local authorities receive a flood warning message, (2) clicking on the message gives the user access to the flood management dashboard, and (3) information about recorded and forecasted water levels, interactive flood maps, and rainfall forecasts is given

event described above, the authorities and residents had 11 h to respond suitably and take necessary precautions for the coming rain.

The FEWS installed in Parramatta performs well for all six characteristic components of a flood warning system mentioned above and defined by the Australian authority (Attorney-General's Department 2009). The predictive component (1) is covered by the 3Di model, which is forced by forecasts from a local meteorology bureau. The interpretation phase (2) is based on automatically generated flood maps with predefined trigger levels. Once these trigger levels are reached, messages are sent with the information needed for the local authorities to respond accordingly. If necessary, the residents are warned as well (3, 4, 5). The results can be thoroughly analyzed afterward (6). It is a key that after a flood event occurs, the system can be triggered again with the actual measured precipitation levels, and the results can be compared with the observations. Additionally, precipitation forecasting is uncertain due to rapidly changing conditions and limited resolutions. In particular, severe precipitation events can have strong local variations.

7.4 Wadi Flows and Hydrometric Network Development in Oman

As is the characteristic of arid and semiarid climates, precipitation events in Oman are highly variable both temporally and spatially. A wadi may flood several times in one year and see no flow over the next several years. There is also high spatial variability in precipitation intensity. One basin or subcatchment may produce major flooding, while the adjacent catchments do not have noticeable runoff. The flooding durations are short in general. An entire flood may occur within a few hours. Most flood hydrographs, particularly those representing the upper hard rock reaches of wadis, peak very quickly and dissipate rapidly. Heavy sediment loads, both bed loads and suspended loads, characterize wadis in Oman, particularly when floods are at such levels that they cut into higher terraces of the alluvium. However, the infiltration rate, in general, is high in downstream alluvial reaches (Al Hinai and Abdala 2020).

The annual average wadi flow is 330 Mm^3. Eighty-five percent of wadis in Oman flow from mountainous areas toward the plains and finally drain to the sea. The rest drain to the interior (desert) or out of the country. The largest wadis catchments are Andam Halfayen (34,220 km^2) and Al Batha (5,740 km^2).

FEWSs are set up based on hydrometric data networks. In Oman during the 1970s, some scattered water monitoring points started to be installed through different exploration and research projects. In the early 1980s, the expansion of the complete hydrometric network started, and the system reached its maximum size in the late 1990s. The Monitoring Network Department was formed by 1997 to supervise, organize, and assess all monitoring activities in the country. Evaluations and upgrades of the monitoring network took place in 1998, 2005, and 2016. Water balance results for the sultanates were available by 2013. Figure 7.8 illustrates the temporal development of the network. Table 7.1 provides an overview of its spatial distribution.

7.5 The Oman Flash Flood Guidance System

Recently, the Directorate General of Meteorology and the Directorate General of Water Resources Assessment in the Sultanate of Oman defined the cooperation framework that is used to manage and run the Oman Flash Floods Guidance System (OmanFFGS). Such collaborative efforts will allow the use of climate predictions in water management, in addition to improving flood forecasting services.

The Oman Flash Flood Guidance System (OmanFFGS) is hosted by the Oman Multi-Hazard Early Warning Center, Directorate General of Meteorology. It was developed by the Hydrologic Research Center (HRC), a USA-registered non-profit organization. The primary purpose of installing the system was to assist operational forecasters in issuing reliable flash flood warnings. OmanFFGS offers baseline

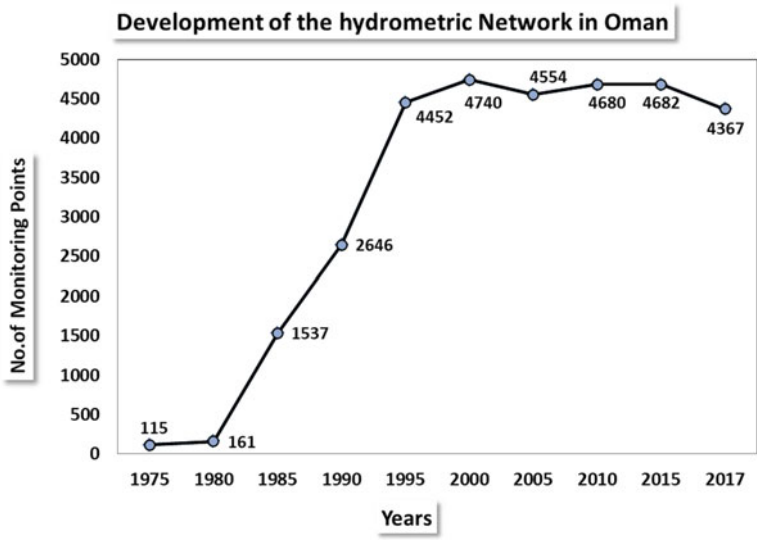

Fig. 7.8 Development of the hydrometric network in Oman between 1975 and 2017

Table 7.1 Recent number of monitoring points per region as of 2017

Hydrometric network by assessment areas										
			Rainfall stations					Salinity		
Assessment areas	Wadi flow	Dams	Gage	Inhacement	Wells	Aflaj	Springs	Well	Falaj	Total
Muscat	17	3	43	8	100	20	6	45	75	317
South Al Batinah	21	10	36	29	112	79	1	22	72	382
North Al Batinah	17	5	45	23	157	29	3	38	24	341
Musandam	7	6	23	0	60	0	0	0	1	97
Al Buraimi	6	6	21	17	169	20	0	9	18	266
Ad Dhahirah	12	1	39	41	238	70	0	25	70	496
Ad Dakhliyah	18	9	57	48	287	117	6	71	119	732
North As Sharqiya	16	4	51	35	164	41	1	15	116	443
South As Sharqiya	11	1	27	0	117	186	0	32	40	414
Al Wusta	0	0	11	0	14	0	0	0	0	25
Dhofar	11	2	60	20	655	0	14	96	0	858
Total	132	47	413	221	2,073	562	31	353	535	4,367
			634					888		

products that must be carefully evaluated by forecasters in real time before a flood warning can be issued. The product console provides a collection of real-time data products in text, image, and CSV file formats with updates every hour.

The Oman Flash Flood Guidance System uses a hydrological model with inputs of rainfall observations, forecasts, and soil properties of each catchment to detect and predict soil oversaturation. The system uses many sources of precipitation data, which can be categorized into two types. The first type includes precipitation input data from near-real-time observations, namely ground-based radars, microwave-adjusted satellite-based precipitation estimates, satellite-based precipitation estimates, and rain gage mean-areal precipitation (see Fig. 7.9). However, the input precipitation data used in flood calculations vary according to the availability and accuracy of the data sources. Currently, ground-based radar data are given the highest priority for use in the calculations when they are available, while rain gage mean-areal precipitation data are given the lowest priority due to the relatively low-density rain gage network. Therefore, the output products should be evaluated according to the assessed accuracy of the input data before they are used for the creation of warnings.

The second type of precipitation input data is rainfall forecasts from atmospheric models. The system is fed by the COSMO model, a nonhydrostatic limited area atmospheric prediction model, which provides two different resolutions: horizontal mesh sizes of 2.8 and 7 km (Fig. 7.10). Currently, this model is in the process of being replaced by the ICON (Icosahedral Nonhydrostatic) limited area atmospheric prediction model.

The OmanFFGS basically uses the same process to generate flood assessment products for both aforementioned precipitation data types. However, the products

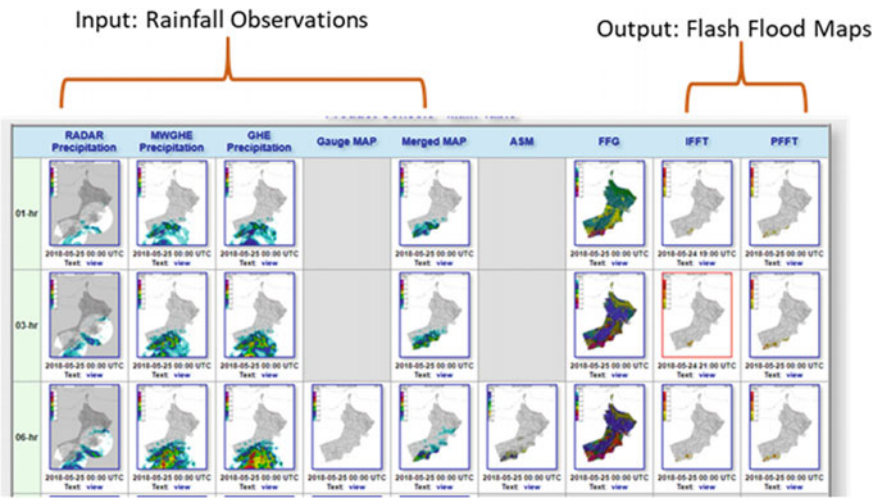

Fig. 7.9 Console of the OmanFFGS rainfall input data from near-real-time observations for Cyclone Mekunu, which occurred in May 2018

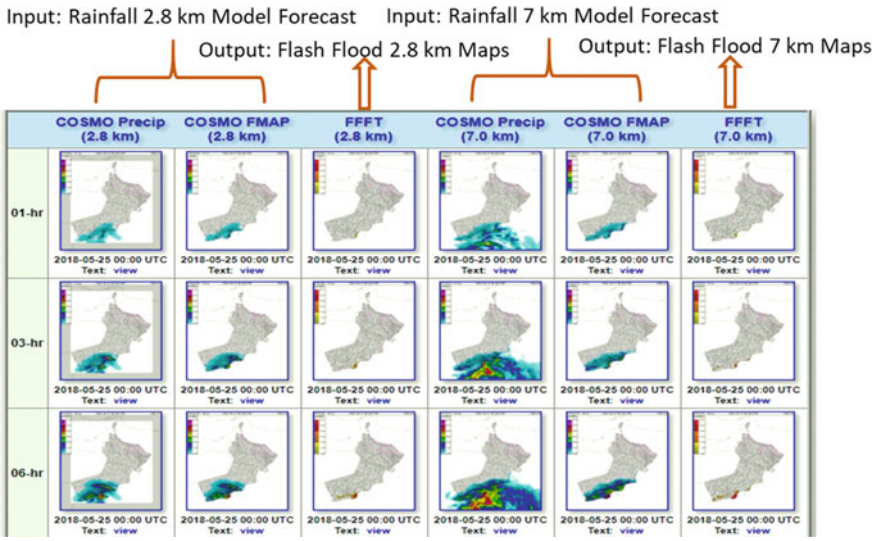

Fig. 7.10 Console of the Oman flash flood guidance system representing rainfall input data from atmospheric models

generated by using the second type should be treated with extra caution due to the high uncertainty present in the data, which might result in a false warning.

Although the system is a large step forward and has been beneficial throughout the last seven years of its operation, the users reported several limitations and challenges. First, the system works best with radar data to indicate whether there will be an imminent flood in the upcoming 1–6 h. However, difficulties have been reported in keeping the radar network running, which eventually resulted in depending on satellite data for the rainfall inputs throughout most of the operational time of the system. Since satellite-based rainfall estimations are less accurate than radar-based rainfall data, the system flood products became less accurate. A higher density of rain gages might provide an alternative solution to this challenge. The Directorate General of Water Resources Assessment has a higher-density rain gage network. Recently, the Directorate General of Meteorology and the Directorate General of Water Resources Assessment agreed on streaming real-time data from the high-density rain gage network of the Directorate General of Water Resources Assessment to be used as input data to run the Oman Flash Flood Guidance System.

From another perspective, many users have requested more than 6 h of flood forecasts with higher confidences. This would require human intervention to modify the precipitation forecast maps. There are currently efforts in this avenue. Other users have requested an interactive background map with the names of dry rivers (wadis), which are not available in the current operational version.

Finally, an essential aspect of any forecasting system is the verification of its products for future improvements and more effective uses as well as verifications of the reliability of the products. Product verification requires water stream and

inundation data, which are collected by the Directorate General of Water Resources Assessment. This is another avenue of potential future collaboration between the system developers, users, and data collectors.

7.6 Conclusions

Advanced technical tools for integrated water resources management are either available or are still in development. A combination of tools can be used for smart sensors with powerful networks. Satellite data are available, and some are available at no charge. Processing, cloud storage and wireless communication advances have enabled powerful tools for simulation, visualization, and modeling that can be utilized by all involved parties. The results can be integrated for optimization and decision-making. Finally, warnings can be issued, and measures can be disseminated to at-risk communities. Due to the ability of previous systems to quickly generate reliable results, new modeling tools allow a much more flexible approach to flood management as well as to natural disaster management and long-term planning.

An application of a flood early warning system in an urban area was presented, concerning an implementation that is installed in the region of the city of Parramatta, Australia. This system fulfills the six components of FEWSs that are described in Manual 21 (Attorney-General's Department 2009). The case study illustrates the advantages of having such a system installed. The system allows the production of up-to-date flood maps based on actual precipitation events that occur, including the spatial and temporal variations associated with such events. The system allows more targeted actions to be taken in communication and safety precautions. Moreover, it gives the local authorities and residents more time to take action.

With the Flash Flood Guidance System of Oman, a countrywide installed network was presented. The hydrometric network has proven to be an appropriate tool for monitoring flash floods. With the existing network, it is possible to project flood events. Thus, the described system may form a convenient foundation for the development and use of an efficient FEWS.

A recent review of the United Nations University (Perera et al. 2019) names technical, financial, institutional, and social challenges concerning the implementation of FEWSs in general. Flash flood management responses require a set of multidisciplinary collaborative efforts in the fields of meteorology, hydrology, and emergency management. In many countries, national meteorological services and national hydrological services do not coordinate closely to improve flash flood forecasting services (WMO 2007).

The case of the FEWS, installed in Parrametta, demonstrates how most technical issues associated with flood warning systems can be addressed and resolved. However, on the technical side, such an implementation also depends on a sufficiently vast and reliable sensor network being installed and being in operation.

Moreover, non-technical issues may be crucial, such as the availability of funds for hardware and software, maintenance, communication, and cooperation between various authorities, the availability of trained competent personnel, and the proactive involvement of the public within the community.

References

3Di (2020) https://docs.3di.lizard.net/. Accessed July 2020

Al-Hinai HY, Abdalla R (2020) Spatial prediction of coastal flood-susceptible areas in Muscat Governorate using an entropy weighted method. WIT Trans Eng Sci 129:121–133

Attorney-General's Department (2009) Manual 21 flood warning. Australian emergency manuals series, Commonwealth of Australia, 2009. Available at http://www.em.gov.au/Documents/Manual%2021-Flood%20Warning(2).PDF

Casulli VA (2009) High-resolution wetting and drying algorithm for free-surface hydrodynamics. Int J Numer Meth Fluids. https://doi.org/10.1002/fld.1896,60,391-408

Casulli V, Stelling GS (2013) A semi-implicit numerical model for urban drainage systems. Int J Numer Meth Fluids 67:441–449

de Risi R, Jalayer F, de Paola F, Lindley S (2018) Delineation of flooding risk hotspots based on digital elevation model, calculated and historical flooding extents: the case of Ouagadougou, Stoch Environ Res Risk Assess. https://doi.org/10.1007/s00477-017-1450-8

Flash® (2020) https://3diwatermanagement.com/blog/flood-resilience-in-action-flash/. Accessed July 2020

Holzbecher E, Barghash H, Hadidi A, Al Balushi K (2019) Application of big data and technologies for integrated water resources management—a survey. In: 5th international conference on social network analysis, management and security (SNAMS 2019). IEEE Proceedings, Granada

ITU-T (2014) Focus group on smart sustainable smart cities, smart water management in cities. https://www.itu.int. Accessed June 2019

Lizard (2020) https://lizard.net/. Accessed July 2020

Mileti DS (1999) Disasters by design: a reassessment of natural hazards in the United States. Joseph Henry Press, Washington D.C.

Morrison T, Molino S (2016) Floodplain management innovation to facilitate city growth. In: Floodplain Management Australia Conference

Perera D, Seidou O, Agnihotri J, Rasmy M, Smakhtin V, Coulibaly P, Mehmood H (2019) Flood early warning systems: a review of benefits, challenges and prospects. UNU-INWEH report series, issue 08, United Nations University, Institute for Water, Environment and Health, Hamilton, Canada

QGIS (2020) https://qgis.org/en/site/. Accessed July 2020

Tingsanchali T (2012) Urban flood disaster management. Proc Eng 32:25–37. https://doi.org/10.1016/j.proeng.2012.01.1233

Umakhanthan K, Ball J (2002) Importance of rainfall models in catchment simulation. In: 13th congress APD-IAHR, Singapore

Volp ND, Prooijen BC, Stelling GS (2013) A finite volume approach for shallow water flow accounting for high-resolution bathymetry and roughness data. Water Resour Res. https://doi.org/10.1002/wrcr.20324C,49,4126-4135

Webber JL, Gibson MJ, Chen AS, Savic D, Fu G, Butler D (2018) Rapid assessment of surface-water flood-management options in urban catchments. Urban Water J 15(3):210–217

Wicht M, Osinska-Skotak K (2016) Identifying urban areas prone to flash floods using GIS—preliminary results. Hydrol Earth Syst Sci Diss 1–22

WMO (2007) Fifteenth world meteorological congress: abridged final report with resolutions. WMO-No. 1026, pp 204–207. ISBN 92–63–11026–3

Chapter 8
Hydrologic Assessment of the Uncertainty of Six Remote Sensing Precipitation Estimates Driven by a Distributed Hydrologic Model in the Blue Nile Basin

Hadir Abdelmoneim, Mohamed R. Soliman, and Hossam M. Moghazy

Abstract Because of the sparseness of the ground monitoring network, precipitation estimations based on satellite products (PESPs) are currently requisite tools for hydrological simulation research and applications. The evaluation of six global high-resolution PESPs (TRMM 3B42V7, GPGP-1DD, TRMM 3B42RT, CMORPH-V1.0, PERSIANN, and PERSIANN-CDR) is the ultimate purpose of this research. Additionally, the distributed Hydrological River Basin Environmental Assessment Model (Hydro-BEAM) is used to investigate their potential effects in streamflow predictions over the Blue Nile basin (BNB) during the period 2001 to 2007. The correctness of the studied PESPs is assessed by applying categorical criteria to appraise their performances in estimating and reproducing precipitation amounts, while statistical indicators are utilized to determine their rain detection capabilities. Our findings reveal that TRMM 3B42V7 outperforms the remaining product in both the estimation of precipitation and the hydrological simulation, as reflected in highest NSE and R^2 values ranges from 0.85 to 0.94. Generally, the TRMM 3B42V7 precipitation product exhibits tremendous potential as a substitute for precipitation estimates in the BNB, which will provide powerful forcing input data for distributed hydrological models. Overall, this study will hopefully provide a better comprehension of the usefulness and uncertainties of various PESPs in streamflow simulations, particularly in this region.

Keywords Satellite · Rainfall · Products · Hydro-BEAM · Blue Nile Basin · Hydrological model

H. Abdelmoneim (✉) · M. R. Soliman · H. M. Moghazy
Faculty of Engineering, Alexandria University, Alexandria, Egypt

M. R. Soliman
Faculty of Engineering, Beirut Arab University, Beirut, Lebanon

T. Sumi et al. (eds.), *Wadi Flash Floods*, Natural Disaster Science and Mitigation Engineering: DPRI Reports, https://doi.org/10.1007/978-981-16-2904-4_8

8.1 Introduction

Precipitation inputs are a vital source for research and applications of hydrologic simulations, specifically in data-scarce areas where the rareness of gauging networks curtails the accessibility of precise and credible rainfall data. However, measured ground gauging data are either sparse in time and space in several areas, or ungauged regions exist in several populous areas of the world, such as developing regions (Behrangi et al. 2011).

Many high-resolution precipitation estimations based on satellite products (PESPs) have been operatively obtainable over a quasi-global scale in recent decades at high temporal (3 h) and spatial (almost 0.25°) resolutions. These products are potential substitutes for rainfall datasets in global hydrometeorological studies and applications. Commonly used satellite precipitation estimates include Tropical Rainfall Measuring Mission (TRMM) data (Huffman et al. 2007), the National Oceanic and Atmospheric Administration (NOAA)'s Climate Prediction Center (CPC) MORPHing technique data (CMORPH) (Joyce et al. 2004), the Global Satellite Mapping of Precipitation (GPM) data (Kubota et al. 2007) and the Precipitation Estimation from Remotely Sensed Imagery using Artificial Neural Networks (PERSIANN) data (Sorooshian et al. 2000). These PESPs are capable of monitoring temporal precipitation variations and spatial patterns at diminutive resolutions. Additionally, they provide useful tools to promote hydrological purposes for fully distributed hydrological models, especially in data-sparse regions and regions with nonexistent data (Sun et al. 2016).

Reviews of recent studies allow the studies to be classified into two categories: the first focuses on evaluating and comparing PESPs against the estimates of local gauging networks (Ali et al. 2017; Habib et al. 2012; Hirpa et al. 2010; Fenta et al. 2018; Gebere et al. 2015; Gebremicael et al. 2017; Jiang et al. 2018; Romilly and Gebremichael 2011). Among these studies, Jiang et al. (2018) used continuous statistical indices (RMSE, CC, and RE) and categorical metrics (POD, FBI, FAR, and ETS) to evaluate the accuracies of two high-resolution PESPs (TRMM 3B42V7 and CMORPH) for the interval 2010 to 2011 in Shanghai. Additionally, Gebremicael et al. (2017) evaluated eight PESPs against in situ rainfall data over the upper Tekeze-Atbara basin, which characterizes by the composite topography of Ethiopia.

The second category involves the evaluation and investigation of the impacts of PESPs through streamflow simulations driving hydrological models over various regions (Alazzy et al. 2017; Bitew and Gebremichael 2011; Bitew et al. 2012; Jiang et al. 2012; Lakew et al. 2017; Sun et al. 2016; Stisen and Sandholt 2010; Tong et al. 2014; Xue et al. 2013; Wang et al. 2015). For instance, Sun et al. (2016) statistically evaluated the four latest PESPs (CMORPH-CRT, CMORPH-CMA, CMORPH-BLD, and TRMM 3B42V7) over the Huaihe River basin in eastern China. Additionally, the authors employed the variable infiltration capacity (VIC) distributed model to predict the river flow rate within the period 2003–2012. The results revealed that CMORPH-CMA had a perfect capability for improving the distribution of precipitation and hydrological applications. They also recommend this CMORPH-CMA as an alternative rainfall input source for this region.

Li et al. (2019) assessed three PESPs (TMPA 3B42V7, PERSIANN-CDR, and GPM IMERG) at daily and monthly timesteps in the lower Mekong River basin, which is located in Southeast Asia. They also investigated the potential of these PESPs to predict streamflows driven by a distributed geomorphology-based hydrological model (GBHM). Their findings revealed that the IMERG product can be used to reproduce precipitation well and accurately, particularly in the detection of heavy rainfall events. The hydrological simulations forced by the three datasets revealed acceptable precisions at major stations. Moreover, simulated results forced by IMERG outperformed the remaining products, as the smallest RRMSE values and largest NSE values were calculated for the IMERG product.

The Blue Nile River is a vital tributary of the Nile River and provides the greatest portion to the flow of the Nile River, approximately 60%. The area of the Blue Nile River suffers from a sparse rain gauge network with an uneven distribution. In addition, the region is characterized by complex topography, a variable climate, and a large geographical area. Hence, the use of PESPs as driving forces for hydrological models is necessary after the determination of the accurate product for this basin. A few prior studies focused on the evaluation of PESPs over small basins in the Ethiopian highland, such as the studies by Bitew and Gebremichael (2011) and Bitew et al. (2012). Additionally, Gebremicael et al. (2017) explored the relationships between PESPs and topography to understand the conceivable miscalculations generated by the rugged land in the area. To the best of our knowledge, no study has evaluated PESPs and investigated their ability to predict streamflow over the entire BNB. Therefore, the present research focuses on the comprehensive hydrologic assessment of the uncertainty of six PESPs (TRMM 3B42V7, TRMM 3B42RT, PERSIANN, PERSIANN-CDR, CMORPH-V1.0, and GPGP-1DD) in the Blue Nile Basin (BNB). This work aims to compare and evaluate the performance of six high-resolution PESPs in capturing the magnitude of rainfall over the BNB against data from land gauges within the period 2001 to 2007. Additionally, the effects of the studied PESPs on hydrologic simulation procedures at the target basin is investigated, driven by the distributed Hydrological River Basin Environmental Assessment Model (Hydro-BEAM), which was established by Kojiri et al. (1998). This attempt is valuable as it relates to the use of high-resolution PESPs for monitoring and predicting streamflows in the BNB and in similar watersheds that are characterized by common climate and topography.

8.2 Materials and Methods

8.2.1 Study Area

The Nile River is a transboundary river, and its tributaries travel through eleven countries. The Nile River has two vital tributaries: the White Nile River and the Blue Nile River. The Blue Nile River, chosen in this paper as the study area, is a

crucial Nile River tributary originating from the Ethiopian Plateau, flowing into Sudan, and meeting the White Nile River at Khartoum to form the main Nile River. This river is considered the Nile River's critical tributary, as it provides a large portion of the flow of the Nile River, approximately 60%. The BNB is located between latitudes 16°2′N and 7°40′N and longitudes 32°30′E and 39°49′E in the Ethiopian Highlands, as shown in Fig. 8.1. The river originates from the outlet of Lake Tana, flowing south in the Ethiopian highlands and then northwest; its length is approximately 900 km from Lake Tana to the Sudanese border, and the river ends when it reaches the White Nile River in Khartoum, Sudan (Samy et al. 2015). The drainage area of the BNB is estimated at approximately 325,000 km^2 (Ragab and Valeriano 2014). The catchment includes a range of topographic conditions, sizes, climatic conditions, slopes, geological features, drainage patterns, vegetation covers, soils, and anthropogenic activity.

The topography of the watershed is split into two distinct features: the first comprises flat topography in the lowlands of Sudan, and the second includes mountainous topography in the Ethiopian Plateau, where the regions containing high, steep mountains, when combined, overlay approximately 65% of the drainage area (Gebrehiwot et al. 2011). The Ethiopian Plateau is situated at altitudes of 2,000–3,000 m, with certain areas reaching heights up to or above 4,000 m, as

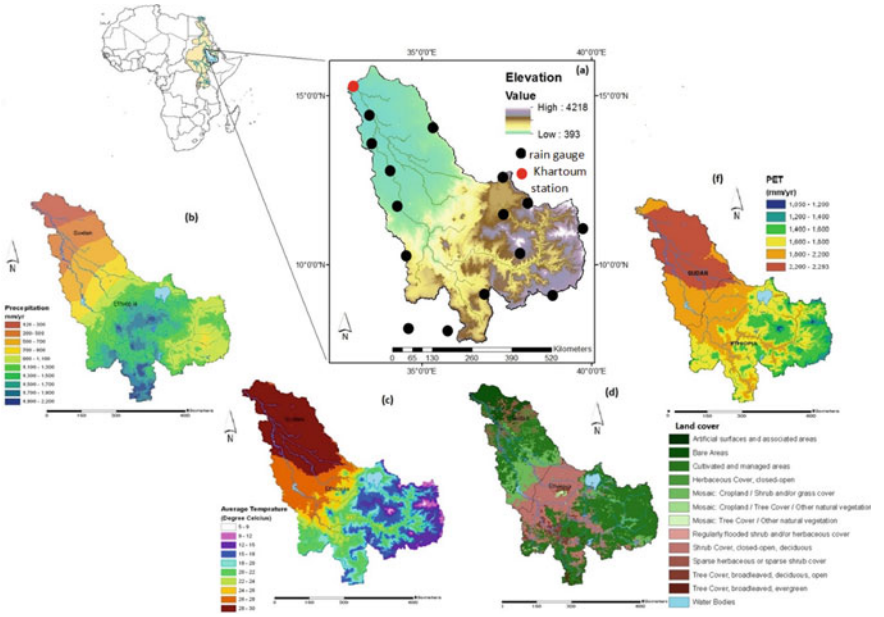

Fig. 8.1 **a** The BNB's location in the Ethiopian Highlands and (right) a DEM map of the BNB; **b** the average annual precipitation distribution over the BNB; **c** the average annual temperature distribution over the BNB; **d** soil types in the BNB; and **f** the average annual evapotranspiration distribution over the BNB (Abd-El Moneim et al. 2019)

illustrated in Fig. 8.1a (Ragab and Valeriano 2014). Precipitation over the BNB varies remarkedly with altitude from nearly below 200 mm/yr in the northeastern part of the basin to 2,000 mm/yr in Ethiopia's highlands, as displayed in Fig. 8.1b (Awulachew et al. 2008). In the northeastern clay plains of Sudan, the greatest mean annual temperatures occur. In Sudan, 24 and 44 °C are the daily minimum and maximum temperatures in May, and 14 and 33 °C are the daily minimum and maximum temperatures in January, respectively. The Ethiopian Plateau region is characterized by lower monthly mean minimum temperatures, ranging from 3 to 21 °C, between December and February, as shown in Fig. 8.1c (Awulachew et al. 2008). The spatial distribution of evapotranspiration in the region is similar to those of rainfall and temperature, with considerable variations across the basin and a notable correlation with altitude, as illustrated in Fig. 8.1f (Awulachew et al. 2008).

8.2.2 In Situ Precipitation and Discharge Datasets

Measured datasets play pivotal roles in the quantitative evaluation of PESPs. Due to the scarcity of data in developing regions, rainfall and Blue Nile flow rate data are collected through a process that requires the study time interval to be set from 2001 to 2007, according to the availability of measured datasets. Additionally, these data were collected on a monthly timestep from published reports by the Ministry of Water Resources and Irrigation (MWRI) in Egypt (MWRI 1998a; b). Monthly rainfall data from 15 ground rain gauges and the monthly discharge data from the Khartoum station are used in the current study, as shown in Fig. 8.1a. Incorrect values, such as negative and missed values, were rejected, which may make the comparison unreliable.

8.2.3 Remote Sensing Precipitation Estimation Products

8.2.3.1 TRMM Products

The National Space Development Agency (NSDA) and the National Aeronautics and Space Administration (NASA) jointly established the TRMM on 27 November 1997. This satellite is primarily intended for weather and climate science monitoring and for observations of tropical precipitation. The main pieces of rainfall equipment on this satellite are the Visible and Infrared Radiometer Network (VIRS), the TRMM Microwave Imager (TMI), and the Precipitation Radar (PR) (Kummerow et al. 1998). The TRMM Multisatellite Precipitation Analysis (TMPA) rainfall products were blended with other high-quality rainfall estimate algorithms, such as infrared-based (IR) and merged active/passive microwave (PMW) rainfall estimations, and these merged data were added to other numerous source dataset rainfall product blends, according to Huffman et al. (2007). The three

following steps are carried out for this product: first, the PMW rainfall estimates are calibrated and combined to produce the utmost reliable PMW estimates; next, the calibrated PMW estimates are utilized to produce IR rainfall estimations; and finally, the PMW and IR rainfall estimations are combined to provide the best TMPA rain estimations (Alazzy et al. 2017). Two versions of TMPA products are accessible with coverage between the longitudinal range 180°W–180°E and the latitudinal range 50°S–50°N as well as a fine spatial resolution (0.25° × 0.25°) and a high temporal resolution (3 h): a post-real-time research version (3B42) and a real-time version (3B42RT). The TRMM 3B42V7 product was adjusted via the monthly deviation of the precipitation dataset from the Global Precipitation Climate Center (GPCC) calibration meteorological stations compared to the TRMM 3B42RT product. Furthermore, this product has many computational enhancements and good data precision (Huang et al. 2014). The principal distinction between the two versions is that the post-real-time research product uses monthly ground rainfall data for bias correction. In this study, the TRMM 3B42V7 and 3B42RT datasets used were obtained from https://giovanni.sci.gsfc.nasa.gov/giovanni/.

8.2.3.2 CMORPH Product

The CMORPH tool of NOAA is a process of rainfall estimation based primarily on passive microwave (PWM) satellite measurements collected from low Earth orbiting (LEO) satellite radiometers; it incorporates a tracking technique using data from infrared (IR) measurements solely to derive a field of cloud motion that is thereafter used to propagate pixels of rainfall (Joyce et al. 2004). The latest satellite rainfall datasets, named the CMORPH-Version 1.0 products, have recently been developed by NOAA-CPC in three product forms: a pure satellite rainfall product (CMORPH-RAW), a gauge-satellite blended product (CMORPH-BLD) and a bias-corrected product (CMORPH-CRT). The CMORPH-RAW is an outcome of satellite-only rainfall estimates created by merging passive microwave-based rainfall estimates the infrared data of various geostationary satellites as well as numerous low orbit satellites. The following can be summarized as the key discrepancies between the ancient version, 0.x, and the new version, 1.0: fixed versions of satellite rainfall datasets and a fixed algorithm were used during the whole TRMM/GPM period (1998–present) in the latest version, 1.0, particularly to ensure the best possible homogeneity, whereas the ancient version, 0.x, has been developed since 2002 using various enhanced algorithms and developing satellite-based inputs of rainfall product versions (Joyce et al. 2010). In this work, the CMORPH-V1.0 RAW datasets were used; these datasets are freely available at ftp://ftp.cpc.ncep.noaa.gov/precip/CMORPHV1.0/.

8.2.3.3 PERSIANN Products

The PERSIANN product (Hsu et al. 1997) is one of the accepted estimates of global precipitation used to estimate historical precipitation from March 2000 until now. For its global precipitation estimations, the product uses the neural network method to derive relationships between IR and PMW estimates from Geostationary Earth Orbiting (GEO) and LEO satellite imagery, respectively (Sorooshian et al. 2000). First, the Grid Satellite (GridSat-B1) IR record archive (Knapp 2008) was used in the latest version of the PERSIANN-Climate Data Record (PERSIANN-CDR) product as an input to the eligible PERSIANN model; then, the Global Precipitation Climatology Project (GPCP) version 2.2 updated the biases in the predicted PERSIANN precipitation values on a monthly time scale (Ashouri et al. 2015). The parameters of the PERSIANN model were pretrained using stage-IV hourly precipitation data from the National Centers for Environmental Prediction (NCEP); later, the model was run using the full GridSat-B1 IR historical record with fixed model parameters as indicated in the calibration scheme by Ashouri et al. (2015). This product is available with a daily temporal resolution and a fine spatial resolution (0.25° × 0.25°). Precipitation datasets are available from 1 January 1983 to the present. In the current research, the two PERSIANN product (PERSIANN and PERSIANN-CDR) datasets that were used were freely obtained from http://chrsdata.eng.uci.edu/.

8.2.3.4 GPCP-1DD Product

The Global Precipitation Climatology Project One Degree Daily (GPCP-1DD) product incorporates IR and PMW precipitation estimates with the GPCC gauging dataset (Huffman et al. 1997). In the GPCP-1DD product, the PMW precipitation estimates depend on the Special Sensor Microwave/Imager (SSM/I) data from the Defense Meteorological Satellite Program (DMSP, US), while the IR data are principally obtained from the precipitation index (PI) data of the Geostationary Operational Satellite (GOES) (Xie and Arkin 1995). This product has the advantage of integrating precipitation estimate information by incorporating the strengths of different data types from multiple data sources. The GPCP-1DD product provides daily data on global precipitation grid with a resolution of 1° × 1°. The GPCP-1DD datasets are available to download from https://ftp://ftp.cgd.ucar.edu/archive/PRECIP/.

Overall, Table 8.1 presents the six PESPs (TRMM 3B42V7, GPGP-1DD, TRMM 3B42RT, CMORPH-V1.0, PERSIANN, and PERSIANN-CDR) used in this work.

Table 8.1 Summaries of the six PESPs evaluated in this work

Datasets	CMORPH-V1.0	TRMM 3B42v7	TRMM 3B42RT	PERSIANN	PERSIANN-CDR	GPCP-1DD
Spatial coverage	180°W–180°E, 50° N–50°S Quasi-global	180°W–180°E, 50°N–50°S Quasi-global	180°W–180°E, 50°N–50°S Quasi-global	180°W–180°E, 60° N–60°S Quasi-global	180°W–180°E, 60° N–60°S Quasi-global	180°W–180°E, 50°N–50°S Quasi-global
Temporal coverage	1998–present	1998–April 2014	March 2000–present	March 2000–present	1983–January 2017	1997–July 2011
Datasets source	TIMI, AMSR-E, SSM/I, SSMIS, AMSU, MHS, IR vectors	TCI, TMI, SSMI, SSMIS, AMSR-E, AMSU, MHS, MW-VAR, (IR). gauge	HQ, Mw-VAR (IR)	(TIMI, AMSR-E, SSM/I, SSMIS, AMSU, MHS)-cal. IR	GRIDSAT-IRWIN, GPCP monthly precipitation	SSMI- and SSMIS-TMPI (IR), TOVAS, AIRS, GPCP monthly
Spatial resolution	0.25° × 0.25°	0.25° × 0.25°	0.25° × 0.25°	0.25° × 0.25°	0.25° × 0.25°	1° × 1°
Temporal resolution	Daily	Daily	Daily	Daily	Daily	Daily
Data download Web site	ftp://ftp.cpc.ncep.noaa.gov/precip/CMORPH_V1.0/RAW/	ftp://ftp.cgd.ucar.edu/archive/PRECIP/TRMM/	https://giovanni.sci.gsfc.nasa.gov/giovanni/	http://chrsdata.eng.uci.edu	http://chrsdata.eng.uci.edu	ftp://meso.gsfc.nasa.gov/pub/1dd-v1.2/

8.2.4 *Hydro-BEAM Model*

Hydro-BEAM is a physically based distributed hydrological model established by Kojiri et al. (1998). The model was confined to environments characterized by moist circumstances until the model was adjusted for simulations of flash flood events in arid wadis (Abdel-Fattah et al. 2015; Saber et al. 2013) and semiarid basins (Abdel-Fattah 2017; Saber and Yilmaz 2016). The model has also been successfully used in numerous hydrological studies under different climatic conditions (e.g., Abd-El Moneim et al. 2017; Saber and Yilmaz 2018; Abdelmoneim et al. 2020). In this study, Hydro-BEAM is used to evaluate the simulated streamflow rates over the BNB based on six PESPs.

The ultimate benefit of the Hydro-BEAM model is the reflection of the spatial variability in catchment features and hydrological processes, where it can reflect hydrological surface and subsurface procedures, such as surface runoff, evapotranspiration, channel flow routing, groundwater flow, and the intake/release of water on spatially distributed meshed cells. To understand differences in infiltration due to changes in land cover, the model identifies three types of land cover (Sapkta et al. 2010). The model consists of four layers, from A to D, which represent the upper layer for the surface and the remaining layers for the subsurface, as shown in Fig. 8.2a.

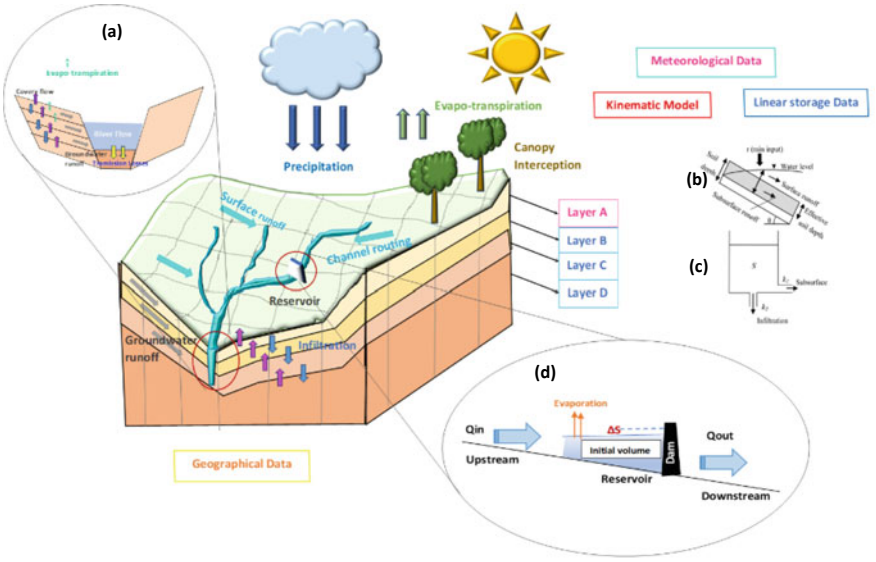

Fig. 8.2 Conceptual representation of Hydro-BEAM: **a** the basic structure of Hydro-BEAM; **b** the kinematic wave model of the surface layer; **c** the subsurface storage tank layer representation; and **d** the reservoir modeling approach (Kojiri et al. 1998; Abdelmoneim et al. 2020)

Each mesh cell includes details such as surface runoff, land use, slope direction, and a channel's absence/presence (Saber 2010). Layer A represents the surface layer, while layers B to D represent the subsurface layers, as denoted in Fig. 8.2b. In this study, Layer D is neglected as it contains deep groundwater, which has a minor effect on the BNB flow rate. The subsurface layer structures (layers B and C) are based on the linear storage model (see Fig. 8.2c). When the water content storage in these layers reaches a saturated state, the water is discharged into the river combined by layer A. The suggested method can be outlined by the following key processes: (1) watershed modeling is carried out using the methodology of the geographical information system (GIS), (2) the kinematic wave approach is used to calculate the stream routing and surface runoff modeling, (3) transmission loss modeling is calculated using the Walter equation (Walters 1990), and (4) canopy interception losses and (5) the linear storage model are applied for the modeling of groundwater. The spatial resolution implemented in the current research for the BNB is 5 km (~0.05°), as indicated in (Abd-El Moneim et al. 2017).

The Blaney-Criddle method was used to determine potential evapotranspiration (ET_0) in the model as follows (Karamouz et al. 2013):

$$ET_0 = p\ (0.46T_{\text{mean}} + 8.13) \tag{8.1}$$

where ET_0 is the potential evapotranspiration (mm/d), T_{mean} is the average temperature (°C), and p is the daily average proportion of daytime hours per year. We can determine the value of p depending on the estimated latitude of the study area (the number of degrees north or south of the equator) (Karamouz et al. 2013). In this study, daily temperature and daily radiation datasets were retrieved from the Climate Forecast System Reanalysis (CFSR). The datasets are available to download from https://globalweather.tamu.edu/#pubs.

Stream routing and surface runoff were calculated using integrated kinematic wave runoff approximations assuming a triangular river cross-section, as shown in Eqs. (8.2, 8.3, 8.4, 8.5):

$$\frac{\partial h}{\partial t} + \frac{\partial q}{\partial x} = fr \tag{8.2}$$

$$q = \alpha(h-d)^{5/3} + ah(h > d) \tag{8.3}$$

$$q = ah \tag{8.4}$$

When $\begin{pmatrix} h \geq d \\ h \leq d \end{pmatrix}$, $d = \lambda D$

$$\alpha = \frac{\sqrt{\sin\theta}}{n}\ , \quad a = Ks\frac{\sin\theta}{\gamma} \tag{8.5}$$

where q is the unit discharge ($m^3/s/m$), h is the depth of the water (m), r is the effective precipitation intensity input (m/s) corresponding to the total rainfall infiltration into the soil after evapotranspiration losses are extracted, f is the ratio of direct runoff, which is equal to the upper soil saturation ratio, layer A (0–1), λ is the porosity, α and m are friction constants, x is the gap to the edge upstream, d is the saturation pondage (m), and D is the thickness of the layer (m).

A multilayer linear storage feature model is implemented on the Hydro-BEAM layers B and C to realistically calculate the base flow procedure. The linear storage function model's continuity equation and its dynamic equation are as follows:

$$\frac{dS}{dt} = I - O \tag{8.6}$$

$$O = kS \tag{8.7}$$

where I is the inflow (m/s), S is the storage of water (m), k is the coefficient of runoff (l/s), and O is the outflow (m/s).

8.2.4.1 Parameters and Calibration

It is noteworthy that the calibration of the model consists of a method that adjusts the parameters to achieve the optimum possible simulation of the realistic runoff measured for some forced data (Jiang et al. 2012). The parameters of the model may display several variations when utilized to simulate the flow rates (Stisen and Sandholt 2010). In the current analysis, the model with individual PESPs as inputs was calibrated with the observed streamflow data in the BNB.

The distributed hydrological model for the BNB was calibrated and validated against the available measured streamflow data from 2001 to 2007. The entire study period was classified into two periods: the calibration period, from 2001 to 2003, and the validation period, from 2004 to 2007. Table 8.2 illustrates the respective ranges of the model parameters used, which are dependent on variables such as land use and soil. The calibration regime returns the best parameter values that maximize the Nash–Sutcliffe efficiency (NSE) between the observed and simulated monthly flow rates (Bitew et al. 2012). Such parameters authorize us to parse the influence of the precipitation data source on the model calibration and validation.

8.2.5 Statistical Metrics for the Performance Evaluation

Several commonly utilized statistical indicators were employed to qualitatively analyze the overall performance of the six studied PESPs versus the gauge-based precipitation measurements. In the current analysis, three different statistical criteria

Table 8.2 Calibration parameters of the hydrological model for various PESPs

Parameters	Symbol	Value range	Units
Horizontal coefficient of permeability	B-layer C-layer	0.2 0.025	
Vertical coefficient of permeability	B-layer	0.4	
Layer thickness	A-layer	0.4	m
Equivalent roughness coefficient	Grass Forest Urban	0.3 0.7 0.03	$m^{-1/3}$ s
Direct runoff constant	Grass Forest Urban	0.5–0.75 0.3–0.5 0.9	
Porosity	B-layer C-layer	15.0 15.0	%
Finite difference interval	Spatial finite difference interval	2,500	m

were implemented to determine the correctness of the six PESPs, as explained in detail below.

8.2.5.1 Continuous Statistical Metrics

Continuous verification metrics were used, including the Pearson correlation coefficient (CC), relative error (RE), and root-mean-square error (RMSE). The CC refers to the rainfall variation synchronicity between the in situ rainfall data and PESPs, the RE describes the extent of the simulated error compared with that in the rain gauges, and the RMSE was employed to assess the averaged error magnitude. These metrics are calculated as follows:

$$\mathrm{CC} = \frac{\sum_{i=1}^{n}\left(G_i - G_i^{'}\right)\left(P_i - P_i^{'}\right)}{\sqrt{\sum_{i=1}^{n}\left(G_i - G_i^{'}\right)^2 \sum_{i=1}^{n}\left(P_i - P_i^{'}\right)^2}} \tag{8.8}$$

$$\mathrm{RE} = \frac{\sum_{i=1}^{n}\left(P_i - G_i\right)}{\sum_{i=1}^{n} G_i} \times 100\% \tag{8.9}$$

$$\mathrm{RMSE} = \sqrt{\frac{\sum_{i=1}^{n}\left(P_i - G_i\right)^2}{n}} \tag{8.10}$$

where P_i and G_i are the ith pair of PESPs and the gauge-based rainfall data, n reflects the cumulative number of timescales, and $P_i^{'}$ and $G_i^{'}$ are the corresponding

average values of the PESP data and the gauge-based data, respectively. The locally measured data and PESP data are considered compatible, without PESP-associated uncertainty, if the RMSE value and RE value are equal to zero and the CC value is equal to 1; this corresponds to higher CCs and lower RMSEs representing higher accuracy of PESP data.

8.2.5.2 Categorical Statistical Metrics

To test the detection capability analysis of PESPs against locally measured data at various precipitation thresholds, four categorical statistics were utilized based on the 2×2 contingency table. The following indices were used: the detection probability (POD), the frequency bias index (FBI), the false alarm rate (FAR), and the equitable threat score (ETS) POD, also called the hit rate. These indices were used to calculate the occurrences of rainfall by satellites and determine whether rainfall occurrences were detected correctly. FAR denotes that occurrences of rainfall were detected incorrectly. Furthermore, ETS indicates how well PESPs conformed to the measurements of the rain gauges. These indices were calculated as follows:

$$\mathrm{POD} = \frac{H}{H+M} \tag{8.11}$$

$$\mathrm{FAR} = \frac{F}{H+F} \tag{8.12}$$

$$\mathrm{ETS} = \frac{H - \mathrm{hits}}{H+M+F-\mathrm{hits}} \tag{8.13}$$

$$\mathrm{hits} = \frac{(H+M)(H+F)}{H+M+F+Z}$$

$$\mathrm{FBI} = \frac{H+F}{H+M} \tag{8.14}$$

where H is the correct detection of the measured precipitation number (hits), F is the precipitation number detected but not measured, and M is the precipitation number measured but not detected (misses). The ideal POD, FBI, FAR, and ETS values are 1, 1, 0, and 1, respectively. More information and explanations are described in Schaefer (1990), Wilks (2006) and Sun et al. (2016).

8.2.5.3 Statistical Evaluation of the Hydrological Model

In both the observed streamflows and the resultant streamflow simulations, statistical evaluation indices were applied to assess the uncertainty and the performance

of six PESPs. The criteria for model performance were tested using three widely utilized statistical indicators for simulations of hydrological models. First, NSE was used to match simulated flows with their statistical goodness values. NSE varies from $-\infty$ to 1, with greater values signifying stronger correspondences (Legates and McCabe 1999). If NSE $\leq$ 0, then the model lacks skill concerning the observed mean as a predictor (Lakew et al. 2017). Additionally, the percent bias (Bias) and the determination coefficient (R^2) were utilized to assess the agreement between the simulated and measured discharges. These statistical indices were calculated using Eqs. (8.15), (8.16), and (8.17), respectively, as follows:

$$\mathrm{NSE} = 1 - \frac{\sum_{i=1}^{n}\left(Q_{\mathrm{obs}} - Q_{\mathrm{sim}}\right)^2}{\sum_{i=1}^{n}\left(Q_{\mathrm{obs}} - Q'_{\mathrm{obs}}\right)^2} \tag{8.15}$$

$$R^2 = \frac{\sum_{i=1}^{n}\left(Q_{\mathrm{obs}} - Q'_{\mathrm{obs}}\right)\left(Q_{\mathrm{sim}} - Q'_{\mathrm{sim}}\right)^2}{\sum_{i=1}^{n}\left(Q_{\mathrm{obs}} - Q'_{\mathrm{obs}}\right)^2 \sum_{i=1}^{n}\left(Q_{\mathrm{sim}} - Q'_{\mathrm{sim}}\right)^2} \tag{8.16}$$

$$\mathrm{Bias} = \frac{\sum_{i=1}^{n}\left(Q_{\mathrm{sim}} - Q_{\mathrm{obs}}\right)}{\sum_{i=1}^{n} Q_{\mathrm{obs}}} \times 100\% \tag{8.17}$$

where Q_{sim} and Q'_{sim} are the simulated streamflow and the average simulated streamflow, respectively, and Q_{obs} and Q'_{obs} are the measured streamflow and the average measured streamflow, respectively. When the values of NSE = 1, R^2 = 1, and Bias = 0%, the optimum result occurs.

8.3 Results and Discussions

8.3.1 Comparison and Assessment of PESPs

The PESP precision against the in situ rain data was first tested over the BNB to understand the adverse effects of these products on hydrologic models and their correlated uncertainties. The comparative analysis was carried out using statistical approaches to explore and distinguish precipitation patterns and quantify errors over the BNB for six PESPs. The BNB climate is typified by a dry winter season, little spring rain, and a wet summer season (Awulachew et al. 2008). In the summer months between June and September, approximately 70% of the annual precipitation falls (Awulachew et al. 2008). In this study, one year is split into three periods: the dry season (known in Ethiopia as the Bega) (October–February), the period of little rainfall (known in Ethiopia as the Belg) (March–May), and the wet season (known in Ethiopia as the Kremt). Figure 8.3 displays the spatial distribution maps of the annual average rainfall (column (a)), the dry season (column (b)), the season of little rain (column (c)), and the wet season (column (d)) obtained from

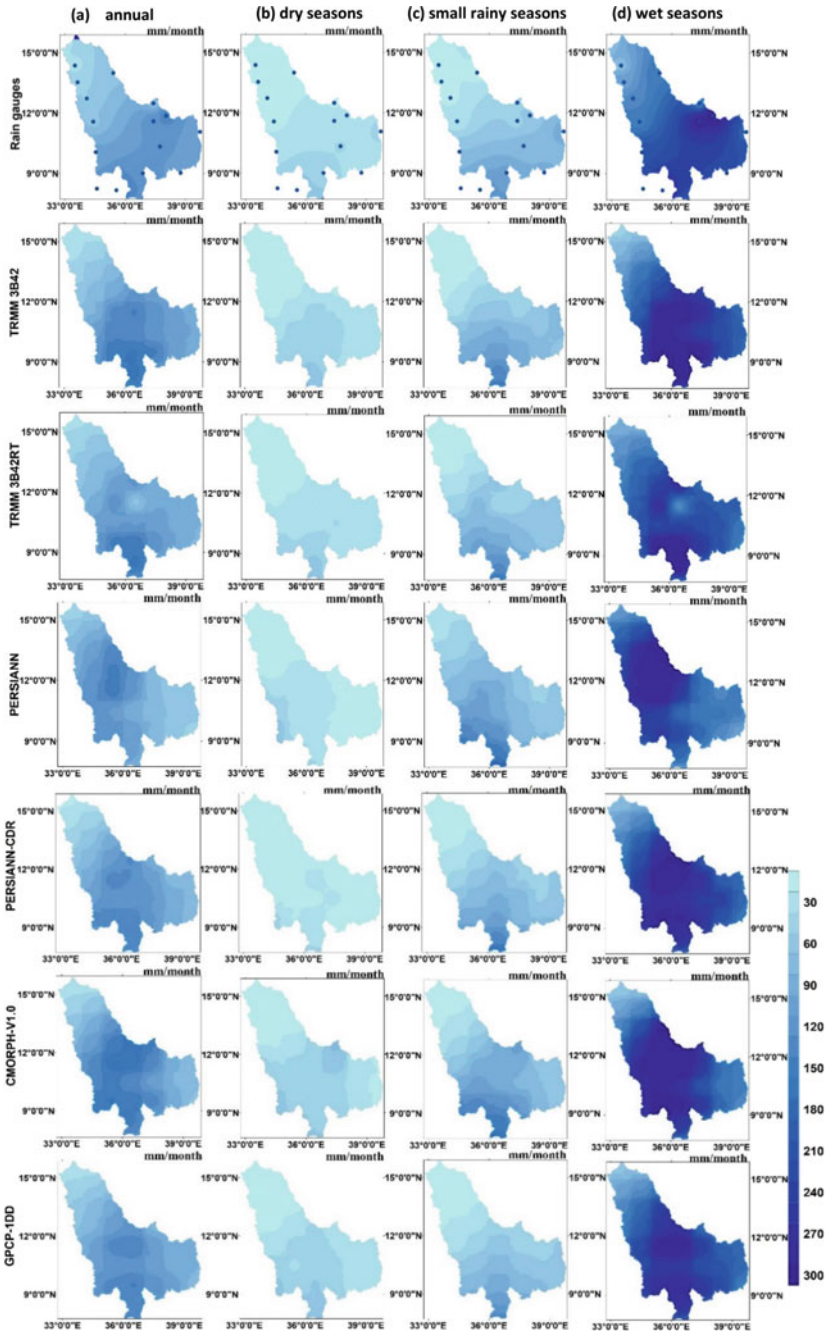

Fig. 8.3 Distribution maps of annual average (column (a)), dry season (column (b)), small rainy season (column (c)) and rainy season (column (d)) rainfall amounts obtained from PESPs over the BNB during 2001–2007 (mm/month)

PESPs over the BNB during the period from 2001–2007. Most PESPs (except PERSIANN) typically displayed harmonious patterns of precipitation, with precipitation events decreasing from south to north. However, high precipitation quantities are concentrated in the southern BNB zone in the elevated mountainous areas, and precipitation obviously depends on the basin's elevation. The precipitation distribution maps also show increases in precipitation in summer (the wet season), especially in August, but precipitation is seen to decrease in winter (the dry season). In both the seasonal and annual spatial patterns, TRMM 3B42V7 reproduced the spatial distributions well against the gauge-based observations. Conversely, the annual and seasonal precipitation patterns obtained with PERSIANN were very distinct with different precipitation intensity distributions.

Figure 8.4 shows the relative volume contributions and the frequency distributions of monthly rainfall at point-based gauge locations in various rainfall event ranges. The monthly precipitation was classified into four groups: 0, 0–100, 100–200, and >200 mm/month. All six PESPs underestimated no rainfall events at the occurrence frequency, while they overestimated small, heavy, and torrential precipitation occurrences (0–100 and >200 mm/month). In terms of moderate rainfall events, all PESPs overestimated their frequencies. The TRMM 3B42V7 estimations were close to the rainfall gauge data for the volume contribution distribution; however, there were some differences compared with the observed gauge-based data. The different performances of volume contributions among PESPs significantly influenced the following hydrological simulations, as most hydrological processes in distributed hydrological models are sensitive to the total precipitation amount and to the distribution of rainfall intensity (Sun et al. 2016). Overall, TRMM 3B42V7 had a greater agreement than the other products when comparing both occurrence frequency and relative volume contribution rate data for moderate

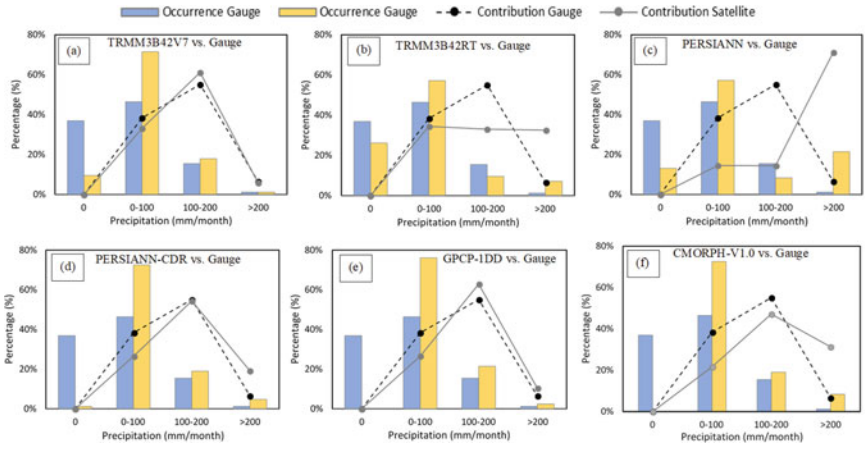

Fig. 8.4 The occurrence frequencies (bars) of each monthly PESP estimate and their relative volume contributions (lines) to the total rainfall for the 2001–2007 period

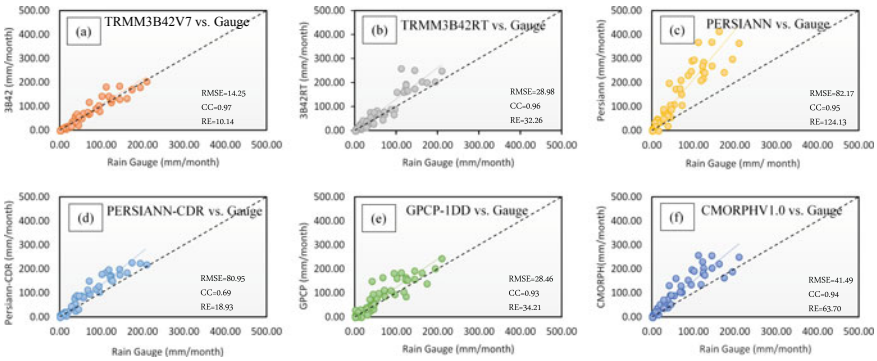

Fig. 8.5 Scatterplots showing monthly precipitation between in situ rainfall observations and PESPs in the BNB during 2001–2007

and extreme rainfall events with rain gauge-based data. TRMM 3B42RT, however, had better agreement with the gauge-based data for no rainfall events and small rainfall events.

Figure 8.5 shows the average monthly precipitation scatterplots of six PESPs against in situ rainfall observations and provides further insight into the characteristics of the variations between the six studied PESPs (TRMM 3B42V7, TRMM 3B42RT, GPCP-1DD, CMORPH-V1.0, PERSIANN, and PERSIANN-CDR) and the in situ rainfall observations during the period from 2001 to 2007 over the BNB. In addition, the statistical indicators of the monthly scale estimations of six PESPs are briefly described in Table 8.3. Good agreement can be observed for all PESPs compared with the gauging measurements except PERSIANN. Among these PESPs, TRMM 3B42V7 exhibited the best correspondence against the rain gauge observation data, which is reflected in its CC value of 0.97, the highest among all products, and its RMSE of 14.25 mm/month and RE of 10.14%, the smallest among all products (Fig. 8.5a). Additionally, TRMM 3B42RT and GPCP-1DD showed good performance against the rain gauge observations, with CC values of 0.96 and 0.93 and RMSE values of 28.98 mm/month and 28.46 mm/month, respectively (Fig. 8.5b, e). In contrast, PERSIANN missed the monthly variance for the target basin and presented the poorest values: an RMSE of 82.17 mm/month and an RE of 124.13% (Fig. 8.5c).

Table 8.3 Statistics of in situ rainfall measurements and PESPs at the monthly timestep

	TRMM 3B42V7	TRMM 3B42RT	CMORPH-V1.0	GPCP-1DD	PERSIANN	PERSIANN-CDR
CC	0.97	0.96	0.94	0.93	0.95	0.69
RMSE	14.25	28.98	41.49	28.46	82.17	80.95
RE (%)	10.14	32.26	63.70	34.21	124.13	18.93

For the categorical statistics, the overall accuracy of the precipitation products (based on POD, FBI, FAR, and ETS) decreased as the rainfall threshold rose, indicating that the studied PESPs are less skilled at estimating the exact magnitudes of intense precipitation events. Figure 8.6 illustrates the precipitation detection analysis events over the BNB at several precipitation thresholds, 30 mm/month, 60 mm/month, 90 mm/month, 120 mm/month, and 150 mm/month, using categorical statistics (POD, FBI, FAR, and ETS). All PESPs showed POD scores greater than 0.9 (except GPCP-1DD) (Fig. 8.6a). However, for FAR, TRMM 3B42V7 showed the lowest value across all precipitation ranges; meanwhile, the best score was observed for TRMM 3B42RT for the threshold of 90 mm/month (Fig. 8.6b). In general, TRMM 3B42V7 had the best FAR, ETS and FBI values, indicating that it exhibited the best performance across all precipitation ranges. At the same time, PERSIANN demonstrated the weakest performance for the categorical statistics.

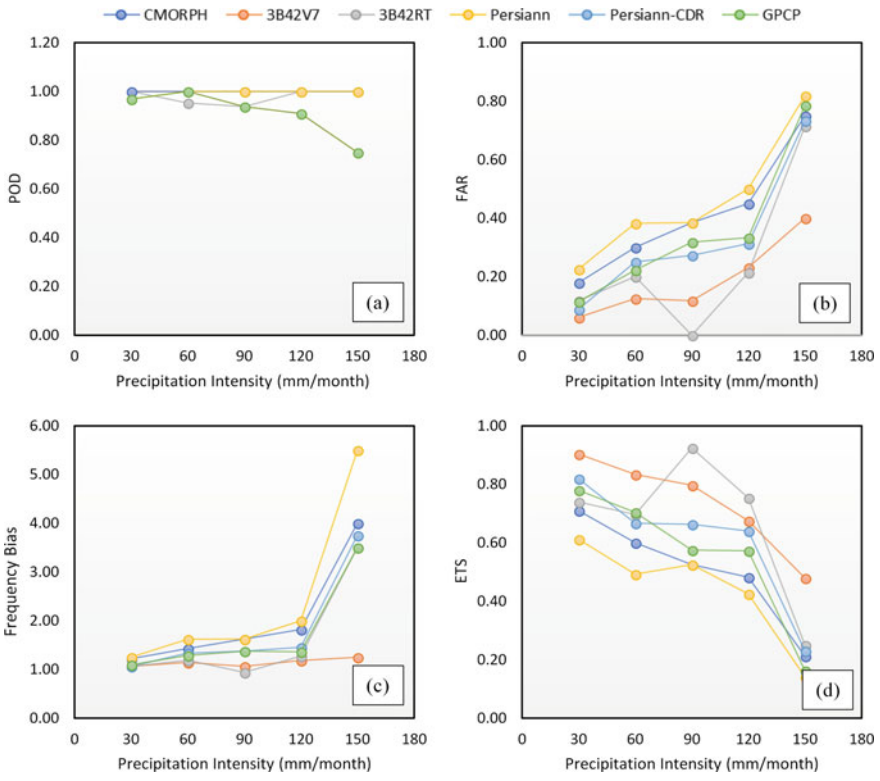

Fig. 8.6 **a** POD, **b** FAR, **c** FBI, and **d** ETS values of the six monthly PESPs against rain gauge observations at 30 mm/month, 60 mm/month, 90 mm/month, 120 mm/month and 150 mm/month threshold values over the BNB during 2001–2007

8.3.2 Comparison and Hydrologic Evaluations of Streamflow

According to Bitew and Gebremichael (2011), there are two advantages to evaluating PESPs based on their predictive flow rate performances in a hydrologic modeling framework. One of them is that PESPs are evaluated as a driving input variable in a hydrological model concerning a specific application. In the prior section, all PESPs were compared against the gauge-based observations; the subsequent phase was designed to evaluate how these PESPs influenced streamflow simulations by driving the Hydro-BEAM model over the BNB. The streamflow simulation using the Hydro-BEAM Model was calibrated by comparing the measured discharge to examine the efficacy of the six studied PESPs over BNB during the calibration period. The Hydro-BEAM model was then forced by CMORPH-V1.0-RAW, TRMM 3B42V7, TRMM 3B42RT, PERSIANN, PERSIANN-CDR, and GPCP-1DD as inputs for seven years (2001–2007) by maximizing the NSE value and the previous model parameter values. Figure 8.7 shows the monthly measured discharge hydrograph compared with the simulated hydrographs in the calibration (from 2001 to 2003) and validation (2004–2007) periods at Khartoum Station. Overall, the simulated hydrographs are noted to be in good agreement with the observed hydrograph, but in some cases, the simulated flows are either underestimated or overestimated compared to the high peaks observed. However, the simulated streamflows presented the relatively low performances of some PESPs in the validation period.

The exceedance probability between the monthly measured and simulated discharges is dependent on the rain gauge observations, and the six studied PESPs, used as rainfall drivers in the BNB for the interval 2001–2007, are shown in Fig. 8.8. In the calibration period, the exceedance probability plots indicated underestimations of high streamflows for all PESPs and overestimations of low streamflows for all PESPs (Fig. 8.8a). On the other hand, in the validation period, all PESPs showed underestimations of high streamflows and overestimations of low streamflows (except PERSIANN and CMORPH-V1.0) (Fig. 8.8b). As the statistical measures briefly described in Table 8.4, the three statistical indices used to measure the efficiency of the model showed perfect agreement between the observed and simulated hydrographs during the calibration period and reasonable simulations conducted during the validation period. According to the statistical metrics that reflect the model performances, the Hydro-BEAM model can capture the timing, occurrence, and magnitude of the rainfall events shown in the monthly observed hydrograph quite well. Although these metric indices were reasonable for the validation period, they were not as good as those obtained during the calibration period, which indicates better agreement during this period.

The simulation forced by the TRMM 3B42V7 product had the best NSE (0.88 and 0.85), Bias (10.35% and − 2.87%), and R^2 (0.94 and 0.92) values during the calibration and validation periods, respectively. The predicted streamflow results were in good correspondence with the observed streamflow data (see Fig. 8.7a,

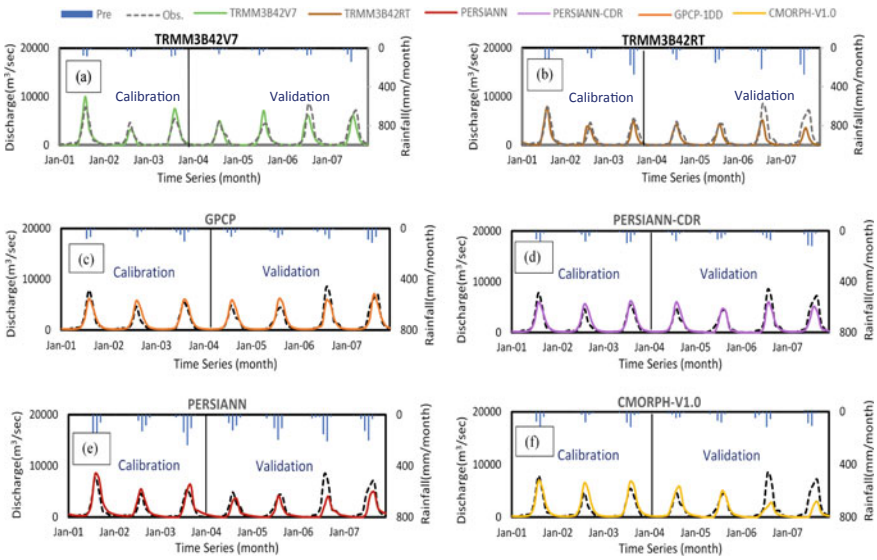

Fig. 8.7 Hydrographs of Hydro-BEAM-simulated and measured monthly discharges for the calibration (2001–2003) and validation (2004–2007) periods (separated by the vertical line)

Table 8.4). The GPCP-1DD- and TRMM 3B42RT-forced simulations also showed good agreements with the observed streamflow throughout the calibration period, with NSE values of 0.87 and 0.87, Bias values of 12.23 and 17.31%, and R^2 values of 0.94 and 0.95, respectively. These products exhibit slightly less performances in the validation period, with NSE values of 0.85 and 0.84, R^2 values of 0.92 and 0.92, and Bias values of 1.15% and 2.95%, respectively (Fig. 8.7b, c; Table 8.4). Conversely, the PERSIANN and CMORPH-V1.0 simulations showed fair performances, with NSE values of 0.59 and 0.42, Bias values of −38.01% and −31.86%,

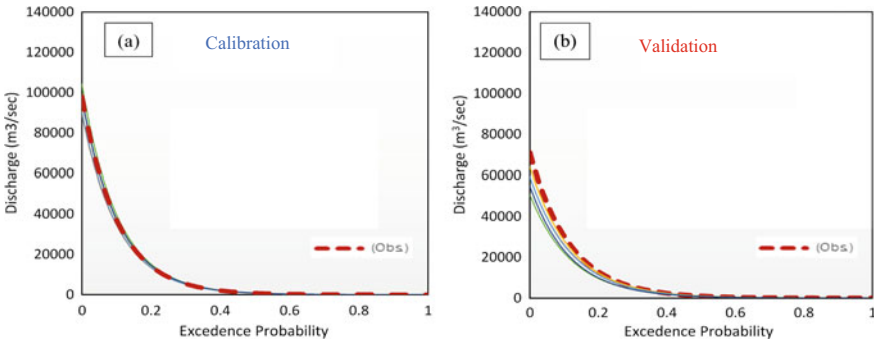

Fig. 8.8 Exceedance probabilities of monthly discharge in the **a** calibration period and **b** validation period

Table 8.4 Statistical monthly summary measures of PESP inputs and corresponding streamflows during the calibration and validation periods

Datasets	Calibration			Validation		
	NSE	R^2	Bias (%)	NSE	R^2	Bias (%)
TRMM 3B42V7	0.88	0.94	10.35	0.85	0.92	− 2.87
GPCP-1DD	0.87	0.94	12.23	0.85	0.92	1.15
TRMM 3B42RT	0.87	0.95	17.31	0.84	0.92	2.95
PERSIANN-CDR	0.86	0.94	11.30	0.83	0.93	− 17.28
PERSIANN	0.79	0.94	25.79	0.59	0.84	− 38.01
CMORPH-V1.0	0.78	0.94	27.67	0.42	0.68	− 31.86

and R^2 values of 0.84 and 0.68 in the validation period, respectively (Fig. 8.7e, f; Table 8.4). Generally, the TRMM 3B42V7 simulations gave the best performance with the Hydro-BEAM model among all PESPs over the BNB during the simulation period (2001–2007). The PERSIANN and CMORPH-V1.0 are not recommended for direct use, as they showed lower abilities to simulate streamflow over the target basin. Therefore, bias removal in PESPs is key to enhancing the truthfulness of hydrologic simulations (Bitew and Gebremichael 2011).

8.4 Conclusions

PESPs are recognized as viable sources of precipitation data for use in various hydrologic models for water resource management worldwide and for regional and global hydrologic applications, particularly in data-sparse regions with poor or nonexistent rain gauge measurements. In the current study, a comprehensive analysis was performed to better understand the reliability, precision, and applicability of six PESPs (TRMM 3B42V7, TRMM 3B42RT, PERSIANN, PERSIANN-CDR, CMORPH-V1.0, and GPGP-1DD) against rain gauge measurements over the BNB during 2001–2007. Precipitation distribution maps over the BNB were presented based on the six PESPs, which are obviously dependent on the basin's elevation. It can also be noticed that the precipitation variation increased in summer (the wet season), especially in August, but decreased in winter (the dry season). Statistical analysis indicated that most PESPs could capture the occurrence, timing, and magnitude of precipitation events. In particular, TRMM 3B42V7 typically presented a stronger ability to detect precipitation events than did the other products and correlated well with rain gauge measurements. Moreover, the best FAR, ETS, and FBI were obtained for TRMM 3B42V7 across all precipitation thresholds. Conversely, PERSIANN mostly displayed the lowest estimations of the entire precipitation (Bias), with a high RMSE. Additionally, PERSIANN showed the worst results for the categorical statistics, although it had a better POD score than did the other products.

For streamflow modeling, the predictive capacity of each PESP was examined using the Hydro-BEAM model after a calibration with the observed measurements was conducted. In general, all products achieved reasonable NSE and R^2 values for their estimations of streamflow series at the monthly timestep during the calibration and validation periods (except CMORPH-V1.0 in the validation period). The streamflow simulation results based on TRMM 3B42V7 provided the best correspondence with the measured discharge series compared with the other PESPs. Moreover, the results revealed that TRMM 3B42V7 may be another potential source of data for the area characterized by sparse rainfall gauges in the BNB. In contrast, the PERSIANN and CMORPH-V1.0 products demonstrated lower potentials for utility in hydrologic applications over the BNB.

In summary, the six studied PESPs showed considerable potential for hydrological applications and research. Among the six PESPs, TRMM 3B42V7 exhibited the best performance when compared with observed, gauge-based data in terms of all analyzed criteria over the BNB region, followed by GPCP-1DD and TRMM 3B42RT. By contrast, CMORPH-V1.0 showed fair agreement compared to the other products. The evaluation of the six PESP-based simulations performed for the BNB may not be valid for other areas characterized by different hydroclimatic regimes. In general, this research hopefully offers a good understanding of the utility and uncertainties of various PESPs in streamflow simulations and forecasts and water resource planning and management with satellite-based rainfall data, particularly in data-scarce catchments. Future studies are required to disclose PESP applications under the conditions of climate change, different initial conditions, and among various basins, especially those in data-sparse and ungauged regions.

References

Abd-El Moneim H, Soliman MR, Moghazy HM (2017) Numerical simulation of Blue Nile Basin using distributed hydrological model. In: 11th international conference on the role of engineering towards a better environment (RETBE' 17)

Abd-El Moneim H, Soliman MR, Moghazy HM (2019) Hydrologic evaluation of TRMM multi-satellite precipitation analysis products over Blue Nile Basin. In: 2nd international conference of chemical, energy and environmental engineering (ICCEEE2019), pp 33–44

Abdel-Fattah M (2017) A hydrological and geomorphometric approach to understanding the generation of wadi flash floods. A Hydrological and Geomorphometric Approach to. https://doi.org/10.3390/w9070553

Abdel-Fattah M, Kantoush S, Sumi T (2015) Integrated management of flash flood in wadi system of Egypt: disaster prevention and water harvesting. Annu Disas Prev Res Inst, Kyoto Univ 58:485–496

Abdelmoneim H, Soliman MR, Moghazy HM (2020) Evaluation of TRMM 3B42V7 and CHIRPS satellite precipitation products as an input for hydrological model over eastern Nile Basin. Earth Syst Environ 4:685–698. https://doi.org/10.1007/s41748-020-00185-3

Alazzy AA, Lü H, Chen R et al (2017) Evaluation of satellite precipitation products and their potential influence on hydrological modeling over the Ganzi River Basin of the Tibetan Plateau. Adv Meteorol 2017. https://doi.org/10.1155/2017/3695285

Ali AF, Xiao C, Anjum MN et al (2017) Evaluation and comparison of TRMM multi-satellite precipitation products with reference to rain gauge observations in Hunza River basin, Karakoram Range, northern Pakistan. Sustain 9. https://doi.org/10.3390/su9111954

Ashouri H, Hsu KL, Sorooshian S et al (2015) PERSIANN-CDR: daily precipitation climate data record from multisatellite observations for hydrological and climate studies. Bull Am Meteorol Soc 96:69–83. https://doi.org/10.1175/BAMS-D-13-00068.1

Awulachew SB, McCartney M, Steenhuis TS, Ahmed AA (2008) A review of hydrology, sediment and water resource use in the Blue Nile Basin (IWMI Working Paper 131)

Behrangi A, Khakbaz B, Jaw TC et al (2011) Hydrologic evaluation of satellite precipitation products over a mid-size basin. J Hydrol 397:225–237. https://doi.org/10.1016/j.jhydrol.2010.11.043

Bitew MM, Gebremichael M (2011) Evaluation of satellite rainfall products through hydrologic simulation in a fully distributed hydrologic model. Water Resour Res 47:1–11. https://doi.org/10.1029/2010WR009917

Bitew MM, Gebremichael M, Ghebremichael LT, Bayissa YA (2012) Evaluation of high-resolution satellite rainfall products through streamflow simulation in a hydrological modeling of a small mountainous watershed in Ethiopia. J Hydrometeorol 13:338–350. https://doi.org/10.1175/2011JHM1292.1

Fenta AA, Yasuda H, Shimizu K et al (2018) Evaluation of satellite rainfall estimates over the Lake Tana basin at the source region of the Blue Nile River. Atmos Res 212:43–53. https://doi.org/10.1016/j.atmosres.2018.05.009

Gebere SB, Alamirew T, Merkel BJ, Melesse AM (2015) Performance of high resolution satellite rainfall products over data scarce parts of eastern ethiopia. Remote Sens 7:11639–11663. https://doi.org/10.3390/rs70911639

Gebrehiwot SG, Ilstedt U, Gärdenas AI, Bishop K (2011) Hydrological characterization of watersheds in the Blue Nile Basin, Ethiopia. Hydrol Earth Syst Sci 15:11–20. https://doi.org/10.5194/hess-15-11-2011

Gebremicael TG, Mohamed YA, Van Der Zaag P, Amdom G (2017) Comparison and validation of eight satellite rainfall products over the rugged topography of Tekeze-Atbara Basin at different spatial and temporal scales. Hydrol Earth Syst Sci Discuss 1–31. https://doi.org/10.5194/hess-2017-504

Habib E, Haile AT, Tian Y, Joyce RJ (2012) Evaluation of the high-resolution CMORPH satellite rainfall product using dense rain gauge observations and radar-based estimates. J Hydrometeorol 13:1784–1798. https://doi.org/10.1175/JHM-D-12-017.1

Hirpa FA, Gebremichael M, Hopson T (2010) Evaluation of high-resolution satellite precipitation products over very complex terrain in Ethiopia. J Appl Meteorol Climatol 49:1044–1051. https://doi.org/10.1175/2009JAMC2298.1

Hsu K, Gao X, Sorooshian S, Gupta HV (1997) Precipitation estimation from remotely sensed information using artificial neural networks. J Appl Meteorol 36:1176–1190. https://doi.org/10.1175/1520-0450(1997)036%3c1176:PEFRSI%3e2.0.CO;2

Huang Y, Chen S, Cao Q et al (2014) Evaluation of version-7 TRMM multi-satellite precipitation analysis product during the Beijing extreme heavy rainfall event of 21 July 2012. Water (switzerland) 6:32–44. https://doi.org/10.3390/w6010032

Huffman GJ, Adler RF, Arkin P et al (1997) The global precipitation climatology project (GPCP) combined precipitation dataset. Bull Am Meteorol Soc 78:5–20. https://doi.org/10.1175/1520-0477(1997)078%3c0005:TGPCPG%3e2.0.CO;2

Huffman GJ, Bolvin DT, Nelkin EJ et al (2007) The TRMM multisatellite precipitation analysis (TMPA): quasi-global, multiyear, combined-sensor precipitation estimates at fine scales. J Hydrometeorol 8:38–55. https://doi.org/10.1175/JHM560.1

Jiang Q, Li W, Wen J et al (2018) Accuracy evaluation of two high-resolution satellite-based rainfall products: TRMM 3B42V7 and CMORPH in Shanghai. Water (Switzerland) 10. https://doi.org/10.3390/w10010040

Jiang S, Ren L, Hong Y et al (2012) Comprehensive evaluation of multi-satellite precipitation products with a dense rain gauge network and optimally merging their simulated hydrological

flows using the Bayesian model averaging method. J Hydrol 452–453:213–225. https://doi.org/10.1016/j.jhydrol.2012.05.055

Joyce RJ, Janowiak JE, Arkin PA, Xie P (2004) CMORPH: a method that produces global precipitation estimates from passive microwave and infrared data at high spatial and temporal resolution. J Hydrometeorol 5:487–503. https://doi.org/10.1175/1525-7541(2004)005%3c0487:CAMTPG%3e2.0.CO;2

Joyce RJ, Xie P, Yarosh Y et al (2010) CMORPH: a "Morphing" approach for high resolution precipitation product generation

Karamouz M, Nazif S, Falahi M (2013) Hydrology and hydroclimatology_ principles and applications. CRC Press, U.S.

Knapp KR (2008) Scientific data stewardship of international satellite cloud climatology project B1 global geostationary observations. J Appl Remote Sens 2:023548. https://doi.org/10.1117/1.3043461

Kojiri T, Tokai A, Kinai Y (1998) Assessment of river basin environment through simulation with water quality and quantity. Annu Disaster Prev Res Inst Kyoto Univ 41:119–134

Kubota T, Hashizume H, Shige S et al (2007) Global precipitation map using satelliteborne microwave radiometers by the GSMaP project: production and validation. In: IEEE transactions on geoscience and remote sensing abbreviated. Institute of Electrical and Electronics Engineers Inc, pp 2259–2275

Kummerow C, Barnes W, Kozu T et al (1998) The tropical rainfall measuring mission (TRMM) sensor package. J Atmos Ocean Technol 15:809–817. https://doi.org/10.1175/1520-0426(1998)015%3c0809:TTRMMT%3e2.0.CO;2

Lakew HB, Moges SA, Asfaw DH (2017) Hydrological evaluation of satellite and reanalysis precipitation products in the Upper Blue Nile Basin: a case study of Gilgel Abbay. Hydrology 4:39. https://doi.org/10.3390/hydrology4030039

Legates DR, McCabe GJ Jr (1999) Evaluating the use of "Goodness of Fit" measures in hydrologic and hydroclimatic model validation. Water Resour Res 35:233–241. https://doi.org/10.1029/1998WR900018

Li Y, Wang W, Lu H et al (2019) Evaluation of three satellite-based precipitation products over the lower Mekong River Basin using rain gauge observations and hydrological modeling. IEEE J Sel Top Appl Earth Obs Remote Sens 12:2357–2373. https://doi.org/10.1109/jstars.2019.2915840

MWRI (1998a) Measured discharges of the Nile and /its tributaries every 5 years. Egypt

MWRI (1998b) Monthly and annual rainfall totals and number of rainy days at stations in and near the Nile Basin for every 5 years. Egypt

Ragab O, Valeriano OCS (2014) Flood forecasting in Blue Nile Basin using a process-based distributed hydrological model and satellite distributed hydrological model and satellite derived precipitation product. In: ASEE 2014 Zone I conference, USA

Romilly TG, Gebremichael M (2011) Evaluation of satellite rainfall estimates over Ethiopian river basins. Hydrol Earth Syst Sci 15:1505–1514. https://doi.org/10.5194/hess-15-1505-2011

Saber M (2010) Hydrological approaches of Wadi system considering flash floods in arid regions. Kyoto University, Japan

Saber M, Yilmaz K (2016) Bias correction of satellite-based rainfall estimates for modeling flash floods in semi-arid regions: application to Karpuz River, Turkey. Nat Hazards Earth Syst Sci Discuss 1–35. https://doi.org/10.5194/nhess-2016-339

Saber M, Yilmaz KK (2018) Evaluation and bias correction of satellite-based rainfall estimates for modelling flash floods over the Mediterranean region: application to Karpuz River Basin, Turkey. Water (Switzerland) 10. https://doi.org/10.3390/w10050657

Samy A, Valeriano OCS, Negm A (2015) Variability of hydrological modeling of the Blue Nile. Int J Environ Chem Ecol Geol Geophys Eng 9:225–229. https://doi.org/10.scholar.waset.org/1999.6/10000744

Saber M, Hamaguchi T, Kojiri T et al (2013) A physically based distributed hydrological model of wadi system to simulate flash floods in arid regions. Arab J Geosci 58:485–496. https://doi.org/10.1007/s12517-013-1190-0

Sapkta M, Hamaguchi T et al. (2010) Hydrological simulations in red river basin using super high resolution GCM outputs with geostatistical process. Annuals of Disas Prev Res Inst, Kyoto Unv., No. 53 B

Schaefer JT (1990) The critical success index as an indicator of warning skill. Weather Forecast 5:570–575. https://doi.org/10.1175/1520-0434(1990)005%3c0570:TCSIAA%3e2.0.CO;2

Sorooshian S, Hsu K, Gao X et al (2000) Evaluation of PERSIANN system satellite based estimates of tropical rainfall. Bull Am Meteorol Soc 81:2035–2046. https://doi.org/10.1175/1520-0477(2000)081%3c2035:EOPSSE%3e2.3.CO;2

Stisen S, Sandholt I (2010) Evaluation of remote-sensing-based rainfall products through predictive capability in hydrological runoff modelling. Hydrol Process 24:879–891. https://doi.org/10.1002/hyp.7529

Sun R, Yuan H, Liu X, Jiang X (2016) Evaluation of the latest satellite-gauge precipitation products and their hydrologic applications over the Huaihe River basin. J Hydrol 536:302–319. https://doi.org/10.1016/j.jhydrol.2016.02.054

Tong K, Su F, Yang D, Hao Z (2014) Evaluation ofsatellite precipitation retrievals and their potential utilities in hydrologic modeling over the Tibetan Plateau. J Hydrol 519:423–437. https://doi.org/10.1016/j.jhydrol.2014.07.044

Walters BMO (1990) Transmission losses in arid region. J Hydraulic Eng 116:129–138

Wang S, Liu S, Mo X et al (2015) Evaluation of remotely sensed precipitation and its performance for streamflow simulations in basins of the Southeast Tibetan Plateau. J Hydrometeorol 16:2577–2594. https://doi.org/10.1175/JHM-D-14-0166.1

Wilks DS (2006) Statistical methods in the atmospheric sciences, 2nd edn

Xie P, Arkin PA (1995) An Intercomparison of gauge observations and satellite estimates of monthly precipitation. J Appl Meteorol 34:1143–1160. https://doi.org/10.1175/1520-0442(1996)009%3c0840:AOGMPU%3e2.0.CO;2

Xue X, Hong Y, Limaye AS et al (2013) Statistical and hydrological evaluation of TRMM-based multi-satellite precipitation analysis over the Wangchu Basin of Bhutan: are the latest satellite precipitation products 3B42V7 ready for use in ungauged basins? J Hydrol 499:91–99. https://doi.org/10.1016/j.jhydrol.2013.06.042

Chapter 9
Innovative Monitoring Techniques for Wadi Flash Flood by Using Image-Based Analysis

Mahmood M. Al-Mamari, Sameh A. Kantoush, and Tetsuya Sumi

Abstract Flash floods in wadi systems are a very important environmental issue, and their monitoring is necessary for many applications, including water resource management, irrigation and flood control. However, monitoring networks are very rare and lack spatial distribution features. In this study, image-based techniques were used to quantify and monitor flash floods in wadi channels by using two different methods. In the first section, we employed photogrammetry processing technique to quantify post-peak flood discharges by using a drone survey to build a digital elevation model (DEM) with a high resolution and calibrated and validated the model with a field survey (levelling measurements). This technique used drone-collected images to construct a DEM for extracting a cross-sectional profile and elevation points to calculate the peak discharge using the slope-area method with the Manning equation. In the second section, we combined the previous technique with the large-scale particle image velocimetry (LSPIV) technique to measure flash flood discharge by installing a fixed camera on a road bridge crossing a wadi channel and using a digitally extracted cross section from the DEM in the analysis. The results of those techniques show a high efficiency that is equivalent to that of conventional methods.

Keywords Flash flood · Wadi · Monitoring · Image analysis · Photogrammetry · LSPIV

M. M. Al-Mamari (✉) · S. A. Kantoush · T. Sumi
Disaster Prevention Research Institute (DPRI), Kyoto University, Kyoto 611-0011, Japan
e-mail: almamari.mahmood.78c@st.kyoto-u.ac.jp

S. A. Kantoush
e-mail: kantoush.samehahmed.2n@kyoto-u.ac.jp

T. Sumi
e-mail: sumi.tetsuya.2s@kyoto-u.ac.jp

T. Sumi et al. (eds.), *Wadi Flash Floods*, Natural Disaster Science and Mitigation Engineering: DPRI Reports, https://doi.org/10.1007/978-981-16-2904-4_9

9.1 Introduction

Precipitation is the main source of water in semiarid and arid regions. The variables of rainfall patterns are intricate with irregular frequencies. However, the intensity and duration of rainfall play the main roles in hydraulic processes in dry environments. Arid regions have many challenges associated with water stress and desertification due to high temperatures and water demands (Sen 2008). Effective water resource management is very important for human and environmental sustainability. In recent years, extreme rainfall events have increased; consequently, flash floods occur more frequently with high discharges. Additionally, massive destruction to infrastructure and properties and human losses have occurred in the last decade in arid regions due to hazardous disasters such as flash floods. However, many countries in dry environments face water resource shortages and drought because of improper management and monitoring. In Middle East countries and North Africa, the term 'wadi' is used to refer to an ephemeral channel or valley. Wadi systems are different from river systems due to their scientific and flow dynamics. Run-off in wadi is mainly dependent on the availability of rainfall events, with rapid peaks of water occurring in streams for short periods. The critical issue concerning wadi flash floods is the availability of hydrological data, and observational data is lacking in this area. There are several challenges involved in wadi monitoring; for instance, access to gauges during flash floods can be impossible, and technical problems with inapplicable instruments measuring flow dynamics (discontinued flow) and sediment load (instrument protection housing clogged up with sediment) can occur, as well as the destruction of hydrometric stations.

Recently, many studies have been conducted to simulate flash floods in wadi basins; however, the efficiency of these models is limited by the observed data (Abdel-Fattah and Kantoush 2016). Many arid countries have requested inexpensive and adaptable techniques for qualitative and quantitative hydrology and water resources due to the ephemeral conditions of wadi basins. To manage and monitor wadi flash floods in arid regions, this chapter presents new methods and approaches by using image-based techniques. Therefore, the monitoring and measurement of wadis are tools used to improve and achieve better management systems. The use of image-based techniques to monitor and quantify flash floods will assist in upgrading hydrological databases with higher accuracies, faster analyses and early warning systems. Therefore, we can integrate our water resource management by mitigation structures, water resource policies/strategies and aquifer management recharge. Additionally, these techniques will provide real-time visual warning systems for flash floods in basins, which will help to prevent and warn downstream communities about strengthening flash floods, and can be used to manage dam operations for the release and storage of water in dam reservoirs during severe conditions.

First, we will discuss image analysis for monitoring wadi flash floods in arid regions. Wadi flash floods are rapid run-off events of peak discharges over dry channel beds. Typically, these events are under-monitored and under-investigated

and are forecasted based on rainfall magnitudes (Smith et al. 2014). In general, the impacts of climate change are expected to include the potential for more changes in rainfall intensities and temperature levels. Accurate field observations of wadi flash floods will provide a scientific understanding of flood characterizations that can help improve future flood forecasting and management. The use of direct and indirect measurements of discharge was possible with image-based techniques. The aim of this section is to provide alternative techniques to estimate peak post-flood discharge in wadi systems.

In the second section, we will discuss the large-scale particle image velocimetry (LSPIV) technique to monitor and measure flash flood discharge as a new method for wadi systems. LSPIV is a method used to measure surface flow velocity by using pairs of images extracted from recorded videos of flash floods. The first systematic study using LSPIV was carried out in 1998 by Fujita et al. (1998) for river systems. This technique is a noncontact measurement that can monitor flash floods from safe places and can provide a real-time monitoring system. The main advantages of this technique are the inexpensiveness, adequate accuracy and geographic extent of the measured surface water. This technology has been widely investigated in river basins (Harpold et al. 2006; Sun et al. 2010; Coz et al. 2010). This paper reports and investigates the performance of using image-based techniques in wadi systems to quantify post-peak discharges and real-time flow rates. The accuracy of LSPIV was evaluated in wadi flash floods, and the outputs seem to be very plausible (Al-Mamari et al. 2019). LSPIV can measure flash flood discharge with an accuracy comparable to that of local point measurements (current meter, transducer sensor and radar water level), which are the most common monitoring methods employed to measure water levels and compute discharges by using a rating curve. In addition, the conventional method of monitoring wadi flash floods is always influenced by technical issues due to dry seasons and the lack of recorded data as well as changing sediment loads and bed channels. Therefore, this work shows that innovative monitoring techniques can be used to obtain noncontact measurements and extract powerful information and data from wadi channels. The case study was from Wadi Aluqq in Oman, where a flood event occurred in October 2018 with a medium flow. We successfully estimated the flow rate at three phases (rising, peak and recession) and compared the results with those obtained from the conventional method (slope-area method). The resultant flood discharge from the rating curve was 6.3 m^3/s, and the LSPIV-estimated discharge showed very good agreement, with a value of approximately 6.4 m^3/s. The proposed monitoring techniques could provide high-quality measurements of wadi flow discharges without the need to visit the field during flash flood events, which is challenging work.

9.1.1 Conventional Monitoring Techniques and Methods in Wadi Systems

Water resource management requires highly precise observation data collected using different equipment and methods for monitoring and early warning systems to prevent threats to humans and infrastructure. Many techniques have been utilized to monitor wadi flash floods, such as crest stage indicators (gauges), water level transducers and radar water levels (Fig. 9.1) (Public Authority for Water Resource 1983). However, these techniques represent local point observations, which deliver some uncertainty when used to calculate discharge. The slope area method is an indirect measurement used to estimate peak discharge after a flood occurs by using a channel geometry technique that was developed in the Western USA (Johnson 1977). We define the relationship between the channel geometry and flood level, which is utilized to develop a rating curve based on the accumulation of slope-area measurements. This method is applied by using the Manning equation and the principle of conveyance. For this method, three or more cross sections of the wadi channel are required with estimated roughness coefficients. The accuracy of this method is dependent on the visibility and availability of flood markers, which present water level markers in the channel embankment (Dalyrmple and Benson 1967). Therefore, the combination of observed data obtained by monitoring techniques (transducer water levels and radar water levels) and rating curves can be used to analyse daily or hourly discharge in wadi channels. Figure 9.2 shows the equipment used to conduct the slope-area method in a wadi channel. Recently, survey instruments have been improved with higher accuracies and easier-to-obtain surface levelling. However, the main disadvantage of these devices is that they are very expensive and highly sensitive to weather conditions.

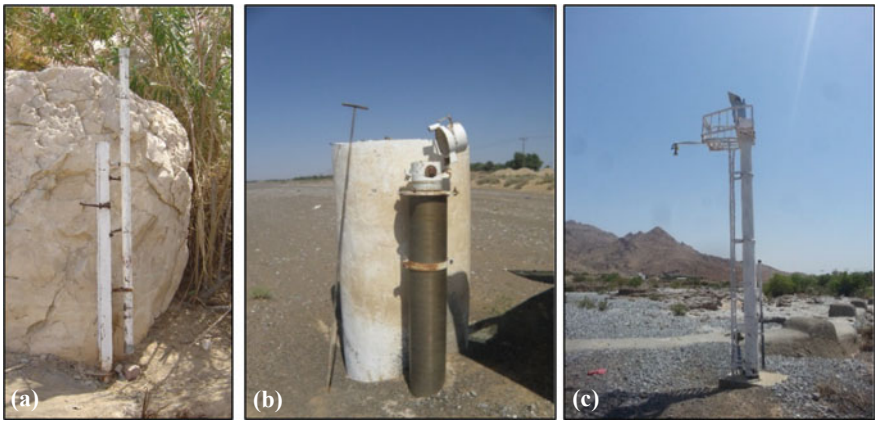

Fig. 9.1 **a** Crest stage indicator; **b** transducer inside a protection screening filter; **c** radar water level

Fig. 9.2 Slope-area method using levelling instruments

Current meter measurements were used to measure the flow rates of low discharges (base flows) in wadis (Fig. 9.3). To measure the average discharge, we divide the width of the surface flow in the wadi channel into several sections and measure the velocity of each section; then, we multiply the average velocity by the cross-sectional area to give the total discharge. Wadi systems in arid regions are characterized by high drainage densities with complex topographic features. Therefore, these systems require widespread hydrologic monitoring networks to achieve integral water resource balance in wadi basins.

Fig. 9.3 Current meter measurement method

9.2 Image-Based Techniques

Currently, image processing analysis is a widespread technique used to extract large amounts of data and information. In the literature, there are several examples of using image-based techniques for monitoring water surfaces (Muto et al. 2002; Fujita et al. 2019; Detert and Weitbrecht 2015). Huang et al. (2018) developed an automated discharge imaging system to estimate floods during typhoon events by using LSPIV in river systems. Objective detection methods have been created based on improvements in image analysis and enhancement over water surfaces; these methods are used to study water and environmental pollution (Zhang et al. 2019). Image-based techniques have been used to investigate and quantify many natural phenomena. Additionally, this new method can show one- and two-dimensional visualizations of different applications. There are many factors that must be considered in image processing, such as the image resolution, image acquisition tools and image analysis software. In addition, image analysis goes through three general stages for image treatment: preprocessing, enhancement and information extraction (Anbarjafari 2014).

9.2.1 Estimation of Peak Discharge Using the Slope-Area Method and Image Processing

It is quite a challenge to manage and develop flash flood monitoring systems in arid regions due to the large-scale catchments and the lack of financial investments in the water sector. The slope-area method is a conventional technique used to quantify peak post-flood discharges in wadi systems; this method requires time and equipment for surveying. However, this method is an indirect measurement that has been used to study low-flow and ephemeral rivers and is currently less frequently used due to the large amount of required statistical analysis (Griffiths and McKerchar 2015). In this section, we used observed and field-measured data to calculate peak discharge in a wadi system and compared the data with the new method involving image processing. This approach was approved by Castillo et al. (2018) to be more suitable to provide sufficient cross-sectional measurements with less time and lower costs than the conventional method. With the high growth of unmanned aerial vehicle (UAV) technology, also called drones, UAVs have been utilized as instruments to extract information such as channel morphology and flood markers. In this research, we presented a novel technique for quantifying the post-flood peak discharge in a wadi system using imagery acquired by UAVs with photogrammetry analysis.

9.3 Methodology

9.3.1 Study Area and Data Collection

The study area is Wadi Aluqq, a part of the Wadi Samail catchment in northern Oman with a drainage area of 136 km^2 (Fig. 9.4). The main types of channel bed material in this basin include gravel and sand. This research was applied on a small-scale reach of a wadi channel that was surveyed by drone and satellite levelling instruments. Thirty-five images were acquired for the study reach by using a drone camera. The zenith of the camera was perpendicular to the channel bed with approximately 50% overlap between images. The camera resolution was 20 MP, or 5472 × 3648 pixels, which had a high efficiency in detecting high details of the wadi channel bed. Four ground control points (GCPs) were located over the reach and were marked with visible spray marks. These GCPs were distributed over the reach to calibrate the photogrammetry analysis and georeferenced into real-world units. Agisoft Metashape is a commercially available software that is used to generate dense cloud points to formulate a digital elevation model (DEM). A DEM was constructed based on the formulation of textural features and the detection of structural properties with a differentiation of features with similar spectra in the same region. Spray marks were placed on all elevation points obtained by the levelling instrument. We used the DEM to extract the same cross-sectional location for the levelling survey. Figure 9.5 shows the methodology approach used to estimate peak discharge with different techniques.

The peak discharge was calculated from the cross sections using the slope area method equations. A satellite levelling instrument was used to obtain three cross sections and flood markers. Additionally, 51 channel bed elevation points for the three cross sections with 22 flood marker elevation points were used to compute the peak discharge by using the slope-area method and Manning equation. The water slope surface was calculated from the flood marker elevation points. Wadi channel flow is a part of the hydrological process for which measurements represent the flood catchment scale. Water level gauging stations were used to detect high water marks with which to extract cross sections from DEMs (drone surveys) and measure the water depth of flows in wadi channels.

The cross section was divided into small areas to estimate the discharge and reduce the uncertainty in the vertical velocity profile. In the first step involving the camera installation and set-up, the camera was mounted on a road bridge across the wadi channel. The camera view covered the channel width with a visible selected GCP. The installed camera was operated by a power supply from batteries and used a memory card to record the flood events. On 28 October 2018, we recorded a flash flood event with approximately five hours of continuously recorded discharge. The discharge was estimated to be 6.3 m^3/s from a rating curve that was constructed based on different slope area measurements.

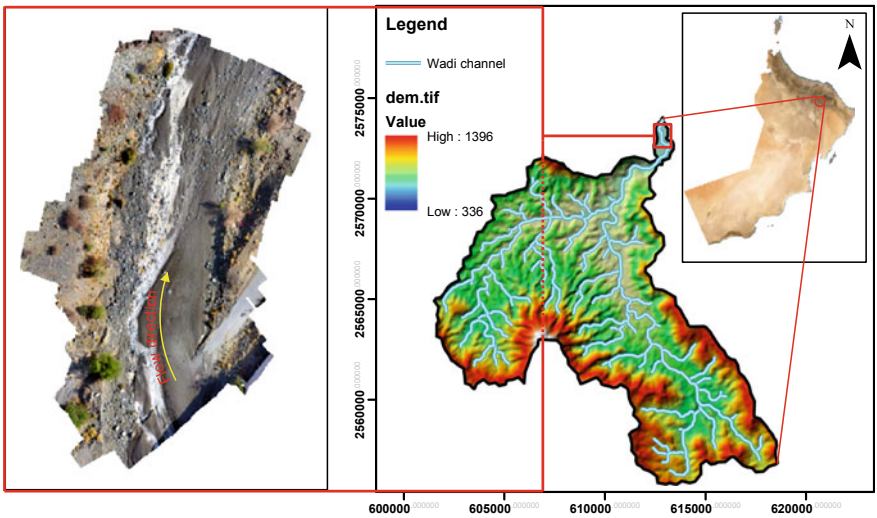

Fig. 9.4 **a** Drone survey of wadi channel bed; **b** location of Wadi Aluqq showing topographic elevation

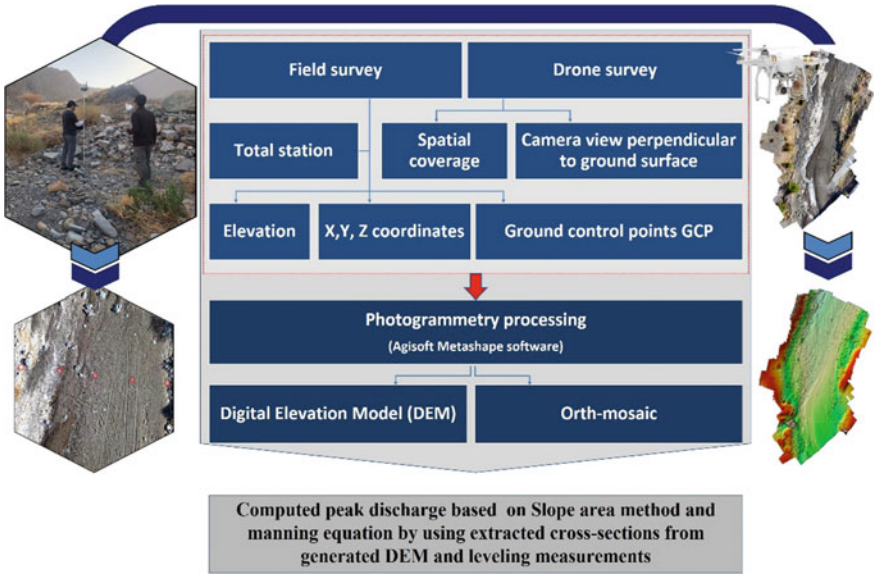

Fig. 9.5 Methodology for generating a digital elevation model (DEM)

9.3.2 Image Preprocessing

The recorded video of the flash flood was converted into frames. The specification of the video was 30 frames per second (fps) with an image resolution of 1280 × 720 pixels. We enhanced the images by changing the contrast setting to improve the sediment tracers and natural floating debris to be clearer and more visible, which helped drive the flow patterns and directions when computing the surface velocity (Kantoush 2009). We selected six natural GCP features (stable rocks within the channel). The images were orthorectified to a plan-to-plan view by using the GCPs, and each pixel was projected and georeferenced based on the correction from the GCPs.

9.3.3 Computation of Surface Flow Velocities by LSPIV

The commercial software used to analyse surface flow velocity in this paper was Dantec Dynamics A/S, Denmark. In addition, there are other options of open-source software that can be used for such analyses, such as Fudda-LSPIV and PIV ImageJ. Series of images were uploaded into the software with a time interval of 0.03 s between frames. We analysed the images with the cross-correlation function for the LSPIV technique, dynamic filtration and statistical analysis of the images to obtain the computed flow velocity and flow pattern (Fujita et al. 1998). Natural tracers provided detection marks with which to involve the movements in an interrogation area (IA) by following the detection pixel with marker movements from the first frame to the second frame. In addition, the IA was surrounded by the search area (SA) to identify the vector pattern that moved out of this area (Coz et al. 2010). The outline of the IA was delimited by 64 × 64 pixels with 50% overlap to formulate correlation coefficients. The resulting surface flow velocities were averaged for all frames to obtain a statistical analysis that included the mean velocity, correlation coefficient, standard deviation and variance over all pixels to avoid uncertainty from invisible tracers in the water surface.

9.3.4 Calculation of Discharge

Figure 9.6a shows the visibility of the displacement of foam on the water surface. The white line shows the location of the cross section, which was used to calculate the discharge and analyse the surface flow velocities. We validated our results using three approaches (slope-area method, velocity–area method and average cross section). The Manning equation was utilized to estimate the flow velocity between three cross sections from field survey data (slope-area method). The velocity–area method was applied to calculate the discharge. We used 42 segments to measure the

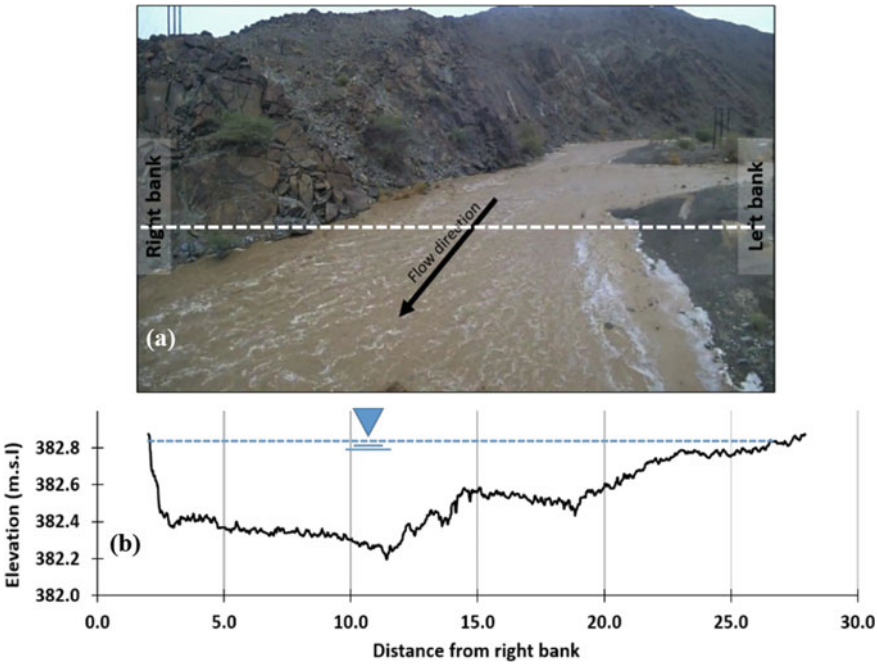

Fig. 9.6 **a** Original image showing the location of the cross-sectional velocity vectors; **b** the cross-sectional profile extracted from the DEM

surface velocity, v_i, with width, Δy_i, along the surveyed cross section. We summed the discharges as $Q = \sum_{i=1}^{n} \alpha v_i h_i \Delta y_i$, where h_i was the water depth, defined based on the availability at each time step of the measured velocity to calculate discharge; v_i is a function of the surface velocity; and α is the correction factor of 0.8 (Hauet et al. 2008). Figure 9.6b shows the bathymetry of the wadi cross section extracted from the digital elevation model (DEM). In addition, we obtained the levels of water markers from the field survey and validated them with the measured water levels.

9.4 Results

The accuracy of the photogrammetry analysis is shown in Fig. 9.7; the accuracy was determined by checking the correlation between the measured and computed elevation (DEM) of the cross section. With 15 elevation points, the results had a good fit, with $R^2 = 0.99$. However, we determined the mean square error (MSR) for those points, which was equal to less than one centimetre (MSE = 0.027). Figure 9.7 shows that the obtained cross section (CS) from the field survey and extracted CS from the DEM matched well, but the CS from the DEM had high and

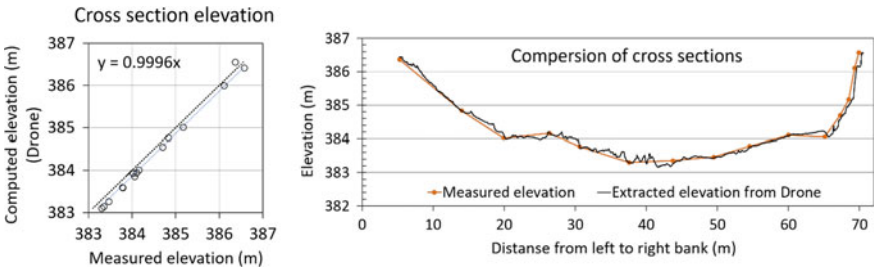

Fig. 9.7 Comparison between the generated DEM and measured cross section

precise elevation details over the whole cross section. We assume the peak discharge had uniform flow. Three cross sections were used to calculate the peak flood discharge, as presented in Fig. 9.8. The calculated peak discharge from the image processing technique was compared with the calculated peak discharge from the satellite levelling survey (Fig. 9.9). The DEM cross section included more details regarding the channel bed that could give reasonable estimations of peak discharge. Moreover, using drones for field surveys can clarify flood marks more easily than using conventional methods.

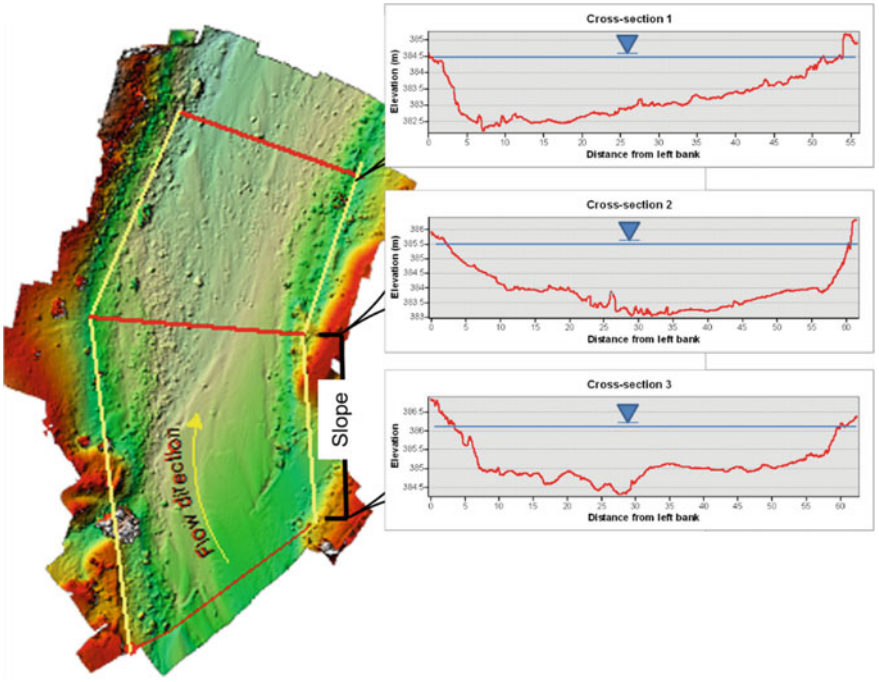

Fig. 9.8 Three cross sections used to estimate the peak discharge

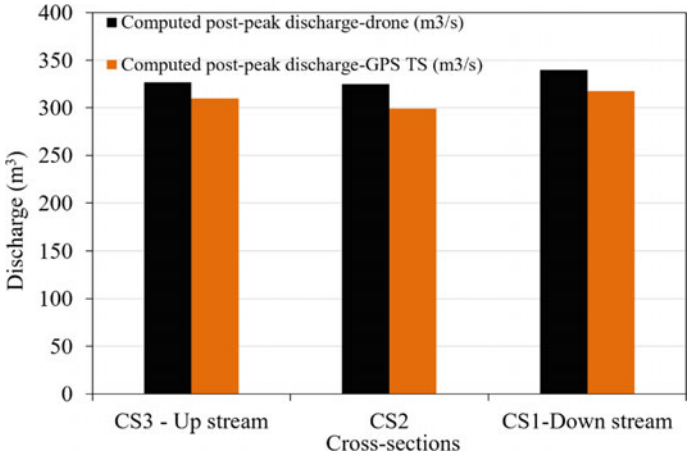

Fig. 9.9 Comparison between estimated discharges from the generated DEM and the measured elevation values

Additionally, the cross sections obtained through the levelling survey produced an underestimated peak discharge due to the unclear topography of the channel bed. The channel bed roughness was estimated based on soil materials in the wadi reach. To calculate cross-sectional areas, we used ArcGIS software and drew the *x*-, *y*- and *z*-axes as polygons. The peak discharge estimated from the DEM was higher in all three cross sections than those obtained in the levelling survey. However, the satellite levelling survey simplified the cross sections of the wadi channel by obtaining elevation points for general topographical shapes with limited data points. The peak discharge obtained by this survey had similar results to that obtained by the drone survey.

9.4.1 LSPIV Velocity Result

Figure 9.10 shows the average velocity pattern in the surface velocities measured by LSPIV. The computational analysis provided LSPIV velocities over all flood surface extents. The averaged cross-sectional velocity obtained using LSPIV (0.83 m/s) was compared with the velocity obtained with the slope-area method, which was computed based on the slopes between the cross sections and water marker elevations (Manning equation) and was equal to 0.7 m/s. Overall, there is reasonable agreement between both techniques, and the relation between the surface flow velocity and cross-sectional profile is shown in Fig. 9.11. We can see that there was a decrease in the velocity on the right bank during the peak and recession phases due to the effects of the channel bank (rock).

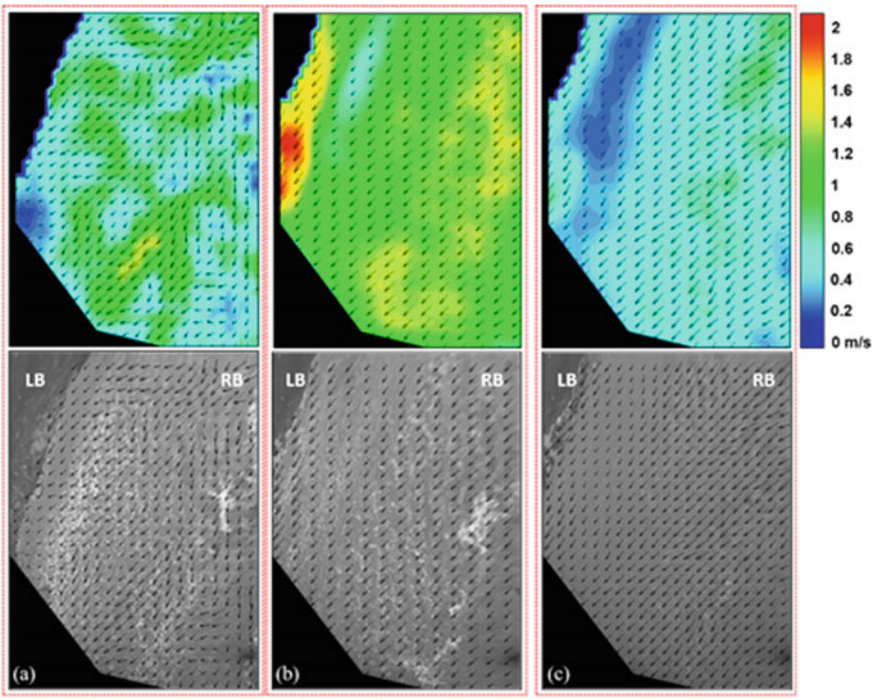

Fig. 9.10 Average flow patterns with velocity colour maps and orthorectified images using LSPIV for **a** the rising phase, **b** the peak phase and **c** the recession limbs of the flood event on 28 October 2018, where LB is the left bank and RB is the right bank (Al-Mamari et al. 2019 MDPI—hydrology)

9.4.2 LSPIV Discharge Result

The LSPIV analysis of discharge was divided into three phases (rising, peak and recession). Figure 9.12 shows the LSPIV-estimated discharge compared with the computed discharge measured by the rating curve using field measurements. The LSPIV computation was used to calculate the discharges with the mean surface flow velocity and cross-sectional surface velocity distributions in different time intervals. The mean velocity of the LSPIV-estimated discharge showed underestimated values compared to those obtained from the conventional method; on the other hand, the cross-sectional surface velocity of the LSPIV-estimated discharge (approximately 6.48 m^3/s) showed very good agreement with the computed discharge from the rating curve and field measurements, which equalled 6.34 m^3/s.

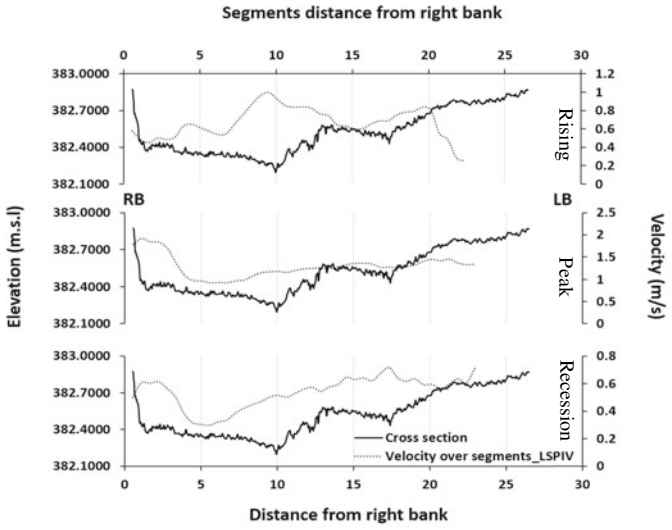

Fig. 9.11 Relation between the surface flow velocity and cross-sectional profile (Al-Mamari et al. 2019 MDPI—hydrology)

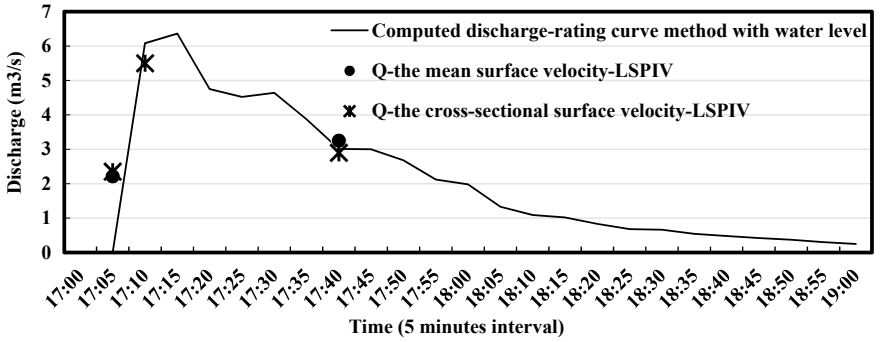

Fig. 9.12 Result of computed discharge from the LSPIV and slope-area methods (Al-Mamari et al. 2019 MDPI—hydrology)

9.5 Conclusions

Hydrological data is an important component in evaluating and managing water resources. In this paper, the investigation of post-peak flood discharge and a real-time discharge measurement method for wadi flash floods in arid regions using photogrammetry and LSPIV techniques was presented. Image-based techniques have been used to quantify post-peak flood discharge for wadi systems by generating DEMs from drone images with fully automated processing workflows.

To generate a DEM, several images with approximately 50% overlap between them and ground control points are required to improve the processing performance. We calibrated and validated the new approach by using a levelling field survey. Based on the analysis, the mean square error between the extracted cross sections from the field survey and the DEM was very small and was equal to 0.027. The new method is easy and has acceptable accuracy compared with other, conventional methods. The combination of techniques proved that image processing can provide sufficient data and information. Photogrammetry analysis is very sensitive to shadows created by vegetation or any objects. The LSPIV technique was utilized to measure the surface flow velocity with a cross-sectional profile from the DEM. The results show good agreement between the surface flow velocity and slope-area method; the estimated peak discharge in the LSPIV method was 6.4 m^3/s, and that from the slope-area method was 6.3 m^3/s. However, the investigation of estimated discharge was very efficient and can be improved with a high-resolution camera and optimal camera angle. This technique will provide an opportunity to measure post-peak flood discharges in any topographic conditions and represents a cost-effective technique to monitor flash floods. However, these techniques require a visible tracer and floating objects in the water surface to detect discharge velocities. Future research will be concerned with developing a real-time monitoring system in wadi basins for multitask purposes, such as early warning systems and online real-time measurements.

References

Abdel-Fattah M, Kantoush S (2016) Hydrological modelling of flash flood in Wadi Samail, Oman. Annual of Disaster Prevention Research Institute, Kyoto University

Al-Mamari MM, Kantoush S, Kobayashi S, Sumi T, Saber M (2019) Real-time measurement of flash-flood in a wadi area by LSPIV and STIV. Hydrology 6:27

Anbarjafari G (2014) https://sisu.ut.ee/imageprocessing/book/1. University of Tartu

Castillo C, Marín-Moreno VJ, Pérez R, Muñoz-Salinas R, Taguas EV (2018) Accurate automated assessment of gully cross-section geometry using the photogrammetric interface FreeXSapp. Earth Surf Process Landforms 43(8):1726–1736

Coz J, Hauet A, Pierrefeu G, Dramais G, Camenen B (2010) Performance of image-based velocimetry (LSPIV) applied to flash-flood discharge measurements in Mediterranean. J Hydrol 394:42–52

Dalyrmple T, Benson MA (1967) Measurement of peak discharge by the slope-area method, USGS

Detert M, Weitbrecht V (2015) A low-cost airborne velocimetry system: proof of concept. J Hydraul Res 53(4):532–539

Fujita I, Notoya Y, Tain K, Tateguchi S (2019) Efficient and accurate estimation of water surface velocity in STIV. Environ Fluid Mech 19(5):1363–1378

Fujita I, Muste M, Kruger A (1998) Large-scale particle image velocimetry for flow analysis in hydraulic engineering applications. J Hydraul Res 36(3):397–414

Griffiths GA, McKerchar AI (2015) Estimation of flood peak discharge by the slope-area method. J Hydrol 54(2):153–160

Harpold AA, Mostaghimi S, Vlachos PP, Brannan K, Dillaha T (2006) Stream discharge measurement using a large-scale particle image velocimetry (LSPIV) prototype. Transactions of the ASABE 49:1791–1805

Hauet A, Creutin JD, Belleudy P (2008) Sensitivity study of large-scale particle image velocimetry measurement of river discharge using numerical simulation. J Hydrol 349(1–2):178–190

Huang WC, Young CC, Liu WC (2018) Application of an automated discharge imaging system and LSPIV during typhoon events in Taiwan. Water 10(3)

Johnson MV (1977) Channel geometry and wadi flows, Batinah coast, Sultanate of Oman

Kantoush SA, Schleiss AJ (2009) Large-scale PIV surface flow measurements in shallow basins with different geometries. J Vis 12(4):361–373

Muto Y, Baba Y, Aya S (2002) Velocity measurements in open channel flow with rectangular embayments formed by Spur dykes. Annual of Disaster Prevention Research Institute, Kyoto University

Public Authority for Water Resource (1983) Surface water gauging station network of the Sultanate of Oman. PAWR 83–2

Sen Z (2008) WADI/hydrology. CRC Press

Smith MW, Carrivick JL, Hooke J, Kirkby MJ (2014) Reconstructing flash flood magnitudes using 'structure-from-motion': a rapid assessment tool 519(2014):1914–1927

Sun X, Shiono K, Chandler JH, Rameshwaran P, Sellin RHJ, Fujita I (2010) Discharge estimation in small irregular river using LSPIV. In: Proceedings of the Institution of Civil Engineers-Water Management. Vol 163, no 5, pp 247–254

Zhang L, Zhang Y, Zhang Z, Shen J, Wang H (2019) Real-time water surface object detection based on improved faster R-CNN. Sensors 19(16):3523

Chapter 10
A Temporally Varied Rainfall Simulator for Flash Flood Studies

Mohammad Ebrahim Banihabib and Bahman Vaziri

Abstract Experimental studies of flash floods require rainfall simulations. For this reason, various rainfall simulators have been designed, built, and employed in previous studies. These previous rainfall simulators have provided good simulations of constant rainfall intensities; however, these simulators cannot generate temporally varied rainstorms. Thus, the effect of the temporal distribution of a rainstorm on flash flooding cannot be studied using current rainfall simulators. To achieve accurate and reliable results in flash flood studies, simulating rainstorms that are similar to natural precipitation events is essential, and natural rainfall varies temporally. Thus, a rainstorm simulator was designed and built using cascading tanks to generate rainstorm hyetographs that cannot be obtained using traditional rainfall simulators. The result of the rainstorm generated by the proposed instrument and its numerical model showed that the instrument can simulate the temporal distributions of rainstorms with an accuracy of 95 percent. Consequently, the proposed instrument and its numerical model can be applied for generating artificial rainstorm hyetographs in experimental and field studies of flash floods.

Keywords Rainfall simulator · Rainfall hyetograph · Cascade reservoir routing · Rainfall temporal distribution flash flood

M. E. Banihabib (✉)
Department of Water Engineering, Aburaihan Campus, University of Tehran, Tehran, Iran
e-mail: banihabib@ut.ac.ir

B. Vaziri
Water Resources Engineering, Department of Water Engineering, Aburaihan Campus, University of Tehran, Tehran, Iran
e-mail: b.vaziri@ut.ac.ir

T. Sumi et al. (eds.), *Wadi Flash Floods*, Natural Disaster Science and Mitigation Engineering: DPRI Reports, https://doi.org/10.1007/978-981-16-2904-4_10

10.1 Introduction

Flash floods are frequently reported in arid and semiarid regions in Iran, Iraq, Egypt, and Oman (Al-Rawas and Valeo 2009; Banihabib and Tanhapour 2020; de Vries et al. 2013; Mustafa et al. 2019). For example, debris floods are flash floods that occur in the mountainous areas of Mazandaran and Golestan Provinces, Iran (Banihabib and Tanhapour 2020). Flash floods were also reported in various provinces in Iran during the period from 1962 to 2002 (Tabari and Willems 2016). In this period, the total flood damage was appraised to be US$138 million. Roughani et al. (2007) reported that heavy rainfall was a key factor in the flash floods that occurred in this period. Recently, in March–April 2019, widespread flash floods damaged most provinces of Iran, causing over $3.5 billion U.S. dollars in destruction (Aminyavari et al. 2019).

Flash floods are triggered by highly intense rainstorms in arid and semiarid areas, and flood hyetographs typically display fast growth, even for large catchments. Thus, the temporal characteristics of rainstorms are the main characteristics used to study the temporal distributions of flash floods (Mays 2001). For example, even though major dissimilarities between the rainstorm depths of the coastal and mountainous zones were reported, a strong consistency in only the temporal distributions of rainstorms that caused flash floods in Oman was observed (Al-Rawas and Valeo 2009). In another study, Mustafa et al. (2019) showed that the intensity rates and temporal distributions of rainstorms are among the key features of flash floods in Iraq's north region.

Rainfall simulators are useful devices for generating artificial rain, and they are used in various rainfall-runoff and soil erosion studies. In addition, data obtained from studies that use these devices can be employed for the verification, calibration, and evaluation of soil erosion and flash flood prediction models (Sangüesa et al. 2010). Therefore, rainfall simulators are widely used as a useful instrument in flash flood field experiments. To date, these devices have been widely employed in various studies to determine soil erosion, runoff, and rainfall percolation in soil (Esteves et al. 2000; Fernández-Gálvez et al. 2008; Foster et al. 2000; Grierson and Oades 1977; Moore et al. 1983).

Aoki and Sereno (2006) employed a small rainfall simulator to study the infiltration of water into the earth in a 0.0625 m^2 square plot. The height of this rainstorm simulator was 1.5 m, and the required pressure to form raindrops was provided by a water tank. Cornelis et al. (2004) used a wind tunnel and a rainstorm simulator to study the effects of wind and rainstorm characteristics on the amount of soil erosion. In their research, the employed rainstorm simulator had sprinklers that were able to simulate precipitation with different constant intensities using a pressurized water system. Simulations of rainfall by these devices are often performed using one of two different methods: nozzle rainfall simulations and drop-forming simulations (Corona et al. 2013). In the first method, the simulation of rainstorms is performed by the use of water distribution nozzles. In this method, pressurized nozzles are embedded in the device, allowing the adjustment of the

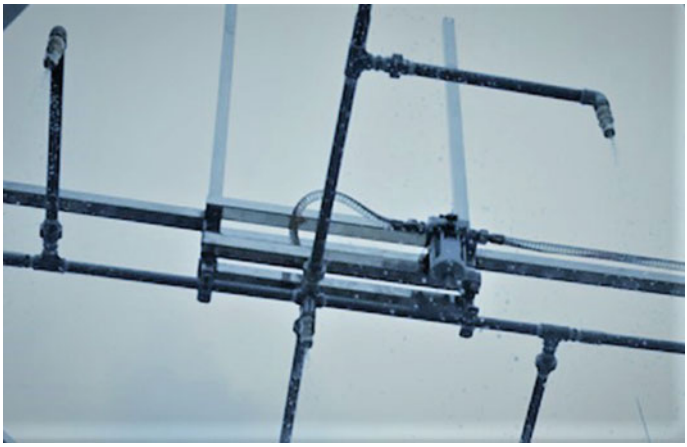

Fig. 10.1 A nozzle rainstorm simulator

simulated rainstorm intensity based on the water pressure in the system. A device of this type is shown in Fig. 10.1.

In the second type, artificial raindrops fall using gravity from holes installed in the device. Generally, the simulated precipitation intensity of these instruments is adjusted by a device known as a Mariotte bottle. A device of this type is shown in Fig. 10.2. This kind of simulator consists of two main parts, a Mariotte bottle for adjusting the amount of water that is let out and the water drainage holes (Huang et al. 2013). The Mariotte bottle is a device used for adjusting a constant rate of flow from a cylindrical or cubic tank and a pipe through which air enters the tank with vertical movement inside the bottle. The amount of air entering the bottle can be adjusted, which leads to the adjustment of the rainfall rate out of the bottle.

Although these simulation technologies can satisfactorily simulate rainfall of a certain intensity, they are not capable of making rainfall hyetographs (temporal variations in rainfall). Under natural conditions, the intensity of rainfall during a storm period is not constant, and rainstorms always start with low intensity. After a while the precipitation reaches its peak; then, the intensity decreases, and finally, the rainstorm stops. Ensuring the accuracy and similarity of simulated rainfall events to the temporal distributions of actual rainfall events is crucial for obtaining precise and reliable results in flash flood and soil erosion studies. Therefore, the invention of new methods for simulating the temporal distributions of rainstorms is necessary. Accordingly, the main purpose of this research is to design and examine a rainfall generator to produce various rainfall hyetographs for a more accurate examination of the different temporal distributions of rainstorms in flash flood studies.

Fig. 10.2 A constant rainstorm simulator

10.2 Material and Methods

The main disadvantage of existing rainfall simulators is that they can only generate a constant rainfall intensity. By designing and constructing hyetograph-generating devices, as shown in Fig. 10.3, the proposed rainfall simulator can simulate temporally varied precipitation using drop-forming simulator technology and a cascading tank model. The cascading tank model has previously been used by some researchers for flood simulations [8], and in this research, the model was developed for temporally varied rainstorm simulations. The hyetograph-generating device is made up of two main parts, including two tanks: one for water retention and another tank for rainfall generation. The outflow can be adjusted by a valve in the first tank outlet which controls the rising limb of the generated rainfall hyetograph, and the drop holes in the second tank produce and control the receding limb of the generated rainfall hyetograph. At the end of the valve, a shower head is installed to prevent turbulence in the water surface of the second tank. At the bottom of the second tank, there are 50 holes, each with a diameter of 1 mm. The simulated rainfall intensity is a function of the area of these holes and the water head in the tank. The discharge of water from these holes can be adjusted by changing the area of the outlet holes to simulate precipitation with varying intensities. Additionally, to adjust the precipitation intensity, the diameter of the outlet holes can be adjusted by inserting plastic threads of different thicknesses in these holes.

To simulate specific precipitation with the device, reservoir flood routing is required in the tanks. The output discharge from the tanks can be obtained from Eq. (10.1) (Almutairi and Zribi 2006):

$$Q_t = CA\sqrt{2gh_t} \tag{10.1}$$

Fig. 10.3 The rainstorm hyetograph-generating device

where Q_t is the flow discharge from the tank at time t, C is the orifice coefficient, A is the orifice area, g is the gravitational acceleration and h_t is the water head in the tank at time t. Further, according to the definition of discharge, the outflow from the tank is equivalent to the water storage variation in the tank in a given time increment and can thus be expressed in terms of the water depth variation, as presented in Eq. (10.2):

$$Q_t = \frac{\mathrm{d}V}{\mathrm{d}t} = \pi r^2 \frac{\mathrm{d}h}{\mathrm{d}t} \tag{10.2}$$

where V is the water volume in the tank, r is the tank radius, h is the height of the water in the tank and t is time.

Since the walls of the tank used in the device have a small slope, the radius value in Eq. (10.2) at moment t is a function of the value of h and can be calculated according to Eq. (10.3):

$$r = R1 + \frac{R2 - R1}{H} h_t \tag{10.3}$$

where r is the tank radius at time t, $R1$ is the radius of the tank bottom, $R2$ is the radius of the tank surface at the highest point and H is the height of the tank. By replacing Eqs. (10.1) and (10.3) in Eq. (10.2), we obtain Eq. (10.4) as follows:

$$CA\sqrt{2gh_t} = \pi\left(R1 + \frac{R2 - R1}{H}h_t\right)^2\frac{\Delta h}{\Delta t} \tag{10.4}$$

By measuring the variations in the water head in the tank at specified intervals, it is possible to determine the value of C by calibration in Eq. (10.4). Additionally, to measure the error indexes of the model calibration and validation, the mean absolute relative error (MARE) was used, as shown in Eq. (10.5):

$$\text{MARE} = \frac{\sum_{i=1}^{n}|X_o - X_c|/X_o}{n} \tag{10.5}$$

where X_O is the value of the observed water depth, X_C is the value of the calculated water depth and n is the number of measured water depths. Thus, by determining the water head value in the tank, it is possible to calculate the amount of water outflow from the tanks using Eq. (10.1) and thus calculate the rainstorm intensity and eventually define a simulated rainfall hyetograph. Therefore, the device can be adjusted to generate various rainfall hyetographs.

10.3 Results and Discussion

In this study, the calibration of the device was carried out only with a fully open valve in the first tank and with a hole diameter of 1 mm. The generated hyetograph was obtained under these circumstances. However, depending on the needs of the researcher, it is possible to similarly calibrate and produce different hyetographs. For this purpose, the values of the water heads were recorded in both tanks at a time interval of 30 s. Since the value of parameter C is not constant and is a function of the water head in the tank, the best equation was obtained for estimating the value of parameter C for each tank using regression analysis. Equations (10.6) and (10.7) were derived for the first and second tanks using regression analysis, respectively. As shown in Eqs. (10.6) and (10.7), the value of C is a function of the ratio of the water head to the diameter of the hole. Equations (10.6) and (10.7) are expressed as follows:

$$C_1 = 1.3\left(\frac{h_1}{D_1}\right)^{-0.275} \tag{10.6}$$

$$C_2 = 2.3\left(\frac{h_2}{D_2}\right)^{-0.25} \tag{10.7}$$

where C_1 and C_2 are the orifice coefficients in the first and second tanks, respectively; h_1 and h_2 are the water heads in the first and second tanks, respectively; D_1 is the diameter of the water outlet orifice in the first tank; and D_2 is the equivalent diameter of the holes in the second tank.

In the next step, based on the values obtained for the parameters C_1 and C_2 from Eqs. (10.6) and (10.7), the values of the parameter h were calculated using Eq. (10.4) for each tank and compared with the observed values of h. The results are shown in Figs. 10.4, 10.5, 10.6 and 10.7.

In Fig. 10.4, the values of the observation water heads and those calculated Eq. (10.4) are displayed over time for the first tank. The value of C_1 is calculated using Eq. (10.6). As shown, the calculated water head values for the first tank at the beginning of the graph have acceptable agreement with the observed data, and this trend continues up to 250 s. After this time, there is a difference between the observed and calculated values in the middle of the chart; however, these values approach each other again, and the calculated water head values agree with the observed values. Additionally, in Fig. 10.5, the calculated water head values versus the observed values are displayed on the vertical and horizontal axes, respectively. As shown in Fig. 10.5, the data are generally close to a perfect line, and there are only some differences between the observed and calculated data in the middle and the end of the graph. This indicates that the high water head values calculated using Eq. (10.4) are a good estimation relative to the observed water head values. The differences between the calculated and observed values in the middle and the end regions of both plots can be attributed to errors in measuring the water levels in the tanks. The exact magnitudes of these errors were calculated using Eq. (10.5), and according to the observed data, the average error was 4.5% for the first tank. Therefore, the simulated water head values can be used to estimate the actual water head values in the first tank of the device with acceptable accuracy.

Figures 10.6 and 10.7 are the same as Figs. 10.4 and 10.5 but display values for the second tank; the observed water head values and the values calculated using

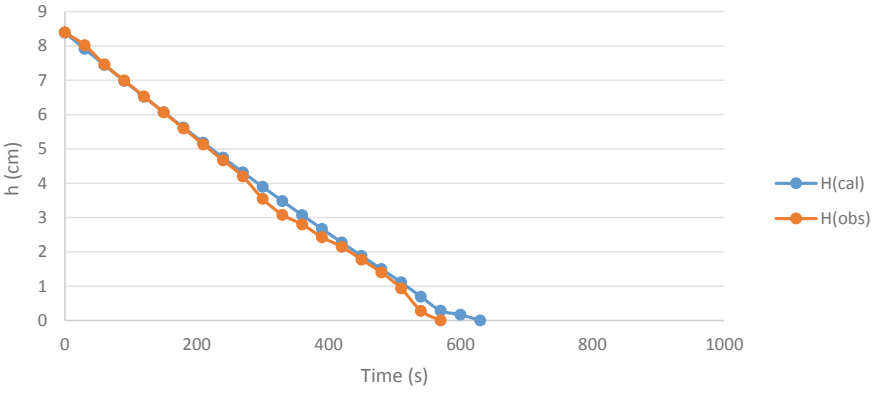

Fig. 10.4 The observed and calculated water head values versus time in the first tank

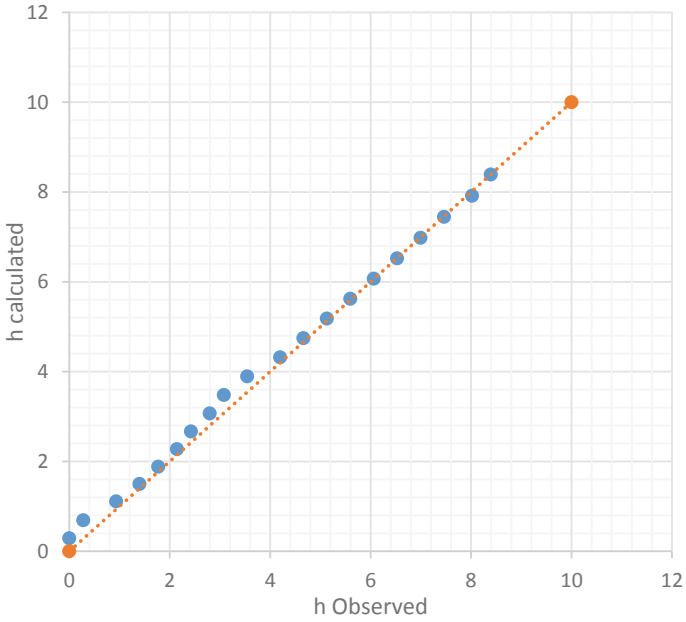

Fig. 10.5 The observed water head values versus the calculated water head values in the first tank

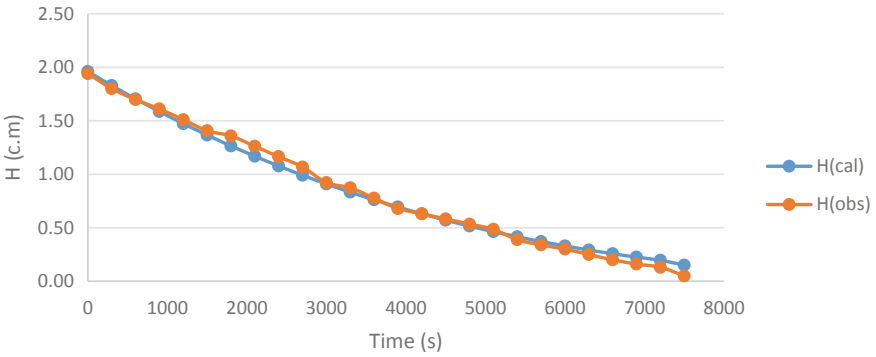

Fig. 10.6 The observed and calculated water head values versus time in the second tank

Eq. (10.4) based on the values of the C_2 parameters for the second tank are displayed over time. As shown in Fig. 10.6, the calculated water head values agreed well with the observed values, except for those in the middle and the end of the diagram. In addition, in Fig. 10.7, the calculated versus observed water head values are similar to a perfect line except for at the beginning and the end of the chart. As previously stated, the differences between the calculated and observed values in the divergent parts of both charts can be attributed to errors in measuring the water

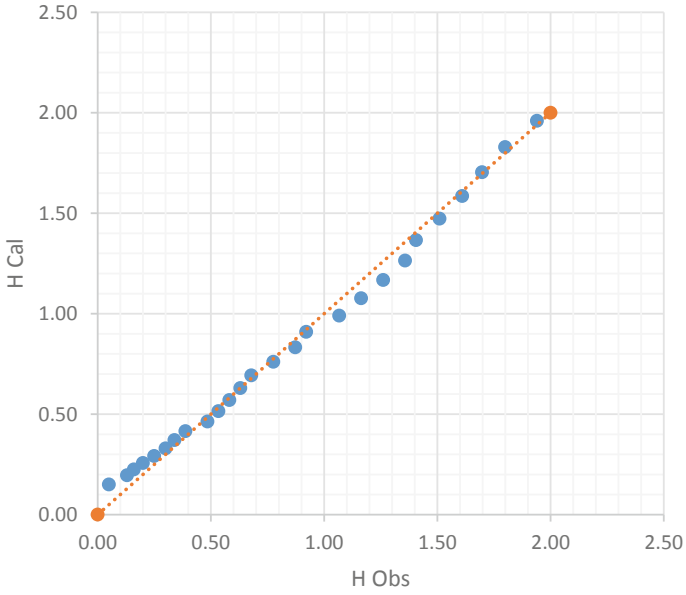

Fig. 10.7 The observed water head values versus the calculated water head values in the second tank

levels in the tank. The error calculated from Eq. (10.5) is equal to 4.9% for the second tank. Therefore, as shown in Figs. 10.6 and 10.7 as well as the calculated error rate, the calculated water head values represent acceptable estimations with good accuracy for the simulation of the water heads in the second tank.

By calculating C_1 and C_2 using Eqs. (10.6) and (10.7) for each tank and replacing these values in Eq. (10.4), it is possible to estimate the water head value in each tank, and accordingly, the different rainstorm hyetographs can be estimated for various initial water heads in the first tank. To show the rainstorm hyetograph of the device, a water level of 9 cm in the first tank was considered as the initial head value. Using this head, the water levels in the tanks were calculated from Eq. (10.4) within a 30-s time interval, and finally, the rainstorm hyetograph was simulated. Figures 10.8, 10.9 and 10.10 show the trends of the water head changes in the first and second tanks and the rainstorm hyetographs, respectively.

Figure 10.8 shows the water head variation in the first tank over time. As shown in this chart, the water head in the first tank begins to drop from the initial head (9 cm) and continues to drop with a constant gradient. Finally, the water volume of the first tank is totally discharged into the second tank after nearly 700 s. This flow time, as shown in Figs. 10.9 and 10.10, directly affects the time it takes to reach the peak in the output hyetograph and the peak flow time of the flash floods in the experiments. When water is discharged from the first tank, the water head in the second tank gradually rises. Finally, as the first tank completely empties, the water head reaches its maximum in the second tank. Since the discharge from the holes is

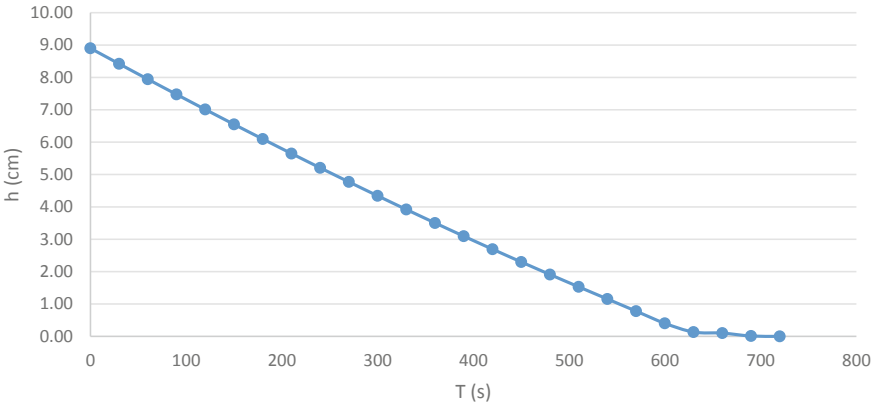

Fig. 10.8 The water head changes in the first tank

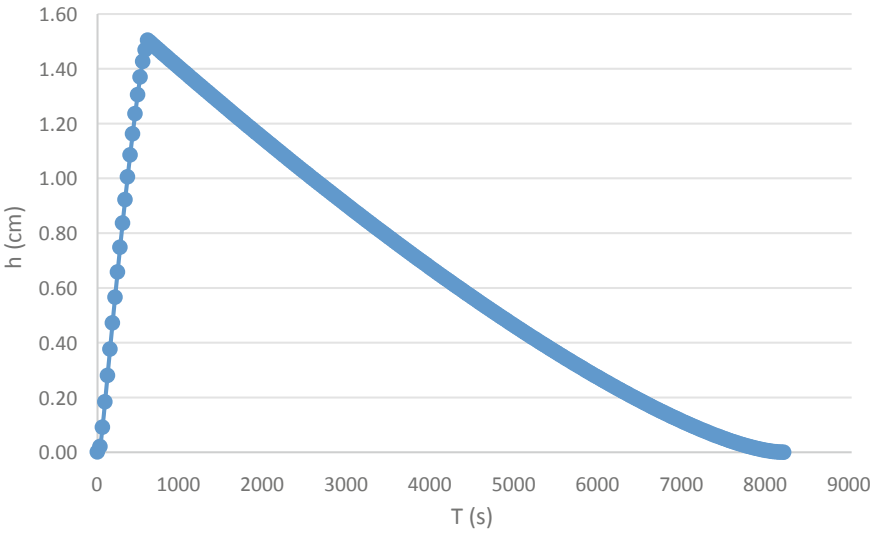

Fig. 10.9 The water head changes in the second tank over time

a function of this second-tank water head according to Eq. (10.1), by reaching the maximum water head value in the second tank, the water outflow from the second tank of the device (rainstorm intensity) reaches its maximum. Therefore, the highest rainstorm intensity is observed at this point. Moreover, it can be concluded that the duration of water discharging from the first tank directly affects the shape of the rainstorm hyetograph, and thus, with the adjustment of the valve installed on the outlet of the first tank, it is possible to create different rainstorm hyetographs with different times to the peaks.

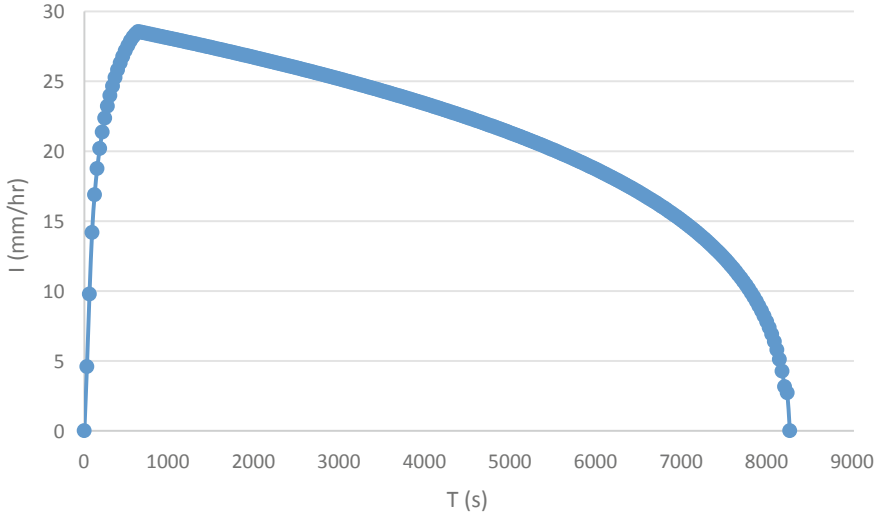

Fig. 10.10 The simulated rainstorm hyetograph

In Fig. 10.9, the water level variation in the second tank of the device is shown. After the discharge duration of the first tank (700 s), as shown in Fig. 10.5, the water head in the second tank reaches a peak, and after 8000 s, the second tank is completely discharged. This discharge duration is a function of the diameter of the outlet holes of the second tank. By changing this diameter, the intensity and duration of a rainstorm can be determined.

The reviewed reports and studies show an increasing number of flash floods, especially in arid and semiarid zones. A sensitivity analysis of the influencing factors of flash floods shows that the temporal distribution of rainstorms are one of the key factors affecting the occurrence of flash floods. The temporal distributions of rainstorms is the second key factor in characterizing flash floods after antecedent moisture conditions (Lázaro et al. 2014). Zhai et al. (2018) reported that the influences of both soil moisture and the temporal patterns of rainfall on flash floods have not been adequately studied thus far (Zhai et al. 2018). Figure 10.10 shows the temporal patterns of the rainstorm intensity simulated by the device. In this figure, the rainstorm intensities in millimeters per hour and the time in seconds are shown in the vertical axis and the horizontal axis, respectively. As shown in Fig. 10.10, the simulated rainstorm intensity reached its peak as the water head in the second tank reached its peak, and finally, the rainfall intensity reached zero as the second tank fully emptied. By adjusting the valve of the device, various temporal rainstorm patterns can be produced by the device, and the numerical model obtained in this research can be used to find the proper adjustment of the valve for producing rainstorms with a certain temporal pattern for flash flood studies.

10.4 Conclusions

Flash flood studies require a new device to expand previous experimental and field studies on the impacts of the various temporal patterns of rainstorms on flash flood characteristics. Current simulation devices can simulate constant-intensity precipitation well; nonetheless, reported studies show the need for more studies on the effects of temporal variations in rainstorms in producing flash floods. In this research, a rainfall hyetograph-generating device is designed and examined based on drop-generating and cascading tanks to produce various rainfall hyetographs for more accurate simulations of rainstorms with different temporal variations. Accordingly, by placing two cascading reservoirs and using reservoir routing in the cascading tanks, a simulator was designed and constructed that could generate hyetographs. Then, the device was calibrated based on observed data. The results of the precipitation values generated with this device showed that it is possible to simulate rainstorms with varied intensities over time as well as produce different hyetographs in terms of the duration to the peak and the rainstorm duration with an accuracy of 95%. Consequently, this device can simulate rainstorms more accurately and can be used to obtain more accurate tests in flash flood studies.

References

Al-Rawas GA, Valeo C (2009) Characteristics of rainstorm temporal distributions in arid mountainous and coastal regions. J Hydrol 376:318–326

Almutairi NB, Zribi M (2006) Sliding mode control of coupled tanks. Mechatronics 16:427–441

Aminyavari S, Saghafian B, Sharifi E (2019) Assessment of precipitation estimation from the NWP models and satellite products for the spring 2019 severe floods in Iran. Remote Sens 11:2741

Aoki AM, Sereno R (2006) Evaluación de la infiltración como indicador de calidad de suelo mediante un microsimulador de lluvias. Agriscientia 23

Banihabib ME, Tanhapour M (2020) An empirical equation to determine the threshold for rainfall-induced landslides developing to debris flows. Landslides

Cornelis WM, Erpul G, Gabriels D (2004) The ICE wind tunnel for wind and water interaction research. Wind Rain Interact Erosion 195–224

Corona R, Wilson T, D'Adderio LP, Porcù F, Montaldo N, Albertson J (2013) On the estimation of surface runoff through a new plot scale rainfall simulator in Sardinia. Italy Procedia Environ Sci 19:875–884

de Vries AJ, Tyrlis E, Edry D, Krichak S, Steil B, Lelieveld J (2013) Extreme precipitation events in the middle east: dynamics of the active red sea trough. J Geophys Res Atmos 118:7087–7108

Esteves M, Planchon O, Lapetite JM, Silvera N, Cadet P (2000) The 'EMIRE'large rainfall simulator: design and field testing. Earth Surf Process Landforms: J Br Geomorphol Res Group 25:681–690

Fernández-Gálvez J, Barahona E, Mingorance M (2008) Measurement of infiltration in small field plots by a portable rainfall simulator: application to trace-element mobility. Water Air Soil Pollution 191:257–264

Foster I, Fullen M, Brandsma R, Chapman A (2000) Drip-screen rainfall simulators for hydro-and pedo-geomorphological research: the Coventry experience. Earth Surf Process Landforms: J Br Geomorphol Res Group 25:691–707

Grierson I, Oades J (1977) A rainfall simulator for field studies of run-off and soil erosion. J Agric Eng Res 22:37–44

Huang J, Wu P, Zhao X (2013) Effects of rainfall intensity, underlying surface and slope gradient on soil infiltration under simulated rainfall experiments. Catena 104:93–102

Lázaro JM, Navarro JAS, Gil AG, Romero VE (2014) Sensitivity analysis of main variables present in flash flood processes application in two spanish catchments: Arás and Aguilón. Environ Earth Sci 71:2925–2939

Mays L (2001) General characteristics of arid and semiarid regions. Urban drainage in arid and semiarid regions

Moore ID, Hirschi MC, Barfield BJ (1983) Kentucky rainfall simulator. Trans ASAE 26:1085–1089

Mustafa AM, Muhammed H, Szydłowski M (2019) Extreme rainfalls as a cause of urban flash floods; a case study of the Erbil-Kurdistan region of Iraq. Acta Scientiarum Polonorum Formatio Circumiectus 18:113–132

Roughani M, Ghafouri M, Tabatabaei M (2007) An innovative methodology for the prioritization of sub-catchments for flood control. Int J Appl Earth Obs Geoinf 9:79–87

Sangüesa C, Arumí J, Pizarro R, Link O (2010) A rainfall simulator for the in situ study of superficial runoff and soil erosion. Chilean J Agric Res 70:178–182

Tabari H, Willems P (2016) Daily precipitation extremes in Iran: decadal anomalies and possible drivers. JAWRA J Am Water Resour Assoc 52:541–559

Zhai X, Guo L, Liu R, Zhang Y (2018) Rainfall threshold determination for flash flood warning in mountainous catchments with consideration of antecedent soil moisture and rainfall pattern. Nat Hazards 94:605–625

Part IV
Disaster Risk Reduction and Mitigation

Chapter 11
The Role of Urban Planning and Landscape Tools Concerning Flash Flood Risk Reduction Within Arid and Semiarid Regions

Karim I. Abdrabo, Sameh A. Kantosh, Mohamed Saber, Tetsuya Sumi, Dina Elleithy, Omar M. Habiba, and Bahaa Alboshy

Abstract This chapter highlights some substantial questions inquired by researchers to comprehend the flood risks (FRs) that occur in their cities as follows: (1) What is the impact of flooding on urban areas? (2) what effect does urbanization have on FR? (3) What are the existing nonstructural and structural mitigation measures for urban flooding? and (4) What is the role of urban planning and landscape tools in flood risk reduction (FRR) for cities as well as their inhabitants? The main messages in this chapter could be summarized as follows:

K. I. Abdrabo (✉)
Faculty of Urban and Regional Planning, Cairo University, Giza 12613, Egypt
e-mail: m.karim.ibrahim@cu.edu.eg

K. I. Abdrabo · D. Elleithy
Department of Urban Management, Graduate School of Engineering, Kyoto University, Kyoto 615-8245, Japan
e-mail: Dina.elleithy@eng.asu.edu.eg

S. A. Kantosh · M. Saber · T. Sumi · O. M. Habiba
Disaster Prevention Research Institute (DPRI), Kyoto University, Kyoto 611-0011, Japan
e-mail: kantoush.samehahmed.2n@kyoto-u.ac.jp

M. Saber
e-mail: mohamedmd.saber.3u@kyoto-u.ac.jp

T. Sumi
e-mail: sumi.tetsuya.2s@kyoto-u.ac.jp

O. M. Habiba
e-mail: habiba.omarmohamedali.8s@kyoto-u.ac.jp

D. Elleithy
Irrigation and Hydraulics, Department of Civil Engineering, Faculty of Engineering, Ain Shams University, Cairo 11535, Egypt

B. Alboshy
Architectural Engineering Department, Faculty of Engineering, Tanta University, Tanta 31733, Egypt
e-mail: bahaa.elboshi@f-eng.tanta.edu.eg

T. Sumi et al. (eds.), *Wadi Flash Floods*, Natural Disaster Science and Mitigation Engineering: DPRI Reports, https://doi.org/10.1007/978-981-16-2904-4_11

(1) Comprehension of both the sources and types of flooding is vital if proper FRR measures are to be determined, (2) Unplanned urban growth could seriously put lives and properties at high risk (3) Land use planning and regulation, and Sustainable infrastructure for stormwater management through landscape architecture are fundamental measures for future FRR (4) The application of the urban planning approach for FRR in arid and semiarid regions has not yet received adequate attention and facing many challenges for its implementation, and finally (5) the combination of structural and nonstructural mitigation measures in spatial planning could be much more effective than using one type of measure alone.

Keywords Flash flood · Urban flood · Urban planning · Landscape · Flood risk reduction · Arid and semiarid regions · Urbanization · Mitigation measures

11.1 Introduction

The United Nations (UN) indicated that 43% of natural disasters worldwide, from 1995 to 2015, were caused by **floods**, which impacted approximately 56% of all people affected by natural disasters and caused casualties for approximately 26% of them (Bertilsson et al. 2019). High losses in both lives and the economy will decrease the capability of communities' sustainability.

Rapid urban expansion, economic development and population growth significantly contribute to increasing **the area exposed** to natural hazards, especially **floods** (Kaspersen et al. 2017; Mojaddadi et al. 2017). Consequently, in the future, the environment, people, and property will experience persistent risks. **Exposure is** one of the three main components of FR and has been defined as the assets that could be affected due to their locations in flood-prone areas (UNISDR 2017). The other two components of FR are **hazard** and **vulnerability** (Len et al. 2018). If one of these elements is missing, the flood risk is not defined. The flood **hazard** is related to the potential danger that the natural phenomenon presents, which is inherent to the event itself; in this study, the hazards are characterized by inundation scenarios (Schanze 2006). **Vulnerability** is defined as a propensity or disposition to being adversely affected by an event. This definition includes the characteristics of a person or a group, and the characteristics of their situations, that influence their capacity to anticipate, cope with, resist, and recover from the adverse effects of physical events (Cardona et al. 2012). Decision makers need to be supported to take appropriate measures aimed at reducing flood risk in an effective and sustainable manner (Fernandez et al. 2016).

However, the main problem facing FRR mitigation measure processes involves the limitations of structural "hard" measures (i.e., storm surge barriers and floodwalls) against unexpected flooding events, despite the modernization of flood prevention measures (Kang et al. 2009). Moreover, "soft" strategies (i.e., building codes, land use and nature-based measures) can play critical roles in reducing FR (Du et al. 2020). Additionally, these "soft" measures do not require extensive

investment in hard-engineered infrastructures, as structural measures typically do, but instead rely instead on a good understanding of flood hazards and adequate forecasting systems.

Spatial planning is increasingly considered an important tool for FRR. Its main advantage is its capability of regulating the use of space for the long term. Appropriate land use allocation can minimize or even prevent exposure to natural hazards in current and future situations. Coordinated regulations are needed to incorporate disaster risk reduction strategies in spatial planning (Sutanta et al. 2010). Flood risk management and river ecosystem conservation have not been traditionally considered components of the urban planning process. This fact is due in large part to the division of academic fields. Those who deal with flooding and water quality are trained in river engineering, hydrology, geology, chemistry, or geophysics, whereas urban planners are most likely trained in architecture, traditional landscape, road engineering or social sciences. This missing or insufficient link to water management can be considered a fundamental flaw in the urban planning system to date (Huang and Shen 2019).

Accordingly, this chapter aims to shed light on the most common **spatial planning tools for FRR**, which have become important tools used by city planners and decision makers to manage FR. The chapter begins with an understanding of the types and sources of flooding, followed by descriptions of the flooding impacts, especially in urbanized areas. Then, descriptions and comparisons of different types of mitigation measures are provided. The next section describes the significant role of spatial planning tools in FRR. The final section provides conclusions.

11.1.1 Flood Causes, Classifications, and Types

Urban floods are a consequence of compounding hydrological and meteorological extremes in addition to human activities (Jha et al. 2012), as shown in Fig. 11.1. For example, extreme precipitation and flows and informal urban sprawl in floodplains increase urban flood risk. Usually, people moving from rural to urban areas or within urban areas settle in areas prone to floods. The absence of flood countermeasures may cause an increase in inhabitants' vulnerability in these areas. Land use changes can reduce the permeability of soils, which increases surface runoff and overloads drainage systems; consequently, the flood risk may increase (Jha et al. 2012). Additionally, flood triggers accumulate, which accelerates their impacts. This evolving challenge requires a better understanding of FR and more effective management by policy makers.

Floods are usually classified according to the duration of the flood event and its appearance as follows (Şen 2018):

(1) Long-standing floods: May extend to a week or longer
(2) Short-standing floods or "flash floods": Usually extend to approximately 6 h or less

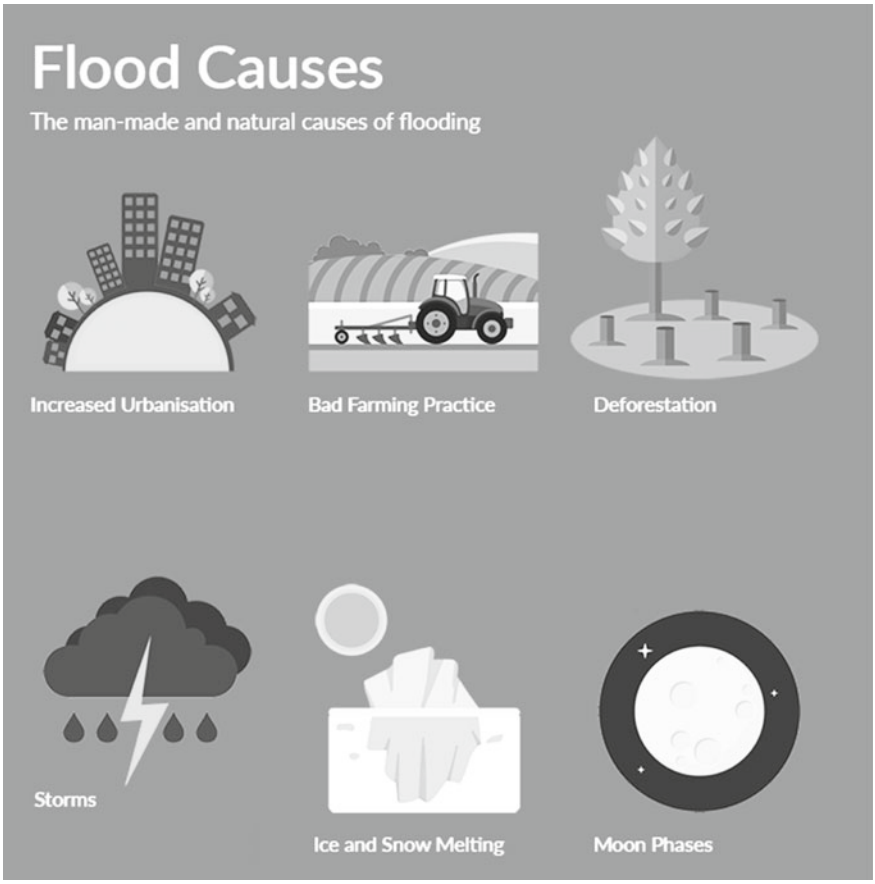

Fig. 11.1 Flood causes (man-made and natural causes) (Modified from: Flood infographic: types, causes and cost of flooding 2016)

In contrast, floods are also classified by their appearances into four types as follows (Şen 2018):

(1) River or stream floods
(2) Urban floods that occur in creeks or streets in urban areas
(3) Dry water-collector floods such as mountain sides and slopes
(4) Coastal floods caused by low atmospheric pressure on the sea surface

Below, Fig. 11.2 and Table 11.1 show the different types of floods. The causes and durations of each flood type are presented.

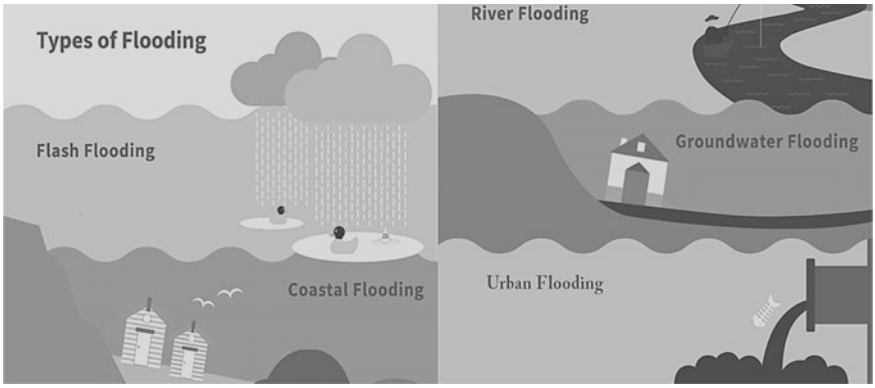

Fig. 11.2 The different types of floods (Modified from: Types of Flooding in the UK 2018)

11.1.2 Urbanization and Flood Risk (FR) Impact

Floods are one of the most frequent and devastating natural disasters worldwide, causing significant economic damage and loss of life. Accordingly, urban flooding has become very costly and difficult to manage, especially in developing countries that suffer from high concentrations of people and property. In addition to the direct impact of floods, floods have long-term indirect consequences, such as loss of educational opportunities, disease, and reduced nutrition, which may impede the achievement of developmental goals.

Several types of floods can occur in urban areas, such as river, coastal, pluvial and groundwater floods. In urban areas, there is a shortage of available areas that can be used for excessive water storage. High rainfall intensities and lack of adequate capacities for drainage systems can cause flooding in urban areas. Continuous and extended urban expansion reduces the permeability of land soil, increasing the runoff and flooding risk. Deficient or inappropriate land use planning is mainly responsible for increasing the urban FR, while many urban areas are facing the challenges of rising populations and high demands for newly developed areas (Abdrabo et al. 2020; Saber et al. 2020). However, while existing laws and regulations control the construction of new infrastructure and different building types, there is often no enforcement in place to ensure proper application because of different factors, such as economic factors, political factors, capacity constraints or resource constraints. Consequently, water flow paths in urban areas can be obstructed, causing floods (Jha et al. 2012).

Urbanization is accompanied by changes in natural landscapes and changes in land use and land cover (LULC), which increase impermeable areas and runoff, reduce infiltration, and change the frequency of flood incidences, as shown in Fig. 11.3. Hollis, in 1975, anticipated that the incidence of floods might increase up to ten times due to extensive urbanization, while for floods of 100-year return

Table 11.1 The different types of floods and their causes and duration

Flooding type	Causes		Period
	Natural	Anthropogenic	
Urban flood	Fluvial Coastal Flash Pluvial Groundwater	- Inappropriate drainage and sewage capacity for the rainfall amount - Lack of land cover permeability due to increased urbanization - Drainage system failure and lack of appropriate interventions	Various timescales starting from hours and extending to days
Pluvial flood	Convective, thunderstorms severe rainfall, breakage of ice jam glacial lake burst earthquakes resulting in landslides	- Land use changes - Urbanization - Increase in surface runoff	Varied periods depending on existing conditions
Coastal flood (tsunami, storm surge)	Earthquakes Submarine volcaniceruptions subsidence coastal erosion	- Urban sprawl in coastal zones - Damaging of coastal natural flora (e.g., mangroves)	Events usually occur in short time periods and may take a long time to recede
Groundwater flood	High water table level combined with heavy rainfall embedded effect	- Development in low-lying areas - Interference with natural aquifers	Long durations
Flash flood	Can be caused by river pluvial or coastal systems; convective thunderstorms; glacial lake outburst floods (GLOFs)	- Sudden failure of water-retaining structures - Inadequate drainage infrastructure	Typically, last a few hours

Source Data source: Jha et al. 2012

periods or greater, the severity could be doubled if 30% of roads were paved (Wheater and Evans 2009).

Floods pose a range of threats to human life, health, and well-being. In 2010, reported floods directly caused over 8000 lost lives. While direct deaths from flooding have declined over time as measures to prevent flooding have been employed, the economic loss is growing, particularly in developed countries, as shown in Fig. 11.4.

Unplanned urban growth creates indigent areas that lack suitable residences, services, and infrastructure, making these areas, and especially the children, elderly

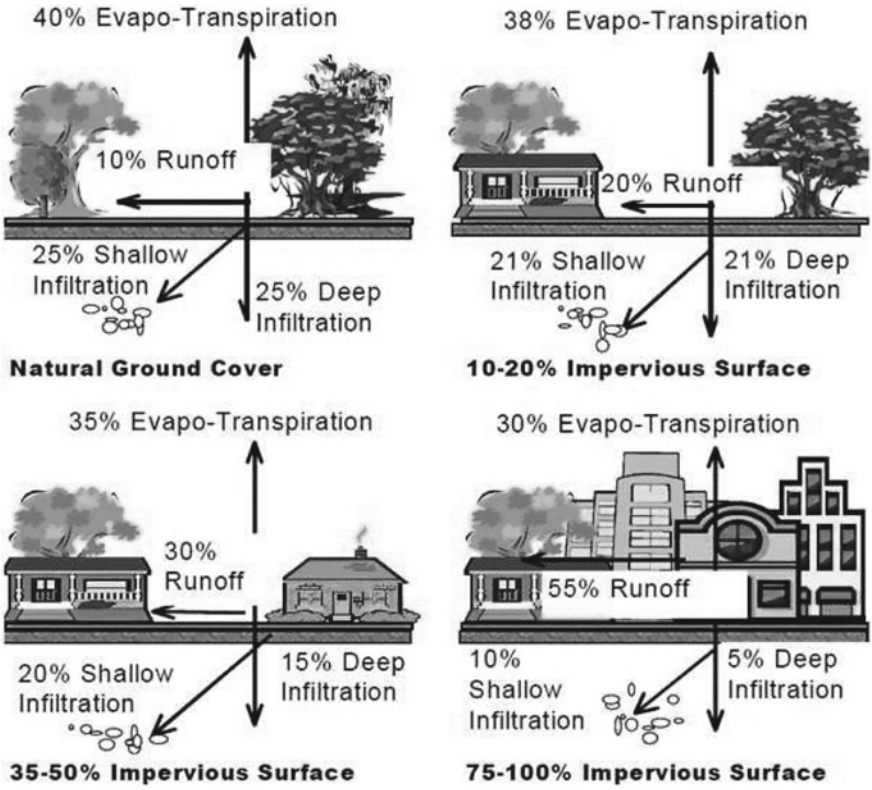

Fig. 11.3 Urbanization impact on water cycle changes (Modified from: NEMO 2018)

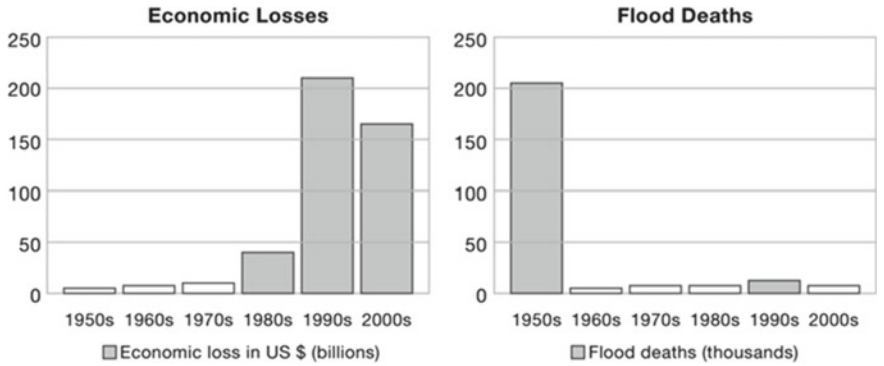

Fig. 11.4 Reported economic losses and deaths resulting from flood events. *Source* based on EM-DAT/CRED (Different natural disasters on a global scale 2016)

people, and women who live in them, more **vulnerable to floods**. The most operative way to manage FR is to embrace an integrated approach that combines structural **and nonstructural mitigation measures** (Jha et al. 2012). Flooding is the phenomenon with the greatest impact on the human population worldwide, with more than 2.8 billion people affected by floods since 1990 (EM-DAT 2016). However, the effect of flooding is mainly concentrated in the economic sector rather than in losses of lives when compared to other natural disasters, such as earthquakes. A comparison between floods and other types of natural disasters is shown in Fig. 11.5.

Egypt, for instance, is an arid and semiarid Arabian country that suffers from devastating flooding events, with an estimated total economic loss of approximately 1.2 billion USD/year in both the coastal and Nile wadi systems in the period from 1975 to 2014 (Abdel-Fattah et al. 2015). Flash floods in Egypt, although short-lasting, can be enormously harmful and represent a threat to property as well as lives. Most of the viable highways and other significant infrastructures are constructed across wadis. Many factors have pushed people to live in flood-prone areas. Recently, floods have become more frequent, causing fatalities and substantial damage in Egypt (Abdel-Fattah et al. 2015; Mohamed 2019). For example, urban floods in Alexandria have caused severe damage and losses, and the city has shown a lack of resilience in facing several events (Fig. 11.6).

Alexandria faced its worst flooding events on 25 October and 4 November 2015; nearly 60% of the city was flooded, the flood inundation ranged from 0.5 to 1.0 m, and lowland areas remained affected for up to 15 days. These flooding events occurred due to heavy rainfall of nearly 32 mm; these rainfall events were considered rare and historically significant (Zevenbergen et al. 2017). A recent study published in 2019 investigated extreme rainfall events that caused urban flooding in Alexandria, and the losses caused by these events are shown in Table 11.2 (Elboshy et al. 2019).

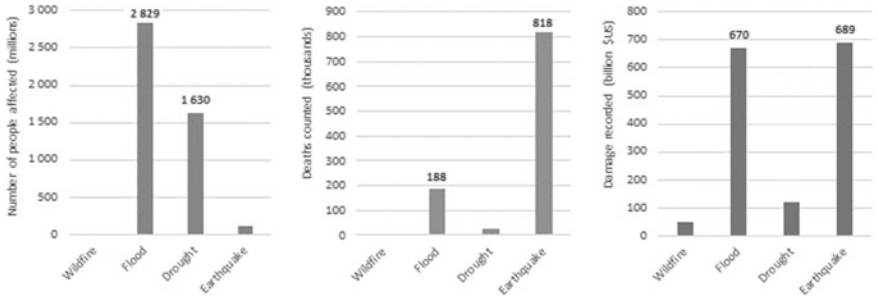

Fig. 11.5 Comparison of the damage caused by different natural disasters on a global scale (Data source: EM-DAT—2016) (Different natural disasters on a global scale 2016)

Fig. 11.6 Devasting urban flash floods in Alexandria, Egypt during the 2015 event (Reprinted from: Ashraf Abdalhameed 2015)

Table 11.2 Recorded hazardous flood events in Alexandria

Date	Rainfall rate	Rainfall duration	Economic loss	Human loss
31 December 1991	74 mm	N/A	N/A	80 died
26 January 2004	N/A	N/A	N/A	
12 December 2010	N/A	N/A	N/A	15 died 11 injured
14 November 2011	N/A	N/A	N/A	
29 September 2015	5 mm	2 h	N/A	
25 October 2015	53 mm	18 h	9.7 million dollars	13 died 16 injured
4 November 2015	227 mm	12 h	N/A	N/A

Source Data source: Elboshy et al. 2019

11.1.3 Flood Risk Management (FRM)

The FRM cycle consists of five main steps as follows: risk assessment, risk treatment (strategy), strategy implementation, strategy monitoring and evaluation, and risk goals and policy development and adjustments. In addition to these, risk communication participation is conducted in all steps, as shown in Fig. 11.7. Among these 5 steps, there are two main steps facing many challenges: flood risk assessment (FRA) and risk treatment (strategy).

FRAs are expected to enhance the effectiveness of disaster management, reduce the destructive socioeconomic impacts of floods and direct urban growth to safe areas (Cools et al. 2012). Therefore, FRAs are essential for identifying flood risk-prone areas in arid urban environments to mitigate flood risks and support-related decision making (Amundrud and Aven 2015; Psomiadis et al. 2016). An FRA defines the risk associated with floods for any city as a creation of both the city's exposure to the flood hazard and the vulnerability of society to the hazard. FRAs propose that the three main factors participating in a region's flood risk are hazard, exposure, and vulnerability (Center Asian Disaster Preparedness

Fig. 11.7 Unified urban flood management (The Authors)

2005; Zhang et al. 2003). However, one of the main problems facing FRA is the inadequate level of vulnerability analysis and mapping, especially in arid regions (de Brito et al. 2017). Although there are many studies in this regard, most of the previous studies have focused on only FRA at regional scales. There is a notable limitation in FRA studies at the local scale.

Regarding risk treatment, which mostly concerns reducing current and future flood damage and the costs inherent in doing so, actions need to be taken. The main challenge in this step is that most governments depend mainly on structural flood mitigation measures. However, in some applications, it was found that nonstructural measures can facilitate the implementation of structural measures and ensure the achievement of structural objectives. Additionally, despite several decades of experience in urban planning tools and stormwater management strategy implementation for FRR in many developed countries, the application of such approaches in arid and semiarid regions has not yet received adequate attention.

11.2 Mitigation Measures for Flood Risk Reduction

It is well known that FRR **measures** can be divided into **structural** and **non-structural** measures. **Structural measures** are generally major public projects that require formal approval from one or more government units, moderate-to-major planning and design efforts, and moderate-to-large capital investments, operation, and maintenance commitments. Examples of structural measures used primarily to control the quantity of urban surface water are the construction of detention/retention facilities, building banks or dams, upstream storage and diversion works, channel modifications or enclosures, dikes and floodwalls, bridges, channel improvement, and culvert alteration or replacement. Structural measures used mainly for controlling the quality of urban surface water are sedimentation basins, artificial or restored wetlands, and infiltration systems (Faisal et al. 1999). On the other hand, **nonstructural measures** usually include little or no construction and can often be implemented quickly by individuals, business, or other private entities. Typically, nonstructural measures require small-to-moderate capital investments. Nonstructural measures can be subdivided into land use regulation, institutional control, elevation of buildings, land acquisition and relocation, flood proofing, flood prediction and warning systems and emergency action plans, and flood insurance programs (Andjelkovic 2001; Faisal et al. 1999). Nonstructural measures aim to keep people safe from flooding by improving urban development planning and management. Structural measures are typically protective measures, while non-structural measures are reduction measures. Experiences show that FRR must avoid single sectorial solutions. A comprehensive integrated strategy combining both structural and nonstructural mitigation measures should be linked to existing urban planning and management policies.

11.2.1 Shortcomings of Structural and Nonstructural Mitigation Measures

Structural measures can directly decrease the magnitude of flooding. However, there are many shortcomings of structural measures, as follows:

- Structural measures can be overtopped by events outside their design capacity.
- Many structural measures also transfer flood risk from one location to another.
- The redirection of water flows also frequently has environmental impacts. In some circumstances, this is acceptable and appropriate, while in others, it may not be. In all cases, a residual flood risk remains.
- Structural solutions can also have a high upfront cost, can sometimes induce complacency by their presence, and can result in increased impacts if they fail or are overtopped, as was tragically illustrated in the tsunami in Japan in 2011.

Nonstructural measures do not usually require large investments upfront, but they often rely on a good understanding of flood hazards and adequate forecasting systems. However, there are many shortcomings of nonstructural measures, as follows:

- Many nonstructural measures lie in the need to engage the involvement and agreement of stakeholders and their institutions.
- Most nonstructural measures are designed to minimize but not prevent damage; therefore, most people would instinctively prefer a structural measure.

11.2.2 Nonstructural Mitigation Measures

The nonstructural measures shown in Fig. 11.8 and Table 11.3 can be categorized by their purposes into three main categories, as follows:

- Emergency planning and management including warning, evacuation, preparedness, and flood insurance.
- Flood avoidance and reduction via (1) land use planning such as (a) land use plans, (b) park and forestation plans, (c) land acquisition, and (d) relocation plans; (2) architectural planning measures such as (a) elevating buildings, (b) dry and wet flood proofing techniques, (c) facility maintenance and repair, (d) structural retrofitting or reinforcement, (e) building greening and (f) placement of pavements with water permeability.
- Speeding up recovery to increase resilience by enhancing building design and construction–"building back better".

11.2.3 Urban Planning and Landscape Tools for Flood Risk Reduction

Urban planning tools have recently played a central role in FRR scientific research. These tools can radically reduce the impact of extreme rainfall on public safety. In this part of the book, we will present some interventions that mainly lie under flood avoidance and reduction categories, such as (A) land use control, (B) building codes, (C) flood proofing and building elevation, and (D) sustainable infrastructure for stormwater management.

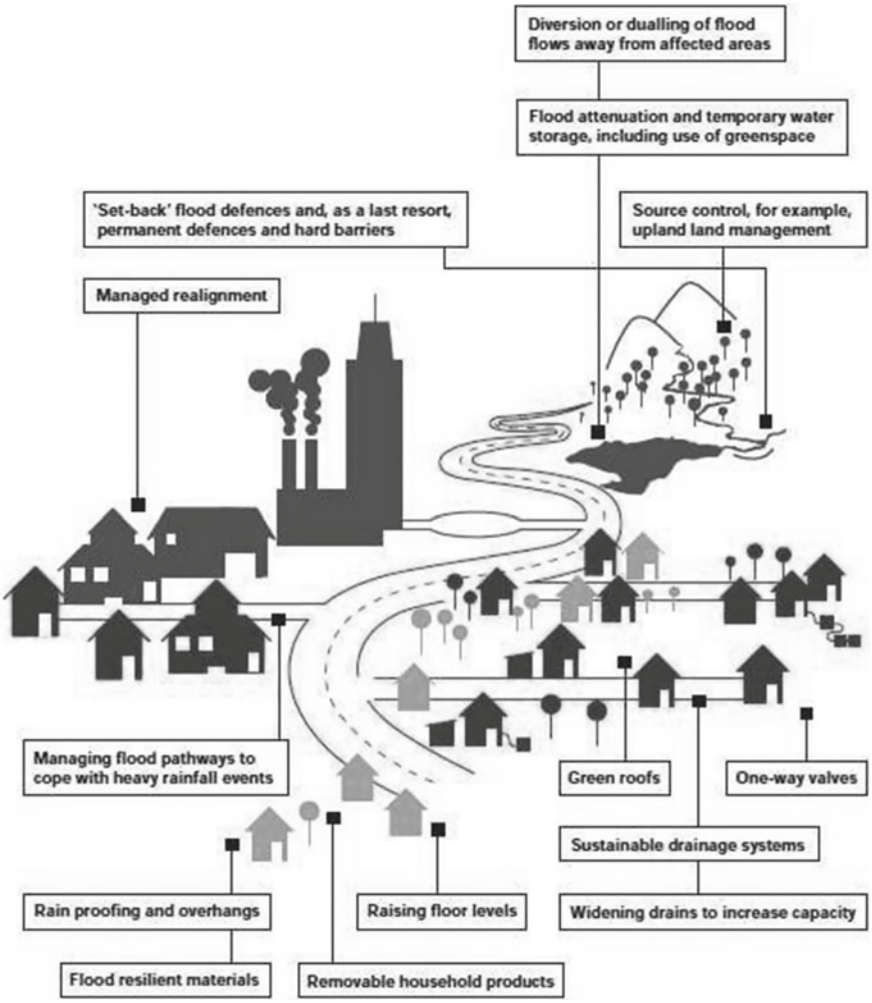

Fig. 11.8 Multiscale nonstructural mitigation measures (Modifed from: Shaw et al. 2007)

11.2.3.1 Land Use Control and Flood Zoning

One of the most operative methods of decreasing FR damage is to control development on a floodplain through land use planning, which requires the involvement of all levels of stakeholders (Şen 2018). According to the UN International Strategy for Disaster Reduction (ISDR) (2004) insufficient or nonexistent land use planning increases the vulnerability of communities exposed to natural hazards. Urban land tends to be the most vulnerable land to catastrophes wrought by floods, yet there are inadequate measures in place to reduce the impacts of floods on local populations. Although spatial planning is responsible for decisions regarding the long-term

Table 11.3 Categories of nonstructural mitigation measures for FRR

Category	Subcategory			Contents and characters
Flood avoidance and reduction	Land use plans	District plan		- Development control in high-flood-risk areas
		Land use control		- Control the area outside of the administrative authority boundary - Guide layouts of streets, infrastructures, lot sizes and shapes, and drainage installations
		Water circulation plan		- Plan urban rain circulation system
	Park and forestation plans	Open and green areas development		- Apply eco-friendly standards and design techniques for natural drainage
		Waterfront park development		- Develop waterfront parks and restrict residential or commercial developments
	Land acquisition and relocation plans	Land acquisition and development	Public development	- Central and local governments acquire land and plan development
			Public/ private development Sale of development rights	
		Land rehabilitation and relocation	Successive residence	- Rehabilitate the flooded districts to maintain existing buildings
			Individual relocation	- Partial relocation after the rehabilitation of high-flood-risk districts
			Complete relocation	- Land acquisition of high-flood risk areas to complete relocation
	Building code			- Develop manuals or guidelines for flood prevention standards for each district or building
	Elevating buildings			- Elevate the ground floors above the inundation line - Install pilots or piers and elevate the inner floors of buildings by filling land.

(continued)

Table 11.3 (continued)

Category	Subcategory	Contents and characters
	Dry and wet flood proofing techniques	Dry flood proofing - sealing the exterior walls to prevent the entry of floodwater - sealing all openings below the flood line - For wet flood proofing, allow the entry of floodwater but keep the same level of pressures between the inside and outside building to mitigate damages on the structure including the foundation
	Facility maintenance, repair, and structural retrofitting or reinforcement	- Repair, maintain or protect facilities from floods - Structural retrofitting to prevent buildings being washed away - Build waterproof walls or fences
	Sustainable infrastructure for stormwater management, building greening, and pavements	- Install roof gardens, vertical garden walls, etc., directly or indirectly to mitigate flood damage - Pave façade, part, or whole of buildings with water-permeable materials
Speeding up recovery	Flood prevention standards	- Increase resistance by enhancing building design and construction after disasters occur
	Restoration policy and risk finance	
Emergency planning and management	Statutes and ordinances	
	Public information and education	- Emergency action plans - Disaster prevention education
	Flood prediction, warning, and evacuation systems	- Including evacuation facilities and flood maps
	Flood insurance	- Evaluation system of flood risk, flood mapping, and coordination with urban architectural plans

Source Data source: Kang et al. 2009

utilization of land and has not been directly responsible for disaster risk reduction, it has a fundamental role in disaster risk reduction. Four likely roles of spatial planning in FRR, as identified by Fleischhauer (2008), are as follows:

- **Eliminate future urban expansion in flood-prone zones** by determining the locations in which building is or is not allowed according to the flood risk degree of each location, especially concerning the history of flood incidences, as shown in Fig. 11.9.
- **Classify different land use settings for flood-prone areas** by identifying sensitive or important societal or environmental features since each disaster has its own acceptable risk to different land use classes.
- **Regulate land use or zoning plans** by identifying appropriate area(s)/location (s) for specific land uses with legally necessary statuses. In areas vulnerable to floods, the regulation of building density is essential to decrease the impact of building collapse. Simply, land regulation determines where urban development should go (Pyke and Andelman 2007).
- **Achieve flood hazard alteration** by promoting a soft engineering method to decrease FR.

Spatial planning processes need to integrate several factors and datasets. Topographical and natural feature maps are considered base maps that enable a spatial understanding of all other features, such as buildings, infrastructure, open spaces, green belts, nature reserves and watercourses. The division of maps into layers helps policy makers interpret community needs and address potential hazards and risks. Using geographical information systems (GISs) has become essential for

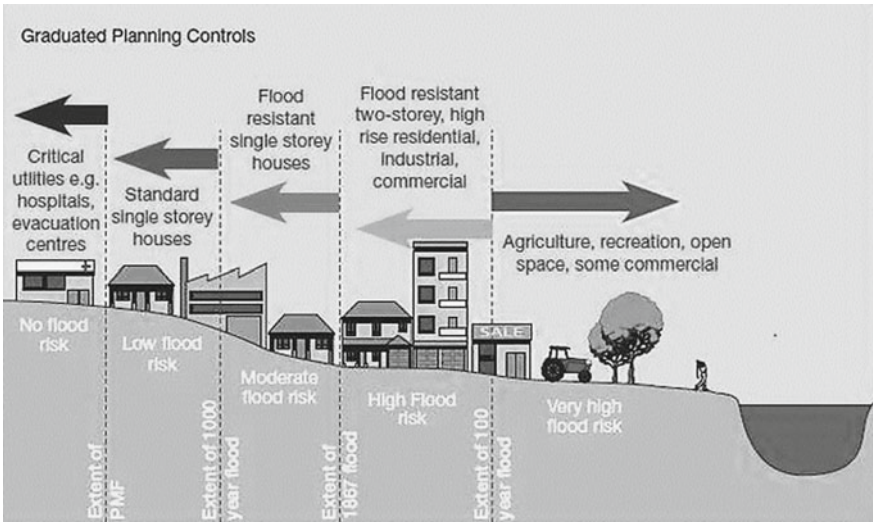

Fig. 11.9 Land use planning controls according to flood risk degree (Modifed from: How can flooding be stopped? 2020)

different governmental entities to capture relevant urban data spatially and address growing issues.

Environmental economists have emphasized the importance of spatial measures as part of a more "risk-based" approach in flood management, wherein spatial measures can be integrated with structural flood measures to reduce flood risk. However, the cost and expected benefits are the main determinants of differentiation between different structural and spatial measures (Liao 2012).

11.2.3.2 Flood Proofing and Elevating Buildings

The damage to infrastructure elements and houses in flood events can be caused by direct water forces, erosion, or a combination of both (Santato et al. 2013). There are many techniques for the flood proofing of properties. (1) Elevation: lifting the buildings or infrastructure elements higher than expected flood level, which prevents them from intersecting with the path of water movement. Also, building elevated walkways improves accessibility to important buildings such as flood shelters. (2) Flood walls: built to keep floodwaters from reaching buildings. (3) Dry flood proofing: making the walls of buildings and the openings resistance to water. (4) Wet flood proofing: minimizing the damage that occurs when water enters the building, as shown in Fig. 11.10.

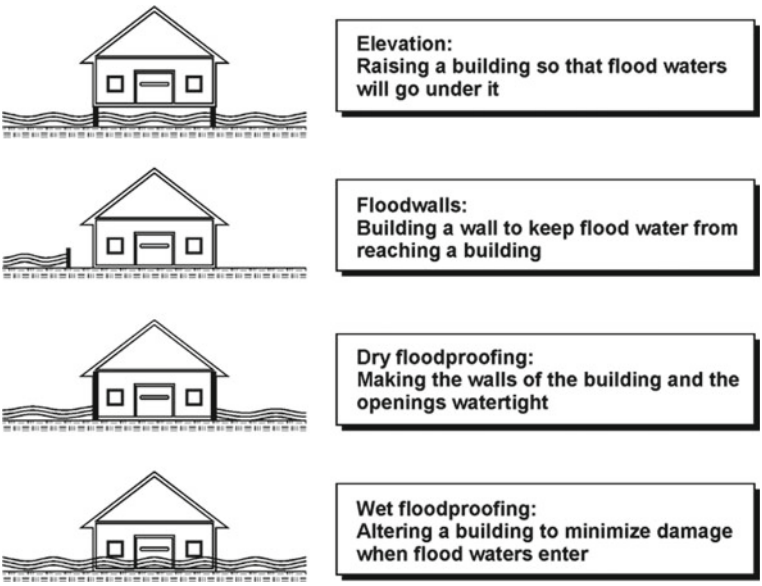

Fig. 11.10 Techniques to fight floods in cities. (Modifed from: UNESCO. Fighting floods in cities; Project training material for disaster reduction; Report, Delft, Holland 1995)

11.2.3.3 Creation of Regulations and Enforcement Procedures

Integrating land use planning with flood risk management by identifying flood zones and determining the developmental frameworks achieves appropriate land use planning and patterns of development. However, the effectiveness of these plans requires appropriate regulations to control or restrict development. Such regulations will need to interact with existing land use control, planning and building control legislation and will be naturally limited by the strength of current land use planning procedures. For example, in Germany, flood legislation was built upon an already stringent planning control system with good compliance and is expected to have a long-term impact on flood risk. The regulations usually cover the following aspects (Andjelkovic 2001):

- Selecting the appropriate uses for new development areas and associated permitted zones
- Flood risk assessment requirements for any new developments
- Design and building standards for flood zones such as materials, access points, and minimum floor level
- Mandatory drainage and surface water management plans
- Mandatory retrofitting of flood protection measures

11.2.3.4 Sustainable Infrastructure for Stormwater Management

Sustainable drainage is a strategy usually applied to urban areas that are prone to different flooding types due to heavy rain. In urban areas, built-up areas and paved roads are impermeable to water, and rain is channeled straight into drainage networks that can quickly become submerged. The main concept of sustainable infrastructure is to utilize landscape elements and make the water from roofs and roads drain underground rather than occupy the water system (Jia et al. 2015), as shown in Fig. 11.11.

The complexity of urban stormwater management has been increasing over recent decades, and many concepts, tools and techniques have been utilized to reduce flood risk. These concepts, tools and techniques have been used by experts of different disciplines in different regions of the world. Additionally, different disciplines are integrated into this issue, such as the urban drainage discipline, architecture, landscape architecture, urban design and planning, sociology, ecology, and economics. This section will discuss some of the urban planning tools, strategies and techniques for FRR in urban areas as follows: best management practices (BMPs) and low impact development (LID) between 1949 and 1990 in the USA; water-sensitive urban design (WSUD) in the 1990s in Australia; sustainable urban drainage systems (SUDS) in the 2000s in the UK; green infrastructure (GI) and green-gray infrastructure; integrated urban water management (IUWM) and sponge cities in 2014–2015 in China. The main common goals for all these tools, strategies and techniques are as follows:

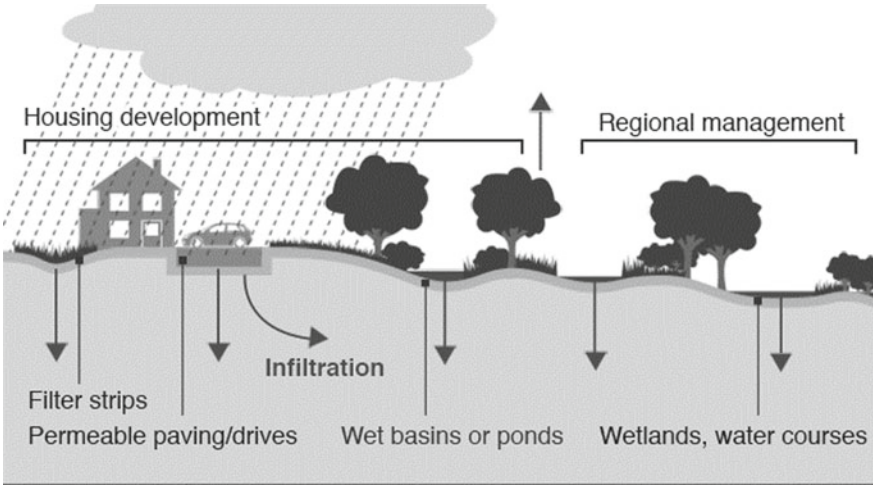

Fig. 11.11 Main concept of **sustainable infrastructure for stormwater management** (Modifed from: How can flooding be stopped? 2020)

- Reduce runoff volumes and flow rates from impermeable surfaces
- Control the impact of urbanization on flooding
- Provide opportunities for using runoff water at the point of fall
- Improve water quality and reduce pollution from runoff water
- Protect natural flow system in watercourses
- Provide an attractive habitat for wildlife in urban watercourses
- Provide opportunities for evapotranspiration from vegetation and surface water
- Support natural groundwater/aquifer recharge.

Best Management Practices (BMPs) and Low Impact Development (LID)

By the early 1990s, the term BMP had been adopted in almost every jurisdiction's stormwater design manual, and consequently, BMPs were implemented across North America. LID is considered as a sub-strategy of BMPs. The main goal of LID was to achieve a natural hydrology system by integrating control measures. Natural hydrology refers to the predevelopment runoff, infiltration, and evapotranspiration volumes that achieve the site's balance through a functionally equivalent landscape. The LID layout applies a cascading flow system to minimize the direct connectivity between adjacent impervious areas. LID mainly concerns the spread of runoff flows produced from upper impermeable surfaces onto lower permeable areas, such as absorbent landscaping areas, for additional infiltration benefits and water quality enhancement. LID depends on small-scale stormwater treatment devices such as bioretention systems, green roofs, and swales located at or near the source of runoff (Fletcher et al. 2015).

The LID–BMP implementation should be fully coordinated with the local construction plan and integrated, if possible, into the site landscaping scheme. The LID–BMP planning strategy includes the following: (1) preserving the original terrain, (2) limiting the ratio of impervious surface areas, (3) avoiding the direct connection of impervious areas, (4) selecting the most suitable BMP types according to local conditions in terms of both technical and social/economic factors, and (5) setting an appropriate goal for LID–BMP implementation (Fletcher et al. 2015).

Water-Sensitive Urban Design (WSUD)

The objectives of the WSUD strategy are to manage the water balance of an urban area, maintain and improve water quality, support water conservation, and maintain water-related environmental and recreational issues. The WSUD approach aims to minimize the hydrological impacts of urban development. Stormwater management as a main target of WSUD includes different objectives, such as providing flood control, flow management, water quality improvements and opportunities to harvest stormwater (Fletcher et al. 2015).

Sustainable Urban Drainage System (SUDS)

SUDS contains various techniques to drain rainfall water in a sustainable manner. The techniques used depend on replicating as closely as possible the natural, pre-development drainage conditions of a site, consistent with the previously described principles behind LID. Typically, SUDS are designed as a sequence of practices and technologies that work together to form stormwater management (Fletcher et al. 2015).

Integrated Urban Water Management (IUWM)

The concept of integrated urban water management (IUWM) integrates the management of water supply systems, groundwater, wastewater networks, and stormwater drainage, considering the roles and cooperation between the different institutions involved in urban water management. The IUWM is based on considering all parts of the water cycle regardless of whether that water cycle is natural or constructed and surface or subsurface, recognizing these factors as an integrated system, considering all requirements for water, both anthropogenic and ecological, and considering the local context. Additionally, the IUWM concept accounts for environmental, social, cultural and economic perspectives and needs and strives for sustainability by achieving a balance among these perspectives (Jia et al. 2012).

11.2.3.5 Sustainable Infrastructure Tools for Stormwater Management

To apply the different sustainable infrastructure strategies discussed in the previous section, different tools have been used and integrated to achieve the desired objective (Hamburg: Hamburg University of Technology (TUHH) n.d.). In the following section, these different tools are divided into three categories: recharge (infiltration) tools, detention tools, and retention tools, as shown in Fig. 11.12.

Recharge Infiltration Tools

Infiltration tools involve stormwater runoff soaking into the ground to reduce the volume of rainfall water runoff on the surface.

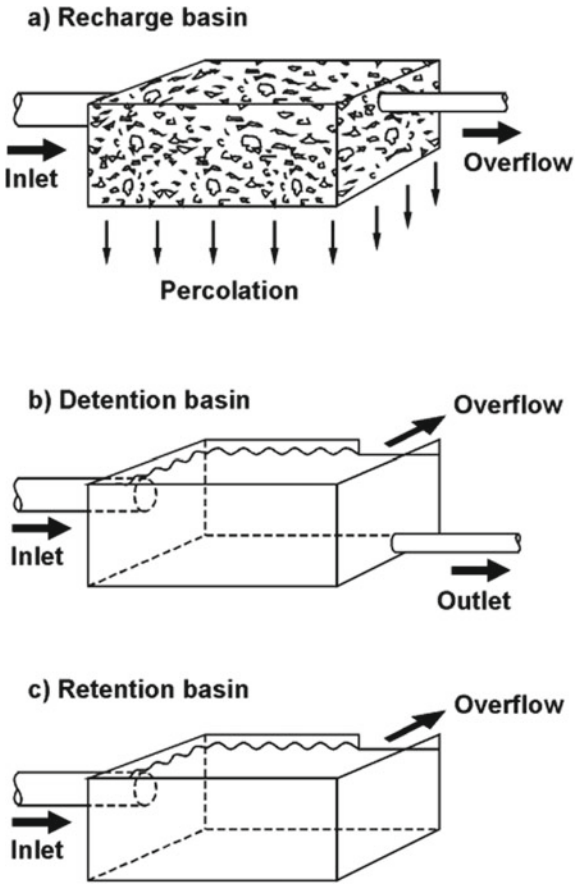

Fig. 11.12 Sustainable infrastructure for stormwater management tools (Modifed from: Hamburg: Hamburg University of Technology (TUHH) n.d.)

A. Bioswales

Bioswales are vegetated channels with permeable soils that infiltrate runoff water from upgradient impermeable areas (Blanco et al. 2011), as shown in Fig. 11.13.

B. Stormwater Planters

Stormwater planters have an essential role in the sustainability of urban areas by reducing stormwater runoff and water pollution. In addition, stormwater planters play an important role in creating a greener and healthier built environment by providing space for plants and trees near buildings and along streets (Rehan 2013).

Stormwater planters are similar to rain gardens: They are designed to capture runoff and filter out sediment and pollutants, as shown in Fig. 11.14.

C. Permeable Pavements

Permeable pavements refer to the use of a special technique to pave urban paths that permits stormwater runoff to infiltrate through the surface into the sublayers and/or underlying strata, as shown in Fig. 11.15.

Different alternatives can be used as permeable pavements, such as permeable concrete block pavers, brick pavers, stone chips, gravel, porous concrete, and porous asphalt. Additionally, grass can be used with or without reinforcement in areas with suitable climates and low traffic loading. Permeable paving is generally constructed on a coarse gravel subbase that creates temporary storage facilities and allows stormwater runoff to infiltrate into the underlying stratum, promoting the recharge of the groundwater table. Stored rainwater can be reused for several domestic purposes.

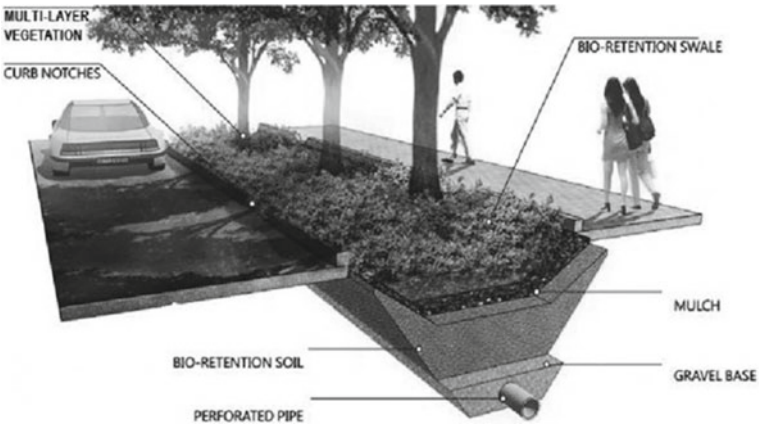

Fig. 11.13 Bioswales design (Modified from: Brankovic and Protic)

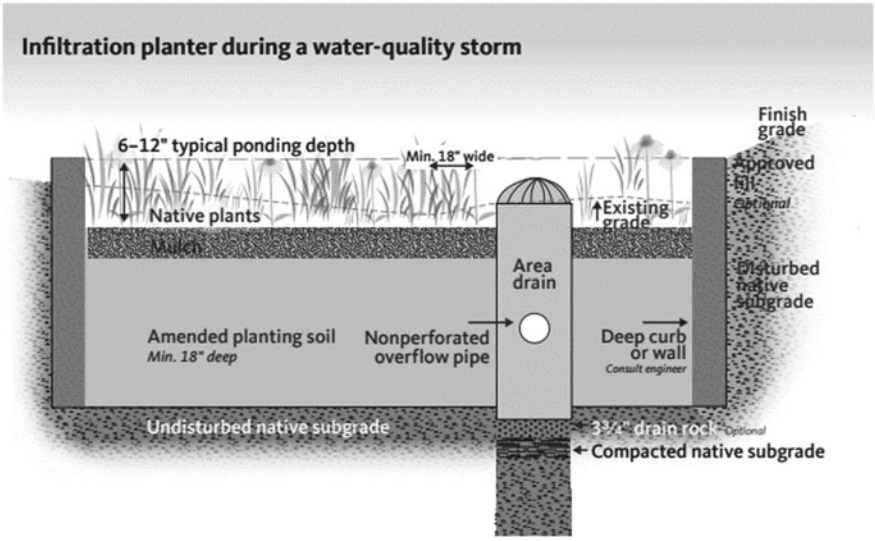

Fig. 11.14 Infiltration stormwater planter design (Modified from: Cahill et al. 2011)

Fig. 11.15 Permeable concrete block pavers with open joints and slotted ends filled with pea-sized gravel (Modified from: Armitage et al. 2013)

Detention Tools

Detention tools are used to slow down stormwater runoff before subsequent transfer downstream. The following section discusses different detention tools.

A. Detention Ponds

Detention ponds are large depressions that work as temporary storage for stormwater runoff and reduce flood peaks. Detention ponds are known as dry ponds and provide only flood control measures. The estimation of detention pond volume

depends on comparing the runoff volumes before and after development in urban areas. The ponds are intended to drain stormwater within a given period to make their volumes available for the next storm event. As shown in the diagram below, outlet pipes are placed at the bottom elevation of detention ponds to allow the ponds to drain dry.

B. Subsurface Storage

The subsurface storage of stormwater involves underground structures that are used to temporarily detain and release stormwater. These structures can include vaults, stone storage, pipe storage, and plastic grid storage. Successful stormwater management plans will combine materials and designs that are specifically appropriate to each site, as shown in Fig. 11.16.

Retention Tools

Retention tools are used for the retention of rainfall water to protect receiving watercourses during floods if long-term storage and additional infiltration are not feasible on site. The following section discusses different retention tools.

A. Retention Ponds (retention basins)

Retention ponds are formed by excavating below the natural groundwater level and/or lining the bases of ponds to retain stormwater. In contrast to dry detention ponds, retention ponds hold permanent pools of water and are referred to as wet ponds. Usually, the main reason to construct retention ponds involves high

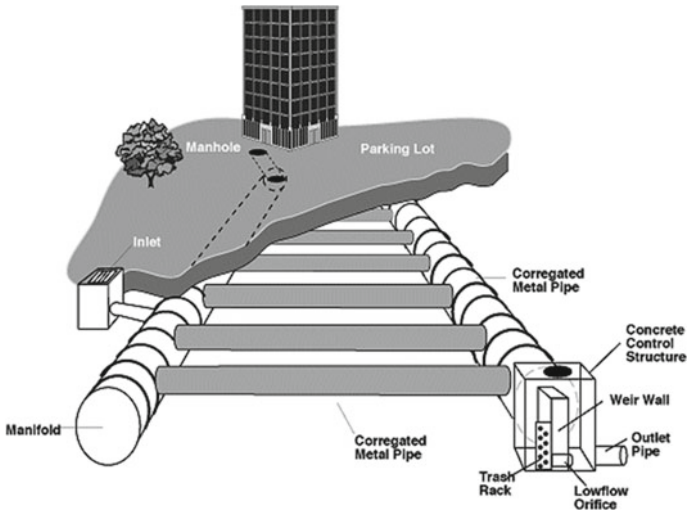

Fig. 11.16 Subsurface storage stormwater components (Modified from: Underground Storage)

groundwater tables. The bottom of the ponds is excavated below the water table elevation to establish a permanent pool. The outlet of the pond is placed above the desired pool elevation. The volume of the permanent pool is estimated by a desired residence time to allow microbes and vegetation in the water to consume nutrients and to allow suspended pollutants to settle.

B. Constructed Wetland

Constructed wetland technology is considered to be a comprehensive approach integrating wastewater treatment, flood protection and stormwater management. Gray water is collected from households and subjected to a primary treatment system (usually a septic tank) and is then transported to the constructed wetland via an inlet to pass through the filter media, allowing the settlement of solids and trapping bacterial populations on the surface of the media and plant stems. Wastewater then reaches the outlet with higher quality and can be reused, as shown in Fig. 11.17.

C. Green Roofs

Green roofs are a technique involving covering rooftops with lightweight plants that enable rainfall infiltration and recover evapotranspiration. As shown in Fig. 11.18, green roofs basically consist of a vegetation layer, a substrate layer that is important to retain water and in which the vegetation is anchored and a drainage layer to drain the excess water. Grasses, perennial herbs and shrubs make up the main constituents of vegetation (Mentens et al. 2006).

Green roofs reduce stormwater through three processes: delaying the initial time of runoff by absorbing water in the green roof system; reducing the total runoff by retaining a portion of the rainfall water; and distributing the runoff over a long time period through a relatively slow release of the excess water that is temporarily stored in the pores of the substrate.

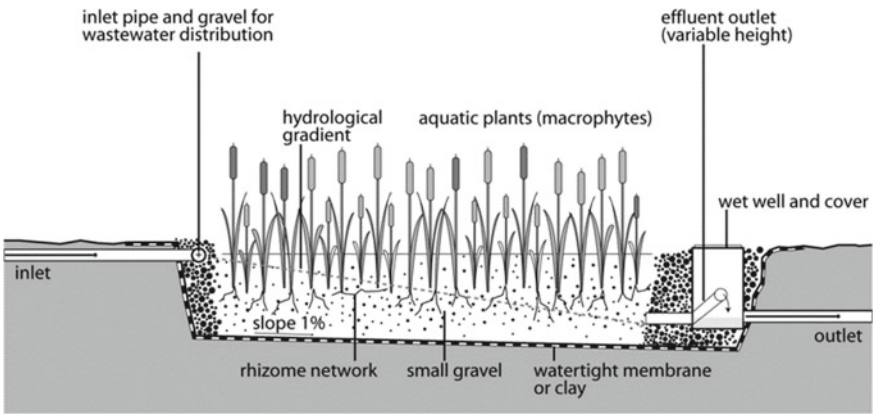

Fig. 11.17 Horizontal subsurface flow in a constructed wetland (Modified from: Tilley 2014)

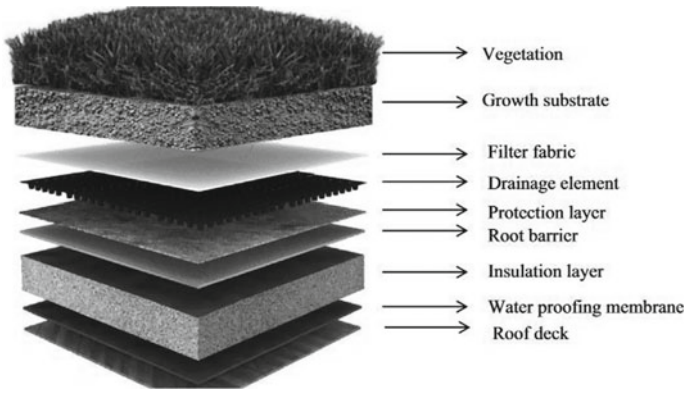

Fig. 11.18 Green roof structure (Modified from: InsulationCorp 2018)

D. Rainwater Harvesting

Rainwater harvesting involves the collection and use of rainfall water from any catchment area, such as roofs, to reduce site runoff and the need for runoff-control devices and to minimize the need for utility-provided water. Rainwater collection has been widely used in arid regions. Particularly in areas where populations are dispersed, rainwater collection constitutes a low-cost alternative to provide needed water. In moist climate zones, rainwater collection is an efficient supplemental water source, as shown in Fig. 11.19 (Annie Kane and The Fifth Estate 2015).

11.3 Implementation of Specific Urban Water Management in Arid and Semiarid Regions

The application of such approaches in arid and semiarid regions has not yet received adequate attention. Therefore, due to the limitations of existing case studies, this section will briefly present 3 case studies involving the implementation of urban water management strategies and techniques in the semiarid region of China and the USA in addition to Egypt.

11.3.1 Sponge City—China

The Sponge City Program (SCP) was embraced by the Chinese government in 2014. This program aims mainly to provide nature-based solutions for urban water-related issues. The main goals were to absorb and reuse 70% of stormwater in urban areas by improving and enhancing the infiltration rate and storing and

Fig. 11.19 Rainwater harvesting example (Modified from: Annie Kane and The Fifth Estate 2015)

purifying rainwater for reuse. The main techniques adopted in this program are the replacement of impervious infrastructure systems, green roofs, parks, and water-front areas following a sustainable or greener approach, as shown in Figs. 11.20 and 11.21 (DSD). The harvested rainwater, after suitable treatment, can be used as far as possible as a water resource. Approximately 50–100 million US$ for each pilot city has been invested in the SCP by the Chinese central government, which allows more cities to join the program (Nguyen et al. 2019).

LID—USA

By the early 1990s, LID was implemented across North America. The main aims of LID are slowing the flow of stormwater and reducing erosion and flood-related dangers. This aim can be achieved by spreading stormwater out, which reduces the flow speed. Thus, the stormwater is absorbed into the ground as recharge. Green roofs (Fig. 11.22), rain gardens, porous pavements, planter boxes (Fig. 11.23), bioswales, and detention/retention ponds (Fig. 11.24) have been adopted in Denver, CO and other cities by the United States Environmental Protection Agency (EPA). Rain gardens are placed near paved surfaces, such as parking lots, to catch runoff. Additionally, rainwater is stored in planter boxes and then channeled into rain gardens. Bioswales/bioretention cells are used to purify contaminants and pollutants from stormwater runoff (Agency 2017).

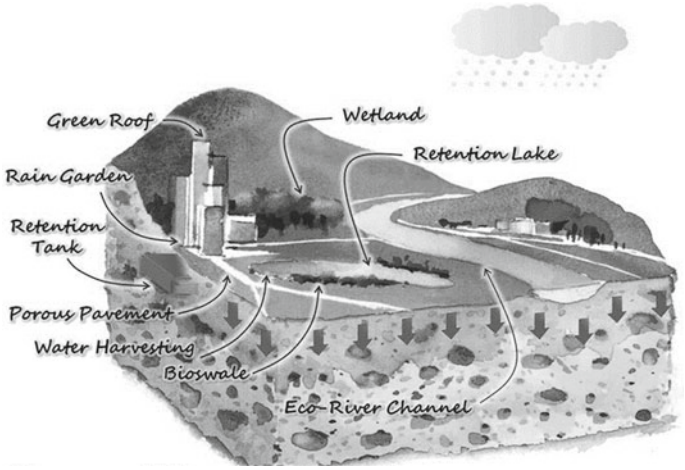

Fig. 11.20 Schematic diagram of the sponge city main concept (Modified from: DSD)

Fig. 11.21 Green roof at Shatin Sewage Treatment Works (Modified from: DSD)

Detention/retention ponds are used due to an increase in flash flood events in **Denver**. Detention and retention ponds provide locations for the collection and infiltration of rainwater into aquifers. The main difference between detention and retention ponds is that during scarce rainfall, detention ponds stay dry, while retention ponds include constant amounts of water, as shown in Fig. 11.24. (Agency 2017)

Fig. 11.22 Green roof technique in Denver, CO, USA, for stormwater management (Modified from: Agency 2017)

Fig. 11.23 Rain gardens, porous pavements, and planter box techniques in Denver, CO, USA, for stormwater management (Modified from: Agency 2017)

Fig. 11.24 Bioswale and detention/retention pond techniques in Denver, CO, USA, for stormwater management (Modified from: Agency 2017)

Fig. 11.25 Bioswales, storm planters, and infiltration tools in New Cairo city

11.3.2 Recharge Infiltration—Egypt

For the first time in Egypt, in 2020, officials began to pay attention to nonstructural mitigation measures for FRR in urban areas, especially new cities. Bioswales, storm planters, and infiltration tools were used in New Cairo city to decrease the volume of stormwater runoff on the surface since the city has recently suffered repeatedly from urban flooding, as shown in Fig. 11.25.

11.4 Conclusion

Solutions for flood management in urban areas are regularly complex because the urbanization process does not result from the optimal use of space or integrated planning. Structural mitigation measures are still common, especially in developing urban environments where flooding disasters and water-related issues must be addressed. Despite several decades of experience in the use of urban planning tools and stormwater management strategy implementation for FRR in many developed

countries around the world, such as the USA, UK, Australia, China, and Netherlands, the application of such approaches in arid and semiarid regions has not yet received adequate attention yet.

The effectiveness of stormwater strategies is flow-path dependent. It is necessary to develop cascading flows to drain storm runoff from impervious surfaces upstream onto pervious areas downstream for more infiltration. When LID, SUDS, Sponge Cities and GI are implemented in arid and semiarid climates, native plants that can cope with drought and are low-maintenance must be chosen due to the dry climate and large temperature differences between summer and winter.

Many challenges are faced when implementing the urban planning approach in flood risk reduction. These challenges include political interventions, unsatisfactory resources, and state inaction to involve civil society in planning and environmental processes. Land use planning and regulation are fundamental measures for future FRR to mitigate the devastating impacts of flooding, particularly in rapidly urbanizing areas.

Accordingly, the integration of a disaster risk reduction strategy combining both structural and nonstructural mitigation measures into spatial planning is vital. This integrated strategy could be much more effective than using one type of measure alone. Therefore, it is essential to simulate the future impacts of flood disasters. Spatial plans should be assessed alongside integrated risk maps to understand the possible consequences of disasters on land use allocation. Planning exercises must be conducted with the contribution of all relevant agencies to develop a framework for holistic flood management within the country. The new city plans must include such urban and landscape tools for FRR in the current and future situations while considering the uniqueness of the local context.

References

Abdel-Fattah M, Kantoush S, Sumi T (2015) Integrated management of flash flood in wadi system of Egypt: disaster prevention and water harvesting

Abdrabo KI, Kantoush SA, Saber M, Sumi T, Habiba OM, Elleithy D, Elboshy B (2020) Integrated methodology for urban flood risk mapping at the microscale in ungauged regions: a case study of Hurghada, Egypt. Remote Sens 12(21):3548

Agency USEP (2017) Low-impact development and green infrastructure in the semi-arid west. Retrieved from https://www.epa.gov/green-infrastructure/green-infrastructure-semi-arid-west

Amundrud Ø, Aven T (2015) On how to understand and acknowledge risk. Reliab Eng Syst Saf 142:42–47. https://doi.org/10.1016/j.ress.2015.04.021

Andjelkovic I (2001) Non-structural measures in urban flood management; IHP-V technical documents in hydrology No. 50. UNESCO, Paris, France

Annie Kane and The Fifth Estate. 2015. Rainwater harvesting could save australia billions. Retrieved from (https://www.eco-business.com/news/rainwater-harvesting-could-save-australia-billions/?fbclid=IwAR3vRFZTGWqaaiv-LOqsxb0aAgZhGkAKGgtiwGCixhnWzc8wmUHt9U7SAS8)

Armitage N, Vice M, Fisher-Jeffes L, Winter K, Spiegel A, Dunstan J (2013) The South African guidelines for sustainable drainage systems. Report TT558/13. Pretoria: water research commission

Ashraf Abdalhameed (2015) The floods killing 6 persons in Alexandria. Alarabia news. Retrieved from https://www.alarabiya.net/arab-and-orld/egypt/2015/10/25/

Bertilsson L, Wiklund K, de Moura Tebaldi I, Rezende OM, Veról AP, Miguez MG (2019) Urban flood resilience—a multi-criteria index to integrate flood resilience into urban planning. J Hydrol 573:970–982

Blanco H, McCarney P, Parnell S, Schmidt M, Seto K (2011) The role of urban land in climate change. Climate change and cities: first assessment report of the urban climate change research network. Cambridge University Press, Cambridge, UK

Cahill MR, Godwin D, Sowles M (2011) Stormwater planters: Oregon sea grant

Cardona O-D, van Aalst MK, Birkmann J, Fordham M, McGregor G, Mechler R (2012) Determinants of risk: exposure and vulnerability

Center Asian Disaster Preparedness (2005) Integrated flood risk management in Asia: A Primer. Retrieved from

Cools J, Vanderkimpen P, El Afandi G, Abdelkhalek A, Fockedey S, El Sammany M, Huygens M (2012) An early warning system for flash floods in hyper-arid Egypt. Nat Hazards Earth Syst Sci 12(2):443–457. https://doi.org/10.5194/nhess-12-443-2012

de Brito MM, Evers M, Höllermann B (2017) Prioritization of flood vulnerability, coping capacity and exposure indicators through the Delphi technique: A case study in Taquari-Antas basin, Brazil. Int J Disaster Risk Reduct 24:119–128. https://doi.org/10.1016/j.ijdrr.2017.05.027

Different natural disasters on a global scale (2016). Retrieved from https://emdat.be/

DSD. The Sustainability Report 2016-17 of Drainage Services Department. Retrieved from https://www.dsd.gov.hk/Documents/SustainabilityReports/1617/en/sponge_city.html

Du S, Scussolini P, Ward PJ, Zhang M, Wen J, Wang L, Ke Q (2020) Hard or soft flood adaptation? Advantages of a hybrid strategy for Shanghai. Glob Environ Change 61:102037

Elboshy B, Kanae S, Gamaleldin M, Ayad H, Osaragi T, Elbarki W (2019) A framework for pluvial flood risk assessment in Alexandria considering the coping capacity. Environ Syst Decis 39(1):77–94

Faisal I, Kabir M, Nishat A (1999) Non-structural flood mitigation measures for Dhaka City. Urban Water 1(2):145–153

Fernandez P, Mourato S, Moreira M, Pereira L (2016) A new approach for computing a flood vulnerability index using cluster analysis. Phys Chem Earth, Parts A/B/C 94:47–55

Fleischhauer M (2008) The role of spatial planning in strengthening urban resilience. Resilience of cities to terrorist and other threats, pp 273–298. Springer

Fletcher TD, Shuster W, Hunt WF, Ashley R, Butler D, Arthur S, Bertrand-Krajewski J-L (2015) SUDS, LID, BMPs, WSUD and more—the evolution and application of terminology surrounding urban drainage. Urban Water J 12(7):525–542

Flood infographic: types, causes and cost of flooding (2016) Retrieved from https://www.fluvial-innovations.co.uk/2016/12/22/flood-infographic-types-causes-cost/

How can flooding be stopped? (2020) Retrieved from https://www.bbc.com/news/uk-25929644

InsulationCorp (2018) Green Roofs. Insulation Company of America. Retrieved from (https://insulationcorp.com/green-roofs/)

Jha AK, Bloch R, Lamond J (2012) Cities and flooding: a guide to integrated urban flood risk management for the 21st century. The World Bank

Jia H, Lu Y, Shaw LY, Chen Y (2012) Planning of LID–BMPs for urban runoff control: the case of Beijing Olympic Village. Sep Purif Technol 84:112–119

Jia H, Yao H, Tang Y, Shaw LY, Field R, Tafuri AN (2015) LID-BMPs planning for urban runoff control and the case study in China. J Environ Manage 149:65–76

Kang S-J, Lee S-J, Lee K-H (2009) A study on the implementation of non-structural measures to reduce urban flood damage. J Asian Archit Build Eng 8(2):385–392

Kaspersen PS, Ravn NH, Arnbjerg-Nielsen K, Madsen H, Drews M (2017) Comparison of the impacts of urban development and climate change on exposing European cities to pluvial flooding. Hydrol Earth Syst Sci 21(8):4131–4147

Len NLS, Bolong N, Roslee R, Tongkul F, Mirasa AK, Ayog JL (2018) Flood vulnerability of critical infrastructures-review. Malays J Geosci 2(1):31–34

Liao K-H (2012) A theory on urban resilience to floods—a basis for alternative planning practices. Ecol Soc 17(4)
Mentens J, Raes D, Hermy M (2006) Green roofs as a tool for solving the rainwater runoff problem in the urbanized 21st century? Landscape Urban Plann 77(3):217–226
Mohamed WME (2019) Planning and Urban Policies and Mechanisms for Environmental Disasters. Environ Plann Infrast. Cairo. un published
Mojaddadi H, Pradhan B, Nampak H, Ahmad N, Ghazali AHB (2017) Ensemble machine-learning-based geospatial approach for flood risk assessment using multi-sensor remote-sensing data and GIS. Geomatics, Nat Hazards Risk 8(2):1080–1102
NEMO C (2018) How urbanization affects the water cycle. Retrieved from www.waterboards.ca.gov
Nguyen TT, Ngo HH, Guo W, Wang XC, Ren N, Li G, Liang H (2019) Implementation of a specific urban water management-Sponge City. Sci Total Environ 652:147–162
Psomiadis E, Dercas N, Dalezios NR, Spyropoulos NV (2016) The role of spatial and spectral resolution on the effectiveness of satellite-based vegetation indices. Paper presented at the Remote Sensing for Agriculture, Ecosystems, and Hydrology XVIII
Pyke CR, Andelman SJ (2007) Land use and land cover tools for climate adaptation. Clim Change 80(3–4):239–251
Rehan RM (2013) Sustainable streetscape as an effective tool in sustainable urban design. Hbrc J 9 (2):173–186
Saber M, Abdrabo KI, Habiba OM, Kantosh SA, Sumi T (2020) Impacts of triple factors on flash flood vulnerability in Egypt: urban growth, extreme climate, and mismanagement. Geosciences 10(1):24
Santato S, Bender S, Schaller M (2013) The European floods directive and opportunities offered by land use planning. CSC Report, 12
Schanze J (2006) Flood risk management—a basic framework. Flood risk management: hazards, vulnerability and mitigation measures, pp 1–20. Springer
Şen Z (2018) Flood modeling, prediction and mitigation. Springer
Shaw R, Colley M, Connell R (2007) Climate change adaptation by design: a guide for sustainable communities. Town and Country Planning Association
Sutanta H, Bishop I, Rajabifard A (2010) Integrating spatial planning and disaster risk reduction at the local level in the context of spatially enabled government
Tilley E (2014) Compendium of sanitation systems and technologies. Eawag
Types of Flooding in the UK (2018) Retrieved from https://www.cleansafeservices.co.uk/types-of-flooding-in-the-uk/
Wheater H, Evans E (2009) Land use, water management and future flood risk. Land Use Policy 26:S251–S264
Brankovic MD, Protic IB. Bioswales as elements of green infrastructure—foreign practice and possibilities of use in the district of the City of Nis, Serbia
Hamburg: Hamburg University of Technology (TUHH) (n.d.) Detention and Retention Basins. Flood Manager. Retrieved from (http://daad.wb.tu-harburg.de/tutorial/integrated-flood-management-ifm-policy-and-planning-aspects/environmental-aspects/flood-management-interventions/detention-and-retention-basins/)
Underground Storage. Retrieved from https://www.lakesuperiorstreams.org/stormwater/toolkit/underground.html
Zevenbergen C, Bhattacharya B, Wahaab R, Elbarki W, Busker T, Rodriguez CS (2017) In the aftermath of the October 2015 alexandria flood challenges of an Arab city to deal with extreme rainfall storms. Nat Hazards 86(2):901–917
Zhang K, Chui TFM (2019) Linking hydrological and bioecological benefits of green infrastructures across spatial scales—a literature review. Sci Total Environ 646:1219–1231
Zhang J, Hori T, Tatano H, Okada N, Zhang C, Matsumoto T (2003) GIS and flood inundation model-based flood risk assessment in urbanized floodplain. Paper presented at the Proceedings of the International Conference of GIS and Remote Sensing in Hydrology

Chapter 12
Measuring Vulnerability to Flash Flood of Urban Dwellers

Md. Enamul Huq, Zhenfeng Shao, Ahmed Abdullah Al Dughairi, Md. Nazirul Islam Sarker, Cai Bowen, Abdullah Al Mamun, Nayyer Saleem, Akib Javed, and Md. Mahabubur Rahman

Abstract Flash floods are unexpected, localized flood events that occur when an exceptional amount of rain falls happens over a short period of time. In South Asia, it is mostly disastrous, for example, in 2017 flash floods killed approximately 1200 people from India, Nepal, and Bangladesh. However, it is also common in Dhaka megacity, Bangladesh due to its geographic location, monsoon climatic condition

Md. E. Huq (✉)
College of Environmental Science, Hohai University, Nanjing, China
e-mail: enamul.huq@hhu.edu.cn

Z. Shao · N. Saleem · A. Javed
State Key Laboratory of Information Engineering in Surveying, Mapping and Remote Sensing, Wuhan University, 129 LuoyuRoad, Wuhan 430079, Hubei, China
e-mail: shaozhenfeng@whu.edu.cn

N. Saleem
e-mail: saleemnayyer@whu.edu.cn

A. Javed
e-mail: akibjaved@whu.edu.cn

A. A. Al Dughairi
Department of Geography, Faculty of Arabic Language and Social Studies, Qassim University, Qassim Burydah, Kingdom of Saudi Arabia

Md. N. I. Sarker
School of Political Science and Public Administration, Neijiang Normal University, Sichuan, China

C. Bowen
School of Remote Sensing and Information Engineering, Wuhan University, Wuhan, China
e-mail: caibowen@whu.edu.cn

A. Al Mamun
Department of Mechanical Manufacturing Engineering, School of Mechanical and Automotive Engineering, South China University of Technology, Tianhe District, 381 Wushan Road, Guangzhou 510641, Guangdong, China

Md. M. Rahman
Department of Computer Science and Engineering, Bangladesh University of Business and Technology, Dhaka, Bangladesh

T. Sumi et al. (eds.), *Wadi Flash Floods*, Natural Disaster Science and Mitigation Engineering: DPRI Reports, https://doi.org/10.1007/978-981-16-2904-4_12

and surrounding rivers. Though it is impossible to avoid them, the losses and damages of hazards can be reduced effectively by using appropriate techniques. This study aims to determine the responsible factors and measure the household vulnerability to flash flood as a tool of mitigation. The study has been conducted based on primary data. Therefore, data were collected from both slum and non-slum population to cover the entire urban habitats. Data were collected with a structured questionnaire based on five factors (social, economic, institutional, structural, and environmental) of vulnerability to flash flood. The key feature of this paper is to provide an insight into real picture of vulnerability to flash flood for urban habitants. Moreover, this practical approach is useful to quantify hazard-induced vulnerabilities not only for Dhaka megacity but also for other cities of the globe.

Keywords Flash flood · Factors of vulnerability · Urban · Slum · Non-slum · Dhaka megacity

12.1 Introduction

Bangladesh is known as a disaster-oriented country. Various kinds of natural hazards, such as floods, droughts, riverbank erosion, cyclones, and storm surges, occur in Bangladesh almost every year. Geographically, Bangladesh is a low, riparian country characterized by floodplains. For this reason, Bangladesh is exposed to floods as well as flash floods. As a result, the rural and urban areas of Bangladesh are vulnerable to flash flood disasters. Dhaka is the capital of Bangladesh. It is the largest and only megacity in the country. Due to rapid urbanization, the city has evolved into a megacity containing over 10 million people and accounting for 33% of the national urban population (Fakhruddin et al. 2019). Flooding is perhaps the best-known hazard for this megacity (Barua et al. 2016; Braun and Aßheuer 2011). Among other factors, the excessive population and a high number of residents living in slum areas (approximately 43% of the total city population) (Ahmed 2016) have made city dwellers more vulnerable to flash floods. Low socioeconomic status and dilapidated housing conditions are considered the main determinants of vulnerability to flash floods or other hazards. Vulnerability is differentiated socially and geographically. It is recognized that identifying and understanding the factors of vulnerability are imperative for assessing vulnerability (Chen et al. 2019; Huq et al. 2020b; Shao et al. 2020; Zakour and Swager 2018). The vulnerability of a population to large-scale hazards can be reduced by applying disaster management efforts. The measurement of local-level vulnerability is an important tool for identifying households' and local communities' capacities for managing disastrous situations (Adger 2006; Berrouet et al. 2018; Nayyer et al. 2019). Moreover, poor people who have no adequate protective power and insufficient abilities to cope with damage to their belongings and income are the most vulnerable to flash flood disasters (Aroca-Jiménez et al. 2018).

Very few previous documents have measured vulnerability linked to flash floods, and generally pursued fragmented methods in which all the components of vulnerability were not thoroughly measured. Normally, vulnerability analysis exclusively covers the physical (Shah et al. 2018), social extent (Ogie and Pradhan 2019), physical infrastructure, and socioecological dimensions together (Hayes et al. 2019; Pandey et al. 2015). Some studies (Ahsan and Warner 2014; Aroca-Jiménez et al. 2018; Okayo et al. 2015) have included economic factor but within a limited number of indicators compared to the social factor. Subsequently, it is cumbersome to properly present the exact socio-financial framework and spatial differences of vulnerability. Indicators used in vulnerability assessments should comprise various factors that influence people's lives or society's social and financial dimensions. However, the indicator selection of existing studies still lacks these aspects, which leads to errors in vulnerability assessment. Since vulnerability assessment and adaptation are context-specific, they must focus on local socioeconomic and socioecological conditions to explore society's real pictures (Aroca-Jiménez et al. 2020; Kamruzzaman et al. 2020). Ruin et al. (2008) investigated flood exposure in France by connecting key parameters of floods and the vulnerability of victimized society. The authors incorporated several indicators into their vulnerability assessment of flood risk by highlighting dimensions of social life and geophysics. Shrestha et al. (2008) assessed flood vulnerability and pointed out two main dimensions: physical vulnerability and social vulnerability. Recently, Aroca-Jiménez et al. (2020) assessed urban flash floods by developing the integrated socioeconomic vulnerability index (ISEV), which comprises the main key components of vulnerability, including exposure, sensitivity, and resilience. The ISEV index also focuses on the socioeconomic dimension of the urban environment. In another study, de Andrade and Szlafsztein (2018) notably assessed vulnerability to seasonal and flash floods using perceptible and imperceptible elements of the index. Similarly, Pham et al. (2020) assessed vulnerability to flash floods and landslides at the household level in Vietnam. They mainly evaluated the extent of the vulnerability of marginal farmers living in remote areas to the harmful effects of natural hazards. Aroca-Jiménez et al. (2018) proposed a quantitative approach for exploring specific economic factors of flood vulnerability in Castilla y León, Spain.

It is evident from various studies that flash floods cause damage to physical infrastructures such as roads, communication infrastructure, local water supply systems, and housing. Therefore, the inhabitants of urban areas are not free from flash flood risks. However, only a few studies have focused on household vulnerability in urban areas that frequently face flash flooding or on the components and key factors of vulnerability in urban settings. Moreover, household vulnerability indices are not usually focused on or available for flash flood events in urban areas. Therefore, this study aims to identify the factors responsible for creating household vulnerability to flash floods and to reduce the existing or potential vulnerabilities of the slum and non-slum areas in Dhaka megacity.

12.2 Flash Floods in Bangladesh

Flash flood is a common natural hazard worldwide that causes huge damage to assets and life. Flash floods are considered to be among the most serious natural hazards that cause high mortality (>5000 people/year) (Wmo and Gwp 2016). The recent 2019 floods in Bangladesh affected 2.1 million people and killed 104 people across 24 districts (Uddin et al. 2019). Every year, flash floods cover approximately 20.5% of Bangladesh and cause notable damage to livelihoods, assets, property, and lives (Ahmed et al. 2017). In 2014, people gained similar flash flood experiences when floods caused substantial damage to thousands of acres of cropland and forced the migration of 0.5 million people. A flood in 2015 killed 22 people and affected 1.8 million people (Gain et al. 2017). Similarly, floods in 2014 also caused huge damage to the assets and property of 4.6 million people, along with causing a large amount of riverbank erosion (Alam et al. 2020). Generally, heavy rainfall causes flash floods in Bangladesh; flash floods result from heavy rainfall in the hilly areas of Bangladesh and in neighboring countries. Forecasting flash flood events is challenging due to the spatial patterns, areal coverages, and genesis patterns of the events.

Flash floods inundate crops and other possessions. People have very little capacity to protect their crops and other resources. Additionally, affected people have very little knowledge about the adverse health consequences of flash floods. A pilot project was conducted in 2013 in Korchar Haor, Bangladesh, to develop an effective early warning system for flash floods by using a wireless sensor network (WSN) to provide residents of the area with a two-and-a-half to three-hour warning of the imminent arrival of a flash flood (Chowdhury and Hassan 2017).

Due to the topographical position of Bangladesh, conventional flood mitigation measures are not suitable in the country. Flood management practitioners have adopted a few structural approaches, such as establishing embankment and drainage systems, using low-level submersible embankments, evacuating unwanted rainwater, and providing drainage by pumping out accumulated water, to mitigate floods in Bangladesh (Sarker and Rashid 2013). Other strategies, for example, river dredging, reducing sand bars, and repairing river basins and embankments, have also been applied as structural flood management measures. Similarly, urban areas are protected by conventional practices such as constructed embankments and drainage systems, and pump-based drainage facilities (Haque 2016). Households usually build ponds and construct plinths around the banks of these pond as preventive measures against floodwater intrusion. In rural and coastal areas, school buildings and various community buildings are used as flood and cyclone shelters during natural hazards. People can use these shelters to save their lives and property (Chowdhury and Hassan 2017; Rahman and Salehin 2013).

12.3 Methods and Materials

12.3.1 Study Area

Dhaka is purposively selected as an area of study because it is the largest administrative, commercial, and industrial center and the capital of Bangladesh (Bahauddin et al. 2014). A few rivers are located in Dhaka, such as the Buriganga, Turag, Tongi Khal, and Balu Rivers in its southwest, north, and east. Urban floods are a key challenge for urban areas in Asia (Gain et al. 2015). Like other cities, the megacity Dhaka also faces the problem of flash floods. The city is located between the latitudes 23°39' and 23° 54′N and the longitudes 90°20' and 90° 28′E (Fig. 12.1a). The specific study area is located in the northern part of Khilgoan Thana, between latitudes of 23°44' and 23°47′N and between longitudes of 90°24' and 90°27′E. Ward number 03 was selected as the specific study area. The specific studied area is shown in Fig. 12.1b. This part of the city was selected because it is a flash flood-prone area that is not protected by an embankment or dam, and, almost every year, this area faces flash floods.

12.3.2 Climatic Conditions

Dhaka megacity lies in a subtropical monsoon climate zone. The region experiences six different seasons. From May to October, almost every year, Dhaka suffers from heavy rainfall due to a few key reasons, such as winter monsoon weather, early thunderstorms, and the summer season. Dhaka experiences an average of 2000 mm

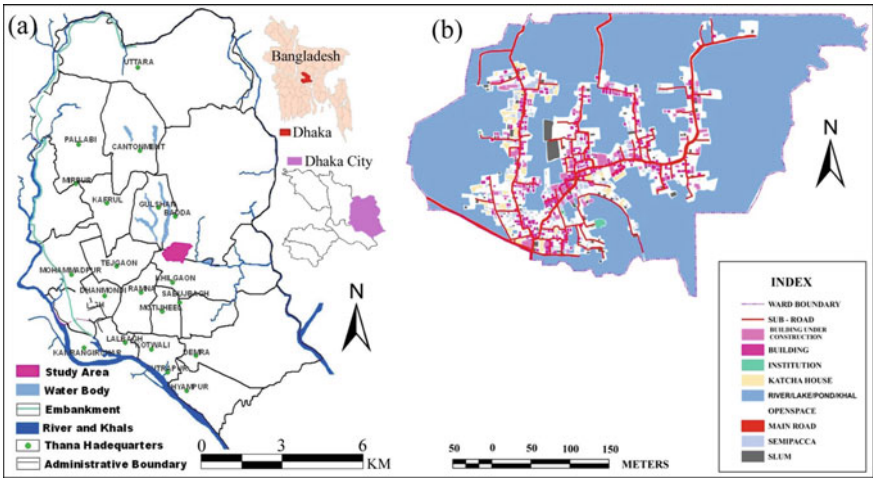

Fig. 12.1 **a** Map of the location of Dhaka megacity and **b** map of the specific study area

of rainfall per year, and 90% of the rainfall occurs from May to October. Heavy downpours are common during the monsoon season. The highest temperatures rise to 42 °C in March and April, and the lowest temperatures reach 5 °C in December and January every year. The monthly precipitation of the area fluctuates from 80 to 130 mm (Rahman and Islam 2019). Table 12.1 shows the detailed climatic conditions of Dhaka megacity.

12.3.3 Frequency of Devastating Floods

Dhaka city dwellers are facing flash floods since long ago, and it is not a new threat for the residents. The city has been facing floods since its early stages. Historical data show that Dhaka city faced heavy floods in 1787 and 1788. During those floods, the streets were so inundated that the city's inhabitants continued their communications by boats within the city (Dewan et al. 2005). Again, in 1833–34, 1870, the 1950s, and the 1960s, Dhaka and its adjacent areas were severely affected by floods. Similar situations occurred in 1954, 1955, 1970, 1974, 1980, 1987, 1988, 1998, 2004, and 2007 due to overflows of the rivers surrounding the city. Dhaka faced catastrophic floods in 1988 and 1998. The flood in 1988 was very remarkable among the floods in recent history due to its devastation; almost 60% of city dwellers were affected in 85% of the area of Dhaka city (Gain et al. 2015; Huq and Alam 2003; Masuya et al. 2015; Rahman and Islam 2019). The main flood-prone areas of Dhaka city are the low-lying areas of Motijheel, Badda, Jatrabari, Khilgaon, Baridhara, Shipahibag, and Sabujbag, where some commercial areas are also regularly inundated. Dhaka is recognized as a moderate- to very high-level flood-prone area. Only a small part (8.04%) of the city is categorized as least vulnerable to flood hazards. On the other hand, 28.70% of greater Dhaka is highly vulnerable to flood hazards (Ahmed 2016). Among that 28.70%, slum dwellers are most vulnerable because they often have low levels of education, economically poor, and living in marginal areas.

12.3.4 Topography and Geological Conditions

Dhaka lies at a low altitude in the Ganges Delta. The ground, which is flat and close to sea level, is characterized by tropical vegetation and moist soils. Dhaka is exposed to floods during the monsoon seasons due to heavy rainfall and cyclones and its position at the southern tip of the Madhapur tract. The city's core geomorphic units are the high terrain of Dhaka, the lowlands or floodplains, and newly built canals (Masood and Takeuchi 2012; Taylor 1849). The town and its surroundings are protected by two unique geological units, namely, Madhupur clays and alluvial accretion from the recent era. The Madhapur clays, which are ancient sediments, exposed due to standard topography and erosion around the city center.

Table 12.1 Climatic conditions of the study area (Khatun et al. 2016)

Parameter	Jan	Feb	Mar	Apr	May	Jun	Jul	Aug	Sep	Oct	Nov	Dec
Average rainfall (mm)	6.5	20.2	52.3	124.0	283	398	391.4	328	264	160	25.3	7.4
Rainy day/m	1	2	4	8	14	19	22	22	16	9	2	1
Temperature												
High (°C)	34.2	36.6	40.6	42.3	40.6	38.4	35.2	35.9	35.3	38.8	33.3	31.2
Low (°C)	5.6	4.5	10.4	15.6	18.4	20.4	21.7	21.0	22.0	10.4	10.6	6.7
Average (°C)	18.8	21.5	26.1	28.7	28.9	28.7	28.7	28.7	28.7	27.4	23.6	19.8
Relative humidity (%)	70.7	66.0	63.0	71.0	79.0	86.0	87.0	863.0	86.0	81.0	75.0	74.0
Evaporation (mm)	104.0	79.0	81.0	77.0	78.0	83.0	87.0	130.0	118.0	106.0	75.0	105.0
Wind velocity (2 km/hr)	2.0	2.0	3.0	5.0	5.0	4.0	4.0	4.0	3.0	2.0	1.0	1.0

Other major topographic features of the city include the low-lying swamplands and marshlands situated within and around the city (Taylor 1840). Three individual bodies are seen at the subsurface level of the sedimentary chain and at a depth of 300 m. The Domitila foundation of the Plio-Pleistocene period, consisting of medium to heavy sands and occasional gravels, is trickily shrouded by Madhupur clays. No surface folding is seen in the structures and lines of the city center. Additionally, N–S, E–W, NE–SW, and NW–SE patterns have been characterized by a significant number of faults and lineaments (Shams 1999; Sufia et al. 2009), which compose the major faults bordering the city.

12.3.5 Data Collection and Analysis

Data were gathered to fulfill the research objectives. Based on the surveyed literature, a questionnaire was created in this research to collect primary data. Before starting the questionnaire survey, a reconnaissance survey was carried out to understand the physical environment, human characteristics, settlement patterns, socioeconomic structures, and disaster history of the study area. During the survey, the real scenarios of the flood-prone lowlands (Fig. 12.2a) housing types (Fig. 12.2b), poor environmental conditions (Fig. 12.2c) and sanitation systems in the slum area (Fig. 12.2d) were captured. A questionnaire was developed for the collection of data after enough theoretical knowledge was obtained about the vulnerability to floods and the factors responsible for flood vulnerability. Then, the questionnaire was modified for the final survey. The factors responsible for flash floods include social factors, economic factors, structural factors, institutional factors, and environmental factors. Data were collected from a total of 300 households through the questionnaire survey. For the survey, the study area was selected purposively, and the surveyed households were selected by simple random sampling.

12.3.6 Sampling Design

Dhaka city and its eastern region were selected purposively. Ward number 3, part of Khilgoan Thana, was also selected purposively. This ward consists of 12,490 households (UNICEF 2009). It was impossible to survey all households in the ward. Therefore, with the ward map (Fig. 12.1b), 145 buildings were selected among the 311 buildings and 30 slum clusters were selected among the total 88 slum clusters by applying simple random sampling methods. The selected 145 buildings and 30 slum clusters contained 960 and 830 households, respectively. Among the total households, the sample size in this study was determined with the Kothari (2004) formula. Then, the households to be surveyed were selected by simple random sampling. The following table (Table 12.2) shows the sampling methods followed in the research.

Fig. 12.2 Pictures of the study area captured during the survey: **a** flood-prone lowlands; **b** housing types; **c**, poor environmental conditions and **d** a sanitation system in a slum area

Table 12.2 Sampling statistics for the study area

Surveyed part	Location	Total number of households	Sample size	% of total households
30 clusters	Slum	830	150	18.07%
145 buildings	Non-slum	960	150	15.62%
Total	**2**	**1790**	**300**	**16.85%**

12.3.7 Determination of Sample Size

There are multiple ways to determine the sample size. Time and money are matters of consideration in this regard. This study's sample size was determined based on Eq. 12.1 (Kothari 2004):

$$n = \frac{z^2 \times p \times q \times N}{e^2(N-1) + z^2 \times p \times q} \tag{12.1}$$

where n = the sample size; N = the size of the population; e = the acceptable error; p = the sample proportion; $q = 1 - p$; and z = the value of the standard variant at a given confidence level.

In the slum area, total population (N) = 830; the acceptable error $e = 0.02$; the sample proportion $p = 0.02$; $q = 1 - \mathrm{p}$; the value of a typical variant for the specified confidence level (95%) was $z = 1.96$; and the sample size, n, was calculated as follows.

$$n = \frac{1.96^2 \times 0.02 \times (1 - 0.02) \times 830}{0.02^2(830 - 1) + 1.96^2 \times 0.02 \times (1 - 0.02)}$$

$$n = \frac{62.495}{0.331 + 0.075}$$

$$\mathbf{n} = 153.928$$

In the non-slum area, the total population (N) = 960; the acceptable error $e = 0.02$; the sample proportion $p = 0.02$; $q = 1 - p$; and the value of a typical variant for the specified confidence level (95%) was $z = 1.96$; sample size, n, was calculated as follows.

$$n = \frac{1.96^2 \times 0.02 \times (1 - 0.02) \times 960}{0.02^2(960 - 1) + 1.96^2 \times 0.02 \times (1 - 0.02)}$$

$$n = \frac{72.283}{0.383 + 0.075}$$

$$\mathbf{n} = 157.832$$

Finally, sample sizes of 150 for both the slum and non-slum areas were determined for the questionnaire survey. The total percentages of the sample sizes relative to the total number of slum and non-slum households were 16.85% and 18.07%, respectively (Table 12.2).

After editing and coding, collected data were given as input to a computer. Then, all the data were analyzed distinctly. The spatial data were investigated with Arc/GIS 9.3, and the temporal data were analyzed using statistical computer software with Statistical Software for Social Sciences (SPSS). Finally, both types of analyzed data were presented as maps, tables, and graphs. Figure 12.3 reveals the main steps of the research methodology.

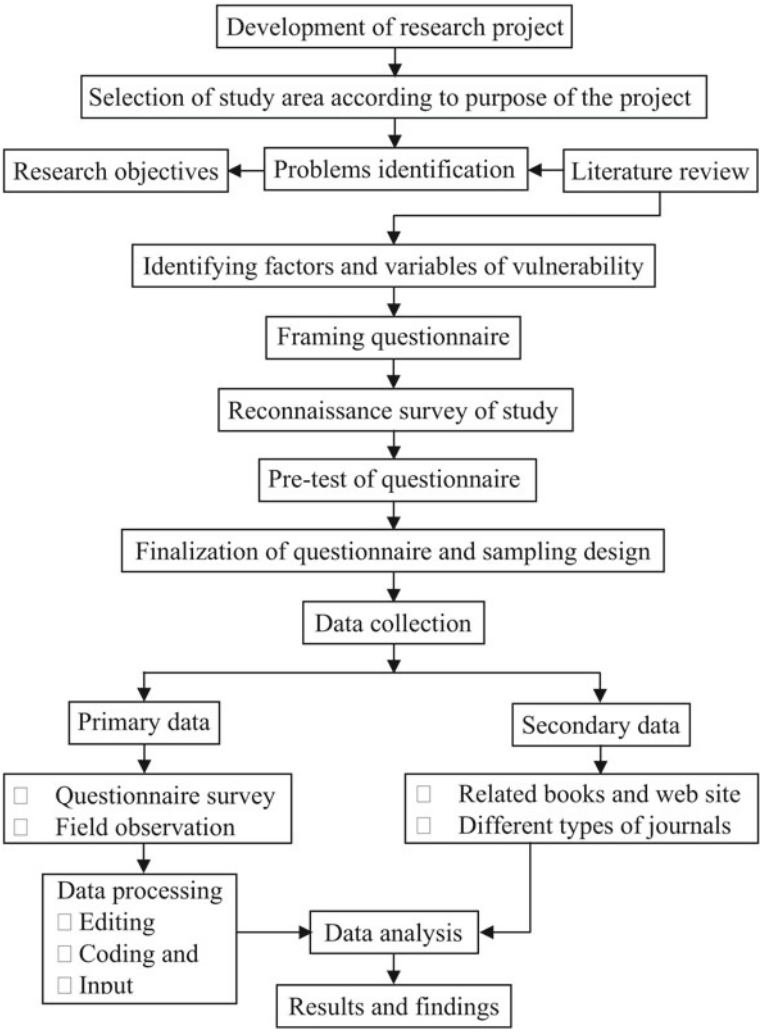

Fig. 12.3 Flow chart of the research methodology of this study

12.3.8 Methods for Vulnerability Mapping

In this study, the five considered factors were assigned weights from 1 to 9 by Saaty's (2008) rating scale (Table 12.3). There is no specific rule for the comparison of factors; therefore, it was considered that the social factor is more important due to its significant consequences for flash floods. Hence, social vulnerability was given a weight of 9. There were five identified factors that affect the vulnerability of a household to flash floods. Economic vulnerability is considered a very much more

important factor for flash floods than structural vulnerability. Therefore, a weight of 7 was allocated for the economic factor, and a weight of 5 was assigned for the structural factor. The environmental factor has less influence on flash flood vulnerability; thus, its weight was defined as 2. Likewise, it was quantified that institutional vulnerability is more important than the environmental factor in influencing household vulnerability to flash floods. A value of 3 was assigned for institutional vulnerability. Table 12.3 exhibits the assigned weights of all factors.

A normalization function (Eq. 12.2) was used to rearrange the factors' vulnerability scores as follows:

$$\text{Normalized output} = \frac{\text{input} - \text{minimal value}}{\text{maximal value} - \text{minimal value}}, \tag{12.2}$$

First, this normalization function was applied to all five factors. The individual factors' median values were used to shift the output away from 0 (Eq. 12.3).

$$\text{Updated variable} = \text{normalized variable} + \text{median of variable}. \tag{12.3}$$

Therefore, all factors had a central tendency near 1. The index was again normalized and multiplied by 100 to obtain an output between 0 and 100.

12.4 Results

12.4.1 Measuring Social Vulnerability

Measuring social vulnerability to flash floods is a vital step for measuring the overall vulnerability of the community. Social vulnerability to flash floods is mostly evident after a hazard event has occurred (de Moor et al. 2018; Dintwa et al. 2019; Emrich and Cutter 2011; Huq et al. 2020a). The aims of measuring social vulnerability are to recognize and understand the populations that are very vulnerable and susceptible to the influences of flash floods.

12.4.1.1 Education and Occupation

Flash floods turn into flood disasters not only due to inundation of the land but also due to the vulnerability of a population based on certain socioeconomic circumstances. Poor education is one of these circumstances that is partly responsible for the flood vulnerability of urban inhabitants. Households with higher-educated members are less vulnerable to flash floods than households including members with lower education levels (Huang et al. 2012; Mavhura et al. 2017). Flash floods are serious natural hazards in Dhaka, Bangladesh. People living in slums in this area also have lower levels of education (Huq et al. 2020b). These low-educated people

Table 12.3 Assigned weights of the influencing factors (Saaty 2008)

No	Theme	Assigned weight
1	Social	9
2	Economic	7
4	Structural	5
5	Institutional	3
6	Environmental	8

1, 3, 5, 7, and 9 indicate equal, more, much more, very much more, and absolutely more important, respectively, while 2, 4, 6, 8 indicate intermediate values. Saaty's pairwise rating scale was followed for this assessment

migrate from villages to the city to seek jobs and better lives. They also mainly rely on informal jobs for their daily foods. As a result, they are extremely vulnerable to the flash floods that commonly occur in the area. Most of the survey respondents in the slum area (approximately 46.7%) had no formal academic education, while 36% of the respondents had primary-level educations, and only 6% of respondents' educational levels were Secondary School Certificate (SSC) or Higher Secondary Certificate (HSC). The remaining 11.3% of respondents' educational qualifications ranged from class five to class ten (Table 12.4). In the surveyed slum clusters, no residents were found to have a bachelor's or master's degree. Table 12.4 also shows that in the non-slum area, approximately half (nearly 48.7%) of the respondents had bachelor's or master's degrees, and 42.7% of the respondents' educational levels were SSC or HSC. Only 2% of these respondents were illiterate, 4% had primary educations, and 2.7% had class-ten educations.

Occupations can be directly related to hazards. For example, some workers become jobless during floods (Huq and Hossain 2012). Paavola (2008) demonstrated that job diversity and different income sources allow people to build stable livelihoods and cope with various risk issues; therefore, with diversified income sources, risks (e.g., those created by flash floods or climate change) could be controlled and recovered easily and quickly. Among the poorest day laborers, construction workers and rickshaw pullers are most vulnerable to flash floods. In slum areas, most people are normally engaged with informal activities such as rickshaw pulling, day labor, petty businesses, and small job services. From the empirical data (Table 12.4), it can be observed that the most common occupation for household heads in the slum area was day labor (approximately 46.0%). These day laborers worked in restaurants, factories, hawking rings, bus drivers, and so on. However, in the studied slum clusters, the occupation of many household heads was rickshaw pulling (approximately 28.7%). Nearly 8.7% of the surveyed household heads had no job, and 10.0% of the household heads were engaged with petty business. The remaining approximately 3% of household heads were homemakers. In the non-slum area, about 50.7% of household heads were engaged with the service sector (government, private, etc.). Of the household heads in the non-slum

Table 12.4 Distribution of respondents' educational qualifications and occupations

Education			Occupation		
Educational qualification	Slum	Non-slum	Type of occupation	Slum	Non-slum
	Percent	Percent		Percent	Percent
			Service	00	50.7
			Business	10.0	32.7
Illiterate	46.7	2.0	Homemaker	2.7	9.3
>1 <5	36.0	4.0	Unemployment	8.7	7.3
>5 <10	11.3	2.7	Rickshaw-puller	28.7	00
SSC and HSC	6.0	42.7	Day-labor	46.0	00
Bachelor and Masters	00	48.7	Housemaid	4.0	00
Total	**100.0**	**100.0**	**Total**	**100.0**	**100.0**

area, 30% were businesspeople, more than 9% were homemakers, and 7.3% were unemployed (Table 12.4). From the above data, an evident discrepancy between the levels of education of people living in the slum area and people living in the non-slum area can be observed. Most of the non-slum habitants were engaged with formal professions. In contrast, few dwellers of the slum area were involved with the formal sector. These low-paying jobs cause residents of the slum area to be more vulnerable to flash flood hazards, and any kind of hazard or disaster, than non-slum people.

12.4.1.2 Gender

Gender inequality was also widespread in the study area, as women normally cannot go outside for earnings. Moreover, women feel unsafe when men temporarily travel to other places, leaving them at home (Kamal et al. 2018). For this reason, women tend to be socially vulnerable due to their social environment. The experimental field observation data showed that the male–female ratio was almost the same irrespective of area. Out of the surveyed people living in the slum area, about 51.9% (based on the questionnaire survey) were male, and 48.1% were female. In the non-slum area, approximately 50.7% (based on the results of the questionnaire survey) were male, and the remaining 49.3% were female (Table 12.5). The vulnerability levels of the residents of studied slum and non-slum areas were almost the same in consideration of gender.

12.4.1.3 Age Structure

Elderly individuals and children are generally considered as vulnerable groups (Cutter et al. 2003). Additionally, some studies have directly used elderly individuals to assess vulnerability because they live alone (Huq and Hossain 2015). The

Table 12.5 Gender distribution of residents of the slum and non-slum areas

Type of household head	Slum		Non-slum	
	Frequency	Percent	Frequency	Percent
Male	387	51.9	322	50.7
Female	359	48.1	313	49.3
Total	**746**	**100.0**	**635**	**100.0**

present study followed the method of Sebald (2010) to show vulnerability due to age. In the Bangladesh context, this study categorized the age groups as 0–18 years, 18–55 years, and above 55 years for both the slum and non-slum areas. From Fig. 12.4, it seems that in the slum area, the active age covered 53.9% of all surveyed household members in slum clusters (based on a questionnaire survey). Of the remaining surveyed individuals, 41.8% were inactive groups (i.e., children) and 4.3% were elderly individuals. Figure 12.4 also shows that in the non-slum area, the dominant age group was the active group, encompassing nearly 58.0% of the total household members; 36.2% were in the inactive group, and the remaining 5.8% were elderly individuals. These age groups are more vulnerable to flood disasters because they are dependent on others. The age group comprising individuals above 55 years is more vulnerable than all other age groups because these individuals are physically unable to move into safe areas during floods and to collect relief from relief distributors. The number of elderly persons was greater in the non-slum area than in the slum area, but the number of inactive people was greater in the slum area (41.8%) than in the non-slum area (36.2%). From this viewpoint, it can be said that people living in slums are less vulnerable than those living in non-slums.

12.4.1.4 Existence of Disable Persons

The presence of a disabled person makes a family vulnerable to hazards. This variable is significantly responsible for creating flood vulnerability because during a flash flood event, sensible and physically fit people cannot move easily. Thus, people with disabilities cannot move to safe places without the help of others. Therefore, disability is a vital cause that can increase the vulnerability of a family. The study found that in the slum area, approximately 20% of households had disabled persons, whereas more than 80% of households did not. In contrast, in the non-slum areas, more than 10% of households contained disable persons, while around 90% of households had no disabled persons (Fig. 12.5).

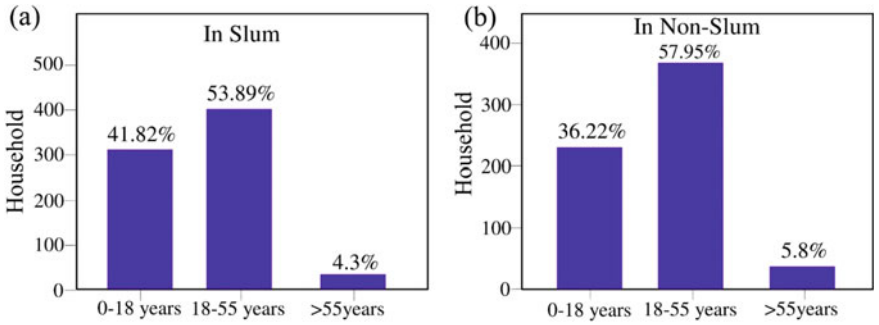

Fig. 12.4 Age structure of the urban inhabitants **a** the studied slum area and **b** the studied non-slum area

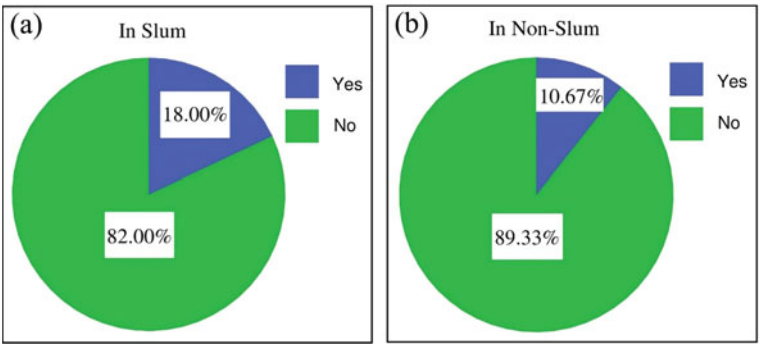

Fig. 12.5 Existence of disable persons in **a** the slum area and **b** the non-slum area

12.4.1.5 Preparation

Low awareness of and preparedness for natural disasters cause vulnerability (Bouzelha et al. 2018). Many criteria can be included to identify the preparedness level of a household or community for facing future flood hazards or any kind of hazard. The present study selected reserves of dry food at the household level to evaluate the preparedness level of the households. Food scarcity is common for slum dwellers because their livelihood resources are very limited (Pham et al. 2019). In Dhaka city, residents of the slum area who have no good jobs and poor access to other resources are faced food scarcities. Table 12.6 shows that in the slum area, most households (80.7%) had no food reserves to consume during a flash flood, and only 19.3% of households kept dry food. In contrast, all inhabitants of the non-slum area (of the surveyed households) kept dry food to consume on disaster days. Most of the slum dwellers were not aware of or prepared for tackling any type of misfortune. Therefore, residents of the slum area are more vulnerable than residents of the non-slum area to the destructive hazards of flash floods or cyclones.

Table 12.6 Reserves of dry food

Reserve status of dry food	Slum		Non-slum	
	Frequency	Percent	Frequency	Percent
Yes	29	19.3	150	100
No	121	80.7	00	00
Total	**150**	**100.0**	**150**	**100.0**

12.4.1.6 Social Network

The ability of a household to recover from a disaster can reduce the vulnerability of the household. Social networks are the main influencing factor that strengthens the adaptive ability of a household (Few and Tran 2010). The power of resilience depends on social or neighborhood networks (Huq 2017). Several organizations help people lead their livelihoods smoothly, such as laborer's unions and women's unions. The members of these organizations can receive useful information associated with current news, such as information on natural disasters (flash floods). Simultaneously, the involvement of residents with these groups also helps them to create closer social bonds with other societies and people, thus, facilitating residents to seek support or help during a crisis. In Dhaka megacity, people mostly receive this kind of assistance from local governmental organizations. This service is not enough, but it has contributed slightly in lessening the impacts of natural hazards on households.

Furthermore, in Bangladesh, particularly Dhaka city, the social network may be an operative channel used to obtain new information and pursue common support, for instance, work sharing. Similarly, people can look for support (getting loans or labor) from their families or neighbors within their communities (Huq and Hossain 2015); this factor was chosen in this study as a criterion used to evaluate the social network of an area. That is, in times of financial emergency, where do residents go for rescue? Social capital refers to mutual support among neighbors, family members' assistance, and widespread social networks. It is a vital safety net that vulnerable households can use to cope with flash floods (Gain et al. 2015). Table 12.7 shows that in the slum area, nearly 40.7% of household heads go to their relatives living in Dhaka to remedy their financial problems. Approximately, one-fourth of household heads (roughly 24.0%) go to their neighbors to solve their financial problems. The remaining 12.7, 4.0, and 11.3% of household heads go to their relatives living beyond Dhaka, to the bank, and to NGOs, respectively. Among the total non-slum households, nearly one-fourth of household heads (around 26.7%) go to their relatives living in Dhaka to meet their financial problems, and more than one-third of household heads (approximately 36.7%) go to their relatives living beyond Dhaka to solve their financial problems. The remaining 3.3, 20.0, and 13.3% of household heads go to their neighbors, banks, and NGOs, respectively, for financial help (Table 12.7). These results demonstrate an interesting matter: very few non-slum dwellers go to their neighbors to solve their financial problems.

Table 12.7 Sources of financial help

Sources of help	Slum		Non-slum	
	Frequency	Percent	Frequency	Percent
Relatives (Dhaka)	61	40.7	40	26.7
Relatives (beyond Dhaka)	19	12.7	55	36.7
Neighbors	36	24.0	5	3.3
Bank	6	4.0	30	20.0
NGO	17	11.3	20	13.3
Local loan agency	11	7.3	00	00
Total	**150**	**100.0**	**150**	**100.0**

The condition of the social network of slum dwellers was found to be much better than that of non-slum dwellers.

12.4.2 Measuring Economic Vulnerability

12.4.2.1 Income

People of different income groups are affected by flash floods (Huq 2013). Additionally, a resident who makes money from different sources holds more adaptive capability than a resident who earns money from limited income sources (Abdul-Razak and Kruse 2017). The incomes of urban dwellers mainly rely on business or formal jobs, not on agricultural farming. Thus, during unexpected flash floods, people can become extremely vulnerable to losses of income and livelihood assets (Kamal et al. 2018). Therefore, to show the vulnerability of slum and non-slum dwellers, this study categorized the income levels of slum and non-slum dwellers differently; to quantify the vulnerability level of each group, the number of classes was uniform. In the surveyed slum areas, the highest monthly household income was 52,000 BDT, and the lowest was 3500 BDT. In the slum area surveyed, nearly 9% of the total samples belonged to the lowest income group, with monthly income values between 3500 and 5500 BDT. The largest number of households' (almost 23.3% of all surveyed households) monthly income values were between 7501 and 9500 BDT, while 16.0 and 14.7% of households' monthly total income values were between 5501–7500 BDT and 11,501–13,500 BDT, respectively. Approximately, 15.3% of households earned more than 15,500 BDT per month. The remaining 14.0 and 8.0% of households had monthly income levels between 9501–11,500 BDT and 13,501–15,500 BDT, respectively (Fig. 12.6). In the non-slum area, the highest monthly household income was 125,000 BDT, and the lowest was 12,000 BDT. The surveyed field data of the non-slum area portrayed that more than one-fourth (approximately 26.7%) of the households had monthly income levels above 42,000 BDT. Around 16.0% of the households' monthly

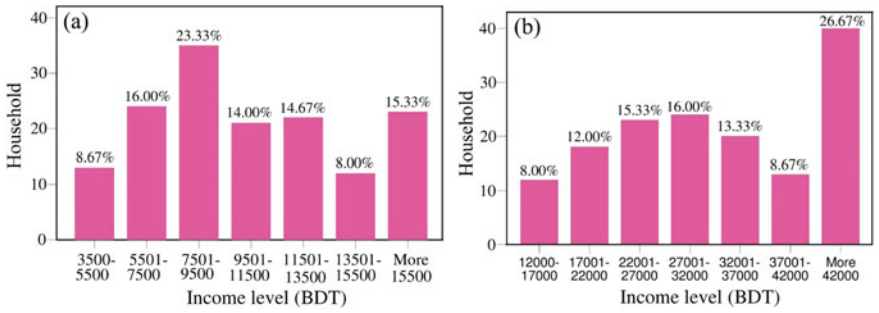

Fig. 12.6 Monthly household income levels

income values were between 27,001 and 32,000 BDT, while 15.3 and 13.3% of the households' monthly income levels were between 22,001–27,000 BDT and 32,001–37,000 BDT, respectively. Approximately, 8.0 and 12.0% of households earned 12,000–17,000 BDT and 17,001–22,000 BDT monthly (Fig. 12.6). It seems that slum dwellers are much more vulnerable to any crisis than non-slum dwellers are in terms of income.

12.4.2.2 Housing Land Ownership and Savings

Land ownership, or the lack thereof, is another factor responsible for creating vulnerability. It is the key aspect affecting the vulnerability levels of different social groups. Land ownership for housing is vital for people to confirm their livelihoods since it is considered one of the basic needs for humans and increases landowners' incentives for investment in long-term development (Amoako and Inkoom 2018). Additionally, owning land is a significant asset that can aid in obtaining a loan from microfinance organizations. Land ownership assists households in ensuring food safety as landowners have wealth to invest. Incidentally, the surveyed households in the slum area had no percentage of land ownership, which is a leading cause affecting their vulnerability levels. Poor urban households often have no land ownership for housing. Thus, these households are highly vulnerable. The surveyed data showed that members of each household in the slum area were living as tenants.

In the non-slum area, only 29.3% of those interviewed, owned their land for housing, while most (approximately 70.7%) did not own land for housing. The majority of those interviewed lived as tenants or in relatives' houses (Table 12.8). Moreover, the savings of a household can be used to determine the power of resilience of the household (Sarker et al. 2020). Usually, slum dwellers cannot afford to keep any savings with which to face future calamity because of their poverty levels. Table 12.8 reveals that in the slum area, only 24.7% of households had savings to face disaster days, whereas most (above 75%) of the households had

Table 12.8 Land ownership (housing)

Status	Slum		Non-slum	
	Land ownership (%)	Savings status (%)	Land ownership (%)	Savings status (%)
Yes	00	24.7	29.3	92.0
No	100.0	75.3	70.7	8.0
Total	**100.0**	**100.0**	**100.0**	**100.0**

no savings to face calamity. Most (approximately 92%) of the non-slum households saved money for the future and kept their savings in various places, such as banks, post offices, NGOs, and with relatives. Only 8% of households in the non-slum area had no savings (Table 12.8). In terms of land ownership, people living in slum areas are more vulnerable than people living in non-slum areas. Inhabitants of slum areas cannot save money due to their economic crises, lack of income sources, and high expenditures.

12.4.2.3 Insurance

Having health, house, flood, or vehicle insurance can reduce the vulnerability of a household to hazards (Dintwa et al. 2019). The serious sickness of a family member is a key concern for the other members of a household because it influences their morale and spirits. Sicknesses also affect a family's economic standing, as sicknesses are unwanted and extensively influence consumption and wages. It has two important financial/economic impacts: extra expenditures for treatment and medical services and income drops owing to labor deficiencies. Sicknesses increase the poverty levels of low-income households and push the household members to poor health due to unforeseen costs.

These consequences cause the exposure of households to natural hazards in developing countries due to these households having almost no health insurance. Those seeking care from the Health Ministry of Bangladesh without health insurance might face significant difficulties and high-cost medical services and health care (Andaleeb et al. 2007). The data obtained from the survey regarding insurance express that the insurance scenarios in the slum area are reversed from those in the non-slum area. In the slum area, only 19.3% of households had insurance, while 80.67% had no insurance. Here, insurance means any type of insurance in any format, including health insurance, vehicle insurance, fire insurance, etc. In the non-slum area, a greater number (almost 72.7%) of households had insurance, and the remaining 27.3% had no insurance (Fig. 12.7). It can be concluded that slum dwellers have poor savings and insurance levels due to their poverty levels. Many members of the population living without health insurance or any other type of insurance causes the community to be highly vulnerable to flash floods.

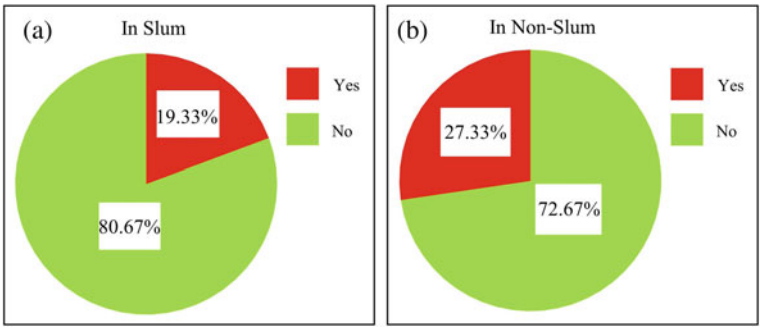

Fig. 12.7 Insurance statuses for **a** individuals living in the studied slum area and **b** those living in the studied non-slum area

12.4.2.4 Vehicle Ownership

In hazardous and disastrous situations, cars or other vehicles are very useful for relocating from a dangerous place to a safe place. Those who own a vehicle that can be used for moving makes them less vulnerable than those who have no personal vehicle. Therefore, the present study selected ownership of vehicle as a variable of vulnerability. The surveyed empirical data show that in the slum area, most (almost 88%) of the surveyed household heads did not own vehicles, and only 12% of households had bicycles or rickshaws. In the non-slum area, most (about 57.3%) of the households had no vehicle, while approximately 32% had motorcycles. The remaining 7.3 and 3.3% of households had private cars and bicycles, respectively (Table 12.9). Due to the unavailability of vehicles, both slum and non-slum habitats are vulnerable to flash floods.

12.4.3 Measuring Structural Vulnerability

Structural factor also affects the vulnerability of people to flash floods. The types of housing, shelter availability, road networks, transportation systems, existing evacuation roads, embankments to protect from floods, drainage density, and

Table 12.9 Ownership of vehicles

Types of vehicle	Slum		Non-slum	
	Frequency	Percent	Frequency	Percent
Motorcycle	00	00	48	32.0
Private car	00	00	11	7.3
Bicycle	18	12.0	5	3.3
Nothing	132	88.0	86	57.3
Total	**150**	**100.0**	**150**	**100.0**

geographical positions in an area are typically considered to be variables/indicators of structural vulnerability. Four key variables: housing types, shelter availability, road networks, and transportation systems were selected in this study to assess the structural vulnerability of households to flash floods in Dhaka megacity.

12.4.3.1 Housing Quality

Housing quality is one of the most important variables of structural factors. It can increase or decrease the level of flash flood vulnerability of a household. The structure of a house and its physical location significantly influence to spread of the hazard impacts. For example, households located along rivers are susceptible to flash floods (Adelekan 2011). A building can be situated in a flash flood hazard zone, but developing its structure can reduce its vulnerability (Zakour and Swager 2018). The surveyed data show that approximately 75.3% of slum households lived in kutcha[1] houses, while only 24.7% lived in semi-pucca[2] houses. Figure 12.8a, b shows the housing types in the study area. Table 12.10 reveals that no surveyed residents in the non-slum area lived in semi-pucca or kutcha houses. All the surveyed residents of the non-slum area were living in pucca[3] houses. It is obvious that fragile housing types make slum dwellers more vulnerable to flash floods. The findings of Braun and Aßheuer (2011) revealed that approximately 50% of respondents narrated a flash flood that hit them severely and reached above 2.5 feet inside their living rooms. Their residences remained inundated with floodwaters for half a month. Moreover, the floodwaters remained adjacent to their homes for nearly a month.

12.4.3.2 Sheltering During Flash Flood Events

The sheltering system is another variable responsible for influencing vulnerability. People who go to shelters during flash floods are less vulnerable than those that do not. The government and NGOs provide sheltering facilities. Therefore, the people who go to these shelters are much more secure than those who do not. The field data disclose that more than 55% of slum households have gone to shelters during floods, while 44.7% of households have not gone to shelters during floods. Only approximately 24% of non-slum household members went to shelters during a catastrophic flood, such as the 1998 flood, and the remaining 76% of household members did not go to shelters during floods (Fig. 12.9). Braun and Aßheuer (2011) also found that almost 50% of surveyed households were compelled to give up their homes and take shelter in government schools on elevated roads, or at

[1]Walls made by tin, lightwood, bamboo or plastic; straw or tin roof materials.

[2]Walls made by brick of metallic structure; tin roof material.

[3]Walls made by brick; concrete slab or cement tiles roof materials.

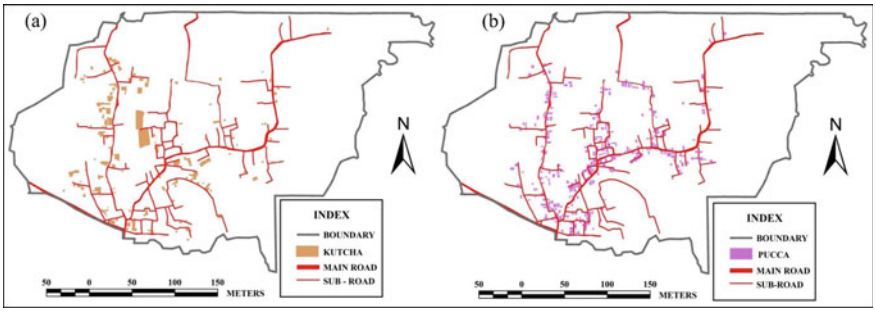

Fig. 12.8 **a** Kutcha houses and **b** pucca houses in the study area

Table 12.10 Housing type of study area

Housing type	Slum		Non-slum	
	Frequency	Percent	Frequency	Percent
Pucca	00	00	150	100
Semi-Pucca	37	24.7	00	00
Kutcha	113	75.3	00	00
Total	**150**	**100.0**	**150**	**100.0**

relatives' houses or dams. Sheltering places do not always provide better facilities than housing; this is why non-slum dwellers are reluctant to go to shelter places. Slum dwellers keep fewer assets in their houses and thus can move easily in disastrous situations and go to sheltering places.

12.4.3.3 Road Network

Road networks play a great role in affecting household vulnerability to flash floods. With a dilapidated road network, people cannot move easily in a normal situation. The study area's road network is not good (Fig. 12.10a); the existing roads are narrow and clumsy. Additionally, in the slum area, approximately 52.7% of respondents thought that their locality's existing road network was not good. Above 30% of the total respondents mentioned that the road network was good. More than 16% of respondents believed that the area's road network was very bad (Fig. 12.10b). However, approximately 41.3% of respondents in non-slum areas noted that the existing road network was not good because they lived away from the main roads. In contrast, 52.7% of respondents lived near the main road, so they thought that the existing road was good, and the remaining 6% of respondents indicated that the existing road network was very bad (Fig. 12.10c).

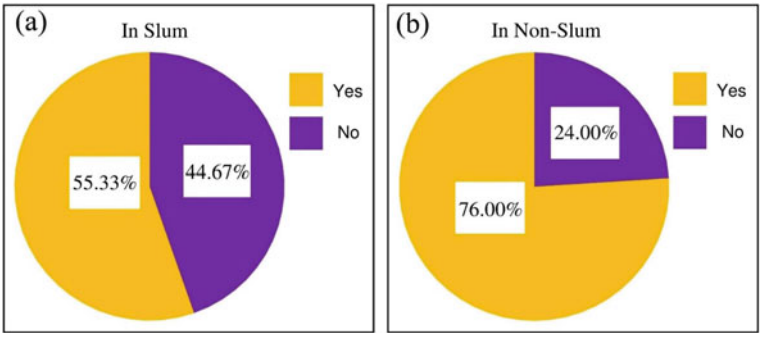

Fig. 12.9 Sheltering during floods: **a** the percentage of people living in the studied slum area who went to shelters during flash floods; **b** the percentage people living in the studied non-slum area who went to shelters during flash floods

12.4.3.4 Transportation System

The transportation system is another significant structural variable affecting household vulnerability to flash floods. Table 12.11 exhibits that 47.3% of respondents living in the slum area thought that the transportation system was not good, although more than 35% of respondents thought that the transportation network was good. Only 17.3% of respondents believed that the transportation system was very bad. Nearly 62.7% of those interviewed in the non-slum area felt that the transportation system was good, but 30% believed that the transportation system was not good. The remaining 7.3% of respondents indicated that the transportation system was very bad (Table 12.11). Due to the uneven road network and poor transportation services, people living in both the slum and non-slum areas are vulnerable to flash floods.

12.4.4 Institutional Vulnerability

The institutional setup of a community can significantly influence the vulnerability of the community to flash floods (Huq 2017). The presence of an emergency management committee can help to reduce vulnerability during a disastrous situation. The major institutional vulnerability factors are early warning systems, services for emergency situations, and governance. In this study, only two variables (aid during floods and warning before floods) were considered when estimating people's vulnerability levels to flash floods.

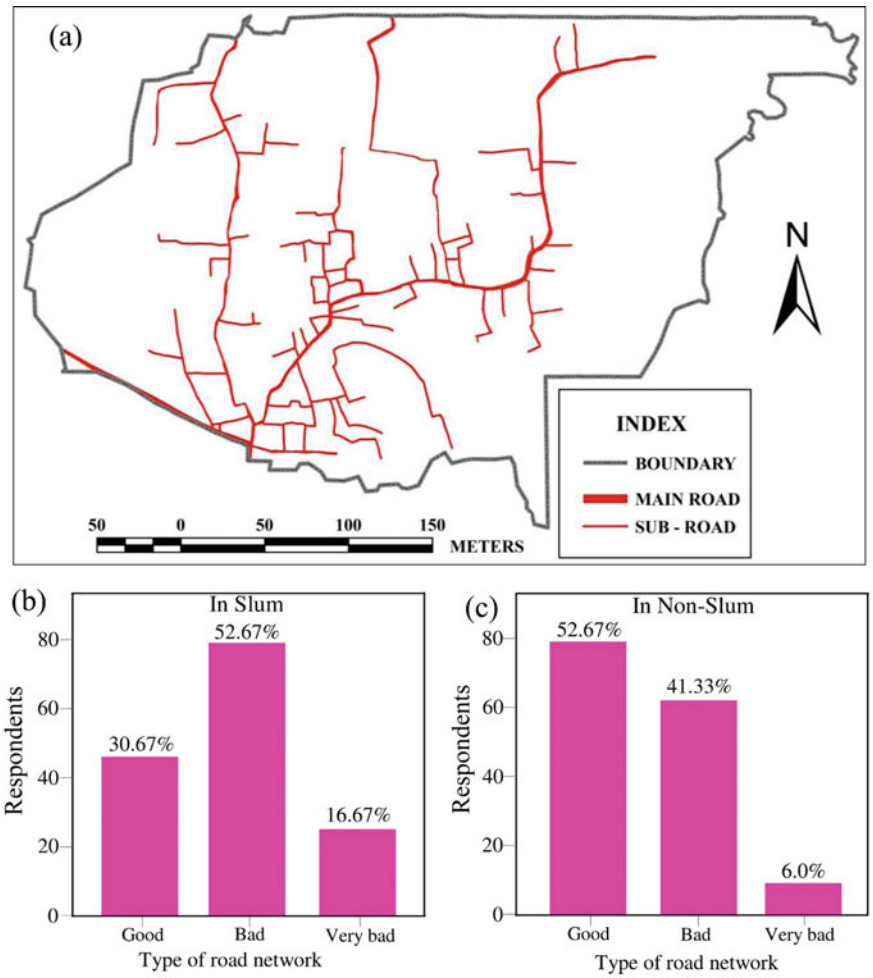

Fig. 12.10 **a** Condition of the road network in the study area; **b** and **c** respondents' opinions about the road network in the study area

Table 12.11 Condition of the transportation system

Transportation system	Slum		Non-slum	
	Frequency	Percent	Frequency	Percent
Good	53	35.3	94	62.7
Not good	71	47.3	45	30.0
Very bad	26	17.3	11	7.3
Total	**150**	**100.0**	**150**	**100.0**

12.4.4.1 Aid During Flash Flood Events

Flash flood-affected households receive help from different kinds of governmental and nongovernmental organizations. Middle-earning households are considered more often because they are unwilling to accept aid/relief, unlike people experiencing poverty who do not hesitate to obtain relief from the government and NGOs. In addition, during the questionnaire survey, the local people claimed that the flood relief programs were not distributed accurately, and even wealthy people were nominated for relief by local leaders who were associated with the regent government party (Kamal et al. 2018). The field data (Fig. 12.11a) show that among the surveyed slum households, most of the households (approximately 72.7%) did not receive any aid during flash floods because they were not able to go to the place where the relief was distributed. The rest of surveyed households (only 27.3%) received help. A greater number of households (almost 62%) in the non-slum area did not receive help (Fig. 12.11b). Because the relief distribution was not sufficient, it was impossible to provide aid to every affected family. Therefore, the majority of households did not receive help during floods; the remaining 38% of the total households in the non-slum area received help during floods. Nevertheless, the aid amounts distributed were very small. As a result, almost all households (who received help) were dissatisfied with the help.

12.4.4.2 Warning Before Flash Flood

To reduce household vulnerability to flash floods, early warning systems are essential. Flash floods can destroy many lives and assets within a few hours, but if the respective authority can provide timely forecasts of flash floods, the loss of lives can be reduced and asset damage can be condensed. Table 12.12 reveals that of the respondents living in slums, the majority (nearly 62.7%) were not given forecasts before flash flood events. These respondents had low awareness and insufficient electronic devices (television, radio) that can provide information about flash floods. In comparison, 24% of respondents received forecasts 1–3 days before flood events. Only 10.7 and 2.7% of respondents received forecasts 4–6 days before and more than six days before a flood event, respectively. A total of 16.7% of those living in non-slum areas did not receive any warning before flash floods occurred, while approximately half of the respondents (about 48%) received forecasts 4–6 days before floods occurred. The remaining 32.7 and 2.7% of respondents were warned about flash floods 1–3 days before and more than six days before the floods occurred, respectively (Table 12.12). The results show that slum dwellers are institutionally much more highly vulnerable than non-slum dwellers.

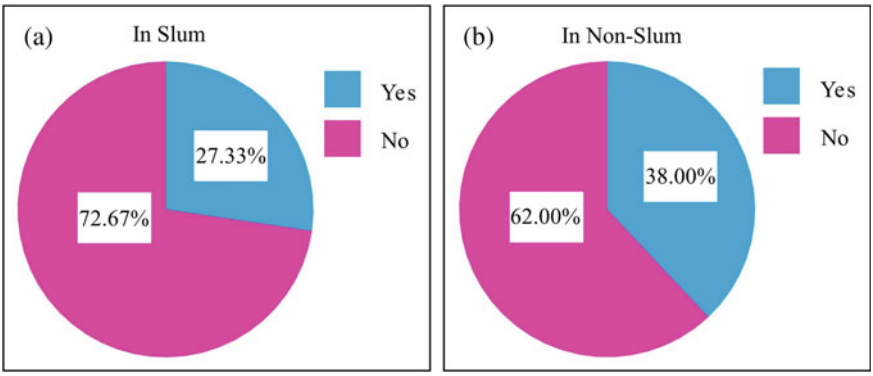

Fig. 12.11 Aid during flood events for **a** those living in the studied slum area and **b** those living in the studied non-slum area

Table 12.12 Warnings received before flash flood events

Timing of warning	Slum		Non-slum	
	Frequency	Percent	Frequency	Percent
None	94	62.7	25	16.7
1–3 days before	36	24.0	49	32.7
4–6 days before	16	10.7	72	48.0
More than 6 days before	4	2.7	4	2.7
Total	**150**	**100.0**	**150**	**100.0**

12.4.5 Measuring Environmental Vulnerability

Sanitation problems are major environmental concerns for city dwellers. Very few households in the studied city area enjoy water supply facilities. Poor drainage systems and sanitation can amplify the flash flood vulnerability levels of people living in the city. Floods can contaminate water and damage water pipes, tanks, and pump equipment (Mavhura et al. 2017). This study considered only sanitation and water supply to evaluate Dhaka megacity inhabitants' flash flood vulnerability levels.

12.4.5.1 Sanitation

If a household contains a fragile or poor sanitation system, the household can be easily affected by floods because floodwater can abolish weak systems easily. There are shortages of potable water in the study region during and after long floods. Sanitation and hygiene services are similarly influenced by floods, as broken

sanitation systems expand pollutants into surface water, which is usually used for showers and other domestic purposes (Richmond et al. 2018). Slum dwellers commonly use communal toilets, twin-pit toilets, and pit latrines. Hanging toilets still exist in some slum clusters. The surveyed data show that approximately 80% of the slum households used communal[4] sanitary latrines, whereas 5.3% had no toilet facilities, and the remaining 15.3% of households used hanging toilets (Table 12.13). Around 77.3% of non-slum inhabitants used twin-pit toilets, 13.3% of households used single-pit[5] toilets, and the remaining 9.3% of households used both single-pit and twin-pit lavatories (Table 12.13). This kind of hanging toilet can be easily affected by flash floods and, as a result, might threaten the water supply due to pollution. Additionally, due to damage to their toilets incurred during floods, the surveyed slum dwellers defecated in floodwaters, which is, in fact, harmful to human health. Slum dwellers might be easily affected by contaminated floodwaters in terms of sanitation facilities.

12.4.5.2 Water Facility

Water pollution is another environmental problem for city dwellers. The capability of residents to access hygienic drinking water is an important feature affecting vulnerability to flash floods or any other natural calamities. Moreover, the lack of water resources is another barrier preventing poor people from adapting during floods (Masciopinto et al. 2019). The formal organization (the city corporation) is the most commonly stated water supplier in the community, as residents have low and poor access to this service. Table 12.14 reveals that in the studied slum area, more than half of households (nearly 53.3%) used supplied water for drinking, and approximately one-fourth of households drank boiled water. The remaining 17.3 and 4.0% of households used tap and filtered water, respectively, for drinking. Most (almost 69.3%) household members in the studied non-slum areas drank boiled and filtered water, and the remaining 12.0 and 18.7% of habitants drank only boiled water and filtered water with a high-quality filter, respectively (Table 12.14). Drinking supplied and tap water causes the residents of slums to be vulnerable to water-borne diseases.

12.4.6 Spatial Map of Vulnerability

To evaluate flash flood vulnerability and the intensity and frequency of flood hazards (Hung et al. 2016), vulnerability maps of floods, exposure, and disaster risk reduction (Adnan et al. 2020; Tapsell et al. 2010) have been produced in previous

[4]Toilets were used by several households.

[5]The commode is considered as a single pit toilet.

Table 12.13 Sanitation coverage in the study area

Slum		Non-slum	
Toilet type	Percent	Toilet type	Percent
Communal sanitary latrine	79.3	Twin-pit	77.3
No toilet	5.3	Single-pit	13.3
Hanging	15.3	Single + twin-pit	9.3
Total	**100.0**		**100.0**

Table 12.14 Types of drinking water in the study area

Slum		Non-slum	
Type of drinking water	Percent	Type of drinking water	Percent
Filtered	4.0	Filtered	18.7
Boiled	25.3		
Tap	17.3	Boiled	12.0
Supply	53.3	Boiled + normal filter	69.3
Total	**100.0**		**100.0**

studies. Not only flash flood events are responsible for flood disasters; socioeconomic, structural, institutional setup, and environmental conditions also influence flood disasters. In the study region, most households in the slum area were, structurally, very highly vulnerable to future flash floods. Uneven road networks and poor transportation services cause residents living in both slum and non-slum areas to be vulnerable to flash floods. Most slum inhabitants were not aware of or prepared to address any misfortunes. Therefore, people living in slums were more vulnerable to sudden flood hazards than those living in non-slum. The present study demonstrates that most slum inhabitants are socially vulnerable to flash floods, but very few non-slum inhabitants are socially vulnerable to flash floods. Economic factor has a dominating role, influencing people's vulnerability levels to flash flood hazards. Remarkably, the institutional vulnerability levels of people living in slums and non-slums were similar because residents of both areas live under the same institutional framework and consider the issue of institutional vulnerability virtually useless in their regular lives compared to higher-priority economic factors. The environment has great importance for humans, but slum inhabitants live in environmentally risky areas. Slum dwellers might easily be affected by contaminated floodwater in terms of sanitation facilities. In contrast, non-slum inhabitants are environmentally more secure.

The goal of this study is to assess urban households' flash flood vulnerability levels, representing people's vulnerability to flash floods in Dhaka megacity. The map of the spatial vulnerability of residents to flash floods was developed via the aggregation of all vulnerability factors. Figure 12.12 shows that inhabitants of the middle portion of the study area are highly vulnerable to flash floods. The majority

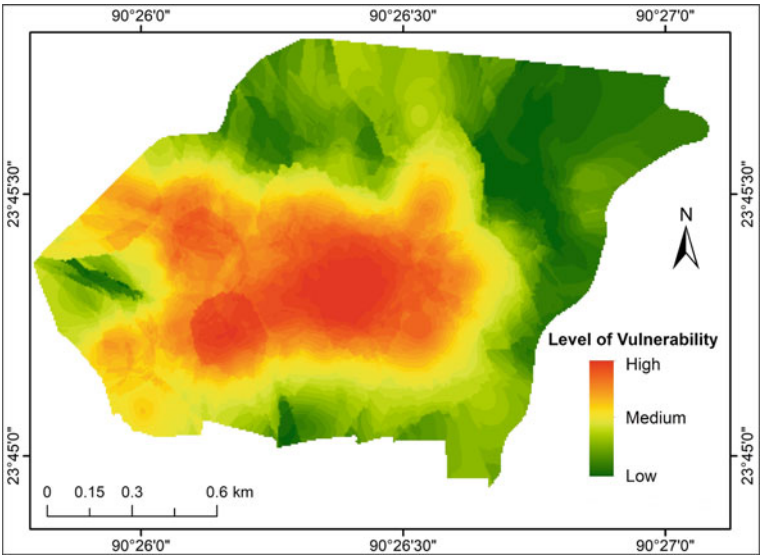

Fig. 12.12 Overall household vulnerability of urban people to floods (based on Huq et al. (2020c))

of people in the study area are moderately vulnerable. Northeastern residents are less vulnerable to future floods than residents in other areas. The vulnerability maps were derived from the household survey data and prepared with a fixed spatial vulnerability scale. Therefore, the maps do not symbolize the individual attributes of inhabitants.

12.5 Discussion

Certainly, flash flood is a key problem for the residents of Dhaka city. Most people are anxious about flash floods because during these crises, they have limited access to essential needs, such as food, potable water, and shelter. During and after flood events, finding a dry place to sleep, drying clothes, drinking water, making money, continuing jobs, and accessing food become difficult. Not only flash flood events are responsible for flood disasters; socioeconomic, structural, institutional setup and environmental conditions are also responsible for influencing these disasters. The present study demonstrates that most slum inhabitants are highly socially vulnerable to flash floods due to various social causes, such as poor educational quality, insecure jobs, large family size, and gender influence. On the other hand, the high educational quality, formal professions, and small families of non-slum dwellers cause very few residents of the studied non-slum area to be socially vulnerable to flash flood hazards. The lower educational quality of the slum habitants amplifies

their vulnerability to flash floods. The non-slum inhabitants are less vulnerable than slum dwellers due to educational quality (Table 12.4). Due to their low educational quality levels, most slum dwellers work as day laborers and thus cannot switch over their occupations in disastrous situations. This is the vital cause of their high vulnerability levels. Considering occupation, in the slum area, most of the household heads work as day laborers or rickshaw pullers. Therefore, when flash floods occur, the day laborers and rickshaw pullers are affected first. Alternatively, those living in the non-slum area are engaged with service and business (Table 12.4). For this reason, the non-slum inhabitants are less vulnerable than slum dwellers are in terms of occupation.

Age plays a large role in intensifying flood vulnerability. Both the slum and non-slum areas are dominated by the working-age group (average 55.95%), but percentage of the dependent age groups is not negligible (Fig. 12.4). The preparation levels of the slum dwellers are insufficient; approximately 80.7% of households did not have sufficient preparations to face flash floods. As a result, flash floods can attack them easily. Almost all households of the non-slum area kept dry foods to face disastrous situations (Table 12.6), which makes them less vulnerable to these situations than slum dwellers are. Immediate recovery power can minimize the vulnerability of people to flash flood events. The power of resilience depends on the presence of networks within social systems or neighborhoods. The social networking of slum dwellers is better than that of non-slum dwellers. A great number (40.7%) of those living in slum area households go to their relatives living in Dhaka for help, while only 26.7% of non-slum residents go to their relatives living in Dhaka for help. Interestingly, only 12.7% of those in slum households go to their relatives living beyond Dhaka, whereas a large (36.7%) number of those in non-slums go to their relatives living outside Dhaka to solve their financial problems (Table 12.7). Water-borne sicknesses, flooding in workplaces, or the inability to reach workplaces may take place due to flooded roads; these were the key causes of the inability of people to carry on their jobs during flash flood events. These events significantly influence income loss for most households. Since approximately half of the surveyed households did not save money or reserve food, several families were faced with extreme trouble and could not afford food and medicine during flood events.

Economic factor has a significant role in affecting people's vulnerability levels to flash flood hazards. This study shows that most slum community households are, economically, very highly vulnerable due to their low-income levels. No slum dwellers surveyed in this study area owned any land. A large number (75.3%) of households in the slum area kept no savings with which to face future floods or any kind of calamity (Table 12.5). More than 80% of households did not have any kind of insurance with which to defend against disasters (Fig. 12.7). The results of Vo (2016) recommended that enhancement of insurance registration amount is very important for reducing household vulnerability. The results of this study support the findings of Vo (2016). In the non-slum area, only 8% of households were, economically, considered to be under very highly vulnerable conditions. Because, only 8% of the total monthly income levels of the households were between only 12,000

and 17,000 BDT, and approximately 8% of the households had no savings (Fig. 12.6 and Table 12.8). In consideration of insurance, non-slum inhabitants had better positions than slum dwellers. Slum dwellers were found to be in highly vulnerable conditions due to their low-income levels. It was found that most people from flash flood-affected regions were engaged with informal jobs. These low-diversified livelihoods cause residents to be more vulnerable to flash floods. The outcomes of the current study are consistent with those of other studies (Kamal et al. 2018). The loan status of the surveyed residents was good because most (about 56%) households in the slum area had no loans; however, other economic supports, such as land ownership, savings conditions, insurance, and vehicle ownership, were found to be very poor.

Structural components were also responsible for raising or lowering people's flash flood vulnerability levels. In Dhaka megacity, most households in the slum areas are structurally very highly vulnerable to future flash floods. The empirical data show that the housing conditions of slum dwellers are very poor. The largest portion (around 75.3%) of the total surveyed slum area residents live in kutcha houses. In the non-slum area, almost all (approximately 100%) of the inhabitants live in pucca houses (Table 12.10). Additionally, Few and Tran (2010) noted that household structure and household location are also important issues affecting the preparation for and prevention of hazard events. According to most respondents' statements, their locality's road network and transportation system were not good (Fig. 12.10 and Table 12.11). This makes these populations vulnerable to flash floods because they cannot move to a safe place easily during floods. Most of the victims of flood events living in non-slum areas stay at their own affected houses due to worries about their existing property being stolen.

The present study reveals that slum and non-slum residents are mostly vulnerable to flash flood hazards due to inadequate institutional facilities, as the majority of households in slum and non-slum areas (about 72.7% and 62%, respectively) do not receive any help or relief (e.g., food, drinking water, medical facilities) from the government or NGOs during flash floods (Fig. 12.11). Early warning system is considered as an important tool for reducing the impacts of disasters. Only few slum and non-slum dwellers reported obtaining early warnings before flash floods (Table 12.12). The survey results of Kamal et al. (2018) showed that only 7.5% of households obtained weather forecasts and attempted to take essential preparation measures for impending flash floods. Approximately 65% of households did not initiate for protection or preparation measures for potential flash floods. Most people were not aware of effective preparation measures that can be taken to save themselves and avoid losses resulting from flash floods. However, some inhabitants took preparation measures, such as establishing house structures, keeping reserves of dry food, and saving money.

Environmental factor also can intensify the flash flood hazard. The analytical result revealed that most households (about 64.7%) of the slum are very highly vulnerable to environmental conditions. Because, most of the households of slums use the communal toilet (Table 12.13). A maximum of non-slum inhabitants is moderately vulnerable in terms of environmental conditions. The analytical data

show the majority (roughly 77.3%) households of non-slum use twin-pit type toilets (Table 12.13). In the slum and non-slum area, none of the households uses tube-well water for their daily activities. The household survey results of Pham et al. (2020) demonstrated that nearly 90% of the community uses natural water for drinking and household purpose. Thus, it makes them vulnerable to health-associated issues due to poor food quality and water safety, and water-borne illnesses are related to water pollution during the flood.

12.6 Vulnerability Reduction

The present study recommends an inclusive array of strategies that should be implemented or considered to reduce vulnerability in Dhaka megacity. It is essential to raise people's education levels with free or low-cost educational institutions. Simultaneously, the local government needs to assist people by establishing professional training, for instance, in handcrafts. This might help them increase the income of inhabitants, thus, assisting them in escaping from poverty. The local and central governments can also inspire inhabitants via various measures, such as making and protecting strong dams along rivers, improving potable water quality, building water reservoirs, introducing water treatment plants, providing flash flood early warning systems, and developing infrastructure. Finally, financial assistance must also be provided during flash floods. The following options could be considered to reduce city inhabitants' vulnerability levels and lessen the damage derived from physical, social, institutional, and economic phenomena during flash flood events.

- To undertake a maximum range of communal contributions, invaded communities should be empowered to reduce their vulnerability.
- To reduce economic vulnerability, we need to create different economic activities and income sources for city dwellers.
- Women are often identified as a group that is highly vulnerable to flash flood hazards, so women should be considered a target group in disaster-related programs.

To allow urban areas to become less vulnerable to flash flooding, the following measures should be considered:

Options	Possible measures for reducing flash flood vulnerability levels in urban areas
Threshold ability (damage inhibition)	– Construction of dams – Enhancing river volume – Underground floodways – Improving urban drainage density – Reducing stormwater runoff
Coping ability	– Emergency strategies and timely flash flood warnings

(continued)

(continued)

Options	Possible measures for reducing flash flood vulnerability levels in urban areas
(damage reduction)	– Better communication with inhabitants – Elevated major infrastructure and buildings – Flash flood-proof infrastructure and buildings
Recovery ability (damage reduction)	– Insurance – Emergency funds – Forming flash flood relief organizations
Adaptive ability (damage reduction)	– Integrating flash flood management and spatial planning – Floodplain zoning – Socioeconomic problem subsidies

12.7 Conclusions

Flash flood is a very common and familiar issue in Bangladesh. Dhaka city is not free from the impacts of flash flooding. Residents of slums commonly have low levels of education and are financially poor. Normally, these residents reside in marginalized zones that are in bad conditions and sometimes located in risky areas. Thus, these populations are most vulnerable to flash floods. From the current study's findings, it is obvious that slum inhabitants are more vulnerable to flash flood hazards than non-slum inhabitants are. This study focused on measuring the levels of people's vulnerability to flash flood hazards in urban areas. There is an urgency to conduct more research on this key issue while focusing on residents of slum and non-slum areas in other cities. Paying more attention to the relative importance of various factors, such as social, economic, structural, institutional, political, geographic, and environmental factors, would allow the specific nature of people's vulnerability levels to different hazards to be measured.

There are two kinds of floods in Dhaka megacity: river floods/annual floods and flash floods resulting from heavy rainfall events. In the current study, only flash floods were considered. Risk comprises three components, vulnerability, exposure, and hazard, but this study covers only vulnerability. In future studies, analyses of river floods/annual floods can be conducted while including all the risk components. Secondary data was not available for this study. Parameters/factors are important tools used to assess vulnerability, but identifying these variables is a complex process that requires adherence to certain quality criteria. This study surveyed only 300 households, an estimated 16.85% of the total population. To mitigate hazards and reduce vulnerability, regular action is needed over a large spatial scale.

This study was exclusively limited to only flash flood-oriented areas. To evaluate vulnerability to flash floods, five factors of vulnerability were applied; other factors could not be applied due to data unavailability. Further studies including other

factors of vulnerability can be conducted. Further research should be conducted incorporating spatial data for the mapping of vulnerability levels in Dhaka megacity and other cities.

References

Abdul-Razak M, Kruse S (2017) The adaptive capacity of smallholder farmers to climate change in the northern region of ghana climate. Risk Manage 17:104–122

Adelekan IO (2011) Vulnerability assessment of an urban flood in Nigeria: Abeokuta flood 2007 Natural Hazards 56:215-231

Adger WN (2006) Vulnerability. Global Environ Change 16:268–281

Adnan K, Ying L, Sarker S, Yu M, Eliw M, Sultanuzzaman M, Huq M (2020) Simultaneous adoption of risk management strategies to manage the catastrophic risk of maize farmers in Bangladesh. Geo J

Ahmed I (2016) Building resilience of urban slums in Dhaka, Bangladesh. Procedia Soc Behav Sci 218:202–213

Ahmed MR, Rahaman KR, Kok A, Hassan QK (2017) Remote sensing-based quantification of the impact of flash flooding on the rice production: a case study over northeastern Bangladesh. Sensors 17:2347

Ahsan MN, Warner J (2014) The socioeconomic vulnerability index: a pragmatic approach for assessing climate change led risks—a case study in the south-western coastal Bangladesh. Int J Disaster Risk Reduct 8:32–49

Alam A, Ahmed B, Sammonds P (2020) Flash flood susceptibility assessment using the parameters of drainage basin morphometry in SE Bangladesh. Quat Int

Amoako C, Inkoom DKB (2018) The production of flood vulnerability in Accra, Ghana: re-thinking flooding and informal urbanisation. Urban Studies 55:2903–2922

Andaleeb SS, Siddiqui N, Khandakar S (2007) Patient satisfaction with health services in Bangladesh. Health Policy Plan 22:263–273

Aroca-Jiménez E, Bodoque JM, García JA, Díez-Herrero A (2018) A quantitative methodology for the assessment of the regional economic vulnerability to flash floods. J Hydrol 565:386–399

Aroca-Jiménez E, Bodoque JM, García JA (2020) How to construct and validate an integrated socio-economic vulnerability index: implementation at regional scale in urban areas prone to flash flooding. Sci Total Environ 746:140905

Bahauddin KM, Rahman MM, Ahmed F (2014) Towards urban city with sustainable buildings a model for Dhaka City Bangladesh. Environ Urbanization Asia 5:119–130

Barua U, Akther MS, Islam I (2016) flood risk reduction approaches in Dhaka, Bangladesh. In: Shaw R, Atta ur R, Surjan A, Parvin GA (eds) Urban disasters and resilience in Asia, pp 209–226. Butterworth-Heinemann

Berrouet LM, Machado J, Villegas-Palacio C (2018) Vulnerability of socio—ecological systems: a conceptual. Framework Ecol Indic 84:632–647

Bouzelha K, Hammoum H, Saradouni F, Benamar A (2018) Assessment of the vulnerability index of small dams to natural hazards: case study. In: Makhlouf ASH, Aliofkhazraei M (eds) Handbook of materials failure analysis, pp 329–350. Butterworth-Heinemann

Braun B, Aßheuer T (2011) Floods in megacity environments: vulnerability and coping strategies of slum dwellers in Dhaka/Bangladesh. Nat Hazards 58:771–787

Chen G, Huang K, Zou M, Yang Y, Dong H (2019) A methodology for quantitative vulnerability assessment of coupled multi-hazard in chemical industrial park. J Loss Prev Process Ind 58:30–41

Chowdhury EH, Hassan QK (2017) Use of remote sensing data in comprehending an extremely unusual flooding event over southwest Bangladesh. Nat Hazards 88:1805–1823

Cutter SL, Boruff BJ, Shirley WL (2003) Social vulnerability to environmental hazards. Soc Sci Q 84:242–261

de Andrade MMN, Szlafsztein CF (2018) Vulnerability assessment including tangible and intangible components in the index composition: an amazon case study of flooding and flash flooding. Sci Total Environ 630:903–912

de Moor EL, Denollet J, Laceulle OM (2018) Social inhibition, sense of belonging and vulnerability to internalizing problems. J Affect Disord 225:207–213

Dewan AM, Kankam-Yeboah K, Nishigaki M (2005) Assessing flood hazard in greater Dhaka, Bangladesh using SAR imageries with GIS. J Appl Sci(Pakistan) 5:702–707

Dintwa KF, Letamo G, Navaneetham K (2019) Quantifying social vulnerability to natural hazards in Botswana: an application of cutter model. Int J Disaster Risk Reduct 37:101189

Emrich CT, Cutter SL (2011) Social vulnerability to climate-sensitive hazards in the southern United States Weather. Climate Society 3:193–208

Fakhruddin B, Reinen-Hamill R, Robertson R (2019) Extent and evaluation of vulnerability for disaster risk reduction of urban Nuku'alofa, Tonga. Progress Disaster Sci 100017

Few R, Tran PG (2010) Climatic hazards, health risk and response in Vietnam: case studies on social dimensions of vulnerability. Glob Environ Change 20:529–538

Gain AK, Mojtahed V, Biscaro C, Balbi S, Giupponi C (2015) An integrated approach of flood risk assessment in the eastern part of Dhaka City. Nat Hazards 79:1499–1530

Gain AK, Mondal MS, Rahman R (2017) From flood control to water management: a journey of Bangladesh towards integrated water resources management. Water 9:55

Haque CE (2016) We are more scared of the power elites than the floods": adaptive capacity and resilience of wetland community to flash flood disasters in Bangladesh. Int J Disaster Risk Reduct 19:145–158

Hayes S, Desha C, Burke M, Gibbs M, Chester M (2019) Leveraging socio-ecological resilience theory to build climate resilience in transport infrastructure. Transp Rev 39:677–699

Huang D, Zhang R, Huo Z, Mao F, Youhao E, Zheng W (2012) An assessment of multidimensional flood vulnerability at the provincial scale in China based on the DEA method. Nat Hazards 64:1575–1586

Hung L-S, Wang C, Yarnal B (2016) Vulnerability of families and households to natural hazards: a case study of storm surge flooding in Sarasota County. Florida Appl Geogr 76:184–197

Huq ME (2013) Flood hazard, vulnerability and adaptation of slum dwellers in Dhaka. Lambert Academic Publishing, Germany

Huq ME (2017) Analyzing vulnerability to flood hazard of urban people: evidences from Dhaka megacity Bangladesh. Int J Earth Sci Eng 10:585–594

Huq S, Alam M (2003) Flood management and vulnerability of Dhaka City Building Safer Cities: the future of disaster risk Washington, DC, pp 121–135

Huq ME, Hossain MA (2012) Flood hazard and vulnerability of slum dwellers in Dhaka Stamford. J Environ Human Habitat 1:36–47

Huq ME, Hossain MA (2015) Vulnerability framework for flood disaster management. J Geo-Environ 11:51–67

Huq ME et al. (2020a) Measuring vulnerability to environmental hazards: qualitative to quantitative. In: Fahad S, Hasanuzzaman M, Alam M, Ullah H, Saeed M, Ali Khan I, Adnan M (eds) Environment, climate, plant and vegetation growth, pp 421-452. Springer International Publishing, Cham. https://doi.org/10.1007/978-3-030-49732-3_17

Huq ME, Shoeb AZM, Javed A, Shao Z, Hossain MA, Sarven MS (2020b) Measuring vulnerability for city dwellers exposed to flood hazard: a case study of Dhaka City, Bangladesh. In: International conference on urban intelligence and applications, pp 207–215

Huq ME et al (2020) Assessing vulnerability for inhabitants of Dhaka city considering flood-hazard exposure. Geofizika 37(2):97–130. https://doi.org/10.15233/gfz.2020.37.5

Kamal AM, Shamsudduha M, Ahmed B, Hassan SK, Islam MS, Kelman I, Fordham M (2018) Resilience to flash floods in wetland communities of northeastern Bangladesh. Int J Disaster Risk Reduction 31:478–488

Kamruzzaman M, Saad Awadh A, Madallah A, Nasser A, Muhammad Hameed S, Md. Enamul H (2020) Water resource evaluation and identifying groundwater potential zones in arid area using remote sensing and geographic information system. J Comput Sci 16. https://doi.org/10.3844/jcssp.2020.266.279

Khatun MA, Rashid MB, Hygen HO (2016) Climate of Bangladesh MET report, 2387–4201

Kothari CR (2004) Research methodology: methods and techniques. New Age International

Masciopinto C et al (2019) Human health risk assessment for the occurrence of enteric viruses in drinking water from wells: role of flood runoff injections. Sci Total Environ 666:559–571

Masood M, Takeuchi K (2012) Assessment of flood hazard, vulnerability and risk of mid-eastern Dhaka using DEM and 1D hydrodynamic model. Natural Hazards 61:757–770

Masuya A, Dewan A, Corner RJ (2015) Population evacuation: evaluating spatial distribution of flood shelters and vulnerable residential units in Dhaka with geographic information systems. Nat Hazards 78:1859–1882

Mavhura E, Manyena B, Collins AE (2017) An approach for measuring social vulnerability in context: the case of flood hazards in Muzarabani district. Zimbabwe Geoforum 86:103–117

Nayyer S, Huq M, Nana Yaw Danquah T, Akib J, Asif S (2019) Parameters derived from and/or used with digital elevation models (DEMs) for landslide susceptibility mapping and landslide risk assessment: a review ISPRS. Int J Geo-Inf 8

Ogie RI, Pradhan B (2019) Natural hazards and social vulnerability of place: the strength-based approach applied to Wollongong Australia. Int J Disaster Risk Sci 10:404–420

Okayo J, Odera P, Omuterema S (2015) Socio-economic characteristics of the community that determine ability to uptake precautionary measures to mitigate flood disaster in Kano Plains. Kisumu County, Kenya Geoenviron Disasters 2:4–28

Paavola J (2008) Livelihoods, vulnerability and adaptation to climate change in Morogoro Tanzania. Environ Sci Policy 11:642–654

Pandey R et al. (2015) Socio-ecological vulnerability of smallholders due to climate change in mountains: agroforestry as an adaptation measure. Change Adapt Socio-Ecol Syst 1

Pham NTT, Nong D, Garschagen M (2019) Farmers' decisions to adapt to flash floods and landslides in the Northern Mountainous Regions of Vietnam. J Environ Manage 252:109672

Pham NTT, Nong D, Sathyan AR, Garschagen M (2020) Vulnerability assessment of households to flash floods and landslides in the poor upland regions of Vietnam. Climate Risk Manage 28:100215

Rahman R, Salehin M (2013) Flood risks and reduction approaches in Bangladesh. In: Disaster risk reduction approaches in Bangladesh, pp 65–90. Springer

Rahman MA, Islam S (2019) Climate change adaptation in urban areas: a critical assessment of the structural and non-structural flood protection measures in Dhaka. In: Confronting climate change in Bangladesh, pp 161–173. Springer

Richmond A, Myers I, Namuli H (2018) Urban informality and vulnerability: a case study in Kampala, Uganda. Urban Science 2:22

Ruin I, Creutin J-D, Anquetin S, Lutoff C (2008) Human exposure to flash floods—relation between flood parameters and human vulnerability during a storm of September 2002 in Southern France. J Hydrol 361:199–213

Saaty TL (2008) Decision Making with the Analytic Hierarchy Process. Int J Serv Sci 1:83–98

Sarker AA, Rashid AM (2013) Landslide and flashflood in Bangladesh. In: Disaster risk reduction approaches in Bangladesh, pp 165–189. Springer

Sarker M, Bo Y, Yang L, ME H, MM K (2020) Climate change adaptation and resilience through big data. Int J Adv Comput Sci Appl 11:533–539

Sebald C (2010) Towards an integrated flood vulnerability index: a flood vulnerability assessment. Master of Science (MSc)

Shah AA, Ye J, Abid M, Khan J, Amir SM (2018) Flood hazards: household vulnerability and resilience in disaster-prone districts of Khyber Pakhtunkhwa province, Pakistan. Nat Hazards 93:147–165

Shams N (1999) Urban geology of Dhaka city for geohazard mitigation and development planning. University of Dhaka, Dhaka

Shao Z, Huq ME, Cai B, Altan O, Li Y (2020) Integrated remote sensing and GIS approach using Fuzzy-AHP to delineate and identify groundwater potential zones in semi-arid Shanxi Province, China. Environ Modell Softw 134:104868

Shrestha AB, Shah SH, Karim R (2008) Resource manual on flash flood risk management. Internat. Centre for Integrated Mountain Development, ICIMOD Kathmandu,

Sufia S, GM TI, Zahidul I (2009) Pre-and post-urban wetland area in Dhaka City, Bangladesh: a remote sensing and GIS analysis. J Water Resour Prot 2009

Tapsell S, McCarthy S, Faulkner H, Alexander M (2010) Social vulnerability to natural hazards. CapHaz-Net WP4 Report. Flood Hazard Research Centre—FHRC, Middlesex University, London. http://caphaz-net.org/outcomes-results/CapHaz-Net_WP4_Social-Vulnerability2.pdf. Access on Sept 2012

Taylor J (1840) A sketch of the topography and statistics of Dacca. Military Orphan Press, GH Huttmann

Taylor J (1849) Topography of Dhaka East India Company, Dhaka

Uddin K, Matin MA, Meyer FJ (2019) Operational flood mapping using multi-temporal sentinel-1 SAR images: a case study from Bangladesh. Remote Sensing 11:1581

UNICEF (2009) Bangladesh Bureau of Statistics. 2018 Bangladesh Drinking Water Quality Survey

Vo T (2016) Risk aversion and the impact of health insurance on household vulnerability: new evidence from rural Vietnam

Wmo G, Gwp G (2016) Handbook of drought indicators and indices geneva: world meteorological organization (WMO) and global water partnership (GWP)

Zakour MJ, Swager CM (2018) Vulnerability-plus theory: the integration of community disaster vulnerability and resiliency theories. In: Zakour MJ, Mock NB, Kadetz P (eds) Creating Katrina, Rebuilding Resilience. Butterworth-Heinemann, pp 45–78

Chapter 13
Flash Flood Modeling and Mitigation in Arid and Semiarid Basins: Case Studies from Oman and Brazil

Mohamed Saber, Sameh A. Kantoush, Mohammed Abdel-Fattah, Tetsuya Sumi, Jose Andres Moya, and Karim Abdrabo

Abstract The behaviors and impacts of flash floods (FF) are different based on the climatic regions. To understand such difference, two case studies were selected for the analysis: Wadi Uday, Oman and Sume Basin, Paraiba, Brazil. The rainfall-runoff inundation model (RRI) was used to simulate the discharge and flood inundation of the recent flood events to understand the severity and frequency of flash floods to better assess the current mitigation measures. The current FF situations in arid and semiarid basins were analyzed, and the hazards associated with flood phenomenon were assessed for various calculated rainfall return periods using RRI model. To this end, a flash flood index (average water depth per total basin area) was calculated as a basis to understand the impact of flash floods. A coupling of this index with the FF histories was included to provide a comprehensive overview of the FF vulnerability of arid and semiarid basins. We concluded that

M. Saber (✉) · S. A. Kantoush · T. Sumi
Disaster Prevention Research Institute (DPRI), Kyoto University, Kyoto 611-0011, Japan
e-mail: mohamedmd.saber.3u@kyoto-u.ac.jp

S. A. Kantoush
e-mail: kantoush.samehahmed.2n@kyoto-u.ac.jp

T. Sumi
e-mail: sumi.tetsuya.2s@kyoto-u.ac.jp

M. Abdel-Fattah
Civil Engineering and Quantity Surveying Department, Military Technological College, P.O. Box: 262, Muscat 111, Oman
e-mail: Mohammed.Soliman@mtc.edu.om

K. Abdrabo
Faculty of Urban and Regional Planning, Cairo University, Giza 12613, Egypt
e-mail: m.karim.ibrahim@cu.edu.eg

J. A. Moya · K. Abdrabo
Department of Urban Management, Graduate School of Engineering, Kyoto University, Kyoto 615-8245, Japan

T. Sumi et al. (eds.), *Wadi Flash Floods*, Natural Disaster Science and Mitigation Engineering: DPRI Reports, https://doi.org/10.1007/978-981-16-2904-4_13

FFs tend to be more severe and extreme in arid regions than in semiarid regions, despite the lower frequency of FFs and the water scarcity in arid regions. Distributed dams also proved to be more effective in preventing FFs in arid regions than in semiarid regions.

Keywords Wadi flash flood · Arid and semiarid basins · Mitigation measures · Hydrological modeling · Flood index · Concentrated and distributed dams · Oman · Brazil

13.1 Introduction

However, arid and semiarid areas make up approximately one-third of the total area of the world, and there are implications caused by the expansion of urban regions due to the increase in population (Huang et al. 2016; Metzger et al. 2020) that consequently lead to intensified flash flood risks. Despite this, previous studies addressing flash floods in these regions are still limited. A spatiotemporal analysis of rainfall variability over the Middle East and North Africa (MENA) region showed high spatiotemporal variability over the region in terms of the frequency and intensity of flash flood events (Saber et al. 2017, 2020). Additionally, the maximum rainfall in storms and the number of extreme rainfall events will increase in the future (Tanaka* et al. 2020), leading to higher risks of wadi-related flash floods in such regions.

The lack of high-quality data on wadi flash flood events in both arid and semiarid regions hinders efforts to mitigate flooding risks (Abdrabo et al. 2020; Chimnonyerem n.d.; Wheater et al. 2007; Rogger et al. 2014; Saber and Habib 2016; Abdel-Fattah et al. 2017; Saber et al. 2010). Most previous studies have mainly focused on arid or semiarid case studies separately; however, a few previous studies have focused on both regions. Therefore, understanding the difference between arid and semiarid regions as well as assessing the flash flood risks using distributed hydrological models is crucial for better flood risk reduction and proposing proper mitigation measures in such regions.

Flash flood hazards and risk assessments have been discussed in some previous studies in arid and semiarid regions, and these studies have addressed the impact of extreme rainfall variability in urban regions (Pathirana et al. 2014; Saber et al. 2020). However, the optimal methods for managing flood hazards in both regions are not very clear. The challenges of applying the concept of flood-risk management in practice might be attributed to the lack of proper planning approaches that take the flood issues into account or the lack these approaches being used in practice. The uncertainty of using floodplain mapping to efficiently capture the likelihoods of losses of property and human lives has caused real problems for local communities. In many cases, structural mitigation measures in arid and semiarid regions are not always optimum solutions. The core problem, as summarized in a World Bank report (Jha et al. 2012), is that poorly designed and managed urbanization

contributes to the growing flood risk due to unsuitable land-use changes. Urban expansion often occurs in a pattern of unplanned development in flood-prone regions (Huang and Shen 2019; Abdel-Fattah et al. 2017).

Flash floods have been highlighted in the twenty-first century for the damage they have caused, particularly in the more arid regions of the world, as climate change intensifies. In northern Brazil, for instance, which is the most populated semiarid region in the world (Cutter et al. 2013) at 30 million people, a sizeable portion of the population lives at risk due to flash floods (Alcantara et al. 2013). Families often must walk several kilometers every day to obtain water, which increases their vulnerability (Lindoso et al. 2018; Lindoso and Filho n.d.). On the other hand, Oman has experienced major flash floods, such as the Gonu Cyclone in 2007, which caused 4 billion USD worth of infrastructure damage and 49 deaths (Wang and Zhao 2008). It was stated that urbanization in Wadi Uday within this time period (1960–2003) was dramatically increasing (Al-Rawas 2011, 2013). Such urbanization expansions contribute directly to increasing the disastrous impacts of flash floods. In addition, there is a lack of substantial research focusing on flash flood disaster impacts and mitigation measures in both arid and semiarid basins. In the Sume Basin in the State of Paraiba, Brazil, the areas of corn and bean plantations, which account for the economic sustainability of many residents, have also increased in recent history. In addition, water has become increasingly scarce, which has placed increased importance on dams and flood mitigation measures. In light of this, the government has set up websites that make real-time measurements of the fullness of reservoirs.

The main objective of this study is to holistically compare arid and semiarid basins, considering characteristics such as the climate, aridity, hydrology, etc., of the two types of basins in addition to understanding flash flood phenomena in selected basins in Oman and Brazil. With this framework, a hydrological rainfall-runoff model was applied to assess the flood hazard levels based on calculations of the flood index (average water inundation depth per basin area). Abdel-Fattah et al. (2021) studied flash floods in wadi systems considering different scenarios of mitigation measures, stating that both distributed and single dam structures each have some advantages and disadvantages depending on the purposes and objectives of the proposed dams. Therefore, this study also compared the efficiency of different mitigation measures for flash floods, considering both concentrated and distributed dam scenarios to evaluate which scenario is more advantageous for the region from a comprehensive perspective.

13.2 Comparison Between Arid and Semiarid Basins

Approximately one-third of the land in the world is deemed to be arid or semiarid according to the Food and Agriculture Organization (FAO) of the United Nations. Both climate types are characterized by severe drought and rare precipitation (Lin 1999) and are generally vulnerable to flash floods. The two regions were compared

Table 13.1 General comparison between arid and semiarid areas

Type	Semiarid		Arid
Temperature (°C)	23–27		45–48
Annual average rainfall (mm)	200–400		<200
Evaporation (mm)	2,000		2,500–3,000
Aridity index (AI)	0.2 < AI < 0.5		AI < 0.2
Global land area	17.70%		12.10%
Annual runoff depth (mm)	10–50		<10
Mitigation measures	Flood protection dams	recharge dams	Storage dams, groundwater recharge dams
Infiltration	>Arid regions		<Semiarid regions
Drainage density	<4 km/km^2		10 km/km^2
Vegetation cover	>Arid regions		<Semiarid regions

Source (Data source): Moya et al. (2017)

and summarized as shown in Table 13.1. Arid and semiarid basins were compared in terms of hydrology, climatology, precipitation, and geomorphology. This comparison covered many aspects as follows: temperature, annual average rainfall, evaporation, the aridity index, global land area, annual runoff depth, mitigation measures, infiltration rate, drainage density and vegetation cover. There is a long-standing perception that intense rainfall-runoff events are more common in semiarid regions than in arid regions despite a lack of documentation. Arid and semiarid areas typically lack the vegetation cover, mature soil profiles, and humus layers that generally intercept and store precipitation, enhance infiltration and attenuate storm runoff in areas with moist climates. Compared with semiarid climates, sparsely vegetated soils in arid areas are commonly thin or absent and exhibit low rates of infiltration of rainfall due to soil-particle compaction by raindrop impacts (Anon 2000). Drainage density factor values in arid climates are typically regarded as low (<4 km/km^2), while those in semiarid regions average approximately 10 km/km^2, indicative of the maximum event runoff, short distances to drainage ways, and high potentials for high-magnitude discharge event (Knighton 1984).

13.2.1 Climate Conditions

Both arid and semiarid basins are affected by drought and very infrequent rainfall coupled with high temperatures (Lin 1999). Records indeed show the existence of prolonged drought periods that can extend for several years in some cases, as evidenced in. Oman is no exception, with potential evaporation that ranges from 2,000 to 3,000 mm and temperature varying from 3 °C in the mountains in winter

to temperatures exceeding 45 °C and reaching up to 48 °C in summer. In Brazil, annual average temperatures usually range from 24 to 26 °C, and temperatures exceed this range in places where the altitude is below 200 or, in some cases, 300 m (Malveira et al. 2012). However, climate change is making temperatures higher; in the last 41 years, maximum temperatures in the Northeastern Region of Brazil have increased from 1.5 to 2 °C (F. Lacerda Meteorology-ITEP). For the Sume Basin, average annual temperatures vary from 23 to 27 °C, with daily temperatures having a 10 °C range of variance (Alcantara et al. 2013). The aridity index was calculated for each basin according to UNEP by the following formula:

$$AI = \frac{P}{\text{PET}} \tag{13.1}$$

where P stands for the average annual precipitation and PET is the potential evapotranspiration. The AI was calculated to be 0.036 for the Wadi Uday basin and 0.25 for the Sume Basin.

13.2.2 Precipitation

Precipitation in arid and semiarid areas tends to present high variance (Geber et al. 2008) and randomness factors. In Wadi Uday, the rainy season occurs from November to April in winter and is often caused by thunderstorms, while the dry season occurs in summer from May to October, during which large rainfall events still sparsely occur (Ministry of Regional Municipalities and Water Resources 2009). According to the Ministry of Regional Municipalities and Water Resources, the annual average rainfall measured from 1995 to 2008 was 90 mm. Oman has been the subject of many tropical cyclones that often develop in the Arabian Sea, causing heavy rain and floods (Saleh and Al-Hatrushi n.d.), as evidenced in Fig. 13.1. Records also show the existence of prolonged drought periods, as exemplified in, which can extend for several years in some cases. Rainfall variability is very high in Oman, with the average yearly rainfall ranging from 76.9 mm in the interior of the country to a high of 181.9 mm in the Dhofar Mountains, according to data collected from 1997 to 2003 (Kwarteng et al. 2009).

The average annual rainfall in the Sume Basin tends to vary from 550 to 600 mm based on the last 50 years of measurements. The semiarid climate in this basin is characterized by irregular rainfall and a clear divide between two seasons: the dry season, which ranges from June until January, and the rainy season, which extends from February until May. The region is well-known for its remarkable rainfall intensity variability associated with the low total annual rainfall values that characterize much of the Northeastern Region of Brazil (Silva et al. 2007). Especially due to the Intertropical Convergence Zone (ITCZ), there is high rainfall variability in this region; along the coast, the annual average rainfall surpasses

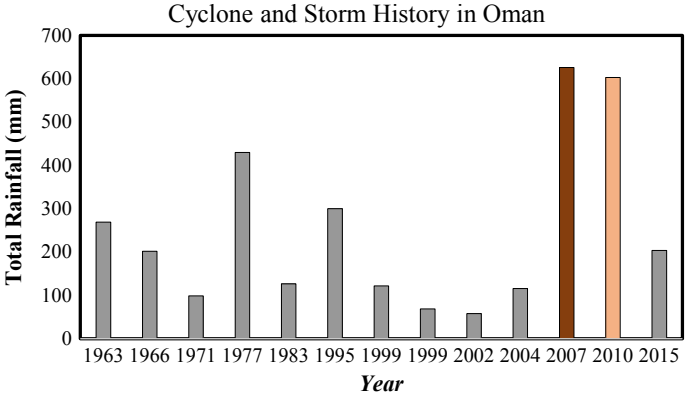

Fig. 13.1 List of cyclones in Oman from 1963 until 2015; 2007 and 2010, highlighted, stand for the Gonu and Phet cyclones, respectively. *Source data* Al Barwani, A., 2015. Flash flood mitigation and harvesting Oman case study, first international symposium on flash floods (ISFF). DPRI, Kyoto University, Kyoto, Japan

1,000 mm, while toward the backland, the average hovers at approximately 500 mm (Silva et al. 2007).

The PERSSIAN CDR data (Ashouri et al. 2015) from 1983 to 2019 were analyzed for both countries, and we found that the annual trend of rainfall in Brazil is decreasing, but in Oman, it is slightly increasing. The maximum annual average rainfall over Oman is limited to less than 200 mm/year, but in Brazil, it is over 2,000 mm/year (Figs. 13.2 and 13.3).

13.2.3 Flash Floods in Arid and Semiarid Basins

Flash floods are defined as floods that rapidly develop within a very small amount of time, usually a few minutes or hours, due to excessive rainfall (Abdel-Fattah et al. 2015). There are many types of floods that are very destructive with different features and characteristics, such as coastal flooding of land areas around coasts due to high tides and/or heavy rainfall; river flooding where the water level surpasses the top of a riverbank due to excessive rainfall; urban/pluvial flooding, which occurs in urban areas due to heavy rainfall, exceeding the capacity of the drainage systems; and reservoir flooding, which occurs as a result of dam failures. Additionally, wadi-related flash floods occur in catchments, urban areas or both due to extreme rainfall events in most cases. With climate change in recent years, flash floods have intensified; in Oman, for instance, major flash floods occurred in 1989, 1997, 2002, 2003, 2007, 2010, 2015 and 2016, as shown in Table 13.2. There are some other common characteristics of flash floods in arid and semiarid areas, such as the difficulty of forecasting flash floods due to the suddenness of flash flood

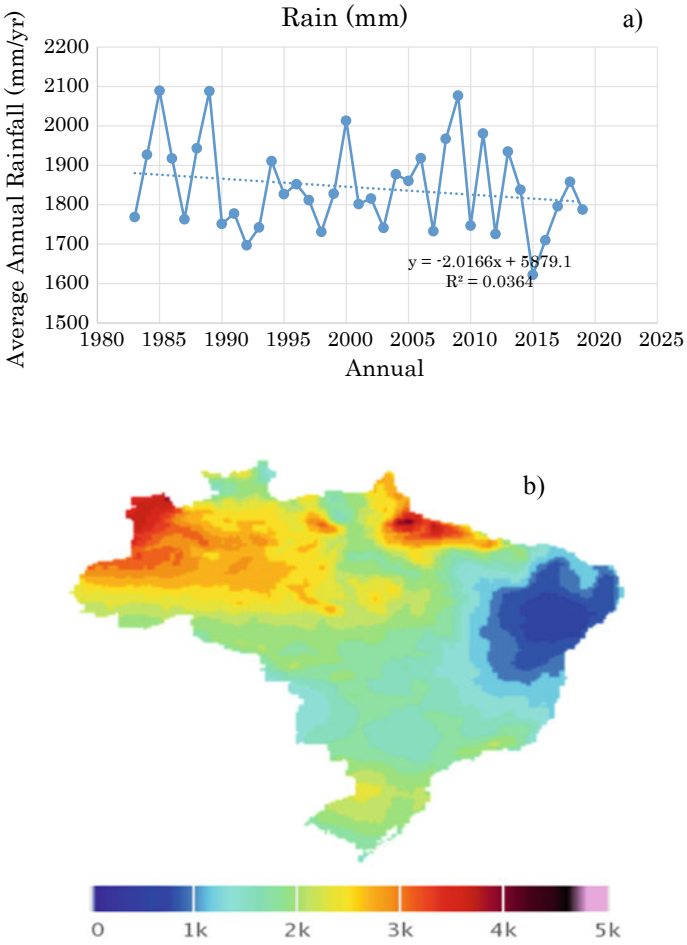

Fig. 13.2 Annual average precipitation from PERSSIAN-climatology data over Brazil: **a** time series annual average, **b** total average from 1983 to 2019. *Source data* Ashouri et al. (2015). For citation "PERSIANN-CDR: daily precipitation climate data record from multisatellite observations for hydrological and climate studies." *Bulletin of the American Meteorological Society* 96.1 (2015): 69–83

occurrences, the scarcity of data, and the area distribution being statistically random (Lin 1999). In Brazil, many flash floods are caused by the breakage or spilling of dams or levies. Flash floods can also carry downed trees, boulders, and debris along wadi beds to alluvial fans, as is often seen in many wadis, such as Wadi Uday and Wadi Samail (Al-Rawas 2013).

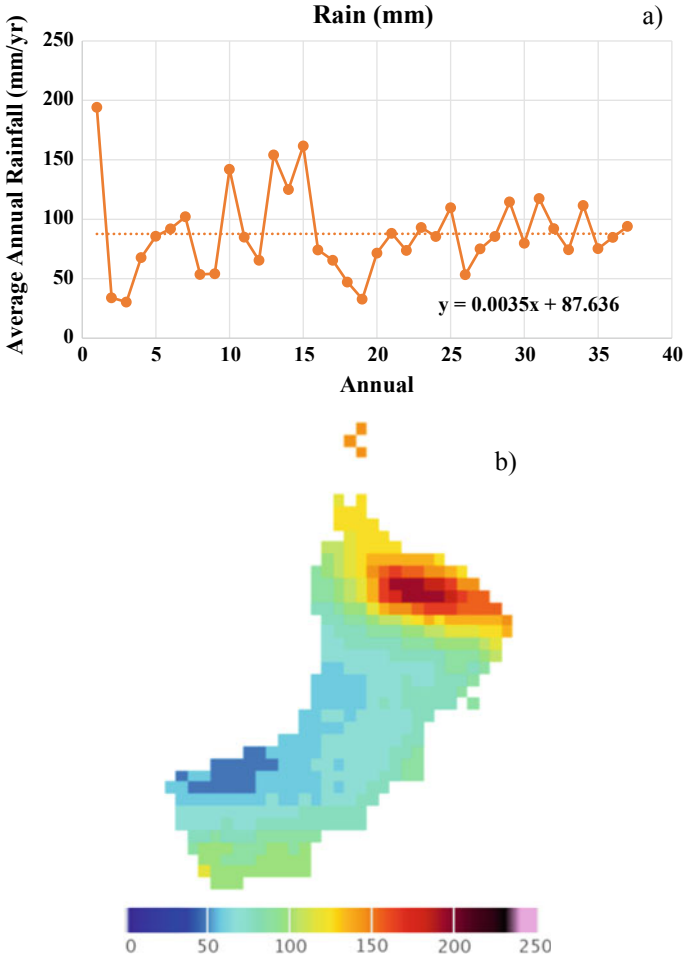

Fig. 13.3 Annual average precipitation from PERSSIAN-climatology data over Oman: **an** annual average time series, **b** total average from 1983 to 2019. *Source data* Ashouri et al. (2015)

13.2.4 Current Mitigation Measures in Arid and Semiarid Basins

Mitigation measures for flash floods have played an increasingly pivotal role in recent years, with the intensification of flash floods coupled with urban expansion into flood-risk areas (Abdel-Fattah et al. 2021; Al-Rawas 2013). Partially stemming from this, the Omani government created a seven-dam project in the Wadi Uday basin. This study considered the similar conditions of the seven dams, as shown in Fig. 13.4 and Table 13.3.

Table 13.2 History of flash floods in Oman

Year	Location	Began	Ended	Duration (days)	Missing	Displaced	Area (km^2)
1989	Muscat	14 Sept	16 Sept	3	2	NA	72,160
1997	Dibba	21 June	23 June	3	4	NA	21,980
2002	Salalah	10 May	12 May	3	9	100	9,460
2003	Nizwa Muscat/ Muscat, Dhofar	14 April	19 April	6	30	NA	23,060
2005	Batinah Nizwa Musandam	01 March	23 March	23	7	700	489,000
2007	Muscat	06 July	12 July	7	61	60,000	373,000
2010	Muscat	May 31	June 6	7	24	NA	150,000
2015	Masirah Island/ Muscat	8 June	12 June	5	105	50,000	50,000

Source Moya (2017)

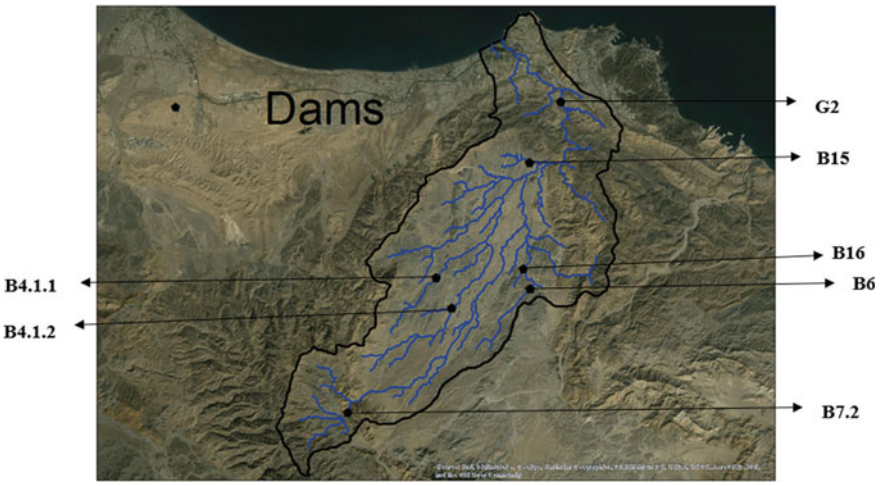

Fig. 13.4 Dam locations in the Wadi Uday basin. *Source* Moya (2017)

Flash flood measures in arid and semiarid areas can mainly be divided into 2 categories: structural and nonstructural measures, as shown in Table 13.4. According to the Ministry of Regional Municipalities and Water Resources (MRMWR), the established dams in Oman are not limited to flood protection dams but also include groundwater recharge and storage dams. In Wadi Uday basin, for

Table 13.3 List of dams and their characteristics in the Wadi Uday basin

Dam ID	Dam name	Dam height (m)	Dam coordinates	Dam type	Reservoir storage volume (10^6 m^3)
B15	Al Amerat Heights	22	Lat: 23.54° Long: 58.49°	Embankment	22
G2	Wadi Uday Gorge	45	Lat: 23.58° Long: 58.52°	Embankment	26
B6	Al Jufainah	28	Lat: 58.5° Long: 23.45°	Embankment	16
B7.2	Al Humaniyah	58	Lat: 23.36° Long: 58.36°	Concrete	8.6
B4.1.1	Madinat Al Nahdah N	16	Lat: 23.46° Long: 58.42°	Embankment	4
B4.1.2	Madinat Al Nahdah S	20	Lat: 23.44° Long: 58.43°	Embankment	6
B16	Al Mahag	18	Lat: 58.5° Long: 23.46°	Embankment	5

Source data Ministry of Regional Municipalities and Water Resources, Oman

instance, after the destruction caused by the Gonu Cyclone, 16 dams were examined for a project to build 7 flood protection dams (currently, only one has been built). In Brazil's case, the main mitigation measures mainly consist of flood-risk maps and evacuation measures as well as storage reservoirs of various sizes (Malveira et al. 2012). Although there are tens of thousands of storage dams in the Northeastern Region of Brazil, only some of these storage dams have flood mitigation functions.

Table 13.4 Structural and nonstructural measures for flash flood mitigation

Structural	Nonstructural
Improve channel drainage efficiency by increasing channel width and depth	Monitor and forecast water situations and rainfall in the target basin
Flood protection dams	Accelerate drainage of water in low-lying areas
Flood walls and levees	Reduction of flood peaks that pass close to communities by diverting upstream water
Floodways	Land-use zoning and flood-risk maps
Embankments	Floodplain management

Source Moya (2017)

13.3 Study Areas

13.3.1 Semiarid Region: Sume Basin, Brazil

The Sume Basin is located in the Northeastern Region of Brazil, as shown in Fig. 13.5, which has an area of 1.6 million km^2; 86% of this area is deemed to be semiarid (Marengo et al. 2008). This region is often referred to as the drought polygon due to its particular fragility and poor level of development, which is exacerbated by the frequent droughts that occur in the area. The Northeastern Region of Brazil is formed by nine states, and the Sume Basin is located in the state of Paraiba, as shown in Fig. 13.5. The basin itself has an area of approximately 128 km^2, and according to a 2014 IBGE report (Brazilian Institute of Geography and Statistics), the population contained in this basin is 51,000. The hydrographic basin constituting the Sume Basin is located between the municipalities of Sume and Monteiro, bounded by the coordinates of 7°40′ south latitude and 37°0′ east longitude (Cadier and Jose de Freitas 1982). The Sume Basin is divided into three subbasins: Jatoba, Umburana and Gangorra.

To run the RRI model, daily rainfall data from the Superintendence for the Development of the Northeast (SUDENE) were used for the 1985 floods, which had huge impacts in the majority of the Northeastern Region of Brazil. Rainfall return

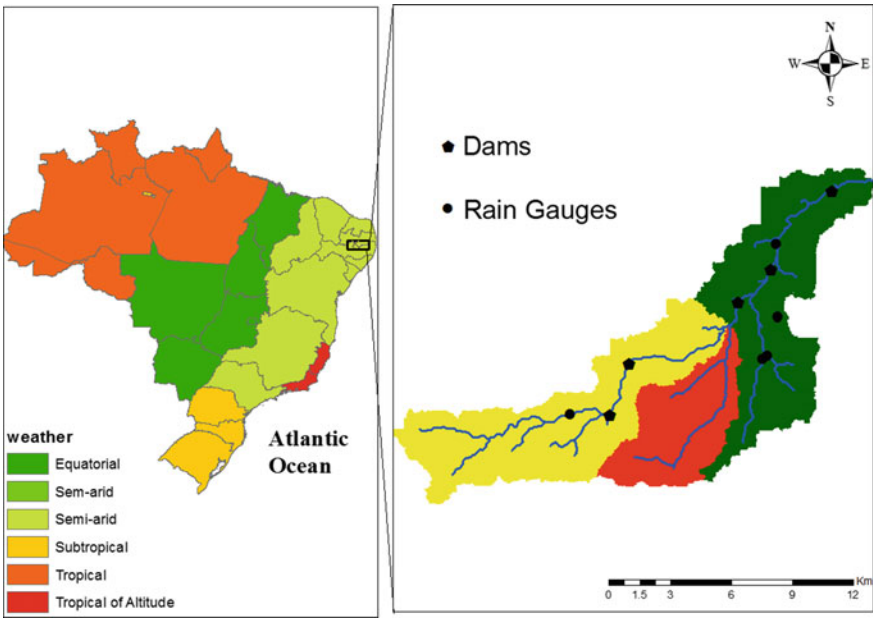

Fig. 13.5 Map of the Sume Basin in Paraiba, Brazil, showing the locations of dams and rain gauges. Reprinted (modified) from Moya et al. (2017)

periods were also calculated using rainfall data from SUDENE. GSMaP data were also used to simulate the floods that occurred in 2014 in Sume. This simulation was run using the rainfall intensity values calculated from the 1985 floods and a 100-year rainfall return period. For topographic data, a 30-s resolution, which is equivalent to approximately 1 km per cell, was used from the HydroSHEDS data.

13.3.2 Wadi Uday Basin

The Wadi Uday basin is located in the Muscat governorate of Oman, which is the fastest-growing part of the country (Al-Rawas 2013), with a population of 1,288,300 according to a 2015 census made by the National Centre for Statistics and Information. The basin itself has an area of 372 km^2, with a total urbanized area of approximately 85 km^2, which represents approximately 22% of the total watershed area. Wadi Uday is bounded by the coordinates 23°40′ north latitude and 58°35′ east longitude. Figure 13.6a shows the watershed delineation and its geographical location in the Middle East, as well as the rain gauges that were used to collect rainfall measurements in the basin. The basin is also almost entirely surrounded by mountains, which greatly increases the risk of flash floods.

The Gonu Cyclone in June 2007 was the event chosen for the calibration, using data from the MRMWR measured from the rain gauges shown in Fig. 13.6b. For the model validation, a major flood event that occurred in December 2006 was chosen, and the same sources of data were used. The main geologic base of the soil in this basin is made up of basaltic, limestone and sandstone rock according to data from the MRMWR.

13.4 Data Processing and Methods

First, the available rainfall and discharge data were collected. Data collected from 1983 to 2015 by 6 rain gauges were used for Wadi Uday in Oman, and data collected from 1982 until 1991 were taken from 5 rain gauges for Sume Basin in Brazil. In addition to satellite-based rainfall data, GSMaP data were also used in Oman to simulate the 2007 Gonu Cyclone and the March 1985 large floods in Brazil.

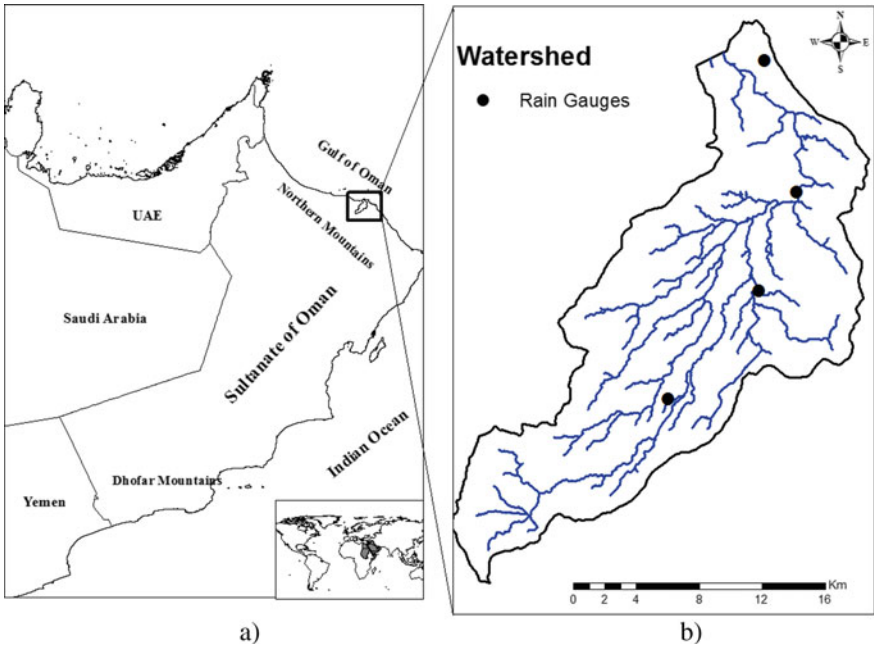

Fig. 13.6 Map of Wadi Uday basin in Muscat, Oman (**a**), showing the locations of dams and rain gauges (**b**). *Source data* Ministry of Regional Municipalities and Water Resources, Oman (*source* Moya 2017)

13.4.1 Hydrological Rainfall Runoff Inundation Model (RRI)

The hydrological model utilized in this study is called the RRI, which is capable of simulating rainfall runoff and flood inundation simultaneously. The model deals with slopes and river channels separately, although they are both positioned in the same grid cells. In the model, the channel is discretized as a single line vector of the overlying slope grid cells (Sayama 2013, 2015). The channel represents an extra flow path between grid cells overlying the actual river course. Lateral flows are simulated on the cells on a 2D basis, and slope grid cells on the river channel have two water depths: one allocated for the channel and another for the slope.

Channel flow in the RRI model is calculated with the 1D diffusive wave model. The RRI model also simulates lateral subsurface flow, vertical infiltration flow and surface flow. This study focused on the case where there was no lateral saturated hydraulic conductivity to consider saturated subsurface and saturation excess overland flow. A particularity of the RRI model is that it can simulate both surface and subsurface flow with the same algorithm (Sayama 2013, 2015).

The RRI model can also be used to simulate several mitigation measures, such as dams, diversion channels and channel improvements. To assess the current mitigation measures more accurately in arid and semiarid basins, this study also attempted, unsuccessfully, to change the dam subroutine embedded in the model to allow it to simulate dams with different discharge rates (as opposed to the normal RRI function, which sets discharge at a fixed rate and includes circular storage reservoirs). It is worth mentioning that the RRI model was efficiently applied in flash flood simulations in Oman (Abdel-Fattah et al. 2016, 2018).

13.4.1.1 Governing Equations

The model used to calculate lateral flows on slope grid cells is called the "storage cell-based inundation model" (Hunter et al. 2007) and is based on Eq. (13.2), describing mass balance, and Eq. (13.3), describing the momentum equation. These equations can be expressed as follows:

$$\frac{\partial h}{\partial t} + \frac{\partial q_x}{\partial x} + \frac{\partial q_y}{\partial y} = r \tag{13.2}$$

$$\frac{\partial q_x}{\partial t} + \frac{\partial u q_x}{\partial x} + \frac{\partial v q_y}{\partial y} = -gh\frac{\partial H}{\partial x} - \frac{\partial \tau_x}{\partial p_w} \tag{13.3}$$

where h is the height of water of the surface, q_x and q_y are the unit width discharges in the x and y directions, u and v are the flow velocities in the x and y directions, r is the rainfall intensity, H is the height of water from the datum, p_w is the density of water, g is the gravitational acceleration, and τ_x and τ_y are the shear stresses in the x and y directions. These equations are then calculated using Manning's equation (Sayama 2013, 2015), after which the following equations are derived.

$$q_x = -\frac{1}{n}h^{5/3}\sqrt{\left|\frac{\partial H}{\partial x}\right|}\operatorname{sgn}\left(\frac{\partial H}{\partial x}\right) \tag{13.4}$$

$$q_y = -\frac{1}{n}h^{5/3}\sqrt{\left|\frac{\partial H}{\partial y}\right|}\operatorname{sgn}\left(\frac{\partial H}{\partial y}\right) \tag{13.5}$$

13.5 Model Calibration and Validation in Arid and Semiarid Regions

13.5.1 Calibration (Gonu 2007) and Parameter Setting

Calibration was performed by comparing the discharge results from the RRI simulation to the actual measured discharge for the June 2007 Gonu Cyclone. The model was calibrated for 3 cases: case A for only overland flow, case B for vertical infiltration and case C for saturated subsurface (Sayama 2013, 2015). Due to the topographical particularities of the selected arid and semiarid basins, this study focused on case C. To perform the calibration, first, various parameters were adjusted until the simulated and measured discharge curves resembled each other, as shown in Fig. 13.7. The effect of each parameter as well as the values that were finally selected for the arid and semiarid basins are listed in Table 13.5.

Here, the suction at the vertical wetting front, S_f, is inactive, and the vertical saturated hydraulic conductivity, k_v, is zero, therefore, these parameters were omitted from the table.

Both daily and hourly calibrations were performed, and one large difference between these calibrations was the gap between the peak discharges of the measured and simulated values before calibration; this gap was much steeper in the hourly case. This was reflected in the values of the parameters, particularly the values for the roughness of the river and slope, which were significantly lower for the hourly calibration case than for the daily case. The final calibration result is shown in Fig. 13.8. The formulas that were used to assess the accuracy of these results are listed below:

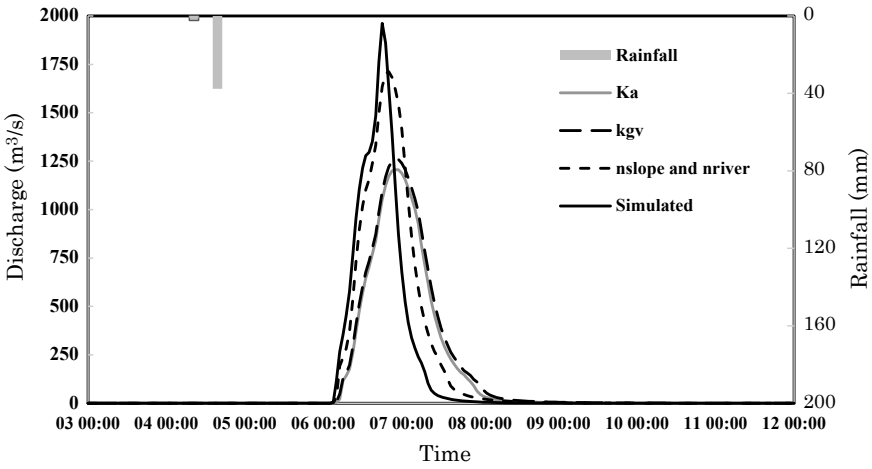

Fig. 13.7 Different calibration attempts together with the final simulated curve; the legend shows which parameter was changed for each line to increase or decrease the peak discharge

Table 13.5 Value and effect of each parameter after calibration

Parameter	Value	Effect
$n_{\text{river}}(m^{-1/3}s)$ (Roughness of river)	0.02	Considerable decrease in peak discharge
$n_{\text{slope}}(m^{-1/3}s)$ (Roughness of slope)	0.05	Decrease in peak discharge
d (m) (Soil depth)	0.7	Slight decrease in peak discharge
φ(Porosity)	0.3	Slight decrease in peak discharge
k (ms^{-1}) (Lat. sat. hydr. conduc.)	0	Low discharge peak
k_{gv} (Groundwater hydr. conduc.)	2x	Considerable overall decrease of discharge curve
River settings	$C_w = 6.5$ $S_w = 0.56$ $C_D = 0.22$ $S_D = 0.32$	

Source Moya (2017)

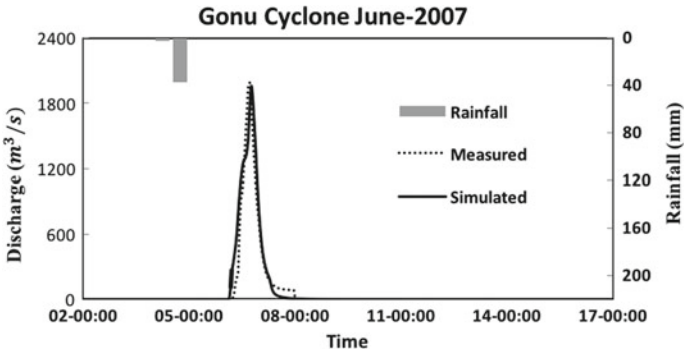

Fig. 13.8 Discharge peak from the measured data, as well as simulated values before and after calibration. *Source* Moya (2017)

$$\text{PBIAS} = \frac{\sum(Q_{\text{meas}} - Q_{\text{sim.}})}{\sum Q_{\text{meas}}} * 100 \tag{13.6}$$

$$\text{NSE} = 1 - \frac{\sum (Q_{\text{meas}} - Q_{\text{sim.}})^2}{\sum \left(Q_{\text{meas}} - Q_{\text{sim.}}^{\text{mean}}\right)^2} \tag{13.7}$$

where $Q_{\text{sim.}}$ stands for the simulated discharge and Q_{meas} is the measured discharge. The peak bias for the Gonu Cyclone event at Wadi Uday was calculated to be approximately 6%, and the Nash–Sutcliffe model efficiency coefficient was approximately 0.98. The width and depth of the channel were determined by

comparing the simulated values with real values obtained from Google Maps. The channel in Wadi Uday was found to be rather deep and quite wide, especially in the upstream part, whereas the Sume channel in Brazil tended to be very flat and narrow. The flood depth level that was measured downstream was also used to prove that the calibration results here were valid. In the Sume Basin, due to a lack of measured discharge data, the results were not calibrated or validated.

13.5.2 Validation (2006 December Floods)

The December 2006 floods were selected to validate the calibration, following a similar procedure as mentioned in the beginning of this chapter, as shown in Fig. 13.9 in the appendix. The *PBIAS* used for the validation was estimated to be approximately 28%. This exemplifies the reliability of the obtained parameters.

13.6 Comparison of Flash Flood Mitigation Scenarios

13.6.1 Proposed Mitigation Scenarios

Below are the main mitigation scenarios that were proposed, mainly for the distributed and concentrated structures in both the Wadi Uday basin and Sume Basin (Moya et al. 2017). The main point behind how the reservoir volumes were selected is that the total volume of all the reservoirs summed together always remained the same. The reservoir storage volume was chosen according to the topography of the

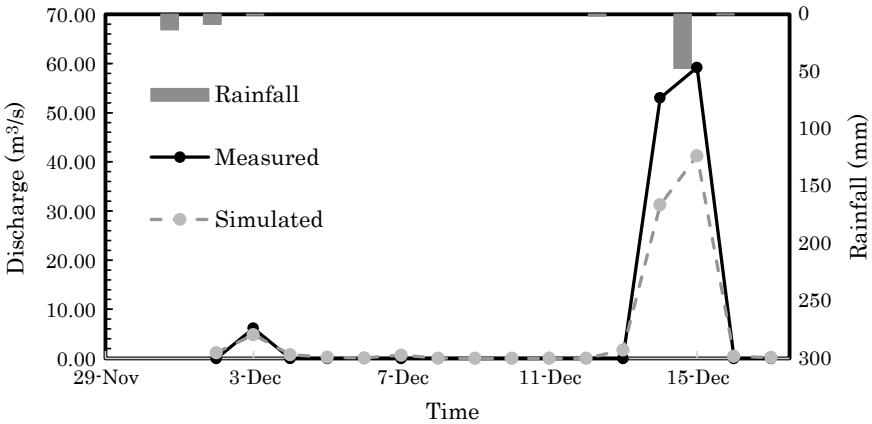

Fig. 13.9 Discharge peak curve of the December 2006 floods obtained after using the calibrated parameters from 2007 Gonu cyclone calibration

basin. In Fig. 13.10, the concentrated dams that were proposed for each case study are shown, and their specifications are described in Tables 13.6 and 13.7. The distributed dams and information on the Sume Basin are displayed in Fig. 13.11 and Table 13.8.

13.6.2 Impact of Mitigation Measures

The main five scenarios compared were the scenario without mitigation measures, with 1 dam, concentrated dams, distributed dams, and channel improvement. In Fig. 13.12, the hydrograph of the Gonu Cyclone event in 2007 shows the efficiency of concentrated versus distributed mitigation structures based on daily data that were measured at a point downstream. In Fig. 13.13, the different water levels at the same point downstream are shown to illustrate how the various mitigation measures applied managed to decrease the maximum flood depth. The distribution maps were visualized for the flow discharge (Fig. 13.14) and flow depth with distributed and concentrated dams at Wadi Uday (Figs. 13.15 and 13.16). Both distributed and concentrated dams seemed to be more efficient in the Wadi Uday basin in terms of lowering both the discharge and flood depth, which could be attributed to the geomorphologic differences between the two channels. The main conclusion that can be drawn from these pictures is that distributed dams may be more effective in reducing flood depths and peak discharges. This could be because distributed dams can stop water at different time sets compared to the concentrated dam strategy, which might hold the flood water at a single point in time.

Similarly, the flood depth and discharge values as well as maps showing the distributions of these data based on measurements made at a downstream point were also performed in the Sume Basin. Figures 13.17 and 13.18 exhibit the hydrographs of the flow discharge and flow depth, respectively. The distribution

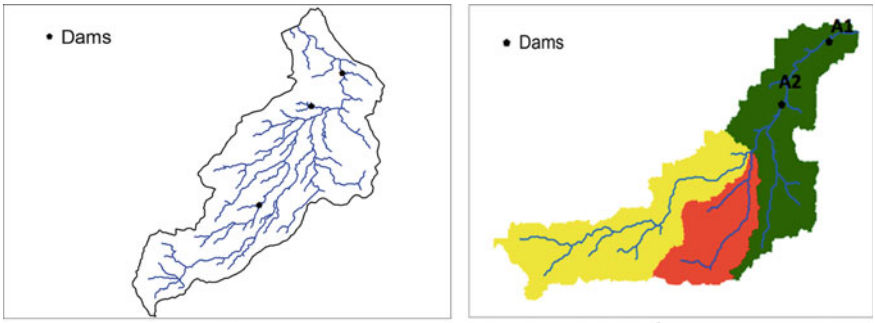

Fig. 13.10 Location of concentrated dams in the Wadi Uday basin (**a**) and Sume Basin (**b**). *Source* Moya (2017)

Table 13.6 Information on concentrated dams in the Wadi Uday basin

Dam ID	Dam name	Dam height (m)	Dam coordinates	Dam type	Reservoir storage volume (10^6 m^3)
B15	Al Amerat Heights	22	Lat: 23.54° Long: 58.49°	Embankment	48
G2	Wadi Uday Gorge	45	Lat: 23.58° Long: 58.52°	Embankment	22
B4.1.2	Madinat Al Nahdah S	20	Lat: 23.44° Long: 58.43°	Embankment	19

Source data Ministry of Regional Municipalities and Water Resources, Oman

Table 13.7 Information on concentrated dams in the Sume basin

Dam ID	Storage volume (10^6 m^3)
A1	35
A2	10

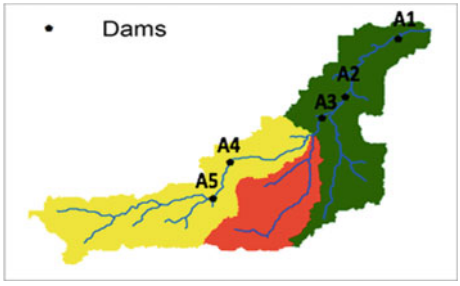

Fig. 13.11 Location of distributed dams in the Sume basin. Reprinted (modified) from Moya et al. (2017) copyright 2021

Table 13.8 Information on distributed dams in the Sume basin

Dam ID	Storage volume (10^6 m^3)
A1	25
A2	5
A3	5
A4	5
A5	5

Source Ministry of Regional Municipalities and Water Resources, Oman

maps of discharge (Fig. 13.19) and flow depth with concentrated and distributed dams are also visualized (Figs. 13.20 and 13.21).

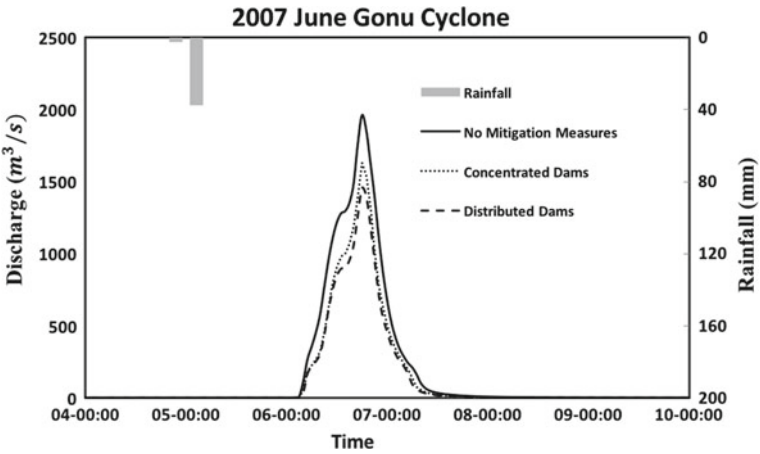

Fig. 13.12 Hydrograph showing the discharge peak in Wadi Uday considering various mitigation scenarios

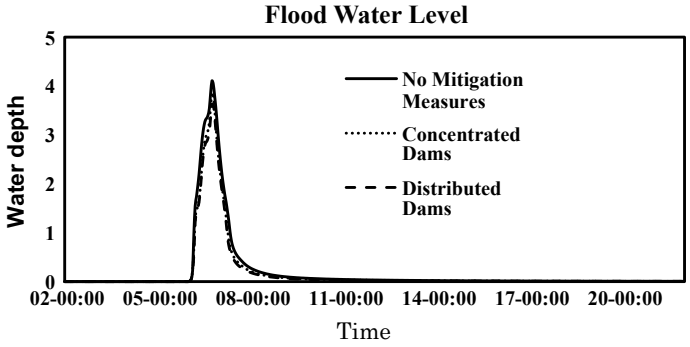

Fig. 13.13 Flood depth during the Gonu Cyclone in Wadi Uday measured at a point downstream

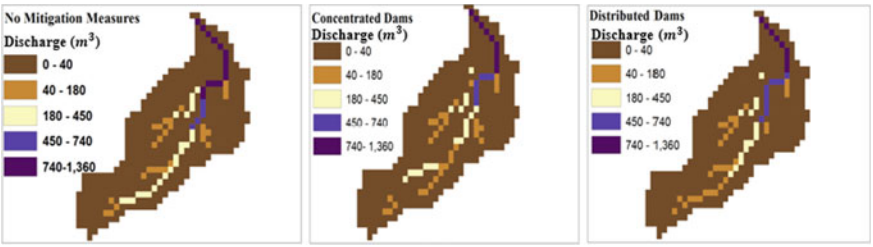

Fig. 13.14 Discharge maps of Wadi Uday for the 100-year rainfall return period under different mitigation scenarios

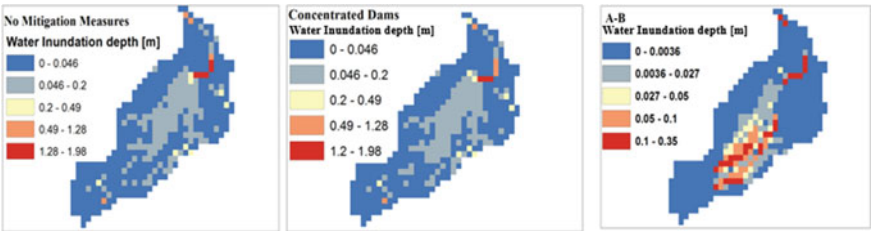

Fig. 13.15 Flood depths with concentrated dams; A–B represents the difference between the flood depths under the situation in which mitigation measures are taken and the situation in which mitigation measures are taken in Wadi Uday for the 100-rainfall return period

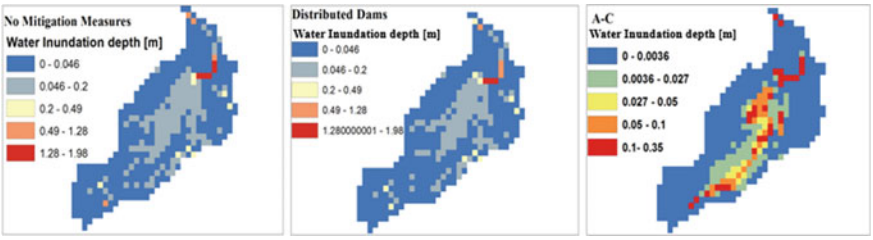

Fig. 13.16 Flood depths with distributed dams; A–C represents the difference between the flood depths under the situation in which mitigation measures are taken and the situation in which no mitigation measures are taken in Wadi Uday for the 100-year rainfall return period

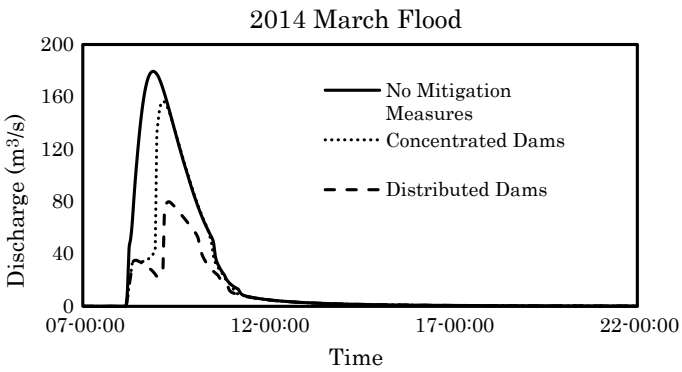

Fig. 13.17 Hydrograph of discharge peaks in Sume basin considering various mitigation scenarios

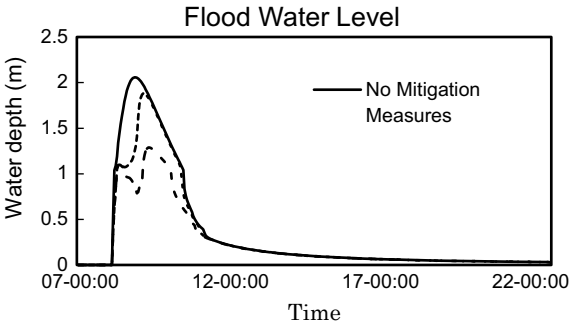

Fig. 13.18 Flood depth during the Gonu Cyclone in the Sume basin measured at a point downstream

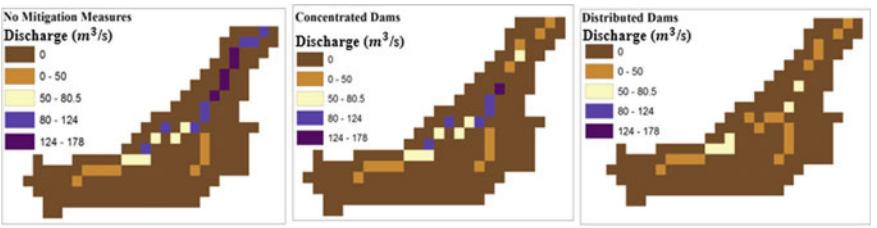

Fig. 13.19 Discharge maps in the Sume basin under different mitigation scenarios for the 100-year rainfall return period

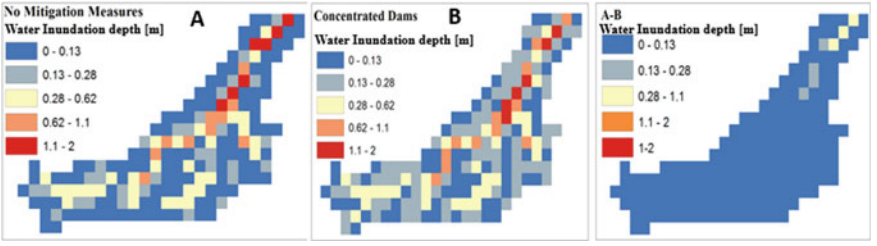

Fig. 13.20 Flood depths with concentrated dams; A-B represents the difference between the flood depths under the situation in which mitigation measures are taken and the situation in which no mitigation measures are taken in the Sume Basin based on the March 2014 flood event

13.7 Flood Index

The rainfall return period was calculated considering June 2007 Gonu Cyclone in Oman, and the March 1985 flood event in the Northeastern Region of Brazil. The rainfall return period was calculated using the following equation:

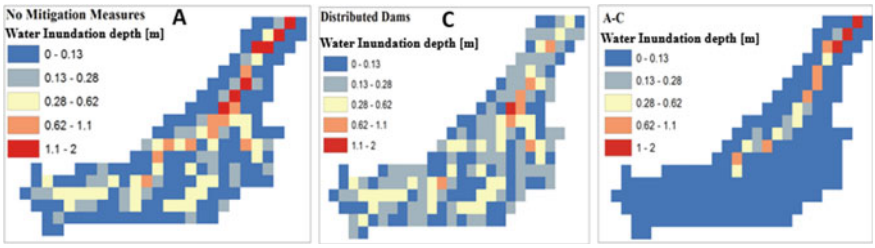

Fig. 13.21 Flood depths with distributed dams; A-C represents the difference between the flood depths under the situation in which mitigation measures are taken and the situation in which no mitigation measures are taken in the Sume Basin based on the March 2014 flood event

$$F_a = \frac{100(2n-1)}{2y} \tag{13.8}$$

$$\text{FFI} = \frac{\sum_{i=1}^{N} I_D}{N} \tag{13.9}$$

where F_a is the probability of occurrence, n is the total number of years and y is the total number of events. Using this rainfall return period, the flood index was estimated in the Sume Basin and in the Wadi Uday basin, as shown in Fig. 13.22. To calculate this flood index, Eq. 13.6 was used, where I_D is the average inundation depth and N is the total number of cells. The difference in the span of the return period graphs is due to the lack of available data for the Sume Basin in Brazil.

13.8 Conclusions and Recommendations

As shown in the previous section, concentrated dams did not reduce the inundation water level or total area as much as distributed dams did, and by observing the flood index, channel improvements were 20% more efficient in reducing the inundation depth of flash floods than the construction of dams. Furthermore, concentrated dams were much more efficient in arid basins than in semiarid basins. Concentrated dams seem to be less efficient in semiarid Brazil because of the flat terrain and localized rain. One common point among both basins, however, is that in both cases, channel improvements were always effective; this is mainly attributed to the accumulation of sedimentation in the channels and embankments, which can make the rivers more prone to flash floods.

The RRI model was used because of its ability to simulate results, including mitigation measures, within a very short time span. Both data input and output visualization can be performed very quickly using this model, and the results can be easily compared and validated by utilizing results from other hydrological models.

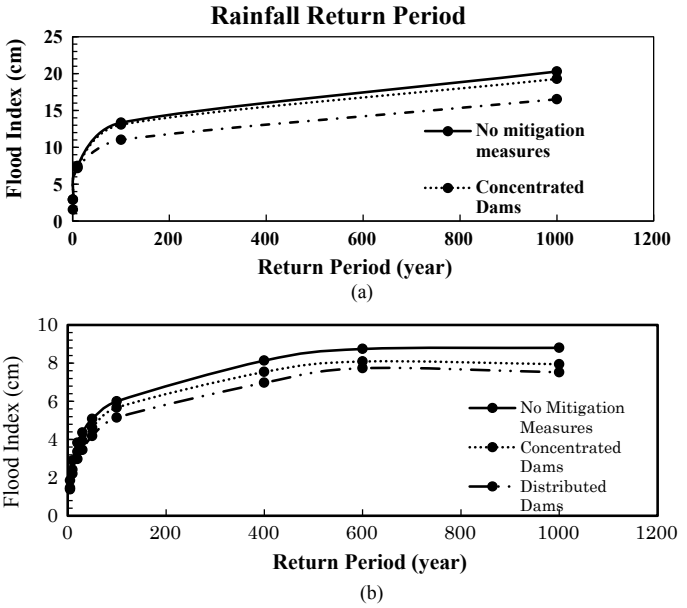

Fig. 13.22 Flood index curves plotted according to the rainfall return period for **a** Sume Basin, Brazil, and **b** Wadi Uday, Oman

The model was found to be suitable for simulations in arid and semiarid basins, as it provided accurate results after being calibrated and validated.

Despite the slight decrease in efficiency from a flood mitigation perspective, concentrated dams present other advantages. From an economic standpoint, they are much more affordable to construct since they centralize the necessary infrastructure, as seen in the construction of saddle dams, diversion channels and land survey costs for dams. Concentrated dams are also more efficient for groundwater recharge and are less harmful to the environment since concentrated dams require fewer construction materials. Additionally, concentrated dams are more easily accessible and maintained. Nevertheless, distributed dams also have advantages such as fostering local development in the local regions and providing more upstream protection from flash floods.

Overall, there seems to be a lack of academic papers that thoroughly compare arid and semiarid regions, especially from the perspective of hydrology and vulnerability to flash floods. Indeed, this might be because reliable data for flash floods in arid and semiarid basins are lacking; deeper investigation and research in disaster prevention in these regions only started in approximately 1980. One key difference this study found between semiarid Brazil and arid Oman is that the way each of these regions tackles flood problems is quite different. In northeastern Brazil, flash floods are mostly mitigated at a local level, with the subbasin being the main point of focus. In Oman, on the other hand, there is more of an integrated mitigation

strategy plan at a national level considering the entire basin. This study concluded that Oman's more unified mitigation strategy was more efficient in preventing flash floods, especially because it took into account the topography of each basin; in the Brazilian semiarid region, mitigation measures are often relegated to nonstructural measures such as land evacuation plans and flood-risk maps. The frequency of flash floods is lower in arid basins than in semiarid basins; however, the magnitudes of flash floods are higher in the former. In recent times, Oman has had an unprecedented string of flash floods due to cyclones and thunderstorms that have combined to cause very intense precipitation events. Despite the recentness of this phenomenon affecting Oman, the government has developed a successful plan based on distributed structural measures, as seen in the previously mentioned seven-dam project in Wadi Uday. Such policies can be a great lesson for semiarid Brazil, which lacks inclusive and comprehensive structural measures to address the flash flood phenomenon.

References

Abdel-Fattah M, Kantoush S, Sumi T (2015) Integrated management of flash flood in wadi system of Egypt: disaster prevention and water harvesting

Abdel-Fattah M, Kantoush S, Saber M, Sumi T (2016) Hydrological modelling of flash flood at wadi samail, Oman

Abdel-Fattah M, Saber M, Kantoush SA, Khalil MF, Sumi T, Sefelnasr AM (2017) A hydrological and geomorphometric approach to understanding the generation of wadi flash floods. Water 9 (7):553. https://doi.org/10.3390/w9070553

Abdel-Fattah M, Kantoush SA, Saber M, Sumi T (2018) Rainfall-runoff modeling for extreme flash floods in wadi samail, Oman. J Jpn Soc Civ Eng Ser B1 (Hydraul Eng) 74(5):I_691–I_696. https://doi.org/10.2208/jscejhe.74.5_I_691

Abdel-Fattah M, Kantoush S, Saber M, Sumi T (2021) Evaluation of structural measures for flash flood mitigation in wadi abadi region of Egypt. J Hydrol Eng. https://doi.org/10.1061/(ASCE)HE.1943-5584.0002034

Abdrabo KI, Kantoush SA, Saber M, Sumi T, Habiba OM, Elleithy D, Elboshy B (2020) Integrated methodology for urban flood risk mapping at the microscale in ungauged regions: a case study of Hurghada, Egypt. Remote Sens 12(21):3548. https://doi.org/10.3390/rs12213548

Al Barwani AS (2016) Omani experience in flash floods, disaster risk reduction and water harvesting. In: Proceedings of the second international symposium on flash floods in wadi systems: disaster risk reduction and water harvesting in the Arab region, pp 19–24

Alcantara HM, Cunha JEB, Galvao CO, Taveira IML (2013) Decisions on land conservation practices in a semi-arid region considering hydrological and social drivers. IAHS-AISH Publ 359:352–357

Al-Rawas GAA (2011) Flash flood modelling in Oman Wadis. Library and Archives Canada, Bibliothèque et Archives Canada, Ottawa

Al-Rawas GAA (2013) Urbanization impact on rainfall runoff modeling; an integration of remote sensing and GIS approach. In: Proceedings of the international conference on water resources and environment research

Anon (2000) The disparity between extreme rainfall events and rare floods—with emphasis on the Semi-arid American West. Hydrol Process 13

Cadier E, Jose de Freitas B (1982) Bacia Representativa de Sumé: Primeira Estimativa Dos Recursos de Água

Chimnonyerem UN (n.d.) Meeting the challenges of flood risk assessment in data poor developing countries, with particular reference to flood risk management in Lagos, Nigeria, p 375

Cutter SL, Munich Re Foundation Chair on Social Vulnerability, and Summer Academy on Social Vulnerability (eds) (2013) From social vulnerability to resilience: measuring progress toward disaster risk reduction outcomes of the 7th UNU-EHS summer academy of the Munich Re Foundation Chair on Social Vulnerability, 1–7 July 2012, Hohenkammer, Germany

Geber BDA, de Melo JSP, Giongo PR, Lira Júnior MdA, da Silva APN (2008) Relação Entre Condições Hídricas e o Crescimento Vegetal Da Cana-de-Açúcar No Município Itambé, Pernambuco. Revista Caatinga 21(5):171–77

Huang G, Shen Z (eds) (2019) Urban planning and water-related disaster management. Springer International Publishing, Cham

Huang J, Haipeng Yu, Guan X, Wang G, Guo R (2016) Accelerated dryland expansion under climate change. Nat Clim Chang 6(2):166–171. https://doi.org/10.1038/nclimate2837

Hunter NM, Bates PD, Horritt MS, Wilson MD (2007) Simple spatially-distributed models for predicting flood inundation: a review. Geomorphology 90(3–4):208–225. https://doi.org/10.1016/j.geomorph.2006.10.021

Jha AK, Bloch R, Lamond J (2012) Cities and flooding: a guide to integrated urban flood risk management for the 21st century. The World Bank

Knighton D (1984) Fluvial forms and processes. Edward Arnold Inc., New York

Kwarteng AY, Dorvlo AS, Vijaya Kumar GT (2009) Analysis of a 27-Year rainfall data (1977–2003) in the Sultanate of Oman. Int J Climatol 29(4):605–617. https://doi.org/10.1002/joc.1727

Lin X (1999) Flash floods in arid and semi-arid zones. Technical Documents in Hydrology

Lindoso D, Eiró F, Bursztyn M, Rodrigues-Filho S, Nasuti S (2018) Harvesting water for living with drought: insights from the Brazilian human coexistence with semi-aridity approach towards achieving the sustainable development goals. Sustainability 10(3):622. https://doi.org/10.3390/su10030622

Lindoso DP, Pereira Filho SR (n.d.) Vulnerabilidade e adaptação da vida às secas, 519

Malveira VTC, de Araújo JC, Güntner A (2012) Hydrological impact of a high-density reservoir network in semiarid Northeastern Brazil. J Hydrol Eng 17(1):109–117. https://doi.org/10.1061/(ASCE)HE.1943-5584.0000404

Marengo JA, Nobre CA, Tomasella J, Oyama MD, de Oliveira GS, de Oliveira R, Camargo H, Alves LM, Foster Brown I (2008) The drought of amazonia in 2005. J Clim 21(3):495–516. https://doi.org/10.1175/2007JCLI1600.1

Metzger A, Marra F, Smith JA, Morin E (2020) Flood frequency estimation and uncertainty in arid/semi-arid regions. J Hydrol 590:125254. https://doi.org/10.1016/j.jhydrol.2020.125254

Ministry of Regional Municipalities and Water Resources (2009) Wadi Aday flood protection dams. 1. Oman.

Moya J, Kantoush SA, Abdel-Fattah M, Sumi T, Saber M (2017) A comparative study between flash floods in arid and semi-arid basins with respect to economic mitigation measures, pp 21–22

Pathirana A, Denekew HB, Veerbeek W, Zevenbergen C, Banda AT (2014) Impact of urban growth-driven landuse change on microclimate and extreme precipitation—a sensitivity study. Atmos Res 138:59–72

Rogger M, Viglione A, Derx J, Bloeschl G (2014) Step changes in the flood frequency curve-quantifying effects of catchments storage thresholds. EGUGA 12100

Saber M, Abdrabo KI, Habiba OM, Kantosh SA, Sumi T (2020) Impacts of triple factors on flash flood vulnerability in Egypt: urban growth, extreme climate, and mismanagement. Geosciences 10(1):24

Saber M, Habib E (2016) Flash floods modelling for wadi system: challenges and trends. In: Landscape dynamics, soils and hydrological processes in varied climates. Springer, Berlin, pp 317–339

Saber M, Hamaguchi T, Kojiri T, Tanaka K (2010) Flash flooding simulation using hydrological modeling of wadi basins at Nile river based on satellite remote sensing data

Saber M, Kantoush S, Abdel-Fattah M, Sumi T (2017) Assessing flash floods prone regions at wadi basins in Aswan, Egypt. 京都大学防災研究所年報. B= Disaster Prev Res Inst Annuals B 60(B):853–863

Saleh AS, Al-Hatrushi SM (n.d.) Torrential flood hazards assessment, management, and mitigation, in wadi aday, Muscat area, Sultanate of Oman. GIS RS Approach 17

Sayama T (2013) Rainfall-runoff-inundation (RRI) model ver. 1.4. 2. International Center for Water Hazard and Risk Management (ICHARM), Public Works Research Institute (PWRI)

Sayama T (2015) Rainfall-runoff-inundation (RRI) model manual, version 1.4. 2, International Center for Water Hazard and Risk Management (ICHARM), Public Works Research Institute (PWRI)

Silva JC, Heldwein AB, Martins FB, Trentin G, Grimm EL (2007) Análise de distribuição de chuva para Santa Maria, RS. Revista Brasileira de Engenharia Agrícola e Ambiental 11(1):67–72. https://doi.org/10.1590/S1415-43662007000100009

Tanaka* K, Omar H, Tanaka S (2020) Changes in extreme rainfall in arid and semi-arid region projected by super high resolution AGCM. In: Fifth international conference on engineering geophysics (ICEG). Society of Exploration Geophysicists, Al Ain, UAE, pp 296–299

Wang D, Zhao H (2008) Estimation of phytoplankton responses to hurricane Gonu over the Arabian Sea based on ocean color data. Sensors 8(8):4878–4893. https://doi.org/10.3390/s8084878

Wheater H, Sorooshian S, Sharma KD (2007) Hydrological modelling in arid and semi-arid areas. Cambridge University Press

Chapter 14
Assessment of Exposure to Flash Flooding in an Arid Environment: A Case Study of the Jeddah City Neighborhood Abruq Ar Rughamah, Saudi Arabia

Saeed Alharbi and Gerald Mills

Abstract In arid areas, flash floods represent one of the most severe hazards for people and infrastructure alike. The associated risks are compounded by increasing exposure and vulnerability through rapid and unregulated urbanization, poor infrastructure, and sociocultural factors, among other elements. This research explores the flash flooding risk in the Saudi Arabian city of Jeddah with a particular focus on the Abruq Ar Rughamah neighborhood, which experienced a destructive flood in November 2009 that resulted in 116 deaths and 1,200 families becoming homeless. The neighborhood is an interesting case study as it has two distinctive urban layouts representing planned and irregular settlement types. In this paper, the focus is placed on exposure to flash flood hazards using a geographic information system to study urban layouts, building types, and resident populations in conjunction with data from satellites, flood mapping studies, and topographic data. The results show that most of the study area is located along a natural flood path. The regions that were affected by the 2009 disaster received no comprehensive site rehabilitation. This paper concludes that it is important to develop a risk management strategy that includes limiting urban expansion in flood-prone areas and redesigning neighborhoods to increase flood resilience.

Keywords Urbanization · Flood hazard · Urban planning · Unplanned area

S. Alharbi (✉) · G. Mills
School of Geography, College of Social Sciences and Law, University College Dublin, Dublin, Ireland
e-mail: saeed-abdulaali.alharbi@ucdconnect.ie

G. Mills
e-mail: gerald.mills@ucd.ie

T. Sumi et al. (eds.), *Wadi Flash Floods*, Natural Disaster Science and Mitigation Engineering: DPRI Reports, https://doi.org/10.1007/978-981-16-2904-4_14

14.1 Introduction

Urbanization has two distinct but related meanings. The first is the demographic shift in the global population from rural to urban living. Since the mid-twentieth century, the global urban population has expanded rapidly; in 1900, just 15% of the world's population of 1.6 billion lived in cities (Spence et al. 2009), and now, more than half of the 7 billion on the planet live in cities. Moreover, it is projected that the quantity of individuals living in cities will increase to over six billion by 2045 due to both migration and natural population increases (World Bank 2018). The second is the transformation of the landscape as the natural land surface cover is replaced by closely spaced buildings and impermeable surfaces. Much of this urbanization is concentrated in areas that are exposed to natural hazards such as flooding, extreme weather, and geological events (e.g., Small and Naumann 2001), placing a larger number of people at risk. Some of these risks are accentuated by environmental changes at global, regional, and urban levels, many of which are linked to human activities. For example, most cities are located on coastlines near sea level and are projected to experience the effects of sea-level rise due to global warming (Neumann et al. 2015). In addition, impermeable urban surface cover is linked to rising air temperatures (the urban heat island effect) and increased flooding, as storage has decreased while runoff has surged. The types of hazards to which cities are exposed vary with climate and topography; thus, each city may require a unique solution to reduce its risk. However, the great majority of current global urbanization is taking place in economically developing regions (Henderson et al. 2017) where growth is often unplanned and unmanaged (Ali et al. 2015) and the capacity to respond to hazard events is limited.

Saudi Arabia is in an arid and semiarid climatic region. The weather is unpredictable, and the geomorphology is specific, so the region is prone to occasional floods. Settlements, agriculture, roads, and infrastructure together increase the potential for flood hazards because they cause floodwater to be unable to leak into the subsoil, which in turn increases the volumes and speeds of water flows. The expanding population puts pressure on these regions as per capita water use increases, resulting in limited water resources (Wheater 2002; Nemec and Rodier 1979).

Floods are one of the major effects of indiscriminate urbanization, and Jeddah is exposed to different levels of flooding. On November 25, 2009, flash floods occurred in Jeddah during one of the most exceedingly terrible and damaging flood events throughout the entire existence of the city. The official death toll totaled 116 people (Alsaggaf 2012). In addition to claiming lives, the floods also wrecked more than 4,000 cars and caused more than 1,200 families to become homeless; the resulting damage ran into the millions (Alsaggaf 2012). The depths of this flood were 1.34 m in the main channel of the valley and approximately 2 m on the streets, confirming that it was not only natural causes that led to this disaster but also the profound effect of urbanization (El-Hames and Al-Wagdany 2012). The impact of the floods was most severe in the Abruq Ar Rughamah neighborhood.

While there was little research on the topic prior to the disaster (Ameur 2016), following the Jeddah catastrophe, a number of studies focused on the extent of flood damage and explained the outcome in terms of physical processes, such as the intensity of rainfall and the local topography. In the research following the flood event, detailed mapping was performed to assess and analyze flood risk using satellite images and digital elevation models (DEMs). Al Saud (2010, 2015) used high-resolution images before and after the event to identify the affected areas. The study used data derived from climatic records from ground-based stations, remotely sensed data, and additional information such as geological and topographic maps, DEMs at 2 and 30 m accuracies, satellite images, and software (ENVI-4.3, ERDAS9.3, Arc-GIS 9.3). Moreover, the author examined physical and anthropogenic factors such as drainage systems, rainfall distribution, geomorphologic and geological characteristics, and urban expansion. An overview of the flooding experienced in 2009 and 2011 in Jeddah was also included; the study covered the conveyance of floods and torrents and various aspects such as transported water and sediment, injected flows, impact flows, restricted rainwater, and water bodies and flows in urban areas. Al-Saud also used a hydrological analysis of DEMs that included the slopes of basins in the study area, cross sections, channel slopes, and depressions, as well as a geometric analysis of the drainage systems (length/width ratios, shape factors, widths/outlets, and width ratios). The study also presented analyses of drainage systems (morphometric analysis), stream order, and, finally, the meandering ratio. Furthermore, it included an assessment and examination of the localities damaged by the floods in both 2009 and 2011 in terms of the levels of risk. The study also included an overview of the existing flood control measures in the study area in terms of small-scale flood control measures, such as pipes for water tunneling, and large-scale flood control measures, including dams and old water channels. Additionally, erroneous flood control was also noted, including depression dumping, the closure of valley passageways, soil obstacles, and narrow tunnels. Proposed projects and programs were discussed that included some objectives to reduce the impacts of flooding in at-risk areas: setting up infrastructures in urban areas to drain water, stabilizing flood plains, constructing retaining walls, creating channels, constructing dams, cleaning channels, constructing tunnels adjacent to roads, and controlling encroachment on the passageways of valleys.

Moreover, Subyani (2012) used a DEM to identify geomorphological hazards in the study area by determining the slope and considered the level of risk to be connected to the slope percentage. In terms of hydrology, he used buffering tools in a GIS environment to identify vulnerable areas and linked land use with the overall risk of flooding; all low-lying urban areas of the city are considered to be at high risk of flooding. Furthermore, he assessed flood vulnerability in arid areas to aid decision-makers and contributed to flooding protection plans by predicting a yearly maximum 24-h precipitation value alongside 25-, 50-, 100-, and 200-year forecasts using Gumbel's extreme value distribution (EV1) and log-Pearson type III model at 18 rainfall stations around select valleys in western Saudi Arabia.

Additionally, the study by Elfeki et al. (2011) used simulation models to estimate the flood hydrograph of the 2009 storm to determine the impact of floods on

urban areas in Jeddah. Two hydrologic models were used to estimate the floods caused by the 2009 storm: the HEC-HMS 3.3 hydrological modeling system and the WMS 7.1 watershed modeling system were consulted, and a diffusive wave model was developed. In addition, both models and satellite images integrated with GIS were examined to capture the water depths and inundation zone. In their study, Hadadin et al. (2013) applied the synthetic unit hydrograph hypothesis to determine the peak release of the stream during the Jeddah flood; this value is necessary in the establishment of the flood hydrography to evaluate water resources and design different hydraulic structures. Two prediction models were used in the study, the Snyder approach and a routing unit hydrograph, to analyze 12 streams east of Jeddah. The study concluded that there is a strong relationship between the density of drainage systems and the ability of water to infiltrate. Furthermore, El-Hames and Al-Wagdany (2012) also worked on rebuilding the characteristics and hydrograph of the 2009 flood by using HEC-RAS software as well as a dimensionless hydrograph, the Soil Conservation Service (SCS) curve number, GIS, and a DEM. The study found that in the case of the natural conditions of the 2009 flood, the height of the water reached 1.34 m in the main channel and two meters in the neighborhood due to its narrow streets; the floodwater was discovered to have risen to 2.1 m at street entrances. The study contradicted assumptions that the disaster was due to natural causes. The urbanization of hot arid environments with a BWh climate types in the Köppen classification has generally received little attention, although these regions also experience rapid urban growth. These areas are characterized by high temperatures and infrequent rainfall events that result in sparse vegetative cover. The hydrological systems of these regions often consist of wide and shallow channels that are usually dry (wadis) but respond to rapid and intense rainfall events that generate flash floods. These events are difficult to prepare for because they are rare, difficult to predict and provide little lead times for warnings and evacuations (Lin 1999). Moreover, urbanization in areas prone to flash flooding exacerbates flood hazards by obstructing and redirecting flows and enhances risk by increasing exposure.

This paper offers an assessment of the exposure and vulnerability to flash flood hazards in Jeddah city, Saudi Arabia, an area that has experienced many flooding events over the last two decades. The focus is on the role of physical planning (including building construction and urban layout) in managing risk. To illustrate these factors, the November 2009 flood event is selected and the Abruq Ar-Rughamah neighborhood is chosen as the case study; this neighborhood has two distinctive urban forms representing formal (planned) and informal (irregular) settlement types.

14.2 Jeddah Case Study

The city of Jeddah covers an area of 748 km^2 along a thin and gently inclining coastal plain between the Red Sea line and the Al-Hejaz slope (Fig. 14.1). Its climate is hot and dry; during the summer months, temperatures can exceed 40 °C, while the relative humidity (RH) can approach saturation (Subyani 2009). Rainfall, when it occurs, takes place mostly during the winter period and is associated with convective activity triggered by the passage of low-pressure systems moving in from the west (Haggag and El-Badry 2013). Although Jeddah receives just over 50 mm of rainfall annually, much of it arrives as intense rainfall events of limited spatial extent; at Jeddah Airport, the mean annual rainfall is 63 mm, but the mean daily maximum is almost 36 mm. Uplift over the Al-Hejaz escarpment results in much higher rainfall amounts over these uplifted regions, in excess of 220 mm/year (Haggag and El-Badry 2013). The generated precipitation travels through nearly 80 drainage systems that convey runoff from the escarpments in the east through Jeddah into the Red Sea in the west (Qari 2008). Since 2005, Jeddah has experienced several flood events (Tekeli 2017); one of the most devastating events took place from 24 to November 26, 2009 and severely impacted the Abruq Ar-Rughamah neighborhood in the southern part of the city.

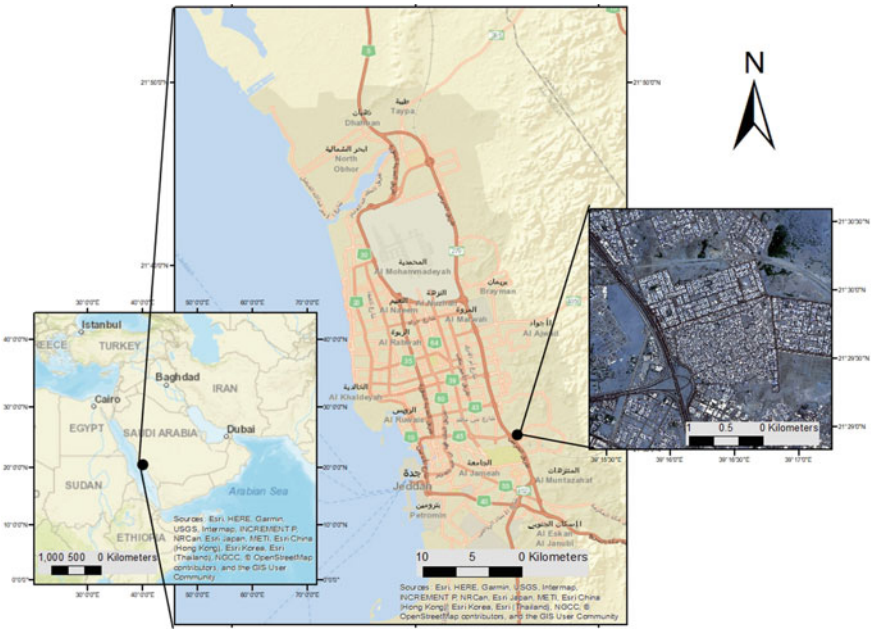

Fig. 14.1 Location of Jeddah's urban area between the Red Sea coast to the west and the Hejaz escarpment to the east. The red boundary indicates the Abruq Ar Rughamah neighborhood

The population of Jeddah is increasing rapidly; its population has doubled since 1990 and now stands at over 4.1 million. In 2010, Jeddah had a population of 3.5 million, approximately half of whom were non-Saudis and 40% were female. This population occupied 702,527 dwellings (that is, almost five persons per dwelling). Not surprisingly, population growth has resulted in considerable pressure to build houses. At the edges of the city, urban growth occurs in both planned developments and informal settlements. The former are subject to official planning and building permits, while the latter have no legal status and the land on which they are built is cheaper. The two types of urban growth are also distinguished by building construction types and layout. In general, formal settlements are laid out on grids with wide roads and buildings constructed from modern materials. Many newer buildings are multistory apartments that have steel/concrete supports. By comparison, informal settlements are laid out in a haphazard fashion; the buildings are typically one story, enclosed by walls, and are built using bricks/adobe and wooden supports. The streets in these settlements are short and narrow (Fig. 14.2a). Informal settlements are the preferred destination for low-income residents, as the rents are lower in the informal settlements than in the planned developments. Approximately

Fig. 14.2 **a** Traditional buildings and the shape of the streets in the informal settlement area. **b** A villa, one of the common types of residential buildings in Jeddah. **c** A scene depicting a formal settlement, showing the building types and the shape of the streets. **d** Basic structure of modern buildings constructed using concrete columns

one-third of the population lives in approximately 70 of these types of informal settlements (Aleqtisadia 2018).

The Abruq Ar Rughamah neighborhood is located in eastern Jeddah and is built on the basin of the Qus wadi (Fig. 14.1). On November 25, 2009, the flash floods that occurred in Jeddah were most severe in this neighborhood; 116 people lost their lives, 1,200 families were made homeless, and property was damaged and destroyed (Alsaggaf 2012). This neighborhood makes an ideal case study because it is composed of informal and formal settlement types, both of which were severely affected by the flood event. Figure 14.3 shows a satellite image (SPOT-70 0.6M) of the study area from 2016; superimposed on this image are the river channels within the Qus wadi and the area that was severely affected due to the flash flood in 2009 (Al Saud 2015).

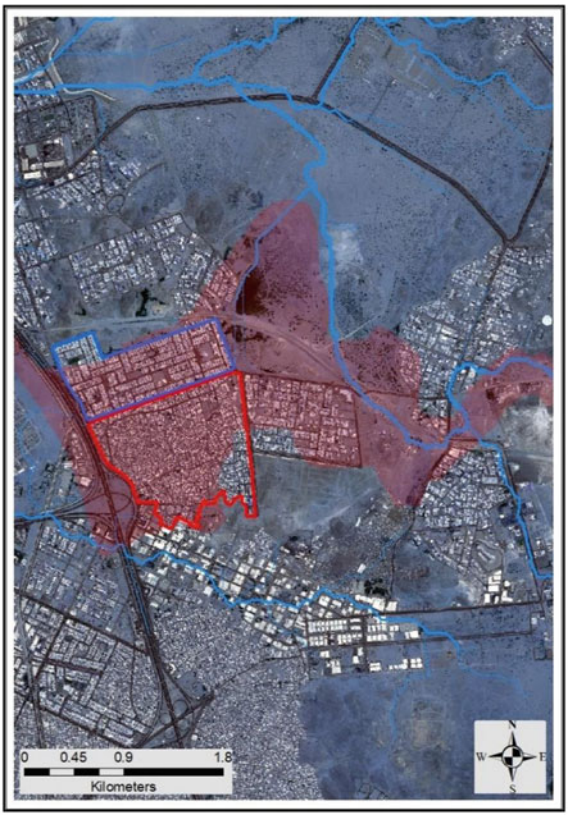

Fig. 14.3 Abruq Ar Rughamah neighborhood. The red boundary shows the informal settlement type area, and the dark blue boundary shows the formal settlement type area. The red shading shows the area affected by the 2009 flood, and the light blue lines depict the stream system

14.3 Data and Methods

The main source of data for this study is the 2010 Saudi census (Saudi Arabia General Authority of Statistics) and the associated geographic files. The census is collected from households but is typically available only at the level of the governate (of which there are 118), the region (13), and the state. Jeddah is a governate within the Makkah region. For enumeration purposes, each governate is divided into neighborhoods, sectors, and blocks based on the road network. A block describes a building or a number of contiguous buildings that are not separated by streets and can form irregularly shaped polygons. For this study, the census data for the Abruq Ar Rughamah neighborhood were collated at the block scale. These data are unique, as they were manually entered from the original census returns specifically for this project. Given the time taken to generate these data, relevant variables were created from the full census form. The variables included information on geography, types of houses, nature of occupancies, communication systems, and population that could be used to assess the levels of risk. The geographic location can be used to evaluate exposure to flood risk, while housing type is a measure of each dwelling's strength and its ability to withstand the effects of a flash flood. The census distinguishes between five types of dwellings: traditional, villa, apartment, tent, and shanty; the first three types are present in this neighborhood (see Fig. 14.2). Both the villa and apartment types are classed as modern buildings, owing to the construction techniques and materials used. The age profile, and in particular the male to female ratio, is a measure of the daytime residential population, while communication infrastructure can be used to evaluate the potential for a warning system. The block information is linked to a digital map so that these data can be analyzed geographically. The layout of the blocks and the road network can also be examined using a geographic information system (GIS). The road design plays an important role in blocking and redirecting floodwaters. Moreover, the road width can play a role in accentuating hazards by narrowing channels and raising water levels. During the 2009 event, it was estimated that the depth of the floodwaters was 1.34 m in the main channel of the Qus wadi but approximately 2 m in the streets within the informal settlement area (El-Hames and Al-Wagdany 2012). Finally, the presence of cars along roads will contribute further to hazards by restricting flows along streets and providing debris that can damage walls and dwellings. In the following section, descriptions of these attributes are given in relation to the formal and informal areas of the Abruq Ar Rughamah neighborhood.

14.4 Results

Figure 14.4 and Table 14.1 show the attributes of the neighborhood, depicting the physical forms (building type and road density) and population exposure in the formal and informal areas. There is little difference between the two areas in terms of population exposure: both are densely occupied (>12,000 persons per sq. km), the majority of the occupants are male, and approximately 20% are either elderly (>60 years) or young (<6 years). Most of in the formal settlement live in rented accommodations, whereas approximately half of the occupants living in the informal settlement own their dwellings. Figure 14.4 shows that the population densities and the distributions of old and young individuals are evenly dispersed within each settlement.

In terms of comparative physical geographies, the formal and informal settlements differ significantly. The planned settlement area has long roads, wide streets, and few traditional buildings. Although the built fraction of the landscape in the informal settlement area is nearly the same as that in the formal settlement area, the street lengths in the informal settlement area are, on average, one-quarter of the length of those in the formal settlement area, and the streets are much narrower in the former area than in the latter. Figure 14.2 confirms these basic features. The

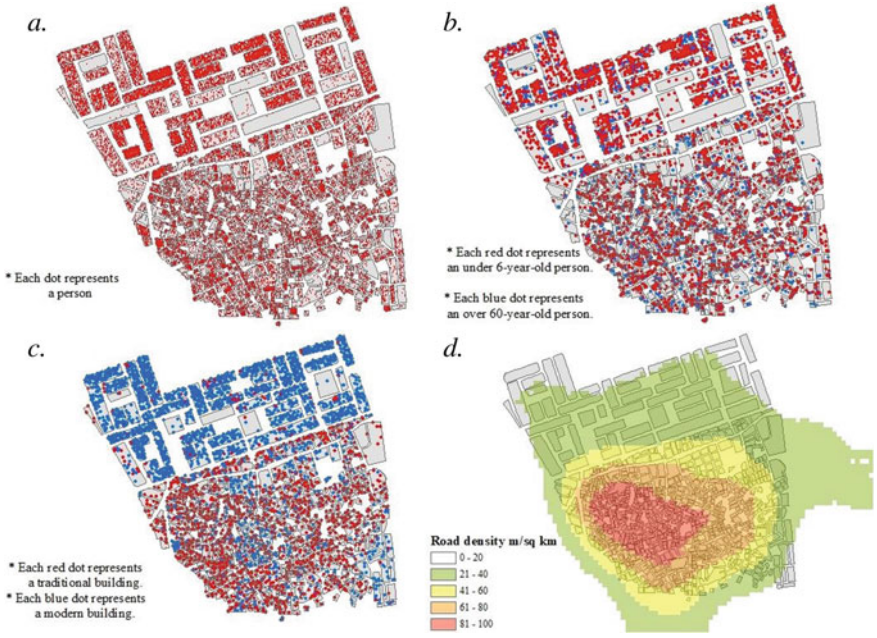

Fig. 14.4 Physical and human geographical aspects of the Abruq Ar Rughamah neighborhood: **a** population distribution; **b** dependent population (those under 6 and over 60 years of age); **c** distribution of modern and traditional buildings, and **d** road density

Table 14.1 Properties of the Abruq Ar Rughamah neighborhood

Attribute	Formal	Informal
Physical geography		
Area	0.80 km^2	1.31 km^2
Built fraction	0.62	0.68
Traditional housing unit	116	22,80
Modern housing unit	2,444	976
Average street width	17 m	5.7 m
Average street length	106 m	25 m
Population geography		
Population	10,375	16,169
Population density	13,036 cap. km^{-2}	12,360 cap. km^{-2}
Male	5,583 (54%)	9,423 (58%)
Female	4,792 (46%)	6,746 (42%)
Under 6 years old	1,907 (18%)	2,370 (15%)
Over 60 years old	413 (4%)	589 (4%)
Tenants	1,845	1,572
Owners	624	1,511

planned development area consists of buildings that form rectangular blocks arranged as a grid; the wide roads are aligned with the natural slope so that flood water can move through the settlement with few impediments. The buildings in this region are strong and have multiple floors, enabling evacuation to higher floors. The unplanned development area has many roads (see Fig. 14.2a and c) that are short and narrow with no dominant directions; thus, floodwaters that enter the settlement area are obstructed, and the water level rises. Moreover, the buildings and walls in this settlement area are weaker and more prone to damage than those in the planned development area.

An additional factor that contributes to flood risk in the neighborhood is parked cars. As a result of the availability of cheap fuel and cars in Saudi Arabia, the majority of residents depend on cars for travel; in 2014, there were 336 vehicles per 1,000 persons. It is important to consider that since 2018, Saudi Arabia has begun to allow women to drive, suggesting that the number of cars owned by each family may increase. Therefore, while cars could be used as a means of evacuation if there were sufficient warnings, cars are easily movable and often become debris when floods occur. During the 2009 flood disaster, many roads became impassable due to blockages created by cars; this was especially true in areas with narrow streets (Fig. 14.5). A simple geographic analysis of car locations based on a 2016 satellite image showed that there were approximately 4,500 cars in the informal settlement area, corresponding to a density of over 5,000 vehicles per km^2 if the built area is excluded. A typical car is nearly 2 m wide or one-third of the average street width in

the informal settlement; in other words, the same density of cars occupies less road space in the formal settlement area than in the informal settlement area.

14.5 Discussion

The Abruq Ar Rughamah neighborhood represents a good case study of urbanization and exposure to flash flood hazards. The neighborhood has experienced two recent flash flood events (in 2009 and 2011) due to its location in the Qus Valley basin; however, Fig. 14.6 shows that urbanization continues as before. The expansion of Jeddah into flood risk zones suggests that the likelihood of flood recurrence is not properly accounted for in land management planning. There is a critical need for a flash flood hazard map that outlines the likely return period for flood events of varying magnitudes. These maps should be central to all urban plans and should be made available to the local population to increase residents' awareness of flood risks and encourage their participation in flood risk management. If further urbanization takes place in at-risk zones, the nature of the flood hazard should be explicitly addressed in urban planning and design. Measures could include upstream dam construction and/or drainage channels to control the path of floodwater and divert it from settled areas. It is also possible to create retention reservoirs to collect some of the flood water temporarily or permanently so that it can be used later, reducing the volume of floodwater and the speed of runoff. Ideally, these systems would be part of land-use plans and urban design prior to urbanization.

Fig. 14.5 A photograph of the 2009 flood disaster in the study area showing the impact of cars forming debris that leads to the obstruction of the entry of rescue teams (Alriyadh Newspaper 2018)

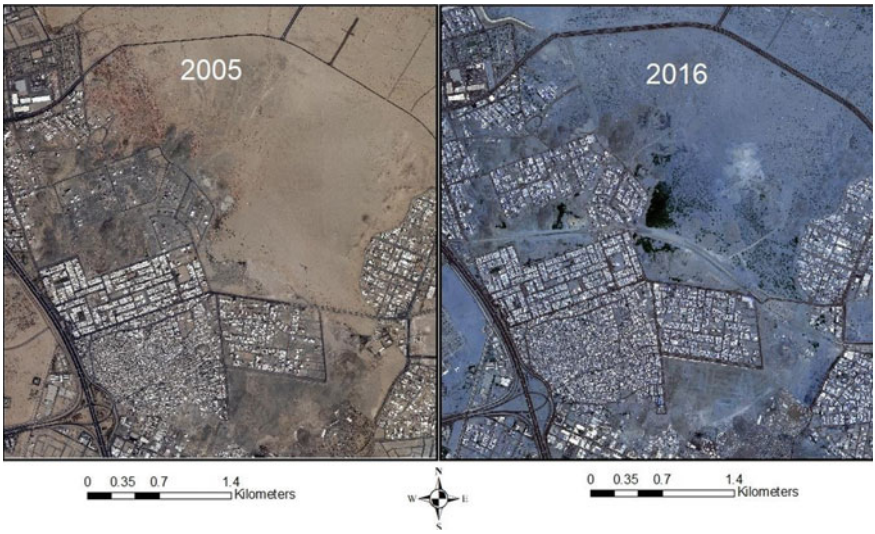

Fig. 14.6 Footprint of urbanization in 2005 and 2016

In addition to design changes, there is also a need for an early warning system that is linked to actions at the neighborhood and household levels. The absence of such a system in the 2009 flash flood event has been noted (Momani and Fadil 2010). Such a system would include meteorological and hydrological observations and modeling coupled with an effective communication system. Smartphone technology, which is widely available in Saudi Arabia, provides an opportunity for direct communication with affected households (Alkhunaizan and Love 2013). The final component of the system requires actions on behalf of household members in response to threats. It is clear from the above analysis that the flood risk differs greatly depending on the physical characteristics of a settlement; thus, the required actions will also differ.

Abruq Ar Rughamah was selected for this study because it is composed of both formal and informal settlements. Although the entire neighborhood is exposed to flood hazards, informal settlements, which mostly feature traditional houses, are more vulnerable to floods for a number of reasons. First, the physical geography of informal settlements enhances the flood hazard by impeding water flow, and the weaker construction materials used to build informal settlements point to a greater likelihood of structural damage. Second, the opportunities to evacuate are reduced in informal settlement areas; for example, the haphazard building layouts increase the presence of flood water in the streets, which transports debris (including cars). Modifying existing neighborhoods to cope with floods is difficult and would result in changes to buildings and their layouts for the following reasons.

- Official building permits are based on the Saudi Code of Building (sbc.gov.sa 2018), which stipulates the quality of construction materials to be used. This

code has not been applied to 'traditional' houses that use low-cost materials and do not have legal status. Strengthening buildings in these settlements should be a priority and may comprise the removal/rebuilding of dangerous structures that pose risks.

- Redesigning the layout would have to include creating new streets that are wide and aligned with the natural slope to provide a path through the built-up area. Protective barriers along these streets could limit damage to other parts of the settlement area. Such a dramatic redesign would also entail the removal of some buildings.

Other factors that increase the risk in informal settlement areas are cars parked on narrow roads. These factors impede the movement of emergency vehicles, act as waterborne debris during floods (damaging walls and buildings), and hamper clean-up efforts. Rules about parking that greatly reduce the street space occupied by vehicles are a priority; this may mean setting aside parking areas on the downstream side of the settlement area.

Flood risk assessments must account for community responses (Cutter 1996; Messner and Meyer 2005), but the census data used here offered limited insights into this component of flood risk. Although these data showed that the populations of the informal and formal settlements differed little in terms of demography, further work is needed to examine flood awareness and coping strategies.

14.6 Conclusions

Given the roles played by physical and human factors in this study, both of which led to increased vulnerability and exposure in the study area, this study recommends the redesign of unplanned parts of the city to improve the adaptability of these areas to flood risks. This would include opening drainage channels, especially in the irregular part of the neighborhood, and widening some narrow roads. This study also stresses the importance of finding urgent solutions for traditional buildings, as these buildings increase hazards both in flood scenarios and other natural disasters, such as earthquakes, due to their structural weaknesses.

Acknowledgments We thank the Ministry of Education in Saudi Arabia for sponsoring the author's PhD program. Appreciation is also expressed for the cooperation of the General Authority for Statistics in Saudi Arabia in providing the census data exclusively for this project.

References

Al Saud M (2010) Map of flood and torrents in City of Jeddah (in Arabic). J Geogr Res 91

Al Saud MM (2015) Flood control management for the city and surroundings of Jeddah. Springer, Saudi Arabia

Aleqtisadia Nwspaper (2018) الأحياء العشوائية في جدة.. وجودة الحياة المفقودة. 11 Aug 2011 [online]. Available from: http://www.aleqt.com/2011/08/14/article_569299.html. Accessed 7 Mar 2018

Ali A, Iqbal S, Ul Amin N, Malik H (2015) Urbanization and disaster risk in Pakistan. Acta Tehnice Corviniensis–Bull Eng 8(3):161–163. ISSN: 2067-3809

Alkhunaizan A, Love S (2013) Effect of demography on mobile commerce frequency of actual use in Saudi Arabia. In: Advances in information systems and technologies. Springer, Berlin, Heidelberg, pp 125–131

Alriyadh Newspaper (2018) 28 Nov 2009 [online]. صور كارثةجدة في. Available from: http://www.alriyadh.com/477736. Accessed 8 Mar 2018

Alsaggaf Y (2012) Social media and political participation in Saudi Arabia: the case of the 2009 Floods in Jeddah. Paper presented at the 8th international conference on culture, technology, communication (CaTaC'12), Aarhus University, Aarhus, Denmark

Ameur F (2016) Floods in Jeddah, Saudi Arabia: unusual phenomenon and huge losses. What prognoses. In: E3S web of conferences, vol 7. EDP Sciences, p 04019

Cutter SL (1996) Vulnerability to environmental hazards. Prog Hum Geogr 20(4):529–539

Elfeki AM, Ewea HA, Al-Amri N (2011) Simulation of urban flooding by diffusive wave model: Jeddah flood 2009 case study. In: First international geomatics symposium in Saudi Arabia, May 2011, King Abdel Aziz University, Jeddah

El-Hames A, Al-Wagdany A (2012) Reconstruction of flood characteristics in urbanized arid regions: case study of the flood of 25 November 2009 in Jeddah, Saudi Arabia. Hydrol Sci J 57 (3):507–516. https://doi.org/10.1080/02626667.2012.665995

Hadadin N, Tarawneh Z, Shatanawi K, Banihani Q, Hamdi MR (2013) Hydrological analysis for floodplain hazard of Jeddah's drainage basin, Saudi Arabia. Arab J Sci Eng (Springer Science & Business Media BV) 38(12)

Haggag M, El-Badry H (2013) Mesoscale numerical study of quasi-stationary convective system over Jeddah in November 2009. Atmos Clim Sci 3(1):73–86

Henderson V, Squires T, Storeygard A, Weil D (2017) On the spatial distribution of development. The roles of nature and history. In: The long economic and political shadow of history, vol 1. CEPR Press, London, pp 7–17. Available from: Vox EU E-book

Lin X (1999) Flash floods in arid and semi-arid zones. In: Technical documents in hydrology, no 23. UNESCO

Messner F, Meyer V (2005) Flood damage, vulnerability and risk perception—challenges for flood damage research. UFZ discussion papers 13/2005, Helmholtz Centre for Environmental Research (UFZ), Division of Social Sciences (ÖKUS)

Momani N, Fadil A (2010) Changing public policy due to Saudi City of Jeddah flood disaster. J Soc Sci 6(3):424–428

Nemec J, Rodier JA (1979) Streamflow characteristics in areas of low precipitation. In: Proceedings of a symposium on the hydrology of areas of low precipitation, Canberra, IAHS publ. no. 128, pp 125–140

Neumann B, Vafeidis AT, Zimmermann J, Nicholls RJ (2015) Future coastal population growth and exposure to sea-level rise and coastal flooding—a global assessment. PloS one 10(3): e0118571. https://doi.org/10.1371/journal.pone.0118571

Qari M (2008) Geomorphology of Jeddah Governate, with emphasis on drainage system. JKAU; Earth Sci 20(1):93–116

Sbc.gov.sa (2018) كود البناء السعودي. [online]. Available from: http://www.sbc.gov.sa/En/Pages/default.aspx. Accessed 12 Mar 2018

Small C, Naumann T (2001) The global distribution of human population and recent volcanism. Glob Environ Change Part b Environ Hazards 3(3–4):93–109

Spence M, Annez P, Buckley R (2009) Urbanization and growth. World Bank and Commission on Urbanization and Growth. Environment and Urbanization ASIA vol 1(2), p 227

Subyani AM (2012) Flood vulnerability assessment in arid areas, Western Saudi Arabia. Int J River Basin Manage 10(2):197–203

Subyani M (2009) Hydrologic behavior and flood probability for selected arid basins in Makkah area Western Saudi Arabia. Arab J Geosci 4(5–6):817–824

Tekeli AE (2017) Exploring jeddah floods by tropical rainfall measuring mission analysis. Water 9 (8):612

Wheater HS (2002) Hydrological processes in arid and semi arid areas. In: Wheater HS, Al-Weshah RA (eds) Hydrology of wadi systems. UNESCO, pp 5–22

World Bank (2018) Urban development [online]. Available from: http://www.worldbank.org/en/topic/urbandevelopment. Accessed 14 Mar 2018

Part V
Reservoir Sedimentation and Sediment Yield

Chapter 15
Integrated Study of Flash Floods in Wadi Basins Considering Sedimentation and Climate Change: An International Collaboration Project

Mohamed Saber, Sameh A. Kantoush, Tetsuya Sumi, Yusuke Ogiso, Tahani Alharrasi, Takahiro Koshiba, Mohammed Abdel-Fattah, Ali Al-Maktoumi, Osman A. Abdalla, Yasuhiro Takemon, Daisuke Nohara, Sohei Kobayashi, Mahmood Almamari, Khalid Al Hooti, Ahmed Al Barwani, Hilal Almamari, Dina Ellithey, Ekkehard Holzbecher, and Ahmed Hadidi

Abstract Recently, Wadi flash floods (WFFs) have happened frequently in arid environments, resulting in great damage the society and the environment. In Oman, severe WFFs have occurred repeatedly within the last 10 years causing a huge impact on human lives and properties. This paper aims at introducing the framework of an international collaboration project between Japan and Oman for WFF management considering sediment dynamics and climate changes. Four research groups were established: climate change (G1), rainfall-runoff modeling (G2), sediment yield and transport (G3), and sedimentation and infiltration processes (G4). Several field investigations were conducted since 2017 until now. The detailed field survey to assess the deposited sediment in a dry reservoir by using sediment bars, and infiltration test, as well as drone survey were addressed. Some of the prelim-

M. Saber (✉) · S. A. Kantoush · T. Sumi · Y. Ogiso · T. Alharrasi · T. Koshiba · M. Abdel-Fattah · Y. Takemon · D. Nohara · S. Kobayashi · M. Almamari · D. Ellithey
Disaster Prevention Research Institute (DPRI), Kyoto University, Kyoto 611-0011, Japan
e-mail: mohamedmd.saber.3u@kyoto-u.ac.jp

A. Al-Maktoumi
Soils, Water, and Agricultural Engineering, College of Agriculture and Marine Sciences, Sultan Qaboos University, Al Khoud, P.O. Box 34, Postal Code 123 Muscat, Oman

O. A. Abdalla · H. Almamari
Water Research Center, Sultan Qaboos University (SQU), Sultan Qaboos University, Al Khoud, P.O. Box 17, Postal Code 123 Muscat, Oman

K. Al Hooti · A. Al Barwani
Ministry of Regional Municipalities and Water Resources, Muscat, Oman

E. Holzbecher · A. Hadidi
Department of Applied Geology, The German University of Technology in Oman, Muscat, Oman

T. Sumi et al. (eds.), *Wadi Flash Floods*, Natural Disaster Science and Mitigation Engineering: DPRI Reports, https://doi.org/10.1007/978-981-16-2904-4_15

inary results and findings from the field investigation is discussed. The results show there is an adverse impact of sedimentation clogging on the infiltration process at the reservoirs. Based on the historical rainfall data analysis, there is a systematic increasing trend of the annual average precipitation with remarkable cycles over the MENA region and Oman. The knowledge obtained from this project is expected to be valuable to understanding sediment dynamics at Wadi basins.

Keywords Collaboration project · Wadi flash floods · Sedimentation · Climate change · Arid regions

15.1 Introduction

Information about hydrological processes in arid regions is scarce—although the associated problems are severe, particularly the management of water resources and soil erosion (Reid and Frostick 1987). Sediment yield data from a humid and a semiarid region was compared (Wolman and Miller 1960), and the conclusion of the study was the greatest part of the sediment removed from both drainage basins was carried by small to moderate flows with a recurrence interval of fewer than five years. This shows a large proportion of sediment yield and the erosion caused by an extremely short-lasting storm is a substantive property of rivers in arid and semiarid regions (Walling and Kleo 1979). Yet there has been surprisingly little attention paid to sedimentation assessments and impacts associated with flash floods in arid regions, especially in the Arab regions with hyperaridic conditions. Several studies have highlighted the importance of sediment monitoring during flash floods to operate and take countermeasures in recharge dams, but the sediment observations have not been recorded and documented adequately (Reid and Frostick 1987). Monitoring the sediments coming from upstream reaches in Wadi basins during the flash floods is extremely difficult in arid regions for two main reasons, the difficulty to access Wadi stream during the floods, and the missing of monitoring tools for sediment transport in most Wadi systems. A large quantity of sediments usually comes with the flash floods and is controlled by several factors such as geological and topographical features of the basins, the land uses and soil type variability, and the intensity and frequency of extreme rainfall, as well as the human impact. Therefore, to assess the sedimentation for any river basin regardless of the climatic conditions, such factors should be investigated to understand the interrelation with sediment yield.

Most of the arid and semiarid regions suffer from several challenges including (a) limited hydrological models due to the lack of monitoring networks, (b) a shortage of water resources—the available surface water is limited due to the paucity and high variability of rainfall events, and subsurface water is very important but suffers from quality problems and depletion due to mismanagement, and (c) the disaster of Wadi flash floods (WFFs) or drought conditions (Saber and Habib 2016). These problems are accompanied by practical difficulties involving

water resources management, planning, and development in arid areas. Several studies and efforts have been performed in WFF modeling to understand behaviors and characteristics (Saber 2010; Saber et al. 2013; Abdel-Fattah et al. 2017), mitigation strategies and water management (Sumi et al. 2013; Abdel-Fattah et al. 2015), and evaluation and bias corrections of satellite-based rainfall for flash flood simulations (Saber and Yilmaz 2018), but the assessments of sedimentation impacts associated with extreme events under climate change impacts are still negligible in Wadi basins.

Recently, WFFs have happened frequently and are becoming more devastating in arid regions, especially when considering climate change and sedimentation impacts. Oman has experienced severe flash floods such as (Cyclone Guno, June 2007 and Cyclone Phet, June 2010). Figure 15.1a shows rainfall totals around the Gulf of Oman between May 31 and June 7, 2007 (Cyclone Guno). For instance, the Cyclone Guno ($Q = 900\ m^3/s$) caused 50 fatalities and $3.9 billion worth of economic losses (Al Barwani 2015). Great damage to infrastructures (Fig. 15.1b), housing, and agricultural lands was recorded from Cyclone Guno. The red areas show where rainfall exceeded 200 mm (8 inches). The most recent cyclone that happened from May 25 to May 26, 2018 was named Cyclone Mekunu. It was much more powerful than previously recorded events in Southern Oman, and it extended to the neighboring countries as well. It reached category 3 as reported by the Ministry of Regional Municipalities and Water Resources (MRMWR). The cyclone endured from May 23 to May 27, 2018, with a total rainfall of about 617 mm. The maximum rainfall was of about 505 mm in just two days (May 25 and 26, 2018) as recorded by the rain gauges.

Wadi systems in arid regions (Fig. 15.2a) are not only characterized by extreme disasters (e.g., flash floods, drought) but also a lack of monitoring networks and integrated management strategies for water as well as sediments. Flash floods have become more frequent, especially in connection with extreme events like cyclones (Fig. 15.2b). In Oman, mitigation structures for flood control and groundwater

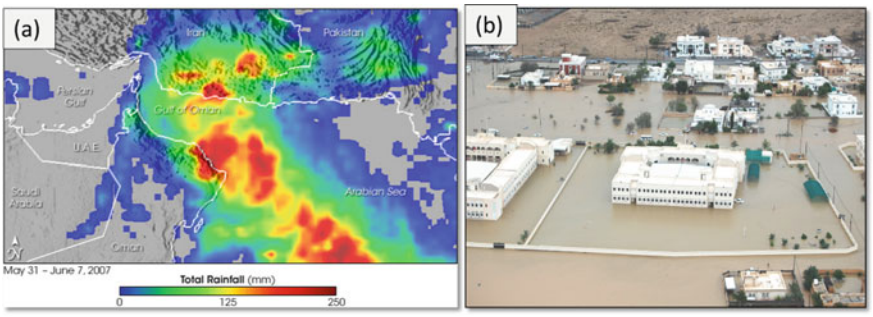

Fig. 15.1 **a** Total rainfall of Cyclone Guno in Oman between May 31 and June 7, 2007 (http://earthobservatory.nasa.gov/NaturalHazards/natural_hazards_v2.php3?img_id=14295). **b** An example of the resulting damage in Muscat City (Al Barwani 2015). *Source* Reprinted from Saber et al. (2018) Copy right 2018

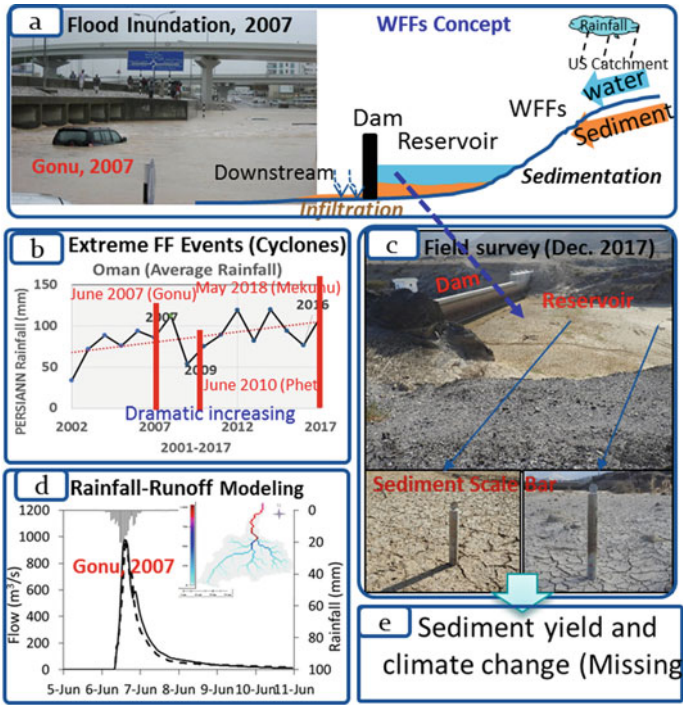

Fig. 15.2 Wadi flash flood concept (**a**), problematics (**b**), achievements (**c** and **d**), and gaps (**e**)

recharge have been installed. However, issues of sedimentation were underestimated, leading to environmental problems due to reservoir sedimentation (Fig. 15.2c). This was examined in field investigations in December 2017 and September 2018. Oman is one of the countries that could experience critical sedimentation volumes (Fig. 15.3a) by the year 2050 (ICOLD 2009). The current conditions of sedimentation exhibit real problems at many reservoirs (Fig. 15.3b). In this paper, we present the concept and framework for an international collaborative research project between Japan and Oman. In addition, we refer to efforts done in preparation for the project to prove the feasibility of the implementation and applicability of transferring the technology to developing countries.

Sedimentation is the most serious technical problem in reservoir management, especially in arid regions with increasing extreme flash floods. There are several reasons why sedimentation is so important in Wadi basins:

- The lack of previous studies, especially regarding the impacts on reservoir and infiltration.
- The deterioration of dams' ability to store water and the influence on their function for flood protection.

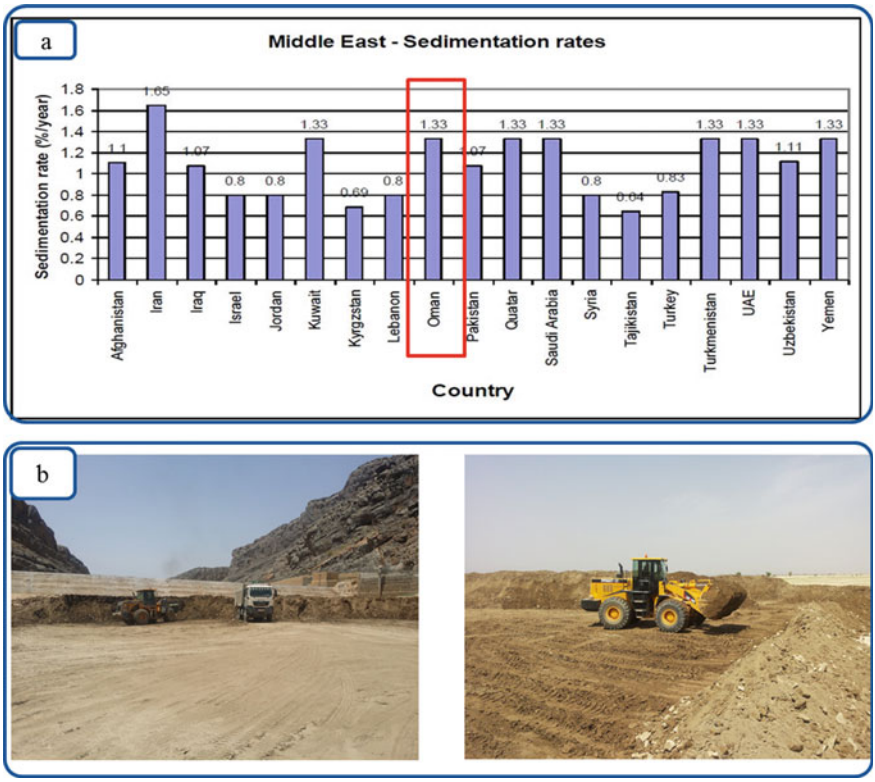

Fig. 15.3 a Actual and predicted sedimentation in the Middle East. *Source* Reprinted from (ICOLD 2009). **b** Reservoir sedimentation at Wadi Tanuf, Nizwa (right photo) and Wadi Al Kabir, Ibri (left photo), Oman

- The decrease of infiltration at the recharge zone at the downstream, consequently affecting the groundwater recharge.
- The increase of probability of the disaster impacts of WFFs.

In dry environments such as Wadi basins, the aforementioned problems are expected to be more serious and destructive than for perennial rivers, particularly with respect to climate change. Therefore, the assessment of the adverse impacts of sedimentation at Wadi basins is desperately crucial to bring forth a secure integrated water and sediment management strategy. The project's key scientific questions were

- What is the impact of climate change on extreme rainfall events?
- How can sediment yield be predicted based on understanding flash floods' spatiotemporal variability and sediment dynamics?
- What are the impacts of sedimentation on the infiltration processes?

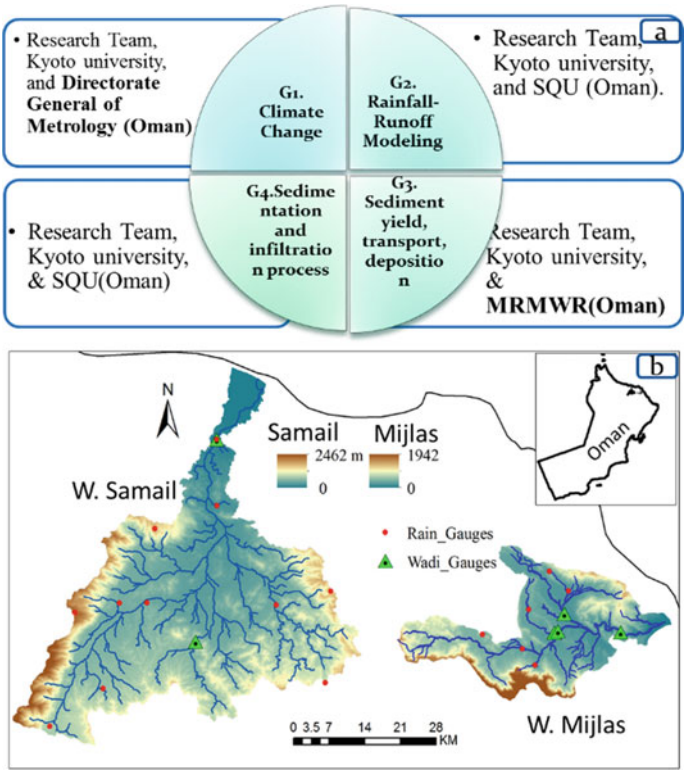

Fig. 15.4 a Research groups and roles in Japan and Oman. **b** Study areas of Wadis Samail and Mijlas in Oman

To address the raised questions and overcome the related problems of WFFs in arid regions, a project was initiated based on the international collaboration between Japan and Oman. The project consisted of four research groups (Fig. 15.4a): climate change (G1), rainfall-runoff modeling (G2), sediment yield and transport (G3), and sedimentation and infiltration processes (G4).

The target Wadi basins for the implementation of the project were Wadi Samail and Mijlas (Fig. 15.4b). The selection criteria included the possibility of monitoring data and the availability of facilities for the field surveys and the conduct of field investigations. Other aspects were (a) the knowledge that Oman is a Middle East leading country in the implementation of a unique flash flood management strategy, (b) the long history of collaboration with Kyoto University, Japan, since 2015, and (c) the expertise of Kyoto University concerning approaches for WFF simulation and sedimentation issues.

The main objectives of this project were to.

- Analyze the extreme rainfall events from historical records and assess the impacts of climate change (G1)

- Combine the developed sediment transport model with the developed hydrological models to simulate water discharge and sediment transport (G2 & G3)
- Assess sedimentation impacts on infiltration process by detailed field surveys (G4)
- Utilize the high-resolution satellite data (Interferometric Synthetic Aperture Radar [InSAR], ALOS Phased Array type L-band Synthetic Aperture Radar [PALSAR], etc.) to assess the sediment deposition, erosion, and sediment yield, and then validate by field investigation (G3 & G4)

15.2 Project Approach: Feasibility, Design, and Implementation

15.2.1 Research Approach and Implementation

The project aimed to develop an integrated concept of combined rainfall-runoff modeling with satellite-based data (InSAR, GSMaP) and field investigations to assess the sediment yield associated with WFF water. There was a special focus on understanding climate change impacts as well as sediment dynamics and its impacts on infiltration. The merit of this research project is unique since it assessed WFFs and sediment dynamics under climate change based on extensive field investigations. We started our collaborative network with Sultan Qaboos University (SQU), the Directorate General of Metrology (DGM), and MRMWR in Oman in 2015 and performed field investigations in 2016, 2017, and 2018 for several Wadis. A detailed presentation of each research group is given below.

15.2.1.1 Climate Change (G1)

The frequency of WFFs has dramatically increased within the last ten years (Saber et al. 2018); this might be as a result of climate change or human impacts. Understanding climate change is desperately needed and should be addressed in WFF studies. We started a rainfall analysis for the extreme events in arid regions (Fig. 15.5a), and the details will be addressed in Sect. 15.4. Analysis of the historical extreme events as well as future events will be conducted to understand the occurrence, rainfall variability, and climate change impacts on both intensity and magnitudes of WFFs. Downscaling and bias corrections of global circulation model outputs using the regional climate model to create different scenarios of climate change will be conducted. This will guide us to answer the question of how and why WFFs are recently becoming more frequent and devastating.

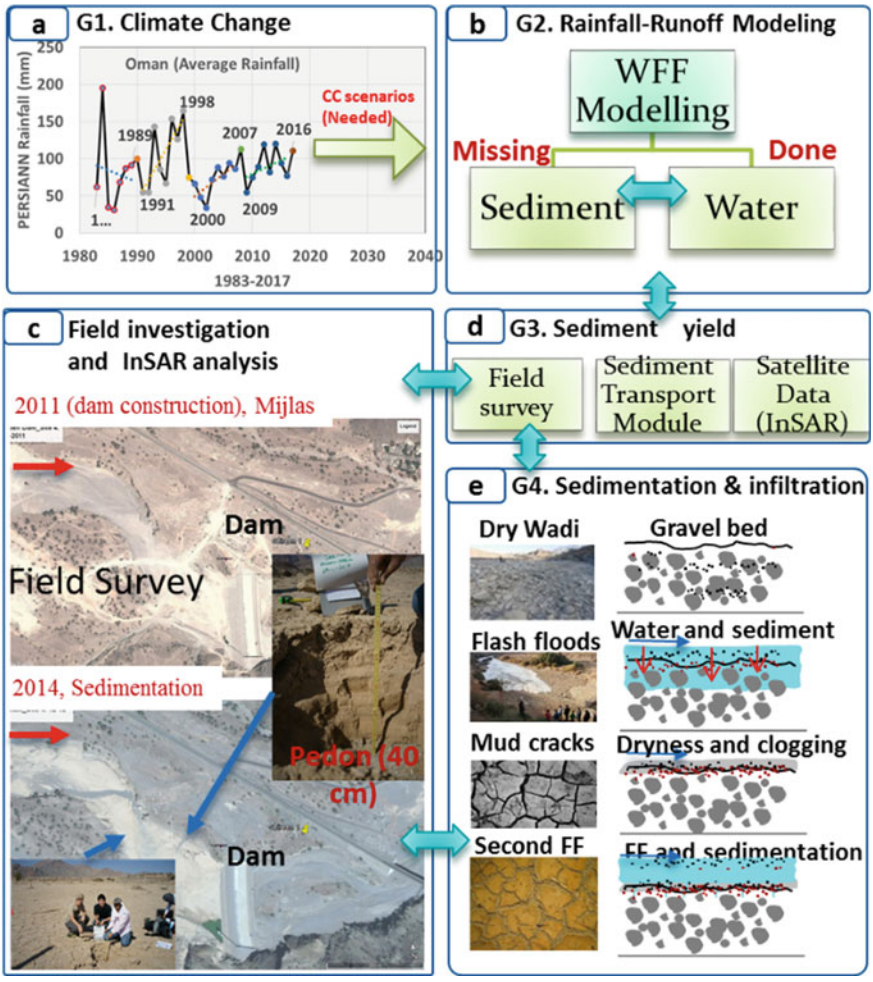

Fig. 15.5 Research plan and methodology

15.2.1.2 Rainfall-Runoff Modeling (G2)

We developed and set up several hydrological and hydrodynamic models for WFFs in different Wadi basins in Oman for instance the Hydrological River Basin Environmental Assessment Model for Wadi systems (Hydro-BEAM-WaS) (Kojiri et al. 2008; Saber et al. 2010a, b, 2013; Sato et al. 2013), a rainfall-runoff model (Sayama et al. 2012; Abdel-Fattah et al. 2018), and TELEMAC-2D (Riadh et al. 2014; Ogiso et al. 2017). The models have not yet been combined with a sediment transport module in arid regions (Fig. 15.5b). A sediment transport model will be

developed (G3) (Fig. 15.5d) and coupled with the hydrological model to simultaneously simulate both sediment and water (G2). Field investigations were conducted by G3 and G4 for validation (Fig. 15.5c–e).

15.2.1.3 Sediment Yield and Transport (G3)

Globally, sedimentation is the most serious technical problem in reservoir management, but in arid regions, the challenge becomes much more serious with increasing extreme flash floods. Two approaches will be used to estimate sediment yields and numerical simulations. The sediment transport module will be implemented to predict the sediment volumes associated with WFFs (linked with G2). The satellite data (InSAR, PALSAR-2) will be utilized to quantify sediment volume and determine the morphological changes along Wadi channels and then validated by field investigations (G3 & G4) (Fig. 15.5d, e). The researchers in SQU and MRMWR have already conducted several studies for sedimentation and pedon analysis (Al-Maktoumi et al. 2014, 2015).

15.2.1.4 Sedimentation and Infiltration Processes (G4)

We will assess the influence of sedimentation on infiltration processes in the selected Wadi basins (sediment clogging in Fig. 15.5e). This group will focus on conducting field surveys to investigate the sedimentation at Wadi basins (Fig. 15.5c). A disk infiltrometer will be used to measure the impacts of sedimentation clogging on the infiltration rates at the reservoirs. This will help in understanding the adverse impacts on groundwater recharge and trapping efficiency of dams.

15.2.2 Project Potentiality and Feasibility

Oman is a Middle East leading country in the implementation of a unique flash flood management strategy. Japan is also a world leader in the field of sediment management techniques on the river basin scale. Therefore, transferring such technologies to developing countries is crucial. The project was initiated based on the long history of activities such as meetings, conferences, and detailed research among the counterparts. There are, however, several factors controlling the applicability of the project and implementation. The Kyoto University team started a collaboration with the Arab countries (e.g., Egypt, Oman) in 2009 with establishing the Japan–Egypt Hydro Network (Sumi et al. 2013). Then, several field surveys were conducted for the target Wadis (Samail & Mijlas) in 2010, 2014, 2016, 2017, 2018 to better understand Wadi characteristics (Saber et al. 2018). The Japanese research group modified, calibrated, and validated hydrological models for WFFs.

Fig. 15.6 a The third international symposium on flash floods (ISFF) symposium, GUTech, Oman, showing the research teams from Oman and Japan. **b** The third ISFF outcomes in the news. *Source* of (**b**): http://www.omanobserver.om/guidelines-mooted-managing-flash-floods/

Moreover, the Kyoto University research team initiated a series of conferences titled the International Symposium on Flash Floods in Wadi Systems (ISFF). The first ISFF was organized in Kyoto University (2015), the second ISFF in Egypt (2016), the third ISFF in Oman in 2017 (Fig. 15.6a) (ISFF 2017), and the fourth ISFF in Casablanca, Morocco (2018) (ISFF 2018). The fifth ISFF is scheduled to take place in Kyoto in 2020.

Through discussions at the third ISFF, the Japanese research team and the international counterparts from Oman, Morocco, and the other countries agreed to continue discussions, cooperate to share experiences, and develop outstanding methodologies for sediment yield and sedimentation throughout such international collaboration. These activities were reported by an Omani newspaper (Fig. 15.6b) (http://www.omanobserver.om/guidelines-mooted-managing-flash-floods/) and a TV program (https://youtu.be/GojslFCBHYM/) that is widely recognized locally.

The project is expected to enable undergraduate students and young researchers through the efforts of the international collaboration. Students from both Oman and Japan are involved in the project. For instance, there are three master's students from Oman working under the project topics, as well as Japanese students. Based on these factors, the project is expected to be feasible and applicable mainly for hydrological investigations of WFFs to complete the missing gaps related to sedimentation and climate change.

The significance and the expected outcomes of this project are an increased understanding of WFFs spatiotemporal variability with implications of climate change, upgrading current hydrological models to simulate WFF water and sediment, validating high-resolution satellite products for sediment yield assessments, and clarifying the adverse impacts of sedimentation on infiltration processes. Additionally, learning lessons from the international collaboration project is beneficial for further understanding of climate change and drought/flood cycles. Also, since Japan is a world leader in the field of sediment management techniques on the river basin scale, transferring such technologies to developing countries is important. Mutual benefits from learning lessons from Oman and transferring Japanese advanced technologies will be accomplished.

15.3 Field Survey and Preliminary Results

In the ungauged Wadi systems, field surveys were essential for better understanding the real physical conditions of WFF phenomena and, mainly, the sedimentation issues in arid regions. Therefore, two field surveys were conducted for Wadis Mijlas and Samail in Oman in December 2017 and September 2018, respectively, to study sedimentation issues and their impact on reservoir capacity and identify flash flood marks. Several measures have been implemented such as Wadi channel leveling, the use of sedimentation pedons to study the vertical layers of sedimentation at the reservoirs by collecting sediments samples for further laboratory analysis and detecting flash flood marks. Additionally, drone surveys, infiltration tests, and field questionnaires about flash floods were conducted. The sedimentation volume at the reservoir along Wadi Mijlas was estimated from the sedimentation measure bars installed in the reservoir before the dam construction. Currently, InSAR data is being processed to assess the sedimentation changes. Numerical models were set up to estimate sediment transport. All these outcomes will be compared and validated by the field investigation findings. Details of the field investigations are presented in the following subsections.

15.3.1 Sedimentation Measures

Several sedimentation bars were installed by MRMWR. We measured the level of these bars and estimated how much sediments were deposited from 2011 to 2017 (Fig. 15.7). The sedimentation volume at the reservoir along Wadi Mijlas was estimated from the sedimentation measure bars installed in the reservoir before the dam construction. The sedimentation volume due to four flash flood events over the seven years was estimated to be about 8433 m3 at Asserin Down Dam 1 and about 15,041 m^3 at Asserin Up Dam 2.

15.3.2 Pedon Survey

Several sediment pedons were dug at Asserin Up Dam (Fig. 15.8a) along the reservoir to analyze the sediment grain size and organic contents and check the layers of sediments accumulated during the previous flash floods. Samples were collected from each layer for detailed laboratory analyses (grain size analysis, microscopic analysis, ash separation, and organic contents assessment). All layers were analyzed and described in the field to understand the correlation with rainfall data. At Asserin Up Dam, we found six layers as shown in pedons 1, 2, and 3 (Fig. 15.8c). The layers were separated and distinguished by two techniques:

Fig. 15.7 Sedimentation measures at the reservoir of Asserin Up Dam at the upstream of Wadi Mijlas (photographs taken by the Kyoto University team: field survey from Nov. 29 to Dec. 2, 2017). Reprinted from Saber et al. (2018), Copyright 2018

vertical grain size variations and the occurrence of mud cracks at the top of a layer (Fig. 15.8b).

Based on the measure bars and sediment pedons analyzed, the sediment thickness along the central line of the reservoir was estimated for the six layers. This will be very beneficial in calibrating the sediment transport model in the reservoir (Fig. 15.9).

15.3.3 Morphometric Changes

An investigation of the morphometric changes along Wadi channels is required to understand the sediment yield, transport, and erodibility at the basins. We tried to assess and investigate the depositions and erosions along Wadi channels. Wadi channel leveling was conducted in the field to assess the Wadi channel elevations at different flash flood events. Also, we used Google Earth maps to check the Wadi channels' morphometric changes due to the impact of flash floods. For instance, the sedimentation changes at the dams before and after the constructions showing the spatial topographic changes at the reservoir at both dams along Wadi Mijlas

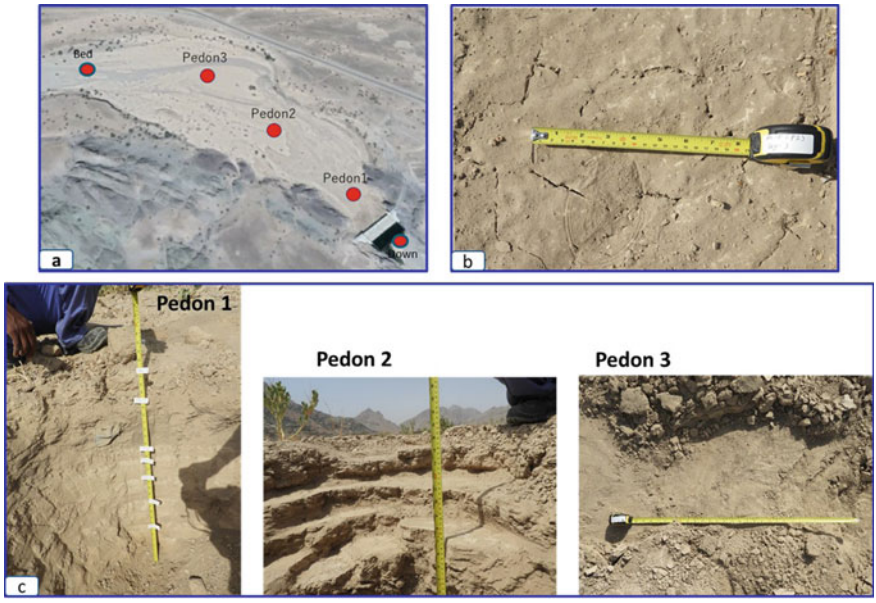

Fig. 15.8 a Pedon sites at Asserin Up Dam, Wadi Mijlas. **b** Observed mud cracks at the top of layer 3, pedon 2. **c** Three investigated pedons: pedons 1, 2, and 3

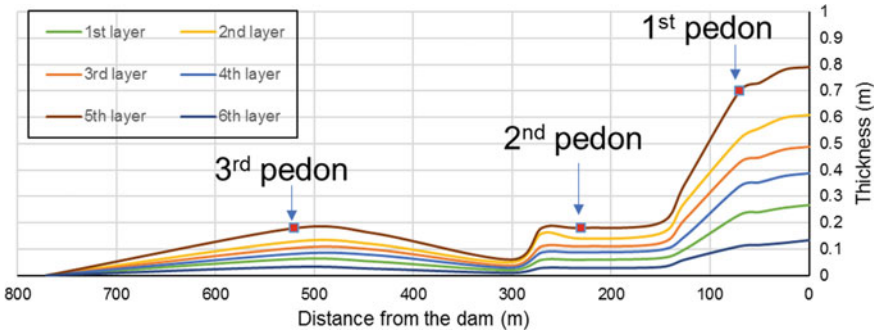

Fig. 15.9 Sediment thickness changes along the central line of the reservoir at Wadi Mijlas (Asserin Up Dam)

(Fig. 15.10). Along the Wadi channels, the impact of Cyclone Guno was observed, examining changes on the channel morphology as shown on Google Earth maps before and after the flash floods (Fig. 15.11). Currently, we are analyzing synthetic-aperture radar images to assess the sediment changes at the catchments after the flash floods.

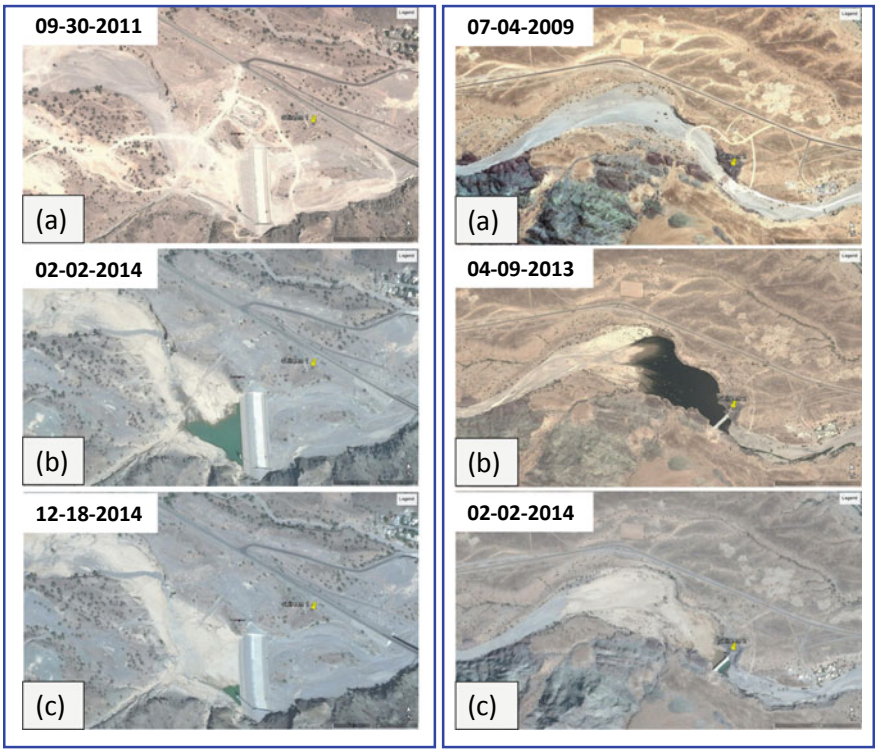

Fig. 15.10 Left Panel: Asserin Dam 1 (downstream) construction and sedimentation impacts. **a** The completion of the dam construction in 2011. **b** The sedimentation impacts on the reservoir in February 2014. **c** The sedimentation impacts on the reservoir in December 2014. Right Panel: Asserin Dam 2 (upstream) construction and sedimentation impacts. **a** Before the dam construction in 2009. **b** After flash floods and sediment deposition on the reservoir in April 2013. **c** Dryness of the reservoir in February 2014. Reprinted from Saber et al. (2018), Copyright 2018

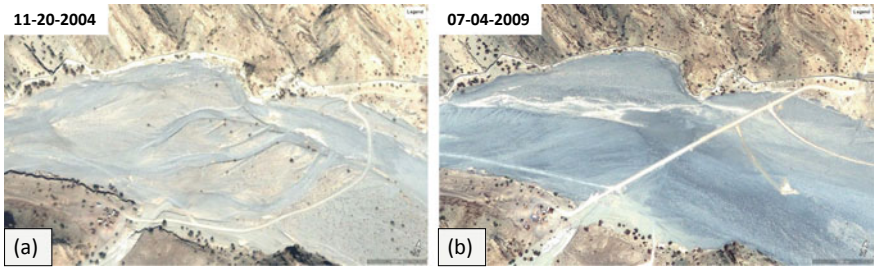

Fig. 15.11 Wadi channel morphology changes after Cyclone Guno in 2007. The sedimentation bars in photograph (**a**) disappeared after the extreme floods revealed the massive transported sediment and the difference in the soil colors, as observed in photograph (**b**). Reprinted from Saber et al. (2018), Copyright 2018

15.3.4 Infiltration Tests

During the field investigations, we observed the clogging phenomena of sedimentation at the reservoir (Fig. 15.12), both upstream and downstream of the dams at Wadi Mijlas. Therefore, we conducted several infiltration tests vertically as a unique approach to understand the sediment dynamics as well as impacts on the groundwater recharge.

Using the disk infiltrometer, we conducted several tests at the investigated pedons, considering different layers to understand sedimentation impacts on the infiltration. The objectives of the infiltration tests were to measure the change of infiltration rate by sedimentation and assess the influence of clogging. The saturated hydraulic conductivity (Ks) was determined using tension infiltrometers (Reynolds and Elrick 1991) at the target sites (pedons). About 13 infiltration tests were conducted at several layers as shown in Fig. 15.13. As preliminary results, we found the sedimentation decreases the infiltration. Concerning the infiltration tests, however, further discussion is still in progress. The relationship between pedon sediments and infiltration tests was also investigated.

At pedon 2, the results of the infiltration test and grain size analysis showed the relationship between the soil texture and K_{sat}: K_{sat} decreases at the layers from upstream to downstream with depth (Fig. 15.14). It was also found that Ksat declines when the grain size decreases. The findings of the study by (Mazaheri and Mahmoodabadi 2012) agrees with these results indicating the soil particle distribution affects the infiltration rate. Furthermore, the longitudinal change of K_{sat}

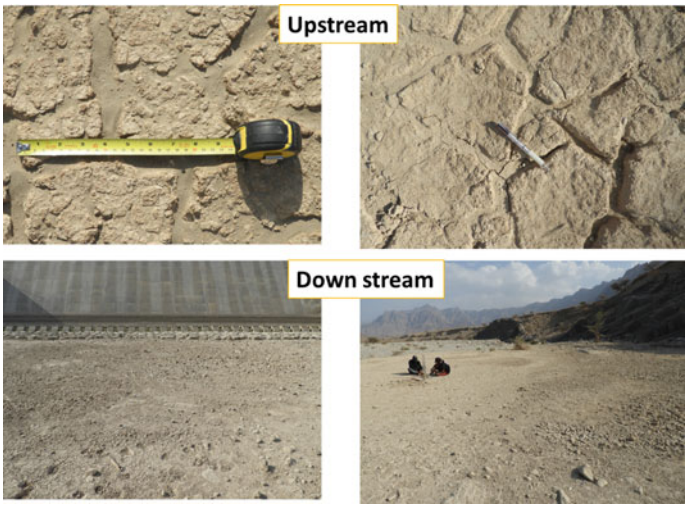

Fig. 15.12 Sediment clogging upstream (the two upper photographs) and downstream (the two lower photographs)

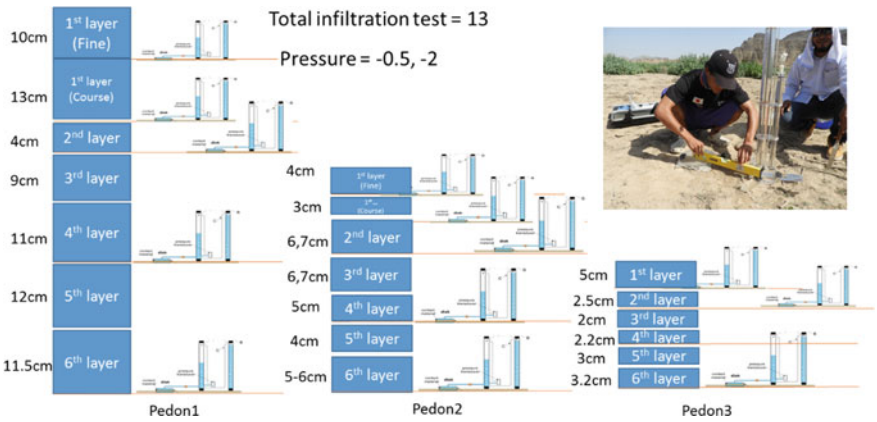

Fig. 15.13 Infiltration tests at several layers of the three pedons, Asserin Up Dam

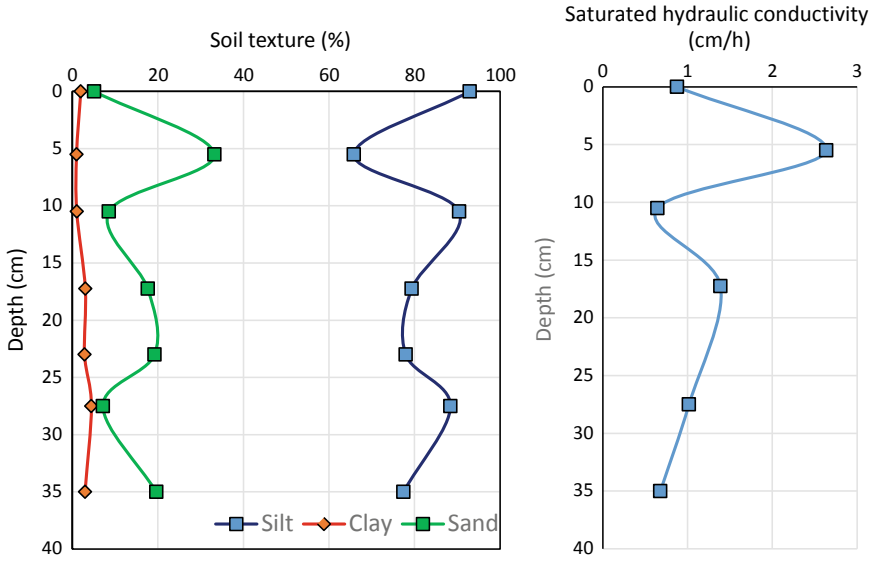

Fig. 15.14 Soil texture and saturated hydraulic conductivity at pedon 2

along the tested sites was observed (Fig. 15.15). This revealed the impact of sedimentation on the infiltration rate. Also, K_{sat} of the surface layer decrease from upstream to downstream, which is also related to the soil texture. Further analysis of all the layers by using the infiltration model to simulate such changes are still running.

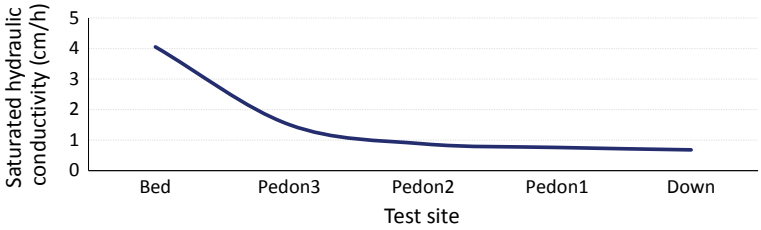

Fig. 15.15 Longitudinal change of saturated hydraulic conductivity at the pedon sites (see Fig. 15.8a)

15.3.5 Drone Surveys

Over two days we conducted drone surveys using Phantom 4 Pro at different locations and sites (Fig. 15.16) including Asserin Up Dam, Asserin Down Dam, Al Sawaqim, the monitoring station, the old monitoring station along Wadi Mijlas, the newly proposed dam, and also at the Wadi gauge station site. The reservoir of Asserin Up Dam was selected to develop the bathymetry DEM (Fig. 15.16). The drone images were analyzed to produce a very high-resolution DEM at the reservoir (Fig. 15.17), with about 0.5 m spatial resolution, that will be very useful to enhance the topographic data inputs for the hydrological models. The drone images were processed using the Photo Scan software. This DEM will be very crucial to enhancing the input topographic maps for the hydrological model and consequently reducing the model uncertainty related to topographic data accuracy. These results will be used for the future modeling of sediment transport models and also for future sediment changes over the target basins by comparing them with future results to assess the extent of the deposited sediments for any future flash flood events.

Fig. 15.16 Satellite image showing the sites for the drone survey of Wadi Mijlas, Oman, on the right and the drone photograph of Asserin Up Dam, Wadi Mijlas, Oman on the left

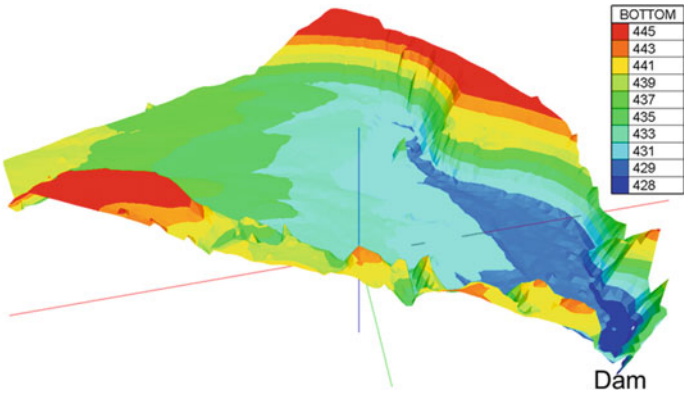

Fig. 15.17 High-resolution digital elevation model generated from unmanned ground vehicles will be used to enhance the input topographic maps for sediment transport modeling

15.4 Climate Change and Extreme Rainfall Events

As a part of this project, the impacts of climate change on WFFs was addressed. We analyzed long-term rainfall data to understand the temporal variability over the Arab region and Oman. The satellite rainfall data of the Precipitation Estimation from Remotely Sensed Information using Artificial Neural Networks (PERSIANN) was used (Sorooshian et al. 2000; Ashouri et al. 2015). The results of the analysis of PERSIANN rainfall data from 1983 to 2017 exhibited the whole Arab region had experienced systematic cycles of increasing trends of rainfall about every seven years (Fig. 15.18a) and the same behaviors were recorded for Oman, except the first cycles showed extreme increasing and then decreasing trends in the rainfall data (Fig. 15.18b). To understand the temporal variability for such kinds of systematic cycles of extreme events, additional historical data from the Climate Change Knowledge Portal was freely downloaded and used (WorldBankGroup 2019). The data was derived from observational data, and it provided quality controlled rainfall values from thousands of weather stations worldwide. It was developed by the Climatic Research Unit of the University of East Anglia and reformatted by the International Water Management Institute. The Persian data showed an acceptable agreement between the annual Persian data and historical rainfall data with a correlation coefficient of 0.7693 (Fig. 15.18c). The future climate scenarios will be discussed in a separate research paper to deeply understand the spatial and temporal variability of rainfall over the Arab region and Oman for a long-term period including the past, recent, and future extreme rainfall events.

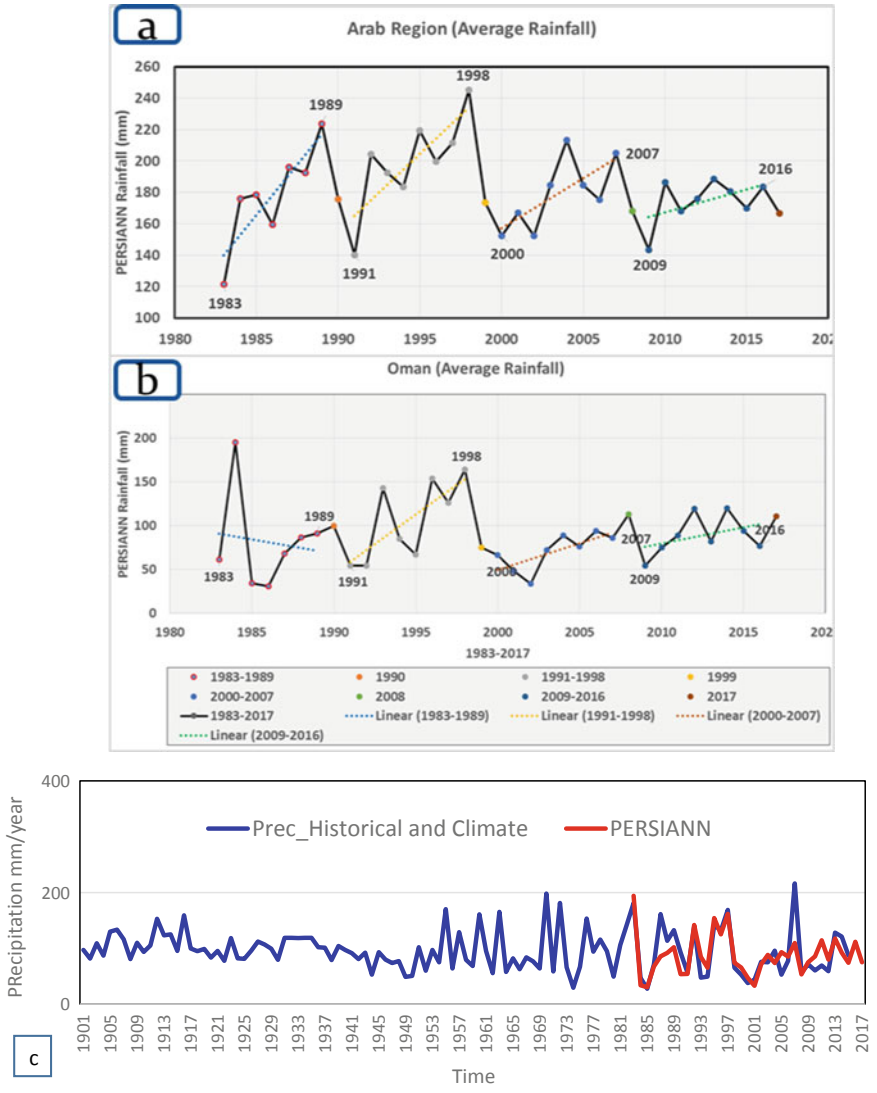

Fig. 15.18 Annual rainfall analysis of precipitation estimation from remotely sensed information using artificial neural networks (PERSIANN) rainfall data from 1983 to 2017 over **a** the Arab region and **b** Oman and **c** the comparison of long-term historical data of Oman with PERSIANN data from 1983 to 2017

15.5 Conclusions and Ongoing Work

In this paper, an international collaboration project is presented and discussed. The collaboration was initiated between the Kyoto University team and the Omani team (in collaboration with SQU, MRMWR, and DGM) to develop an effective hydrological approach for WFFs in arid regions, considering climate change and sedimentation impacts. Four research groups were established to focus on analyzing historical rainfall data to assess extreme events variability and global circulation models for future climate scenarios (G1), developing the hydrological models to simulate water discharge and sediment transport (G2), and assessing sediment yield (G3) by satellite data (e.g., InSAR) and hydrological surveys by conducting investigations for sedimentation impacts on infiltration process (G4). The outcomes will be solutions to overcome challenges related to WFFs and the proposition of a secure long-term sustainable management of water and sediments, as well as the transfer of Japanese technologies. Both the Japanese and the Omani teams are working together to achieve the project tasks, providing approaches and methods to overcome WFF challenges in arid regions.

To therefore understand flash flood phenomena in arid regions in terms of water and sediment management, two field surveys were conducted for Wadis Mijlas and Samail in Oman in December 2017 and September 2018, respectively, to study the sedimentation issues and their impacts on reservoir capacity. Several measures were implemented such as Wadi channel leveling, and the use of sedimentation pedons to study the vertical layers of sedimentation at the reservoir by collecting sediment samples for further laboratory analysis and detecting of flash flood marks. Additionally, drone surveys, infiltration tests, and field questionnaires about flash floods were conducted. The infiltration tests showed the relationship between the sedimentation layers and the Ksat at several vertical sediment layers of three pedons. A high-resolution digital elevation model was generated from the drone images to be used for the sediment transport modeling. Long-term satellite precipitation data and historical data were used to analyze the temporal variability in the whole Arab region and also at Oman, and the results exhibit interesting systematic cycles every seven years. Thus, additional detailed analyses of these data and climate change scenarios are still ongoing. Thus, this study is quite crucial in assessing the sedimentation in the field survey, numerical modeling, and satellite data, as well as in proposing the best sediment management techniques in Wadi basins. Further field surveys will be conducted in the near future to extend the analysis, especially concerning long-term rainfall analysis and climate change impacts.

Acknowledgements This research was funded by the International Collaborative Research, grant number 30W-01, and General Collaborative Research, grant number 30A-01, internal funds of Disaster Prevention Research Institute (DPRI) at Kyoto University, Japan. The support and provided facilities for the field investigations and data collection from Sultan Qaboos University and the Ministry of Regional Municipalities and Water Resources is highly appreciated.

References

Abdel-Fattah M, Kantoush SA, Saber M, Sumi T (2018) Rainfall-runoff modeling for extreme flash floods in wadi samail, oman. J Jpn Soc Civil Eng Ser B1 (Hydraulic Engineering) 74(5)

Abdel-Fattah M, Kantoush S, Sumi T (2015) Integrated management of flash flood in Wadi system of egypt: disaster prevention and water harvesting. Ann Disas Prev Res Inst Kyoto Uni 58 B:485–496

Abdel-Fattah M, Saber M, Kantoush SA, Khalil MF, Sumi T, Sefelnasr AM (2017) A hydrological and geomorphometric approach to understanding the generation of Wadi flash floods. Water 9 (7):553

Al-Maktoumi A, Al-Ismaily S, Kacimov A, Al-Busaidi H, Al-Saqri S, Al-Hadabi M (2014) Soil substrate as a cascade of capillary barriers for conserving water in a desert environment: lessons learned from arid nature. J Arid Land 6(6):690–703

Al-Maktoumi A, Kacimov A, Al-Ismaily S, Al-Busaidi H, Al-Saqri S (2015) Infiltration into two-layered soil: the green-Ampt and Averyanov models revisited. Transp Porous Media 109 (1):169–193

Al Barwani A (2015) Flash flood mitigation and harvesting oman case study. In: First international symposium on flash floods (ISFF), Kyoto, Japan

Ashouri H, Hsu KL, Sorooshian S, Braithwaite DK, Knapp KR, Cecil LD, Nelson BR, Prat OP (2015) PERSIANN-CDR: daily precipitation climate data record from multisatellite observations for hydrological and climate studies. Bull Am Meteor Soc 96(1):69–83. https://doi.org/10.1175/bams-d-13-00068.1

ICOLD, CIGB (2009) Sedimentation and sustainable use of reservoir and river systems. Draft ICOLD Bull. Sedimentation Committee. Google Scholar

ISFF, 3rd. (2017) 3rd International Symposium on Flash Floods in Wadi Systems (3rd ISFF). http://isff2017.gutech.edu.om/

ISFF, 4th. (2018) 4th International Symposium on Flash Floods in Wadi Systems (4th ISFF)

Kojiri T, Hamaguchi T, Ode M (2008) Assessment of global warming impacts on water resources and ecology of a river basin in Japan. J Hydro-Environ Res 1(3):164–175

Mazaheri MR, Mahmoodabadi M (2012) Study on infiltration rate based on primary particle size distribution data in arid and semiarid region soils. Arab J Geosci 5(5):1039–1046

Ogiso Y, Sumi T, Kantoush S, Saber M, Abdel-Fattah M (2017) Risk assessment of flash floods in the valley of the kings, Egypt

Reid I, Frostick LE (1987) Flow dynamics and suspended sediment properties in arid zone flash floods. Hydrol Process 1(3):239–253

Reynolds WD, Elrick DE (1991) Determination of hydraulic conductivity using a tension infiltrometer. Soil Sci Soc Am J 55(3):633–639

Riadh A, Goeury C, Hervouet JM (2014) Telemac modelling system: TELEMAC-2D software v7. 0 user's Manual. Recherche et développement, Électricité de France: Chatou, France

Saber M, Hamagutchi T, Kojiri T, Tanaka K (2010a) Hydrological modeling of distributed runoff throughout comparative study between some Arabian wadi basins. Ann J Hydraul Eng JSCE 54:85–90

Saber M, Hamaguchi T, Kojiri T, Tanaka K, Sumi T (2013) A physically based distributed hydrological model of wadi system to simulate flash floods in arid regions. Arab J Geosci 1–18. https://doi.org/10.1007/s12517-013-1190-0

Saber M (2010) Hydrological approaches of Wadi system considering flash floods in arid regions

Saber M, Habib E (2016) Flash floods modelling for Wadi system: challenges and trends. In: Landscape dynamics, soils and hydrological processes in varied climates, pp 317–339. Springer

Saber M, Hamaguchi T, Kojiri T, Tanaka K (2010b) Flash flooding simulation using hydrological modeling of Wadi basins at Nile River based on satellite remote sensing data

Saber M, Kantoush S, Sumi T, Abdel-fattah M, Alharrasi T, Koshiba T, Ogiso Y, Almamari M (2018) Field investigation on Wadi system in Arid Regions: flash flood indicators and sedimentation impacts. Disaster Prev Res Inst Ann 61B

Saber M, Yilmaz KK (2018) Evaluation and bias correction of satellite-based rainfall estimates for modelling flash floods over the mediterranean region: application to Karpuz River basin, Turkey. Water 10(5):657

Sato Y, Kojiri T, Michihiro Y, Suzuki Y, Nakakita E (2013) Assessment of climate change impacts on river discharge in Japan using the super-high-resolution MRI-AGCM. Hydrol Process 27(23):3264–3279

Sayama T, Ozawa Go, Kawakami T, Nabesaka S, Fukami K (2012) Rainfall–runoff–inundation analysis of the 2010 Pakistan flood in the Kabul River basin. Hydrol Sci J 57(2):298–312

Sorooshian S, Hsu KL, Gao X, Gupta HV, Imam B, Braithwaite D (2000) Evaluation of PERSIANN system satellite-based estimates of tropical rainfall. Bull Am Meteor Soc 81 (9):2035–2046

Sumi T, Saber M, Kantoush SA (2013) Japan-Egypt hydro network: Science and technology collaborative research for flash flood management. J Disaster Res 8(1):28–36

Walling DE, Kleo AHA (1979) Sediment yields of rivers in areas of low precipitation: a global view. In: Proceedings... The Hydrology of areas of low precipitation

Wolman MG, Miller JP (1960) Magnitude and frequency of forces in geomorphic processes. J Geol 68(1):54–74

WorldBankGroup (2019) Accessed March, 2019. https://climateknowledgeportal.worldbank.org/

Chapter 16
Sediment Transport in Shallow Waters as a Multiphysics Approach

Ekkehard Holzbecher and Ahmed Hadidi

Abstract Suspended particle and bed-load transport are usually high during flooding events. For that reason, sediment transport is an important feature to be taken into account when studying floods. Measures that aim to mitigate the negative impacts of floods depend on such studies. Sediment transport phenomena are complex due to their coupling behavior with fluid flow. Due to the erosion and sedimentation of particulate matter, the ground surface changes during the passing of a flood. The courses of unregulated rivers and wadis after floods are different than those before floods. Flowing water transports sediments, and vice versa; sediment redistribution affects the flow of water due to changes in the ground surface and other factors. Computer simulations of sediment transport must take the coupling between water flow and transport processes into account. Here, a multiphysics approach in such a coupled model is presented. Shallow water equations (SWE) representing water height and velocity are coupled with equations for suspended particulate matter and bed loads. Using COMSOL Multiphysics software, an implementation is presented that demonstrates the capability and feasibility of the proposed approach. The approach is applied to the problems of scouring and sedimentation at obstacles, which are particularly important for ensuring the stability of bridges across rivers and wadis.

Keywords Sediment transport modeling · Multiphysics · Scour

16.1 Introduction

Sediment transport in surface water bodies is a topic that is gaining increasing relevance and scientific interest. With a focus on sedimentation and resuspension, applied research has been performed concerning rivers (Sibetheros et al. 2013; Zavattero et al. 2016), channels (Visescu et al. 2016), coastal zones (Amoudry and

E. Holzbecher (✉) · A. Hadidi
Department of Applied Geology, German University of Technology in Oman, Muscat, Oman
e-mail: ekkehard.holzbecher@gutech.edu.om

T. Sumi et al. (eds.), *Wadi Flash Floods*, Natural Disaster Science and Mitigation Engineering: DPRI Reports, https://doi.org/10.1007/978-981-16-2904-4_16

Souza 2011; Aoki et al. 2015), reservoirs (Kondolf et al. 2014; Sumi and Hirose 2009), and floodwaters (Eaton and Lapointe 2001; Berghout and Meddi 2016). Here, the focus lies on the floodwaters, although the discussed methods can also be applied to other fields.

In reservoirs, the deposition of sediments is a general problem; the water storage capacity may be reduced drastically due to sediment deposition. Groundwater recharge can be reduced or completely inhibited due to the deposition of fine particles. This is a crucial issue at dams that are also designed for groundwater recharge, as shown by a case study in Oman (Prathapar an Bawain 2014). Additionally, in Oman, Saber et al. (2019) examined various aspects of reservoir sedimentation. Few studies have attempted to estimate the overall sediment budgets of reservoirs. From extensive observations on beach profiles along the Batinah coast in northern Oman, Kwarteng et al. (2016) estimated that approximately 960,000 m^3 per year of sediments are supplied from the coastal plain, of which roughly half is currently trapped by numerous dams built in the area. While onshore withheld sediments cause problems for the long-term operation of dams, sediment deficits along coasts may lead to serious beach erosion problems.

The topics of suspended and bed-load transport have been investigated for a long time, and associated studies have mainly dealt with perennial flow channels and steady flows. There are far fewer studies on ephemeral streams and transient regimes, as these appear in connection with floods. There are a few case studies from the Negev Desert (Reid et al. 1998) and from Saudi Arabia (Nouh 1988a, b). In their review, Karimaee Tabarestani and Zarrati (2015) clearly stated that sediment transport under unsteady conditions is very different than that under steady flow.

Scott (2006) points to the fact that for high sediment loads appearing in ephemeral streams, the flow regime may become non-Newtonian. In sediment-laden water bodies, deposition causes problems if it occurs in incorrect places. Navigation may become hindered or even impossible, as shown by Ezzeldin et al. (2019). On the other hand, unwanted scouring may emerge due to sediment removal and cause problems concerning the stability of bridge piers and foundations (Pizarro et al. 2020).

Numerical models can play an important role in understanding these processes. The locations and amounts of erosion and sedimentation can be identified using numerical models. With validated numerical models, potential measures to mitigate flood damage can be simulated, examined, and evaluated on computers.

However, simulation techniques and tools for the implementation of such models are still in development and have not yet been well established. The physics of the situation in question is complex. Some water flow models are also extended to treat sediment transport processes. If there is erosion or deposition at the bottom of a channel, the depth of the water column changes, and thus, the flow regime is altered. This two-way coupling of flow and transport must be incorporated using a multiphysics approach; water flows and sediment transport must be simulated simultaneously.

16.2 Modeling

Here, we present a multiphysics approach in which the coupling between flow and transport is taken into account. As a first approach, we attempt to minimize complexity, and with it, the required computational resources. For flow modeling, we choose the shallow water equations (SWE), a system of two coupled differential equations. These equations constitute a minimalistic approach, as the vertical direction is not explicitly considered, and thus, the problem setting is reduced to 2D or even 1D in rivers and channels. The sediment transport is described by two equations: one for the suspended particle load in the water column and one for the bed load. The latter is formulated as an expression of the bottom elevation.

For an initial check of the ability of such an analytical system of minimal complexity to simulate flow and transport, a test case is simulated. The situation is simple, consisting of a circular obstacle placed into a uniform 2D flow field. It is shown that it is possible to capture both erosion and deposition at different locations along the obstacle wall by a multiphysics modeling approach.

Fluid flow modeling is based on the mathematical analytical formulations represented by differential equations. The Saint–Venant equations, also known as the shallow water equations for depth-averaged flow in one or two spatial dimensions, can be written as:

$$\frac{\partial}{\partial t}(H-d)+\nabla\cdot(H\mathbf{u})=0 \tag{16.1}$$

$$\frac{\partial \mathbf{u}}{\partial t}+(\mathbf{u}\cdot\nabla)\mathbf{u}+g\nabla H-\mathbf{F}=0 \tag{16.2}$$

with total water depth H, water depth d below a reference level, velocity vector $\mathbf{u}$, and acceleration due to gravity g (Takase et al. 2011). In vector **F,** the contributions of all other forces are gathered. The equations are derived from the volume and momentum conservation principles and are formulated using depth-averaged velocities. The system comprising Eqs. (16.1) and (16.2) is nonlinear. The derivation is based on several assumptions: (1) the fluid is incompressible, (2) in the vertical direction, there is a hydrostatic pressure distribution, (3) depth-averaged values can be used for all properties and velocities, (4) the bottom slopes are small, (5) there are no density effects from variable fluid density or fluid viscosity, (6) the eddy viscosity is much larger than the molecular viscosity, and (6) the atmospheric pressure gradient can be ignored. Despite these numerous assumptions, the validity of SWEs for many application cases is widely accepted.

Friction at the walls, i.e., the interfaces between fluids and solids, can be taken into account by an additional term in Eq. (16.2) (Brufau and García-Navarro 2000; Duran 2015):

$$\frac{\partial \mathbf{u}}{\partial t} + (\mathbf{u} \cdot \nabla)\mathbf{u} + g\nabla H + g\eta n^2 \frac{|\mathbf{u}|}{\eta^{4/3}}\mathbf{u} - \mathbf{F} = 0 \tag{16.3}$$

with water height η above a reference height and Manning coefficient n. In 1D, i.e., for rivers, channels, and channel systems, Eqs. (16.1) and (16.3) constitute a coupled system for H and u. In 2D, the equations are used to determine three variables, H and two components of $\mathbf{u}$.

For sediment transport, we choose the concentration of suspended material, c, as the dependent variable. Following the methods used in Li and Duffy (2011), the differential equation reads as follows:

$$\frac{\partial Hc}{\partial t} + \nabla \cdot (Hc\mathbf{u}) - E + D = 0 \tag{16.4}$$

where E and D denote the erosion and deposition terms, which will be outlined below. Using the product rule, Eq. (16.4) can be rewritten as follows.

$$H\frac{\partial c}{\partial t} + c\frac{\partial H}{\partial t} + H\nabla \cdot (c\mathbf{u}) + c\nabla \cdot (H\mathbf{u}) - E + D = 0 \tag{16.5}$$

Both terms with leading factor c cancel out because of Eq. (16.1). The remainder can be written as follows.

$$\frac{\partial c}{\partial t} + \nabla \cdot (c\mathbf{u}) - \frac{1}{H}(E - D) = 0 \tag{16.6}$$

The corresponding conservative form is given as follows.

$$\frac{\partial c}{\partial t} + (\mathbf{u} \cdot \nabla)c - \frac{1}{H}(E - D) = 0 \tag{16.7}$$

Note that the sediment load is represented as a concentration with mass/volume units. In Eq. (16.7), diffusion is not considered. Analogous to mass transport, diffusive processes are taken into account by an additional term.

$$\frac{\partial c}{\partial t} - \nabla(\mathbf{D}\nabla c) + (\mathbf{u} \cdot \nabla)c - \frac{1}{H}(E - D) = 0 \tag{16.8}$$

Here, $\mathbf{D}$ denotes the dispersion tensor, in which all types of diffusive processes are gathered (Rowinski and Kalinowska 2006). In the following equation, we consider turbulent diffusivity as the most relevant part, described as follows:

$$\mathbf{D} = \frac{\upsilon}{\mathrm{Sc}}\mathbf{I} \tag{16.9}$$

with turbulent viscosity υ and turbulent Schmidt number Sc. $\mathbf{I}$ denotes the 2D unit matrix.

Except for the consideration of diffusion, the presented approach is similar to those outlined in Cao et al. (2004), Li and Duffy (2011), and Rowan and Seaid (2017). Analogous to the cited references, the changes in the bed that occur due to settling and resuspension are thus governed by the formula:

$$\frac{\partial d}{\partial t} - \frac{1}{1-\theta}(E - D) = 0 \tag{16.10}$$

where θ denotes the bed-load porosity.

The system comprising Eqs. (16.1), (16.3), (16.7), and (16.10) is a coupled multiphysics approach. The terms H and $\mathbf{u}$ appear in Eq. (16.7), forming the link between the flow and transport processes. As the next section shows, there are further dependencies in the exchange terms D and E, constituting a coupling between Eqs. (16.7) and (16.10). The back-coupling is given as the depth, d, which appears in Eq. (16.1).

16.3 Sedimentation and Erosion Approaches

For the settling and resuspension terms, several approaches can be found in the current literature. For D, Li and Duffy (2011) propose the following equation:

$$D = \beta v_s c \tag{16.11}$$

with the settling velocity v_s. The amount of settling material is proportional to the settling velocity and the concentration of suspended material. The β factor thus has the dimension of length^{-1} and is the mean travel length in the vertical direction. In our first approach, we use an expression in which β is set to $H/2$, the mean settling depth.

$$D/H = 2v_s c/H \tag{16.12}$$

The model allows working with a constant settling velocity, but more complex approaches can also be utilized. For example, the more general approach,

$$D = v_s c_s (1 - c_s)^m \tag{16.13}$$

proposed by Cao et al. (2004) can be included easily. The sediment concentration near-bed c_s is proportional to the sediment concentration with a proportionality factor, α, greater than 1: $c_s = \alpha c$. Rowan and Seaid (2017) suggested the use of Eq. (16.13) with power $m = 1.4$ for noncohesive materials. Also dealing with 1D settings in channels and channel networks, Zhang et al. (2014) made D dependent on the carrying capacity, c_*:

$$D = v_s \alpha (c - c_*) \tag{16.14}$$

with

$$c_* = K\left(u^3/gRv_s\right)^m \tag{16.15}$$

depending on the hydraulic radius, R, and the parameters K and m. Li and Duffy (2011) extended the 1D approach for use in 2D systems, using the following expressions for β and v_s:

$$\beta = \min\{2, (1-\theta)/c\} \tag{16.16}$$

$$v_s = \sqrt{(13.95v/\delta)^2 + 1.09g\delta\left(\rho_s/\rho_f - 1\right)} - 13.95v/\delta \tag{16.17}$$

with particle diameter δ, kinematic viscosity v, and particle and fluid densities ρ_s and ρ_f, respectively. For resuspension, Li and Duffy (2011) proposed the following equation:

$$E = \alpha(\Theta - \Theta_c)H|\mathbf{u}| \tag{16.18}$$

with coefficient α and Shields parameters Θ and Θ_c, defined by $\Theta = u_*^2/sg\delta$, and the following equations.

$$u_* = \sqrt{gh\left(S_{fx}^2 + S_{fy}^2\right)} \tag{16.19}$$

$$S_{fx} = nu_x|\mathbf{u}|/h^{4/3} \quad S_{fy} = nu_y|\mathbf{u}|/h^{4/3} \tag{16.20}$$

$$s = \rho_s/\rho_f - 1 \tag{16.21}$$

The term Θ_c denotes the critical Shields parameter, which must be exceeded by Θ for resuspension (erosion) to become active. In his classical paper, Shields (1936) demonstrated that Θ_c depends on the grain size Reynolds number. Cao et al. (2004) used a similar relation to that shown in Eq. (16.18) and considered the dependence of α on parameters δ, s, Θ_c, and fluid velocity.

In the presented approaches, the terms are dependent on particle size and density. For the general modeling approach, heterogeneous sediment must be partitioned into several classes of different sizes and weights, similar to the implementation in SISYPHE (TELEMAC 2020). The numerical calculation must then be performed for each different sediment class. In the presented numerical approach, this can be included easily. For each class, a differential equation,

as formulated in Eq. (16.8), must be added. In Eq. (16.10), the contributions of the various sediment fractions must be added. For the first demonstration of the approach, we restrict our simulations to a single sediment type.

16.4 Demonstration Model

The capability of the modeling approach is demonstrated for the problem of scouring as a result of flooding. In their recent review on the science behind scours at bridge foundations, Pizzaro et al. (2020) identified scouring as an erosional process and characterized it as the interaction between any type of underwater structure and the water flowing in a river or wadi channel. According to Pizzaro et al. (2020), scouring is by far the leading cause of bridge failure worldwide and thus causes significant direct losses of infrastructure and disruption of road networks.

In Oman, it is reported that the 1996 cyclone washed away roads and 21 bridges. Resulting from Cyclone Gonu, which hit the Oman coast in 2007, "roads and bridges were washed out, and major sites in the capital area were totally isolated and inaccessible for days" (Al-Shaqsi 2010). Investigations of scours and their underlying processes are thus topics of high relevance. Figure 16.1 shows the early stage of an advancing flood at a bridge pier.

Measures that aim to avoid damage to bridges during flood events are considered during the design phase of bridge construction or when reinforcing the foundations of existing bridges. The calculations are usually based on a designed flood event with a specified magnitude and a return period of 100 or 200 years. The depth of the scour is then calculated under the assumption of a one-to-one relationship between the flood discharge and the steady-state scour depth (Pizarro et al. 2020). This approach leaves several processes out of consideration that acts simultaneously during the passing of a flood.

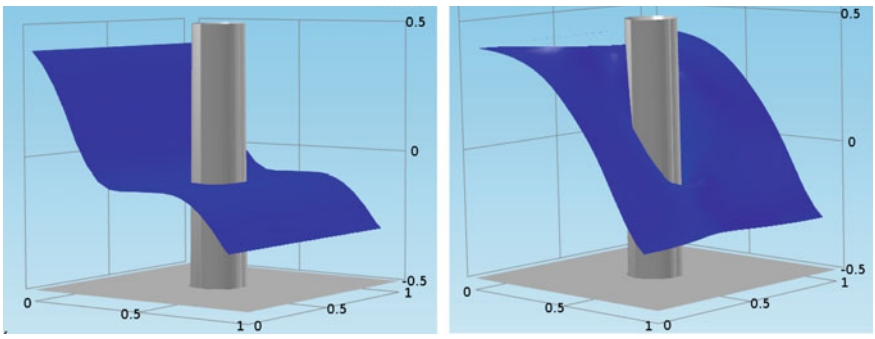

Fig. 16.1 Sketch of a flood passing a bridge pier

Using numerical models, it is possible to simulate the simultaneous actions of numerous processes. Sedimentation and erosion are processes that appear at different locations in rivers or wadis during flood events. In computer models, suspended loads of different sizes and bed loads can be treated in parallel. Concerning floods, it is crucial to examine transient development and not long-term equilibrium.

To demonstrate how the proposed numerical approach performs concerning scour development near an obstacle, we deal with a simple geometric setup. The model region is given by a square cavity that is open on two opposite sides and closed on the other sides. In the center, a circular obstacle is located, representing a bridge pier. The situation is sketched in Fig. 16.2.

It is assumed that there is a sudden increase in the water column height at the inflow boundary. The inflowing water has a constant load of particulate matter. The initial values of the water table and depth are constants. The initial particulate load concentration is zero.

The numerical simulations are performed using the COMSOL Multiphysics (2020) program. This is a versatile and flexible software applicable for coupled partial differential equations solved by the finite element method. The program is currently used for all kinds of multiphysics applications in the fields of engineering, physics, chemistry, biology, medicine, hydraulics, etc. It is operated via a graphical user interface that allows comfortable handling and coupling of multiple physics modes.

The entire system can be implemented in COMSOL Multiphysics using pde-modes. We utilized a physics mode for the SWE (Schlegel 2012), i.e., Eqs. (16.1) and (16.2). The particulate load in the water column, following Eq. (16.7), is modeled by the solute transport mode. For simplicity, only one sediment class is considered. The settling velocity is considered in a loss term according to Eq. (16.12). Finally, the coefficient form pde of COMSOL Multiphysics is utilized to include the bed load represented by Eq. (16.10) in the model. All input parameters are gathered in Table 16.1.

For extreme flood events, Lumbroso and Gaume (2012) examined common guidance documents to determine the distributions of the mean maximum velocity, Manning parameter, and Froude number. According to their presentation, the 50% threshold of the mean maximum velocity is 1 m/s; that of the Manning parameter is

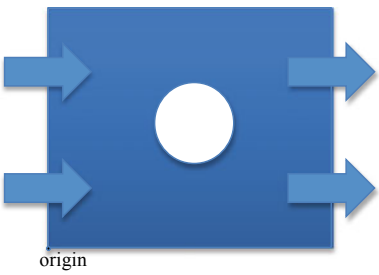

Fig. 16.2 Sketch of a flood domain with a cylindrical obstacle

Table 16.1 Parameters of the demonstrated model

Parameter (symbol)	Value (unit)	Parameter (symbol)	Value (unit)
Length	1 m	Initial particulate load	0
Width	1 m	Settling velocity v_s	0.01 m/s
Obstacle radius	0.1 m	Particle diffusivity	10^{-9} m^2/s
Initial bed below reference	0.5 m	Turbulent viscosity υ	0.0025 m^2/s
Initial water table above reference	0.5 m	Turbulent Schmidt number Sc	0.71
Inflow water table above reference	1 m	Critical Shields parameter Θ_c	0.4
Velocity at outlet	1 m/s	Particle diameter δ	0.0001 m
Manning parameter n	0.03 $s/m^{1/3}$	Resuspension parameter α	$5 \cdot 10^{-4}$
Froude number	0.26/0.31	Specific gravity ρ_s/ρ_f	2.65

0.04 $s/m^{1/3}$; and that of the Froude number is approximately 0.5. The lower Froude numbers used in our simulation, calculated on the basis of the initial and inflow depths, are more representative of common flood events. Following the methods of Li and Duffy (2011), several parameter values were taken from Cao et al. (2004). To emphasize the flow and transport coupling, we increased the resuspension parameter from the value used by the authors of previous studies.

For the SWE and transport equation, linear elements are used, and for the bed equation, quadratic elements are used. The finite element mesh is refined at the obstacle boundaries. When constructing the mesh, maximum element side lengths of only 0.01 m at the upstream side and 0.005 m at the downstream side were allowed. The resulting mesh, consisting of 2476 elements, is shown in Fig. 16.3. The discretization of the entire system of coupled differential equations has 10,468 degrees of freedom.

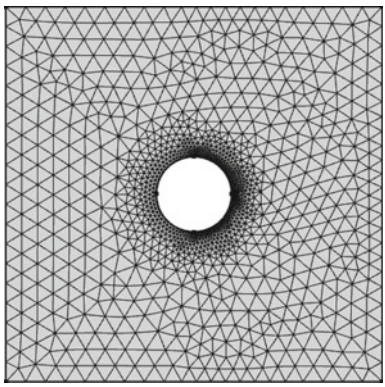

Fig. 16.3 Model finite element mesh

It is well known that the numerical solution of the advection–diffusion transport equation may suffer from severe instabilities. Straightforward modeling, either using finite differences or finite element techniques, may produce spurious oscillations. The numerical solution of SWEs (16.1) and (16.2) may have the same problem, as examined by Holzbecher and Hadidi (2017). To suppress these instabilities, various stabilization schemes have been proposed.

For the transport equation, the most basic stabilization method is the introduction of artificial diffusivity (Quarteroni 2017). In CFD implementations, an artificial viscosity, v, can be introduced, which appears in an additional term on the left side of Eq. (16.2) (Chen et al. 2013).

$$\frac{\partial \mathbf{u}}{\partial t} + (\mathbf{u} \cdot \nabla)\mathbf{u} + g\nabla H - v\nabla^2 \mathbf{u} - \mathbf{F} = 0 \tag{16.22}$$

In straightforward implementations of numerical methods, stability problems are likely to occur. Using basic stabilization methods, nonphysical terms, such as artificial diffusivity and viscosity, are introduced, which may lead to increased smoothing of steep gradients (Margolin 2019). For this reason, more sophisticated schemes have been proposed. To avoid stabilization problems in our demonstration case, several of these schemes are utilized: streamline stabilization, shock wave capturing, and artificial kinematic viscosity for the SWEs and streamline and crosswind diffusion for the transport equation. COMSOL Multiphysics offers options to easily include these schemes in the finite element formulation.

16.5 Results

Figure 16.4 shows the outcome of the numerical model outlined above. The subfigures show the water table and bottom elevation at four different time instants. For better visualization, the water table is shifted by −0.6 m.

At time $t = 0.1$ s, the wave that is initiated by the elevated water table at the inlet is moving into the domain, with the wave front reaching the obstacle. The bottom of the domain is still almost flat as in the initial state. At time $t = 0.3$ s, the wave trough has passed the obstacle. The water depth is increased at the upstream edge of the obstacle and at the outlet and is decreased behind the obstacle. The bottom surface begins to show slight changes from the initial constant state.

At $t = 0.5$ s, the water depth distant from the obstacle fluctuates slightly around the same value; at the outlet, it is slightly higher than at the inlet, while a slight wave trough is seen in between the outlet and inlet. At the upstream edge of the obstacle, the water level is still higher, and the water level is lower behind the downstream edge of the obstacle. The changes at the bottom elevation have become more pronounced: at the flanks, the digging of scours can be observed, while the bottom of the domain is elevated in the wake of the obstacle.

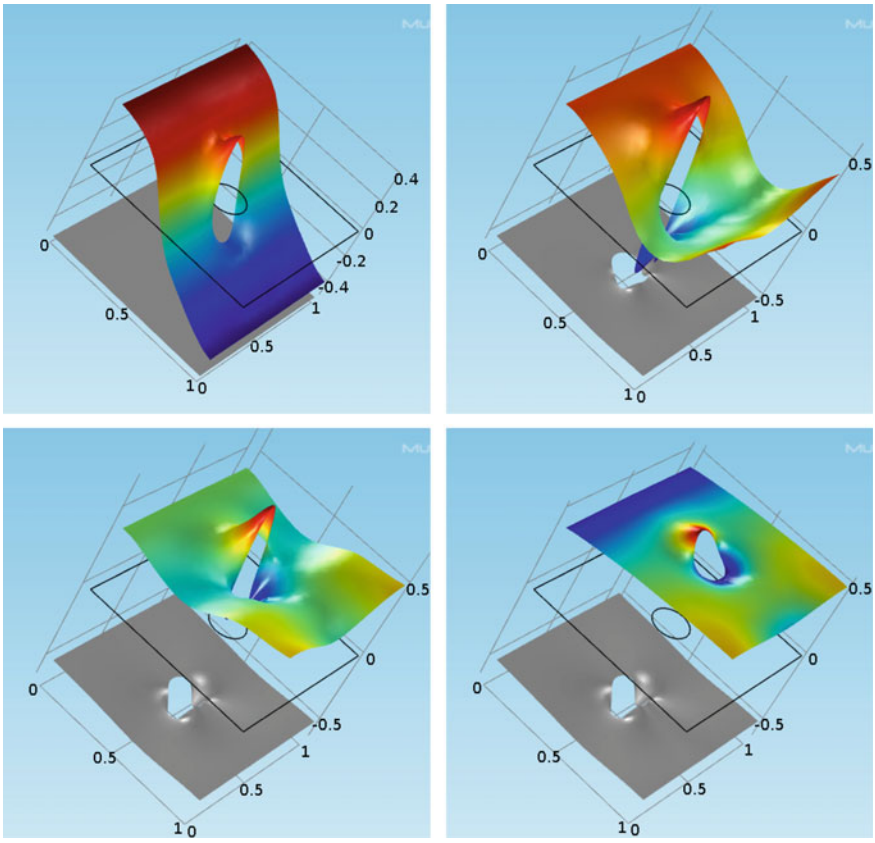

Fig. 16.4 Water table (color) and ground surface (gray) at different time instants: t = 0.1 (top left), 0.3 (top right), 0.5 (bottom left), and 0.9 (bottom right) s; all units in m

In the subfigure for t = 0.9 s, the general observation is still the same. The water table deviations from a constant value decrease. Depth extremes are still present at the obstacle boundaries: The highest value appears upstream, and the lowest value appears downstream. The changes in the bottom elevation increase further: Trough-building is observed at the flanks and sedimentation is observed in the wake.

These findings are highlighted in Fig. 16.5, which depicts the water table and bottom elevation changes at two positions as functions of time. The flank position is located directly at the obstacle boundary at the most transverse point relative to the main flow axis. The downstream position is located slightly beyond the obstacle, downstream near the flow axis. The water depth increases from 1 m to approximately 1.65 m at both positions. The graphs clearly show the deepening of the bottom of the domain at the flanks, down to almost 10 cm, and these values nearly stabilize after 0.6 s. The increase in the wake amounts to only a few centimeters but is still increasing at the end of the simulated period.

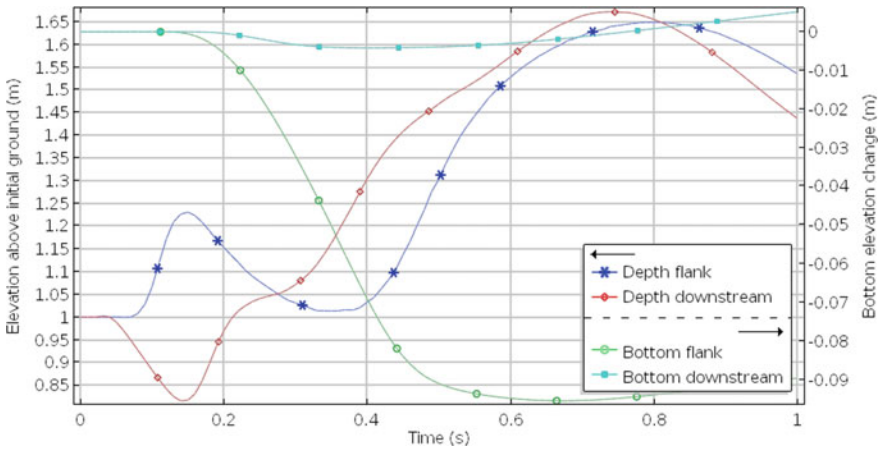

Fig. 16.5 Water table and bottom elevation changes at selected locations

16.6 Conclusions

An ideal–typical situation of scour development near an obstacle was set up in order to examine the capability of the numerical 2D coupled multiphysics approach to simulate basic processes changing the bottom of the water body. Results in Fig. 16.4 identify scours at the flanks of the obstacle and sedimentation downstream. This coincides with field observations, shown in Fig. 16.6 showing an upstream view in a wadi with a stone obstacle. Water-filled scours at the sides of the stone can be identified, while in the backwater (front in the photograph) sediment is deposited.

Further, experimental and numerical research is needed to examine the real capabilities and limits of the approach. In order to improve simulations with respect to field data, the proposed approach offers many options for the consideration of additional dependencies and processes. Sediment transport processes are complex. Even concerning the more specialized topic of scours at bridge foundations, a current review (Pizarro et al. 2020) sees no consensus between scientists of different disciplines (physicists, hydrologists, hydro-, structural, and geotechnical engineers). The cooperation between different scientific branches is thus a challenge. Theoretical and numerical efforts have to be synchronized with experimental studies, in the laboratory and in the field.

Fig. 16.6 Depression and sedimentation around an obstacle; view upstream in Wadi Abyad, Oman

Acknowledgements The presented research is enabled as part of the project funding from The Research Council (TRC) of the Sultanate of Oman under Research Agreement No. ORG/GUTECH /EBR/13/026.

References

Al-Shaqsi S (2010) Care or cry: three years from cyclone Gonu. What have we learnt? Oman Med J 25(3):162–167

Amoudry LO, Souza AJ (2011) Deterministic coastal morphological and sediment transport modelling: a review and discussion, Rev Geophys 49:2, RG2002, 21p

Aoki S, Kato S, Okabe T (2015) Observation of flood-driven sediment transport and deposition off a river mouth. Procedia Eng 116(1):1050–1056

Audusse E, Berthon C, Chalons C, Delestre O, Goutal N, Jodeau M, Sainte-Marie J, Giesselmann J, Sadaka G (2012) Sediment transport modelling: relaxation schemes for Saint-Venant-Exner and three layer models. ESAIM: Proc 38:78–98

Berghout A, Meddi M (2016) Sediment transport modelling in wadi Chemora during flood flow events. J Water Land Dev 31:23–31

Brufau P, García-Navarro P (2000) Two-dimensional dam break flow simulation. Int J Numer Meth Fluids 33:35–57

Cao Z, Pender G, Carling P (2004) Computational dam-break hydraulics over erodible sediment bed. J Hydraul Eng 130(7):689–703

Chen Y, Kurganov A, Lei M, Liu Y (2013) An adaptive artificial viscosity method for the Saint-Venant system. In: Ansorge R et al (eds) Recent developments in the numerics of nonlinear conservation laws, vol 120 of notes on numerical fluid mechanics and multidisciplinary design. Springer-Publ., Berlin, pp 125–141

Duran A (2015) A robust and well balanced scheme for the 2D Saint-Venant system on unstructured meshes with friction source term. Int J Numer Meth Fluids 78(2):89–121
Eaton BC, Lapointe MF (2001) Effects of large floods on sediment transport and reach morphology in the cobble-bed Sainte Marguerite River. Geomorphology 40:291–309
Ezzeldin MM, Rageh O, Saad MI (2019) Navigation channel problems due to sedimentation. In: Arab Academy for Science, Technology and Maritime Transport, the international maritime and logistics conference, Marlog 8'
Holzbecher E, Hadidi A (2017) Some benchmark simulations for flash flood modelling, COMSOL conference, Rotterdam
Kondolf GM et al (2014) Sustainable sediment management in reservoirs and regulated rivers: experiences from five continents. Earth's Future 2:256–280
Kwarteng AY, Al-Hatrushi SM, Illenberger WK, McLachlan A, Sana A, Al-Buloushi AS, Hamed KH (2016) Beach erosion along Al Batinah coast, Sultanate of Oman. Arab J Geosci 9:85
Li S, Duffy CJ (2011) Fully coupled approach to modeling shallow water flow, sediment transport, and bed evolution in rivers. Water Resour Res 47:W03508
Lumbroso D, Gaume E (2012) Reducing the uncertainty in indirect estimates of extreme flash flood discharges. J Hydrol 414–415:16–30
Margolin LG (2019) The reality of artificial viscosity. Shock Waves 29:27–35
COMSOL Multiphysics (2020). http://www.comsol.com
Nouh M (1988) Methods of estimating bed load transport rates applied to ephemeral streams. IAHS Publ 174:107–115
Nouh M (1988) Transport of suspended sediment in ephemeral channels. IAHS Publ 174:97–106
Pizarro A, Manfreda S, Tubaldi E (2020) The science behind scour at bridge foundations: a review. Water 12:374
Prathapar A, Bawain AA (2014) Impact of sedimentation on groundwater recharge at Sahalanowt Dam, Salalah, Oman. Water Int 39(3):381–393
Quarteroni A (2017) Numerical models for differential problems. Springer Publ, Heidelberg
Reid I, Laronne JB, Powell DM (1998) Flash flood and bedload dynamics of desert gravel bed streams. Hydraul Process 12:543–557
Rowan T, Seaid M (2017) Depth-averaged modelling of erosion and sediment transport in free-surface flows, World Academy of Science, Engineering and Technology. Int J Mech Mechatron Eng 11(10):1692–1699
Rowinski PM, Kalinowska MB (2006) Admissible and unadmissible simplifications of pollution transport equations. In: Ferreira R, Alves E, Leal J, Cardoso A (eds) River flow. CRC Press, Boka Raton, pp 199–208
Saber M, Kantoush S, Sumi T, Ogiso Y, Alharrasi T (2019) Reservoir sedimentation at wadi system: cahallenges and management strategies, DPRI Annals 62 B
Schlegel F (2012) Shallow water physics (shweq), COMSOL internal paper, private communication
Scott SH (2006) Predicting sediment transport dynamics in ephemeral channels: a review of literature, ERDC/CHL CHETN-VII-6, US Army Corps of Engineers
Shields A (1936) Anwendung der Ähnlichkeitsmechanik und der Turbulenzforschung auf die Geschiebebewegung, Ph.D. Thesis, Technical University of Berlin, Berlin, Germany
Sibetheros IA, Nerantzaki S, Efstathiou D, Giannakis G, Nikolaidis NP (2013) Sediment transport in the Koiliaris river of Crete. Procedia Technol 8:315–323
Sumi T, Hirose T (2009) Water storage, transport and distribution. In: Takahasi Y (ed) Encyclopedia of life support systems, vol 1. EOLSS Publ
Tabarestani MK, Zarrati AR (2015) Sediment transport during flood event: a review. Int J Environ Sci Technol 12:775–788
Takase S, Kashiyama K, Tanaka S, Tezduyar TE (2011) Space-time SUPG finite element computation of shallow-water flows with moving shorelines. J Comp Mech 48(3):293–306
TELEMAC (2020). http://www.opentelemac.org/

Visescu M, Beilicci E, Beilicci R (2016) Sediment transport modelling with advanced hydroinformatic tool case study—modelling on Bega channel sector. Procedia Eng 161:1715–1721

Zavattero E, Du M, Ma Q, Delestre O, Gourbesville P (2016) 2D sediment transport modelling in high energy river—application to Var river, France. Procedia Eng 154:536–543

Zhang W, Jia Q, Chen X (2014) Numerical simulation of flow and suspended sediment transport in the distributary channel networks. J Appl Math Article ID 948731, 9p

Chapter 17
Water Erosion and Sediment Transport in an Ungauged Semiarid Area: The Case of Hodna Basin in Algeria

Omar Djoukbala, Mahmoud Hasbaia, Oussama Benselama, Boutaghane Hamouda, Salim Djerbouai, and Ahmed Ferhati

Abstract This study aims to estimate the eroded and transported sediment yields from the The Hodna basin (26,000 km^2) situated in central Algeria by two approaches. In the first model, the data of the gauged subbasins are extrapolated to the ungauged areas based on the homogeneity of factors that influence the water erosion-sediment transport process. In this approach, the specific eroded and transported sediment yield in the Hodna basin is estimated to be 425 $t/km^2/yr$. In an alternative approach, the eroded yield is estimated by mapping erosion using the (RUSLE) in a GIS environment. The obtained results show a high eroded sediment yield of approximately 610 $t/km^2/yr$.

The observed difference between the results of the two approaches can be explained by the amount of sediment that is eroded but is not transported by runoff.

These two methods show high eroded and transported sediment yield values in the Hodna basin region; these high yields may seriously threaten the central flat zone with progressive deposition.

Keywords Ungauged watershed · Regionalization · Soil erosion · RUSLE · Hodna · Algeria

This study aims to estimate the eroded and transported sediment yields from the Hodna basin (26,000 km^2) situated in central Algeria by two approaches. In the first model, the data of the gauged subbasins are extrapolated to the ungauged areas based on the homogeneity of factors that influence the water erosion–sediment transport process. In this approach, the specific eroded and transported sediment yield in the

O. Djoukbala (✉)
Department of Hydraulics, University of Sidi Bel Abbès, BP 89, 22000 Sidi Bel Abbes, Algeria

O. Djoukbala · M. Hasbaia · O. Benselama · S. Djerbouai · A. Ferhati
CEHSD Laboratory, University of M'sila, 166 Ichebilia, 28000 M'sila, Algeria

B. Hamouda
Badji-Moukhtar University of Annaba, Annaba, Algeria

T. Sumi et al. (eds.), *Wadi Flash Floods*, Natural Disaster Science and Mitigation Engineering: DPRI Reports, https://doi.org/10.1007/978-981-16-2904-4_17

Hodna basin is estimated to be 425 t/km^2/yr. In an alternative approach, the eroded yield is estimated by mapping erosion using the (RUSLE) in a GIS environment. The obtained results show a high eroded sediment yield of approximately 610 t/km^2/yr.

The observed difference between the results of the two approaches can be explained by the amount of sediment that is eroded but is not transported by runoff.

These two methods show high eroded and transported sediment yield values in the Hodna basin region; these high yields may seriously threaten the central flat zone with progressive deposition.

17.1 Introduction

Soil loss due to water erosion is a real risk to the prosperity of humans and ecosystems. Soil erosion is responsible for approximately 85% of the degradation of our planet (Angima et al. 2003), and it is a complex phenomenon that affects large areas of the world. In fact, water erosion is very severe, especially in the southern Mediterranean, affecting nearly 7 million hectares of agricultural soils in Algeria.

Algeria is one of the regions that are most prone to flooding (Boudani et al. 2020) and water erosion, with a specific soil loss up to 4000 t/km^2/year (Demmak 1982) causing a large loss of fertile soil, which leads to low crop yields and associated environmental degradation. Water erosion is affected by many factors, the most important of which are climatic conditions (rain intensity), soil characteristics, topography, and human activities (Dinka 2020). The transport of eroded sediment depends on the drainage capacity, vegetal cover, and channel slope of the affected watershed.

In Algeria, the first measurements of sediment transport began in 1946 at the Traille gauging station, which controls the upper basin of the Isser wadi (Medinger 1960; Demmak 1982). With the installation of other stations, several studies have been conducted to explore the phenomena of erosion and sediment transport (Hasbaia et al. 2017); these studies have shown high rates of soil erosion and sediment transport in all regions of the country (Table 17.1).

In Algeria, gauging stations ensure that flow discharges (m^3/s) and suspended sediment concentrations (g/l) are measured. The number of samples taken at gauging stations is adapted to the hydrological regime; during low flows with little difference, only one sample is taken every 24 h. However, during the flood period, the sampling rate increases until the sampling frequency reaches every 10, 15, or 30 min during the peak of the flood. The flow discharges are determined directly from the rating curves by the water elevation, which is measured by means of a ladder or float. For each elevation measurement, water samples are taken near the riverbank to estimate the concentrations of suspended sediment. The water samples are filtered through 145-LM filter paper. The collected mass of sediment is weighed after drying at 105 °C for 24 h. The estimated suspended sediment concentration is considered to be the average over the cross section of the river, and the sediment discharge is calculated as the product of this concentration and the flow discharge.

Table 17.1 Specific erosion in Algerian catchments

Authors	Watershed	Period	A (km^2)	P (mm)	Ass (t/km^2/yr)
Hasbaia et al. (2012)	Wadi El Ham	1968–1989	5605	185	530
Bouchelkia et al. (2014)	Wadi Chellif	1972–2000	43,700	–	94.27
Bouguerra et al. (2016)	Wadi Boumessoud	1988–2004	118	396	518
Selmi and Khanchoul (2016)	Wadi Mellegue	1970–2003	4575	270	589.23
Madani Cherif et al. (2017)	Wadi El Hammam	1986–2008	7440	400	111
Achit et al. (2017)	Wadi Sebaou	1968–1999	2500	–	147.32
Hasbaia et al. (2017)	Wadi Soubella	1974–1989	183.5	288.5	126
Balla et al. (2017)	Wadi Reboa	1985–2012	327	458	678
Balla et al. (2017)	Wadi Soultez	1985–2012	207	330	575
Belarbi et al. (2018)	Wadi Tafna	1997–2011	6900	–	196.11
Benselama et al. (2019)	Wadi El Maleh	1981–1998	932.5	383	294

A: area, P: precipitation, Ass: specific soil erosion

In most cases, only suspended loads are measured, and bed load transfer measurements are lacking as they are difficult to measure. However, the suspended fraction is predominant (Lu et al. 2012) and generally accounts for approximately 90% of the total flowing sediments (Walling and Fang 2003).

In gauged areas, instantaneous measures of suspended sediment concentrations and water discharges are used in several approaches to assess and model erosion and sediment transport dynamics. The sediment rating curve (SRC) is one of the most commonly used and validated models for sediment transport studies of Algerian watersheds (Hasbaia et al. 2017; Benselama et al. 2018). The SRC can be applied to evaluate the sediment yield with a known flow and sediment concentration (Zhang et al. 2015). Other approaches are also used for the same purpose, including conceptual, distributed, and semidistributed hydrologic models.

While hydrological data are available for some gauged watersheds, predicting hydrological variables in ungauged watersheds is still a major challenge (Gibson and Hancock 2019). According to Choubin et al. (2019), reliable estimations of stream flow and sediment transport, particularly in ungauged watersheds, are the most important factors for environmental management and planning.

The availability of satellite data, which are currently easily accessible, can help in mapping erosive hazards. Moreover, approaches and models using GIS and remote sensing are increasingly used in Algeria to derive variables that are necessary for estimating soil erosion (Benchettouh et al. 2017; Benselama et al. 2018; Toubal et al. 2018).

The Hodna basin is the fifth-largest watershed in Algeria, with a drainage area of approximately 26,000 km^2. The basin is characterized by a semiarid climate with

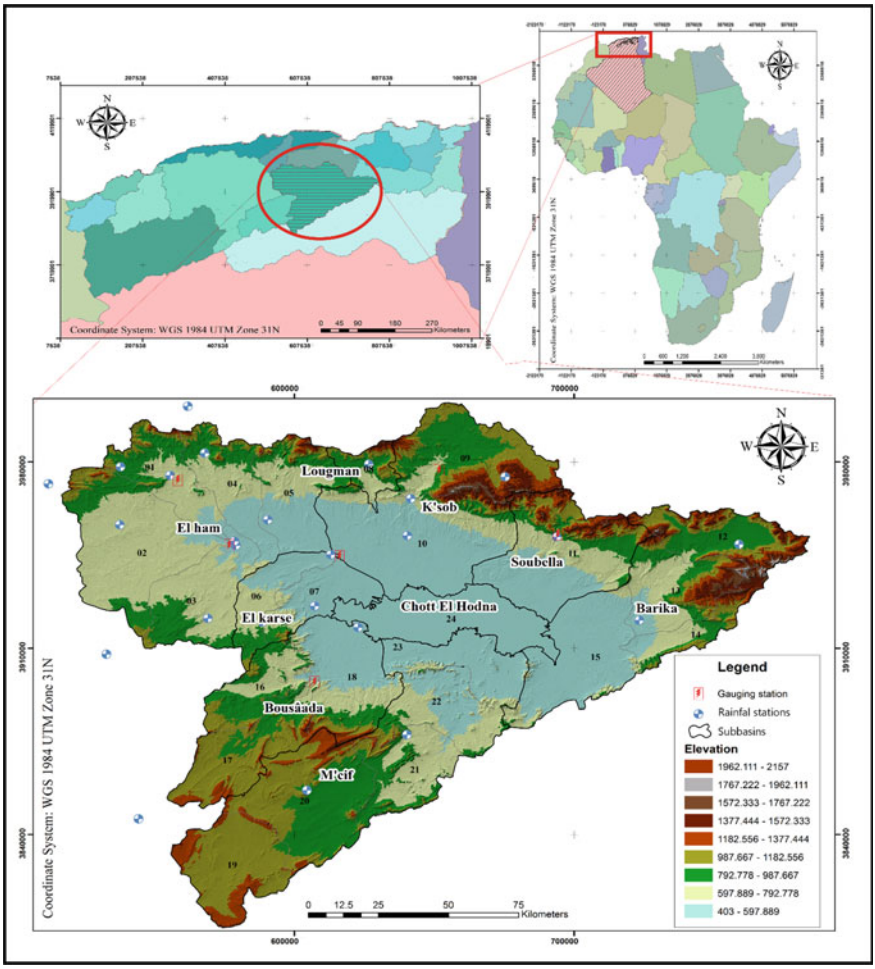

Fig. 17.1 Hodna basin

high temperatures and low rainfall associated with high spatiotemporal variability. The Hodna basin records an average annual rainfall of 363 mm/year, and the maximum daily rainfall is approximately 36.6 mm. The Hodna basin is located in the center of Algeria (Fig. 17.1) between two sets of mountains in the north and the south; it is an endorheic watershed around an almost flat depression at an altitude of 392 m. At the center of this depression, a dry salt lake named "Chott El Hodna" (1150 km^2) receives all water and solid yields from the 13 main subbasins of the watershed, which poses serious problems involving flooding and the deposition of sediment.

The main purpose of this study is to assess the soil degradation and sediment yield in the Hodna basin where 72% of the basin area is ungauged. Two

frameworks are employed. One is based on the regionalization concept and includes extrapolating data from the gauged areas to the ungauged subbasins. The second approach is based on RUSLE mapping and uses remote sensing in a GIS environment.

17.2 Methods and Materials

Study area:
The Hodna basin is the fifth-largest watershed in Algeria, with a drainage area of approximately 26,000 km^2 (Fig. 17.1). It is an interior endorheic watershed situated 150 km south of the Mediterranean coast. It is also organized as a closed, flat area (at an altitude of 392 m) between two sets of mountains to the north and south. This area receives sediment yields and water from all the subbasins of the region, and the center of this basin consists of the Chott El Hodna, a saline lake (1150 km^2).

According to the National Agency of Hydraulic Resources, the Hodna basin can be divided into 23 subbasins, and the 24th, central subbasin is the lake Chott El Hodna (Table 17.2); however, these subbasins can be grouped into eight hydrographic subbasins, each with the same principal thalweg or the same outlet. The semiarid climate of the Hodna basin is characterized by high temperatures and low rainfall associated with high spatiotemporal variability. The months of June, July, and August are the warmest, with temperatures of approximately 40 °C, while the months of December, January, and February record drops in temperature reaching −3 °C. The study area is characterized by high spatiotemporal variability in rainfall, which varies from 130 to 450 mm.

To measure the instantaneous water discharge and suspended sediment concentrations, the Hodna basin is equipped with seven gauging stations; these stations were installed between 1966 and 1970, but not all of the stations are in service. An examination of the available data shows that only data from three stations are reliable: the Medjez station in the wadi K'sob subbasin, the Sidi Ouadah station in the wadi Soubella subbasin, and the Rocade-sud station at the outlet of the wadi El ham subbasin. The Hodna basin is partially gauged, and only 28% of the total surface area is measured; the rest of the watershed (72%) is ungauged.

Methods
In this paper, the sediment yield and specific erosion of the Hodna basin are estimated by two approaches.

The first approach is developed from a regionalization concept based on the similarity of the parameters that influence runoff, sediment transport, and soil loss, especially rainfall behavior and terrain slope. The Hodna subbasins can be organized into two groups: the northern subbasin group and the southern subbasin group. The first subbasin group (northern) is characterized by relatively high rainfall, dense vegetative cover, and a steep land slope. The second subbbasin group

Table 17.2 Hodna subbasins

Subbasins of the Hodna basin		Hydrographic subbasins of the Hodna basin	
Name	Area (km^2)	Name	Area (km^2)
1 El ham	805.80	El ham	6817.61
2 Sbissebe	1851.98		
3 Guernini	1071.31		
4 Djenene	860.47		
5 Torga	1026.94		
6 El karsa	553.12		
7 El leham	647.99	El leham	647.99
8 Lougman	333.75	Lougman	333.75
9 K'sob	1471.20	K'sob	3628.72
10 M'sila	2157.52		
11 Soubella	1768.97	Soubella	1768.97
12 Barika amont	889.77	Barika	3804.24
13 Barika aval	1007.05		
14 Barriche	504.40		
15 Bithem Barika	1403.02		
16 Maiter amont	672.74	Boussaâda	2940.75
17 Boussaâda	1035.15		
18 Maiter aval	1232.86		
19 Ain Rich	1130.88	M'cif	5323.27
20 Chair amont	1597.78		
21 Chair aval	877.75		
22 M'cif amont	924.20		
23 M'cif aval	792.66		
24 Chott El Hodna	1216.81	/	/

(southern) is characterized, contrary to the first group, by low rainfall and gradual land slopes with poor vegetative cover.

The homogeneity of the two main parameters (terrain slope and rainfall) in each group is well-justified, and the vegetative cover has the same trend in the subbasins of each group. An analysis of the terrain slope generated from a digital terrain model of all the subbasins of the Hodna basin confirms that the slopes of all the southern subbasins are less than 10%, contrary to the northern subbasins (Table 17.3). Concerning rainfall, we focused on the spatial distribution of annual rainfall while assuming that the other rainfall parameters (rain intensity, maximum daily rainfall, etc.) have the same distribution.

To identify the two groups, we used an annual rainfall map of the Hodna basin. Then, we measured, for each subbasin, the area fraction with rainfall amounts ranging from 150 to 200 mm and from 300 to 400 mm (Fig. 17.2). Analyzing this

Table 17.3 Terrain slope of the Hodna subbasins

Subbasin	Terrain slope (%)	Group
Lougman	12.14	I slope > 10%
K'sob	11.08	
Soubella	10.78	
Barika	10.23	
El ham	6.53	II Slope < 10%
El Leham	5.98	
Bousâada-Maitar	8.87	
M'cif	7.68	

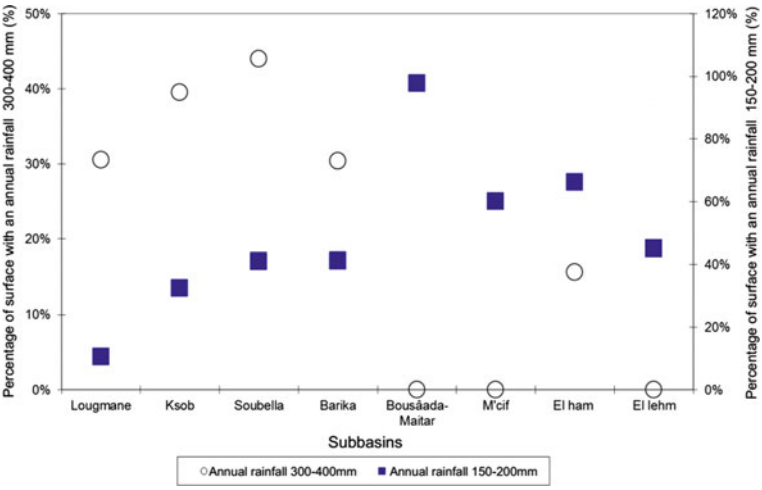

Fig. 17.2 Annual rainfall distributions in Hodna subbasins

latter figure, we clearly observed that most of the northern subbasin areas have annual rainfall between 300 and 400 mm, unlike the southern subbasins, in which the rainfall amount ranges from 150 to 200 mm.

In the northern subbasin group, comprising the four subbasins of K'sob (3628.72 km^2), Lougman (333.75 km^2), Soubella (1768.97 km^2), and Barika (3804.24 km^2), there are only two gauging stations, the K'sob and Sidi Oudah stations, which are installed in the K'sob and Soubella subbasins, respectively. The two other subbasins (Lougman and Barika) are ungauged. The whole area of this subbasin group has a land slope greater than 10%, with average annual rainfall between 300 and 400 mm and relatively dense vegetal cover.

Among the four subbasins of the second group, El ham (6817.61 km^2), Bousaâda (2940.75 km^2), M'cif (5323.27 km^2), and El leham (647.99 km^2), only the El ham subbasin is gauged; it is equipped by the Rocade-sud gauging station situated at its outlet. This subbasin group is characterized by moderate land slopes

and low annual rainfall, with values <10% and between 100 and 200 mm, respectively. The vegetal cover in this group is also poor (Hasbaia et al. 2012).

This regionalization of the Hodna basin allows the extrapolation of the calculated specific soil losses (A) from the gauged subbasins to the ungauged subbasins in the same group. In the northern subbasin group, the sediment yields of the ungauged subbasins (wadi Lougman and wadi Barika) are calculated using the specific erosions of the gauged subbasins, wadi K'sob, and wadi Soubella, respectively. In the southern subbasin group, there is only one gauged basin, wadi El- ham; therefore, the sediment yields of the ungauged subbasins (wadi Bousâada, wadi M'cif, and wadi El leham) are calculated from its specific erosion.

The second approach consists of mapping soil loss due to water erosion in the Hodna watershed using the Revised Universal Soil Loss Equation (RUSLE) (Wischmeier and Smith 1978) in a GIS environment. This equation estimates soil erosion (A) by multiplying the five RUSLE factor maps, defined as the specific soil erosion (A) (t/km^2/yr), the rainfall erosivity (R) (MJ mm/ha/h/yr), the soil erodibility (K) (Mg h/MJ/mm), the topography factor (LS), crop management (C), and erosion control practices (P) (Table 17.4).

$$A = R \times K \times LS \times C \times P \tag{17.1}$$

In this approach, we used the data of 25 rainfall stations situated inside and around the Hodna basin. The rainfall erosivity (Fig. 17.3) was calculated at all stations and spatialized over the whole watershed surface by inverse distance weighting (IDW) interpolation in a GIS environment. To characterize the soil erodibility (K) map (Fig. 17.4), we used the harmonized world soil database (HWSD) (Djoukbala et al. 2019). The map of topographic factors (LS) was obtained from a digital elevation model (DEM) with an accuracy of 30 m in a GIS

Table 17.4 Description of the data used

Parameter	Materials	Resolution (m)	Year	Source
NDVI data	Landsat satellite	30	2019	http://earthexplorer.usgs.gov/
Rainfall data	Monthly/ annual rainfall data	30	1985–2015	National Agency for Hydraulic Resources (NAHR)
Soil properties	(HWSD)	90	–	The Harmonized World Soil Database http://webarchive.iiasa.ac.at/Research/LUC/External-World-soil-database/HTML/
Topographic data	Aster global DEM	30	2019	http://earthexplorer.usgs.gov/

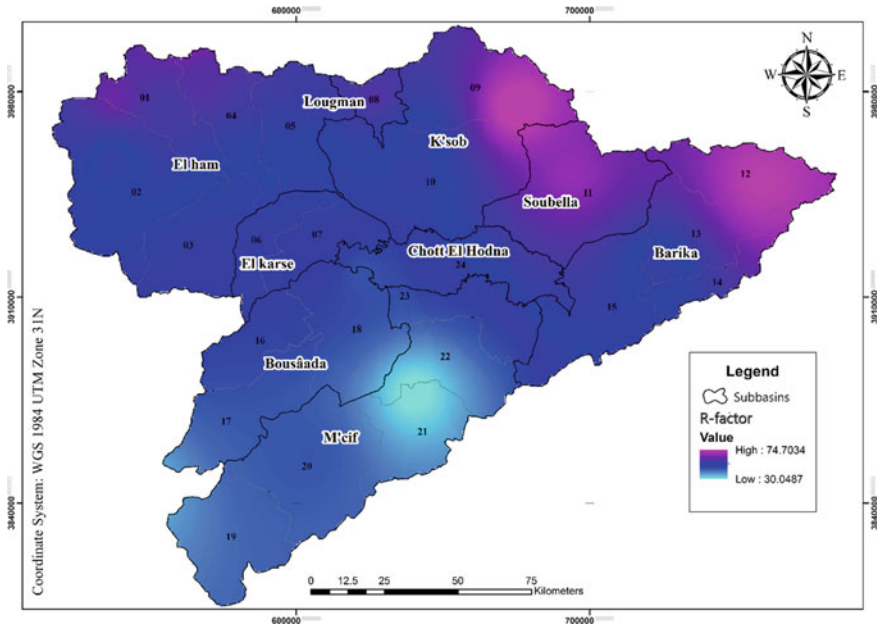

Fig. 17.3 Map of rainfall erosivity

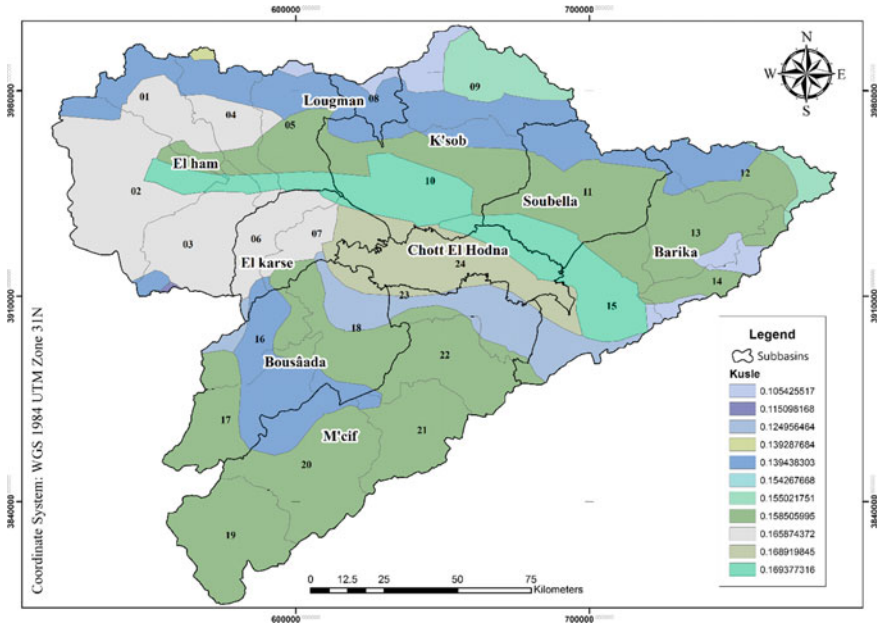

Fig. 17.4 Map of soil erodibility

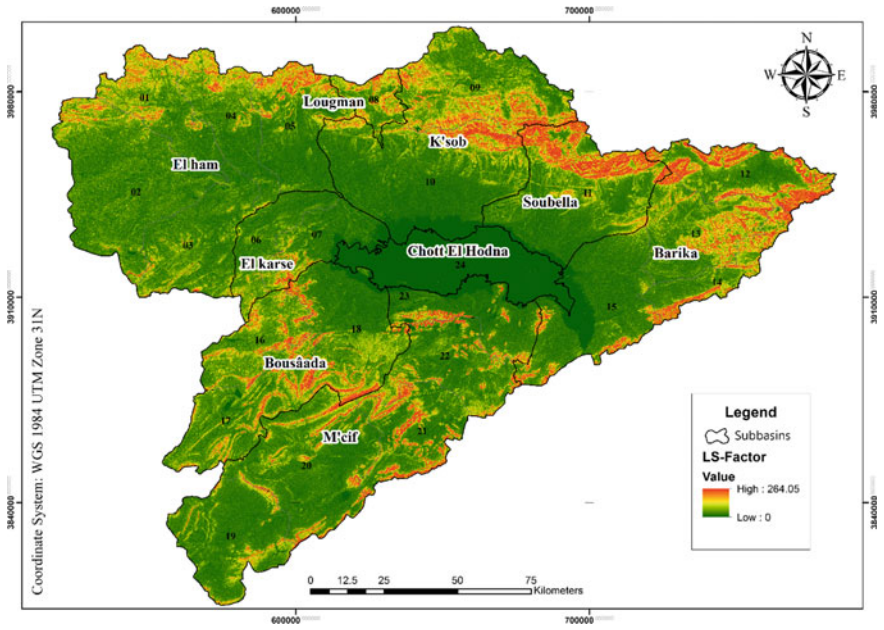

Fig. 17.5 Map of the topographic factor (LS)

environment (Fig. 17.5). To map the crop management factor (C), we used normalized difference vegetation index (NDVI) data (period 2019) obtained by the Landsat 8 satellite. To estimate the values of factor C in the study area (Fig. 17.6), we used the regression between two extreme values. These values are taken from experimental diagram (Gitas et al. 2009). The equation of the regression line found is as follows:

$$C = 0.9167 - NDVI \times 1.1667 \tag{17.2}$$

The erosion control methods in the Hodna basin are very modest; therefore, the factor P is taken to be equal to one. The superposition of the five-factor maps for the Revised Universal Soil Loss Equation allowed the mapping of specific soil loss over the whole surface of the Hodna watershed (Fig. 17.7).

17.3 Results and Discussion

Based on the first approach, we calculated specific soil erosion from the measured data of three gauging stations: Medjez, Sidi Ouadah, and Rocade-sud (Table 17.5). The obtained values were extrapolated to the ungauged subbasins to estimate their sediment yields and corresponding specific soil erosion rates (Table 17.6).

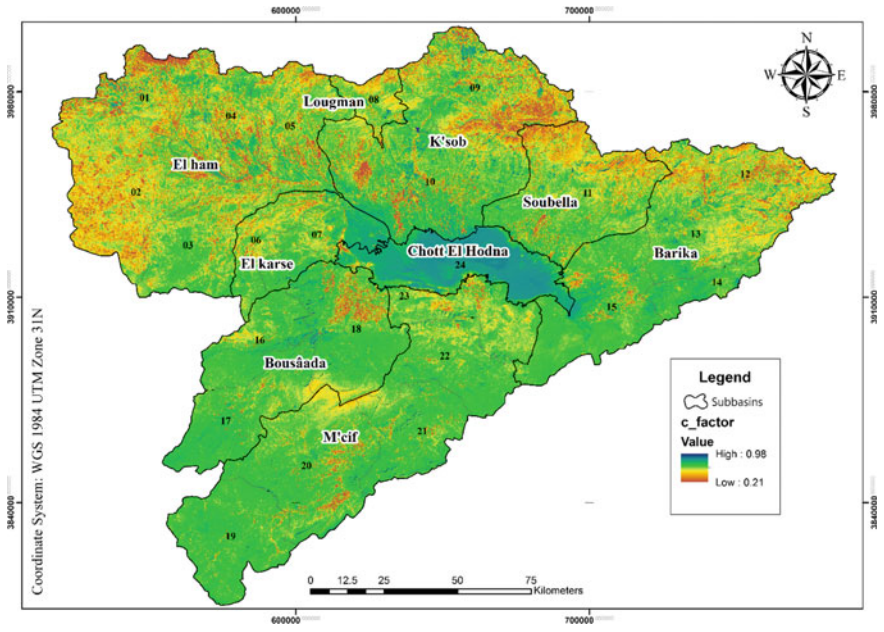

Fig. 17.6 Map of the C-factor

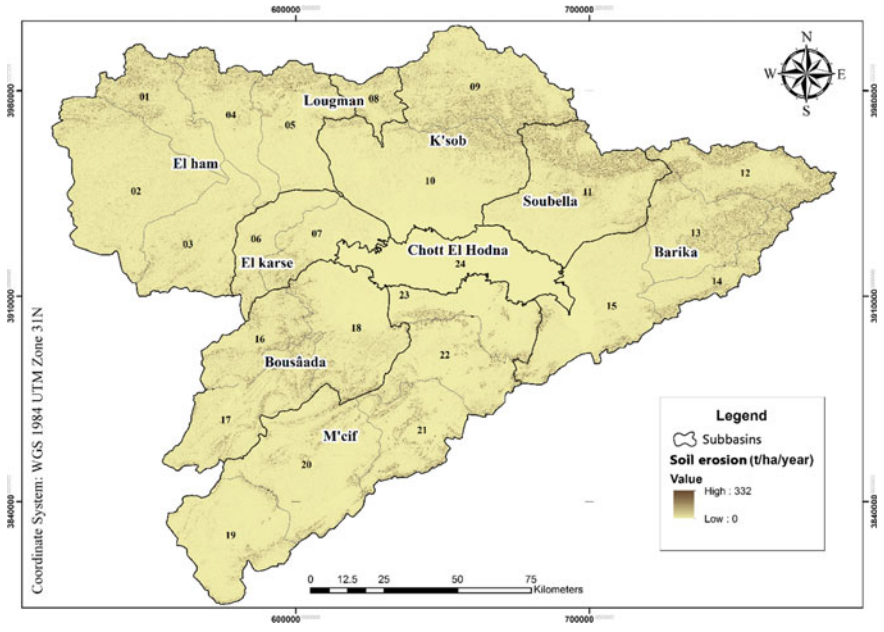

Fig. 17.7 Map of soil loss in Hodna basin

Table 17.5 Specific erosion of gauged subbasins

Subbasin	El Ham	K'sob	Soubella
Specific erosion (t/km^2/yr)	529.26	430.00	239.50

Table 17.6 Specific erosion and sediment yields of the Hodna basin

Approach	I			II	
Subbasin	Water yield (million m^3/yr)	Sediment yield (million t/yr)	Specific erosion (t/km^2/yr)	Specific erosion (t/km^2/yr)	Error (%)
El ham	94.35	2.97	529.26	571.78	7.4
El leham	9.69	0.63	529.26	601.80	12.1
Lougman	9.61	0.14	430.00	528.49	18.6
K'sob	102.88	1.56	430.00	595.67	27.8
Soubella	19.76	0.42	239.50	490.00	51.1
Barika	40.90	0.91	239.50	438.34	45.4
Busaâda	44.84	1.55	529.26	549.86	3.7
M'cif	80.59	2.81	529.26	585.67	9.6

From this regionalization approach, the above numbers show the high dynamics of soil degradation and sediment transport in the Hodna region; approximately, 11 million tons of sediment and 403 million m^3 of water are lost annually, with a specific erosion of 425 t/km^2/yr (among the highest in Algeria) in the whole Hodna basin. Taking into account the temporal variability of the water and sediment yields estimated in the Hodna basin as 120% and 100%, respectively, these yields can reach 860 million m^3 of water and 22 million tons of sediment. The only dam in the Hodna basin, "K'sob," is almost entirely silted, and it mobilizes less than 10 million m^3 of water; therefore, spectacular volumes of water and sediment are spilled into the Chott, causing serious problems involving inundation and sediment deposition. The sediment volume can increase the terrain level of the Chott El Hodna by approximately 2 cm every year, i.e., 20 cm in 10 years on the whole of the supposed flat surface (1150 km^2). If we consider the variation of the topography, all the depressions in this region can be bridged in fewer than ten years, which explains why several roads and bridges were raised several times last year; the villages of the region are also threatened.

The water yield also presents a real danger; it could immerse the entirety of the saline lake Chott El Hodna with a water depth of 74 cm if the terrain is assumed to be flat, which means that any depression is threatened by flooding. Due to this high water yield, the risk of the spread of saline water is also increasing (Hasbaia et al. 2012).

The use of remote sensing (RS) techniques in a geographic information system (GIS) environment allows the quantitative estimation of erosion as well as its spatial distribution at a low cost and with a significant degree of accuracy for large areas,

particularly since policy creators are much more interested in the distribution of erosion risk than in its absolute value (Lu et al. 2004).

The quantitative estimation of soil erosion was carried out by applying empirical point models, which require input parameters including specialized data (slopes, soil texture, rainfall, etc.) characterizing water erosion factors (topography, erodibility, erosivity, etc.) (Le Bissonnais et al. 2004).

According to Wishmeier's equation (RUSLE), the average annual soil loss(A) was estimated from the different factors (rainfall erosivity (R), soil erodibility (K), topography (LS), cropping management (C), and support practice (P)) using spatial analysis with ArcGIS software, which represents a geoenvironmental scenario for the study area. A soil loss map (Fig. 17.7) of the entire watershed area was obtained by the superposition of the generated maps of each previous factor.

The results indicate that the annual rate of soil erosion ranged from 0 to 332 t/ha/yr, with an average of 6.10 t/ha/yr; this value is very close to the results obtained in similar studies in the Hodna region (Djoukbala et al. 2018; Hasbaia et al. 2018).

This approach also demonstrates that the RUSLE model combined with a geographic information system (GIS) is a practical and relevant method for assessing the spatial variability of soil erosion for the efficient and effective management of sediments and water quality.

According to the comparison between the two approaches, the values converge with variable errors from 3 to 50% (Table 17.5). Among the eight subbasins, we note that satisfactory results are obtained for the Busaâda, M'cif, El ham, El leham, and Lougman subbasins, with errors of 3.7%, 9.6%, 7.4%, 12.1%, and 18.6%, respectively, compared with those acquired by the regionalization approach. Diverse results are obtained for the K'sob, Barika, and Soubella subbasins, with errors up to 51%.

This approach shows a very useful tool for predicting sediment degradation in ungauged areas. The comparison of the obtained results in only the gauged areas with reliable measured suspended sediment data shows an error less than 21%. This error is acceptable if we take into account the mass of eroded sediments that do not reach the gauging stations located in the main channels.

17.4 Conclusion

The Hodna basin is a very large basin with an area of 26,000 km^2; it is an endoreic basin that is partially gauged, and only 28% of the basin surface is measured by gauging stations. Estimating sediment yields and erosion risks in this basin presents a very important challenge. To this end, this paper presented two approaches: one based on the regionalization concept and the second based on RUSLE mapping. The soil loss in the Hodna basin presents average values of approximately 425 or 610 t/km^2/yr as calculated by the first and second approaches, respectively. The value obtained from the RUSLE method is approximately 30% greater than that obtained from the regionalization approach. This rate is explained by the mass of

eroded sediments that do not reach the gauging stations in the main channels. In fact, these two approaches are very complementary for estimating both the eroded and transported sediment rates.

The present results are similarly compatible with the results of other studies relating to water erosion assessments carried out in other Algerian basins with similar climatic and environmental characteristics. The specific soil loss has been evaluated as 570, 679, and 1118 t/km^2/yr in the wadi El Ham watershed (Djoukbala et al. 2018), K'sob catchment (Hasbaia et al. 2018), and wadi Boumahdane (Bouguerra et al. 2017), respectively.

References

Achit M, Ballah A, Kamel Toubal A (2017) Etude de l ' ecoulemen t liquide et solide dans le bassin versant de l ' oued se baou au droit de la station hydrometrique de baghlia, Algerie. http://dspace.univ-ouargla.dz/jspui/handle/123456789/13919

Angima SD et al (2003) Soil erosion prediction using RUSLE for central Kenyan highland conditions. Agric Ecosyst Environ 97(1–3):295–308

Balla F, Kabouche N, Khanchoul K, Bouguerra H (2017) Hydro-sedimentary flow modelling in some catchments constantine highlands, Case of Wadis Soultez and Reboa (Algeria). J Water Land Dev 34(1):21–32. http://content.sciendo.com/view/journals/jwld/34/1/article-p21.xml

Belarbi F, Bouchelkia H, Remini B, Benmansour A (2018) Quantification and study of monthly variation of suspended sediment loads in Tafna Basin—Algeria. J Water Land Dev 37(1):29–38. http://content.sciendo.com/view/journals/jwld/37/1/article-p29.xml

Benchettouh A, Kouri L, Jebari S (2017) Spatial estimation of soil erosion risk using RUSLE/GIS techniques and practices conservation suggested for reducing soil erosion in Wadi Mina Watershed (Northwest, Algeria). Arab J Geosci 10(4)

Benselama O, Mohamed M, Mahmoud H, Omar D, Sakher M (2018) Prediction of water erosion sensitive areas in mediterranean watershed, a case study of Wadi El Maleh in North-West of Algeria. Environ Monit Assess 190(12):735. http://link.springer.com/. https://doi.org/10.1007/s10661-018-7117-1

Benselama O, Mohamed M, Mahmoud H, Omar D, Sakher M (2019) Analysis of the suspended sediment yield at different time scales in mediterranean watershed, case of Wadi El Maleh (North-West of Algeria). J Mediterr Earth Sci 11:3–13

Bouchelkia H, Belarbi F, Remini B (2014) Quantification of suspended sediment load by double correlation in the watershed of Chellif (Algeria). J Water Land Dev 21(1):39–46

Boudani MR, Mohamed M, Omar D et al (2020) Development of a minimalist conceptual numerical model for flood forecasting and management under GIS environment. J Water Clim Change

Bouguerra SA, Bouanani A, Baba-Hamed K (2016) Transport Solide Dans Un Cours d'eau En Climat Semi-Aride : Cas Du Bassin Versant de l'Oued Boumessaoud (Nord-Ouest de l'Algérie). Revue des sciences de l'eau 29(3):179. http://id.erudit.org/iderudit/1038923ar

Bouguerra H, Bouanani A, Khanchoul K et al (2017) Mapping erosion prone areas in the Bouhamdane watershed (Algeria) using the revised universal soil loss equation through GIS. J Water L Dev 32:13–23. https://doi.org/10.1515/jwld-2017-0002

Cherif M, Hayet KK, Bouanani A, Terfous A (2017) Prediction of sediment yield at storm period in Northwest Algeria. Arab J Geosci 10(9):1–17

Choubin B et al (2019) Streamflow regionalization using a similarity approach in ungauged basins: application of the geo-environmental signatures in the Karkheh River Basin, Iran. CATENA **182**(February 2018), 104128. https://doi.org/10.1016/j.catena.2019.104128

Demmak A (1982) Contribution à l'étude de l'érosion et Des Transports Solides En Algérie Septentrionale [Contribution to the Study of Erosion and Sediment Transport in Northern Algeria]." PhD Thesis. Manuscript. Paris. Université de Pierre et Marie Curie

Dinka MO (2020) Quantification of soil erosion and sediment yield for ungauged catchment using the RUSLE model: case study for Lake Basaka Catchment in Ethiopia. Lakes Reservoirs: Res Manage (March 2019):1–13. http://doi.wiley.com/. https://doi.org/10.1111/lre.12312

Djoukbala O, Mazour M, Hasbaia M, Benselama O (2018) Estimating of water erosion in semiarid regions using RUSLE equation under GIS environment. Environ Earth Sci 77(9):345. https://doi.org/10.1007/s12665-018-7532-1

Djoukbala O, Hasbaia M, Benselama O, Mazour M (2019) Comparison of the erosion prediction models from USLE, MUSLE and RUSLE in a Mediterranean watershed, case of Wadi Gazouana (NW of Algeria). Model Earth Syst Environ 5(2):725–743. http://link.springer.com/. https://doi.org/10.1007/s40808-018-0562-6

Gibson A, Hancock G (2019) Suspended sediment load estimation in an ungauged river in South-eastern Australia. River Res Appl (October): rra.3558. https://onlinelibrary.wiley.com/doi/abs/. https://doi.org/10.1002/rra.3558

Gitas IZ, Douros K, Minakou C, Silleos GN, Karydas CG (2009) Multi-temporal soil erosion risk assessment in N. Chalkidiki using a modified USLE raster model. EARSel eproceedings 8 (1):40–52

Hasbaia M et al (2012) Study of the water and sediment yields of Hodna Basin in the centre of Algeria, Examination of their impacts key words. In: ICSE6, Paris, pp 103–110

Hasbaia M et al (2018) Prediction of dams silting in semi-arid region using erosion map under GIS environment, case of Ksob watershed in Hodna region (Algeria), pp 781–783. http://link.springer.com/. https://doi.org/10.1007/978-3-319-70548-4_229

Hasbaia M, Hedjazi A, Benayada L (2012) Variabilite de l ' Érosion Hydrique Dans Le Bassin Du Hodna : Cas Du Sous-Bassin Versant de l ' Oued Elham. Revue Marocaine Des Sciences Agronomiques Et Vétérinaires 1(1):28–32

Hasbaia M, Paquier A, Herizi T (2017) Hydrological modeling of sediment transport in the semi-arid region, case of Soubella Watershed in Algeria. In: Water resources in arid areas: the way forward, pp 251–266. http://link.springer.com/. https://doi.org/10.1007/978-3-319-51856-5

Le Bissonnais Y, Dubreuil N, Daroussin J, Gorce M (2004) Modélisation et Cartographie de l'aléa d'érosion Des Sols à l'échelle Régionale. Étude Et Gestion Des Sols 11(3):307–321

Lu D, Li G, Valladares GS, Batistella M (2004) Mapping soil erosion risk in Rondonia, Brazilian Amazonia: using RUSLE. Remote Sens GIS Degrad Dev 15(5):499–512

Lu G et al (2012) Impacts of Danjiangkou Reservoir on sediment regime of the Hanjiang River. Hydrol Res 43(1–2):64–72

Medinger JM (1960) Transport solide des oueds algeriens. Annuaire Hydrologique de l'Algérie (Années 50–59), Alger

Selmi K, Khanchoul K (2016) Sediment load estimation in the Mellegue catchment, Algeria. J Water Land Dev 31(1):129–137

Toubal AK, Achite M, Ouillon S, Dehni A (2018) Soil erodibility mapping using the RUSLE model to prioritize erosion control in the Wadi Sahouat Basin, North-West of Algeria. Environ Monit Assess 190(4)

Walling DE, Fang D (2003) Recent trends in the suspended sediment loads of the World's Rivers. Global Planet Change 39(1–2):111–126

Zhang HY, Shi ZH, Fang NF, Guo MH (2015) Linking watershed geomorphic characteristics to sediment yield: evidence from the Loess Plateau of China. Geomorphology 234:19–27. https://doi.org/10.1016/j.geomorph.2015.01.014

Chapter 18
Reservoir Sediment Management Practices in Sudan: A Case Study of Khashm El-Girba Dam

Elhadi Adam and Mohammed Suleiman

Abstract The sedimentation problem is a hot issue currently affecting the operations of reservoirs and irrigation networks in Sudan. Most of the rivers that cross Sudanese borders come from the Eastern African Plateau, which acts as a sediment source for the Nile River and its tributaries. Khashm el-Girba Dam (KEGD), which crosses the Atbara River in Eastern Sudan, is a multipurpose dam that was constructed in 1964. The Atbara River is a branch of the Nile River system, and the river carries a large amount of sediment during the flood period. Seven years after construction, in 1970, the dam faced a critical problem that could have led to a disaster; it was discovered that, due to sediment deposition, the water storage was not enough to satisfy the downstream requirements. This study discusses the sediment management practices used in KEGD and their impacts on maintaining the reservoir capacity. Practices including operation policy (OP), trap efficiency (TE), sluicing, sediment sluicing, and flushing operation (FO) were discussed. The adopted management practices succeeded in removing a considerable amount of silt and maintaining the lifetime of the reservoir.

Keywords Sluicing · Flushing operation · Bathymetric survey · KEGD

18.1 Introduction

18.1.1 General

Reservoir sedimentation is a global challenge affecting the life cycle and sustainability of reservoirs. Annually, reservoirs lose considerable amounts of storage capacity due to sedimentation. Globally, 1 to 2% of the total storage capacity of reservoirs is lost annually (Yang 2003). Figure 18.1 shows the percentage loss of

E. Adam (✉)
Faculty of Engineering, University of Kassala, Kassala, Sudan

M. Suleiman
Dam Complex of Upper Atbara, MoWRI, Atbara, Sudan

T. Sumi et al. (eds.), *Wadi Flash Floods*, Natural Disaster Science and Mitigation Engineering: DPRI Reports, https://doi.org/10.1007/978-981-16-2904-4_18

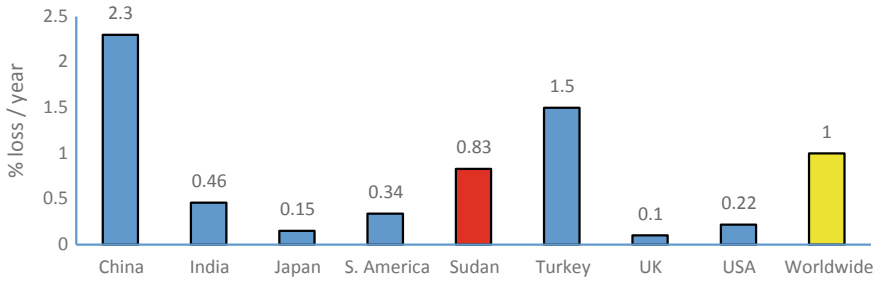

Fig. 18.1 Percentage of annual reservoir loss worldwide. *Source* Yang (2003)

reservoir capacity worldwide. From the figure, China has the highest loss (2.3%), and the Sudan loss rate is approximately 0.83%.

For most dam schemes around the world, there are concerns that the rate of storage capacity loss due to sedimentation is much larger than was catered for in the original dam designs. The majority of dams allow for a dead storage capacity to accommodate the sediment that will be deposited. However, there is no guarantee that sediment will settle in this specified zone, and as a result, the operational life span of a reservoir may be reduced sooner than anticipated.

18.1.2 Sediment Management

Sediment is produced as a result of weathering agents (erosion and the wearing a way of land surfaces) (Strand and Pemberton 1982). Climate change and the increased frequency of climate extremes (floods and drought) have increased the sediment yields from reservoir catchments. Water resource development projects are most affected by sediment transported by water (Raghunath 2006). Catchment characteristics (such as areal extent, soil types, land slopes, vegetation cover, and climatic conditions) play important roles in the sediment generation process and have great influences on sediment movement and distribution (Raghunath 2006). The key factors ensuring the sustainability of reservoirs are achieved by applying reservoir sediment management strategies.

In the literature, worldwide practices have shown a variety of management options. The selection of an appropriate method is region-specific, and a method can be applied in certain regions but not in other regions (Yang 2003). The methods available as enumerated by Annandale et al. (2016) are watershed management in the upper catchment to reduce sediment inflow into a reservoir, construction of small dams upstream to control the sediments entering a reservoir, methods that use flow hydraulics to reduce the load accumulation entering a reservoir and methods consisting of hydraulic dredging of existing sediment. According to Annandale, all of these methods have been tried worldwide, and none of them provide complete mitigation.

Several factors should be considered, such as factors pertaining to sedimentation characteristics (rate of discharge, concentration, etc.), factors pertaining to catchment characteristics (physical and hydrological features, land use/land cover), environmental considerations as well as downstream considerations, and socioeconomic factors. More than one technique or a combination of management strategies may also be applied at a given reservoir, either sequentially or concurrently, to control sediment deposition (Kantoush et al. 2010).

18.1.3 Sediment Management Practices in Sudan

By the end of the 1960s, dam projects of different kinds were constructed in Sudan. These projects play tremendous roles in agricultural development, power generation, flood control and water supply, and many other purposes. However, most of the agricultural development projects in Sudan were situated in semiarid to arid regions. The main water supplies for these projects emerge from the Ethiopian Plateau through the Blue Nile and Atbara Rivers. Rivers coming from this area carry torrential flows with large sediment loads, which are conveyed further downstream to the relatively low-lying lands of Sudan. Drought, which occurred in the 1980s, and the food security practices adopted by the Sudanese government for irrigated areas without consideration of sediment mitigation measures have had great impacts on the increase in sediment loads in reservoirs.

Considerable sediment loads are deposited in the reservoirs and irrigation networks, reducing the capacity of the reservoirs and the efficiency of the irrigation networks. Figure 18.2 shows the volume of discharged sediment carried by the Nile River and its tributaries. As seen in the figure, the Atbara River, on which KEGD was constructed, comes in second after the Blue Nile.

The average annual suspended sediment load in the Nile River has been estimated to be 140×10^6 tons per year (ElMonshed et al. 1997), of which

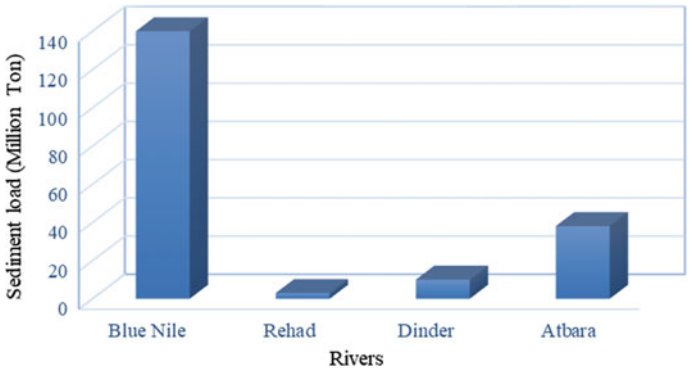

Fig. 18.2 Sediment loads of the Nile River and its tributaries. *Source* Osman (2018)

Table 18.1 Reduction in the storage capacities of Sudanese reservoirs due to sedimentation

Name of dam	River	Year of construction	Design capacity (Billion)	Present capacity (Billion)	Reduction (%)
Sennar	Blue Nile	1925	0.93	0.36	60
Jebel Aulia	White Nile	1939	3	3	0
KEG Dam	Atbara	1964	1.3	0.6	54
Roseires	Blue Nile	1966	3.2 (before heightening)	1.9 (before heightening)	40
Merowe	Main Nile	2009	12.4	11.4	8
Dam Complex of Upper Atbara (DCUA)	Atbara	2015	3.7	2.8 (Survey 2017)	24

approximately 37% is produced by the Atbara River. Table 18.1 shows Sudanese reservoirs and the changes in their capacities that have occurred during their life-times (Osman 2018).

In Sudan, reservoir sedimentation management sometimes has a great negative impact on water resource projects. For example, reservoir management has serious impacts on the hydropower generation potential. To remove sediments from hydropower intakes, the upstream water levels must be lowered and maintained as low as possible to flush the sediment-laden water. This process has great impacts on the head and amount of generated power. However, recently, the heightening of Roseires Dam, as well as the new Great Ethiopian Renaissance Dam (GERD), has added more management abilities to the sedimentation problem in the Roseires reservoir and the irrigation canalization system in Sudan; on the other hand, these changes will reduce soil fertility due to sediment trapping.

In general, the objectives of the reservoir operating rules in Sudan are to preserve a sufficient amount of water to satisfy needs and to minimize sediment deposition. Many sediment management methods have been applied in Sudanese practices to restore reservoir volumes. Among these methods, regulation rules were found to be the most effective. The operation of reservoirs is performed while taking into consideration effective ways to avoid the period of the maximum possible sediment deposition quantity and pass the sediment downstream safely. Drawdown has been practiced in some reservoirs, and other reservoirs use sediment sluicing during the rainy season and begin storing water only after the passage of the peak of the flood season. Sluicing and dredging are practiced in Roseires Dam (Blue Nile), only sluicing is practiced in Sennar Dam (Blue Nile), storing is practiced in Jabel Aulia Dam (White Nile), a combination of sluicing and flushing is practiced in KEGD (Atbara river), and sluicing and sediment sluicing are practiced in Merowe Dam (Main Nile).

18.1.3.1 Roseires Dam

Roseires Dam, on the Blue Nile, was provided with low-level sluicing gates that have discharge capacities capable of passing the average annual river flows. In the case of hydropower generation in Roseires reservoir, the function of the low-level sluices is to pass the bulk of larger sediment particles to minimize the impact of sediment on the turbines. The removal of already-deposited sediments is costly and impractical, and this process is very limited for most of the reservoirs in the Nile. Sediment removal by dredging is regularly performed in the Roseires reservoir in front of the powerhouse intakes before the occurrence of floods. However, in Merowe Dam, the sediment that accumulates in front of the power intakes is removed using sluice gates 26 m below the power intakes.

In the first ten years of its operation, Roseires reservoir lost 17% of its overall capacity, which represents 90% of the to-date storage capacity. By the end of 1992, Roseires reservoir lost 37% of its original capacity, which represents 100% of the dead storage capacity and a considerable part of the live storage capacity.

GERD, after construction, will act as a natural settling basin that will reduce the amount of sediment entering Roseires reservoir, prevent the blockage of irrigation canals and pump station intakes, improve hydropower generation efficiency and effectiveness, prevent the blockage of power plant inlets, and reduce abrasion on turbines.

18.1.3.2 Sennar Dam

Sennar Dam was constructed in 1925. During the period from 1925 to 1981, the rate of sedimentation in Sennar reservoir never exceeded 0.5% per year compared to its original capacity, which represents a 28% reduction in the overall reservoir capacity (Ahmed 2008). During the abovementioned period, the Blue Nile usually flowed naturally (all the inflow discharge was passed) without storing water during the flood period. This perfect performance of the reservoir was attributed to the excellent design of the dam. However, after 95 years, Sennar Dam lost 71% of its original reservoir capacity.

Figure 18.3 shows the operation rules for Sennar Dam. From the figure, the sediment concentration is very high (>6000 ppm) during the start of the flood season (July–August). According to the operation rules for different reservoirs in Sudan, the reservoir level is usually maintained at a minimum level during this period to allow all the sediment-laden water to pass, and then the filling program starts.

18.1.3.3 Merowe Dam

From lessons learned in the sediment management practices of Roseires reservoir, a new technique was applied to Merowe Dam to control the accumulation of

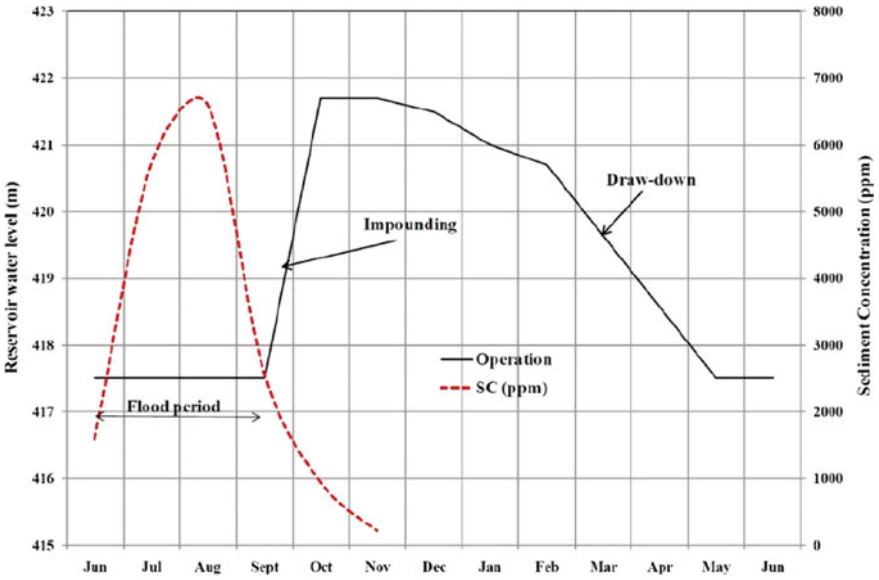

Fig. 18.3 Sennar Dam operation rules. *Source* Osman (2018)

sediment in front of the powerhouse. There are six sediment sluices arranged in the power intake dam 26 m below the intake opening beside the normal sluice gates. The cross sections of these sediment sluices are tapered at the downstream ends. The flow-through each sluice is controlled by main radial gates placed at the downstream ends of the sluices. Due to the high flow velocities (22–24 m/s) and the high sediment concentrations, the sediment sluices are steel-lined (Osman 2018).

18.1.3.4 Irrigation Network Sedimentation

Most of the irrigation water in Sudan is diverted from sediment-laden rivers that originate from the Ethiopian Plateau. The Blue Nile and Atbara Rivers carry flows with high sediment concentrations during the rainy season. Most of these sediment loads are introduced to the irrigation networks of existing agricultural schemes, such as Gezira and Managil.

The Gezira Scheme (GS) is one of the largest agricultural schemes in the world. To restore the canalization system, desilting and aquatic weed clearance have been practiced since the establishment of the scheme in 1925.

The Hydraulic Research Center (HRC) of the Ministry of Water Resources and Irrigation (MoWRI) of Sudan, carried out, from 1988 to 1996, sediment studies in the Gezira canalization system (irrigation water supply from Sennar Dam). The study concluded that 5% of the sediment was deposited in the main canals, 22%

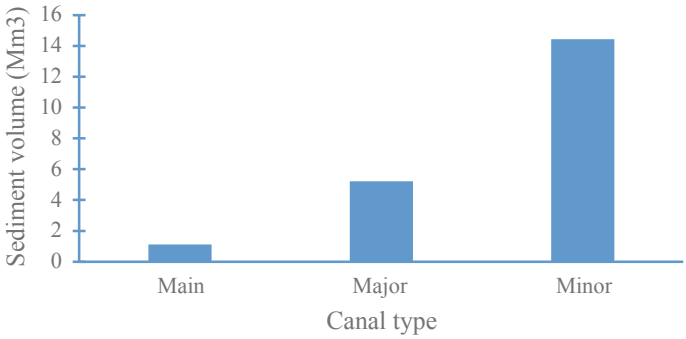

Fig. 18.4 Average quantities of silt removed from canals (2003–2010)

was deposited in the major canals, 33% was deposited in the minor canals, and 40% passed to the fields (Ahmed 2008). The same study was conducted by the HRC for the Halfa Irrigation Scheme (which is irrigated from KEGD), and comparable results were obtained (Fig. 18.4).

At the beginning of the Gezira Scheme, the removal of 5–7 million m^3 of sediment was considered satisfactory (World Bank 2000). In 1999, MoWRI recorded that 41 million m^3 of sediment was removed from the canalization system, but some researchers believe that this value is not realistic or scientific considering the past experience and the amount of sediment that enters the GS annually (Ahmed 2008). This amount of sediment removed causes many irrigation difficulties; during sediment removal, the canalization system is over excavated, and the cross sections of the canals are widened.

Most of the operation and maintenance (O/M) costs of the irrigation networks in the Sudanese irrigation schemes go to sediment and aquatic weed clearance. These two problems create many irrigation difficulties, such as increases in O/M costs, delays in sowing times, water shortages, and decreases in crop productivity, which in turn lead to reductions in crop yields.

The water supply used for irrigation is conveyed through a system of canals that are exposed to sediment deposition from silt-laden water. The growth of aquatic weeds provides traps for suspended silt if the water velocity is low and thus increases siltation in the canals, which might also raise the water level in the fields. Many efforts have been made to mitigate sediment and aquatic weeds in irrigation schemes in Sudan with little success**.** Figure 18.4 shows the average quantities of silt removed from the canals of the New Halfa project during the years 2002–2010; the silt in these canals was delivered by the Atbara River.

18.1.3.5 Khashm El-Girba Dam (KEGD)

In this study, the focus was on sediment management practices in Sudan with special emphasis on sediment management in KEGD.

18.2 Sediment Management in KEGD

18.2.1 Background

Khashm el-Girba Dam (KEGD) was constructed in 1964 across the Atbara River to reserve water for resettlement of the displaced from Wadi Halfa area (North of Sudan) due to the construction of the Aswan High Dam (South of Egypt). The main purposes of KEGD are irrigation, hydropower generation and domestic water supply.

The Atbara River is a tributary of the Nile River that emerges from Ethiopia (Fig. 18.5). The watershed area of the river is 112,000 km^2, the average annual discharge is 12×10^9 m^3 (14% of the average annual flow of the Nile), and the reservoir length is 80 km. The Atbara River is characterized by its potential to carry torrential inflows with significant amounts of silt estimated at 85 Mt. annually (Odeyer 2007; Garzanti et al. 2006). Silt-laden water affects not only KEGD reservoir but also the irrigation networks in the New Halfa Agricultural Scheme.

During dry spells within the rainy seasons, the main source of water supply for irrigation is sediment-laden water, which exposes the irrigation networks to sediment deposition. Some of the consequences of deposited sediment are decreases in irrigation efficiency, increases in maintenance costs, and subsequent decreases in farmer incomes, which lead to socioeconomic problems.

A few years after its construction, KEGD lost a considerable amount of its reservoir capacity. The initial reservoir capacity of KEGD decreased from 1.32×10^9 to 0.62×10^9 m^3 (MoWRI 2009). The annual rate of siltation is estimated to be 0.9%. Due to siltation and the formation of deltas, the reservoir has shrunk in surface area and storage capacity. Figure 18.6 shows how the reservoir capacity depleted overtime during the period from 1964 to 2014. As shown in the figure, the loss rate was very rapid during the early period of operation (1964–1971). After adopting a certain sediment management strategy (sluicing + flushing), which started in 1971 and then stopped and continued in 1974, the rate of sedimentation decreased, and the lifetime of the reservoir was preserved.

One of the techniques used in KEGD to manage sediment was the construction of the Dam Complex of Upper Atbara (DCUA). The DCUA was proposed after the construction of KEGD in 1964 to supplement the content deficit in the KEGD reservoir; it was completed and in operation in 2015. The construction of new dams in the upper catchment area in Ethiopia (e.g., Tekeze) will further reduce the sedimentation problem in the Atbara River.

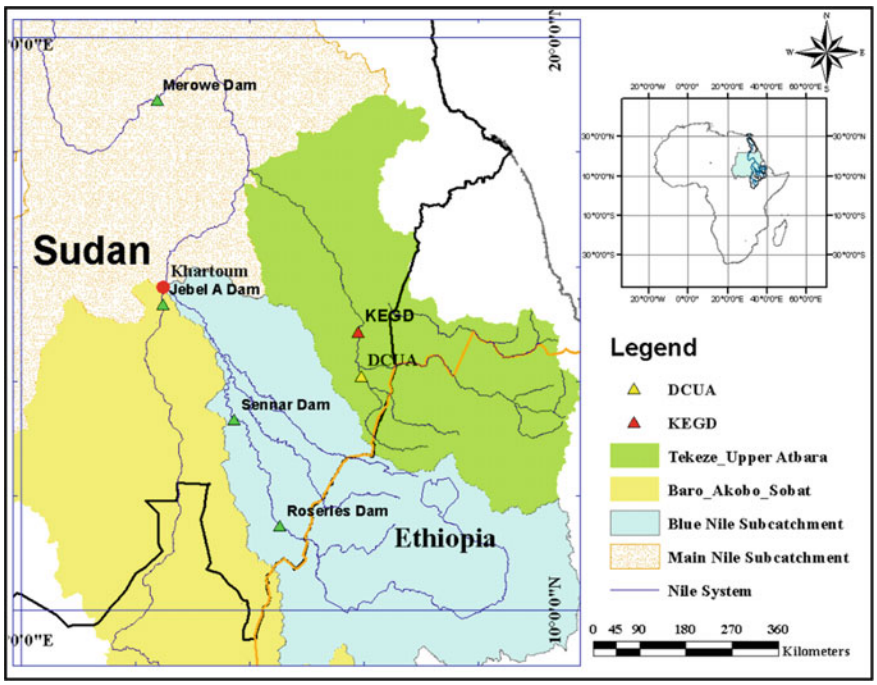

Fig. 18.5 Map of the location of KEGD on Atbara River

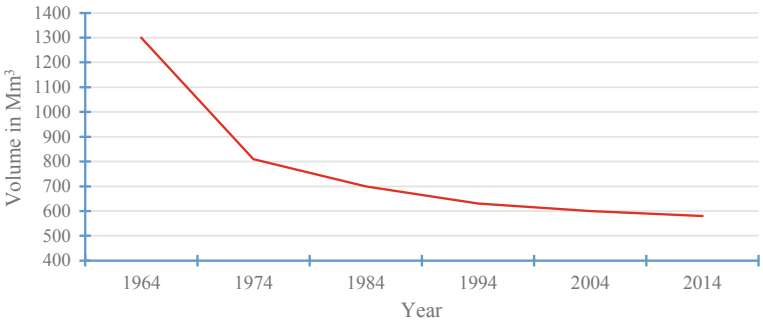

Fig. 18.6 KEGD reservoir storage depletion over time

18.2.2 Sediment Yield and Measurement

Sediment measurements are essential for monitoring the total sediment loads, and having long records of sediment data is very important. Water discharge and sediment concentration must be simultaneously measured over relatively long periods of time. Direct measurements of sediment are considered the most reliable method

for determining sediment yield; these measurements are accomplished by either bathymetric surveys of reservoirs or sampling sediment discharges. Empirical relationships, empirically checked procedures, and trap efficiency can also be used for sediment estimations.

The measurement of suspended sediment in KEGD is practiced during the flood period. Normally, three samples per day are taken, but during a flushing operation (FO), more samples were taken (every three hours). The in situ samples were analyzed by the percentage volume of sediment, while parts of the same samples were sent to a laboratory for weight analysis (gram per liter, g/l or part per million (ppm)).

18.2.3 Trap Efficiency (TE)

When sediment-laden water approaches a reservoir, the velocity of the flow decreases, causing a decrease in the sediment transport capacity of the water. Part of the sediment load passes through the gates and flows downstream, and a considerable amount of sediment is deposited in the reservoir. Trap efficiency (TE) is a measure that expresses how much of the inflowing sediment may be trapped and deposited in a given reservoir.

TE is the ratio of the deposited sediments to the total inflowing sediments over a given period within the economic life of a reservoir (Hadley and Walling 1984). TE depends on several factors, such as particle size, sediment load, and flow characteristics (Ji 2006). From the available literature, two empirical methods can be used to estimate the TE of a reservoir: the Brune curve (1953) and Churchill curve (1948) (Annandale et al. 2016). The Brune curve relates TE to the average annual residence time in the reservoir, and the relative size of the reservoir is determined by dividing the storage volume by the mean annual flow volume entering the reservoir. This ratio is known as the capacity/inflow ratio (Annandale et al. 2016). Brune curves are not applicable for reservoirs with scouring sediment; however, the TE of KEGD can be computed for the period when the sluicing method is applicable (the period from 1964 to 1974, during which there was no flushing operation).

According to the operation rules applied to KEGD, there are three categories of operation: the low-level flood period, filling period, and abstraction or drawdown period. During the low-level period, the reservoir is operated at its lowest level with its deep sluice gates opened to pass floodwaters, and insignificant sediment deposition occurs in the main channel of the reservoir (sluicing period; low TE). During the filling period, a significant amount of sediment is deposited in the reservoir bottom and on its banks, and the TE percentage is expected to have a significant value. The third period has no contribution to sediment deposition due to insignificant inflows and clear water. TE requires an accurate measurement of the sediment that is transported into a reservoir as well as the sediment that is discharged through spillways (Annandale et al. 2016; Atkinson 1996).

18.2.4 Operation Policy of KEGD Reservoir

The operation of the KEGD reservoir is divided into four periods: the first filling, the period between the first and second filling, the second filling, and the abstraction period.

18.2.4.1 The First Filling

In the first filling, the minimum operational level at the beginning of the dam operation on June 30 is 462.00 m. The first filling may begin on July 1 or later if the mean flow of the river has risen above 15 Mm^3/day to raise the reservoir level to 462.00. However, if the level of the reservoir is above 462.00 m at the end of June, water is released so that the level of 462.00 m can be reached and maintained by 10 to 15 July.

18.2.4.2 Period Between the First and the Second Filling (Flood Period)

This period extends from the beginning of July to the end of August, and most sediment-laden water is discharged during this period. This type of operation is known as the sediment sluicing period. Flushing operations are normally conducted during this period, in which the river is allowed to erode itself by leaving the dam gates fully opened. Figure 18.7 explains how the operation rules are implemented as well as the flushing operation and sediment concentration during the flushing operation.

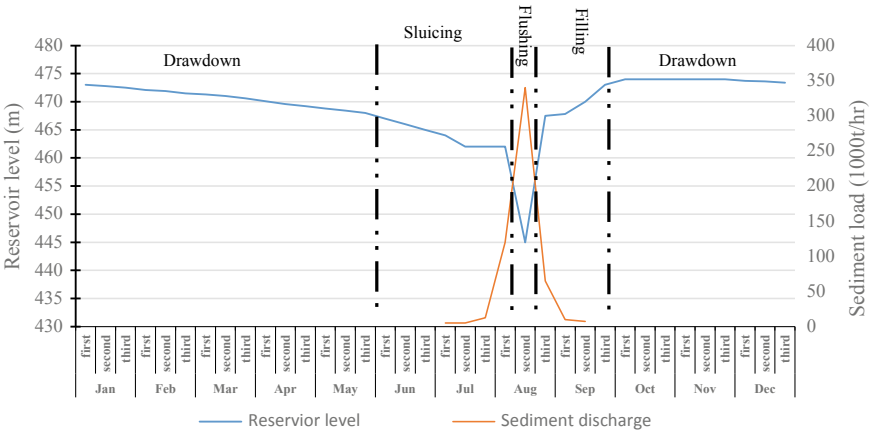

Fig. 18.7 Operation policy of KEGD

18.2.4.3 Second Filling

The second filling begins (a) on August 25 if the inflow either has not risen above 100 Mm^3/day or has previously reached above that rate and fallen, (b) on a date later than August 25 after the inflow has fallen below 100 Mm^3/day. However, for the high flood season, the second filling should start on a date no later than the 6^{th} of September. The second filling takes 45 days to reach the maximum operating pool level at 473.00 a.m.s.l.; this maximum level was raised to 474.00 in 1989 due to sediment deposition. During this period, the water contains some suspended sediment that is deposited in the reservoir bottom and lateral shelves.

18.2.4.4 Abstraction period

After filling the reservoir to a full level of 474.00 m, the inflow exceeds the downstream requirements. The excess surplus is discharged downstream of the dam through deep sluice gates until the inflow equals the requirements. Then, the gates are closed, and the electrical power machines are stopped because irrigation water has the first priority. Abstraction from reservoir storage starts after the inflow water becomes less than the downstream requirements.

All the downstream stakeholders gather in the dam headquarters to decide the abstraction policy based on their needs. The water allocation is confirmed in this meeting. The different stakeholders include representatives of the domestic water supply, crop requirements, sugarcane requirements, freehold, forestry, and downstream requirements.

18.2.5 Sediment Flushing

Sediment flushing describes the process of clearing existing accumulated sediment using the hydraulic method in a reservoir. Sediment flushing is not effective unless the river is left to flow naturally; i.e., if the reservoir is drawn down to a level at which the flow conditions over the deposits reach those of the original river; in such a case, effective erosion over the delta starts from both ends.

18.2.6 Sluicing of Sediments

Sluicing sediment-laden water and storing clean water have been practiced since the beginning of KEGD operations. Sluicing or partial drawdown describes the lowering of water levels in a reservoir for a few weeks or months during the flood season. The principal purpose of sluicing is to pass the high sediment flows carried by flood flows through the lower gates.

18.3 Flushing Operation (FO)

Flushing represents a necessary regular annual activity for keeping silt deposits clear from the water intakes and for preserving reservoir storage (SOGREAH 1971). Flushing operations have been applied successfully in many reservoirs worldwide and have been found to be inexpensive in many cases (Garzanti et al. 2006).

Kantoush et al. (2010) considered flushing to be the only economical approach to swiftly restore the storage capacity of reservoirs with severe deposition. Worldwide experience confirms that low-level outlets that have sufficient capacities to increase drawdown and add more control to water levels during flushing operations will lead to effective flushing (White 2006).

The World Commission on Dams (2006) decided to study the guideline considerations for efficient flushing operations, which include the hydraulic conditions, quantity of water available for flushing, mobility of reservoir sediments, storage capacity of the reservoir, sediment deposition potential, shape of the reservoir basin, operational limitations, downstream impacts, and site-specific factors.

Flushing was introduced for the first time in KEGD for a single year in 1971. Then, FO stopped, but continued in 1974 when the coupling of sluicing and flushing significantly reduced the rate of deposition (Bathymetric Survey of KEG Dam 1990). Twenty million tons of sediment can be removed in one FO in KEGD; i.e., approximately 40 million tons could be removed if FO were carried out twice in the same flood season (Jonson and Phelipon 1974). Figure 18.8 shows the development of the bed level of the reservoir and the accumulation of sediment during the period from 1962 to 2009 in KEGD.

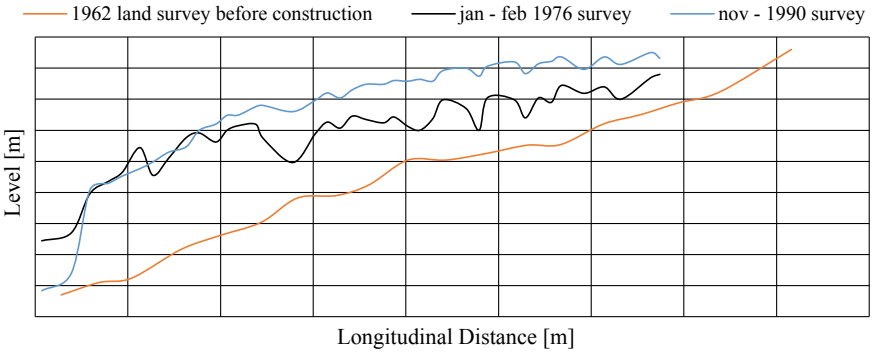

Fig. 18.8 Longitudinal profiles for three different bathymetric surveys. *Source* Reprinted from Mohamed (2013) copyrights 2013

18.3.1 Impacts of Flushing Operations

Although flushing operations are considered the most effective method for managing sediment accumulation in reservoirs, FO might have negative impacts on dams and the environments further downstream. The following section describes some of the negative impacts of FO.

18.3.1.1 Deep Sluice Abrasion

Large quantities of sediment particles that pass through the deep sluice gates during FO cause abrasion to the sill beams and concrete (Fig. 18.9). The only precaution that can be taken to limit this wear is to keep the reservoir level low to limit the flow velocity (Johnson and Phelipon 1974). Abrasion might increase leakage through deep sluices, which is a serious problem affecting preserved stored water. Leakage might cause deformation problems in the dam structure itself.

18.3.1.2 Driftwood

If floods are above average, wood is forced to spill by raising the reservoir level or is forced to pass through deep sluices when floods are below average. However, driftwood accumulates at pump-turbine intakes and compensation gates. This driftwood is sometimes carried by running water back from canals through pumps with the aid of backwaters from compensation gates. Figure 18.10a, b shows pump turbine-intakes blocked by driftwood and silt during 2005.

Figure 18.11 shows the accumulation of sediment downstream of a dam due to insufficient flushing discharge, which seriously affects the downstream environment and ecosystem.

Fig. 18.9 Abrasion to a sill beam and concrete

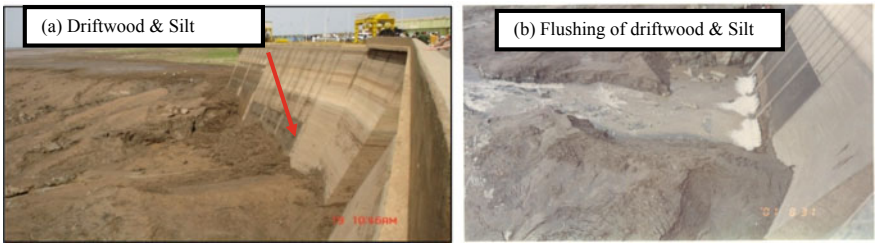

Fig. 18.10 **a** Pump-turbine intakes blocked by driftwood and silt, and **b** flushing of driftwood and silt by backwater (2005)

Fig. 18.11 Accumulation of silt downstream due to insufficient discharge in flush operations

18.4 Bathymetric Survey

The main purpose of conducting bathymetric surveys of a reservoir is to determine the storage capacity, loss of storage volume, and distribution of deposited sediment within the reservoir and to provide data on sediment accumulation by comparison to an earlier survey (usually the original survey).

Bathymetry is the process through which the bed level of a reservoir is mapped. To map a reservoir bed, the topography of a given area is surveyed before a reservoir is filled. Once the reservoir is filled, bathymetric surveys are used to monitor possible changes at the bottom surface. These surveys are useful from time to time because, over time, sediment builds up in reservoirs, and these surveys can help determine the amount of sediment that has been deposited. Different survey methods have been conducted to map the KEGD reservoir. Figure 18.12 shows the results of bathymetric surveys conducted in KEGD, and how the storage drastically changed before the flushing operations were adapted in 1974. From the figure, during the period from 1964 to 1974, a rapid reduction in reservoir capacity occurred. When the flushing operation was introduced in 1974, the sediment accumulation decreased noticeably. After 1990, the reservoir almost reached a state of equilibrium.

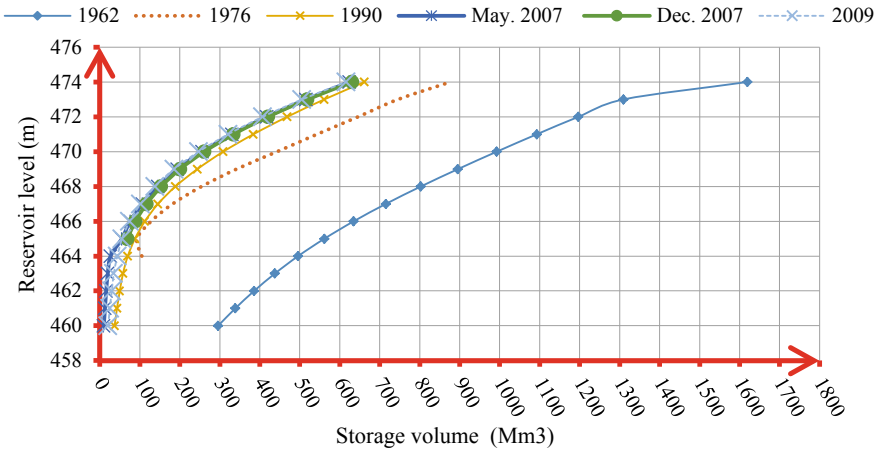

Fig. 18.12 Change in reservoir bed level of KEGD during the period from 1964 to 2009. *Source* Reprinted from Mohamed (2013) copyrights 2013

18.5 Conclusion

The deposition of silt is a serious problem affecting the storage capacities and lifespans of reservoirs. This study was carried out to discuss the sediment management practices in Sudan, with special reference to Khashm el-Girba Dam (KEGD), and the effects of storage management practices on maintaining the lifetime of the reservoir. During the 1990–2009 period, the average annual sediment inflow to the Atbara River was 86 Mt. Nearly 40% of the storage capacity of KEGD has already been filled with sediment soon after dam construction. The coupling of sluicing and flushing in 1974 significantly reduced sediment deposition in the reservoir. The sediment management strategy that followed in KEGD increased the lifetime of the reservoir. Building Tekeze Dam in Ethiopia in 2009 and the Dam Complex of Upper Atbara (DCUA) in Sudan in 2015 further helped regulate Atbara River flows and control the amount of sediment discharged to KEGD.

References

Ahmed AA (2008) Sediment in the Nile River system. Report to UNESCO IHP. International Sediment Initiative. Khartoum Sudan

Annandale W, Gregory LM and Karki P (2016) Extending the life of reservoirs sustainable sediment management for dams and run-of-river hydropower. World Bank Group Report

Atkinson E (1996) TDR project R5839. The feasibility of flushing sediment from reservoirs. HR Wallingford Ltd., Wallingford, pp 1–14

ElMonshid BEF, ElAwad OMA, Ahmed SE (1997) Environmental effect of the Blue Nile Sediment on reservoirs and Irrigation Canals. In: Int. 5th Nile 2002 conf., Addis Ababa, Ethiopia (cross reference)

Garzanti E, Andò S, Vezzoli G, Abdel Megid AA, El Kammar A (2006) Petrology of Nile River sands (Ethiopia and Sudan): sediment budgets and erosion patterns'. Earth Planet Sci Lett 252 (3–4). Available from: http://www.science direct.com/science/journal

Hadley RF, Walling DE (1984) Erosion and sediment yield, some methods of measurement and modeling

Ji U (2006) Numerical model for sediment flushing at the Nakdong River Estuary Barrage. Dissertation submitted for partial fulfillment of the requirements for the Degree of Doctor of Philosophy Colorado State University Fort Collins, Colorado

Johnson G, Phelipon M (1974) R.12251: Khashm El-Girba Dam sediment flushing operation. Sogreah, Grenoble

Kantoush SA, Sumi T, Suzuki T, Murasaki M (2010) The Impacts of sediment flushing on channel evolution and morphological processes: case study of the Kurobe River, Japan: ISBN 978–3–939230–00–7: 1165

Mohamed S (2013) Evaluation of sediment management in Khashm El Girba Dam in Sudan. M. Sc. thesis submitted to the Water Management Institute, University of Gezira, Sudan

MoWRI (2009) Ministry of water resources and irrigation, Sudan. Annual report

Odeyer C (2007) Hydrological report. Dam Complex of Upper Atbara Project. Grenoble Sogreah: 62–64

Osman IS (2018) Sedimentation and mitigation measures in Sudan. International Training Workshop on Integrated Sediment Management in River Basin November 5–10, 2018 Beijing, China

Raghunath HM (2006) Hydrology principal analysis and design New Delhi: new age international publishers: 178–315

SOGREAH (1971) A study of silting and silt control measures for the Khashm El Girba Reservoir, Grenoble: Sogreah: 3–16

Strand RI, Pemberton EL (1982) Reservoir sedimentation: technical Guideline for Bureau of Reclamation.U.S. Bureau of Reclamation Colorado, 2–4

White WR (2006) Flushing of sediment from reservoirs, contributing paper prepared for thematic review IV.5: Operating, Monitoring and Decommissioning of Dams. http://www.dams.org/

World Bank Document (2000) Options for sustainable development of the Gezira scheme, Sudan (cross reference)

World Commission on Dams (2006).

Yang X (2003) World Meteorological Organization, Operational Hydrology Report No. 47: Manual on Sediment Management and Measurement: Geneva

Chapter 19
Determining the Precipitation Intensity Threshold of Debris Flood Occurrence

Mohammad Ebrahim Banihabib and Mitra Tanhapour

Abstract In this chapter, the precipitation threshold at which debris floods occur was evaluated experimentally, and the factors that influence debris flood occurrence, including the bed slope, sediment layer thickness, sediment grain size, length of alluvial flow direction, precipitation intensity, and time of debris flood occurrence, were examined. The impacts of these factors on debris flood initiation were investigated through dimensional analysis. Then, a method was developed to estimate the precipitation intensity threshold based on a set of laboratory tests. Furthermore, different methods for determining the precipitation intensity threshold at which debris floods are initiated were assessed and discussed. The results of the experiments showed that the effect of the sediment layer thickness on debris flood occurrence can be ignored. Moreover, by independently evaluating the effect of each factor on debris flood occurrence, it was found that the sediment length and average diameter of sediments are influential to debris flood initiation. The results of this research provide a better understanding of debris flood mechanisms and occurrence thresholds of debris floods and can be employed to prepare a forecasting model.

Keywords Debris floods · Dimensional analysis · Precipitation intensity thresholds · Sediment layer thickness

M. E. Banihabib (✉)
Department of Water Engineering, University of Tehran, Abouraihan Campus, Tehran, Iran
e-mail: banihabib@ut.ac.ir

M. Tanhapour
Hydraulic Structure, University of Tehran, Abouraihan Campus, Tehran, Iran
e-mail: mitratanhapour@ut.ac.ir

T. Sumi et al. (eds.), *Wadi Flash Floods*, Natural Disaster Science and Mitigation Engineering: DPRI Reports, https://doi.org/10.1007/978-981-16-2904-4_19

19.1 Introduction

Heavy precipitation events lead to flash floods in mountainous areas. Flash floods generally move quickly in rivers due to intensive precipitation in river basins and can trigger landslides suddenly due to heavy rainfall in small basins (He et al. 2018a, b). Intensive rainfall can usually produce flash floods and debris floods. The type of event (debris flood or flash flood) depends on different factors, e.g., the hydrological, geotechnical, and geomorphological characteristics of steep slopes, material sources, the volume of available sediments, and characteristics related to the frequency and magnitude of precipitation events (Borga et al. 2014).

Debris floods are common phenomena in many areas worldwide (Mangeney et al. 2010; Banihabib and Nazarieh 2019; He et al. 2018a, b). Debris floods are the main factor affecting erosion and sedimentation in riverbeds or channels and create many environmental hazards (Berger et al. 2011). These flows generally consist of granular materials and concentrated compositions of water and sediments (Banihabib and Forghani 2017; Banihabib and Masumi 1999). The sediment concentrations of debris floods vary in different circumstances, from loose deposits to flows. There is a wide range of debris flood sediment concentrations, which are reported to range from 2 percent by volume to 80–90% (Banihabib et al. 2020; Takahashi 1981; Coussot and Meunier 1996). For typical events, the water content is small, approximately 10–30%. Furthermore, the range of the particle diameters is approximately 10^{-6} to 10 m (Zhuang et al. 2015). These debris flood features make them potentially powerful and disastrous factors due to their abilities to transport large volumes of coarse-grained materials and destroy facilities, infrastructures, and the environment (Hassan-Esfahani and Banihabib 2016; Iverson and Denlinger 2001). The hazards caused by debris floods are enhanced by their sudden occurrences. Therefore, understanding the processes of debris flood occurrences is necessary not only to obtain insights into the mechanisms of debris flood occurrences but also to predict and avoid hazards (Shu et al 2017; Banihabib and Tanhapour 2020). Due to the complexity of the mechanism of these floods and their high speeds, laboratory methods are appropriate tools for studying debris flood initiation processes (Cogan and Gratchev 2019).

Flash floods and debris floods are among the most destructive natural disasters with the highest risk potentials in the world due to their rapid occurrences, very short time intervals from the moments of precipitation initiation to flood generation, and the spatial distributions of their affected areas (Borga et al. 2014; Kotlyakov et al. 2013; Diakakis and Deligiannakis 2017; Ashley and Ashley 2008). According to Barredo's assessments, flash floods caused 49 fatalities per year in Europe on average during the years from 1950 to 2005 (Barredo 2007). Salvati et al. (2010) reported that more than 2204 landslides and debris floods occurred due to precipitation over a period of 59 years (1950–2008) in Italy and caused 4103 fatalities. Furthermore, studies have illustrated that predicting and warning people about flash floods and debris floods are difficult because of the sophisticated processes of their formations, the uncertainty associated with intense and short-term precipitation

events and the dependency of these types of floods on various physiographic and hydrological factors of river basins (Sun et al. 2012; Diakakis et al. 2020). Therefore, it is indispensable to provide a simple and practical approach for predicting debris floods to detract from the risks and damages caused by them.

Although debris floods often occur due to key factors such as heavy precipitation, abundant sediment, and steep slopes (Jomelli et al. 2015; Banihabib et al. 2020), they can also begin due to landslides, snowmelt, and failure of temporary dams blocking rivers (Procter 2012; Evans et al. 2001). Most previous studies primarily evaluated the influences of one or more specific factors, e.g., bed slope, particle size distribution, and precipitation intensity on debris flood initiation. Hu et al. (2014) used laboratory flumes to study the effects of discharge and slope on the mechanism of debris flood initiation. They found that the effects of slope on erosion and the volume of flow deposits were greater than the effects of flow discharge (Hu et al. 2014). Pellegrino and Schippa (2018) investigated the impacts of particle concentrations and coarse materials on the triggering of debris floods. Based on experimental evidence, they revealed that the viscous features that comprise the stresses and the volumetric viscidity are affected by coarse materials. Moreover, the flow features are sensitive to variations in solid content and particle size (Pellegrino and Schippa 2018). An empirical equation was proposed by Takahashi (1977). He performed a set of experiments to investigate debris flow occurrence under different discharge flow and bed slope values. According to his proposed equation, the concentration of solid materials was obtained based on the bed slope (Takahashi 1977). Dong et al. (2009) presented an equation to obtain the average volume of sediments in debris flows by collecting data on debris floods that occurred due to the Toraji typhoon (Dong et al. 2009). In another study, Takahashi and Kuang (1986) presented equations for the deposition rate and erosion rate of debris floods. Egashira (1993) evaluated the mechanism of debris floods over an erodible bed and proposed a formula for the bed erosion rate.

Most previous studies did not investigate the influence of altering the sediment layer thicknesses on debris flood occurrence. In the present study, a set of laboratory tests were performed at different sediment thicknesses and bed slopes to estimate the precipitation intensity threshold that triggers debris floods. A key piece of information associated with debris flood warning systems is that all precipitation events cannot produce debris floods. Therefore, it is crucial to determine the precipitation intensity threshold that triggers debris floods. In these laboratory tests, the precipitation intensity and the timing of the debris flood occurrence were measured. Then, using dimensional analysis, empirical equations between precipitation intensity (as the dependent variable) and each dimensionless variable, including bed slope, sediment layer thickness, average grain size, and sediment sample length (as the independent variables), were obtained separately. In addition, different methods for deriving the precipitation intensity threshold of debris floods were discussed in this chapter. Finally, the proposed equation obtained in the present research was compared with the equations obtained in other studies.

19.2 Material and Methods

19.2.1 Experimental Facilities

A laboratory flume was used for the tests. Its length, width, and depth were 7.6, 0.3, and 0.25 m, respectively. The laboratory tests were performed in a Plexiglas tilting flume. A gauge was utilized to obtain the slope of the flume, and the gauge could be installed anywhere in the flume. In addition, we applied a rain simulator to produce precipitation over the loose deposit sample. A Casio EX-F1 video camera was used to record the timing of the debris flood occurrences.

19.2.2 A Theory for Initiating Debris Floods

Hirano (1997) demonstrated that the critical conditions for debris flood occurrence may be incurred at the thickness of the sediment layer (D) if the shear stress is greater than the shear strength (Fig. 19.1). He noted that debris floods occur if the cumulative precipitation at the concentration time (T) is more than the specified amount (Eq. (19.1)):

$$R(t,T) = \int_{t-T}^{t} r(t)\mathrm{d}(t) \geq \frac{DK}{L}\tan\theta = R_c \tag{19.1}$$

where L is the alluvial length, θ is the bed slope, R_c is the precipitation threshold of debris flood initiation, D is the depth of loose materials, K is the hydraulic conductivity, t is the time, and $r(t)$ is the precipitation intensity.

To determine the precipitation threshold of debris flood initiation in Eq. (19.1), K and D must be measured; however, the determination of these factors is difficult under field conditions, and they cannot be determined precisely. Therefore, we tested other available factors to obtain the precipitation threshold of debris flood initiation.

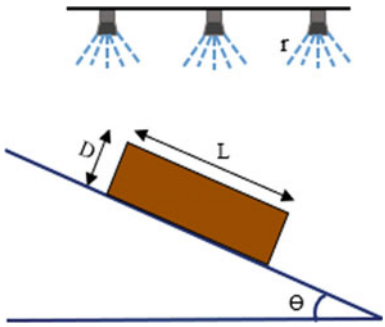

Fig. 19.1 Schematic plan of a slope bed

19.2.3 A Set of Influential Factors

Hydrological, climatic, and topographic factors are the most important factors that are effective in triggering debris floods (Liang et al. 2012; Chang et al. 2010). Generally, physiographic parameters (e.g., loose material, river length, and steep slopes) and hydrological factors (e.g., antecedent soil moisture, and heavy precipitation) influence debris flood initiation (Banihabib and Tanhapour 2019). The influencing factors and their relevant abbreviations and units are shown in Table 19.1. The grain mean diameter was estimated to be 0.7 mm using the sediment aggregate curve. The sediment length was 25 cm (equal to the length of the rain simulator). The layer thickness of the particles ranged from 1 to 3.5 cm. The bed slope was variable between 36° and 58° during the tests.

In the current study, the Buckingham theorem was applied to extract the dimensionless factors and to analyze the factors that influenced the occurrence of debris floods. Based on Hirano's research results, the set of factors used in this study was as follows (Eq. (19.2)):

$$F(I, t, d_{50}, \tan\theta, L, D, g) = 0 \tag{19.2}$$

Based on the Buckingham theorem, with N factors and M main dimensions, we can extract $N - M$ dimensionless factors. If we show dimensionless factors as Π_1, Π_2, etc., Eq. (19.2) can be rewritten as Eq. (19.3):

$$F(\Pi_1, \Pi_2, \Pi_3, ..., \Pi_{N-M}) = 0 \tag{19.3}$$

Length and time are the main dimensions of the factors used in this study. Furthermore, the number of repetitive variables must be equal to the number of main dimensions. Moreover, the timing of debris flood occurrences and gravitational acceleration were considered to be repetitive variables. Based on the mentioned explanations, a total of five dimensionless factors were obtained, which are presented in Eqs. (19.4)–(19.8) as follows:

Table 19.1 Factors that influence the occurrence of debris floods

Factor	Abbreviation	Unit
Precipitation intensity	I	Meter per second
Time	t	Second
Grain mean diameter	d_{50}	Meter
Bed slope	$\tan\theta$	Radian
Sediment layer length	L	Meter
Sediment layer thickness	D	Meter
Gravitational acceleration	g	Meter per second squared

$$\Pi_1 = \tan\theta \tag{19.4}$$

$$\Pi_2 = \frac{\sqrt{g}\,t}{\sqrt{d_{50}}} \tag{19.5}$$

$$\Pi_3 = \frac{\sqrt{g}\,t}{\sqrt{D}} \tag{19.6}$$

$$\Pi_4 = \frac{\sqrt{g}\,t}{\sqrt{L}} \tag{19.7}$$

$$\Pi_5 = \frac{I}{g\,t} \tag{19.8}$$

Thus, the threshold of precipitation intensity at which debris floods are triggered was obtained by other nondimensional variables using regression analyses based on Eq. (19.9):

$$\frac{I}{gt} = F\left(\tan\theta, \frac{\sqrt{g}\,t}{\sqrt{d_{50}}}, \frac{\sqrt{g}\,t}{\sqrt{D}}, \frac{\sqrt{g}\,t}{\sqrt{L}}\right) \tag{19.9}$$

19.2.4 Experiment Procedures

The average size of the sediments used in the laboratory tests was determined using the sieving method, and a sediment gradation curve was obtained (Fig. 19.2). According to Fig. 19.2, more than 90 percent of the sediments consisted of sand, and a small percentage of sediments were fine grains or coarse grains, such as clay and gravel. Thus, based on the ASHTO classification system (Zidan et al. 2019), the sediments were sandy-type with a mean grain size equal to 0.7 mm. The laboratory test steps used to determine the precipitation intensity thresholds at which debris floods were initiation in the different sediment layer thicknesses and bed slopes were as follows.

I. The sediment weight was determined with the scale.
II. To consider the influence of moisture due to antecedent precipitation, a constant moisture content (5% of the dry weight of the sediments) was added to the sediments.
III. The flume slope and camera were set.
IV. The rain simulator and its bases were prepared and placed on the flume. Then, the rain simulator reservoir was filled with water. Finally, the precipitation intensity was adjusted by calipers.
V. The instability of the slope of the particles was determined, and the sediment sample was transferred into the flume/channel.

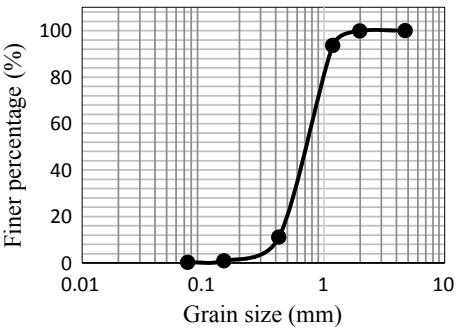

Fig. 19.2 Sediment gradation curve

VI. The rain simulator was laid on its base, and raindrops were poured/fell over the sediments. Then, the time to the failure/collapse of the sediment sample was recorded using a camera.

For each sediment layer thickness, the laboratory tests were repeated a minimum of 7 times. In total, laboratory tests were carried out 57 times for diverse particle layer thicknesses and different bed slopes. This research examined debris floods that occurred on bedrock. For this reason, these experiments were performed using thin sediment layers (Banihabib and Tanhapour 2020).

19.3 Results and Discussion

Debris floods occur due to a set of climatic, topographic, and geological factors, and debris floods have complex relationships with the factors that affect them. Therefore, it is necessary to understand the conditions under which these floods occur and to determine the relations between debris floods and other related factors. Steep slopes, large volumes of loose deposits, and intense precipitation are essential for producing debris floods (Zhuang et al. 2015). To address the effects of these main criteria on debris flood initiation, a series of effective variables, including slope, depth of loose material, mean grain size, length of alluvial material in the flow direction, timing of the debris flood, and precipitation intensity at debris flood initiation, were selected. In this section, first, the influence of each dimensionless factor on the threshold of the precipitation intensity that triggers debris floods was investigated separately. Then, different methods for determining the precipitation intensity threshold of debris floods were examined.

19.3.1 Assessment of the Impacts of Dimensionless Variables on the Precipitation Intensity Threshold

In this section, the impacts of dimensionless variables on debris flood occurrence were examined as a simple regression model. Figure 19.3 illustrates the simple nonlinear regression equation between Π_5 (the dimensionless precipitation intensity) and Π_2 (the dimensionless sediment mean diameter), and their good correlation was observed between them. Based on the observed results of the laboratory tests, a large volume of the soil texture was made up of fine sand particles. These particles are easily eroded by various precipitation intensities due to their negligible cohesion and relatively low weights, while the erosion rates of the coarse-grained particles and the clay materials are lower. This result is consistent with the results of other research (Vaezi and Ebadi 2016; Williams et al. 1997; Papa et al. 2004). Therefore, loose materials and fine sand particles provide suitable conditions for debris flood initiation, and there is a good relation between the precipitation intensity and this dimensionless factor.

Figure 19.4 demonstrates the nonlinear equation between the dimensionless precipitation intensity (Π_5) and the dimensionless sediment layer thickness (Π_3). Based on this figure, it is obvious that there is a fair correlation between these two factors. Generally, the precipitation intensity threshold increases with enhanced sediment layer thickness on a certain slope, which is mostly in agreement with the results of this research. For example, for thin sediment layers (between 1 and 2 cm), the minimum precipitation intensity for debris flood initiation is 109 mm/h, while the required precipitation intensity increases to 153 mm/h for thicker sediment layers (more than 2 cm). It can be deduced that the sediment layer thickness alone is not sufficient to estimate the precipitation intensity threshold, and the sediment layer thickness alone cannot accurately estimate the precipitation intensity.

Figure 19.5 indicates the relationship between the dimensionless precipitation intensity (Π_5) and the dimensionless factor Π_4. According to Fig. 19.5, there is

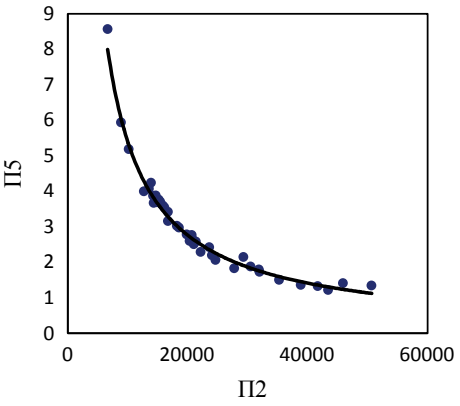

Fig. 19.3 Relation between Π_5 (the dimensionless precipitation intensity) and Π_2 (the dimensionless sediment mean diameter)

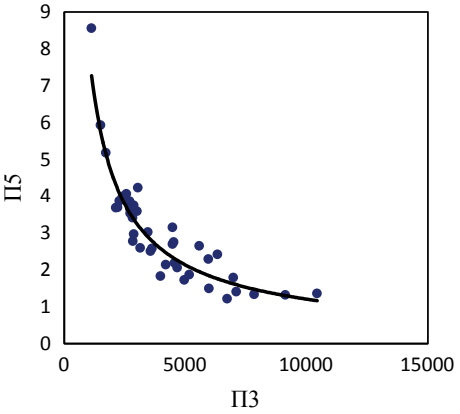

Fig. 19.4 Relation between the dimensionless precipitation intensity (Π_5) and the dimensionless sediment layer thickness (Π_3)

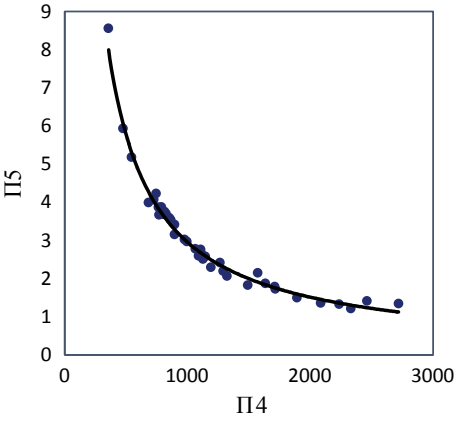

Fig. 19.5 Relation between the dimensionless precipitation intensity (Π_5) and Π_4

good consistency between the observed and estimated results, and the correlation between them is high. The value of the determination coefficient is 0.979. Therefore, it can be inferred that there is a significant relation between the precipitation intensity threshold and sediment layer length.

Figure 19.6 shows the relation between the dimensionless precipitation intensity (Π_5) and bed slope (Π_1). The relation between these two factors is not significant. The results of this research revealed that precipitation intensity and bed slope are the main factors responsible for initiating debris floods, but the role of precipitation intensity on sediment layer failure is greater than the role of the bed slope. When the precipitation intensity increases, more runoff is produced, which leads to the destruction of the sediment layer and the initiation of debris floods. Therefore, by evaluating the relation between the roles of precipitation intensity and bed slope on debris flood initiation, it was found that precipitation intensity is more effective on the occurrence of debris floods than the bed slope is.

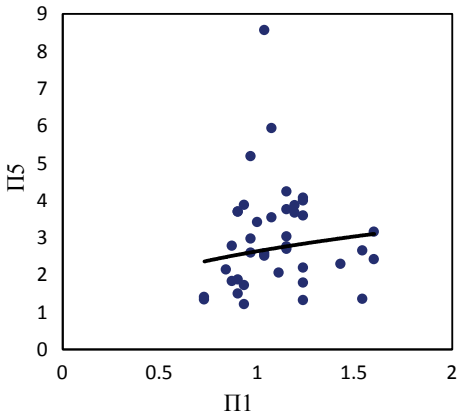

Fig. 19.6 Relation between the dimensionless precipitation intensity (Π_5) and bed slope (Π_1)

19.3.2 Proposed Equation of This Study

The derived equations in the previous section are shown in Table 19.2. More accurate results can be obtained based on the dimensionless sediment layer length and dimensionless sediment mean diameter (Eqs. (19.10) and (19.12)).

Since measuring the sediment mean diameter is easier than measuring the sediment layer length in practical uses, the relationship between Π_5 (the dimensionless precipitation intensity) and Π_2 (the dimensionless sediment mean diameter), represented by Eq. (19.10), is introduced as the proposed equation in this research. After rewriting, the equation is as follows:

$$I = 39482\, g^{0.517}\, t^{0.034}\, d_{50}^{0.483} \tag{19.14}$$

where I is the precipitation intensity (m/s) and the other variables are introduced in Table 19.1. The unit of the precipitation intensity is m/s in Eq. (19.10). Because the precipitation intensity is often expressed in millimeters/hour, its unit was changed to mm/h in Eq. (19.15). Therefore, Eq. (19.10) was rewritten as Eq. (19.15):

$$I = 1421.3\, g^{0.517}\, t^{0.034}\, d_{50}^{0.483} \tag{19.15}$$

Table 19.2 Equations relating the dimensionless precipitation intensity and other dimensionless factors

Number	Equation	R^2	MARE
19.10	$\frac{I}{gt} = 39482 \left(\frac{\sqrt{g}\, t}{\sqrt{d_{50}}}\right)^{-0.966}$	0.98	0.047
19.11	$\frac{I}{gt} = 2387.5 \left(\frac{\sqrt{g}\, t}{\sqrt{D}}\right)^{-0.824}$	0.83	0.163
19.12	$\frac{I}{gt} = 2339.3 \left(\frac{\sqrt{g}\, t}{\sqrt{L}}\right)^{-0.966}$	0.98	0.047
19.13	$\frac{I}{gt} = (\tan\theta)^{0.345}$	0.14	0.5

19.3.3 Different Methods for Determining the Precipitation Intensity Threshold of Debris Floods

Caine (1980) presented an intensity–duration threshold for shallow landslides and debris floods. He collected precipitation intensity–duration data that triggered landslides and debris floods in different areas worldwide. He utilized a series of 73 events to develop a global precipitation intensity–duration threshold equation. His proposed relationship is as follows:

$$I = 14.82\, t^{-0.39} \quad (0.167 \leq t \leq 240) \tag{19.16}$$

where I and t are the precipitation intensity (mm/h) and rainfall duration (h), respectively.

Cogan and Gratchev (2019) proposed an intensity–duration threshold for rainfall-induced landslides using a laboratory study. They carried out a series of 12 experiments to investigate the influences of the precipitation intensity and bed slope on triggering landslides and altered the bed slopes, precipitation intensities, and the amounts of initial moisture in the experiments. Flume experiments were performed for precipitation intensities equal to 40, 70, and 100 mm/h. According to the experiments, the slope angle and the amount of initial moisture were altered in the ranges of 45–55° and 5–12%, respectively. Then, the failure time was recorded in all experiments (Cogan and Gratchev 2019). Finally, the authors developed the intensity–duration threshold based on the observed landslides as follows:

$$I = 80.07\, t^{-0.596} \quad (0.5 \leq t \leq 4) \tag{19.17}$$

where I and t are the same as those introduced in the previous equation.

Zhuang et al. (2015) used 47 debris flood events to determine the intensity–duration threshold in Jiangjia Gully, China. They employed past precipitation events to empirically derive the intensity–duration threshold and historical debris flood events to validate the threshold. They obtained 50, 70, and 90% probability thresholds to forecast debris flood events using the intensity–duration threshold. These probability curves include 50, 70, and 90% of the debris flood event points. These probability thresholds can be employed to forecast debris flood occurrences and to alert the public about possible occurrences. The authors proposed the following thresholds for debris flood occurrence:

$$I = 15.87\, t^{-0.595} \quad (\text{for curve } 50\%) \tag{19.18}$$

$$I = 11.92\, t^{-0.595} \quad (\text{for curve } 70\%) \tag{19.19}$$

$$I = 7.27\, t^{-0.595} \quad (\text{for curve } 90\%) \tag{19.20}$$

Hirano (1997) proposed the system analysis method to obtain the concentration time (T) and critical precipitation (R_c) necessary for debris flood initiation. He determined the cumulative precipitation $R(t, t_0)$ as follows:

$$R(t, t_0) = \int_{t-t_0}^{t} r(\tau) d\tau \tag{19.21}$$

where τ is the shear stress and t is the precipitation duration.

Based on this method, the maximum value of $R(t, t_0)$ for each rainfall duration was plotted versus t_0. According to Fig. 19.7, if there is no error present in the information or data, the lines should cross above point $R_{\max}(T)$ when debris floods occur (Fig. 19.7a) and should cross below point $R_{\max}(T)$ when debris floods do not occur (Fig. 19.7b).

The difference between the upper bound curve of the nonoccurrence plot and the lower bound curve of the occurrence plot is minimal at point $R_{\max}(T)$, which is shown in Fig. 19.8. Consequently, if the cumulative precipitation at the concentration time is greater than the upper bound curve of the nonoccurrence plot, debris floods occur. If the cumulative precipitation at the concentration time does not exceed the lower bound curve of the occurrence plot, debris floods do not occur. The distance between these two curves is a critical area for triggering debris floods (Fig. 19.8) (Hirano 1997).

Tanhapour and Banihabib (2019) investigated the cumulative rainfall thresholds based on Hirano's method (system analysis method) in the northern areas of the Alborz Mountains, Iran, including the Karganrud, Navrud, Neka, and Babolrud basins. They used rainfall data to derive cumulative rainfall thresholds and

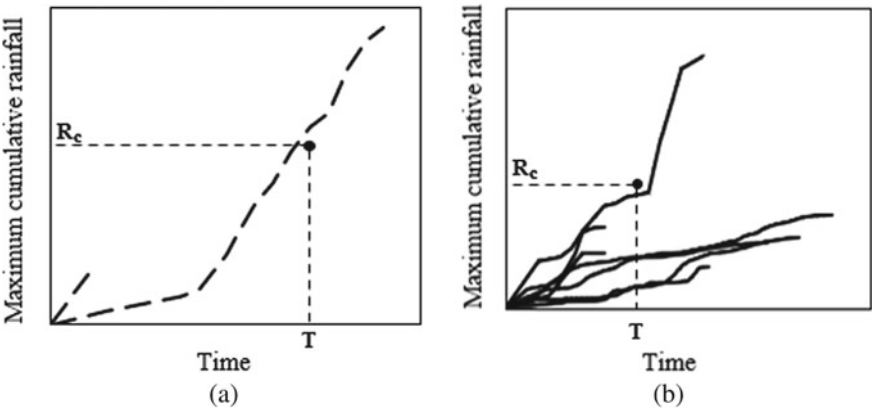

Fig. 19.7 Maximum cumulative precipitation against time for **a** debris flood occurrence and **b** nonoccurrence (Tanhapour and Banihabib 2019)

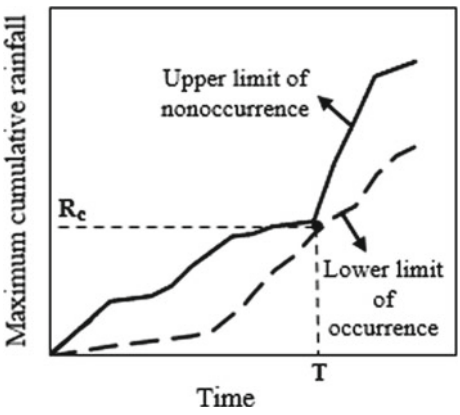

Fig. 19.8 Lower bound of the occurrence curve and the upper bound of the nonoccurrence curve (Tanhapour and Banihabib 2019)

developed a regional intensity–duration threshold for debris flood occurrence (Tanhapour and Banihabib 2019). The threshold curve can be determined using Eq. (19.22):

$$I = 6.14\, t^{-0.536} \quad (0.7 \leq t \leq 15) \tag{19.22}$$

19.3.4 Precipitation Threshold for Flash Floods

In dealing with floods, early warning systems often need an indicator to detect flood events. Precipitation threshold-based methods and assessments of local soil moisture conditions for predicting debris floods and flash floods have long histories. Precipitation thresholds can be used to construct early warning systems for debris floods and flash floods (Bezak et al. 2016). Flash flood predictions depend on various factors, e.g., precipitation, soil moisture, water level, time of occurrence, flood duration, and flood peak time (Ngo et al. 2020). One of the simplest threshold-based approaches for predicting flash floods is to detect extreme weather conditions using weather parameter-based indicators, such as cumulative precipitation. Norbiato et al. (2008) revealed that the inclusion of the effect of initial soil moisture conditions in humid climates is important in assessing the potential of a flash flood occurrence and especially in determining the occurrence and nonoccurrence thresholds. Bezak et al. (2016) proposed intensity–duration–frequency curves and precipitation thresholds for flash floods and landslides.

The usage of simple threshold-based approaches is crucial for several reasons. These thresholds can be applied by flood risk managers in local flood prediction centers. Consequently, communities' preparation levels against floods can be increased. In addition, precipitation threshold-based diagnostic methods and soil moisture indices, which simplify the hydrological status of catchments, provide the possibility of processing local precipitation information and promoting cooperation

between hydrologists and meteorologists (Borga et al. 2014). One of the most important problems associated with this approach (the precipitation threshold approach) is that the false warning ratio is high, which is due to uncertainties in the spatial distributions of rainfall and errors in the precipitation thresholds (Bezak et al. 2016). In this study, a laboratory method was developed to determine the threshold at which debris floods occur, and different approaches used in previous studies were evaluated to determine the rainfall threshold for debris flood occurrences. Depending on the local precipitation characteristics and the physiographic characteristics of the basins, flash floods can lead to debris floods. Generally, determining the precipitation threshold along with a sufficient number of rain gauge stations can be used as part of an early warning system to alert users to the occurrence of flash floods and debris floods.

19.3.5 Comparing the Proposed Equation with the Equations from Previous Studies

In this study, we used 40 debris flood events (70% of all data) to fit the empirical equations and 17 debris flood events (30% of all data) to test the equations. The previous studies' equations describing the precipitation intensity threshold were compared with the equation proposed in this study (Eq. (19.15)) using the laboratory test data displayed in Table 19.3. It was thus found that the MARE coefficients for the equations proposed by Cogan and Gratchev (2019), Tanhapour and Banihabib (2019), Caine (1980), and Zhuang et al. (2015) were 1.86, 0.81, 0.71, and 0.43, respectively, while is the MARE coefficient was equal to 0.047 for the equation proposed in this research. Thus, the equation proposed in this study is better than the equations of previous studies, and the equation proposed here can more accurately estimate the precipitation intensity threshold at which debris floods are generated.

Table 19.3 Precipitation intensity thresholds from other studies with that obtained in this research

Study	Study area	MARE	Equation
Zhuang et al. (2015)	China	0.43	$I = 15.87\, t^{-0.595}$
Caine (1980)	Global	0.71	$I = 14.82\, t^{-0.39}$
Tanhapour and Banihabib (2019)	Northern areas of the Alborz Mountains	0.81	$I = 6.14\, t^{-0.536}$
Cogan and Gratchev (2019)	Based on observed landslides	1.86	$I = 80.07\, t^{-0.596}$
This study	Based on observed debris floods	0.044	$I = 1421.3\, g^{0.517}\, t^{0.034}\, d_{50}^{0.483}$

19.4 Conclusion

In the current study, a laboratory model was employed to determine the precipitation intensity threshold at which debris floods occur using a set of factors, including sediment layer thickness, bed slope, grain mean diameter, length of sediment, precipitation intensity, and time of debris flood occurrence. Furthermore, the equation developed in this study was compared with equations obtained in former studies. To obtain the precipitation threshold at which debris floods are produced, dimensional analysis was applied, and the influences of various dimensionless factors on the precipitation intensity threshold were assessed separately. It was found that dimensionless sediment length and dimensionless sediment mean diameter were the most influential factors on the precipitation intensity threshold, while the influence of the dimensionless sediment layer thickness was the lowest. The results revealed that the equation proposed in this study can be used to estimate the precipitation intensity threshold more accurately than the equations of previous studies. The findings of this study can be used for identifying precipitation intensities that produce debris floods and designing warning systems for debris floods.

References

Ashley ST, Ashley WS (2008) Flood fatalities in the United States. J Appl Meteorol Climatol 47 (3):805–818

Banihabib ME, Masumi A (1999) Effect of high-concentrated sediment transport on inundation of rivers: case study Masuleh Flood. Chapter presented at the 2nd Iranian Hydraulic Conference, Iranian Hydraulic Association, Tehran, Iran

Banihabib ME, Forghani A (2017) An assessment framework for the mitigation effects of check dams on debris flow. CATENA 152:277–284

Banihabib ME, Nazarieh F (2019) A model for simulation of debris flow sedimentation in slit detention-dam reservoirs. J Hydro-Environ Res 27:65–74

Banihabib ME, Tanhapour M (2019) Proposing an empirical equation for estimation of the sediment concentration of debris Flow (Case Study: Jiangjia Gully in China). Iran J Watershed Manag Res 9(18):70–79

Banihabib ME, Tanhapour M (2020) An empirical equation to determine the threshold for rainfall-induced landslides developing to debris flows. Landslides 17:2055–2065

Banihabib ME, Tanhapour M, Roozbahani A (2020) Bayesian networks model for identification of the effective variables in the forecasting of debris flows occurrence. Environ Earth Sci 79:179. https://doi.org/10.1007/s12665-020-08911-w

Barredo JI (2007) Major flood disasters in Europe: 1950–2005. Nat Hazards 42(1):125–148

Berger C, McArdell BW, Schlunegger F (2011) Sediment transfer patterns at the Illgraben catchment, Switzerland: implications for the time scales of debris flow activities. Geomorphology 125(3):421–432

Bezak N, Šraj M, Mikoš M (2016) Copula-based IDF curves and empirical rainfall thresholds for flash floods and rainfall-induced landslides. J Hydrol 541:272–284

Borga M, Stoffel M, Marchi L, Marra F, Jakob M (2014) Hydrogeomorphic response to extreme rainfall in headwater systems: flash floods and debris flows. J Hydrol 518:194–205

Caine N (1980) The rainfall intensity-duration control of shallow landslides and debris flows. Geogr Ann Ser B 62(1–2):23–27

Chang TC, Wang ZY, Chien YH (2010) Hazard assessment model for debris flow prediction. Environ Earth Sci 60(8):1619–1630

Cogan J, Gratchev I (2019) A study on the effect of rainfall and slope characteristics on landslide initiation by means of flume tests. Landslides 16(12):2369–2379

Coussot P, Meunier M (1996) Recognition, classification and mechanical description of debris flows. Earth Sci Rev 40(3–4):209–227

Diakakis M, Deligiannakis G (2017) Flood fatalities in Greece: 1970–2010. J Flood Risk Manag 10(1):115–123

Diakakis M, Deligiannakis G, Antoniadis Z, Melaki M, Katsetsiadou NK, Andreadakis E, ... Gogou M (2020) Proposal of a flash flood impact severity scale for the classification and mapping of flash flood impacts. J Hydrol 590:125452

Dong JJ, Lee CT, Tung YH, Liu CN, Lin KP, Lee JF (2009) The role of the sediment budget in understanding debris flow susceptibility. Earth Surf Proc Land 34(12):1612–1624

Egashira S (1993) Mechanism of sediment deposition from debris flow (part 1). J Jpn Soc Erosion Control Eng 46(1):186

Evans SG, Hungr O, Clague JJ (2001) Dynamics of the 1984 rock avalanche and associated distal debris flow on Mount Cayley, British Columbia, Canada; implications for landslide hazard assessment on dissected volcanoes. Eng Geol 61(1):29–51

Hassan-Esfahani L, Banihabib ME (2016) The impact of slit and detention dams on debris flow control using GSTARS 3.0. Environ Earth Sci 75(4):328

He B, Huang X, Ma M, Chang Q, Tu Y, Li Q, Hong Y (2018a) Analysis of flash flood disaster characteristics in China from 2011 to 2015. Nat Hazards 90(1):407–420

He S, Wang D, Chang S, Fang Y, Lan H (2018b) Effects of the morphology of sediment-transporting channels on the erosion and deposition of debris flows. Environ Earth Sci 77(14):544

Hirano M (1997) Prediction of debris flow for warning and evacuation. In: Recent developments on debris flows. Springer, Berlin, Heidelberg, pp 7–26

Hu W, Xu Q, van Asch TWJ, Zhu X, Xu QQ (2014) Flume tests to study the initiation of huge debris flows after the Wenchuan earthquake in SW China. Eng Geol 182:121–129

Iverson RM, Denlinger RP (2001) Flow of variably fluidized granular masses across three-dimensional terrain: 1. Coulomb mixture theory. J Geophys Res Solid Earth 106(B1):537–552

Jomelli V, Pavlova I, Eckert N, Grancher D, Brunstein D (2015) A new hierarchical Bayesian approach to analyse environmental and climatic influences on debris flow occurrence. Geomorphology 250:407–421

Kotlyakov VM, Desinov LV, Dolgov SV, Koronkevich NI, Likhacheva EA, Makkaveev AN, ... Rudakov VA (2013) Flooding of July 6–7, 2012, in the town of Krymsk. Reg Res Russ 3 (1):32–39

Liang WJ, Zhuang DF, Jiang D, Pan JJ, Ren HY (2012) Assessment of debris flow hazards using a Bayesian Network. Geomorphology 171:94–100

Mangeney A, Roche O, Hungr O, Mangold N, Faccanoni G, Lucas A (2010) Erosion and mobility in granular collapse over sloping beds. J Geophys Res Earth Surf 115(F3):1–21

Ngo TTH, Vu BT, Nguyen TK (2020) Early warning systems for flash floods and debris flows in Vietnam: a review. Geotechnics for sustainable infrastructure development. Springer, Singapore, pp 1233–1240

Norbiato D, Borga M, Degli Esposti S, Gaume E, Anquetin S (2008) Flash flood warning based on rainfall thresholds and soil moisture conditions: An assessment for gauged and ungauged basins. J Hydrol 362(3–4):274–290

Papa M, Egashira S, Itoh T (2004) Critical conditions of bed sediment entrainment due to debris flow. Nat Hazard Earth Syst Sci 4:469–474

Pellegrino AM, Schippa L (2018) A laboratory experience on the effect of grains concentration and coarse sediment on the rheology of natural debris-flows. Environ Earth Sci 77(22):749

Procter C (2012) Debris flow dynamics: a flume study of velocity and super elevation, Doctoral dissertation, Durham University

Salvati P, Bianchi C, Rossi M, Guzzetti F (2010) Societal landslide and flood risk in Italy. Nat Hazard 10(3):465–483
Shu AP, Wang L, Zhang X, Ou GQ, Wang S (2017) Study on the formation and initial transport for non-homogeneous debris flow. Water 9(4):253
Sun D, Zhang D, Cheng X (2012) Framework of national non-structural measures for flash flood disaster prevention in China. Water 4(1):272–282
Takahashi T (1977) A mechanism of occurrence of mud-debris flows and their characteristics in motion. Annu Disaster Prev Res Inst 20:405–435
Takahashi T (1981) Debris Flow. Annu Rev Fluid Mech 13:57–77
Takahashi T, Kuang SF (1986) Formation of debris flow on varied slope bed. Disaster Prev Res Inst Annu 29:345–349
Tanhapour M, Banihabib M (2019) Determination of the rainfall threshold for debris flow occurrence in a part of Alborz mountainous basins. J Watershed Eng Manag 11(3):575–588
Tanhapour M, Banihabib ME, Rouzbahani A (2018) Bayesian network model for the assessment of the effect of antecedent rainfall on debris flow forecasting in Alborz zone of Iran. Iran Water Res Res 13:118–131
Vaezi AR, Ebadi M (2016) Particle size distribution of surface-eroded soil in different rainfall intensities and slope gradients. J Water Soil 31(1):216–229
Williams JJ, Rose CP, Thorne PD, Coates LE, West JR, Harcastle PJ, ... Wilson DJ (1997) Observed suspended sediments in storm conditions. Coast Eng Proc 3257–3269
Zhuang J, Cui P, Wang G, Chen X, Iqbal J, Guo X (2015) Rainfall thresholds for the occurrence of debris flows in the Jiangjia Gully, Yunnan Province, China. Eng Geol 195:335–346
Zidan AF, Aboukhadra AA, Gaber Y (2019) Enhancement of resilient modulus of cohesive soil using an enzymatic preparation. J Central South Univ 26(9):2596–2608

Part VI
Groundwater Management

Chapter 20
Assessment of Groundwater Resources in Water Spring Areas Using Geophysical Methods, Northern UAE

Abdel Azim Ebraheem, Mohsen Sherif, Mohamed Al Mulla, Khaled Alghafli, and Ahmed Sefelnasr

Abstract The Khatt, Madab, and Al Ghmour Springs are important springs in UAE. They are located in the foothills of the Oman Mountains. The water temperature of these springs is relatively high (approximately 39 °C). Overexploitation of fractured aquifers negatively affected the waterflows from these springs. The outflows from these springs are time-dependent and range from 10 to 50 L/s (until 1998) to 1–10 L/s (until 2010). To assess the current conditions of the spring areas, relevant data were carefully reviewed, analyzed, and stored in a GIS database. A 3D-geological model was developed for the Khatt Springs area, which allowed different types of visualizations, calculations, and predictions. In addition, a 2D earth resistivity imaging survey was performed to evaluate the available groundwater resources, characterize the major faults/fractures feeding these springs, and to determine the locations of saturated fractures and karsts and the thicknesses of the unconsolidated materials in the wadis. Borehole and drilling information from observation wells were utilized to enhance the analysis of the earth resistivity imaging data. The described procedures and acquired results indicated that it was

A. A. Ebraheem · M. Sherif · K. Alghafli · A. Sefelnasr (✉)
National Water and Energy Center, United Arab Emirates University, P.O. Box 15551, Al Ain, UAE
e-mail: ahmed.sefelnasr@uaeu.ac.ae

A. A. Ebraheem
e-mail: abdelazim.aly@uaeu.ac.ae

M. Sherif
e-mail: msherif@uaeu.ac.ae

K. Alghafli
e-mail: khaledalghafli@uaeu.ac.ae

M. Sherif
Civil and Environmental Eng. Dept, College of Engineering, United Arab Emirates University, P.O. Box 15551, Al Ain, UAE

M. Al Mulla
Ministry of Energy and Industry, Dubai, UAE
e-mail: Mohamed.Alkokhardi@moei.gov.ae

T. Sumi et al. (eds.), *Wadi Flash Floods*, Natural Disaster Science and Mitigation Engineering: DPRI Reports, https://doi.org/10.1007/978-981-16-2904-4_20

possible to determine the locations of two production wells for feeding Al Ghmour Springs with water during drought periods to keep it alive.

Keywords 2D earth resistivity imaging · 3D geological modeling · Khatt Springs · Madab Springs · Al Ghmour Springs · UAE

20.1 Introduction

There are wide applications of surface geophysical methods for studying water resources in arid and semiarid environments. Geophysical methods allow for continuous scanning of subsurface soils and water saturation, which are of high importance in remote arid areas and wadi systems where information and measurements are scarce or absent. To accomplish the same tasks with piezometers, a large number of piezometers would be required because piezometers only allow observations of conditions at discrete points. In addition, individual techniques for estimating water fluxes in unsaturated zones usually have their own limitations.

The conductivity of water, which is an intrinsic property of the total dissolved solids, indicates how well water conducts electricity. For example, the specific conductivity (SC) of a clay-free gravel layer saturated with saline water could be as high as 100 times the SC of the same gravel layer if it were dry (Hermans et al. 2017). This major difference in SC based on the degree of saturation and the water quality makes geophysical methods very useful for tracing groundwater contaminations and saltwater intrusions in clay-free aquifers. The resistivity of fractured rocks is controlled by the secondary porosity and groundwater salinity (Kalisperi et al. 2018; Khalil et al. 2020). The application of electrical methods for groundwater explorations and assessments has the following advantages (Ebraheem et al. 2014a, b).

- Reduced need for borehole drilling and direct sampling of groundwater,
- Uncostly data acquisition for quick monitoring of large areas as well as optimizing the locations of monitoring wells,
- Electrical conductivity/resistivity is controlled by groundwater salinity, which is readily interpreted in terms of groundwater quality.

The Khatt Springs area includes the most prominent springs in UAE and is located at the western piedmont of the Oman Mountains (Fig. 20.1). These springs are recognized by two main parts (the north Khatt and south Khatt), and the flows from these areas were gauged in 1966. The south Khatt Spring flows directly from the limestone hills, while the north Khatt Spring appears approximately 3 m west of the foothills. Several constructions have been implemented to increase the flow from each spring. The Madab and Al Ghmour Springs are located in the eastern foothills of the Oman Mountains (Fig. 20.1). The water of these springs is characterized by relatively high temperatures (approximately 39 °C) compared to the

temperatures of all other existing groundwater (25–32 °C) within the northern emirates that come from the same domain. The temperature of groundwater may be assumed to increase with depth from a level approximately 20 m below ground level at a gradient of approximately 1 °C per 30 m. The difference between the temperatures of the spring waters and those of the groundwater in the surrounding area suggests that the spring waters originate from a considerable depth, perhaps approximately 300 m below the ground level (Halcrow and Partners 1969; IWACO 1986). The water of these springs has been traditionally used for bathing, medication, and irrigation. Since 1979, the Khatt and Madab Springs have gone through further developments and have become major bathing and recreation sites.

Aflaj (plural of Falaj) is an Arabic term that describes a complex man-made network of tunnels composed of vertical shafts that capture groundwater or base flows at the foothills of mountains and direct the water to the land surface by the force of gravity, without any intervention of machines, mainly for irrigation purposes (Alshahran and Rizk 2020). Aflaj recharge depends on water sources in upstream areas, including groundwater, natural springs, and rainfall (Al Amri et al. 2014). The well locations, channel gradients, aquifer types, and amounts of recharge are the main factors affecting Aflaj discharge rates (Beckers et al. 2013). The climates, geologic settings, and human activities are the main factors affecting the water quality and water use of Aflaj systems (Al Tikriti 2015).

Water outflows from small springs and hand-dug wells are collected in Aflaj. This water is then essentially used for cultivating palm dates and in other market productions. The area of the springs (Ruus Al Jabal Peninsula) consists mainly of highly karstified limestones and dolomites, the thicknesses of which reach 3000 m (Hudson and Chatton 1959). Rainwater percolates through the limestone beds following the joints, fractures, other secondary openings, and the general trend of the folded strata. These strata have north-facing aspect (direction of slope), and the groundwater outflows from these strata emerge through high-level overflow springs, where impermeable rock layers encounter the flow paths of groundwater, or at sea level.

The climate of UAE is generally characterized by hyperarid desert conditions with two main seasons: very hot, sunny summers (May–September, when temperatures often exceed 40 °C) and pleasantly mild, cool winters (October–April, when mean annual average temperatures are approximately 27 °C). Rainfall events are rare and unpredictable with irregular precipitation patterns; however, they occur in the forms of showers or downpours that can sometimes be intense (Tourenq et al. 2011). The mean annual rainfall varies from 150 mm in the mountainous areas to approximately 90 mm on the coast and less than 50 mm in the sandy desert areas.

Due to the drought conditions that prevailed in the period from 1998–2010 and the necessity of intensive groundwater exploitation for irrigation purposes, which has caused severe cones of depression (Fig. 20.2), the outflow from the Khatt Springs was not enough to keep the temperature in the swimming pools at the desired level (Mohamed et al. 2016). The relatively long water residence time in the pools resulted in the deterioration of the environmental conditions in the recreational park around the pools and in the spread of mosquitoes.

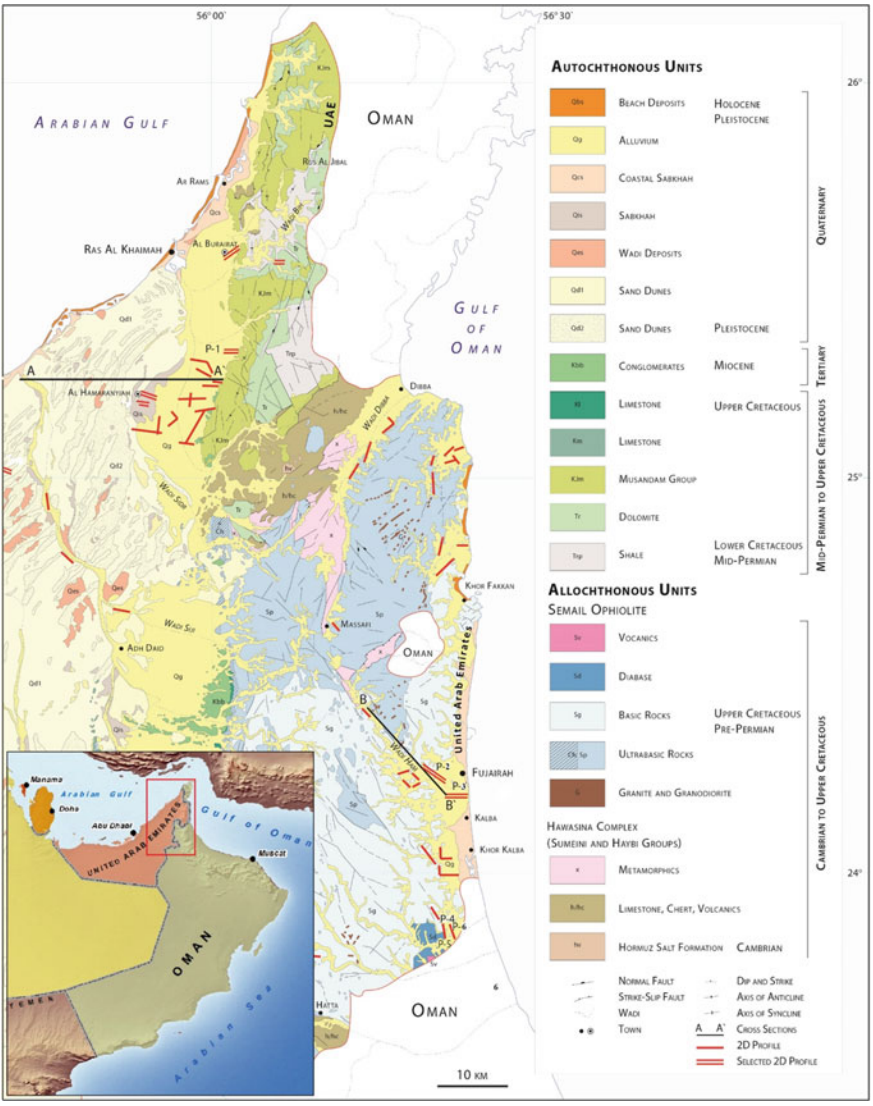

Fig. 20.1 Map of the location of the study area showing the surface geology (*Source* British Geological Survey and Ministry of Energy 2006). The map shows the locations of the cross sections A-A' and B-B' and the 2D earth resistivity imaging profiles

Groundwater levels fluctuate considerably and are controlled by recharge events. The maximum water table increase in this region (approximately 40 m) was observed in March 1997 in well Khat-1 near Khatt Springs (Fig. 20.1).

The impacts of precipitation on fluctuations in the level, flow rate, and temperature of groundwater in the limestone aquifer in the study area have been

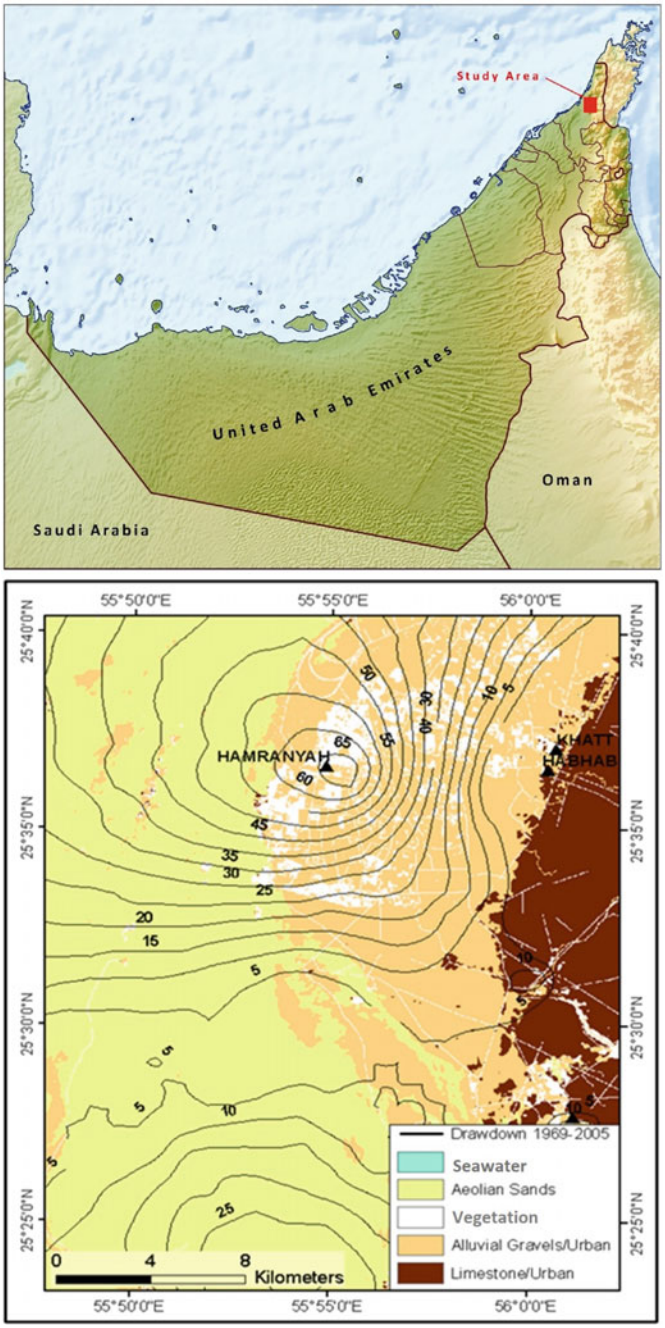

Fig. 20.2 Map illustrating the drawdown of up to 65 m that occurred in the period from 1969 to 2005. Major geomorphologic units and agricultural lands are also shown

Table 20.1 Impacts of the 1999–2010 drought on Khatt Springs

North spring situation in the period from 1979 to 1998	North spring situation in the period from 1999 to 2010
Outflow ranged from 10 to 50 l/s	Outflow ranged from 1 to 10 l/s
Rainfall rate ranged from 60 to 360 mm/year	Rainfall rate ranged from 20 to 150 mm/year
Source water temperature ranged from 39 to 40 °C	Source water temperature from 33 to 37 °C
Irrigation Aflaj work without pumping	Irrigation Aflaj only work with pumping from hand-dug wells

intensively studied since the late 1970s and are summarized in Table 20.1. Groundwater depletion in the areas of the Madab and Al Ghmour Springs is severe, to the extent that water has completely ceased to flow from the Al Ghmour Springs. All the available borehole data, drilling information, and environmental data from 1979 to 2015 were reviewed, analyzed, and stored in a GIS database. Then, the spatial analysis GIS algorithm, enhanced with graphic capabilities, was utilized to analyze and reinterpret these data and to preliminarily assess the current conditions of water resources (water availability and management challenges) in the northern part of UAE. The processed results were implemented in the preparation of a complete dataset as inputs to a 3D geological model for the Khatt Springs area. The main objectives of the present study are as follows.

a) Determining the geological and hydrogeological setting of the Khatt, Ain Madab, and Al Ghmour Springs areas; emphasis was given to the impacts of geological structures on groundwater accumulation and flow patterns.
b) Evaluating the impacts of drought years and groundwater depletion caused by intensive irrigation on the flows and water temperatures of the springs.
c) Application of 2D earth resistivity imaging techniques for mapping the karsts and/or fractures feeding the springs.
d) Applying developed software for digital 3D geological modeling that utilizes cross section-based networks for subsurface interpolation in heterogeneous aquifers.

20.2 Geological and Hydrogeological Settings

The northern Oman Mountains in the Khatt Springs area are composed of Jurassic to Cretaceous Musandam Group limestones. The western Jiri coastal plain consists of Late Tertiary to recent alluvial sediments overlying the Late Cretaceous Juweiza Formation (BGS and MOE 2006; Halcrow and Partners 1969; Sherif et al. 2006, 2018). The Juweiza Formation is composed of a sequence of marl and shale with

intercalations of debris of basic igneous rocks, chert, and limestone (Fig. 20.1). Two major tectonic events have affected the area. The first was in the age of the Upper Cretaceous, when the Hawasina Formations and the Samail Ophiolite were thrust over the Musandam limestone; then, the Mid-Tertiary, the formation of the Oman Mountains occurred due to folding, faulting, and thrusting (Fig. 20.1). As a result of these major structural events, major northeast-trending anticlinal structures were formed, such as the Hagab Mountains thrust fault along the Musandam Mountains, the Jiri plain, the Dibba zone to the southeast, and the Batha Mahani thrust that runs along the valley of the Wadi Tawiyean (Robertson et al. 1990). Accordingly, the Musandam limestones are strongly faulted (Fig. 20.3), with major trends running northeast (parallel to the Dibba zone thrusts), north, and northwest (parallel to the Wadi Ham system).

The topographic setting and structural pattern generally control the thickness of unconsolidated materials. Several subsurface geological cross sections along different directions were constructed using borehole data and drilling information. Two examples of these cross sections in the areas of the Khatt and Ain Madab Springs are shown in Figs. 20.3 and 20.4, respectively. The Masifi Mountains dominate the upstream part of the east coast area, and alluvial plains prevail in the downstream region, in which the sediments are composed of recent Pleistocene wadi gravels. The alluvium gravel layer overlays the consolidated rocks of the Semail Formation with fractured zones at some locations (Fig. 20.5). The two hydraulically connected groundwater aquifers can be characterized as follows.

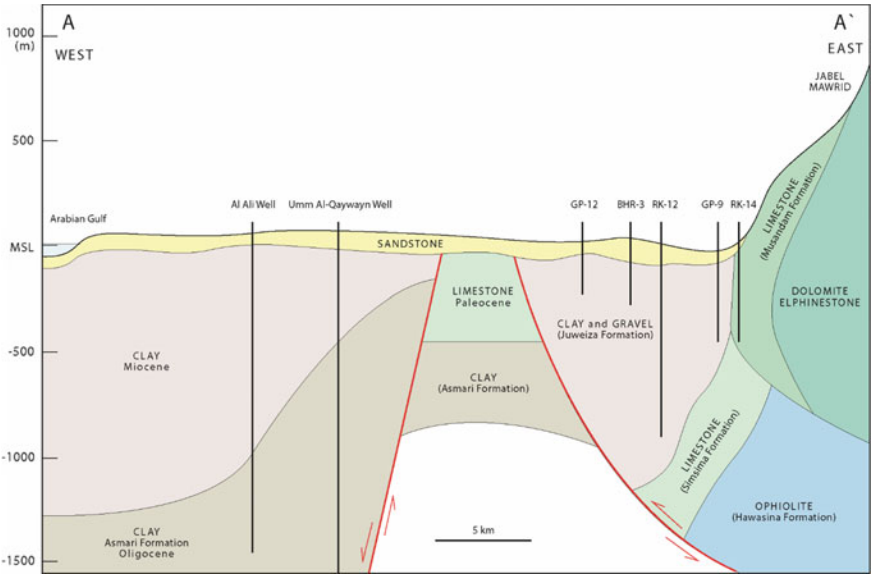

Fig. 20.3 A subsurface geological cross section in the east–west direction (*Source* IWACO 1986). Location of the cross section is shown in Fig. 20.1

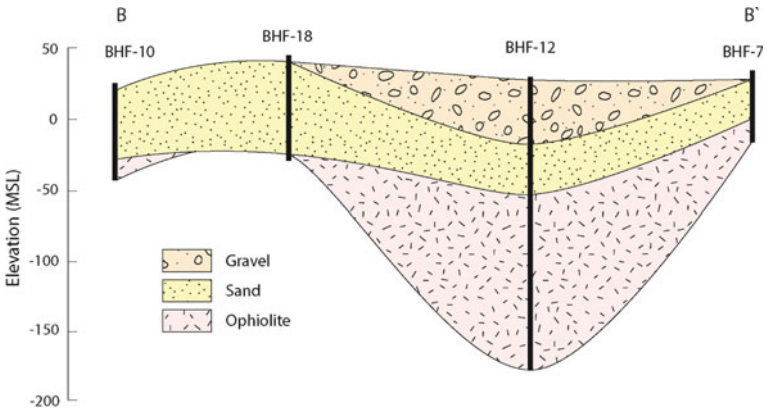

Fig. 20.4 A N–S subsurface geological cross section across the Wadi Ham, approximately 3 km from the Gulf of Oman

Quaternary aquifer: This aquifer is composed of gravel plains of recent silts and conglomerates and meets the mountain front at a high angle. This layer overlies the thick Juweiza Formation on the west coast, which is generally characterized by low permeability and thus acts as an aquitard rather than an aquifer (Fig. 20.3). On the east coast, the aquifer overlies the consolidated rocks of the Semail Formation.

Fractured rock aquifer: The area of the fractured rock aquifer refers to the exposed thick karstified limestone of Jurassic–Cretaceous age in the mountains of the Khatt Springs area (Fig. 20.3) and to the fractured Semail Ophiolite in the areas of the Ain Madab and Al Ghmour spring (Fig. 20.4).

The carbonate layers are composed of well-jointed dolomitic limestone and limestone interbedded with calcareous shales. These beds dip at a very high angle, up to 90°, to the west (Fig. 20.3). The ophiolite layer generally dips toward the east and toward the wadi course (Fig. 20.4).

20.3 Digital 3D Geological Modeling

3D geological modeling is a state-of-the-art technique commonly used in the field of economic geology. It is based on statistical or geostatistical interpolations between stratified scattered boreholes. The method is adequate in areas with sufficient borehole data because it leads to reduced heterogeneity and an inadequate loss of the "real-world" settings of lithostratigraphic layers. The complex structural setting of Quaternary sediments cannot be represented correctly by following only the geostatistical approach (Wycisk et al. 2005). Therefore, the first 3D geological model, comprising approximately 2000 km^2, was developed for the Khatt Springs area based on 39 borehole records. In addition to drilling information, a digital

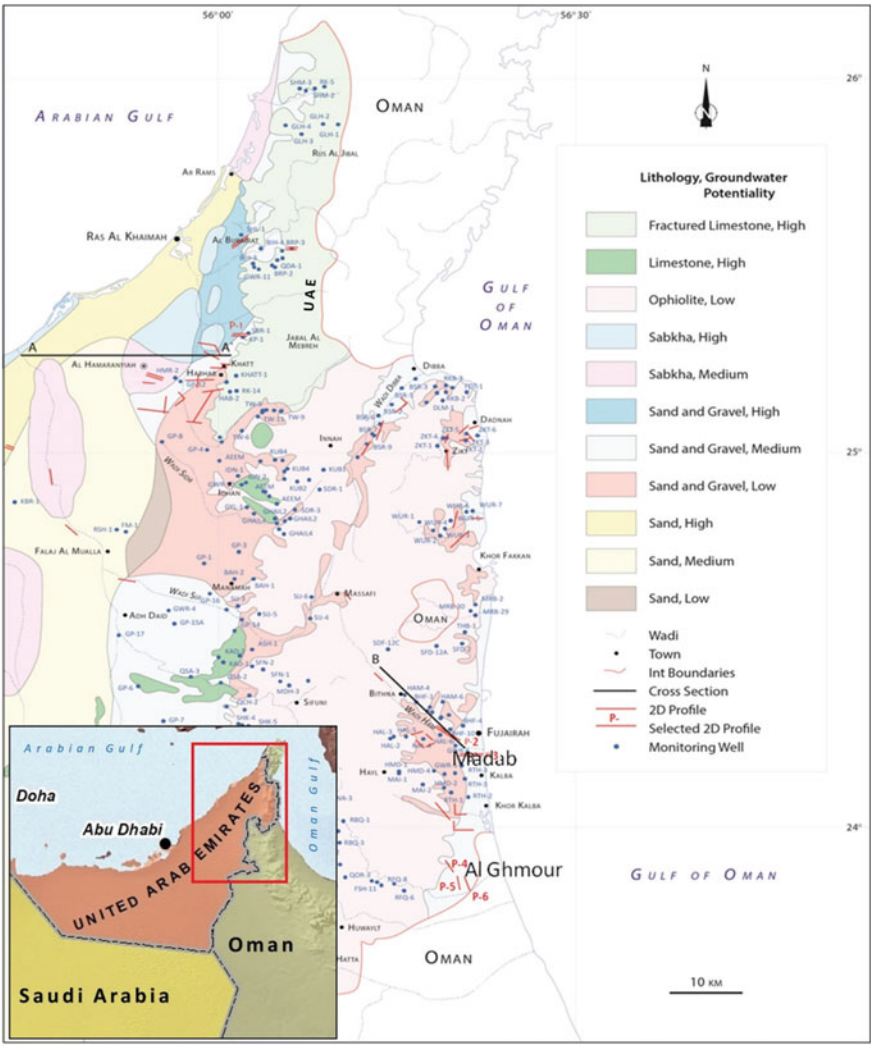

Fig. 20.5 Hydrogeological map of the northern part of UAE (*Source* IWACO 1986)

elevation model (DEM), geophysical logging and profiling information, and geological and hydrogeological maps were also used to develop the 3D database. The developed 3D geological model of the Khatt Springs area allowed different types of visualizations, calculations, and predictions within the hydrogeologic model (Fig. 20.6). Digital, subsurface 3D model results are of specific need in simulations of water resource management options.

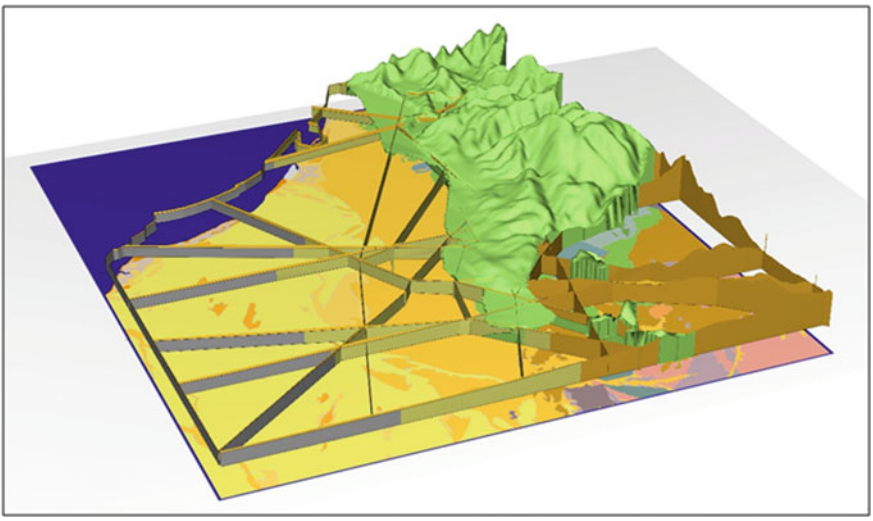

Fig. 20.6 3D geological model constructed for the Khatt Springs area

20.4 DC Earth Resistivity Method

The DC earth resistivity method measures the electrical resistivity distribution in the subsurface by transmitting a current into the ground using two electrodes (C1 and C2; Fig. 20.7) and subsequently measuring the resulting potential difference between a second pair of electrodes (P1 and P2; Fig. 20.7). The apparent resistivity of the subsurface can be calculated using Ohm's law ($R = \Delta V/I$, where R represents the resistance, ΔV depicts the measured potential difference, and I stands for the injected current). Assuming a homogeneous subsurface, these measurements, which are geometrically corrected, can be recognized as apparent resistivity values rather than true resistivity values.

The measured resistivity values are controlled by the earth resistivity, degree of saturation, and groundwater quality (Cartwright and Sherman 1972; Ebraheem et al. 1990, 1997; Haeni et al. 1992). The resistivity value of a fractured zone is dependent on the degree of rock fracturing and on the groundwater salinity. The 2D DC-resistivity profiling method is conducted by applying several measurements along a profile at different offsets (Fig. 20.7). Memory earth resistivity and IP instruments and a switch box were used for eight channels. The switch box was used to automatically control the distances between electrodes. The profiling data were inverted by using an iterative smoothness-constrained least-squares inversion method (deGroot-Hedlin and Constable 1990; Sasaki 1992; Loke 1997; Aizebeokhai 2010) to create a tomogram-like model of resistivity. Linear zones of low resistivity that were continuous with depth were interpreted as fracture zones.

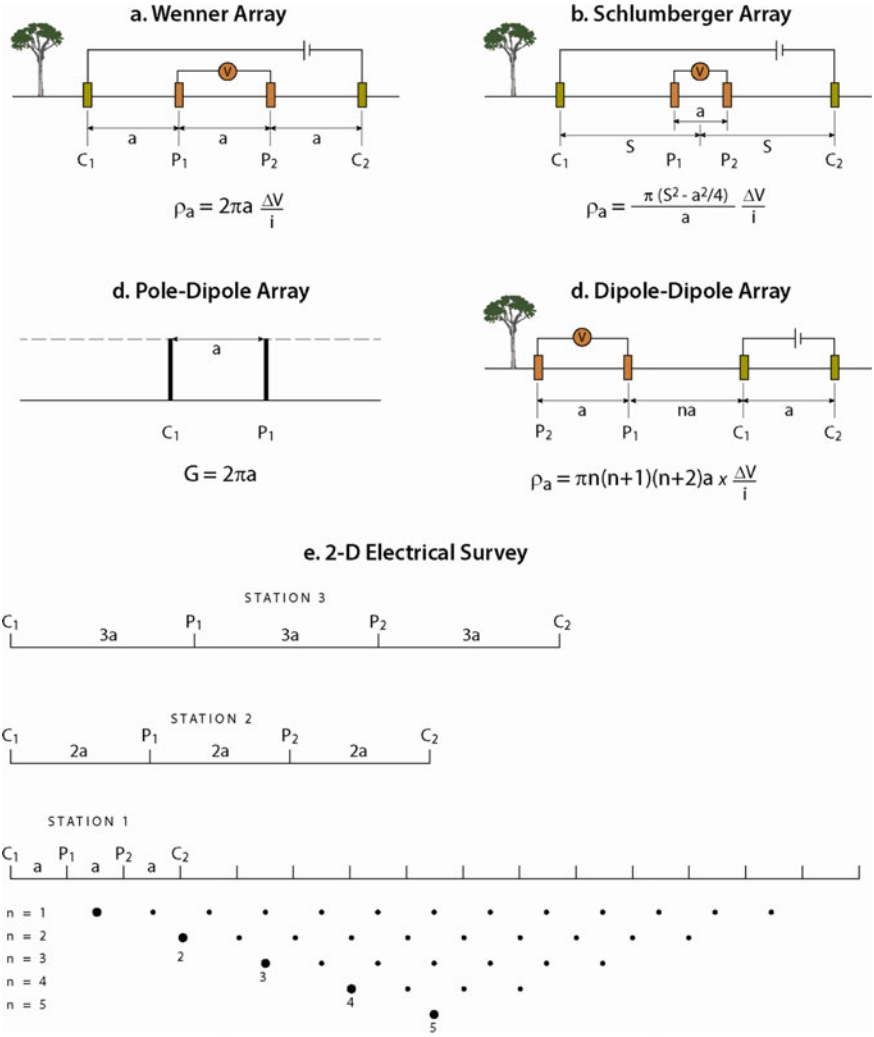

Fig. 20.7 A pattern of electrode arrays implemented in the DC resistivity method and the associated geometrical factors (**a**–**d**) and **e** the arrangement of the electrodes for a 2D electrical survey and the sequence of measurements used to build up a pseudosection (*Source* Ebraheem et al. 2014a, b)

20.5 Data Acquisition and Interpretation

20.5.1 Khatt Springs

With the main purpose of determining the depths and extensions of the fracture zones in the carbonate aquifer feeding the Khatt Springs, measurements of six earth

resistivity profiles were conducted in the Khatt Springs area southeast of Ras Al Khaimah City (Fig. 20.1). An example of an interpreted geophysical profile with a total length of 2220 m (profile P-1; Fig. 20.1) is shown in Fig. 20.8; at this profile, it was possible to determine the areas of saturated cavities and fractures in the Musandam limestone. The obtained results were used to design a production well, KP-1, near profile P-1 (Fig. 20.5). The drilling information of this well-confirmed the obtained interpretation results (Ebraheem et al. 2014a, b).

20.5.2 Ain Madab Springs

Three earth resistivity profiles were conducted in the Madab Springs area (Fig. 20.1). The interpreted results indicate the presence of two layers (an example is shown in Fig. 20.9; profile P-2). The upper layer represents saturated alluvial gravel with slightly brackish water. This layer has a true resistivity ranging from 33 to 100 Ω-m and a thickness ranging from less than 50 to 250 m. This layer overlies the ophiolite layer, which has low permeability except in some places where is fractured. The interpretation of this profile was constrained by comparisons with available lithological logs of existing wells (Ebraheem et al. 2012, 2014a, b).

20.5.3 Al Ghmour Springs

The interpreted results of three resistivity profiles located in the Al Ghmour Springs area also indicated the presence of two layers. As in the Ain Madab Springs area, the upper layer has a true resistivity ranging from 33–100 Ω-m and a thickness ranging from 60 to 250 m; this layer probably consists of alluvial gravels saturated with slightly brackish water (an example of profile P-5 is shown in Fig. 20.10). This layer overlies the ophiolite layer, which is generally a low-permeable or impermeable layer except in places where it is fractured.

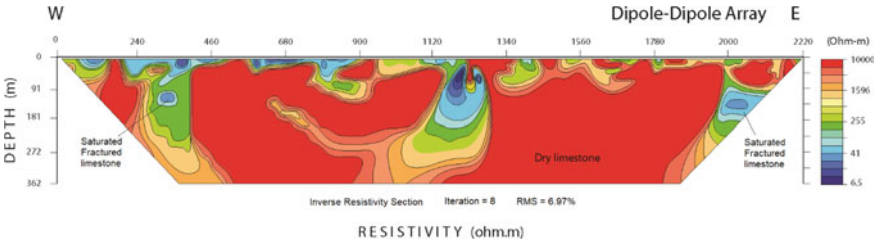

Fig. 20.8 Results of 2D earth resistivity modeling for Profile P-1 in Khatt, Ras Al Khaimah. See Fig. 20.1 for profile location

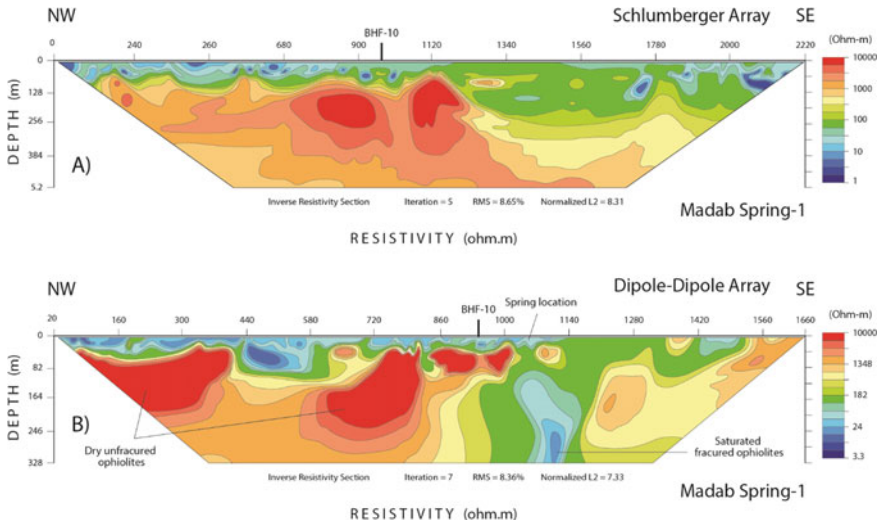

Fig. 20.9 Results of 2D earth resistivity modeling for Profile P-2 in Madab, Fujairah. See Fig. 20.1 for profile locations

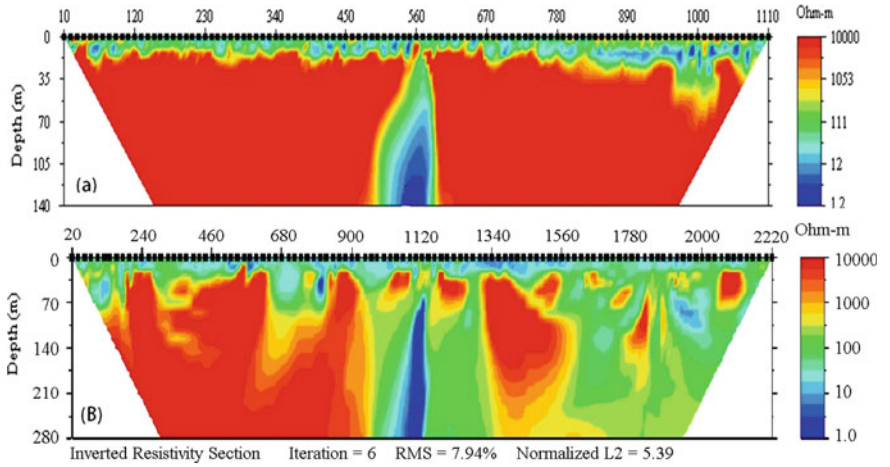

Fig. 20.10 Results of 2D earth sresistivity modeling for Profile P-4 in Al Ghmour, Fujairah using the **a** dipole–dipole array and **b** Schlumberger array. See Fig. 20.1 for profile locations

20.6 Conclusion and Recommendation

A GIS-based comprehensive study was conducted to assess the current situation of water springs in UAE. The investigations included field and laboratory components. Based on the results of the study, the following conclusions could be made.

1. The potentials of limestone aquifers to serve as strategic resources are very high. To develop additional production wells, new locations must be predicted by geophysical investigations as well as by optimized location sites, which in turn must be assessed by geological structure analyses of fractured zones within the outcropping limestone formation. The maximization of expected cavity-building as well as the clustering of fractures can be expected at the zones in which structural elements cross inside wadi courses.
2. For a deeper understanding and long-term development in terms of prognoses, ongoing monitoring of the pressure head of the main free-flowing well near Khatt Springs is strongly recommended due to expected interfering hydraulic effects. This monitoring can be done by flow rate measurements and, more importantly, pressure head measurements.
3. The hydrogeological system in the east coast area is composed of two aquifers. The first is the upper Quaternary aquifer, which is composed of wadi gravel and represents the main aquifer. The second is the lower fractured ophiolite aquifer, which has a low groundwater potentiality in general and modest to high groundwater potentiality in the areas that are strongly affected by regional faulting (e.g., the Wadi Ham).
4. It was possible to determine the locations of two production wells in the Wadi Ham and Ain Madab Springs area for feeding the spring with water during times of drought to keep it alive.
5. The rehabilitation of Al Ghmour Springs as a bathing pool looks very promising and can be reasonably realized. To this end, the following topics must be taken into account.

    - The temperature and pH of the springs indicate a fault/fracture-bounded situation at the higher flank of the wadi shoulder.
    - The spring outlet must be traced toward the bedrock/solid rock position of the morphologically incised depression. The spring outlet must be dug as deep as possible into the unweathered solid rock formation to the deepest position of the fall lines of the incised depression at the entry of the contact zone toward the wadi sediments. To avoid losses of spring water, it is recommended that the water is brought by pipe or by the construction of sealed small canals toward the bathing pool.

References

Aizebeokhai AP (2010) 2D and 3D geoelectrical resistivity imaging. Theory and field design. Scientific Research and Essays 5(23):3592–3605. Online at http://www.academicjournals.org/SRE

Al Amri S, Al Ghafri A, Abd Rahman N (2014) Water management of Falaj Al Khatmain in Sultanate of Oman. J Earth Sci Eng 4:127–133

Al Tikriti W (2015) Origin and technique of the Falaj System: an evidence from the United Arab Emirates, Cultural Heritages of Water. In: The cultural heritages of water in the Middle East and Maghreb, 1st edn. ICOMOS, World Heritage Convention, France, pp 211–222

Alsharhan AS, Rizk ZE (2020) Aflaj systems: history and factors affecting recharge and discharge. In: Water resources and integrated management of the United Arab Emirates. World Water Resources, vol 3. Springer, Cham. https://doi.org/10.1007/978-3-030-31684-6_8

Beckers B, Berking J, Schütt B (2013) Ancient water harvesting methods in the drylands of the Mediterranean and Western Asia. J Anc Stud Berlin 2:145–164

British Geological Survey and Ministry of Energy (2006) Geological map of Northern UAE. Internal Report, Ministry of Energy, Abu Dhabi, UAE

Cartwright K, Sherman F (1972) Electrical earth resistivity surveying in landfill investigations. In: 10th Annual Engineering and Soils Engineering Symposium, Moscow

deGroot-Hedlin C, Constable S (1990) Occam's inversion to generate smooth, two-dimensional models from magnetotelluric data. Geophysics 55(12):1613–1624

Ebraheem AM, Hamburger MW, Bayless ER, Krothe NC (1990) A study of acid mine drainage using earth resistivity measurements. Ground Water 28(3):361–368

Ebraheem AM, Senosy MM, Dahab KA (1997) Geoelectrical and hydrogeochemical studies for delineating groundwater contamination due to salt-water intrusion in the northern part of the Nile Delta. Egypt. Ground Water 35(2):216–222

Ebraheem AM, Sherif M, Al Mulla MM, Akram SF, Shetty AV (2012) A geoelectrical and hydrogeological study for the assessment of groundwater resources in Wadi Bih. UAE. Environ Earth Sci 67(3):845–857

Ebraheem AM, Al Mulla MM, Sherif MM, Awad O, Akram SF, Al Suweidi NB, Shetty A (2014) Mapping groundwater conditions in different geological environments in the northern area of UAE using 2D earth resistivity imaging survey. Environ Earth Sci 72(5):1599–1614. https://doi.org/10.1007/s12665-014-3064-5

Ebraheem AM, Sherif M, Al Mulla MM (2014) Application of 2D earth resistivity imaging for groundwater problems in different geological environment. Environ Earth Sci 72(5):1599–1614

Edwards LS (1977) A modified pseudosection for resistivity and IP. Geophysics 42(5):1020–1036

Haeni FP, Placzek G, Trent RE (1992) Use of ground-penetrating radar to investigate infilled scour holes at bridge foundations. In Hanninen P, Autio S (eds) Fourth international conference on ground penetrating radar, Rovaniemi, Finland, June 8–13, 1992, Proceedings: geological survey of finland special paper vol 16, pp 285–292

Hermans T, Irving J (2017) Facies discrimination with electrical resistivity tomography using a probabilistic methodology: effect of sensitivity and regularization. Near Surf Geophys 15:13–25

Hudson RG, Chatton M (1959) The Musandam Limestone (Jurrassic to Lower Cretaceous) of Oman. Arabia Notes Et Mem. Moyen Orient 7:69–93

IWACO (1986) Groundwater study project 21/81, Drilling of deep water wells at various locations in the UAE. Groundwater Development in the Northern Agricultural Region. Internal Report, vol 7, Ministry of Agriculture and Fisheries, Dubai, UAE

Kalisperi D, Kouli M, Vallianatos F, Soupios P, Kershaw S, Lydakis-Simantiris N (2018) A Transient Electro Magnetic (TEM) method survey in North-Central Coast of Crete, Greece: evidence of seawater intrusion. Geosciences 8:107. https://doi.org/10.3390/geosciences8040107

Khalil MI, Didar-Ul Islam SM, Jamal Uddin Md. Majumder RK (2020) Coastal groundwater aquifer characterization from geoelectrical measurements—a case study at Kalapara, Patuakhali, Bangladesh. J Appl Geol 5(1). https://doi.org/10.22146/jag.55009

Loke MH (1997) Electrical imaging surveys for environmental and engineering studies: a practical guide to 2D and 3D surveys: Unpublished short training course lecture notes. Universiti Sains Malaysia, Penang, Malaysia

Mohamed MM, Al-Suwaidi N, Ebraheem AM, Al Mulla MM (2016) Groundwater modeling as a precursor tool for water resources sustainability in Khatt area, UAE. Environ Erath Sci 75(5). https://doi.org/10.1007/s12665-016-5261-x

Robertson A, Blome CD, Cooper D, Kemp A, Searle M (1990) Evolution of the Arabian continental margin in the Dibba Zone, Northern Oman Mountains. Geological Society, London, Special Publications 49:251–284. https://doi.org/10.1144/GSL.SP.1992.049.01.17

Sasaki Y (1992) Resolution of resistivity tomography inferred from numerical simulation. Geophys Prospect 40:453–464

Sherif M, Al Mahmoudy A, Garamoon H, Kasimov A, Akram S, Ebraheem AM, Shetty A (2006) Geoelectrical and hydrogeochemical studies for delineating ground-water contamination due to salt-water intrusion in the outlet of Wadi Ham. UAE. Environ Geol 49(4):536–551

Sherif M, Ebraheem AM, Al Mulla M, Shetty A (2018) New system for the assessment of annual groundwater recharge from rainfall in the United Arab Emirates. Environ Earth Sci 77:412. https://doi.org/10.1007/s12665-018-7591-3

Sir Williams Halcrow and Partners Consulting Engineers (1969) Water resources of trucial states. Internal report, Ministry of Agriculture and Fisheries, Dubai, UAE

Tourenq C, Brook M, Knutenson S, Shuriqi M, Sawat M, Perry L (2011) Hydrogeology of Wadi Wurayah, United Arab Emirates, and its importance for biodiversity and local communities. Hydrol Sci J 56(8):1407–1422

Wycisk P, Gossel W, Wollmann A, Fabritius H, Hubert T (2005) High-resolution digital 3D models as a base of hydrodynamic calculation in heterogeneous aquifers. In: Proceedings of the 5th International Conference on Aquifer Recharge, 10–16 June, 2005, Berlin, Germany

Chapter 21
Evaluation of the Effect of the Wadi Bih Dam on Groundwater Recharge, UAE

Mohsen Sherif, Abdel Azim Ebraheem, Ampar Shetty, Ahmed Sefelnasr, Khaled Alghafli, and Mohamed Al Asam

Abstract In Ras Al Khaimah, UAE, groundwater from the alluvial aquifer in Wadi Bih was the only source of freshwater for various uses prior to the construction of a seawater desalination plant in 1998. This study was conducted to evaluate the effect of the Wadi Bih dam on groundwater resources and to increase knowledge of the hydrodynamics of the aquifer. A local-scale numerical groundwater flow model was developed and used to investigate the impacts of different groundwater management options on groundwater resources. The calibrated and validated model was defined as the base case, and subsequently, simulations were performed to analyze different management scenarios. The simulations indicated that maximum recharge occurred during years of high rainfall (1995–1998). Minimum recharge occurred in 2000, 2002, and 2004. The major contribution to the water balance was from subsurface inflows from the upper wadi zone and the two tributaries. Overall, the annual water balance was negative in most years, with an average net decline of 0.6 MCM per year, indicating a slow but continuous depletion of groundwater resources. At the end of the simulation, the total groundwater recharge due to rainfall and water storage in the ponding area was 9.81 MCM.

M. Sherif · A. A. Ebraheem · A. Shetty · A. Sefelnasr (✉) · K. Alghafli
National Water and Energy Center, United Arab Emirates University, P.O. Box 15551, Al Ain, UAE
e-mail: ahmed.sefelnasr@uaeu.ac.ae

M. Sherif
e-mail: msherif@uaeu.ac.ae

A. A. Ebraheem
e-mail: abdelazim.aly@uaeu.ac.ae

K. Alghafli
e-mail: khaledalghafli@uaeu.ac.ae

M. Sherif
Civil and Environmental Engineering Department, College of Engineering, United Arab Emirates University, P.O. Box 15551, Al Ain, UAE

M. Al Asam
Department of Water Resources, Ministry of Energy and Industry, Dubai, UAE
e-mail: moh.alzaabi@aurak.ac.ae

T. Sumi et al. (eds.), *Wadi Flash Floods*, Natural Disaster Science and Mitigation Engineering: DPRI Reports, https://doi.org/10.1007/978-981-16-2904-4_21

Keywords Managed aquifer recharge (MAR) · Recharge dam · Numerical groundwater flow model · Wadi Bih · UAE

21.1 Introduction

Natural water resources are scarce in arid and semiarid regions where evaporation significantly exceeds precipitation. Due to the absence of permanent surface water sources in such regions, groundwater constitutes the main source of irrigation water. Groundwater depletion poses a significant threat to water security in arid and semiarid areas, where rivers are usually ephemeral and groundwater is the main source of water. A growing population, rising standards of living, and water-intensive diets lead to an ever-increasing demand for freshwater, which causes considerable stress on groundwater resources. As a result, the overexploitation of groundwater has led to declining water levels in many aquifers in arid regions, such as UAE (Rizk and Alsharhan 2003). The groundwater pumped from these aquifers is attributed mostly to aquifer storage, which typically is not compensated through recharge processes. Generally, aquifer recharge in UAE is restricted to mountainous areas and alluvial gravels at the foothills of mountains. The natural aquifer recharge in UAE is estimated at 174 million m^3, while the agricultural sector only consumes approximately 2.9 billion m^3 through groundwater pumping (EAD 2018). In the mountains, floods are generated from heavy rainfall. A small portion of rainwater percolates into the subsurface, and thus, relatively large flood discharges are produced in wadi channels. The mean annual runoff of major wadis in UAE is approximately 120 MCM (Sherif et al. 2018; Murad et al. 2020). Factors affecting the recharge efficiency include, among others, the geological conditions, hydrogeology, and hydrogeochemistry of the recharge sites, physiography, hydraulic gradients, vegetation cover, types of soil, gravels and loose sediments, fractures and joints, and the secondary porosity of consolidated sediments and rocks. A number of issues are known to reduce recharge efficiency over time, with the key issues being sedimentation and consistently high evapotranspiration.

Consequently, strategies to conserve groundwater and augment the amount of groundwater available for abstraction have gained growing attention over the last decades, with managed aquifer recharge (MAR) being considered an important tool in integrated water resources management (IWRM) (Dillon and Arshad 2016).

One type of MAR technology involves the construction of dams within wadi systems to trap and store surface runoff from flood events for subsequent infiltration to enhance groundwater recharge (Jaafar 2014; Missimer et al. 2015). Wadis are ephemeral streams in arid and semiarid regions, including the Middle East, northern Africa, and southwest Asia (Maliva and Missimer 2012). Typically, alluvial aquifers that occur beneath wadi channels are frequently used to supply water to villages and agricultural areas (Missimer et al. 2015).

In Ras Al Khaimah City, UAE, groundwater abstraction from an alluvial aquifer in Wadi Bih was the only source of freshwater for domestic and other uses before the construction of a seawater desalination plant in 1998. In 1982, the Wadi Bih dam was constructed with the purpose of reducing the risk of flooding and increasing groundwater recharge to the aquifer. However, since the 1990s, a deterioration of the water quality has been observed, which might be attributed to the water mixing with a regional brine that may have increased in volume due to declining water tables resulting from abstractions (Rizk et al. 2007). A growing demand for new settlements and industrial activities as well as for agricultural production puts additional pressure on the groundwater resources in Wadi Bih. The main objective of this study was to assess the effect of the recharge from Wadi Bih dam on the groundwater resources in Wadi Bih. The dam efficiency has not been studied before; however, with increasing pressure on water resources and the observed deterioration of water quality, an improved knowledge of the dam-induced changes to the water balance and the available groundwater resources was deemed necessary to improve groundwater management in the area. As no groundwater-monitoring data from the predam period were available, a simple comparison of pre- and postdam groundwater levels was not possible. Therefore, a numerical groundwater flow model was developed with the additional objectives to reconstruct predevelopment conditions (i.e., no dam and no groundwater abstraction) to assess the effect of groundwater abstraction and the mitigating effect of the dam. These objectives will enable an evaluation of potential management scenarios for the sustainable management of Wadi Bih's groundwater resources.

21.2 Hydrogeological Setting of Wadi Bih

UAE lies in the southeastern part of the Arabian Peninsula, bounded on the north by the Arabian Gulf, on the south and west by the Kingdom of Saudi Arabia, and on the east by Oman and the Gulf of Oman (Fig. 21.1). A major part of the country is covered by sand dunes, but the northern part, where Wadi Bih is located, is characterized by mountains, gravel plains, and drainage basins.

Wadi Bih, in Ras Al Khaimah Emirate, is a large southwest-flowing wadi complex comprising parts of the Ruus Al Jibal Mountains of Oman in its eastern section and alluvial plains to the west and southwest. The drainage network of the Wadi Bih basin is mostly controlled by geologic structures. The wadi comprises an extensive network of valleys covering a surface area of 483 km^2.

The catchment is marked by rough topography with steep slopes and very little vegetation. Elevations range from 2087 m above mean sea level at the highest point (amsl) to 65 m (amsl) near the outlet (Ebraheem et al. 2012; Sherif et al. 2018). The Wadi Bih drainage basin is rectangular in shape, and its drainage basin perimeter (water divide) is 113 km long. The upper portion of the basin consists of narrow valleys with steep slopes leading to distinct channels down to the wadi floor, which is composed of coarse alluvial gravels and boulders. The number and depth of the

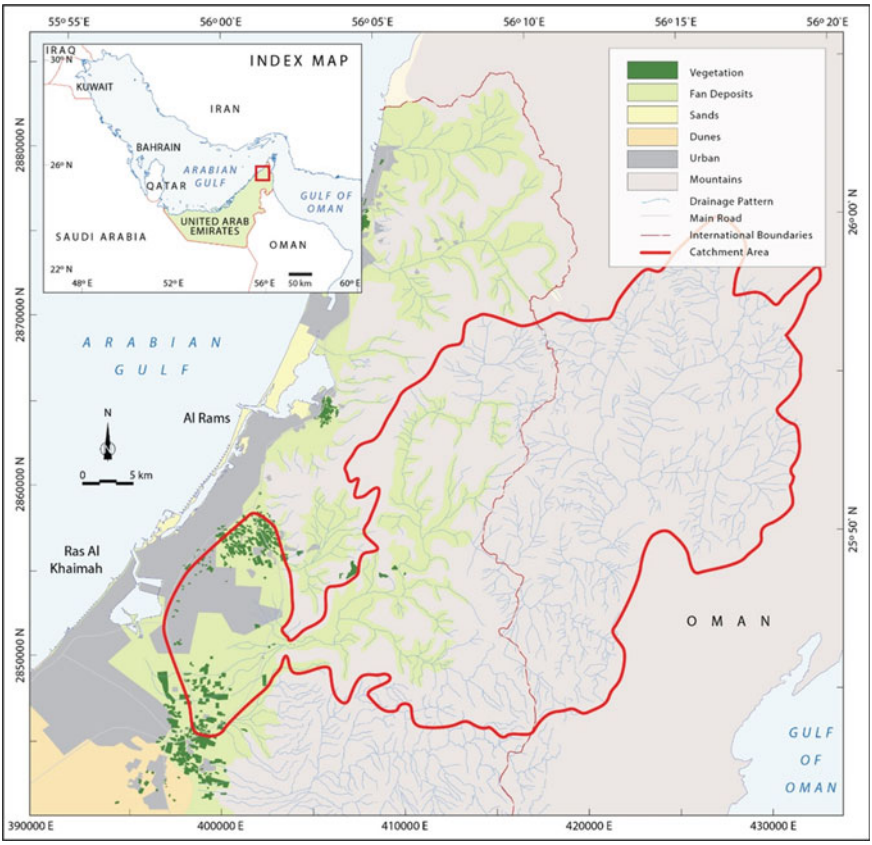

Fig. 21.1 Location and catchment area of Wadi Bih in Ras Al Khaimah Emirate (*Source* Ebraheem et al. 2012)

channels decrease toward the coast. The valley floor of Wadi Bih is a flat, gravelly plain with a triangular shape leading to an alluvial fan.

The catchment of Wadi Bih is mostly dry throughout the year, but occasional intense rainfall can lead to short-duration flash floods. The average annual rainfall in the catchment is 119 mm/year, varying between 6 and 414 mm/year. Rainfall records over the past 15 years indicate that the average annual rainfall has dropped to less than 70 mm/year (Sherif et al. 2009). The surface water flow is estimated to be approximately 1.72 MCM and 10.35 MCM at 3% and 18% of rainfall, respectively. The total annual rainfall in the area is 74 million m^3, of which approximately 9% (6.7 million m^3) recharges the karstified aquifer. This percentage increased to 13% (17.6 million m^3) after the construction of the Wadi Bih dam in 1982 (Rizk 2015). On the other hand, the groundwater extraction from the Wadi Bih limestone aquifer decreased from an average of 9 million m^3/y between 1991 and 1995 to 4.5 million m^3/y between 2010 and 2014. The Wadi Bih dam is 18 m

high and 240 m long and has a reservoir area of 3.2 million square meters (Ebraheem et al. 2012). The constructed storage capacity of the Wadi Bih dam is 7.5 MCM. However, the dam displayed a maximum storage of 6.50 Mm^3, encountered in July 1998 (Sherif et al. 2018), and the dam storage ranges from 0.5 to 2.7 MCM in normal cases. The reservoir of the Wadi Bih dam is filled from time to time due to rain events; therefore, it acts as a mitigation measure and an MAR technique (Fig. 21.2).

The geology of Wadi Bih has been described in detail by Ebraheem et al. (2012). In short, Permian to Early Triassic dolomites and dolomitized limestones represent the main characteristics of the Russ al Jibal group. The sediments were deposited on the continental margin of Arabia as the Bih Formation, Hagil Formation, and Ghail Formation. These formations consist of well-bedded dolomite that is light to dark gray-colored and has frequent joints and fissures. A major fault runs through the dolomite in the north–south direction. The available drilling information from monitoring water wells was used to construct a subsurface geologic cross section, as shown in Fig. 21.3b. The alluvial cover varies in thickness but generally exceeds 80 m and consists of two units. The upper unit consists of loose, superficial Wadi gravels with a thickness ranging from 15 to 20 m. The lower unit is composed of gravel- to boulder-sized debris and is partly cemented by calcite and silica. The depth of this layer base ranges from 80 to 160 m below ground level over the Wadi Bih area.

The aquifer system in the area around the Wadi Bih dam can be classified into two aquifer units: alluvial wadi gravels and underlying weathered and karstified limestone. The superficial gravel layer forms a highly permeable aquifer with variable hydraulic properties. The gravels tend to be unconsolidated near the ground surface, becoming more cemented and consolidated with depth. The wadi sediments range in size from silts to boulders and are derived from rocks within the catchment area. Drilling information from the study area indicates an average thickness of the alluvial cover of 80 m. This alluvial cover can be divided into two units: the upper unit consists of loose gravels with boulders, and the lower unit consists of finer-grained gravels with clays and shales (Ebraheem et al. 2012). The weathered and karstified limestone of the lower aquifer unit has a relatively high groundwater potentiality. The estimated infiltration rate varies from 0 to 56 cm/h, and the lateral hydraulic conductivity ranges from 32 to 67 m/d (Murad et al. 2017). The transmissivity of sediments in the area of interest ranges from 580 to 2800 m^2/d, while the storage coefficient has been estimated at approximately 0.1 (MOEW 2010).

The aquifer system is underlain by consolidated rocks of the limestone Musandam Formation. Several small villages and farms that are located within the study area have their own wells and use groundwater for irrigation purposes. In addition, two well fields have been constructed to supply water for domestic use.

A hydrologic assessment shows that flash flood hazards in the Wadi Bih drainage basin are moderate. Flash flood events are repeated approximately every three to four years. The Wadi Bih dam mitigates flash flood hazards and increases the groundwater recharge potentiality in the vicinity of the dam. Floodwaters in wadis

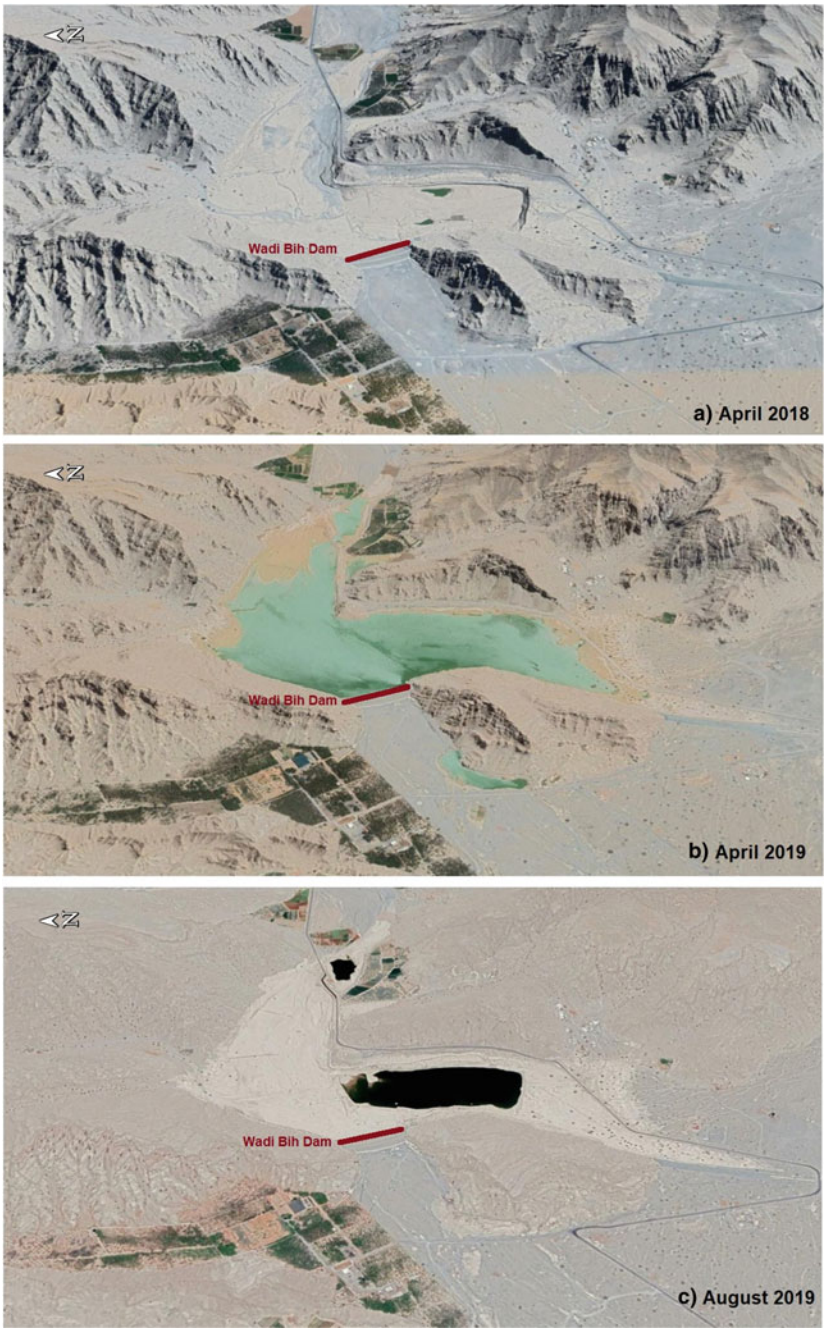

Fig. 21.2 Satellite images showing the Wadi Bih dam and reservoir in three successive time periods illustrating the reservoir before, during, and after filling with water

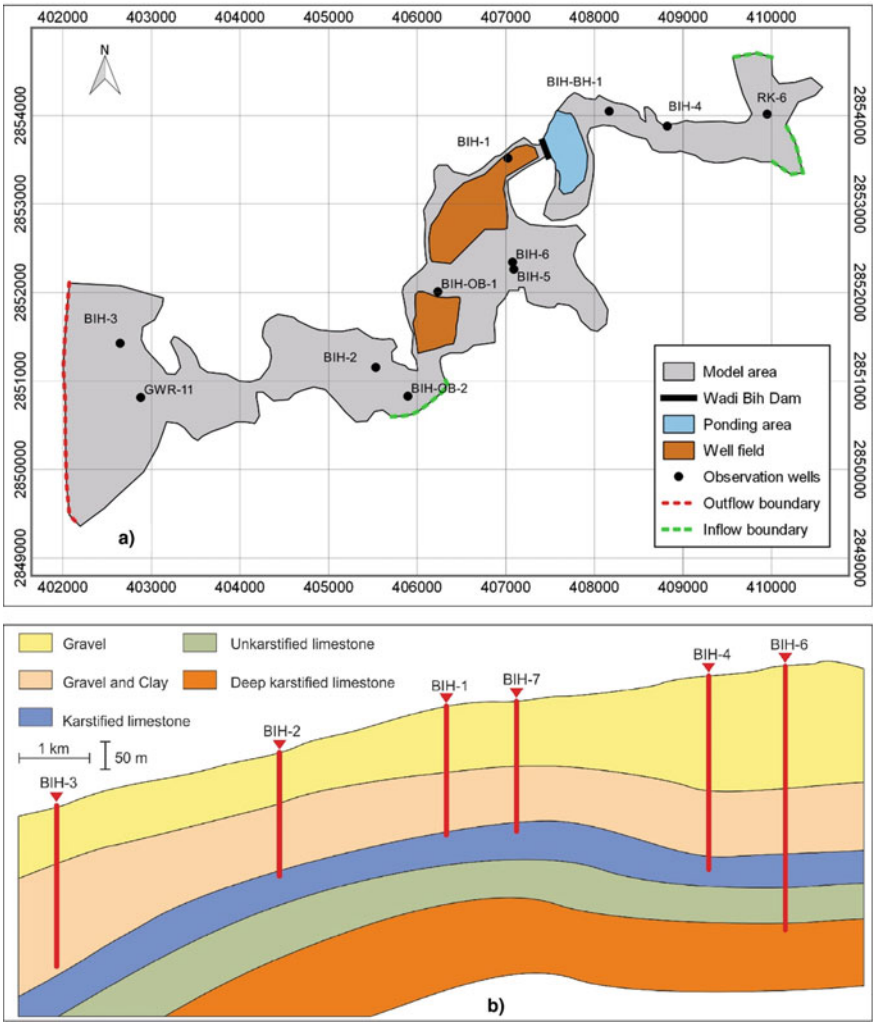

Fig. 21.3 A figure showing **a** the Wadi Bih model domain and locations of observation wells and **b** a cross section along selected wells

typically carry heavy sediment loads. As the floodwater is detained, these sediments settle, leading to clogging of the pore spaces in the upper layers of the reservoir's subsurface and the deposition of silts and sediments on the reservoir bottom. Periodic removal of these sediments enhances the percolation process of water.

21.3 Methodology

A numerical groundwater model of the Wadi Bih dam area was developed, calibrated, and validated using MODFLOW (McDonald and Harbaugh 1988). The mathematical equations used to describe groundwater flow through a porous medium are based mainly on Darcy's law and the continuity equation, which can be described as follows (Freeze and Cherry 1979):

$$\frac{\partial}{\partial x}\left(k_{xx}\frac{\partial h}{\partial x}\right)+\frac{\partial}{\partial y}\left(k_{yy}\frac{\partial h}{\partial y}\right)+\frac{\partial}{\partial z}\left(k_{zz}\frac{\partial h}{\partial z}\right)+q_s=s_s\frac{\partial h}{\partial t}$$

where K_{xx}, $K_{yy,}$ and K_{zz} represent the hydraulic conductivity in the x-, y-, and z-directions, respectively; h is the hydraulic head; q_s stands for the source/sink term; S_s refers to the specific storage; and t describes the time. This equation can be further implemented using finite difference methods through a set of algebraic equations (discrete model) to solve certain groundwater problems.

The model includes the effects of the dam in the form of increased recharge rates across the ponding area and the effects of groundwater abstraction from well fields. In subsequent simulations, the dam and well fields were deactivated to analyze their effects. The methodology is described in more detail below.

21.3.1 Conceptual Model

The developed groundwater model focuses on the area downstream of the Wadi Bih dam and covers an area of 9.60 km^2, as shown in Fig. 21.3a. The model area is bounded by limestone outcrops that act as no-flow boundaries. This boundary was justified because the depth to the groundwater in the area of interest is relatively high; hence, no horizontal flow occurs from the limestone to the Quaternary sediments of the wadi. However, the no-flow boundary is dissected by the wadi tributaries and the outlet of the wadi (green and red dotted lines in Fig. 21.3a, respectively). These were considered inflow and outflow boundaries, respectively. Available bore log information from 11 observation wells illustrated a distinct top unit of gravels and boulders, a middle unit of fine gravels with clay or shale with clay, and a bottom unit of fissured limestone. Three inflows to the modeled area exist, representing the main channel of Wadi Bih, the inflow from Wadi Qadaah, and the inflow from an unnamed tributary. The inflows were defined as specified flux boundaries. The outflow moves through the alluvial fan into the Arabian Gulf; this outflow was defined as a constant head boundary.

Localized recharge occurs through the ponding area of the dam, and diffuse rainfall recharge occurs across the remaining surface area of the model domain. Loss due to evapotranspiration from the water table was considered negligible as the depth to the water table was greater than the extraction depth. Groundwater

abstraction occurs from two well fields located downstream of the dam with a total number of 38 pumping wells (Fig. 21.3a) and from several small farms located within the study area. Figure 21.3b illustrates a subsurface cross section compiled from the bore data of available wells in the area.

21.3.2 Numerical Groundwater Model Set up

A cell size of 100 × 100 m was selected for the numerical model, resulting in 90 columns and 60 rows. The net area of the modeled aquifer was then represented by 960 active cells. The aquifer system is composed of three units, which were represented by three model layers with a total thickness ranging from 80 to 160 m. Specific yield and hydraulic conductivity values were obtained from pumping test data from the monitoring wells (Table 21.1). For each layer, the initial values were assigned through interpolation among the well locations, and the values were then adjusted during calibration. The constant head boundary representing discharge through the alluvial fan to the Arabian Gulf was set along the 0-m groundwater contour line. The inflows through the flux boundaries were initially estimated from water level fluctuations and were then adjusted during calibration.

Recharge to the aquifer was recognized in two zones corresponding to recharge from rainfall and localized recharge from dam storage for the modeling period. Rainfall recharge rates were assigned to all active cells in the model area by applying a recharge factor (i.e., the percentage of rainfall that becomes recharge) to the rainfall data obtained from the Bih rain gauge. These recharge factors were adjusted during calibration. For localized recharge, the ponding area of the dam was delineated for a medium water level, which summed up to an area of 0.31 km^2.

Table 21.1 Calibrated hydraulic conductivity and specific yield values at observation well locations

Well	Hydraulic conductivity (m/day)			Specific yield		
	Layer-1	Layer-2	Layer-3	Layer-1	Layer-2	Layer-3
BIH-1	150.0	10.0	75.0	0.008	0.0001	0.02
BIH-2	100.0	10.0	50.0	0.001	0.0001	0.0005
BIH-3	100.0	10.0	50.0	0.001	0.00001	0.0005
BIH-4	150.0	75.0	75.0	0.008	0.001	0.001
BIH-5	100.0	75.0	75.0	0.008	0.001	0.001
BIH-6	100.0	75.0	75.0	0.008	0.001	0.001
BIH-O.B-1	150.0	75.0	75.0	0.008	0.001	0.001
BIH-O.B-2	150.0	75.0	75.0	0.008	0.001	0.001
BIH-B.H-1	150.0	75.0	75.0	0.008	0.001	0.001
BIH-RK-6	150.0	75.0	75.0	0.008	0.001	0.001
GWR-11	150.0	10.0	50.0	0.001	0.00001	0.0005

Recharge rates were assigned to the cells within the ponding area based on the storage period and on a recharge factor applied to the rainfall data. The recharge factor was adjusted during calibration. Abstraction rates were initially estimated from abstraction data that was obtained from local authorities. As complete records were not available for all wells, these abstraction rates were also adjusted during calibration. Groundwater levels during December 1988 of all available observation wells were used to derive the initial head distribution in the study area, as groundwater extraction before 1990 was limited (Al Asam 1997; Rizk and Alsharhan 2003).

21.3.3 Model Calibration and Validation

The model was calibrated for the period between January 1989 and December 1993 and was subsequently validated with observed water level data from January 1994 to December 2004. Monthly groundwater level data from 7 observation wells were available for the comparison of the simulated heads with the observed heads. The model calibration was achieved by manually adjusting the following parameters (through trial and error): hydraulic conductivity, specific yield, recharge factors (percentage of rainfall), pumping rates, and inflow across boundaries. The model calibration and validation were evaluated using the following standard error statistics (Sorooshian and Gupta 1995): mean error (ME), root mean square error (RMSE), coefficient of determination (R^2), and Nash–Sutcliffe efficiency or model efficiency (EF).

The mean error between the predicted values and observed values can be defined as follows (i = 1 to N):

$$ME = \frac{1}{N}\sum_{i=1}^{N}(O_i - P_i)$$

The standard deviation of the differences between the predicted values and observed values was represented by the root mean square error (RMSE) as follows:

$$RMSE = \sqrt{\frac{1}{N}\sum\nolimits_{i=0}^{N}(O_i - P_i)^2}$$

The coefficient of determination R^2 represents the squared value of the coefficient of correlation and can be described as follows:

$$R^2 = \left(\frac{\sum_{i=0}^{N}\left(O_i - \bar{\mathrm{O}}\right)\left(P_i - \bar{\mathrm{P}}\right)}{\sqrt{\sum_{i=0}^{N}\left(O_i - \bar{\mathrm{O}}\right)^2}\sqrt{\sum_{i=0}^{N}\left(P_i - \bar{\mathrm{P}}\right)^2}} \right)^2$$

Nash and Sutcliffe (1970) described model efficiency as one minus the sum of the absolute squared differences between the predicted and observed values, normalized by the variance of the observed values along the period under interest, as follows:

$$EF = \frac{\sum_{i=1}^{N}(O_i - \bar{O})^2 - \sum_{i=1}^{N}(O_i - P_i)^2}{\sum_{i=1}^{N}(O_i - \bar{O})^2}$$

$$EF = 1 - \frac{\sum_{i=0}^{N}(O_i - P_i)^2}{\sum_{i=0}^{N}(O_i - \bar{O})^2}$$

where N is the total number of observations, O_i is the observed groundwater level of the ith observation, P_i is the estimated groundwater level of the ith observation, and $\bar{O}$ is the mean of the observed groundwater levels.

21.3.4 Simulations

The calibrated and validated model, which comprises groundwater abstraction as well as recharge from the dam and thus represents the actual conditions, was defined as the base case. Subsequently, simulations were performed to analyze the following cases.

21.3.4.1 Effect of the Dam on Groundwater Recharge

To study the effect of the dam on groundwater recharge, the model was run with the localized recharge from the ponding area switched off. The total recharged volume over the simulation period from January 1994 to December 2004 was computed and compared with the base case. The dam efficiency was calculated as the ratio of groundwater recharge from the ponding area to water storage in the reservoir, which was obtained from field observations.

21.3.4.2 Impact of Present Exploitation

To analyze the impact of the present exploitation of the aquifer, the model was run with all abstractions switched off, and the simulated water table was compared with the water table of the base case over the validation period.

21.3.4.3 Comparison of Predevelopment and Postdevelopment States

A predevelopment state is characterized by the absence of both recharge from the dam and groundwater abstractions. To simulate this state, the recharge from the ponding area and all abstractions were switched off, and the simulated water table was compared with that of the base case representing the postdevelopment state.

21.4 Results and Discussion

21.4.1 Calibrated Model Parameters and Model Performance

The calibrated hydraulic conductivity values ranged from 100 to 150 m/d in layer 1 and from 10 to 75 m/d in layers 2 and 3 (Table 21.1). The specific yield values were approximately 0.008 in layer 1 and 0.001 in layers 2 and 3, with a total range from 0.00001 to 0.02 (Table 21.1).

The calibrated rainfall recharge factor is 20% of rainfall. This value falls within the reported values for alluvial gravels in UAE (IWACO 1986; MGGS 1996). The existence of sands and gravels in the studied aquifer system area permits such aquifer recharge. Field observations also indicated the direct effect of rainfall events on groundwater levels (Ebraheem et al. 2012). The localized recharge due to storage in the ponding area was calibrated to 25% of rainfall. Calibrated groundwater abstraction rates increased significantly from 1998. The highest abstraction rates occurred in 2000. After 2001, abstraction rates were steady. The calculated versus observed groundwater levels are represented in Fig. 21.4 for four selected observation wells. As illustrated by the figure, the model very closely simulates the groundwater levels that developed due to groundwater extraction and recharge from dam storage and rainfall events. However, a few discrepancies are apparent, which may be attributed to the accuracies of the observed groundwater levels that used to be measured only once every month and not necessarily on the same day each month. For the validation period, the simulated groundwater levels are also in good agreement with the observed records (Fig. 21.4), confirming that the model can represent the given conditions in the study area.

The predicted and observed water levels were evaluated with standard tests for both the calibration and validation periods. Table 21.2 provides relevant statistics related to the observed and simulated groundwater levels during the calibration and validation periods. The differences between the means, maximums, minimums, and standard deviations of the predicted and observed values are very small for both the calibration and validation periods. The coefficient of determination, R^2, is very close to one in both periods. Apart from high R^2 values, it is prudent to consider additional information provided by the gradient and the intercept of the regression on which the R^2 is based. In the present case of the calibration and validation

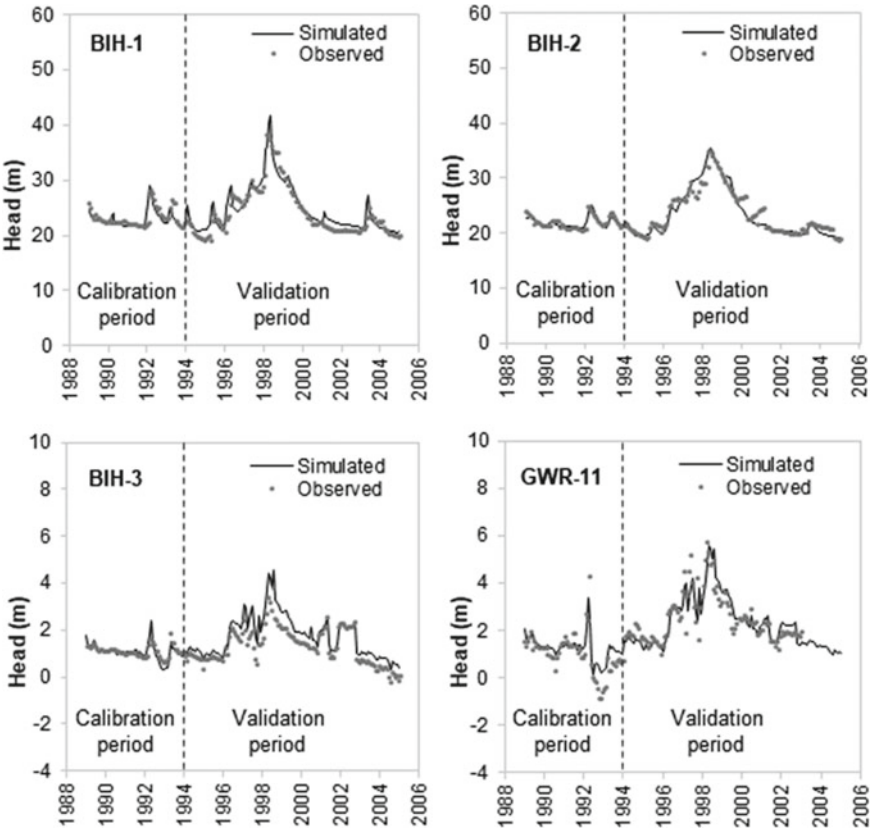

Fig. 21.4 Observed and simulated hydrographs at four observation wells

periods, good agreement of this intercept was observed (Fig. 21.5). The intercept is close to zero, which means that an observed head of zero would also result in a prediction near zero. The gradient is very close to one, showing that the observed and predicted values are very close to each other (Fig. 21.5). Furthermore, the mean error (ME) and RMSE values for the calibration and validation periods are acceptably low (Table 21.2). The model efficiency (EF) estimates the error relative to the natural variation in the observed values; the EF varies from $-\infty$ to 1.00. The EF becomes zero in the case that the square of errors between the predictions and observations equals the variation of the observations. Values of $0.50 \leq \text{EF} \leq 1.00$ are deemed satisfactory (Singh 2011). In this study, the EF values are 0.997 and 0.987 for the calibration and validation periods, respectively, showing good agreement between the predicted and observed groundwater levels. This agreement indicates that the developed model is fit to use for long-term predictions.

Table 21.2 Statistical parameters of observed and simulated groundwater levels

Parameter	Calibration period			Validation period		
	Observed (m)	Calculated (m)	Difference (m)	Observed (m)	Calculated (m)	Difference (m)
Max	28.15	29.10	0.94	38.38	41.59	3.20
Min	−0.87	0.18	1.05	0.03	0.32	0.30
Mean	11.70	11.68	0.02	16.38	16.50	0.13
STDEV	10.81	10.67	0.14	11.49	11.17	0.32
ME		0.027		0.158		
RMSE		0.041		0.030		
EF		0.997		0.986		
R^2		0.997		0.987		

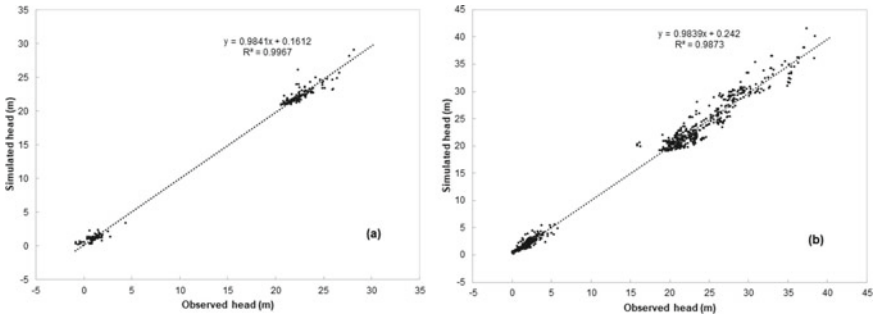

Fig. 21.5 Observed versus simulated heads for the **a** calibration period and **b** validation period

21.4.2 Water Balance

Yearly water balances derived from the model results over the validation period are shown in Fig. 21.6. Maximum recharge occurred during years of high rainfall (1995–1998). Minimum recharge occurred in 2000, 2002, and 2004. The major contribution to the water balance resulted from subsurface inflows from the upper wadi zone and the two tributaries. The net constant head outflow was greater during wet periods than during dry periods. The outflow storage component was also greater during wet periods. Groundwater abstraction increased from 1998 and peaked in 2000, which was a dry year. After that, abstraction remained relatively steady at a rate of approximately 4.3 MCM (million m^3) per year. Overall, the annual water balance was negative in most years, with an average net decline of 0.6 MCM per year, indicating a slow but continuous depletion of groundwater resources.

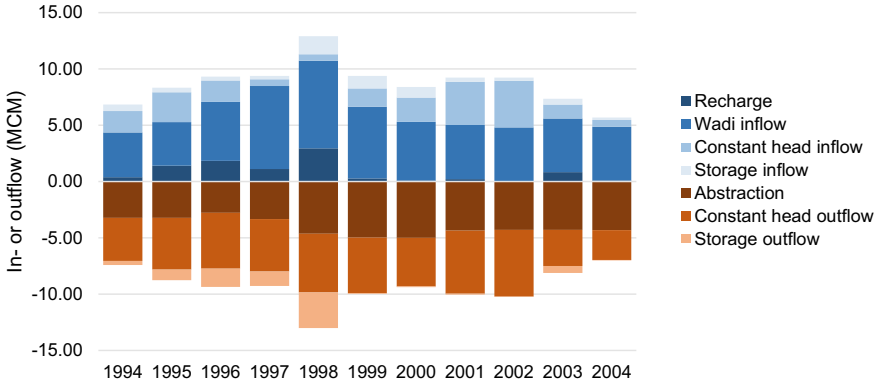

Fig. 21.6 Annual water balances derived from the groundwater model

21.4.3 Effect of the Dam on Groundwater Recharge

To evaluate the effect of the dam on replenishing the groundwater aquifer, a model simulation was conducted without the dam (i.e., no recharge from the ponding area), and the results were compared with the base case representing the actual conditions that included recharge from the dam. At the end of the simulation period (December 2004), the total groundwater recharge due to rainfall and water storage in the ponding area was 9.81 MCM (Fig. 21.6). Without the dam, the total simulated recharge was 2.58 MCM. Thus, the extra groundwater recharge caused by dam construction was 7.22 MCM over a period of 11 years and three months, representing 74% of the total recharge. These results indicate that the majority of groundwater recharge is due to infiltration from the water stored in the ponding area of the dam. This result can mainly be attributed to the increased duration of infiltration, as the average duration of ponding was 60 days per year, while direct recharge from rainfall only occurred during a few rain events per year.

The cumulative recharge curves shown in Fig. 21.7 further illustrate the effect of the dam on groundwater recharge. The figure also shows that the majority of recharge over the simulation period occurred throughout the wet period from 1995 to 1998. The total water storage in the ponding area was estimated to be 22.98 MCM over the simulation period. With the total recharge from the ponding area of 7.22 MCM, the efficiency of the dam, which is the ratio of groundwater recharge to storage, is 31.4%. This result indicates that a major part of the water that infiltrates through the ponding area is stored in the unsaturated zone, resulting in an increase in the moisture content of the soil. Additionally, losses occur through evaporation from the reservoir. The efficiency of the Wadi Bih dam is a medium value compared to findings from other nearby dams. At Wadi Ham, approximately 100 km from the study area, the efficiency of the dam was found to be 47%, and at Wadi Tawiyean (50 km from the study area), it was approximately 22% (Sherif et al. 2017).

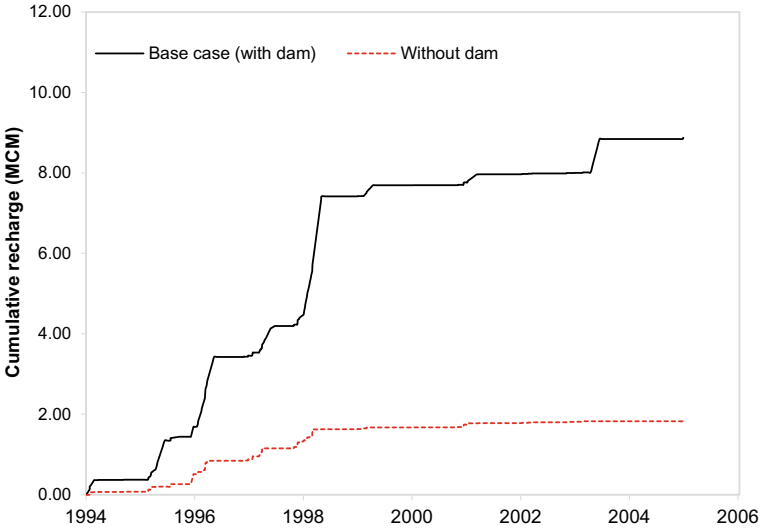

Fig. 21.7 Cumulative recharge with and without dam

21.5 Impact of Present Exploitation

The Wadi Bih model was employed to simulate the impacts of extraction from the well fields in the study area. For this simulation, the extraction values were excluded from the model, and the calculated water table was compared with the base case (Fig. 21.8). The results indicate that without abstraction, water levels would have reached much higher levels. The impact of groundwater abstraction is greater during periods of low groundwater recharge and low water levels. The minimum effects of abstraction are noticed during wet years (1995–1998). Additionally, the minimum impacts of abstraction occur close to the alluvial fan and away from the well fields (wells BIH-3 and GWR-11).

21.5.1 Predevelopment Versus Postdevelopment

A comparison between the predevelopment state (i.e., no abstractions and no dam) and the postdevelopment state (base case) shows that the peaking responses of the water levels in wells located near the ponding area of the dam are due to enhanced recharge from dam storage (Fig. 21.8). Without the dam, the water level response would be much smoother. The comparison also shows that the impact of the dam is small compared to the impact of abstraction. The dam is only able to compensate for a small proportion of the water table decline that occurs due to abstraction. After the wet period, the water table would have stayed at a high level without

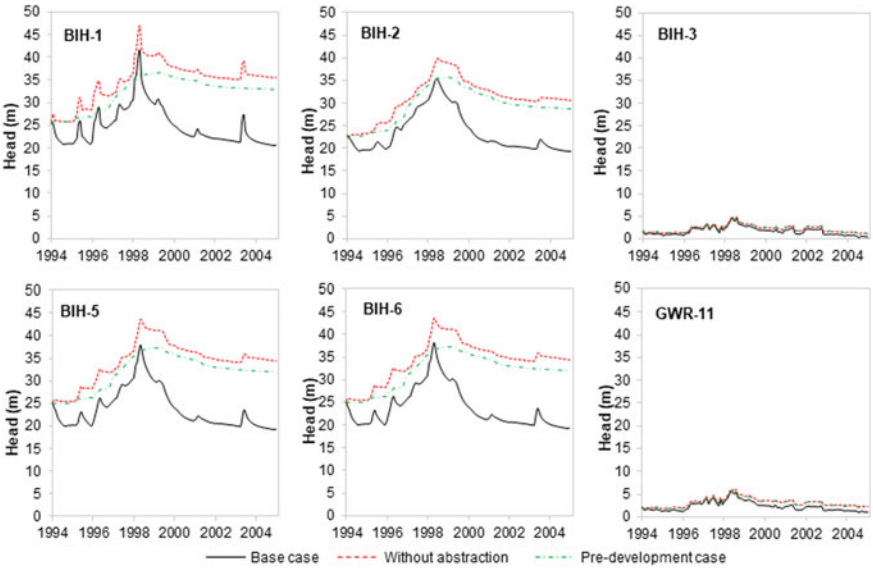

Fig. 21.8 Simulated hydrographs at selected observation wells representing the base case, the case without abstraction, and the predevelopment case (no dam, no abstractions)

abstraction. However, abstraction has led to a decline in the water table to a level prior to that observed during the wet period, with a trend that indicates further decline. At the wells located away from the dam and the well fields (BIH-3 and GWR-11), there are only small differences between pre- and postdevelopment. However, the postdevelopment groundwater levels approach sea level at these wells, which means that further declines in water levels may lead to intrusions of seawater and deterioration of the water quality.

21.6 Conclusion

A numerical groundwater model was developed to evaluate the effects of a groundwater recharge dam in Wadi Bih (UAE) on recharge rates and volumes. Furthermore, the model was employed to reconstruct predevelopment groundwater dynamics to analyze the impact of current groundwater exploitation and the combined impacts of abstraction and recharge from the dam on groundwater resources. Dam-induced recharge was found to have a strong effect on the aquifer's water levels, particularly during years with large amounts of rainfall. Recharge from the ponding areas of the dam was found to contribute 74% of the total recharge. Approximately 31% of the water stored in the reservoir is infiltrated and thus recharges the aquifer. However, the strongest effect on the water levels in the study area is from groundwater abstraction from the well fields. This effect is particularly

pronounced during dry periods when recharge is low. The present exploitation rate leads to a negative water balance, indicating that the current groundwater use is not sustainable. The dam-induced recharge is not sufficient to compensate for the high abstraction rates. These results indicate that to achieve sustainable management of the groundwater resources in Wadi Bih, an integrated solution must be pursued that considers demand management as well as options to further mitigate the impacts of abstraction.

References

Al Asam MS (1997) Application of geophysical and geochemical techniques for the assessment of groundwater recharge from Wadi Al Bih Dams, Ras Al Khaimah, United Arab Emirates. Master's Thesis, United Arab Emirates University

Dillon P, Arshad M (2016) Managed aquifer recharge in integrated water resource management. Integrated groundwater management. Springer, Cham, pp 435–452

EAD (2018) Groundwater Atlas of Abu Dhabi Emirate. Environment Agency—Abu Dhabi, Abu Dhabi

Ebraheem AM, Sherif MM, Al Mulla MM et al (2012) A geoelectrical and hydrogeological study for the assessment of groundwater resources in Wadi Al Bih, UAE. Environ Earth Sci 67:845–857. https://doi.org/10.1007/s12665-012-1527-0

Freeze RA, Cherry JA (1979) Groundwater: Englewood Cliffs. Prentice-Hall, NJ, p 604

IWACO (1986) Groundwater study. Drilling of deep water wells at various locations in the UAE. Ministry of Environment and Water, United Arab Emirates

Jaafar HH (2014) Feasibility of groundwater recharge dam projects in arid environments. J Hydrol 512:16–26. https://doi.org/10.1016/j.jhydrol.2014.02.054

Maliva R, Missimer T (2012) Arid lands water evaluation and management. Springer Science & Business Media

McDonald MG, Harbaugh AW (1988) A modular three-dimensional finite-difference ground-water flow model. U. S. Geological Survey

MGGS (1996) Wadi Bih Catchment study for evaluation of water resources and recharge function of the dam. Project 37/96, Internal Report (vol 1). Groundwater development in the northern agricultural region. Ministry of Environment and Water, Dubai, UAE

Missimer TM, Guo W, Maliva RG et al (2015) Enhancement of wadi recharge using dams coupled with aquifer storage and recovery wells. Environ Earth Sci Heidelb 73:7723–7731. https://doi.org/10.1007/s12665-014-3410-7

MOEW, Ministry of Environment and Water (2010) United Arab Emirates water conservation strategy. Ministry of Environment and Water, Dubai, UAE

Murad A, Gaber A, Mahmoud S, Arman H, Al Dhuhoori A (2017) Investigations of upper most soil zone characterizations and its impact in on recharging the shallow groundwater aquifer in arid region: a case study on Wadi El Bih Dam, Ras Al Khaimah, Northern Emirates, United Arab Emirates (UAE). Proceeding of 12th Guld Water Conference, pp 28–30. March 2017, Manama, Bahrain

Murad A, Hussein S, Arman H, Al Dahahn A (2020) Flash floods in the United Arab Emirates (UAE). In: The Fifth International Symposium on Flash Floods in Wadi Systems, ISFF2020, Kyoto University, Kyoto, Japan

Nash JE, Sutcliffe JV (1970) River flow forecasting through conceptual models part I—a discussion of principles. J Hydrol 10:282–290. https://doi.org/10.1016/0022-1694(70)90255-6

Rizk ZS (2015) Why Wadi Al Bih limestone is the most sustainable aquifer in the United Arab Emirates? Int. J. Sustain Water Environ Syst 7(1):21–28

Rizk ZS, Alsharhan AS (2003) Water resources in the United Arab Emirates. In: Alsharhan AS, Wood WW (eds) Developments in water science. Elsevier, pp 245–264

Rizk ZS, Alsharhan AS, Wood WW (2007) Sources of dissolved solids and water in Wadi Al Bih aquifer, Ras Al Khaimah Emirate, United Arab Emirates. Hydrogeol J 15:1553–1563. https://doi.org/10.1007/s10040-007-0188-7

Sherif M, Akram S, Shetty A (2009) Rainfall analysis for the Northern Wadis of United Arab Emirates: a case study. J Hydrol Eng 14:535–544. https://doi.org/10.1061/(ASCE)HE.1943-5584.0000015

Sherif M, Ebraheem A, Shetty A (2017) Groundwater recharge from dams in United Arab Emirates. In: Proceedings of the world environmental and water resources congress 2017, Sacramento, CA

Sherif M, Ebraheem AM, Al Mulla M, Shetty A (2018) New system for the assessment of annual groundwater recharge from rainfall in the United Arab Emirates. Environ Earth Sci 77:412. https://doi.org/10.1007/s12665-018-7591-3

Singh A (2011) Estimating long-term regional groundwater recharge for the evaluation of potential solution alternatives to waterlogging and salinisation. J Hydrol 406:245–255. https://doi.org/10.1016/j.jhydrol.2011.07.004

Sorooshian S, Gupta VK (1995) Model calibration. In: Singh VP (ed) Computer models of watershed hydrology. Colorado, pp 23–68

Chapter 22
Assessment of the Impacts of Groundwater Overdrafting on Water Quality and Environmental Degradation in the Fares Area, Aswan, Egypt

Mohamed Saber, Omar Ahmed, Esmat A. Keheila, Mohamed Abdel-Moneim Mohamed, Sameh A. Kantoush, Mohammed Abdel-Fattah, and Tetsuya Sumi

Abstract Groundwater contamination and the environmental impact of groundwater uprising due to overpumping are critical issues in Egypt. The main purpose of this study is to evaluate the groundwater quality and the environmental impacts of groundwater uprising in the Fares area of Aswan, Egypt. The environmental impacts of the uprising groundwater level were investigated through field observations and chemical analyses of the surrounding water resources. The results revealed that the use of flood irrigation systems in the upper, newly reclaimed land area is the main cause of the uprising groundwater levels, which causes remarkable environmental degradation in the urban area. Thirty-three samples were collected and chemically analyzed from three groundwater wells. The chemical characterization of the groundwater at Well 1 drastically changed from NaHCO3 to NaCl within a short period of time due to overdrafting. The chemical concentrations of all parameters showed considerable increasing trends and exceeded the standard limits at Well 1. The study stated that the groundwater overdrafting causes extreme changes in the water quality within a very short period of time along with the impacts on the environment. This condition requires attention from decision makers, as the groundwater quality is continuously decreased and the environment is degraded.

Keywords Groundwater Quality · Hydrochemical analysis · Overdrafting · Environmental impacts · Groundwater level uprising · Aswan · Egypt

M. Saber (✉) · S. A. Kantoush · T. Sumi
Disaster Prevention Research Institute (DPRI), Kyoto University, Kyoto 123, Japan
e-mail: mohamedmd.saber.3u@kyoto-u.ac.jp

O. Ahmed · E. A. Keheila · M. A.-M. Mohamed
Geology Department, Faculty of Science, Assiut University, Asyut 71516, Egypt

M. Abdel-Fattah
Civil Engineering and Quantity Surveying Department, Military Technological College, P.O. Box: 262, P.C: 111, Muscat, Oman

T. Sumi et al. (eds.), *Wadi Flash Floods*, Natural Disaster Science and Mitigation Engineering: DPRI Reports, https://doi.org/10.1007/978-981-16-2904-4_22

22.1 Introduction

Groundwater is an important source of fresh water for agricultural, drinking, and domestic uses in many regions of the world (Balachandar et al. 2010). It is estimated that approximately one-third of the world's population uses groundwater for drinking (Nickson et al. 2005). The increase in the population and its needs have led to the deterioration of surface and subsurface waters (Dhiviyaa et al. 2011). In 1999, the United Nations Environment Programme (UNEP) reported that approximately 200 scientists in fifty countries had identified water scarcity as one of the two most worrying problems for the new millennium (United Nations Environmental Program (UNEP) 2002). Groundwater is a major source of drinking water worldwide and plays a vital role in maintaining the ecological value of many areas (IPCC 2001). The reliability of groundwater for drinking lies not only in its widespread occurrence and availability but also in its consistently good quality, all of which makes it an ideal source of drinking water (UNESCO 2000).

In general, the motion of groundwater along its flow paths below ground surfaces increases the concentration of chemical species (Freeze and Cherry 1979; Domenico and Schwartz 1990; Kortatsi 2007), and the concentrations of dissolved ions in groundwater are controlled by the nature of geochemical reactions, lithology, residence time, groundwater flow, solubility of salts, and human activities. Moreover, groundwater quality is influenced by natural geochemical processes, ion exchanges, and human activities such as agriculture, sewage disposal, and the creation of industrial wastes. Recently, several studies have focused on monitoring groundwater quality and evaluating domestic and agricultural activities worldwide (Mitra et al. 2007; Jain et al. 2009; Hakim et al. 2009; Nagarajan et al. 2010). In Egypt, groundwater quality evaluation and monitoring have received little attention; therefore, these types of analyses are urgently needed in Egypt to understand the hydrochemistry and quality changes of groundwater.

The World Health Organization calculated that up to 80% of all sicknesses and diseases in the world are products of inadequate sanitation, polluted water, or water scarcity (WHO 2004). Among fresh waters, only approximately 5% are readily available for beneficial use (Usharani et al. 2010). The microbiological quality of water is measured by analyses and enumerations of indicator microorganisms (Briancesco 2005). Groundwater is a crucial source of drinking water, and its quality has recently become vulnerable due to a combination of over-abstraction and microbiological and chemical contamination (Pedley and Howard 1997; Reid et al. 2003; Aydin. 2007). Additionally, worldwide, 780 million people do not have access to high-quality water sources, and an estimated 2.5 billion people, half of the developing world, lack access to proper sanitation (WHO/UNICEF 2012). Approximately 88% of deaths due to diarrheal illness are attributable to low-quality water, improper sanitation, or poor hygiene (Liu et al. 2010). Diarrheal diseases (e.g., cholera) kill more children than AIDS and malaria, making them the second leading cause of death among children under 5 years old (Liu et al. 2010). More than 1.5 million children die every year from diarrheal diseases (Fenwick 2006).

The most important pathogenic bacteria and viruses that might be transported in groundwater are Salmonella sp., Shigella sp., Escherichia coli and Vibrio sp., and the hepatitis virus, Norwalk virus, echovirus, poliovirus, and coxsackie viruses (Corapcioglu and Haridas 1984; Craun 1984; Gerba et al. 1981).

Although water is a renewable resource, the population of Egypt tripled in 50 years, from 19 million individuals in 1947 to approximately 62 million individuals in 1996, and it is expected to be approximately 95 million by 2025. Consequently, the water demand will increase daily; however, Egypt's share of Nile River water is fixed. Egypt's quota of Nile River water is 55.5 billion cubic meters, so the availability of surface water will become inconvenient, insufficient, or infeasible for consumption with an increasing population, considering that groundwater exhaustion occurs faster than its percolation back into the ground (Trivedy et al. 1987); this effect leads to the increasing importance of groundwater every day. In Egypt, 87.7% of the total water is consumed by agriculture and 5.4% is consumed by industry, while the total human consumption accounts for 6.8% of the total water use (Shalaby 2005). One important issue involves redistributing the population over a large area because 99% of the population is concentrated in the Nile River valley and delta. Therefore, the Egyptian government is determined to increase agricultural production by increasing cultivated areas through the reclamation of new lands in the desert. This particular practice would not only increase the total cultivated area in Egypt but would also relieve the population stress on the narrow Nile Valley land and create new employment opportunities. This paper is a part of a comprehensive study of groundwater quality evaluations and modeling considering the environmental impacts that occur at different locations in Egypt due to the vulnerability of the pollution and the importance of water resources; hydrochemical and bacteriological analyses have been conducted in the Manfalut District of Assiut, Egypt, and researchers have concluded that approximately 55% of the local groundwater wells are not suitable for drinking due to the impacts of chemical and bacteriological contamination (Saber et al. 2014).

During the last decade, a number of inhabitants (farmers) started to reclaim and cultivate new lands in the Fares area of Aswan Governorate, Egypt, because these inhabitants depend mainly on agriculture as a main source of income. Consequently, most of the reclamation and irrigation systems in this region have been implemented without any prior scientific or hydrological surveys. For instance, flood systems are used for irrigation from groundwater wells, which could be very risky for groundwater storage in this area. Therefore, the objectives of the present study are (a) to evaluate the quality of the groundwater in the Fares area of Aswan, which covers both the Nile floodplains and desert fringes, (b) to understand the changes in groundwater chemistry that occur due to groundwater overdrafting, and (c) to maintain the sustainability of groundwater, especially as the groundwater demand in the reclaimed land increases continuously, which may influence the efficiency of the water supply both qualitatively and quantitatively. The evaluation of groundwater quality in the Fares area is challenging, mostly due to the low numbers of existing groundwater wells and a lack of data. Additionally, in the study area, the most critical issue is that the lowland areas suffer from groundwater

uprising, resulting in the loss of many mango gardens and gardens of other fruits as well as damage to the infrastructure of the city, such as houses and buildings. Additionally, the uprising of groundwater has a large environmental impact in terms of health threats and the spread of diseases due to the pollution of surface water. Thus, one of the most important objectives of this study is to assess and evaluate the environmental impacts in the target area that results from the excessive use of groundwater for irrigation.

22.2 Study Area

The study region (Fig. 22.1) is located on the west bank of the Nile River, northwest of Aswan city. The area extends between latitudes 24° 34′–24° 40′ N and longitudes 32° 51′–32° 55′ E. It covers an area of approximately 25 km^2. The total population of the area is approximately 15,000 inhabitants, and most of the economic activity in the study area involves agriculture. The irrigation system is mostly fed by groundwater as well as the canal system. The selected area comprises an arid region that is characterized by a hot and dry climate with no rainfall in summer and a mild climate with rare rainfall in winter. In winter, the average temperatures range from 11 °C at night to 25 °C during the day, and the average summer temperatures range from 25 °C at night to 40 °C during the day.

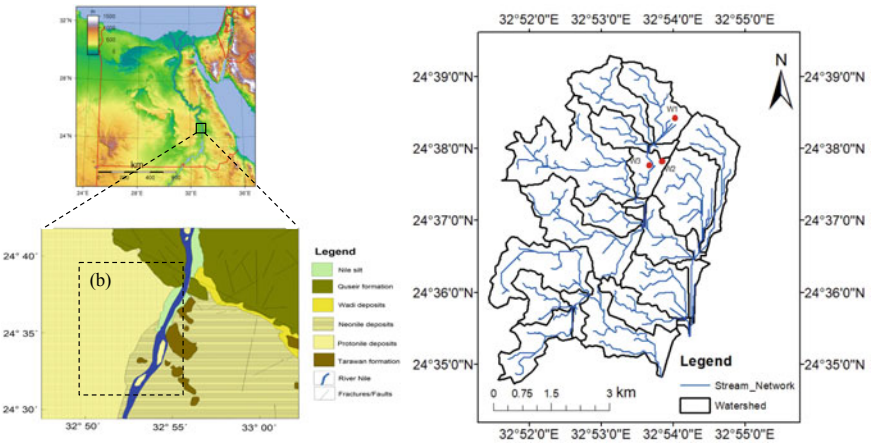

(a) (b)

Fig. 22.1 **a** Location and geological map of the Fares area in Aswan, Egypt (modified after the new geological map of Egypt (Failed 1977; EGPC and Conoco 1987), **b** developed watershed and stream network of the target

22.3 Geological and Hydrogeological Setting

The study area is located in Aswan Governorate, in the western desert and east of the El-Gallba plain (the western part of the Kom Ombo basin) and north of the Wadi of El-Kubanyia. Geologically, it is situated within the African platform; thus, its tectonic framework is related to the last African orogenic belt (Said 1962; Abd El-Razik and Razavaliaev 1972). The borehole lithology in the Fares area collected from a field survey indicates that Quaternary sediments comprising sands constitute the upper layer and are underlain by shaley sand, sandy mud, and medium- to coarse-grained sand, followed by coarse-grained sand and gravels saturated with water.

The area is characterized by gentle northeast slopes oriented toward the Nile River. Additionally, on the western side of the Nile River, there is a wide plain occupying approximately 20 km^2, which is bordered by the western high plateau as well as some sand dunes and reclaimed agricultural land areas. There is also a narrow flat area east of the Nile River bordered by a limestone plateau to the east (Ministry of Water Resources and Irrigation (MWRI) 2007). The topographic features were constructed from surface elevation data during a field trip, showing that the average elevation varies from approximately 86 m above sea level in the eastern part (urbanized city) to approximately 123 m above sea level in the western part (reclaimed lands). The study area is occupied by sedimentary rocks (Fig. 22.1) belonging to the Upper Cretaceous and Quaternary Periods, which represent the main water-bearing unit in the Nile Valley region; these deposits belong to the Proto-Nile River system occupying the present Nile basin and are made up of gravels and coarse-grained sand embedded in a brown matrix (Said 1962, 1981; Ministry of Water Resources and Irrigation (MWRI) 2007).

Climatologically, the area under investigation comprises a part of the arid belt of North Africa, which is characterized by long, hot summers and short, warm winters with rare rainfall. Based on the climatic data obtained from the Egyptian Meteorological Authority and from previously published studies, the average maximum air temperature during the period from 1998 to 2012 ranged between 28.8 °C in winter and 42.4 °C in summer, and the average minimum temperature ranged between 10.7 °C and 27.1 °C in winter. The average annual rainfall value over the area in winter is 0.1 mm and in spring is 0.5 mm; rainfall in autumn is rare. The relative humidity differs from season to season: in the winter, it ranges between 33.9 and 40.3%; in the autumn, it ranges from 26.5 to 30.1%; and the relative humidity decreases in both spring and summer to range between 15 and 20.7%. In the spring and summer, the average wind velocities are 13.7 and 14.4 kt, respectively, whereas in autumn and winter, they are 13.1 and 12.2 kt, respectively. The calculated aridity degree for Aswan Governorate based on the Emberger formula (Emberger 1951) is 0.0153, which indicates typical desert climatic conditions.

22.4 Environmental Investigations

Predicting the environmental consequences of human development and planning appropriate measures to eliminate or reduce these adverse effects and to augment positive effects are formal processes (Dougerty et al. 1995). Groundwater plays an important role in satisfying the water requirements of most arid and semiarid areas. Thus, groundwater sustainability and the preservation of groundwater quality should receive priority attention to enable countries to plan water and land use in an integrated manner and to avoid irreversible environmental damage. Land reclamation projects have been undertaken to increase Egypt's arable land area. In the area of Fares, Aswan, the environmental situation is drastically represented by the rising groundwater level, resulting in environmental impacts on agricultural fields and the houses and property of humans. In this study, several field observations were conducted to understand and determine the reasons for groundwater uprising. The study area is suffering from groundwater uprising, which has affected the urbanized Fares area by causing the collapse of approximately 64 resident homes; 500 homes have been damaged, and the tombs of the city have been affected, forming swamps and covering the low-lying agricultural areas (Fig. 22.2A, B, C, D, and E). Consequently, approximately 500 acres of farmland have been damaged, and groundwater uprising has hindered the establishment of the Kalabsha Corridor project (Fig. 22.2F), which is considered a vital project in Aswan Governorate.

During a field trip, we conducted observations of the affected regions as well as a discussion with the people of Fares to see the extent to which they are suffering from the problem of groundwater level uprising. We found that the impacts of groundwater uprising in the Fares area started in 2010, one year after agriculture activities such as flood irrigation began in the new reclamation areas (upstream area) in the desert. This is also confirmed by the changes in land use and agricultural lands observed from Google Earth images between October 2009 and August 2010, showing the expansion of agricultural lands (Fig. 22.3) within one year and, consequently, the expansion of development in the low-lying areas (agricultural farms, houses, and most infrastructure).

Farmers are using flooding systems to irrigate the new reclamation lands, and unfortunately, these systems are used unwisely and excessively and are undoubtedly a principal cause of the increase in the groundwater level. In addition, these lands have no drainage system. The excessive water from the flood irrigation systems flows directly to the downstream area, which is identified and confirmed in the developed watershed of the area (Fig. 22.1b). The watershed of the study area was developed by GIS and a digital elevation model and illustrates that the water flow direction is from the reclamation area (upper lands, land elevation is 123 m) toward the impacted area in the lowlands (land elevation is 86 m).

Chemical analysis was performed to determine the source of the uprising groundwater in the affected regions and to determine whether this effect originates from the surface drainage system (Nile River) or from the groundwater wells. Water samples were collected and analyzed (Table 22.1) from the impacted areas and from

Fig. 22.2 Field observations show the regions affected by groundwater uprising: **A** graveyard in the Fares area (15/4/2013), **B** affected mango tree farm (water depth approximately 75 cm), **C** residents' home in the Fares area, **D** dug hole showing groundwater uprising, **E** groundwater uprising inside residential houses, and **F** bridge of the Kalabsha Corridor is hindered by groundwater uprising (All photos were taken by Mohamed Saber, during the field survey on 2012)

drainage surface water to distinguish and identify the source of the leaching water. It was found that the seepage water characteristics are mostly similar to the groundwater well characteristics, which confirms that the uprising water in the lowlands (the affected regions) is mainly sourced from groundwater wells.

The recommended solution for reducing groundwater uprising is the construction of a surface drainage system that collects excessive water resulting from surface flood irrigation systems. These surface drainage systems may include land smoothing or grading, field ditches, and open drains or channels that provide an outlet for accumulated water (Ritter and Shirmohammadi 2001; Irwin 1997). The construction of subsurface drainage (tiles) will remove the excess water from the plant zone and lower the water table (Ritter and Shirmohammadi 2001). In addition, dewatering wells can reduce groundwater levels in lowland areas. The most important recommendation of this study is for both farmers and decision makers to use new irrigation systems, such as drip or sprinkler systems, instead of flood

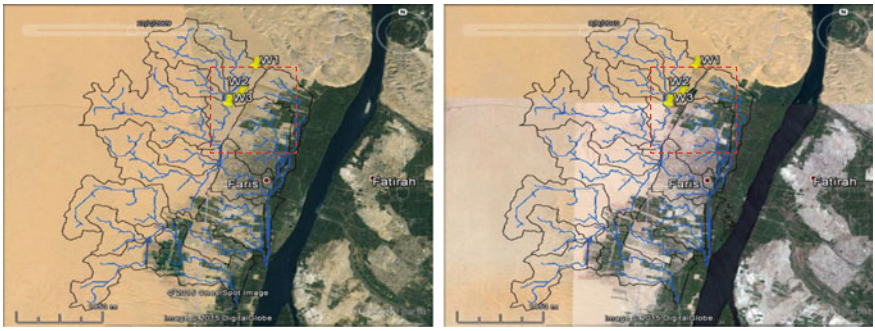

(a) (b)

Fig. 22.3 Google maps of the target area from October 2009 (**a**) to August 2010 (**b**), showing the changes in reclamation areas that occurred within one year

Table 22.1 Chemical analysis of water samples collected from groundwater wells, the Nile River, and seepage water (uprising water)

Parameter	Surface (Nile River)	Seepage (uprising groundwater)	Well 1	Well 2	Well 3
pH	7.5	7.4	7.3	7.24	7.39
TDS	152.3	1180.7	937.2	1297.56	1267.1
HCO4-	116	300	190	220	209
Total hardness	110	296	352.4	407.4	350
Calcium	28.8	67.2	95.1	97	85
Magnesium	9.12	30.7	27.9	39.6	33.5
Sulfate	18	265.5	256.6	338.8	335

irrigation systems, especially on newly reclaimed lands in the desert region. Consequently, the problem of groundwater level uprising would be solved, as well as the sustainable management of the available groundwater in the desert.

22.5 Hydrogeochemical Characteristics

High-quality water is of basic importance to human life and its existence (Lamikarna 1999). The chemistry of groundwater and its nexus to the dominant hydrogeological circumstances have been considered, especially in arid and semi-arid regions. In this paper, we attempt to address the following issues regarding the hydrogeochemistry of the aquifer in the study region: the physical parameters of the

groundwater, chemical parameters of the groundwater, groundwater types, hydrochemical profiles, and hydrochemical genetic classification.

22.5.1 Methodology and Sampling

Thirty-three groundwater samples were collected from three groundwater wells during the period of time from October 2011 to July 2013 and then analyzed for major ions (Ca^{++}, Mg^{++}, Na^{+}, HCO_3^{-}, SO_4^{--}, and Cl^{-}), minor components (Fe^{++}, Mn^{++}, NH_3, NO_2^{-}, and NO_3^{-}), and trace elements (Pb, Cd, and Cr). The techniques and methods followed for the collection and preservation of the samples were in accordance with the 20th edition of the Standard Methods of the American Public Health Association (1998).

22.5.2 Physical Characteristics of Groundwater

In the study area, the groundwater temperature ranges between 27.3 °C (min.) and 31.5 °C (max.). The pH values of the collected groundwater samples ranged between 7 and 8.3, which reflect that the water samples vary from neutral to slightly alkaline groundwater.

22.5.3 Chemical Characteristics of Groundwater

According to Faust and Aly (1981), natural groundwater contains many chemical species in the dissolved state. The occurrence of these constituents results from many physical and chemical weathering processes on geologic formations and from many chemical reactions. Furthermore, the nature of these constituents is a function of the geological type comprising the surrounding area. Glower (1983) reported that anthropogenic changes in groundwater are controlled by humanity's influence, geochemical, physical, and biological processes underground, and hydrogeological conditions.

22.5.3.1 Electrical Conductivity

The electrical conductivity in the study area ranges from 698.78 to 1966 µS/cm. Figure 22.4a illustrates that the EC in Well 1 is lower than that in Well 2 and Well 3. As a result of intensive and prolonged agricultural practices (due to the overdrafting from this well as the farmers use surface flooding systems), the EC exhibits a linear increase from 698.78 µS/cm to 1420 µS/cm within approximately two years.

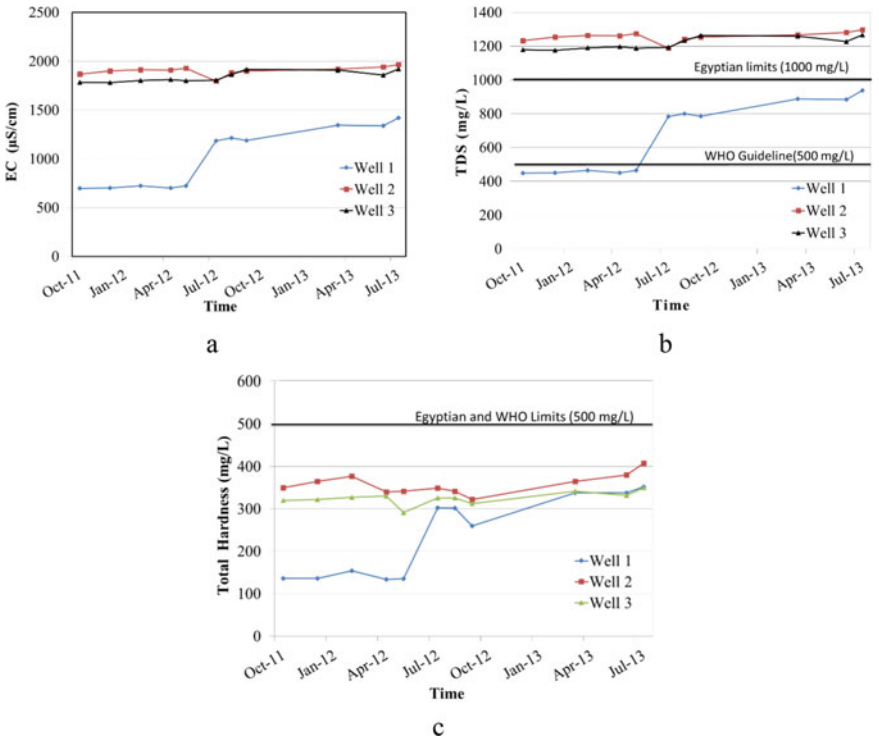

Fig. 22.4 **a** The EC values, **b** TDS values, and **c** total hardness values of the groundwater samples in the study area

22.5.3.2 Total Dissolved Solids (TDS)

Water with a high TDS level may taste salty and be corrosive, resulting in scale formation, which decreases the efficiency of hot water heaters (Sawyer and McCarty 1967). In the study area, the TDS values range from 447.22 to 1297.56 mg/L (Fig. 22.4b). In Well 2 and Well 3, the TDS concentrations are higher than the limits of the WHO and the Egyptian standards. Well 1 water shows a linear increase from acceptable levels to over-the-limit levels.

22.5.3.3 Total Hardness

The hardness of water mainly depends upon the amount of calcium or magnesium salts in the water or both (Rao 2011; Meena and Bhargava 2012). The total hardness concentrations of the sampled water range from 134 to 380 mg/L (Fig. 22.4c), indicating that the groundwater in the study area can be considered

hard water to very hard water. Additionally, in Well 1, the total hardness of the water increases with time due to the overpumping of groundwater.

22.5.3.4 Alkalinity

The alkalinity of water is controlled by the presence of carbonate, bicarbonate, and hydroxide compounds of sodium, calcium, and potassium (Pandey and Pandey 2012). The alkalinity values range from 178 to 226 mg/L. It was found that 85% of the groundwater samples have a total hardness greater than their total alkalinity, which indicates that the groundwater is characterized by permanent (non-carbonate) hardness (Chow 1964).

22.5.3.5 Concentration of Major Ions

The analyzed major cations are calcium (Ca^{2+}), magnesium (Mg^{2+}), sodium (Na^{+}), and potassium (K^{+}), and the major anions are carbonate (CO_3^{2-}), bicarbonate (HCO_3^{-}), chloride (Cl^{-}), and sulfate (SO_4^{2-}). Regarding the calcium ion concentration, in the study area, the calcium concentrations range from 32.19 to 97 mg/L (Fig. 22.5a). The measured calcium concentrations in the three wells were within the acceptable limit, but Well 1 showed an increasing trend with time. The sodium concentration (Fig. 22.5b) ranges from 82 to 283 mg/L. Well 1 shows strong changes with increasing trends due to the intensive and prolonged use of water for irrigation purposes, which led to an increase in the salinity of the well water. Wells 2 and 3 have high concentrations of sodium due to leaching processes. The magnesium concentrations in the groundwater range from 11.5 to 39.6 mg/L (Fig. 22.5c). Low values of magnesium ions were observed in Well 1, and high values were recorded in Wells 2 and 3; this may be attributed to the limestone plateau, which contains magnesium-bearing minerals.

In the study area, the potassium concentrations range between 2.7 mg/L and 10.19 mg/L. The bicarbonate concentration in the groundwater ranges between 178 mg/L and 226 mg/L. The sulfate concentrations range from 68 to 360 mg/L. Well 1 shows low concentrations at the beginning of the analysis, and due to overdrafting, the sulfate concentration exceeded the limit of WHO standards. Wells 2 and 3 show high concentrations of sulfate because of the leaching processes of highly soluble sulfate-bearing minerals such as gypsum and anhydrite (Fig. 22.5d). Chloride concentrations in excess of approximately 250 mg/L can give rise to detectable tastes in water and cause laxative effects (Chand 1999). The chloride ion concentrations in the groundwater range from 63 to 356 mg/L. In most groundwater samples containing high values of sodium, there is also a high concentration of chloride ions. The chloride concentrations of Wells 2 and 3 are higher than the WHO limits, and while the water in Well 1 is lower than the limit, there exists a threat of dramatic increases in concentrations within two years due to overpumping (Fig. 22.5e).

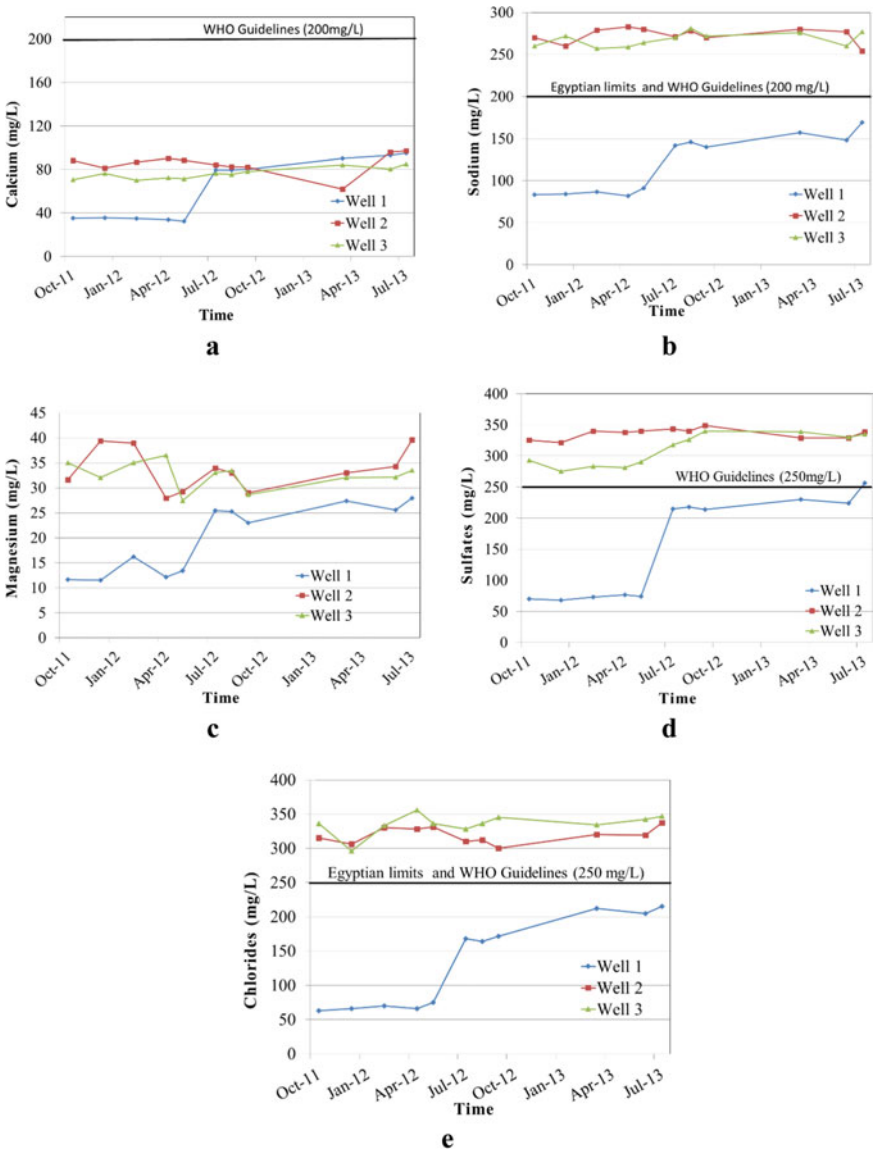

Fig. 22.5 **a** Calcium concentrations, **b** sodium concentrations, **c** magnesium concentrations, **d** sulfate concentrations, and **e** chloride concentrations in the groundwater samples in the study area

Iron occurs in the minerals hematite, magnetite, pyrite, and siderite. The recommended iron level by the United Nations Food and Agriculture Organization (FAO) for irrigation waters is 5 mg/L (American Public Health Association 1998).

Based on the Secondary Drinking Water Standards and regulations recommended by The United States Environmental Protection Agency (EPA), the acceptable limit of Iron is 0.3 mg/L for drinking purposes. In the study area, the iron concentrations range between 0.01 mg/L and 0.1 mg/L. The manganese ion concentrations range from 0.11 mg/L to 0.47 mg/L.

22.6 Water Types

Classification methods are used to differentiate the chemical types of water and identify the dominant types. One of these methods is the Kurlov formula (Kurlov 1928), which is a very useful method for the primary characterization of the chemical composition of water. The ion dominance sequence in Well 1 changed from $HCO_3^- > Cl^- > SO_4^{2-}$/ $Na^+ > Ca^{2+} > Mg^{2+}$ to $Cl^- > SO_4^{2-} > HCO_3^-$/ $Na^+ > Ca^{2+} > Mg^{2+}$ due to overdrafting withdrawal for flood irrigation. In Wells 2 and 3, the abundant sequences for both cations and anions are steady and follow the order $Cl^- > SO_4^{2-} > HCO_3^-$/ $Na^+ > Ca^{2+} > Mg^{2+}$.

22.7 Groundwater Genesis and Hydrochemical Facies

22.7.1 Hydrochemical Parameters

The hydrochemical parameters are calculated by hydrogeochemical indicators such as ionic ratios. These ratios express the relationships between the different ions in terms of mathematical ratios, which are helpful in determining hydrochemical resemblances or differences among different water types. For instance, the ratios are useful in detecting the previous hydrochemical processes that have affected water quality, such as mixing, leaching, and ion exchange. In addition, such ratios may also be useful in distinguishing between groundwater having paleosalinity characteristics and mineralization characteristics resulting from evaporation processes or by seawater contamination.

The ionic concentrations in these ratios are calculated according to their equivalent concentrations (epm), and the ionic ratios are discussed. The value of $Na^+ + K^+/Cl^-$ (meq/L), as a parameter, is very important, as it gives an indication of the genesis and origin of groundwater (marine or fresh water). In marine or seawater, this value ranges between 0.85 and 0.87, while in fresh meteoric water, it is over one. The Na + K/Cl values in the study area range between 1.13 epm and 2.09 epm, indicating that the groundwater samples are of meteoric origin. The ratio of sulfate to chloride (SO_4^{2-}/Cl^- (meq/l) is useful in determining any excess sulfate content in the groundwater due to the dissolution of sulfate minerals or sewage contamination. In the study area, it is obvious that all values of SO_4^{2-}/Cl^- are less

than one, and thus, chloride ions predominate. Low values of this ratio (Ca^{2+}/Mg^{2+} (meq/l)) indicate that the magnesium content exceeds the calcium content. However, high values of this ratio indicate the evaporative dissolution of gypsum and anhydrite or ion exchange. In the study area, all values of the ratio are more than one because the calcium ion concentration is more than that of magnesium ions, which indicates the leaching of calcium-rich sediments. The Na^+/K^+ (meq/l) ratio gives an indication of the extent of the distance between the wells and the recharging sources. If the ratio is less than 50, the wells are near the recharge sources, and if the ratio is more than 50, the wells are far from the recharge sources. In the study area, most of the Na^+/K^+ values of water in Well 1 are less than 50, and this well is near its recharge sources (Fault). In Wells 2 and 3, the Na + /K + ratios are more than 50 due to the long distance between these wells and recharge sources. The ratio of Cl^-/ sum anions (meq/l) reflects the groundwater sources (Hounslow 2018). When the ratio is > 0.8 and TDS > 500, the source is seawater or brine, or evaporates; when the ratio is > 0.8 and TDS < 100, the source is rainwater; and when the ratio is < 0.8 the source is rock weathering. This ratio is less than 0.8 in the groundwater samples of the study area. The standard values for seawater are $rK^+/rCl^- = 0.0181$, $rNa^+/rCl^- = 0.8537$, $rMg^{2+}/rCl^- = 0.1986$ and $rSO_4^{2-}/rCl^- = 0.103$ (Ovchinnikov 1955). According to this method, approximately 85% of samples belong to deep meteoric origin, and 15% belong to shallow meteoric origin.

22.7.2 Hydrochemical Classification

Different methods have been suggested for the chemical classification of groundwater. The trilinear diagram of Piper (1944) is one of the most widely used graphical methods for the classification of natural waters. In the study area, the plotting results of the chemical analysis of the groundwater samples over a period of time illustrate that sodium ions represent the main dominant cations, while chloride ions represent the dominant anions. This reflects that most groundwater samples have sodium chloride facies (Fig. 22.6). In addition, the water type in Well 1 changed from sodium bicarbonate to sodium chloride. This might be attributed to the impact of overdrafting withdrawal from this well.

According to the semilogarithmic diagram (Schoeller 1962), based on the plotted chemical analyses of the groundwater for the periods 10/2011, 7/2012, and 7/2013, the following patterns are recognized. In Well 1, the pattern changed from $HCO_3^- > Cl^- > SO_4^{2-}/ Na^+ > Ca^{2+} > Mg^{2+}$ to $Cl^- > SO_4^{2-} > HCO_3^-/ Na^+ > Ca^{2+} > Mg^{2+}$, which means that the groundwater chemistry changed from NaHCO3 to NaCl. However, in the other two wells, the main patterns are $Cl^- > SO_4^{2-} > HCO_3^-/ Na^+ > Ca^{2+} > Mg^{2+}$, where Na^+ and Cl^- are the dominant ions.

Based on Stiff diagrams (1951), in 10/2011, we found that the alkali contents ($Na^+ + K^+$) were higher than the alkaline earth contents ($Ca^{2+} + Mg^{2+}$), and the

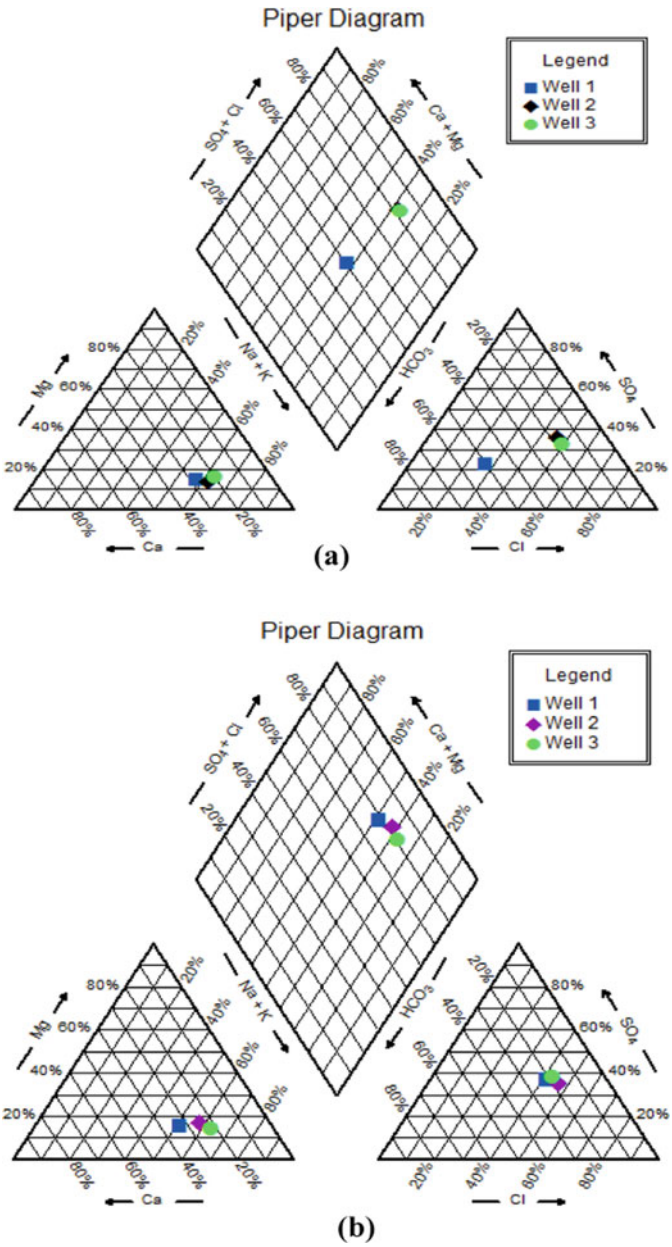

Fig. 22.6 Piper trilinear diagrams in 10/2011 (**a**) and 7/2013 (**b**) showing the changes in chemistry of water in Well 1 (green square) due to the impact of overdrafting withdrawal

strong acid contents ($Cl^- + SO_4^{2-}$) were higher than the weak acid contents ($CO_3^{2-} + HCO_3^-$) in Wells 2 and 3. However, in Well 1, weak acids ($CO_3^{2-} + HCO_3^-$) were more abundant than strong acids ($Cl^- + SO_4^{2-}$). In 7/2012 and 7/2013, all groundwater samples were characterized by the abundance of chloride ions and sodium ions.

22.8 Future Prediction of Water Quality

The previous chemical characterization and analysis revealed that the chemistry of groundwater in Well 1 changed from one phase to another phase due to the impact of overpumping. Therefore, we attempt in this part to discuss and determine the future circumstances of the groundwater of this well. The analyzed data collected during the period of time from October 2011 to June 2013 are used to estimate the linear trends of several chemical parameters at Well 1. We estimated the predicted changes in the chemical characteristics of the groundwater. The TDS values at Well 1 increased with time from 447.2 mg/L to 937.2 mg/L (Fig. 22.7a). Based on the trend line, we expect that the TDS level after 3.3 months (69 days, at 10/2013) will exceed the standard limit (1000 mg/L) of TDS according to the Egyptian Standard of 2007. The TH values at Well 1 also increased with time by a rate of approximately 0.88 mg/L/month (Fig. 22.7a), indicating that after 17.1 months (513 days, at 12/2014), it will exceed the standard limit (500 mg/L). The sodium (Na +) concentrations increased at a rate of approximately 0.144 mg/L/month (Fig. 22.7b), indicating that after 10.4 months (nearly at 5/2014), the sodium (Na +) concentrations will become over the limit (200 mg/L). The calcium (Ca^{++}) concentrations increased with a linear trend rate of approximately 0.144 mg/L/month (Fig. 22.7b), indicating that after 42.2 months (approximately 3.5 years, at 1/2017), the Ca^{++} value will cross the maximum contaminant limit (200 mg/L). The magnesium (Mg^{++}) concentration increased with a linear trend rate of approximately 0.028 mg/L/month (Fig. 22.7b), revealing that after 202.7 months (approximately 17 years, at 10/2030), it will cross the maximum contaminant limit (150 mg/L). The chloride (Cl^-) concentrations increased with a linear trend rate of approximately 0.28 mg/L/month (Fig. 22.7b), indicating that after 6 months (nearly 1/2014), the chloride concentrations will exceed the maximum contaminant limit (250 mg/L). The sulfate (SO_4^{2-}) concentration increased with a linear trend rate of approximately 0.33 mg/L/month (Fig. 22.7b), indicating that after 34 months (approximately 3 years, at 7/2016), it will exceed the 500-mg/L limit. It was found that there are dramatic changes in the quality of the groundwater of Well 1, showing a noticeable increase in parameter values from acceptable values to values over standard limits, resulting in quality deterioration in the near future, within a few years. This may be attributed to the overdrafting of groundwater from this well for agricultural activities, as inhabitants of the area use flooding systems in irrigation.

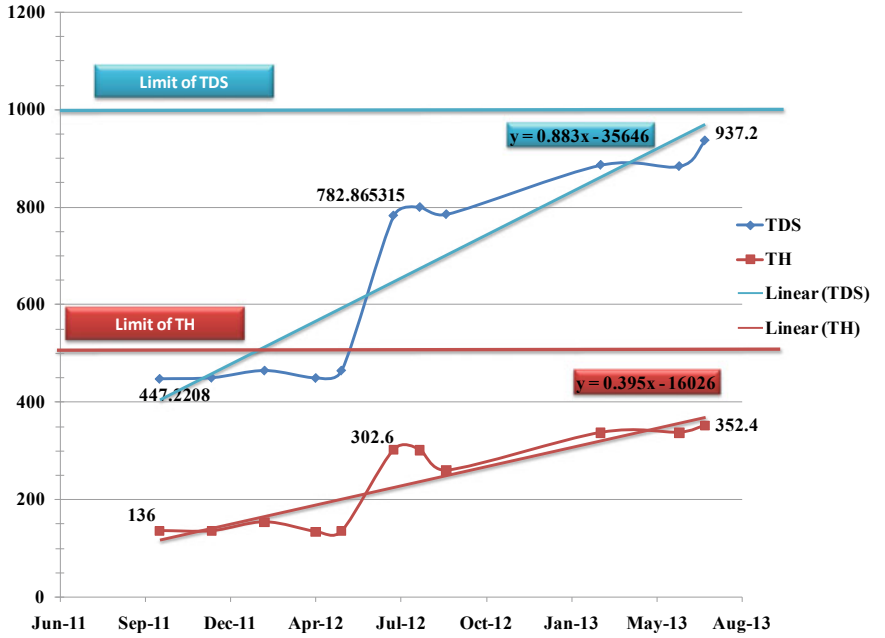
1200
1000
800
600
400
200
0
Limit of TDS
Limit of TH
y = 0.883x - 35646
937.2
782.865315
447.2208
y = 0.395x - 16026
352.4
302.6
136
TDS
TH
Linear (TDS)
Linear (TH)
Jun-11
Sep-11
Dec-11
Apr-12
Jul-12
Oct-12
Jan-13
May-13
Aug-13

(a)

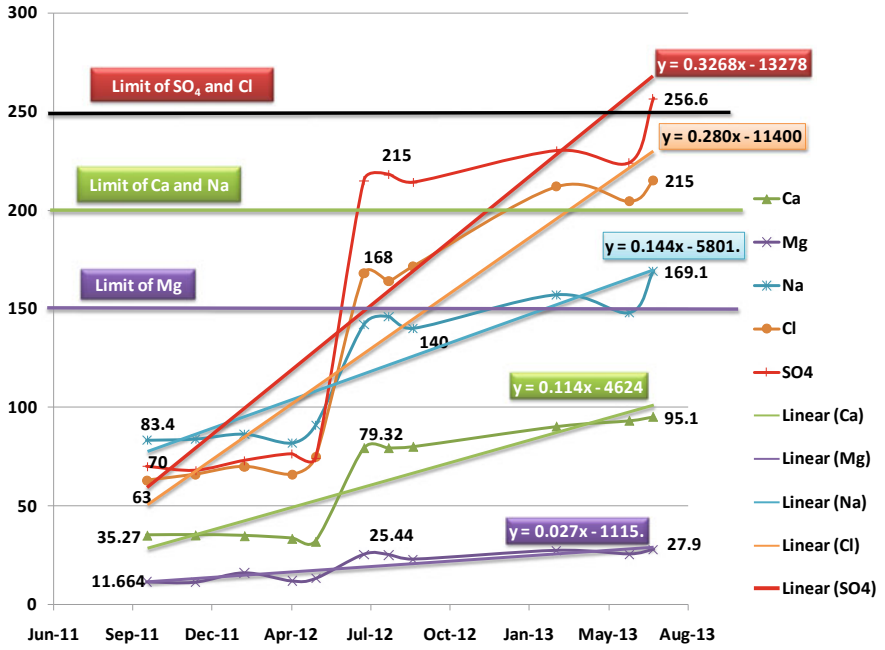
300
250
200
150
100
50
0
Limit of SO4 and Cl
Limit of Ca and Na
Limit of Mg
y = 0.3268x - 13278
256.6
y = 0.280x - 11400
215
215
168
y = 0.144x - 5801.
169.1
140
y = 0.114x - 4624
83.4
70
63
79.32
95.1
35.27
25.44
y = 0.027x - 1115.
27.9
11.664
Ca
Mg
Na
Cl
SO4
Linear (Ca)
Linear (Mg)
Linear (Na)
Linear (Cl)
Linear (SO4)
Jun-11
Sep-11
Dec-11
Apr-12
Jul-12
Oct-12
Jan-13
May-13
Aug-13

(b)

◂**Fig. 22.7** **a** The linear trends of TDS and TH in the water of Well 1, and **b** the linear trends of Ca^{++}, Mg^{++}, Na^{+}, Cl^{-} and SO_4^{--}in the water of Well 1

22.9 Bacteriological Analysis of Groundwater

It is well known that the main threat to human health related to drinking water is microbial contamination. A risk assessment of pathogens and chemicals in drinking water concluded (Regli et al. 1993) that the risk of death from known pathogens in untreated water is 100 to 1000 times greater than the risk of cancer from known disinfection byproducts in chlorinated drinking water, and that the risk of illness from pathogens is 10,000 to 1,000,000 times greater than the risk of cancer from disinfection byproducts in chlorinated drinking water; if the water treatment is inadequate, or if the water distribution system is inadequate, drinking water may contain sufficient numbers of pathogens to cause illness (O'Connor 2000). These pathogenic microorganisms can cause diseases, and the detection of these organisms such as dysentery and typhoid may take long time; in addition, special equipment is required for these detections. For a long time, public health officials/scientists assessed water quality by enumerating fecal coliform and E. coli levels in rivers, estuaries, lakes, and coastal waters (Malakoff 2002; Pandey et al. 2012; Pandey and Soupir 2013). Water that is free of coliform bacteria gives an indication of the validity of that water for human consumption bacteriologically. In contrast, the presence of these bacteria in water is considered proof of pollution and results in the disqualification of that water for drinking. The prevention of waterborne diseases lowers the disease burden in developing countries and improves health, leading to poverty reduction.

In the study area, groundwater samples were collected at different times: 12/2011, 8/2012, 3/2013, and 7/2013. These water samples were analyzed for total heterotrophic bacteria (THB), total coliform, and fecal coliform levels. The spread plate technique was employed to enumerate the bacteria, and the total number of heterotrophic bacteria was determined using nutrient agar medium. The most likely number (MPN) method was employed for the total and fecal coliform levels. In drinking water, total coliform and E. coli should be absent (WHO 1994), so water from most sources is unfit for immediate consumption without some sort of treatment (Raymond 1992). The bacteriological quality of the sampled groundwater samples indicated the absence of total heterotrophic bacteria and total and fecal coliform bacteria, which means that groundwater samples are negative (free from biological contamination) because the aquifer is far enough from the urban area and exists in highlands in the desert.

22.10 Conclusions

In this study, chemical and biological analyses of groundwater aquifers were carried out, in addition to environmental investigations of the impacts of the uprising groundwater level in the target area. The environmental impacts of the uprising groundwater level were discussed and confirmed by watershed analysis using DEM and GIS techniques and by chemical analyses of water samples from uprising water, groundwater wells, and the Nile River water in order to determine the water source and the reason for the uprising water in the low-lying regions. We found that the use of flood irrigation systems in the upper, newly reclaimed lands (in the desert), lakes in agricultural drainage systems, and the absence of sewage networks are the main causes of uprising groundwater levels. Therefore, it is recommended that the use of flood irrigation systems is stopped and that another, new technology system for irrigation is used, in addition to constructing sewage and drainage systems in the whole city area.

A chemical analysis of the groundwater aquifer in the Fares area was conducted and showed that the groundwater in the study area has normal physical properties wherein the water samples varied from neutral to slightly alkaline groundwater. The TDS values ranged from 447.22 to 1297.56 mg/l. It was obvious that water from Well 1 had lower concentrations of TDS than did the waters in the other two wells (Wells 2 and 3). The calcium concentrations ranged from 32.19 to 97 mg/L, the magnesium concentrations ranged from 11.5 to 39.6 mg/L and the total concentrations of sodium and potassium ranged from 84.8 to 292 mg/L. The bicarbonate concentrations ranged from 178 to 226 mg/L, the sulfate concentrations ranged from 68 to 360 mg/L, and the chloride concentrations ranged from 63 to 356 mg/L. Most groundwater samples contained high values of sodium and chloride ions. The most important finding from the chemical analysis is that there were dramatic changes observed in the water quality of Well 1 groundwater, showing a noticeable increase in parameter values from acceptable values to values over standard limits, resulting in quality deterioration in the near future within a few years. This may be attributed to the overdrafting of groundwater from this well for agricultural activities, as inhabitants of the area use flooding systems in irrigation.

Different methods were suggested for the chemical classification of groundwater such as the trilinear diagram of Piper, semilogarithmic diagrams (Schoeller), and Stiff diagrams. They illustrated that sodium ions represent the main dominant cations, while chloride ions are considered the dominant anions. This reflects that most groundwater samples have sodium chloride facies. In addition, the water type in Well 1 changed from sodium bicarbonate to sodium chloride. This might be attributed to the impact of overdrafting withdrawal from this well. The chemical patterns in Well 1 changed from $HCO_3^- > Cl^- > SO_4^{2-}$/ $Na^+ > Ca^{2+} > Mg^{2+}$ to $Cl^- > SO_4^{2-} > HCO3^-$/ $Na^+ > Ca^{2+} > Mg^{2+}$, which means that the groundwater chemistry changed from NaHCO3 to NaCl. However, in the other two wells, the main patterns are $Cl^- > SO_4^{2-} > HCO_3^-$/ $Na^+ > Ca^{2+} > Mg^{2+}$, wherein Na^+ and Cl^- were the dominant ions. The groundwater origin samples show that all of the

collected groundwater samples are of meteoric origin. A total of 85% of the samples belong to deep meteoric origins, and 15% belong to shallow meteoric origins.

Furthermore, a microbiological analysis of the groundwater of the study area was carried out, showing negative results, which means that the groundwater in the study area is free from pathogenic organisms because the wells are far from urbanization areas. Based on this study, we recommend that the people and governorate in Aswan City, Egypt, control and manage the use of groundwater from these wells because the current research states that the quality of the wells will dramatically decrease within the next few years. Additionally, further groundwater modeling analyses regarding the problem of groundwater uprising in the target city constitute our near-future research.

Acknowledgements This work was funded by the TEMPUS Project of Applied Environmental Geosciences and Water Resources Management (JEP-32005-2004), Assiut University, Egypt.

References

Abd El-Razik T, Razavaliaev A (1972) On the tectonic origin of the Nile Valley between Idfu and Qena, Egypt. J Geol 16–2:235–245

American Public Health Association (1998) Standard Methods for the examination of water and waste water, 20st Ed., Washington, DC. (1998)

Aydin (2007) The microbiological and physico-chemical quality of groundwater in West Thrace, Turkey. Pol J Environ Stud 16(3):377

Balachandar D, Sundararaj P, Rutharvel MK, Kumaraswamy K (2010) An investigation of groundwater quality and its suitability to irrigated agriculture in Coimbatore District, Tamil Nadu, India—A GIS approach. Int J Environ Sci 1(2):176–190

Briancesco R (2005) Microbial indicators and fresh water quality assessment. A IST Super Sanita 41:353

Chand D (1999) Fluoride and human health-causes in concern. Indian J Environ Protec 19(2):81–89

Chow (1964) Handbook of Applied Hydrology. McGraw-Hill Book Company

Corapcioglu MY, Haridas A (1984) Transport and fate of microorganisms in porous media: a theoretical investigation. J Hydrol 72:149–169

Craun GE (1984) Health aspects of groundwater pollution. In: Bitton G, Gerba CP (eds) Groundwater pollution microbiology. John Wiley & Sons, Inc., New York, pp 135–179

Dhiviyaa PTS, Venkatesa RT, Punithavathi L, Karunanithi S, Bhaskaran A (2011) Groundwater pollution in the palar riverbed near Vellore, Tamil Nadu, India. Indian J Sci Tech 4–1:19–21

Domenico PA, Schwartz FW (1990) Physical and chemical hydrogeology. Wiley, New York, pp 410–420

Dougerty TC, Hall AW, Wallingford HR (1995) Environmental impact assessment of irrigation and drainage projects

EGPC and Conoco (1977) Aeromagnetic anomaly map of southern Egypt; scale 1:500,000 Complied by the "La Compagnie General De Geophysique" Cairo, Egypt

EGPC and Conoco (1987) Geological map of Egypt, Scale 1:500,000 Cairo, Egypt

Emberger L (1951) Raoirtsur les regions arideset semi-arides de L'Afrique due Nord, les bases ecologiques de la regeneration de la vegetation des zone arides. Internet Urion Biol Sci Ser B Paris 9:50–61

Faust SD, Aly OM (1981) Chemistry of natural waters published by Ann Arbor Science, Michigan, 400

Fenwick A (2006) Waterborne—Could they be consigned to History? Science 313:1077–1081

Freeze RA, Cherry JA (1979) Groundwater. Prentice-Hall, Englewood Cliffs, NJ, USA

Gerba CP, Keswick BH (1981) Survival and transport of enteric viruses and bacteria in groundwater. In: van Duijvenbooden W, Glasbergen P, van Lelyveld H (eds) Studies in environmental science. Elsevier Scientific Publ. Co., The Netherlands, pp 511–515

Glower A (1983) Underground purification capacity. Groundwater in water resources planning published by International Association of Hydrogeologists, UNISCO. Federal republic of Germany, vol 2, pp 1063–1072

Hakim MA, Juraimi AS, Begum M, Hasanuzzaman M, Uddin MK (2009) Suitability evaluation of groundwater for irrigation, drinking and industrial purposes. Am J Environ Sci 5:413–419

Hounslow AW (2018) Water quality data—analysis and interpretation. CRC Press LLC, 85

IPCC (2001) Climate change 2001: the scientific basis. In: Houghton JT, Ding Y, Griggs DJ, Noguer M, van der Linden PJ, Dai X, Maskell K, Johnson CA (eds) Contribution of working group I to the third assessment report of the intergovernmental panel on climate change. Cambridge University Press, Cambridge, United Kingdom and New York, NY, USA, 881pp

Irwin RW (1997) Handbook of drainage principles, publication 73. Toronto ON. Ontario Ministry of Agriculture, Food and Rural Affairs

Jain CK, Bandyopadhyay A, Bhadra A (2009) Hydrochemical appraisal of groundwater and its suitability in the intensive agricultural area of Muzaffarnagar district, Uttar Pradesh, India. Environ Geol 56:901–912

Kortatsi BK (2007) Hydrochemical framework of groundwater in the Ankobra Basin, Ghana. Aquat Geochem 13(4):1–74

Kurlov M (1928) Classification of mineral waters of Siberia, Tomsk, U.S.S.R.

Lamikarna A (1999) Essential microbiology for student and practitioner of Pharmacy, Medicine and Microbiology, 2nd edn, Amkra books Lagos, p 406

Liu L, Johnson HL, Cousens S, Perin J, Scott S, Lawn JE, Rudan I, Campbell H, Cibulskis R, Li M, Mathers C, Black RE (2012) Child health epidemiology reference group of WHO and UNICEF. Global, regional, and national causes of child mortality: an updated systematic analysis for 2010 with time trends since 2000. Extern Web Site Icon Lancet 379(9832):

Malakoff D (2002) Water quality: microbiologists on the trail of polluting bacteria. Science 4 (5564):

Meena BS, Bhargava N (2012) Physiochemical characteristics of groundwater of some villages of Dag Block in Jhalawar district of Rajasthan State (India). Rasayan J Chem 5(4):438–444

Ministry of Water Resources and Irrigation (MWRI) (2007) The final technical report—the results of the groundwater potential study in the desert alternative housing project in Aswan—Urgent Plan—The new Fares, The New Elramady and The New Allaqi

Mitra BK, Sasaki C, Enari K, Matsuyama N, Pongpattanasiri S (2007) Suitability assessment of shallow groundwater for irrigation in sand dune area of northwest Honshu Island, Japan. Int J Agric Res 2:518–527

Nagarajan R, Rajmohan N, Mahendran U, Senthamilkumar S (2010) Evaluation of groundwater quality and its suitability for drinking and agricultural use in Thanjavur city, Tamil Nadu, India. Environ Monit Assess 171:289–308

Nickson RT, McArthur JM, Shrestha B, Kyaw-Nyint TO, Lowrt D (2005) Arsenic and other drinking water quality issues, Muzaffargarh District, Pakistan. Appl Geochem 20:55–68

O'Connor DR (2002) Report of the Walkerton Inquiry – Part 1. Events of May 2000 and Related Issues: Queen's Printer for Ontario

Ovchinnikov AM (1955) General hydrogeology. USSR, Moscow

Pandey R, Pandey SK (2012) Investigations of physico-chemical status of ground water of Singrauli District, Madhya Pradesh, India. Int J Pharmac Sci Res 3(10):

Pandey PK, Soupir ML (2013) Assessing the impacts of E. coli laden streambed sediment on E. coli loads over a range of flows and sediment characteristics. J Am Water Resour Assoc 4 (6):1261–1269

Pandey PK, Soupir ML, Rehmann CR (2012) A model for predicting resuspension of Escherichia coli from streambed sediments. Water Res 4:115–126
Pedley S, Howard G (1997) The public health implication of groundwater microbiology. Q J Eng Geol 30(2):179
Piper AM (1944) A graphic procedure in geochemical interpretation of water analysis. Trans Amer Geophys Union 25:914–928
Rao VB (2011) Physicochemical analysis of selected ground water samples of Vijayawada rural and urban in Krishna district, Andhra Pradesh, India. Int J Environ Sci 2(2):722–726
Raymond FL (1992) Problame dis eandans le monde (problems of water). EB and Sons Ltd., UK, pp 123–126
Regli S, Berger P, Macler B, Haas C (1993) Proposed decision tree for management of risks in drinking water: Consideration for health and socioeconomic factors. In: Craun GF (ed) Safety of water disinfection: balancing chemical and microbial risks. ILSI Press, Washington DC
Reid DC, Edwards AC, Cooper D, Wilson E, Mcgaw BA (2003) The quality of drinking water from private water supplies in Aberdeenshire, UK. Wat Res 37:245
Ritter WF, Shirmohammadi A (2001) Agricultural nonpoint source pollution. Watershed management and hydrology. CRC Press LLC, Florida
Saber M, Abdelshafy M, Faragallah ME, Abd-Alla MH (2014) Hydrochemical and bacteriological analyses of groundwater and its suitability for drinking and agricultural uses at Manfalut District, Assuit, Egypt. Arab J Geosc 7(11):. https://doi.org/10.1007/s12517-013-1103-2
Said R (1962) The geology of Egypt. El Sevier, Amsterdam New York
Said R (1981) The geological evaluation of the River Nile. Springer Verlage, New York, p 151
Sawyer CN, McCarty PL (1967) Chemistry for sanitary engineers, 2nd edn, McGraw-Hill Series in Sanitary Science and Water Resources Engineering. McGraw-Hill, Toronto
Schoeller H (1962) Geochemie des eauxsouterraines. Rev. de I' Institute Francais du Petrole 10:230–244
Shalaby MY (2005) Educational requirements for young graduates for modern irrigation systems on New Lands—Nubaria. Res Bull Soc Protect Environ Rural East Reg 2(2)
Stiff H (1951) The interpretation of chemical water analysis by means of patterns. J Petrol Tech 3:15–17
Trivedy RK, Goel PK, Trishul CL (1987) Practical methods in ecology and environmental science. Environmental Publication, Karad
UNESCO (2000) Groundwater pollution, international hydrological programme
United Nations Environmental Program (UNEP) (1999) Global Environmental outlook 2002. Earthscan, UK.
Usharani K, Umarani K, Ayyasamy PM, Shanthi K, Lakshmanaperumalsamy P (2010) Physico-chemical and bacteriological characteristics of noyyal river and ground water quality of Perur, India. J Appli Sci Environ Manag 14(2):29–35
WHO (1994) Guidelines for Drinking Water Quality, 2nd edn. World Health Organization, Geneva
WHO (2004) Guidelines for drinking-water quality, vol 1. Recommendations, 3rd ed. Geneva, Switzerland
WHO/UNICEF (2012) Progress on drinking water and sanitation: 2012 Update. External Web Site Icon United States: WHO/UNICEF Joint Monitoring Programme for Water Supply and Sanitation